frontiers | Research Topics

Diet-microbe-host interactions in metabolic syndrome

Edited by
Gratiela Gradisteanu Pircalabioru, Anca Stoian,
Mariana Carmen Chifiriuc and Manfredi Rizzo

Published in
Frontiers in Nutrition

ISSN 1664-8714
ISBN 978-2-83251-534-1
DOI 10.3389/978-2-83251-534-1

About Frontiers

Frontiers is more than just an open access publisher of scholarly articles: it is a pioneering approach to the world of academia, radically improving the way scholarly research is managed. The grand vision of Frontiers is a world where all people have an equal opportunity to seek, share and generate knowledge. Frontiers provides immediate and permanent online open access to all its publications, but this alone is not enough to realize our grand goals.

Frontiers journal series

The Frontiers journal series is a multi-tier and interdisciplinary set of open-access, online journals, promising a paradigm shift from the current review, selection and dissemination processes in academic publishing. All Frontiers journals are driven by researchers for researchers; therefore, they constitute a service to the scholarly community. At the same time, the *Frontiers journal series* operates on a revolutionary invention, the tiered publishing system, initially addressing specific communities of scholars, and gradually climbing up to broader public understanding, thus serving the interests of the lay society, too.

Dedication to quality

Each Frontiers article is a landmark of the highest quality, thanks to genuinely collaborative interactions between authors and review editors, who include some of the world's best academicians. Research must be certified by peers before entering a stream of knowledge that may eventually reach the public - and shape society; therefore, Frontiers only applies the most rigorous and unbiased reviews. Frontiers revolutionizes research publishing by freely delivering the most outstanding research, evaluated with no bias from both the academic and social point of view. By applying the most advanced information technologies, Frontiers is catapulting scholarly publishing into a new generation.

What are Frontiers Research Topics?

Frontiers Research Topics are very popular trademarks of the *Frontiers journals series*: they are collections of at least ten articles, all centered on a particular subject. With their unique mix of varied contributions from Original Research to Review Articles, Frontiers Research Topics unify the most influential researchers, the latest key findings and historical advances in a hot research area.

Find out more on how to host your own Frontiers Research Topic or contribute to one as an author by contacting the Frontiers editorial office: frontiersin.org/about/contact

Diet-microbe-host interactions in metabolic syndrome

Topic editors

Gratiela Gradisteanu Pircalabioru — University of Bucharest, Romania
Anca Stoian — Carol Davila University of Medicine and Pharmacy, Romania
Mariana Carmen Chifiriuc — University of Bucharest, Romania
Manfredi Rizzo — University of Palermo, Italy

Citation

Pircalabioru, G. G., Stoian, A., Chifiriuc, M. C., Rizzo, M., eds. (2023). *Diet-microbe-host interactions in metabolic syndrome*. Lausanne: Frontiers Media SA. doi: 10.3389/978-2-83251-534-1

Table of contents

frontiers | Frontiers in Nutrition

TYPE Editorial
PUBLISHED 18 January 2023
DOI 10.3389/fnut.2023.1129200

OPEN ACCESS

EDITED AND REVIEWED BY
Ellen E. Blaak,
Maastricht University, Netherlands

*CORRESPONDENCE
Gratiela Gradisteanu Pircalabioru
✉ gratiela.gradisteanu@icub.unibuc.ro

SPECIALTY SECTION
This article was submitted to Nutrition and Metabolism, a section of the journal Frontiers in Nutrition

RECEIVED 21 December 2022
ACCEPTED 03 January 2023
PUBLISHED 18 January 2023

CITATION
Gradisteanu Pircalabioru G, Rizzo M, Pantea Stoian A and Chifiriuc MC (2023) Editorial: Diet-microbe-host interactions in metabolic syndrome. *Front. Nutr.* 10:1129200. doi: 10.3389/fnut.2023.1129200

Editorial: Diet-microbe-host interactions in metabolic syndrome

Gratiela Gradisteanu Pircalabioru[1,2]*, Manfredi Rizzo[3], Anca Pantea Stoian[4] and Mariana Carmen Chifiriuc[1,2,5,6]

[1]Research Institute of University of Bucharest (ICUB), Bucharest, Romania, [2]Academy of Romanian Scientists, Bucharest, Romania, [3]PROMISE Department, University of Palermo, Palermo, Italy, [4]Department of Diabetes, Nutrition and Metabolic Diseases, Carol Davila University of Medicine and Pharmacy, Bucharest, Romania, [5]Romanian Academy, Bucharest, Romania, [6]Faculty of Biology, University of Bucharest, Bucharest, Romania

KEYWORDS

microbiota, metabolic syndrome, diet, obesity, nutrition

Editorial on the Research Topic
Diet-microbe-host interactions in metabolic syndrome

Affecting around 25% of the world's adult population, metabolic syndrome (MetS) is a cluster of metabolic disorders such as insulin resistance, dysglycemia, dyslipidemia, hypertension and central adiposity with visceral fat accumulation (1, 2). Given its impact on host immunity and metabolism, the gut microbiome is a possible culprit in triggering MetS (3, 4). The scope of the "*Diet-microbe-host interactions in metabolic syndrome*" Research Topic was to report new findings in the field of MetS including microbiota patterns linked to metabolic disease, effects of dietary/probiotic/pre-biotic/post-biotic interventions on MetS complications and inflammatory status, host-microbe interactions in metabolic disease, clinical trials using microbiota targeting, as well as personalized medicine approaches.

In this special e-collection there are 11 papers covering several of the above-mentioned aspects.

Reports of gut dysbiosis associated with Western diet consumption have led to increased interest in the role of the microbiome in the development of obesity and MetS (5). To better study these aspects, it is crucial to develop research models that accurately reflect MetS affected populations. Chehade et al. have formulated a modified Standard American Diet (mSAD) to induce the physiological parameters associated with MetS in mice (*A modified standard American diet induces physiological parameters associated with metabolic syndrome in C57BL/6J mice*). The mSAD administration was associated with altered glucose metabolism, increased body weight and reduced abundance of the *Akkermansia* genus.

Chronic systemic inflammation had long been considered as a major player in the development and progression of non-communicable diseases such as MetS (6). Pro-inflammatory cytokines, other adipokines, along free fatty acids secreted from adipose tissue may activate and/or accelerate the development of insulin resistance and other pathological effects. Dietary manipulations may improve the inflammatory status and the microbiota profile in obesity. A study performed on C57BL/6 mice studied the effects of habitual consumption of the traditional peanut cultivar, HN, and the new high-oleic peanut cultivar, HO, as an integral part of diet-induced obesity (*Metabolic and microbiome alterations following the enrichment of a high-fat diet with high oleic acid peanuts versus the traditional peanuts cultivar in mice*) (Anavi-Cohen et al.). The new high oleic acid cultivar was metabolically superior to the traditional peanut type and was associated with a better inflammatory state and microbiome signature (lower levels of the *Erysipelotrichaceae* family).

In mice, acidic activated charcoal improved high fat die-induced obesity and insulin resistance in a dose-dependent manner without any serious adverse effects. Metabolomic analysis of cecal contents revealed that cholesterol, neutral lipids, and bile acids were excreted at significantly higher levels in the feces of mice under charcoal treatment (*Acidic activated charcoal prevents obesity and insulin resistance in high-fat diet-fed mice*) (Zhang et al.).

Using an animal model for non-alcoholic fatty liver disease (NAFLD), Jian et al. showed that long-term exposure to excessive dietary valine influenced amino acid and fatty acid metabolism by promoting fatty acid synthesis, impairing amino acid metabolism, and inducing amino acid imbalance (*Amino acid and fatty acid metabolism disorders trigger oxidative stress and inflammatory response in excessive dietary valine-induced NAFLD of laying hens*).

Another nutritional supplement, represented by astaxanthin (ATX), a xanthophyll carotenoid, was reported to prevent steatohepatitis and hepatic oxidative stress in mice with diet-induced obesity (*Astaxanthin from Haematococcus pluvialis prevents high-fat diet-induced hepatic steatosis and oxidative stress in mice by gut-liver axis modulating properties*) (Wang, Xu et al.). ATX exerted important effects on the microbiome by significantly inhibiting the growth of obesity-related genera *Parabacteroides* and *Desulfovibrio* while promoting the growth of *Akkermansia* and *Allobaculum* genera.

Polydatin (POD), a natural precursor and glycosylated form of resveratrol had important effects on the microbiome by increasing the abundance of beneficial bacterial genera (*Butyrycimonas, Bifidobacterium*). POD administration altered the glucolipid dysmetabolism, insulin resistance, and non-alcoholic fatty liver disease by reducing the oxidative stress and preventing AMP-activated protein kinase (AMPK) suppression induced by high-fructose diet in mice (*Polydatin, a glycoside of resveratrol, is better than resveratrol in alleviating non-alcoholic fatty liver disease in mice fed a high-fructose diet*) (Zhao et al.).

Treatment with the polyphenol rich Black chokeberry (BCP) reduced body weight, liver, and white adipose tissue weight and alleviated hepatic steatosis and dyslipidemia in rats with obesity [*Modulation of the gut microbiota and lipidomic profiles by black chokeberry (Aronia melanocarpa L.) polyphenols via the glycerophospholipid metabolism signaling pathway*] (Zhu et al.). BCPs supplementation increased the relative abundance of genera such as *Bacteroides, Romboutsia*, *Prevotella*, and *Akkermansia* and decreased the relative abundance of genera *Clostridium* and *Desulfovibrio*.

Short-chain fatty acids (SCFA) such as acetate, propionate and butyrate are produced by bacterial fermentation of non-digestible carbohydrates. HFD (high fat diet) before and during pregnancy significantly induced obesity and worsen glucose tolerance, lipid metabolism and insulin sensitivity in gestational mice. Ding et al. emphasized the importance of the rhythmicity of gut microbiota-derived SCFAs in mediating circadian disruption in response to the HFD in gestational mice (*A high-fat diet disrupts the hepatic and adipose circadian rhythms and modulates the diurnal rhythm of gut microbiota-derived short-chain fatty acids in gestational mice*).

In human studies, anti-inflammatory agents together with dietary interventions may be therapeutically useful in treating and preventing MetS (7, 8). A meta-analysis performed by Wang, Liu et al. (*Effects of dietary intervention on inflammatory markers in metabolic syndrome: A systematic review and meta-analysis*) provided evidence that dietary intervention could improve immunological properties, particularly IL-6, in MetS. Subsequent analysis based on subgroups indicated that these results were affected by dietary patterns in MetS. Despite this, it did not reveal the association between dietary intervention and the IL-1β, CRP, and TNF-α levels. Nevertheless, more research is needed to underpin the mechanisms underlying the effect of dietary intervention on MetS associated inflammatory markers.

In women with obesity, a low-glycemic diet significantly altered the microbiota by lowering the abundance of *Gemmiger formicilis*, *Collinsella aerofaciens*, and *Escherichia coli* (*Beneficial effects of a low-glycemic diet on serum metabolites and gut microbiota in obese women with Prevotella and Bacteriodes enterotypes: A randomized clinical trial*) (Hur et al.). Importantly, the low glycemic diet was more efficient in women with obesity and a *Prevotella* dominant enterotype suggesting that dietary patterns could impact metabolic traits differently in different enterotypes, indicating the need of a personalized diet based on enterotypes. Further studies are needed to find appropriate diets for each enterotype.

The use of microbiome regulation (especially the enrichment of some SCFA-producing bacteria or the targeting of specific SCFA-producing bacteria, such as the representative *A. muciniphila* strain, to improve the intestinal environment to help adults with obesity lose weight) has become an attractive strategy reported in several clinical studies (*The therapeutic effect of SCFA-mediated regulation of the intestinal environment on obesity*) (You et al.). Nevertheless, the microbiota is a complex ecosystem, and whether SCFA play a role directly or by regulating gut microbes remains to be explored.

Dietary interventions are essential tools for modifying the microbiota and improve host health. Future studies characterizing the effects of dietary components through the host-microbe axis are pivotal to provide evidence-based dietary interventions to prevent and ameliorate MetS and other metabolic disorders.

Data availability statement

The original contributions presented in the study are included in the article/supplementary material, further inquiries can be directed to the corresponding author.

Author contributions

GG: draft preparation. AP, MR, and MC: review and editing. All authors contributed to the article and approved the submitted version.

Funding

This research was funded by UEFISCDI (project ID PN-III-P1-1.1-PD-2019-0499, grant numbers 224/2021,

C1.2.PFE-CDI.2021-587, CNFIS-FDI-2022-0675, and AOSR Teams 288/20.02.2022).

Acknowledgments

The research project PD224/2021 (PD-2019-0499) is gratefully acknowledged.

Conflict of interest

The authors declare that the research was conducted in the absence of any commercial or financial relationships that could be construed as a potential conflict of interest.

Publisher's note

All claims expressed in this article are solely those of the authors and do not necessarily represent those of their affiliated organizations, or those of the publisher, the editors and the reviewers. Any product that may be evaluated in this article, or claim that may be made by its manufacturer, is not guaranteed or endorsed by the publisher.

References

1. Giglio RV, Stoian AP, Patti AM, Rizvi AA, Sukhorukov V, Ciaccio M, et al. Genetic and epigenetic biomarkers for diagnosis, prognosis and treatment of metabolic syndrome. *Curr Pharm Des.* (2021) 27:3729–40. doi: 10.2174/1381612827666210412145915

2. Rizvi AA, Stoian AP, Rizzo M. Metabolic syndrome: from molecular mechanisms to novel therapies. *Int J Mol Sci.* (2021) 22:10038. doi: 10.3390/ijms221810038

3. Cătoi AF, Vodnar DC, Corina A, Nikolic D, Citarrella R, Pérez-Martínez P, et al. Gut microbiota, obesity and bariatric surgery: current knowledge and future perspectives. *Curr Pharm Des.* (2019) 25:2038–50. doi: 10.2174/1381612825666190708190437

4. Cătoi AF, Corina A, Katsiki N, Vodnar DC, Andreicuț AD, Stoian AP, et al. Gut microbiota and aging-a focus on centenarians. *Biochim Biophys Acta Mol Basis Dis.* (2020) 1866:165765. doi: 10.1016/j.bbadis.2020.165765

5. Hintze KJ, Benninghoff AD, Cho CE, Ward RE. Modeling the western diet for preclinical investigations. *Adv Nutr.* (2018) 9:263–71. doi: 10.1093/advances/nmy002

6. Lumeng CN, Saltiel AR. Inflammatory links between obesity and metabolic disease. *J Clin Invest.* (2011) 121:2111–7. doi: 10.1172/JCI57132

7. Giglio RV, Carruba G, Cicero AFG, Banach M, Patti AM, Nikolic D, et al. Pasta supplemented with opuntia ficus-indica extract improves metabolic parameters and reduces atherogenic small dense low-density lipoproteins in patients with risk factors for the metabolic syndrome: a four-week intervention study. *Metabolites.* (2020) 10:428. doi: 10.3390/metabo10110428

8. Patti AM, Carruba G, Cicero AFG, Banach M, Nikolic D, Giglio RV, et al. Daily use of extra virgin olive oil with high oleocanthal concentration reduced body weight, waist circumference, alanine transaminase, inflammatory cytokines and hepatic steatosis in subjects with the metabolic syndrome: a 2-month intervention study. *Metabolites.* (2020) 10:392. doi: 10.3390/metabo10100392

frontiers in Nutrition

ORIGINAL RESEARCH
published: 31 March 2022
doi: 10.3389/fnut.2022.846591

Effects of Dietary Intervention on Inflammatory Markers in Metabolic Syndrome: A Systematic Review and Meta-Analysis

Mengjun Wang[1†], Junliang Liu[2†], Zhao Zhang[2], Haixiong Zhang[2], Ning Wang[1], Xi Chen[3], Xuemei Han[2], Qian Lu[2] and Shanshan Chi[2]*

[1] Department of Endocrinology, The First Affiliated Hospital of Xi'an Jiaotong University, Xi'an, China, [2] Department of Endocrinology, 521 Hospital of Norinco Group, Xi'an, China, [3] Department of Epidemiology and Statistics, School of Public Health, Medical College, Zhejiang University, Hangzhou, China

Background: Dietary interventions may modulate inflammatory indicators, but the correlations between dietary intervention and inflammatory markers in metabolic syndrome (MetS) settings remain opaque.

Objective: To evaluate the effects of dietary intervention on interleukin-1β (IL-1β), interleukin-6 (IL-6), tumor necrosis factor-α (TNF-α), and C-reactive protein (CRP) in patients with MetS by systematic review and meta-analysis.

Methods: Databases, including PubMed, Embase, Cochrane Library, Scopus, and Google scholar, were searched from June 2011 to June 2021 for relevant available articles. Standardized mean difference (SMD) was generated as effect size by meta-analysis for continuous variants, including IL-1β, IL-6, TNF-α, and CRP levels. Then, according to study characteristics by dietary patterns of the intervention, subgroup analyses were performed.

Results: Finally, 13 studies comprising a total of 1,101 participants were included for the meta-analysis. IL-6 levels in dietary patients were significantly lower than controls (SMD $= -0.30$, 95% CI $= -0.55, 0.04$, $p = 0.02$, $I^2 = 64\%$). However, IL-1β, TNF-α, and CRP levels did not change significantly compared with the control group. Sensitivity analyses further yielded similar results.

Conclusions: Dietary intervention may help decrease IL-6 rather than IL-1β, TNF-α, or CRP levels in patients with MetS.

Keywords: diets, inflammatory markers, IL-6, metabolic syndrome, meta-analysis

OPEN ACCESS

Edited by:
Gratiela Gradisteanu Pircalabioru, University of Bucharest, Romania

Reviewed by:
Evelyn Frias-Toral, Catholic University of Santiago de Guayaquil, Ecuador
Rosaura Leis, University of Santiago de Compostela, Spain

***Correspondence:**
Zhao Zhang
wmj19871112521@163.com

[†]These authors have contributed equally to this work

Specialty section:
This article was submitted to Nutrition and Metabolism, a section of the journal Frontiers in Nutrition

Received: *31 December 2021*
Accepted: *01 March 2022*
Published: *31 March 2022*

Citation:
Wang M, Liu J, Zhang Z, Zhang H, Wang N, Chen X, Han X, Lu Q and Chi S (2022) Effects of Dietary Intervention on Inflammatory Markers in Metabolic Syndrome: A Systematic Review and Meta-Analysis. Front. Nutr. 9:846591. doi: 10.3389/fnut.2022.846591

INTRODUCTION

Metabolic syndrome (MetS) has become a global epidemic disease due to population aging and lifestyle changes, including diets (1). The various definition and criteria for identifying MetS (2) includes interrelated factors, such as abdominal obesity, insulin resistance, hyperglycemia, hypertension, and dyslipidemia (low high-density lipoprotein and increased triglyceride) (3). Sub-clinical TH1–lymphocyte-mediated innate and chronic low-grade inflammation might partially account for its occurrence (4). The interleukin-1 (IL-1) family, particularly IL-1β, is

a group of cytokines that play a central role in the regulation of responses associated with immune and obesity-associated inflammation (5). IL-6 is a major pro-inflammatory cytokine in chronic inflammation that is closely related to insulin resistance, neurodegeneration, cardiovascular disease (CVD), and malignancy (6). A few pro-inflammatory cytokines [IL-6 and tumor necrosis factor-α (TNF-α)] can promote the upgrade of plasma C-reactive protein (CRP) level (7).

Bad eating habits are the controllable factors accelerating the development of inflammation and related diseases, including MetS (8). According to literature, food can modify inflammatory responses. It is also strongly linked to the pathogenesis of MetS (9). A healthy diet could contribute most to managing obesity and MetS (10). Currently, nutritional epidemiology tends to illustrate the relationship between dietary intervention and inflammatory diseases, but do not demonstrate the exact food species (11).

Although some trials have proved that dietary intervention can reduce the serum level of inflammatory factors, it is still controversial if there is an association between dietary intervention and the serum level of inflammatory factors in patients with MetS.

Hence, in this study, we aimed to perform a systematic review and meta-analysis to investigate the effects of dietary intervention on IL-1β, IL-6, TNF-α, and CRP levels in MetS.

METHODS

The current systematic review and meta-analysis was implemented in accordance with the principles of the Preferred Reporting Items for Systematic Reviews and Meta-Analyses (PRISMA) statement (12).

Literature Search Strategy

Database, including PubMed, Embase, Cochrane Library, Scopus, and Google scholar, were searched from June 15, 2011 to June 15, 2021. We used the following mesh terms: "inflammatory markers," "diet" in combination with "metabolic syndrome."

Study Selection

Inclusion criteria were as follows:

(1) Randomized controlled trial (RCT) studies;
(2) Conducted dietary intervention/s of more than 4 weeks;
(3) Meets the diagnostic criteria of MetS;
(4) Studies that provided numbers, means, and standard difference (SDs) of IL-1β, IL-6, TNF-α, and CRP.

Exclusion criteria were as follows:

(1) literature reviews, *in vitro* study, animal study, or case report;
(2) Included patients who had co-morbidities other than MetS;
(3) (Patients were administrated drugs which might change the levels of cytokines of interest;
(4) No full text.

Data Extraction

The following information were collected: (1) publication data (first author's name, publication year, and country), (2) study design, (3) total number of participants, their age, sex, BMI, and study duration, (4) glucose, insulin, blood lipid levels, and blood pressure status, and (5) mean and standard difference for IL-1β, IL-6, TNF-α, and CRP levels.

Quality Assessment

Qualities of enrolled studies were assessed according to the Cochrane Risk of Bias Tool (13). Two investigators independently assessed the quality and extracted data of all included studies. Any discrepancy was adjudicated by a senior investigator.

Statistical Analysis

Review Manager 5.3 was implemented in our analyses. $p < .05$ was considered to be statistically significant. Standardized mean difference (SMD) was generated as effect size by meta-analysis for continuous variants, including IL-1β, IL-6, TNF-α, and CRP levels. If $I^2 < 50\%$ and $p > 0.01$, a fixed-effect model would be used. Otherwise, a random effect model would be implemented. If $I^2 > 75\%$, further analysis encompassing sensitive analysis, subgroup analysis, or meta-regression was carried out to explore the source of heterogeneity. Publication bias was evaluated by funnel plot and Egger's tests.

RESULTS

Search Results and Characteristics

Eventually, 13 articles (14–26) reporting 1,101 patients were enrolled in this study (**Figure 1**). The baseline characteristics are summarized in **Supplementary Table 1**. Intervention duration varied from 8 weeks to 6 months. Studies followed different MetS diagnostic criteria, namely, six studies used the Adult Treatment Panel III criteria (17, 18, 20, 21, 24, 26); three studies used National Cholesterol Education Programme/Adult Treatment Panel III (NCEP-ATP III) criteria (14, 15, 19); two studies used the Joint Interim Statement (JIS) (16, 23); and two studies used International Diabetes Federation criteria (IDF) (22, 24). The dietary patterns of the intervention received by the intervention groups were as follows: low-calorie diet, fatty acids, berry, and whole wheat. We selected the following inflammatory markers: IL-1β, IL-6, TNF-α, and CRP for analysis. They were measured by enzyme-linked immunosorbent assay (ELISA) in all the studies.

Intervention Details

In the included 13 trails, the following six types of dietary intervention patterns were investigated: berry (16, 20, 26), fatty acids (14, 15, 19), low-calorie diet (22, 23), whole wheat (18,

Abbreviations: MetS, metabolic syndrome; IL-1β, interleukin-1β; IL-6, interleukin-6; TNF-α, tumor necrosis factor-α; CRP, C-reactive protein; SMD, Standardized mean difference; CI, Confidence interval; CVD, cardiovascular disease; RCT, Randomized controlled trial; SDs, standard difference; IDF, International Diabetes Federation criteria; JIS, Joint Interim Statement; ATP III, Adult Treatment Panel III criteria; NCEP ATP III, National Cholesterol Education Program, Adult Treatment Panel III; BMI, body mass index; SBP, systolic blood pressure; DBP, diastolic blood pressure; HDL, high-density lipoprotein; LDL, low-density lipoprotein; FPG, Fasting plasma glucose; NR not reported; ELISA, enzyme-linked immunosorbent assay; PUFAs, polyunsaturated fatty acids; NCDs, non-communicable diseases; IRS-1, insulin receptor substrate 1; DiOGenes, Diet, Obesity, and Genes.

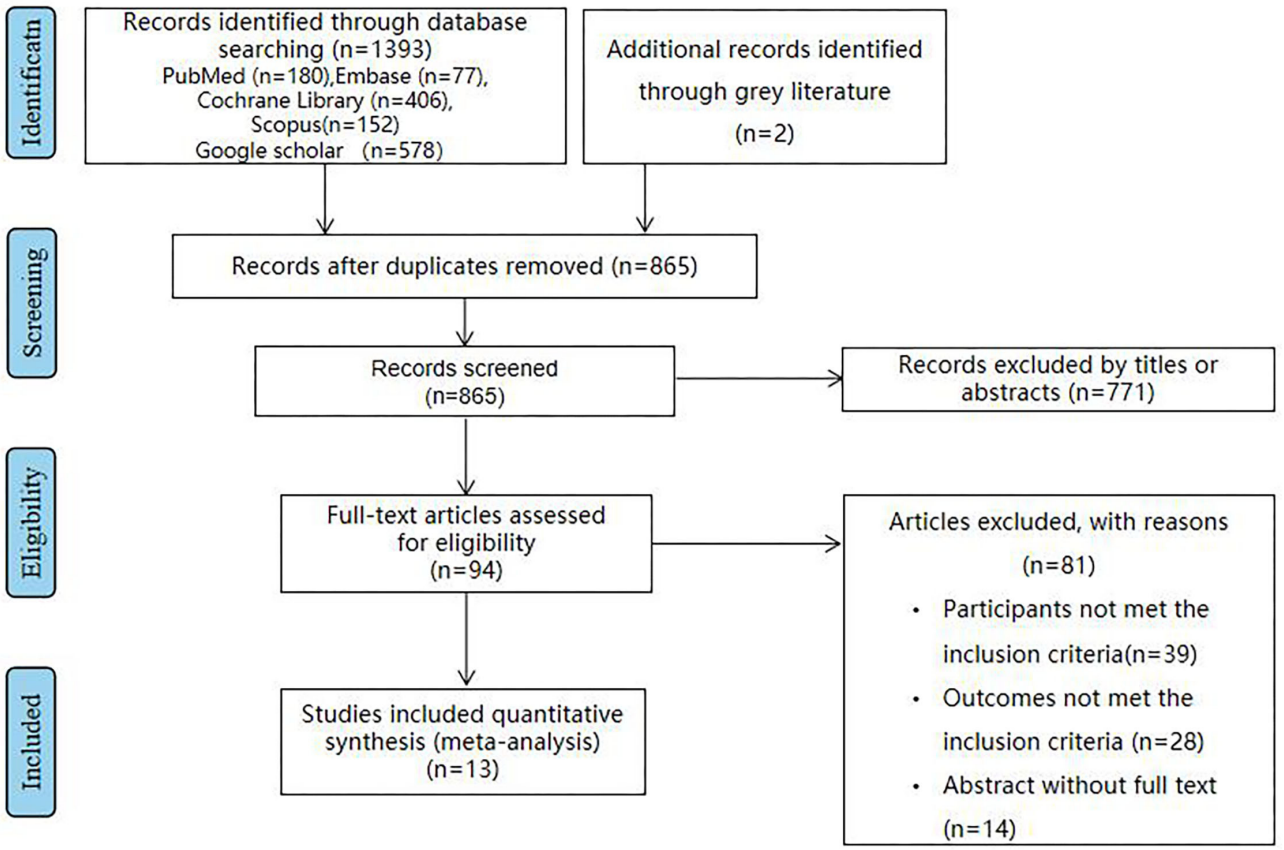

FIGURE 1 | The flowchart shows the article selection process we performed. It shows the process by which relevant studies were retrieved from the databases, assessed, and selected, or excluded. Preferred reporting items for systematic reviews and meta-analyses (PRISMA) diagram for study search was used.

21, 24), whole egg (17), and pistachio nuts (25). The berry intervention patterns included cranberry and black raspberry. Subjects received the same dose of berry diet or placebo. The fatty acids diet intervention patterns referred to diet alone or diet plus omega-3 polyunsaturated fatty acids (PUFAs) supplementation. The low-calorie diet included 50–60% carbohydrate, <30% total fat, and <10% saturated fat. The whole wheat diet included wholegrain or refined cereal products. The whole egg intervention pattern referred to three whole eggs containing 0 g carbohydrate, 16 g protein, and 12 g fat. The pistachio nuts diets referred to participants advised to take pistachios for 20% of total energy.

Quality of the Included Studies

A risk of bias summary is depicted in **Figure 2**, and the risk of bias estimation within each of the studies selected is shown in **Figure 3**. Random sequence generation was adequate in the 5 trials. Three of them have received the maximal score, and none was considered low quality.

Effect of Diet on IL-1β

Based on data from 2 trials (101 participants) (15, 21), we found no effect of diet intervention on IL-1β change compared with control (SMD = −0.08, 95% CI: −0.30, 0.14; **Figure 4**).

Effect of Diet on IL-6

Of the 11 included studies (14–16, 18–25), when all the data were pooled in the meta-analysis, overall IL-6 levels in dietary patients were significantly lower than controls (SMD = −0.30, 95% CI = −0.55, 0.04, p = 0.02, I^2 = 64%). **Figure 5** demonstrates the subgroup analyses for the IL-6 levels of between dietary intervention and the controls. The IL-6 of participants who underwent low-calorie diet, berry, whole wheat, and fatty acids dietary intervention decreased compared with the control group (SMD = −0.17, 95% CI = −0.64, 0.30; SMD = −0.34, 95% CI = −0.76, 0.08; SMD = −0.04, 95% CI = −0.60, 0.52; SMD = −0.75, 95% CI = −1.12, −0.38). **Figure 6** demonstrates the subgroup analyses by MetS assessment method and shows how the NCEP ATP III and JIS assessment decreased compared with the control group (SMD = −0.75, 95% CI = −1.12, −0.38; SMD = −0.55, 95% CI = −1.01, −0.09).

Effect of Diet on TNF-α

As presented in **Figure 7**, our overall pooled analysis did not reveal the association between dietary intervention and the TNF-α levels (15, 17, 18, 20–24, 26) (SMD = −0.11, 95% CI: −0.28, 0.06). According to the assessment method of MetS, the effect estimate did not change considerably (**Figure 8**).

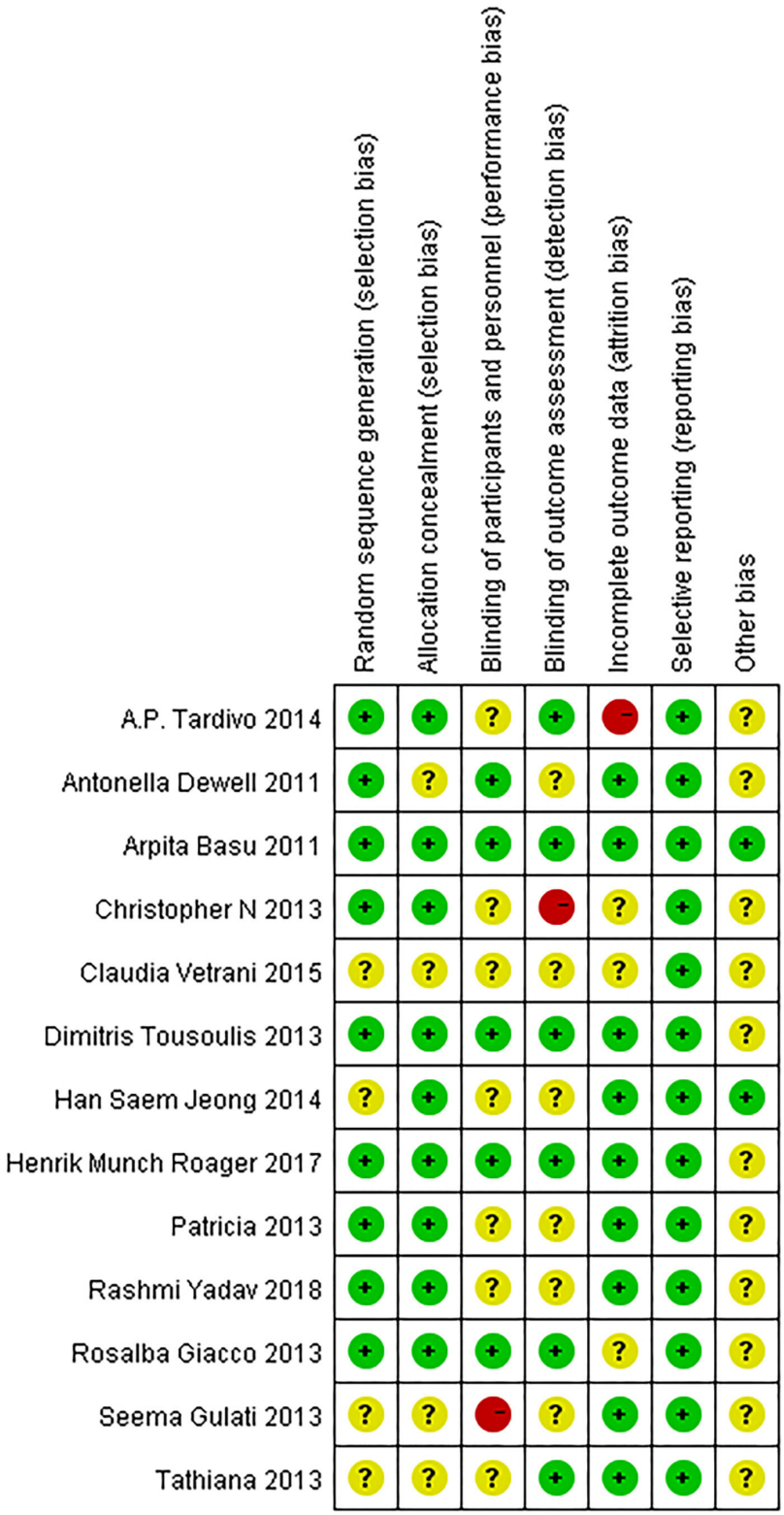

FIGURE 2 | Risk of bias summary.

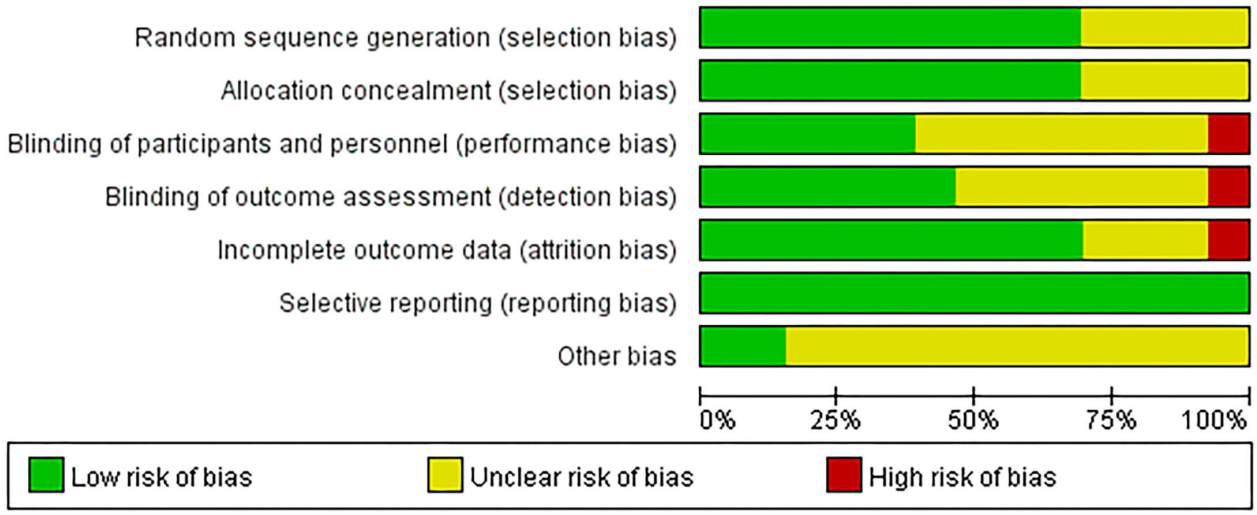

FIGURE 3 | Risk of bias graph.

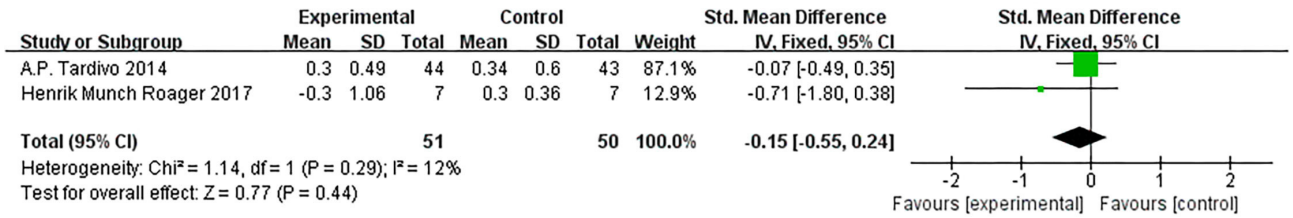

FIGURE 4 | Results of a meta-analysis for the effects of interleukin−1β (IL-1β). Study effect sizes of IL-1β levels differences between metabolic syndrome (MetS) and controls. Each data marker represents a study, and the size of the data marker is proportional to the total number of individuals in that study. The summary effect size for the IL-1β levels of each study is denoted by a diamond. Effect estimates are reported as standardized mean difference (SMD) and 95% confidence intervals. I^2 represents the magnitude of heterogeneity. $p \leq 0.05$ is considered as significant.

Effect of Diet on CRP

Based on data from 8 trials (458 participants) (15, 16, 18, 20–22, 26), changes on CRP due to dietary intervention were not found compared with control (SMD: 0.03, 95% CI: −0.20, 0.25; **Figure 9**). Similarly, the subgroup of MetS definitions did not change (**Figure 10**).

Publication Bias

The scatter funnel plot in IL-6 levels appeared symmetrical, indicating the absence of publication bias. Additionally, Egger's test detected no publication bias ($p = 0.320$). The number of studies that analyzed IL-1β, TNF-α, and CRP levels was <10. Hence, it was inadequate to perform a publication bias test.

DISCUSSION

To our knowledge, this is the first meta-analysis to provide evidence that dietary intervention could improve immunological properties, particularly IL-6, in MetS. Further analysis based on subgroups indicated that these results were affected by diet patterns of MetS. Despite this, it did not reveal the association between dietary intervention and the IL-1β, CRP, and TNF-α levels.

Chronic systemic inflammation had long been considered as a major factor in the development and progression of several non-communicable diseases (NCDs), including MetS, diabetes mellitus, obesity, and cancer (27). This was a low-grade variation in the immune homeostasis that adversely regulated metabolic processes over time (28). The occurrence and development of MetS was related to pro-inflammatory cytokines.

Interleukin-1β could increase insulin resistance and promote apoptosis of β cells in animals (29). Although we did not find that dietary intervention could significantly reduce the level of the pro-inflammatory cytokine IL-1β, the anti-IL-1β agents improve insulin secretion and β cell function and reduce inflammation in humans (30).

Interleukin-6 was shown to be a vital mediator of acute phase response with a pleiotropic effect on inflammation during immune response. We found that IL-6 significantly decreased after dietary intervention, especially with fatty acids diet. It may

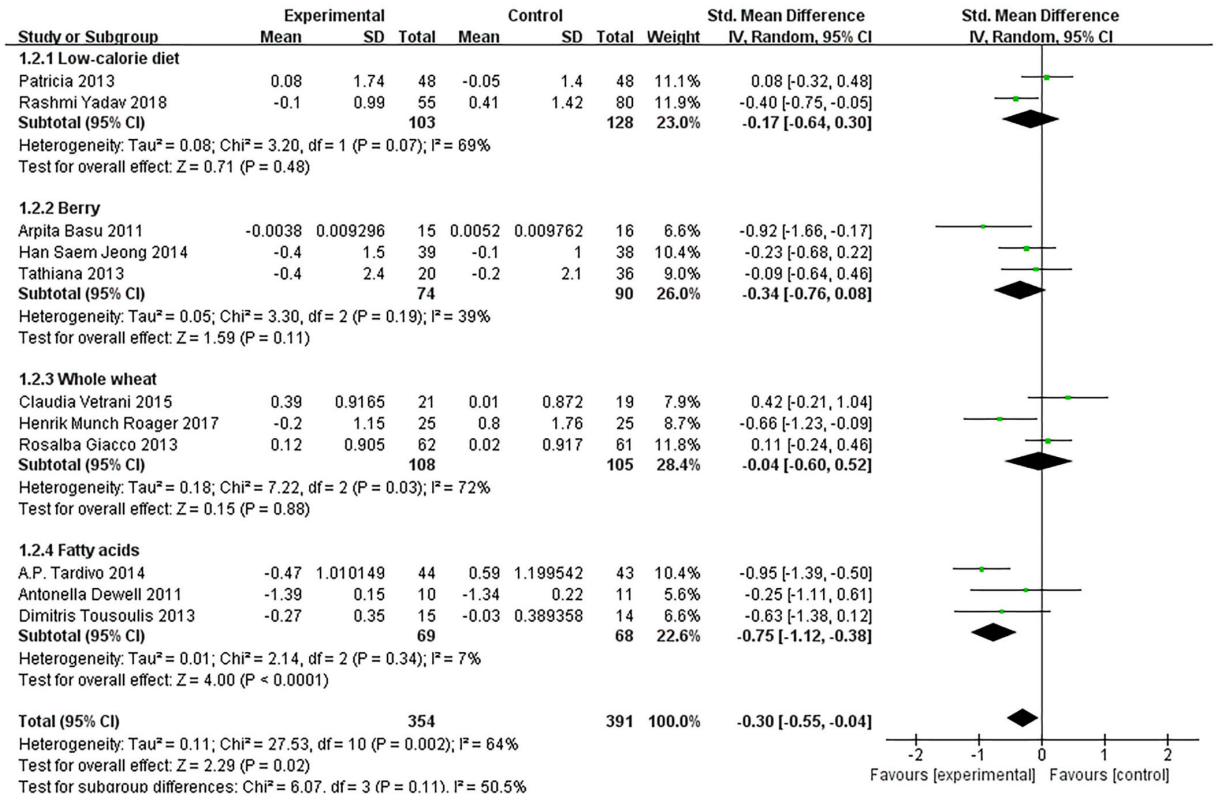

FIGURE 5 | The subgroup analyses for the interleukin-6 (IL-6) levels by dietary intervention. Study effect sizes of the subgroup analyses for the IL-6 levels differences by dietary intervention between MetS and controls.

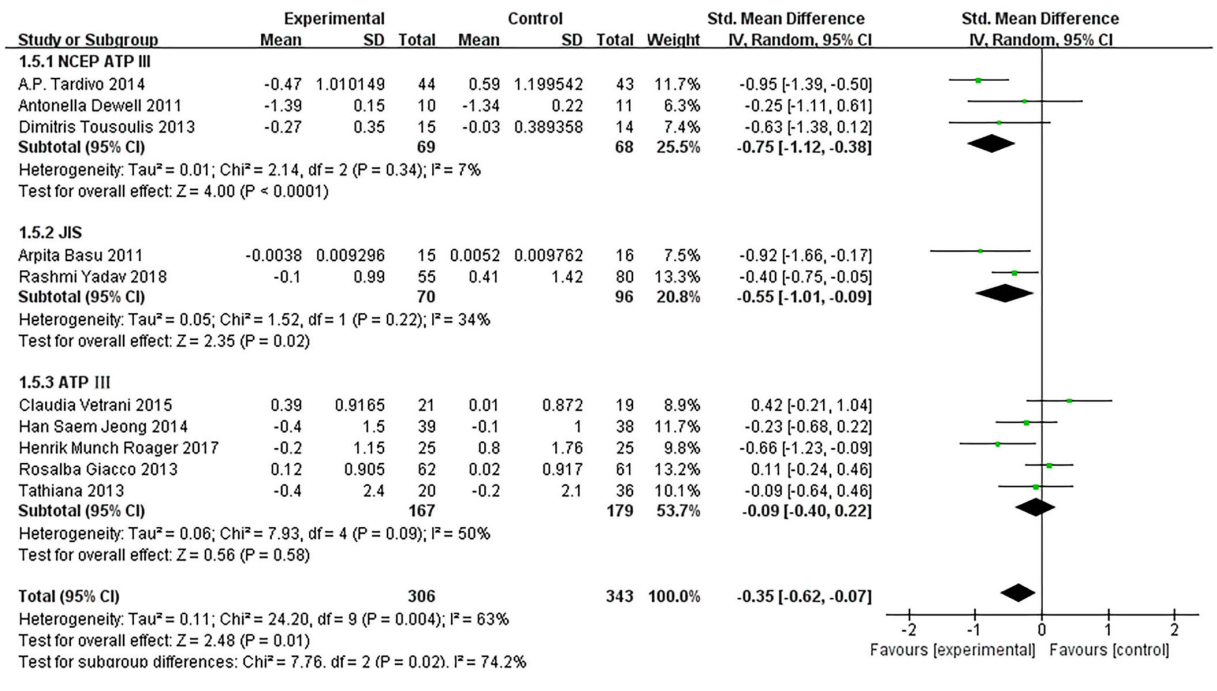

FIGURE 6 | The subgroup analyses for the IL-6 levels by MetS assessment method. Study effect sizes of the subgroup analyses for the IL-6 level differences by MetS assessment method between MetS and controls.

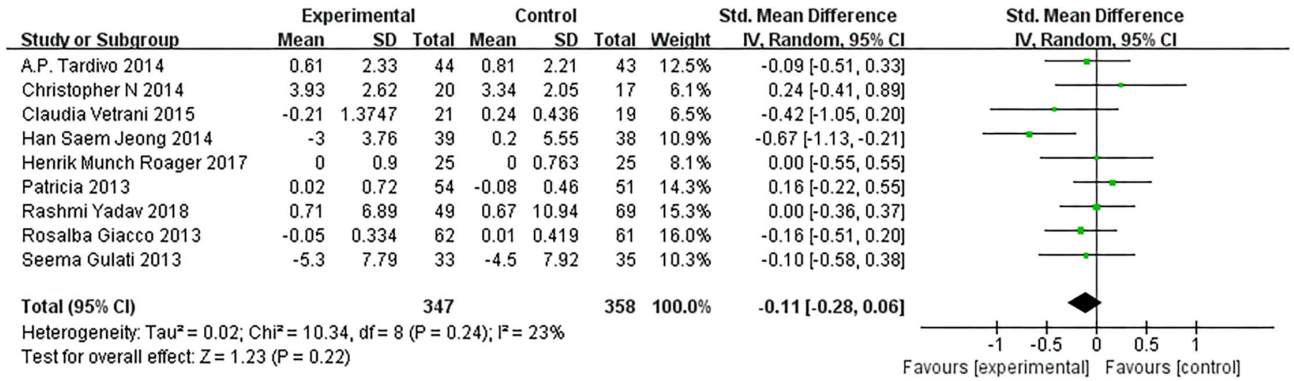

FIGURE 7 | Results of a meta-analysis for the effects of tumor necrosis factor α (TNF-α). Study effect sizes of the subgroup analyses for the TNF-α levels differences between MetS and controls.

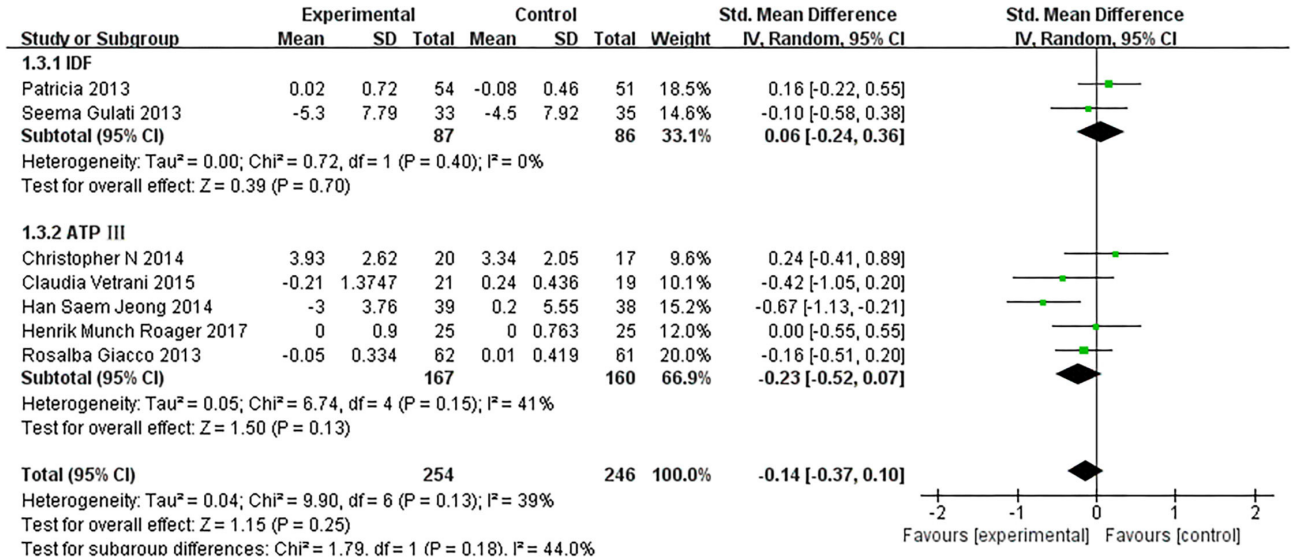

FIGURE 8 | The subgroup analyses for the TNF-α levels by MetS assessment method. Study effect sizes of the subgroup analyses for the TNF-α levels differences by MetS assessment method between MetS and controls.

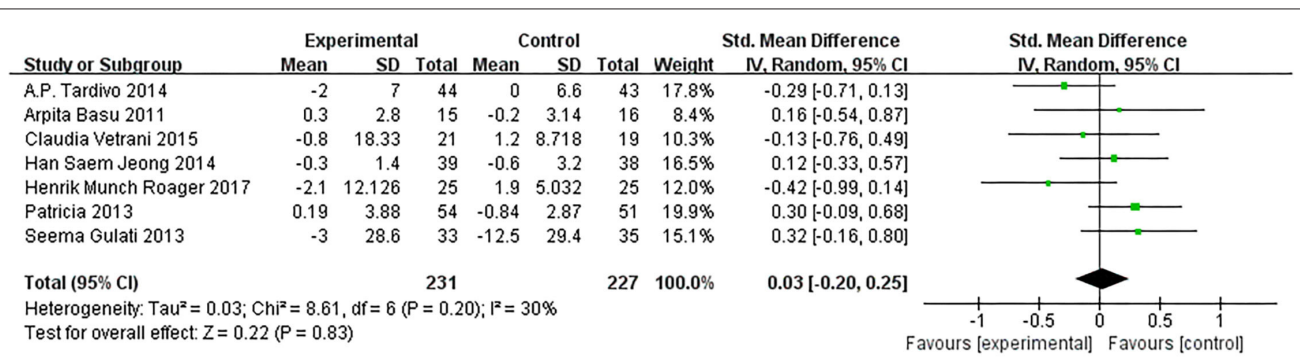

FIGURE 9 | Results of a meta-analysis for the effects of c-reactive protein (CRP). Study effect sizes of the subgroup analyses for the CRP levels differences between MetS and controls.

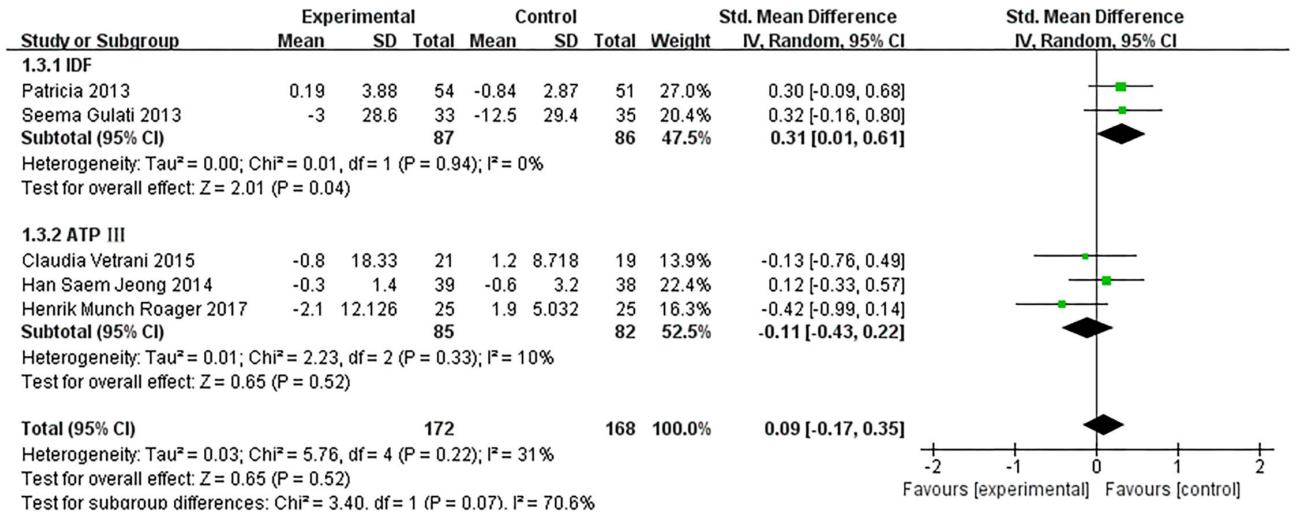

FIGURE 10 | The subgroup analyses for the CRP levels by MetS assessment method. Study effect sizes of the subgroup analyses for the CRP levels differences by MetS assessment method between MetS and controls.

be that dietary intervention can produce immediate changes in MetS, leading to significant changes in IL-6. The JIS and the IDF definitions substantially identify more individuals with MetS than subjects with MetS diagnosed by the NCEP ATP III/ATP III definitions (31). As for the results of subgroup analysis, the NCEP ATP III and JIS assessment show they were statistically significant in identifying patients with MetS, but there was no sufficient evidence.

Tumor necrosis factor-α induced phosphorylation of insulin receptor substrate 1 (IRS-1), preventing insulin from binding to the receptor, which consequently led to insulin resistance (32). In addition, TNF-α and IL-6 mainly came from adipose tissue, which were significantly increased in adults with MetS as they were positively correlated with the degree of obesity (33). Adipose tissue could induce a wide range of acute-phase proteins, such as CRP, fibrinogen, and thrombopoietin, and induce systemic acute phase response (34). These findings supported the role of IL-6, TNF-α, and IL-1β, which are all related to the occurrence of insulin resistance. On the other hand, TNF-α and IL-1β inhibit β Cells and promote their apoptosis (32). Hence, only dietary intervention significantly reduced IL-6 levels, while the rest of the pro-inflammatory cytokines showed a similar trend. We found that these indicators did not reach statistical differences through dietary intervention. This may be due to the patients being in a state of low-grade inflammation. This raises the possibility that data might change significantly if the inclusion standards were to be raised.

Low-calorie diets had been shown to improve the level of inflammatory factors, particularly with advancing age and improving obesity and MetS parameters. However, this was achieved through a significant reduction of total energy intake and supplementing micronutrients (35). The research indicated that after 1 year of low-calorie diet intake, severely obese patients did not show more weight loss, significant changes in MetS indicators, or levels of inflammation markers than those on conventional weight-loss diet (36).

In addition, one of the most commonly used dietary modifications consists of increasing the protein content of the diet. The role of this modification in inflammation was controversial (37). The DiOGenes project reported (apparently for the first time) that dietary protein content influences inflammation, specifically CRP concentrations. This pan-European-controlled dietary intervention study compared a high-protein diet with a low-protein diet in overweight and obese adults and found that the lower protein content appeared to be associated with a further decrease of CRP as compared with the high-protein diet. Excess protein supplementation enhanced phosphorus overload which can lead to acidosis and exacerbated insulin resistance (38). In addition, the meta-analysis by Namazi et al. (39) found no significant association between the pro-inflammatory diet and MetS.

Targeting anti-inflammatory therapies had been applied to patients with MetS. In doing so, the IL1-β inhibitor, Canakinumab, increased insulin secretion (40). In addition, IL-6 inhibitors, tocilizumab, and anti-TNF drugs, were shown to possibly primarily affect insulin-sensitive tissues (41). In the future, the combination of diet and anti-inflammatory drugs may become one of the new approaches to treat MetS.

LIMITATION

Firstly, most eligible studies did not adjust potential confounding factors. Secondly, due to the influence of gender, race, ethnicity, and social factors, our findings should be interpreted in different geographic contexts.

Thirdly, the reason for the analysis might be due to the limited time of intervention for the inclusion of RCT, leading to no significant changes in inflammatory marker levels. In addition, individual differences, different methods of intervention, and sample size might also directly affect the analysis results. Lastly, according to different diagnostic criteria, long-term trends may have confounded the results and limited generalizability.

CONCLUSION

Our study suggests that dietary intervention might decrease IL-6, IL-1β, CRP, and TNF-α in MetS. However, different diets might have different protective mechanisms for MetS. More time and more appropriate dietary patterns are needed to improve the inflammatory state of MetS. In addition, more research is needed to clarify the mechanisms underlying the effect of dietary intervention on this population's inflammatory markers. Anti-inflammatory agents combined with dietary intervention may be therapeutically useful in treating and preventing MetS.

DATA AVAILABILITY STATEMENT

The original contributions presented in the study are included in the article/**Supplementary Material**, further inquiries can be directed to the corresponding author/s.

AUTHOR CONTRIBUTIONS

ZZ contributed to the study design, wrote the manuscript, reviewed and edited the manuscript. MW, JL, ZZ, HZ, XC, and NW conducted the literature search and performed data extraction and data analysis. MW, JL, and XC did the statistical analyses. MW, JL, XC, XH, QL, and SC contributed to the writing of the manuscript. All authors approved the submitted manuscript.

SUPPLEMENTARY MATERIAL

The Supplementary Material for this article can be found online at: https://www.frontiersin.org/articles/10.3389/fnut.2022.846591/full#supplementary-material

REFERENCES

1. Saklayen, M.G. The global epidemic of the metabolic syndrome. *Curr Hypertens. Rep.* (2018) 20:12. doi: 10.1007/s11906-018-0812-z
2. Alberti KG, Zimmet P, Shaw J. IDF epidemiology task force consensus group. the metabolic syndrome—a new worldwide definition. *Lancet.* (2005) 366:1059–62. doi: 10.1016/S0140-6736(05)67402-8
3. Alberti KG, Eckel RH, Grundy SM, Zimmet PZ, Cleeman JI, Donato KA, et al. Harmonizing the metabolic syndrome: a joint interim statement of the international diabetes federation task force on epidemiology and prevention; national heart, lung, and blood institute; American heart association; World heart mfederation; International. *Circulation.* (2009) 120:1640–5. doi: 10.1161/CIRCULATIONAHA.109.192644
4. Alicka M, Marycz K. The effect of chronic inflammation and oxidative and endoplasmic reticulum stress in the course of metabolic syndrome and its therapy. *Stem Cells Int.* (2018) 2018:4274361. doi: 10.1155/2018/4274361
5. Besedovsky HO, Rey AD. Physiologic versus diabetogenic effects of interleukin-1: a question of weight. *Curr Pharm Des.* (2014) 20:4733–40. doi: 10.2174/1381612820666140130204401
6. Yudkin JS, Kumari M, Humphries SE, Mohamed-Ali V. Inflammation, obesity, stress and coronary heart disease: is interleukin-6 the link? *Atherosclerosis.* (2000) 148:209–14. doi: 10.1016/S0021-9150(99)00463-3
7. Marques-Vidal P, Schmid R, Bochud M, Bastardot F, Von Känel R, Paccaud F, et al. Adipocytokines, hepatic and inflammatory biomarkers and incidence of type 2 diabetes. The CoLaus study. *PLoS ONE.* (2012) 7:e51768. doi: 10.1371/journal.pone.0051768
8. O'Neil A, Shivappa N, Jacka FN, Kotowicz MA, Kibbey K, Hebert JR. Pro-inflammatory dietary intake as a risk factor for CVD in men: a 5-year longitudinal study. *Br J Nutr.* (2015) 114:2074–82. doi: 10.1017/S0007114515003815
9. Julibert A, Bibiloni MDM, Mateos D, Angullo E, Tur JA. Dietary fat intake and metabolic syndrome in older adults. *Nutrients.* (2019) 11:1901. doi: 10.3390/nu11081901
10. Martins AD, Majzoub A, Agawal A. Metabolic syndrome and male fertility. *World J Mens Health.* (2019) 37:113–27. doi: 10.5534/wjmh.180055
11. Michels KB, Schulze MB. Can dietary patterns help us detect diet-disease associations? *Nutr Res Rev.* (2005) 18:241–8. doi: 10.1079/NRR2005107
12. Moher D, Liberati A, Tetzlaff J, Altman DG, PRISMA Group. Preferred reporting items for systematic reviews and meta-analyses: the PRISMA statement. *PLoS Med.* (2009) 6:e1000097. doi: 10.1371/journal.pmed.1000097
13. Higgins J, Altman D, Sterne J. Chapter 8: assessing risk of bias in included studies. In: Higgins J, Churchill R, Chandler J, Cumpston M, editors. *Cochrane Handbook for Systematic Reviews of Interventions Version 5.2.0 (Updated June 2017)*. Chichester: Cochrane (2017).
14. Dewell A, Marvasti FF, Harris WS, Tsao P, Gardner CD. Low- and high-dose plant and marine (n-3) fatty acids do not affect plasma inflammatory markers in adults with metabolic syndrome. *J Nutr.* (2011) 141:2166–71. doi: 10.3945/jn.111.142240
15. Tardivo AP, Nahas-Neto J, Orsatti CL, Dias FB, Poloni PF, Schmitt EB, et al. Effects of omega-3 on metabolic markers in postmenopausal women with metabolic syndrome. *Climacteric.* (2015) 18:290–8. doi: 10.3109/13697137.2014.981521
16. Basu A, Betts NM, Ortiz J, Simmons B, Wu M, Lyons TJ. Low-energy cranberry juice decreases lipid oxidation and increases plasma antioxidant capacity in women with metabolic syndrome. *Nutr Res.* (2011) 31:190–6. doi: 10.1016/j.nutres.2011.02.003
17. Blesso CN, Andersen CJ, Barona J, Volk B, Volek JS, Fernandez ML. Effects of carbohydrate restriction and dietary cholesterol provided by eggs on clinical risk factors in metabolic syndrome. *J Clin Lipidol.* (2013) 7:463–71. doi: 10.1016/j.jacl.2013.03.008
18. Vetrani C, Costabile G, Luongo D, Naviglio D, Rivellese AA, Riccardi G, et al. Effects of whole-grain cereal foods on plasma short chain fatty acid concentrations in individuals with the metabolic syndrome. *Nutrition.* (2016) 32:217–21. doi: 10.1016/j.nut.2015.08.006
19. Tousoulis D, Plastiras A, Siasos G, Oikonomou E, Verveniotis A, Kokkou E, et al. Omega-3 PUFAs improved endothelial function and arterial stiffness with a parallel antiinflammatory effect in adults with metabolic syndrome. *Atherosclerosis.* (2014) 232:10–6. doi: 10.1016/j.atherosclerosis.2013.10.014
20. Jeong HS, Hong SJ, Lee TB, Kwon JW, Jeong JT, Joo HJ, et al. Effects of black raspberry on lipid profiles and vascular endothelial function in patients with metabolic syndrome. *Phytother Res.* (2014) 28:1492–8. doi: 10.1002/ptr.5154
21. Roager HM, Vogt JK, Kristensen M, Hansen LBS, Ibrügger S, Mærkedahl RB, et al. Whole grain-rich diet reduces body weight and systemic low-grade inflammation without inducing major changes of the gut microbiome: a randomised cross-over trial. *Gut.* (2019) 68:83–93. doi: 10.1136/gutjnl-2017-314786
22. Lopez-Legarrea P, de la Iglesia R, Abete I, Navas-Carretero S, Martinez JA, Zulet MA. The protein type within a hypocaloric diet affects obesity-related inflammation: the RESMENA project. *Nutrition.* (2014) 30:424–9. doi: 10.1016/j.nut.2013.09.009

23. Yadav R, Yadav RK, Khadgawat R, Pandey RM. Comparative efficacy of a 12 week yoga-based lifestyle intervtention and dietary intervention on adipokines, inflammation, and oxidative stress in adults wih metabolic syndrome: a randomized controlled trial. *Transl Behav Med.* (2019) 9:594–604. doi: 10.1093/tbm/iby060
24. Giacco R, Lappi J, Costabile G, Kolehmainen M, Schwab U, Landberg R, et al. Effects of rye and whole wheat versus refined cereal foods on metabolic risk factors: a randomised controlled two-centre intervention study. *Clin Nutr.* (2013) 32:941–9. doi: 10.1016/j.clnu.2013.01.016
25. Simão TN, Lozovoy MA, Simão AN, Oliveira SR, Venturini D, Morimoto HK, et al. Reduced-energy cranberry juice increases folic acid and adiponectin and reduces homocysteine and oxidative stress in patients with the metabolic syndrome. *Br J Nutr.* (2013) 110:1885–94. doi: 10.1017/S0007114513001207
26. Gulati S, Misra A, Pandey RM, Bhatt SP, Saluja S. Effects of pistachio nuts on body composition, metabolic, inflammatory and oxidative stress parameters in Asian Indians with metabolic syndrome: a 24-wk, randomized control trial. *Nutrition.* (2014) 30:192–7. doi: 10.1016/j.nut.2013.08.005
27. Vissers LE, Waller MA, van der Schouw YT, Hebert JR, Shivappa N, Schoenaker DA, et al. The relationship between the dietary inflammatory index and risk of total cardiovascular disease, ischemic heart disease and cerebrovascular disease: findings from an Australian population-based prospective cohort study of women. *Atherosclerosis.* (2016) 253:164–70. doi: 10.1016/j.atherosclerosis.2016.07.929
28. Lumeng CN, Saltiel AR. Inflammatory links between obesity and metabolic disease. *J Clin Invest.* (2011) 121:2111–7. doi: 10.1172/JCI 57132
29. Ibarra Urizar A, Friberg J, Christensen DP, Lund Christensen G, Billestrup N. Inflammatory cytokines stimulate bone morphogenetic protein-2 expression and release from pancreatic beta cells. *J Interferon Cytokine Res.* (2016) 36:20–9. doi: 10.1089/jir.2014.0199
30. Larsen CM, Faulenbach M, Vaag A, Vølund A, Ehses JA, Seifert B, et al. Interleukin-1-receptor antagonist in type 2 diabetes mellitus. *N Engl J Med.* (2007) 356:1517–26. doi: 10.1056/NEJMoa065213
31. Athyros VG, Ganotakis ES, Tziomalos K, Papageorgiou AA, Anagnostis P, Griva T, et al. Comparison of four definitions of the metabolic syndrome in a Greek (Mediterranean) population. *Curr Med Res Opin.* (2010) 26:713–9. doi: 10.1185/03007991003590597
32. Smitka K, Marešová D. Adipose tissue as an endocrine organ: an update on pro-inflammatory and anti-inflammatory microenvironment. *Prague Med Rep.* (2015) 116:87–111. doi: 10.14712/23362936.2015.49
33. Popko K, Gorska E, Stelmaszczyk-Emmel A, Plywaczewski R, Stoklosa A, Gorecka D, et al. Proinflammatory cytokines Il-6 and TNF-α and the development of inflammation in obese subjects. *Eur J Med Res.* (2010) 15 (Suppl. 2):120–2. doi: 10.1186/2047-783X-15-S2-120
34. Heinrich PC, Castell JV, Andus T. Interleukin-6 and the acute phase response. *Biochem J.* (1990) 265:621–36. doi: 10.1042/bj2650621
35. Sitzmann BD, Brown DI, Garyfallou VT, Kohama SG, Mattison JA, Ingram DK, et al. Impact of moderate calorie restriction on testicular morphology and endocrine function in adult rhesus macaques (Macaca mulatta). *Age.* (2014) 36:183–97. doi: 10.1007/s11357-013-9563-6
36. Stern L, Iqbal N, Seshadri P, Chicano KL, Daily DA, McGrory J, et al. The effects of low-carbohydrate versus conventional weight loss diets in severely obese adults: one-year follow-up of a randomized trial. *Ann Intern Med.* (2004) 140:778–85. doi: 10.7326/0003-4819-140-10-200405180-00007
37. Santesso N, Akl EA, Bianchi M, Mente A, Mustafa R, Heels-Ansdell D, et al. Effects of higher- versus lower-protein diets on health outcomes: a systematic review and meta-analysis. *Eur J Clin Nutr.* (2012) 66:780–8. doi: 10.1038/ejcn.2012.37
38. Mitch WE. Beneficial responses to modified diets in treating patients with chronic kidney disease. *Kidney Int Suppl.* (2005) S133–5. doi: 10.1111/j.1523-1755.2005.09430.x
39. Namazi N, Larijani B, Azadbakht L. Dietary inflammatory index and its association with the risk of cardiovascular diseases, metabolic syndrome, and mortality: a systematic review and meta-analysis. *Horm Metab Res.* (2018) 50:345–58. doi: 10.1055/a-0596-8204
40. Zhao G, Dharmadhikari G, Maedler K, Meyer-Hermann M. Possible role of interleukin-1β in type 2 diabetes onset and implications for anti-inflammatory therapy strategies. *PLoS Comput Biol.* (2014) 10:e1003798. doi: 10.1371/journal.pcbi.1003798
41. Mirjafari H, Ruperto N, Brunner HI. A54: insulin sensitivity is improved in sJIA children with insulin resistance after tocilizumab treatment: results from the TENDER study. *Arthritis Rheumatol.* (2014) 66 (Suppl. 11):S80–1 doi: 10.1002/art.38470

Conflict of Interest: The authors declare that the research was conducted in the absence of any commercial or financial relationships that could be construed as a potential conflict of interest.

Publisher's Note: All claims expressed in this article are solely those of the authors and do not necessarily represent those of their affiliated organizations, or those of the publisher, the editors and the reviewers. Any product that may be evaluated in this article, or claim that may be made by its manufacturer, is not guaranteed or endorsed by the publisher.

frontiers | Frontiers in Nutrition

ORIGINAL RESEARCH
published: 12 April 2022
doi: 10.3389/fnut.2022.840648

Astaxanthin From *Haematococcus pluvialis* Prevents High-Fat Diet-Induced Hepatic Steatosis and Oxidative Stress in Mice by Gut-Liver Axis Modulating Properties

*Meng Wang[1], Wenxin Xu[1], Jie Yu[1], Yingying Liu[1], Haotian Ma[2], Chunli Ji[1], Chunhui Zhang[1], Jinai Xue[1], Runzhi Li[1,3] and Hongli Cui[1,3]**

[1] College of Agriculture, Institute of Molecular Agriculture and Bioenergy, Shanxi Agricultural University, Jinzhong, China, [2] Health Science Center, College of Forensic Sciences, Xi'an Jiaotong University, Xi'an, China, [3] State Key Laboratory of Integrative Sustainable Dryland Agriculture, Shanxi Agricultural University, Taiyuan, China

OPEN ACCESS

Edited by:
Gratiela Gradisteanu Pircalabioru, University of Bucharest, Romania

Reviewed by:
Naoto Nagata, Kanazawa University, Japan
Yuji Naito, Kyoto Prefectural University of Medicine, Japan
Baosheng Ge, China University of Petroleum, China

***Correspondence:**
Hongli Cui
cuihongli@sxau.edu.cn

Specialty section:
This article was submitted to Nutrition and Metabolism, a section of the journal Frontiers in Nutrition

Received: 21 December 2021
Accepted: 01 March 2022
Published: 12 April 2022

Citation:
Wang M, Xu W, Yu J, Liu Y, Ma H, Ji C, Zhang C, Xue J, Li R and Cui H (2022) Astaxanthin From Haematococcus pluvialis Prevents High-Fat Diet-Induced Hepatic Steatosis and Oxidative Stress in Mice by Gut-Liver Axis Modulating Properties. Front. Nutr. 9:840648. doi: 10.3389/fnut.2022.840648

Scope: Evidence is mounting that astaxanthin (ATX), a xanthophyll carotenoid, used as a nutritional supplement to prevent chronic metabolic diseases. The present study aims to identify the potential function of ATX supplementation in preventing steatohepatitis and hepatic oxidative stress in diet-induced obese mice.

Methods and Results: In this study, ATX as dose of 0.25, 0.5, and 0.75% have orally administered to mice along with a high-fat diet (HFD) to investigate the role of ATX in regulating liver lipid metabolism and gut microbiota. The study showed that ATX dose-dependently reduces body weight, lipid droplet formation, hepatic triglycerides and ameliorated hepatic steatosis and oxidative stress. 0.75% ATX altered the levels of 34 lipid metabolites related to hepatic cholesterol and fatty acid metabolism which might be associated with downregulation of lipogenesis-related genes and upregulation of bile acid biosynthesis-related genes. The result also revealed that ATX alleviates HFD-induced gut microbiota dysbiosis by significantly inhibiting the growth of obesity-related *Parabacteroides* and *Desulfovibrio* while promoting the growth of *Allobaculum* and *Akkermansia*.

Conclusion: The study results suggested that dietary ATX may prevent the development of hepatic steatosis and oxidative stress with the risk of metabolic disease by gut-liver axis modulating properties.

Keywords: astaxanthin, oxidative stress, hepatic steatosis, lipid metabolism, gut microbiota

INTRODUCTION

Over the past few decades, obesity has become globally recognized as one of the most common life-threatening chronic metabolic problems, with steadily increasing rates year by year, which are ascribed to the imbalance of energy metabolism and excessive fat accumulation in the body (1, 2). Obesity causes a series of abnormal metabolic complications, including lipid metabolism,

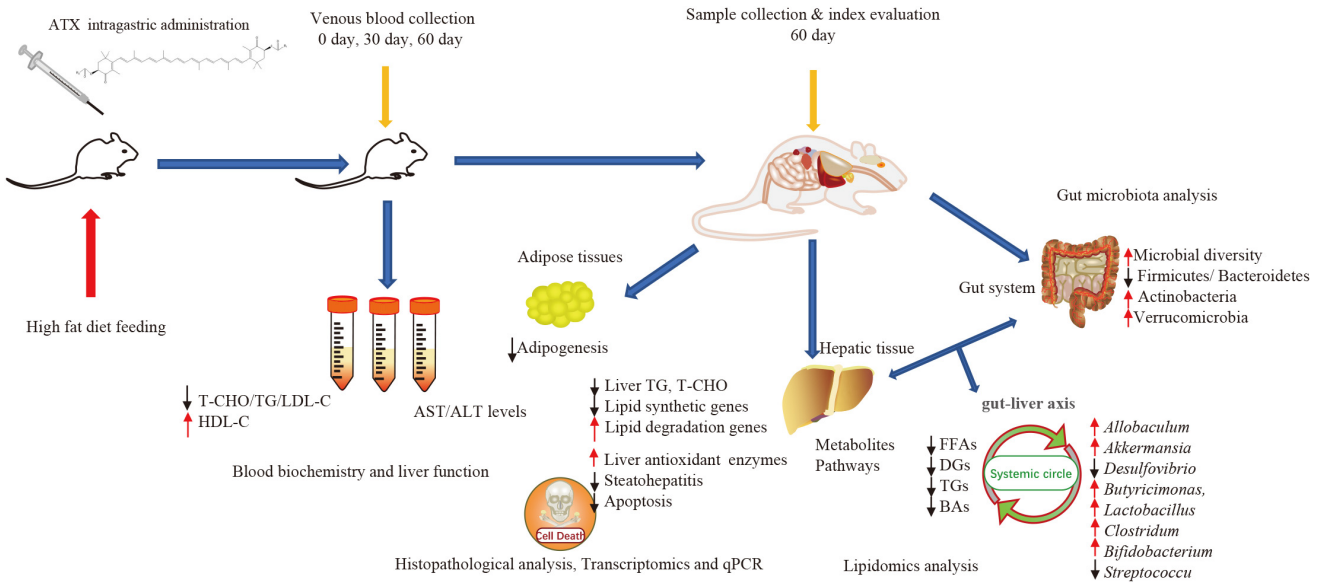

GRAPHICAL ABSTRACT | Astaxanthin (ATX) preventive effects on lipid metabolic disorders, hepatic steatosis, and oxidative stress in high-fat diet-induced mice.

oxidant stress, inflammatory responses, insulin resistance (IR) and steatohepatitis (3, 4). Notably, among patients with NAFLD, obese individuals present more severe histological phenotypes and may suffer from higher mortality and morbidity (5). Recently, according to an epidemiological survey on nutrition and health, the prevalence of obesity has gradually become appeared in younger individuals (6). In modern society, a suboptimal diet and little exercise are among the leading causes of poor health, also increasing triacylglycerol (TG), total cholesterol (TC), free fatty acid (FFA) accumulation, and lipid peroxidation (7, 8). For example, systemic oxidative stress, a key factor in pathological obesity, can be induced by a high-calorie diet through various mechanisms (9, 10).

Currently, the existing anti-obesity medications that have been developed are unsuitable for certain individuals with obesity due to potential side effects and drug tolerability (11, 12). There is, therefore, a key practical value to search for safe and effective functional components from natural foods to prevent obesity and related metabolic diseases when compared with synthetic drugs. With health benefits increasing in the human diet, carotenoids, natural antioxidants distributed in numerous microbes, plants, and animals, have received considerable scholarly attention in recent years (13). Furthermore, an unambiguous association was found between the mechanism of carotenoids regulating liver lipid metabolism and the incidence of obesity-related NAFLD, as demonstrated in many studies (13–15).

Astaxanthin (ATX extracted from *Haematococcus pluvialis*) is a xanthophyll carotenoid in marine organisms and is often used as a nutritious supplementary food in the daily diet. ATX has a protective effect against oxidative stress, inflammation, and metabolic disorders, such as liver fibrosis and type 2 diabetes (16, 17). In our previous study, after 12 weeks of high-fat intake, we found that C57BL/6 mice exhibited a significant reduction in serum TG and TC by administering intragastric ATX treatment (18). Furthermore, ATX also improved lipid metabolism by regulating lipid-related gene and metabolite contents. According to many previous animal experiments, consumption of ATX not only showed no signs of poisoning but also exerted a positive pharmacological effect (19, 20).

Recently, the relationship between gut microbiota and metabolic diseases has attracted attention from the scholarly community because intestinal flora has been confirmed as a target for the prevention and treatment of obesity, metabolic syndrome and cardiovascular diseases (21). Therefore, it is important to investigate how ATX prevents the development of hepatic steatosis and oxidative stress with the risk of metabolic disease. The present study aims to contribute to this growing area of research by exploring the prevention effects on obesity and the development of NAFLD through long-term dietary ATX in mice.

MATERIALS AND METHODS

Chemicals

The detection kits for alanine transaminase (ALT), aspartate transaminase (AST), TG, TC, high-density lipoprotein cholesterol (HDL-C), and low-density lipoprotein cholesterol (LDL-C), and the antioxidant assay kits for SOD, CAT, GSH, T-AOC, and malondialdehyde (MDA) were purchased from Nanjing Jiancheng Bioengineering Institute (Nanjing, China). The superoxide indicator dihydroethidium ROS probe (DHE), 4',6-diamidino-2-phenylindole (DAPI) and YF488 TUNEL assay apoptosis detection kit were purchased from US Everbright, Inc. Other chemicals, solvents and reagents used in the present study were of laboratory analytical grade.

Preparation of Astaxanthin

Astaxanthin oleoresin was provided by Shandong Jinjing Biotechnology Co., Ltd., and the purification was performed in our lab during a previous study (18). After purification, ATX of 94.69% purity was used in the current study.

Animals

The Institutional Animal Care and Use Committee of Shanxi Agricultural University approved all experimental protocols for animal care, handling and experimentation (SXAU-EAW-2018-112). We also confirmed that all experiments were conducted in accordance with relevant guidelines and regulations. Forty-eight male C57BL/6 mice (SPF, 8 weeks old) weighing 20–22 g were obtained from the Experimental Animal Center of Shanxi Medical University. They were housed in individual cages in a specific room (22 ± 2°C) with 55% humidity on a 12 h dark/light schedule and had free access to food and pure water at the Institute of Molecular Agriculture and Bioenergy, Shanxi Agriculture University.

Dosage Information

The design of animal experiments was based on our previous methods (18). After a 2-week acclimation period, mice were randomly assigned to six groups (each comprising eight mice): the normal diet group (ND), the high-fat diet (HFD) group, the solvent group, the HFD + 0.25% ATX group, the HFD + 0.5% ATX group, and the HFD + 0.75% ATX group. The mice in the ND group were fed standard rodent chow containing 3.5 kcal/g with 4.3% fat, 67.2% carbohydrates, and 19.2% protein. The mice in the other group were fed a HFD containing 4.73 kcal/g with 24% fat, 41% carbohydrates, and 24% protein. The mice in the ND group were given distilled water, and the solvent group was gavaged with corn oil. In addition, the mice in the ATX treatment groups were gavaged with 0.25, 0.5, and 0.75% ATX dissolved in corn oil. During the diet phase, all mice were given intragastric treatment once per day at 9:00 a.m., which lasted 9 weeks. The diets were purchased from Beijing Huafukang Bioscience Co., Ltd. **Supplementary Table 1** shows the ingredients of the experimental diets.

Physiological Evaluation

The body weight and food intake were recorded daily for 63 days. To avoid error values, the measurement of weight was repeated three times for each mouse. The energy intake was calculated as food intake × 4.73 kcal g^{-1} for the HFD group and food intake × 3.50 kcal g^{-1} for the ND group, as demonstrated in previously (18). Mice were fasted for 12 h after the last treatment and then euthanized by inhalation with isoflurane. Blood samples were obtained from the retro-orbital veins on Days 0, 30, and 60. The serum was separated by centrifugation at 3,000 rpm for 15 min at 4°C and stored at −20°C until analysis. All other organs, including the liver, heart, kidney, spleen, and adipose tissues, were immediately collected and weighed individually after sacrificing the animals.

Biochemical Analysis

The serum TG, TC, HDL-C, and LDL-C levels and activities of AST (GOT) and ALT were determined using biochemical kits according to the standards and protocols provided by the manufacturer (Nanjing, China). According to the ratio of weight (g): volume (mL) = 1:9, the liver tissues were homogenized with phosphate buffer (PH 7.4) at 4°C and centrifuged at 2,500 rpm for 10 min at 4°C. The supernatant was collected to determine the protein and lipid levels (TG and TC) and enzymatic analyses (T-AOC, SOD, CAT, GSH, MDA, and ROS).

Histopathological Analysis

The dihydroethidium (DHE) probe method was used to qualitatively detect ROS. Five-micron-thick sections of the liver were dyed with DHE, and incubation was performed at 37°C for 10 min in a dark environment. The samples were directly observed under a fluorescence microscope at a measuring emission of 595 nm. The ROS-positive cells had strong red fluorescence. After sacrificing each mouse, fresh epididymal adipose tissue (e-AT) and liver tissues were immersed in 4% paraformaldehyde for 24 h. The tissues were embedded in paraffin, sectioned at a 5 μm thickness and stained with H&E. Meanwhile, the frozen sections were stained with Oil Red O (ORO), which was performed to further detect hepatic vacuolization, inflammatory cell infiltration, and lipid droplets. All of the samples were photographed under a light microscope (Leica, Germany) at 20×/40× magnification.

The above sections were used to examine hepatocellular apoptosis with the YF488 TUNEL assay apoptosis detection kit. After the TUNEL reaction, the sections were mounted using antifade mounting medium with DAPI and observed under an inverted fluorescence microscope at 385 and 485 nm wavelength excitation. The negative cells were dyed with blue fluorescence intensity at 385 nm, while the apoptotic cells exhibited green fluorescence at 485 nm. ImageJ software (National Institutes of Health, United States) was used to measure the cell counting of sections from each group.

$$\text{The apoptosis rate (\%)} = \frac{\text{Apoptotic cell number}}{\text{Total cell number}} \times 100$$

Polymerase Chain Reaction Analysis

Total RNA was extracted from liver tissue using TRIzol reagent (Shenggong BBI Life, Shanghai, China) according to the manufacturer's instructions. Then, cDNA was synthesized from total RNA using the PrimeScript Reverse Transcription reagent kit (Takara, Dalian, China). Quantitative polymerase chain reaction (PCR) was conducted in triplicate for each group to detect gene expression. The quantitative analysis of *AMPK*, *SREBP1c*, *ACC*, *CPT-1*, *PPARα*, *PPARγ*, *LXRα*, *SCD-1*, *PGC-1*, *FAS*, *CYP27A1*, and *CYP7A1* mRNA expression in the liver was measured in triplicate for each group by quantitative PCR. According to the SYBR Premix Ex Taq II (Takara, Dalian, China), the thermal cycle of qPCR was reacted on the CFX 96 Real-Time PCR Detection system (BIO-RAD, Hercules, CA,

United States) under the following conditions: 95°C for 10 min, then 40 cycles of 95°C for 15 s, 60°C for 30 s, and 72°C for 30 s. **Supplementary Table 2** shows the PCR primer sequences of each gene, and the target genes were normalized to the reference gene GAPDH. The $2^{-\Delta\Delta Ct}$ method was used to calculate relative gene expression.

Transcriptomics and Lipidomics Analysis

To investigate lipid metabolism, fresh samples were sent to MetWare Biotechnology Co., Ltd., Wuhan, to apply transcriptomics and metabolomics analyses. The extraction of liver lipids and lipidomic analysis were performed using an LC–MS/MS system following previous works (18). After RNA was extracted from liver biopsy samples, liver transcriptome analysis was conducted by RNA sequencing, as described in detail previously (22, 23).

16S rRNA Sequencing Analysis

The caecal contents were sent to Shanghai Personal Biotechnology Co., Ltd. to investigate microbial diversity through 16S rRNA analysis on the Illumina MiSeq platform. When the microbial DNA was isolated, PCR of the V3–V4 region of the bacterial 16S rRNA gene was performed using the forward primer 5′-ACTCCTACGGGAGGCAGCA-3′ and the reverse primer 5′-GGACTACHVGGGTWTCTAAT-3′ according to the manufacturer's protocol (24, 25). A previous study illustrated the analytical conditions and detailed parameters (18).

Statistical Analysis

All experiments were biologically repeated three times, and the data were analyzed with Social Sciences (SPSS 16.0) statistical software and are presented as the mean ± SD. Multiple comparisons among treatments were statistically analyzed using Duncan's multiple range test in one-way analysis of variance (ANOVA) ($P < 0.05$). Origin 9.1 was used to draw charts.

RESULTS

Effect of Astaxanthin Supplementation on Body Weight and Calorie Intake

A dramatic increment in body weight was observed in the HFD group, while a moderate increase was observed in the ATX treatment groups (**Figure 1A**). Body weight gain plays a pivotal role in evaluating the effect of HFD on obesity and assessing its prevention. **Table 1** presents the initial and final body weights of mice in each group. During feeding induction, the mice gained more weight in the HFD group (15.48 ± 0.22 g) and the solvent group (15.29 ± 0.46 g) than in the ND group (6.62 ± 0.34 g). Meanwhile, ATX supplementation in mice decreased weight gain, and a high dose of ATX significantly ($P < 0.05$) lowered body weight gain (9.60 ± 0.28 g) compared to HFD alone (**Figure 1B**). The energy intake of mice in the HFD group and the solvent group were significantly ($P < 0.05$) higher than the ND group; however, ATX consumption could reduce the energy intake compared to the HFD group regardless of the doses (**Figure 1C**). There was no significant difference in the food efficiency ratio of the mice in each group except for the ND group (**Table 1**).

Effect of Astaxanthin on Wet Liver Weights of and Fat Droplet Deposition

To estimate whether the HFD with ATX supplementation affected visceral organs and fat, the wet weights of adipose tissue and organs were measured in each group, especially the mouse liver (**Figure 1D**). There were no significant differences in the heart, spleen or kidney in each group, similar to our previous results (18) (**Table 2**). Compared to the ND group, the wet liver weights and fat were significantly ($P < 0.05$) increased in the HFD group. ATX supplementation (0.5% and 0.75% w/w) significantly ($P < 0.05$) decreased the wet weights of the liver in high-fat diet-fed mice. In addition, visual adipose tissue, including perirenal and epididymal adipose tissue, was significantly ($P < 0.05$) lowered in the 0.75% ATX group compared to the HFD group (**Figure 1E**).

Liver lipid indicators, namely TG and TC levels, are important parameters for obtaining an understanding of diet-induced fat deposition. The liver turned brown following the accumulation of TG and TC in the HFD group, indicating dyslipidaemia, possibly leading to other diseases. This phenomenon was suppressed in the ATX treatment group compared to the HFD group (**Figure 1F**). The TG and TC levels were examined to further quantify liver fat deposition, as shown in **Figures 1G,H**. The TG and TC levels were significantly ($P < 0.05$) increased by 117.4 and 82% in the HFD group compared to the ND group. However, ATX supplementation effectively decreased fat deposition in a dose-dependent manner compared to the HFD group, among which the TG and TC levels were 40.1 and 40%, respectively.

Effect of Astaxanthin on the Serum Lipid Profiles and Liver Function Indicators of High-Fat Diet-Induced Mice

Table 3 presents the serum lipid profiles of mice at 0, 30, and 60 days. There were no obvious differences in the initial serum lipid profiles among the six groups. The TG, TC, and LDL-C levels of mice were significantly ($P < 0.05$) increased, while the HDL-C level was reduced in the HFD and the solvent groups after 30 and 60 days. Such results indicated that lipid metabolism was disordered. The TC, TG, and LDL-C levels of mice were significantly ($P < 0.05$) decreased in the ATX treatment groups compared to the HFD group after 60 days despite the indistinctive ($P > 0.05$) change on Day 30. The mice in the 0.75% ATX group showed slightly higher serum HDL-C levels than the mice fed a HFD alone, but the variation was not significant on Day 30 ($P > 0.05$). When compared with the HFD group, serum TG levels in the 0.5 and 0.75% ATX groups were significantly decreased by 16.9 and 21.7% on Day 60 ($P < 0.05$), respectively. Serum TC levels in the 0.25, 0.5 and 0.75% ATX groups were significantly reduced to 3.65 ± 0.18, 3.16 ± 0.09, and 2.94 ± 0.38 mmol/L on Day 60 ($P < 0.05$), respectively. Serum LDL-C levels in the 0.5 and 0.75% ATX groups exhibited significant reductions of 35.2 and 39.6% ($P < 0.05$), respectively. No apparent changes

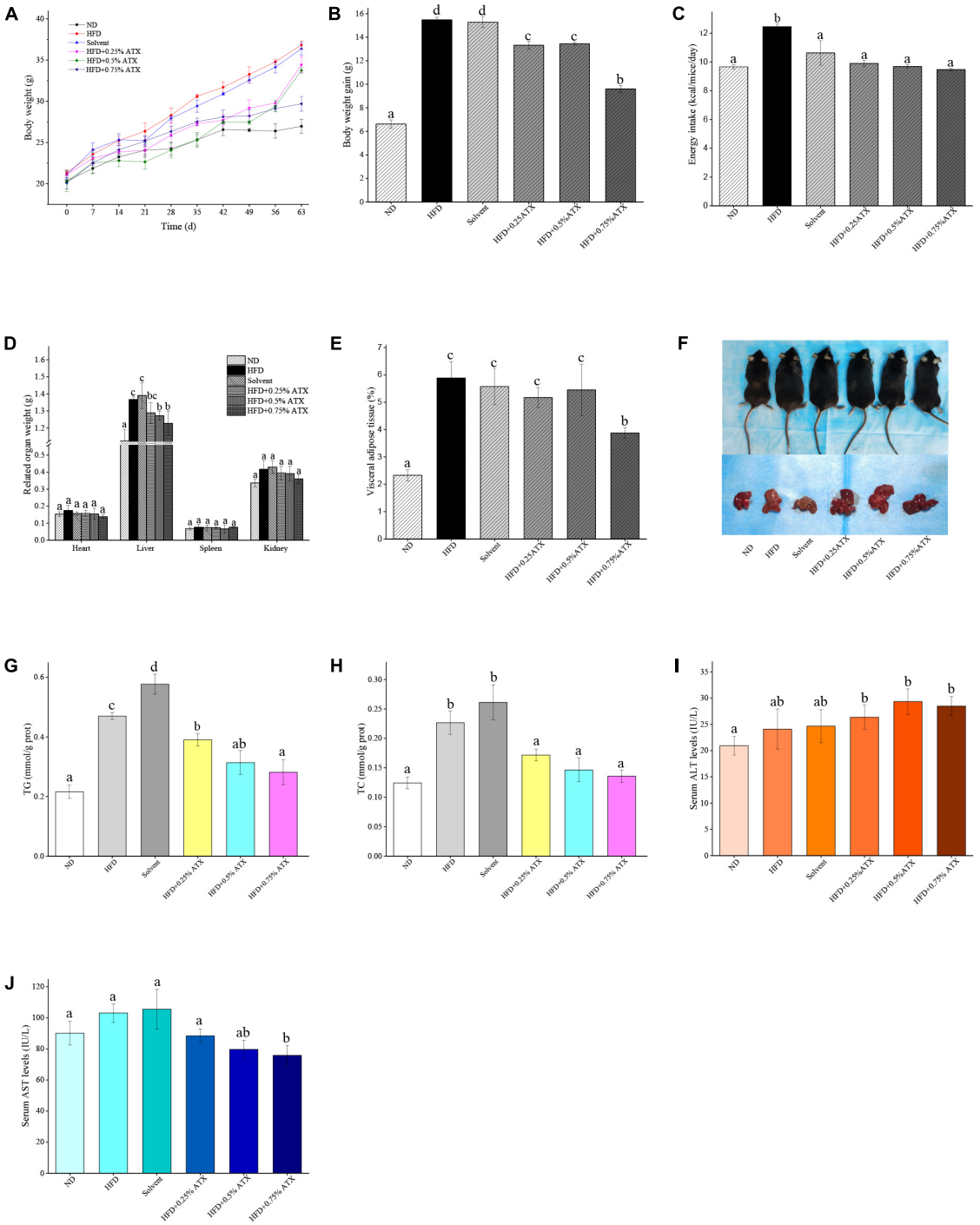

FIGURE 1 | Astaxanthin (ATX) prevented obesity and related indices in HFD-fed mice. **(A)** Body weight. **(B)** Body weight gain. **(C)** Energy intake. **(D)** Related organ weight. **(E)** Visceral adipose tissue. **(F)** Visual appearance pictures of metabolic mice and liver. **(G)** Hepatic TG level. **(H)** Hepatic TC level. **(I)** Serum ALT level. **(J)** Serum AST level. Values are expressed as mean ± SD of triplicate (n = 6). The different letters (a–d) indicate significant differences ($P < 0.05$) according to Duncan's multiple range test in ANOVA.

were monitored after supplementing ATX compared with HFD feeding alone ($P > 0.05$). Therefore, based on the results mentioned above, 0.5 and 0.75% ATX supplementation could efficiently reduce the levels of TG and TC.

In addition, we evaluated serum AST (GOT) and ALT to further explore the liver function induced by HFD and ATX consumption. The serum AST level was increased in the solvent and HFD groups compared with the ND group; however, the

TABLE 1 | Effect of astaxanthin (ATX) supplementation on body weight, energy intake, and food efficiency ratio in high-fat diet-induced mice[a].

Group	ND	HFD	Solvent	HFD+0.25% ATX	HFD+0.5% ATX	HFD+0.75% ATX
Initial body weight (g/mice)	20.35 ± 0.14^{a}	21.35 ± 0.35^{a}	21.09 ± 0.50^{a}	21.11 ± 0.37^{a}	20.32 ± 1.26^{a}	20.08 ± 0.71^{a}
Final body weight (g/mice)	26.97 ± 0.87^{a}	36.83 ± 0.47^{d}	36.38 ± 0.75^{d}	34.79 ± 0.96^{dc}	33.76 ± 0.34^{c}	29.39 ± 0.88^{b}
Weight gain (g/mice)	6.62 ± 0.34^{a}	15.48 ± 0.22^{d}	15.29 ± 0.46^{d}	13.32 ± 0.33^{c}	13.44 ± 0.12^{c}	9.60 ± 0.28^{b}
Energy intake (kcal/mice/day)	9.66 ± 0.14^{a}	12.46 ± 0.19^{b}	10.63 ± 0.85^{a}	9.90 ± 0.21^{a}	9.69 ± 0.12^{a}	9.47 ± 0.08^{a}
Food efficiency ratio (%)[b]	0.47 ± 0.15^{a}	1.05 ± 0.28^{b}	1.36 ± 0.41^{b}	1.06 ± 0.29^{b}	1.06 ± 0.30^{b}	0.96 ± 0.21^{b}

[a]The body weight, energy intake and food efficiency ratio of mice in each group were tested based on one-way ANOVA and the results are expressed as the mean ± SD (n = 6). [b]Food efficiency ratio (%) = (weekly weight gain / weekly food intake) × 100. The values with different labels (a–d) in rows refer to significant difference (P < 0.05).

TABLE 2 | Effect of ATX supplementation on related organ weights and adipose tissue weights in high-fat diet-induced mice[a].

Group	ND	HFD	Solvent	HFD+0.25% ATX	HFD+0.5% ATX	HFD+0.75% ATX
Heart (g)	0.15 ± 0.01^{a}	0.18 ± 0.03^{a}	0.16 ± 0.01^{a}	0.16 ± 0.02^{a}	0.16 ± 0.03^{a}	0.14 ± 0.01^{a}
Liver (g)	1.12 ± 0.07^{a}	1.37 ± 0.02^{c}	1.39 ± 0.08^{c}	1.29 ± 0.06^{bc}	1.27 ± 0.03^{b}	1.23 ± 0.07^{b}
Spleen (g)	0.07 ± 0.01^{a}	0.08 ± 0.02^{a}	0.08 ± 0.02^{a}	0.07 ± 0.01^{a}	0.07 ± 0.02^{a}	0.08 ± 0.01^{a}
Kidney (g)	0.34 ± 0.02^{a}	0.42 ± 0.05^{a}	0.43 ± 0.04^{a}	0.40 ± 0.04^{a}	0.39 ± 0.04^{a}	0.36 ± 0.03^{a}
Visceral adipose tissue (g)	0.63 ± 0.20^{a}	2.17 ± 0.60^{c}	2.03 ± 0.66^{c}	1.84 ± 0.34^{c}	1.78 ± 0.37^{c}	1.15 ± 0.20^{b}

[a]All values are expressed as the mean ± SD (n = 6). Mean separation was performed using Duncan's multiple range test. The different letters (a–c) indicate significant differences (P < 0.05). The visceral adipose tissue included perirenal adipose and epididymal adipose.

TABLE 3 | Effect of ATX supplementation on the levels of serum TG, TC, HDL-C, and LDL-C in the HFD-fed mice.

	ND	HFD	Solvent	HFD+0.25% ATX	HFD+0.5% ATX	HFD+0.75% ATX
TG (mmol/L)						
0 day	0.41 ± 0.09^{a}	0.43 ± 0.18^{a}	0.45 ± 0.28^{a}	0.44 ± 0.23^{a}	0.43 ± 0.10^{a}	0.42 ± 0.11^{a}
30 days	0.48 ± 0.08^{a}	0.72 ± 0.07^{b}	0.70 ± 0.14^{ab}	0.64 ± 0.05^{ab}	0.54 ± 0.08^{ab}	0.45 ± 0.18^{ab}
60 days	0.47 ± 0.13^{a}	0.83 ± 0.12^{c}	0.78 ± 0.21^{ab}	0.74 ± 0.10^{b}	0.69 ± 0.15^{ab}	0.65 ± 0.14^{ab}
TC (mmol/L)						
0 day	3.40 ± 0.28^{a}	3.49 ± 0.10^{a}	3.47 ± 0.13^{a}	3.36 ± 0.23^{a}	3.38 ± 0.18^{a}	3.30 ± 0.10^{a}
30 days	3.36 ± 0.08^{a}	4.19 ± 0.49^{b}	4.08 ± 0.34^{b}	3.56 ± 0.33^{ab}	3.29 ± 0.30^{a}	3.26 ± 0.57^{a}
60 days	3.39 ± 0.12^{a}	4.73 ± 0.38^{b}	4.35 ± 0.41^{b}	3.65 ± 0.18^{a}	3.16 ± 0.09^{a}	2.94 ± 0.38^{a}
HDL-C (mmol/L)						
0 day	0.59 ± 0.08^{a}	0.60 ± 0.06^{a}	0.62 ± 0.12^{a}	0.60 ± 0.14^{a}	0.62 ± 0.09^{a}	0.56 ± 0.08^{a}
30 days	0.49 ± 0.04^{a}	0.36 ± 0.02^{b}	0.36 ± 0.05^{b}	0.33 ± 0.03^{b}	0.31 ± 0.03^{b}	0.31 ± 0.08^{b}
60 days	0.33 ± 0.04^{a}	0.19 ± 0.07^{b}	0.22 ± 0.05^{b}	0.23 ± 0.04^{b}	0.25 ± 0.02^{b}	0.26 ± 0.04^{ab}
LDL-C (mmol/L)						
0 day	0.36 ± 0.04^{a}	0.38 ± 0.04^{a}	0.37 ± 0.03^{a}	0.37 ± 0.04^{a}	0.38 ± 0.04^{a}	0.35 ± 0.04^{a}
30 days	0.39 ± 0.03^{a}	0.83 ± 0.14^{b}	0.74 ± 0.10^{b}	0.63 ± 0.10^{b}	0.51 ± 0.15^{ab}	0.48 ± 0.12^{ab}
60 days	0.57 ± 0.03^{a}	0.91 ± 0.25^{b}	0.84 ± 0.14^{b}	0.70 ± 0.08^{b}	0.59 ± 0.14^{ab}	0.55 ± 0.12^{ab}

Data were expressed as mean ± SD of 6 mice in each group and were analyzed by ANOVA analysis with Duncan's test. Mean values denoted with different superscript letters were significant differences (P < 0.05).

serum ALT level was not apparent in any group (**Figure 1I**). The mice in the 0.75% ATX group displayed significantly lower serum AST levels than the mice in the solvent group, which were reduced by 28.1% (**Figure 1J**).

Effect of Astaxanthin Supplementation on Liver Levels of Oxidation Resistance Markers in High-Fat Diet-Induced Mice

Malondialdehyde and reactive oxygen species (ROS) activities are crucial components contributing to the development of oxidative stress in high-fat diet-fed animals. The levels of antioxidant enzymes, including T-AOC, CAT, SOD, and GSH, were assessed in the liver and exhibited similar trends. The ROS and MDA levels of mice were significantly ($P < 0.05$) increased in the HFD group compared with the ND group (**Figures 2A,B**). According to the ROS qualitative fluorography images, intense red fluorescence was observed in the HFD and the positive control groups (incubated with H_2O_2), while the faint fluorescence in the ATX-treated samples corresponded with the quantitative results (**Figure 2G**). The levels of T-AOC, CAT, SOD, and GSH were significantly ($P < 0.05$) decreased in the HFD group (**Figures 2C–F**); however, the effect of solvent on antioxidant enzymes was not significant ($P > 0.05$). Furthermore,

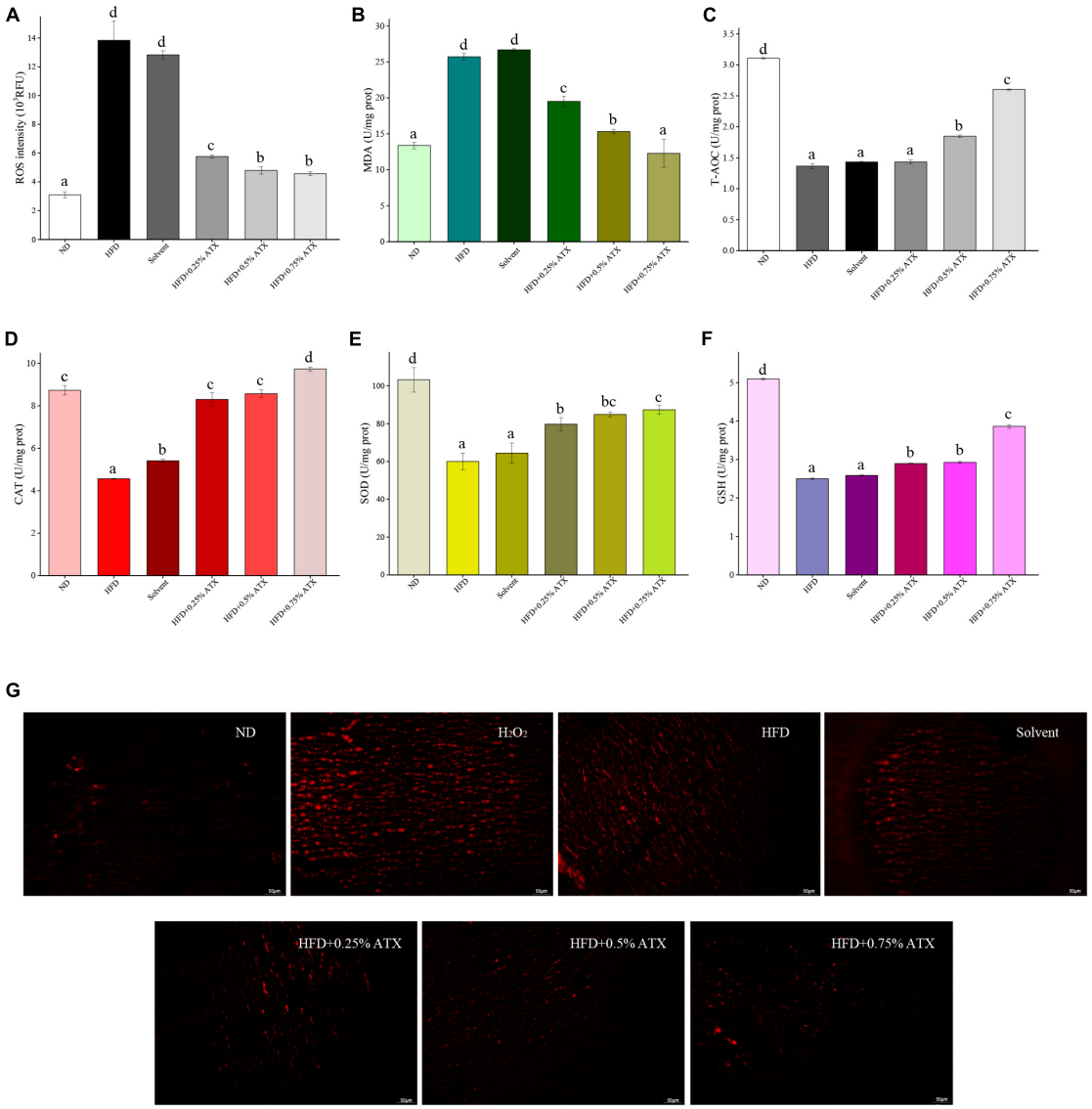

FIGURE 2 | Evaluation of liver oxidation resistance in HFD-induced mice liver tissues. The levels of ROS intensity **(A)**, MDA **(B)**, T-AOC **(C)**, CAT **(D)**, SOD **(E)**, and GSH **(F)** are illustrated in the panel. Values are expressed as mean ± SD of triplicate (n = 6). The different letters (a–d) indicate significant differences ($P < 0.05$) according to Duncan's multiple range test in ANOVA. **(G)** Qualitative detection of ROS by the DHE probe; the ROS-positive cells emitted bright red fluorescence; H_2O_2: as double positive control, and tissues were incubated with 3% H_2O_2.

0.5 and 0.75% ATX supplementation effectively ($P < 0.05$) prevented lipid peroxidation in high-fat diet-fed mice, although the effect was slight in the 0.25% ATX group. When compared to the HFD group, the levels of T-AOC, CAT, SOD, and GSH were increased by 90.6, 113.2, 45.6, and 54.4% in the 0.75% ATX group, respectively.

Histological Assessment of the Liver and Epididymal Adipose Tissue

Photomicrographs of H&E staining were used to observe the pathology in the liver tissues from all experimental groups. In the ND group mice, hepatocytes were fairly uniform, with regularly shaped hepatic plates arranged in an ordered pattern and hepatic cords, except for slight congestion (**Figure 3A**). However, the HFD induced typical lesions in the mouse liver, such as hepatocyte necrosis, inflammatory cell infiltration, congestion of the central veins, ballooning, hepatic sinus expansion and chromatin condensation. In the solvent group, the structure of hepatic plates was irregularly arranged along with fat accumulation, indicating that long-term excessive fat intake disturbed lipid metabolism in the liver. After ATX supplementation following HFD feeding, the pathological characteristics were prevented in the liver tissues, and the steatohepatitis scores were significantly ($P < 0.01$) lowered; in particular, the 0.75% ATX group showed a similar pattern

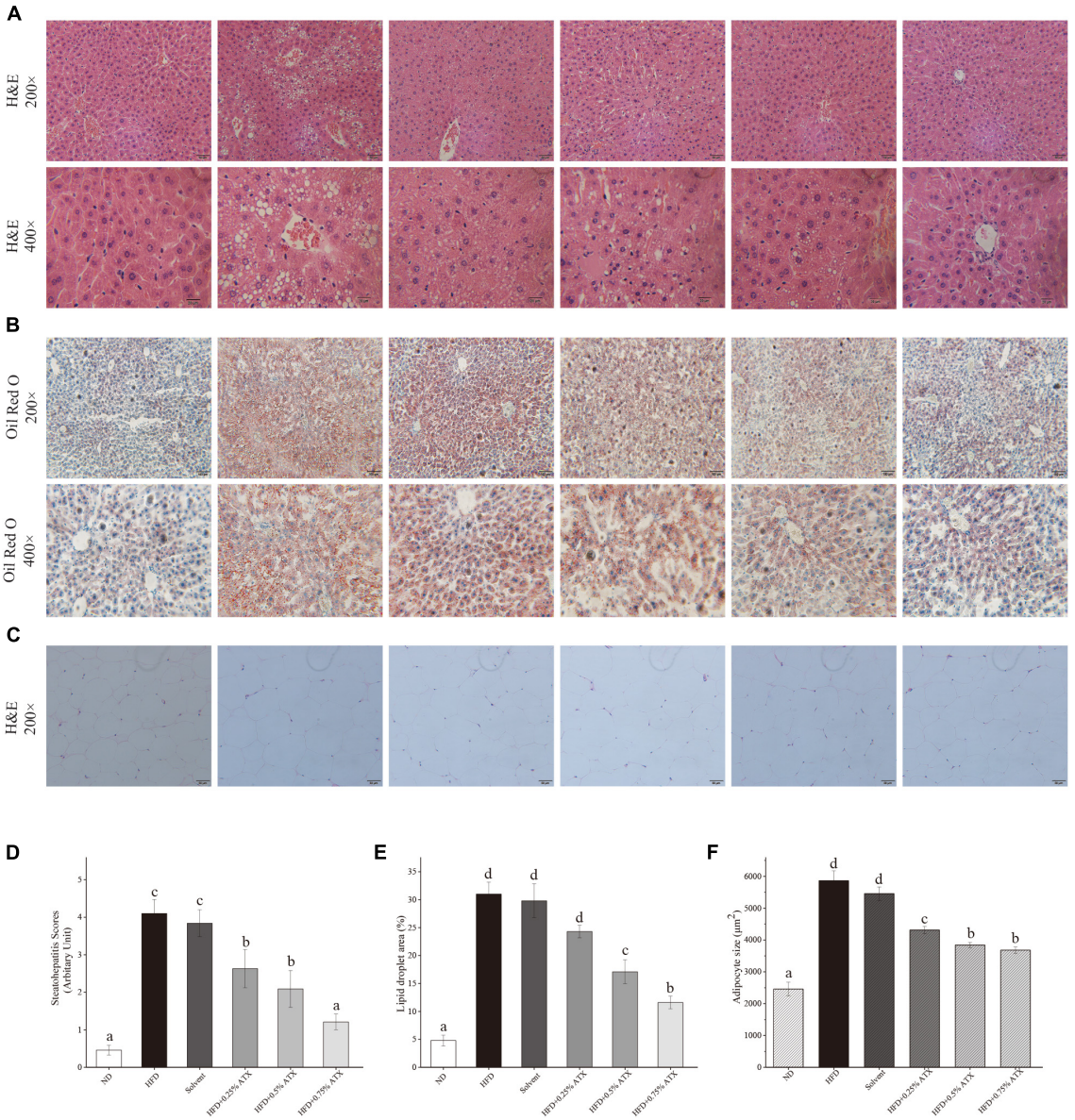

FIGURE 3 | Pathological changes of ATX on liver and epididymal fat in HFD-induced mice. **(A)** Liver sections stained with HE (200×, 400×). **(B)** Liver sections stained with Oil red O (200×, 400×). **(C)** HE-stained e-AT sections (200×). **(D)** Steatohepatitis scores. **(E)** Percentage of the lipid droplet area assessed by Oil red O staining. **(F)** Mean cell area of adipocyte in e-AT. Values are expressed as mean ± SD of triplicate (n = 6). The different letters (a–d) indicate significant differences ($P < 0.05$) according to Duncan's multiple range test in ANOVA.

to the ND group, implying the hepatoprotective effect of ATX (**Figure 3D**).

To further investigate the production of lipid droplets in the liver, Oil Red O staining was performed (**Figure 3B**). More oil red O-stained lipid droplets were observed in the liver tissue of the HFD and solvent groups than in the liver tissue of the ND group, resembling the percentage result of lipid droplets (**Figure 3E**). Conversely, ATX supplementation dose-dependently decreased the production of fatty droplets, in which the area of droplets was significantly lessened in the 0.5 and 0.75% ATX groups. These results confirmed that ATX prevented lipid accumulation and hepatic steatosis, conforming to the results of intrahepatic TG and TC levels. As shown in the e-AT sections of HFD-induced mice (**Figures 3C,F**), the mean adipocyte size increased almost 138.43% compared with that of mice in the ND group. These results were markedly ($P < 0.05$, **Table 2**) related with increasing visual adipose tissue weight.

Apoptotic cells were detected by green fluorescent TUNEL staining, and cell nuclei were stained blue (DAPI). The results showed that the positive apoptosis rate significantly ($P < 0.05$) increased along with the long-term fat infiltration in liver tissue caused by HFD (**Supplementary Figure 1A**). Compared to

that in the HFD group, the number of apoptotic cells stained green was reduced in a dose-dependent manner with ATX supplementation, and the apoptosis rates were decreased by 14.7, 25.1, and 48.5%, respectively (**Supplementary Figure 1B**).

Effect of Astaxanthin Supplementation on the Relative mRNA Expression Levels and Transcriptome Level Verification

To understand the mechanism(s) by which ATX modulates hepatic lipid metabolism in response to a high-fat diet, we analyzed the expression of genes related to lipogenesis and fatty acid β-oxidation in the liver by qRT–PCR. As shown in **Figure 4A**, the expression of *SREBP1c* in the livers of HFD group mice significantly ($P < 0.05$) increased and the expression of *AMPK* and *PPARα* decreased compared to those in ND group mice. However, the expression levels of these key genes were notably altered after ATX supplementation, although no significant differences in the mRNA levels of *AMPK* and *SREBP1c*, the key factors of metabolic energy and transcription factors in lipogenesis, were visualized in either the ND or HFD + 0.75% ATX group. The expression levels of *ACC*, *FAS*, and *SCD-1* were remarkably ($P < 0.05$) decreased, and the expression of lipid oxidation and bile acid metabolism genes *CPT-1*, *LXRα*, *CYP7A1*, and *CYP27A1* was enhanced in the 0.75% ATX group compared with the HFD group. These results indicated that consumption of a HFD contributed to fat synthesis and ultimately disturbed lipid metabolism; furthermore, high-dose ATX could improve the disorder of lipid metabolism by promoting cholesterol metabolism and inhibiting fat synthesis.

To explore how the hepatic lipidome is altered upon ATX intervention, RNA sequencing was used to accurately and quantitatively analyse liver transcriptional changes and lipid metabolism pathways in the liver in response to ATX supplementation. A total of 141 genes were differentially expressed in HFD-induced liver samples compared with ND-induced liver samples (**Supplementary Figures 2A,B**). However, a total of 156 differentially expressed genes, of which 103 were increased and 53 were decreased, were identified in the 0.75% ATX group compared with the HFD group (**Supplementary Figures 2C,D**). Additional screening revealed that 17 genes altered a multitude of biological processes related to the metabolic regulation of lipids, including fatty acid biosynthesis, cholesterol metabolism, lipid storage and bile acid metabolism, through the AMPK/SREBP1c signal pathway (**Figures 4B,C**).

Astaxanthin Supplementation Altered Liver Lipid Metabolism by Lipidomic Analysis

We performed a comprehensive hepatic lipidomic analysis to evaluate whether differences in lipid content or composition may account for differences in hepatic lipid disorders between the HFD group and ATX group. The results of OPLS-DA comparison analysis showed a remarkable separation among the ND, HFD, and HFD + 0.75% ATX groups, indicating that HFD supplementation with ATX altered the compositions of liver lipids (**Figure 5A**). For the liver samples, the validation parameters of fitness ($R^2Y = 0.995$ and $Q^2 = 0.954$) were obtained in ND vs. HFD, as well as fitness ($R^2Y = 0.998$ and $Q^2 = 0.882$) in HFD vs. HFD + 0.75% ATX. A total of 1,012 lipid species were identified in liver samples, which belong to six primary classes of lipids, including glycerophospholipids (GPs), glycerides (GLs), fatty acyls (FAs), sphingolipids (SLs), sterol lipids (STs), and prenol lipids (PRs) (**Supplementary Figure 3**). Values with fold change ≥ 2 (fold change ≤ 0.5) and VIP > 1 were selected to represent metabolic biomarkers, and significant differences were identified at $P < 0.05$. Based on the abovementioned results, we screened 146 and 91 lipid biomarker candidates by applying volcano plots for such distinctions in ND vs. HFD and HFD vs. HFD + 0.75% ATX, respectively (**Figures 5C,D**).

According to the Venn diagram, we found that the accumulated 146 lipid species were significantly different between the ND and HFD groups, while ATX intervention patently changed the levels of 91 lipid species, including 24 ordinary species, compared to the levels in HFD-fed alone (**Figure 5B**). As shown in the heatmap, the HFD increased the levels of 13 metabolites (4 FFAs, 7 TGs, and 2 DGs) and decreased the levels of one metabolite (TG), whereas all of the metabolites were significantly inverted in the HFD + 0.75% ATX group (**Figure 5G**). Furthermore, in our present study, we found that 8 of the other 20 most relevant metabolites (3 BAs, 2 CARs, 2 BMP, and 1 TG) were remarkably downregulated after ATX supplementation; however, there was no significant difference in the ND vs. HFD group. We observed a significantly positive correlation among these 34 metabolite levels associated with lipid metabolism (**Figure 5H**). Thus, these results indicated that the 22 metabolites, including 4 FFAs, 8 TGs, 2 DGs, 3 BAs, 2 CARs, and 2 BMPs, might be potential biomarkers accountable for alleviating the steatohepatitis induced by lipid disturbance. The KEGG database was used to perform pathway analysis of differentially expressed metabolites. The pathways were considerably disrupted in the HFD group, including glycerolipid metabolism, insulin resistance, cholesterol metabolism, fat digestion and absorption, and regulation of lipolysis in adipocytes, when compared with the ND group; however, 0.75% ATX supplementation effectively prevented dysregulation of these pathways and improved bile secretion and primary bile acid biosynthesis (**Figures 5E,F**).

Astaxanthin Supplementation Changed the Structures and Dysbacteriosis of Gut Microbiota in High-Fat Diet-Fed Mice

To investigate how ATX prevents the progression and development of obesity and NAFLD by affecting the gut microbiota, we analyzed the 16S rRNA results clustered into different operational taxonomic units (OTUs) at a 97% similarity level. Of the 8,849 OTUs visualized in the experimental groups, 542 (4.25%) were normal among the ND, HFD, and 0.75% ATX groups. In addition, the number of other OTUs in the ND group, HFD group and 0.75% ATX group was 2,299 (18.03), 2,109 (16.51%), 2,828 (22.18%), respectively, indicating the great differences of gut microbes in the bacterial community (**Figure 6A**). Alpha-diversity analysis was used to identify

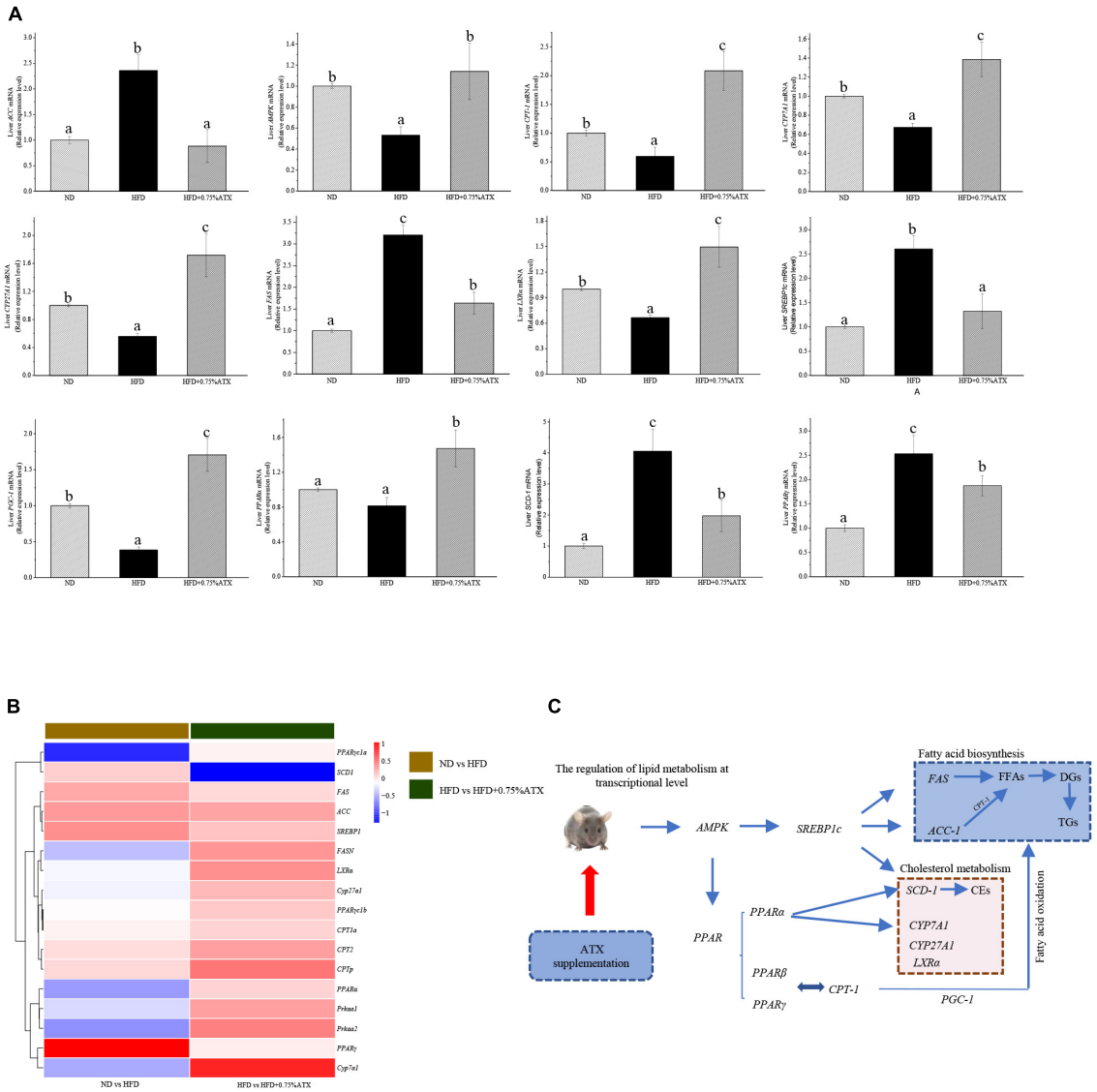

FIGURE 4 | Astaxanthin significantly improved relative gene expression. **(A)** Gene expression levels in AMPK/SREBP1c pathway. **(B)** The heatmap of differential genes expression at the transcriptional level. **(C)** Regulatory effects of ATX supplementation on fatty acid and cholesterol metabolism in mice induced by HFD. Data are shown as mean ± SD of triplicate. The different letters (a–c) indicate significant differences ($P < 0.05$) according to Duncan's multiple range test in ANOVA.

the within-habitat diversity, including richness (the values of Chao1 and observed species), diversity (Shannon and Simpson), and evenness (Pielous' evenness index), of which the richness significantly increased in the HFD and 0.75% ATX groups compared to the ND group; however, the Shannon and Simpson index decreased. The Goods coverage values had no obvious differences in each group (**Figure 6B**). To assess community similarity among samples, we applied principal coordinates analysis (PCoA) to represent the relative abundance of OTUs in each community by two different analyses. The PCoA plot showed that the structure and compositions of gut microbiota in the HFD group (Axis 1, 22.3%, **Figure 6C**) statistically separated from the ND group, and a considerable distinction was observed in the 0.75% ATX group (Axis 2, 8.9%).

At the phylum level, the taxonomic profiles of the gut microbiomes showed significant differences according to increasing ATX supplementation and developing obesity severity, within which *Firmicutes*, *Bacteroidetes*, and *Proteobacteria* were the dominant phyla. The abundance of *Firmicutes*, *Proteobacteria*, *Verrucomicrobia*, and *Actinobacteria* decreased significantly, and the proportions of *Bacteroidetes* increased markedly ($P < 0.05$) in the HFD group compared with those of the ND group (**Figure 6D**), while 0.75% ATX supplementation further reduced the abundance of *Firmicutes* and *Proteobacteria* and remarkably reversed the trend of the other three bacteria. At the genus level, the abundance of genera, including *Bacteroides*, *Allobaculum*, *Desulfovibrio*, *Akkermansia*, *Oscillospira*, *Ruminococcus*, *Parabacteroides*, *Adlercreutzia*,

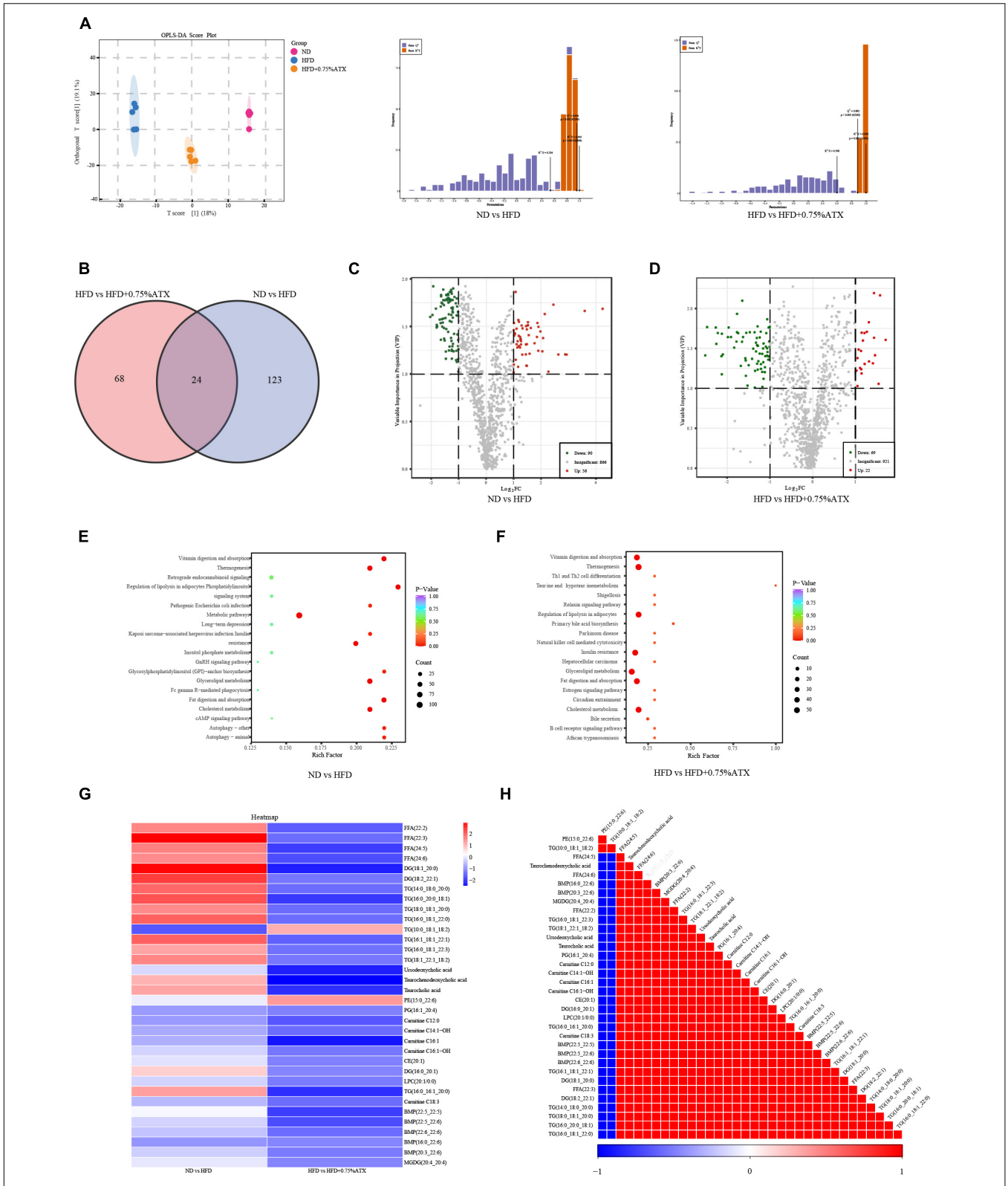

FIGURE 5 | Astaxanthin regulated lipid metabolites in HFD-fed mice. **(A)** OPLS-DA score plot (*left*) and permutation plot (*right*). **(B)** Venn diagram depicting the overlap of significantly changed metabolites between experimental groups. The volcano plot analysis of ND vs. HFD group **(C)** and HFD vs. HFD + 0.75% ATX group **(D)**. Analysis of lipid metabolism pathway of ND vs. HFD **(E)** and HFD vs. HFD + 0.75% ATX **(F)**. **(G)** Heatmap of 34 significantly altered metabolites in ATX-treated HFD-fed mice. Blue: downregulated metabolites. Red: upregulated metabolites. **(H)** The associated heatmap of significantly changed metabolites.

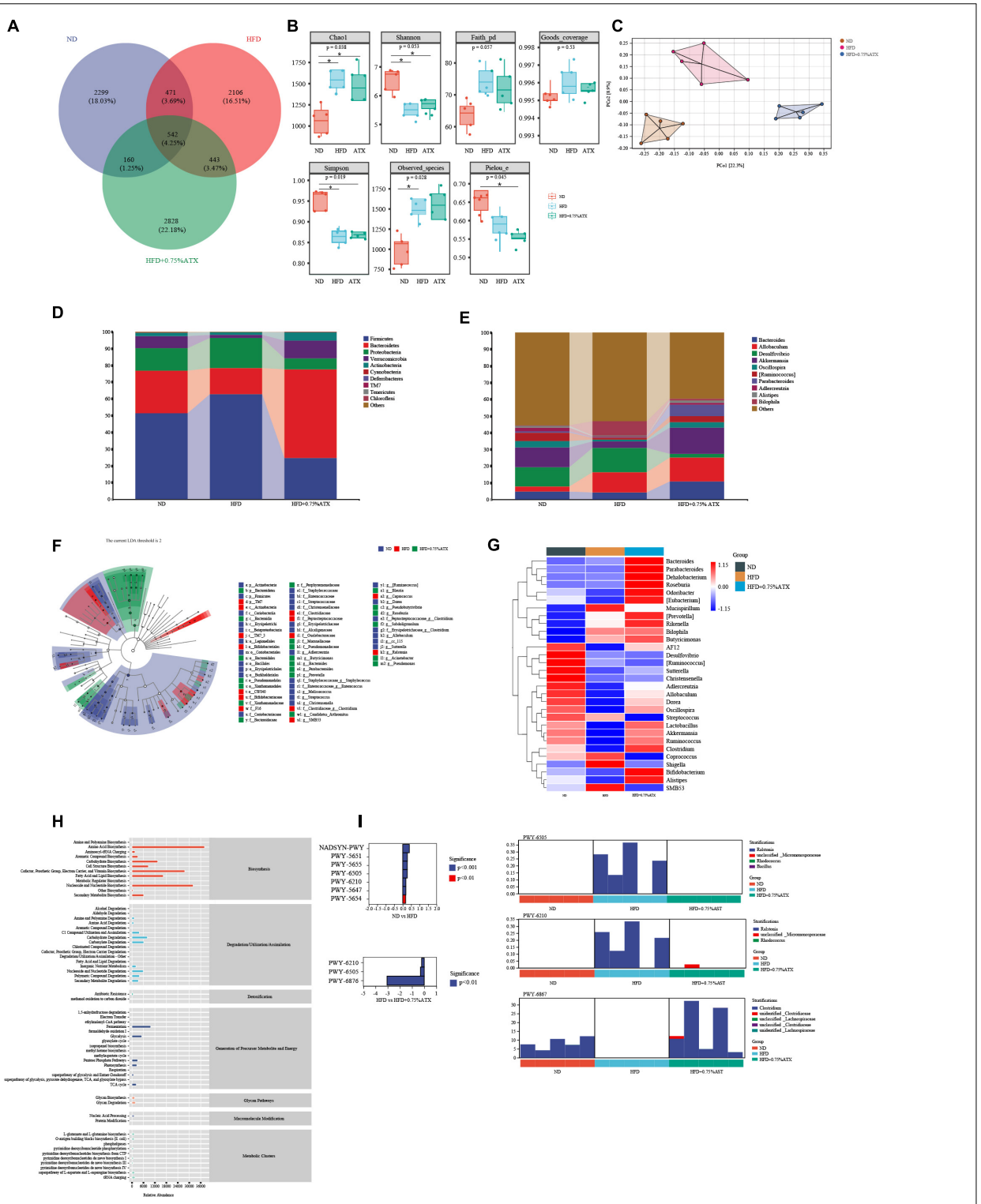

FIGURE 6 | Astaxanthin regulated the gut microbiota. **(A)** The Venn diagram. **(B)** Evaluation of Alpha Diversity Index including Chao1, Simpson, Shannon, Pielou's evenness, observed species, Faith's phylogenetic diversity and Good's coverage index values. Data were analyzed using a one-way ANOVA and are expressed as the mean ± SD. ($n = 5$). "*" $P < 0.05$ versus ATX-treated HFD-fed mice. **(C)** PCoA of unweighted UniFrac distance from beta diversity analysis. **(D)** Phylum abundance graph genus levels. **(E)** Genus abundance graph. **(F)** Species taxonomy branch map based on LEfSe analysis. **(G)** The heatmap of the 30 bacterial genera with the largest differences in abundance were selected, according to the unweighted UniFrac distance of the intestinal content samples. **(H)** Predicted the abundance map of MetaCyc secondary functional pathways. X-coordinate: the abundance of functional pathways, Y-coordinate: the MetaCyc secondary functional pathway. **(I)** Analysis of differences in metabolic pathways (*left*) and species composition in different MetaCyc pathways (*right*).

Alistipes, and *Bilophila,* was significantly altered by a high-fat diet compared with the normal diet and moderately inverted by 0.75% ATX. Compared to the mice induced by HFD alone, the mice supplemented with ATX had significantly upregulated abundances of *Akkermansia* and *Parabacteroides* to 15.74 and 6.73%, respectively (**Figure 6E**). Additionally, to explore high-dimensional biomarkers and identify significant differences at the species level, LEfSe with default parameters was used between the microbial communities compared. The 65 most abundant OTUs were observed at the taxonomic level in the samples, among which beneficial bacteria were significantly reduced in the HFD group compared with the ND group, revealing a serious gut microbial disorder in HFD-fed mice (**Figure 6F**).

Furthermore, 9 of the 30 most prevalent bacterial genera were upregulated and 21 bacterial genera were downregulated in the HFD-fed mice compared with the mice fed a normal diet, while these genera were partially promoted to their original relative abundance levels after ATX supplementation (**Figure 6G**). To characterize the functional role of the related abundant bacterial genera, we found 47 secondary functional pathways from the MetaCyc database of metabolic pathways that are relevant to lipometabolism, including the fatty acid and lipid biosynthesis pathway (abundance value: 16,383.26), carbohydrate degradation (8,059.48), secondary metabolite biosynthesis (6,077.67), glycolysis (5,101.02), secondary metabolite degradation (3,331.28), and pentose phosphate pathways (2,978.49) (**Figure 6H**). According to the MetaCyc profiles, there were significant and apparent differences in the species composition of the eight selected metabolic pathways, among which three pathways, 2-aminophenol degradation (PWY-6210), L-tryptophan degradation XII (PWY-6505) and isopropanol biosynthesis (PWY-6876), were relatively and significantly ($P < 0.05$) different in all of the samples (**Figure 6I**).

DISCUSSION

Obesity and obesity-related complications are classic health problems worldwide. A long-term high-fat diet and an imbalance in energy expenditure are important causes for concern (26). In both obese individuals and animal models of NASH, it could be characterized by excessive intracellular lipid accumulation combined with inflammation, which can ultimately progress into hepatic insulin resistance, mitochondrial dysfunction and cellular injury (27, 28). Emerging evidence shows that ATX, a natural functional food, has been used as a dietary supplement for treating obesity and liver injury and maintaining health (18, 29). For example, Ni's study reported that ATX reduced hepatic steatosis and TG accumulation by decreasing lipid uptake and further improved simple fatty liver whether in a HFD-induced obesity (DIO) model or in genetically obese (*ob*/*ob*) mice (30). Importantly, when compared to vitamin E, ATX was more effective at lipid peroxidation and preventing NASH. In the present study, our results showed that ATX supplementation could prevent obesity and the development of NAFLD by meditating lipid metabolism and gut microbiota. Alternatively, ATX consumption also prevents oxidative stress in the liver and lipid peroxidation by improving antioxidant enzyme activity. According to experimental results, dietary ATX not only significantly decreased body weight gain, adipose tissue weight, and serum TG, TC, and LDL-C levels but also ameliorated abnormal hepatic metabolism following the reduction of liver weight and hepatic TG and TC levels in HFD-induced mice. No significant difference in the food efficiency ratio or serum HDL-C levels was observed in the HFD group with long-term ATX intake. From the physiological and biochemical profiles, ATX exhibited a better preventive effect on dyslipidaemia and abnormal liver function than our previous results (18).

Over the past decade, numerous pieces of evidence have shown that oxidative stress caused by a high-fat diet and specific products of ROS are involved in the development of obesity and fatty liver (31, 32). Thus, balancing the liver oxidative reaction is an important aspect of preventing the development of NAFLD. Studies have shown that oxidative stress is closely related to endoplasmic reticulum (ER) stress in the development and progression of NAFLD and other diseases, while ATX can directly or indirectly moderate ER through antioxidant activity (33, 34). Interestingly, previous study has confirmed that ATX significantly reduced the levels of oxidative stress marker thiobarbituric acid-responsive substances (TBARS) in the liver of NASH mice (30). In our results, both the ROS levels evaluated by the DHE probe and the levels of MDA measured, a lipid peroxidation product, were significantly increased in liver tissues in each experimental group. HFD might have contributed to the increase in these oxidative stress indices and the decrease in antioxidant enzymes, including T-AOC, SOD, CAT, and GSH levels. Our results are consistent with previous studies showing that HFD seriously damaged the antioxidant defense system (32, 35). Regardless of the dose, the MDA levels of all ATX-supplemented groups were reduced, suggesting that ATX suppresses overproduction of ROS induced by obesity. In addition, with dose-dependent increases of the ATX in the diet, the activities of antioxidant enzymes remarkedly improved and were close to normal levels in mice fed HFD. Multiple studies have confirmed that cell apoptosis induced by excessive endogenous cholesterol is associated with increased ROS in tissues (36, 37). As previously discussed, long-term HFD intake advanced total cholesterol and disturbed the oxidative balance in the liver, which was attributed to hepatocellular apoptosis. Based on the TUNEL assay results, we found a large number of apoptotic liver cells in the HFD group, whereas ATX alleviated the degree of necrosis. Nevertheless, the precise intracellular mechanism responsible for this phenomenon was unclear in this study. Moreover, the pathological results showed that ATX could effectively prevent fat accumulation and hepatic steatosis in a dose-dependent manner.

Whether for obesity or the development of NAFLD, one of the root causes is the perturbation in lipid metabolism (38). As reported in previous studies, excessive fat intake induced abnormal bile secretion and disturbed cholesterol levels (39). In addition, FFAs usually trigger the accumulation of DGs and TGs by mediating insulin signal and sensitivity in liver tissue (40). To demonstrate the function of ATX in lipid metabolism, lipidomic analysis revealed that the total levels of hepatic FFAs,

TGs, and DGs were noticeably increased in HFD group mice, indicating that a high-fat diet partly supported our previous results. Interestingly, our results suggested that ATX not only decreased the levels of FFAs and TGs but also specifically reduced the levels of BAs and acyl-carnitines, indicating that both cholesterol metabolism and fatty acid oxidation were improved in mouse livers. Moreover, *SREBP1c*, along with its downstream genes *ACC*, *SCD1* and *FAS*, is an important component in the energy metabolic system and plays a key role in regulating the FFA and TG synthesis mentioned above (38, 41).

To further clarify the association between the development of obesity and the changes in lipid metabolites and related genes, we integrated the transcriptome and qPCR analysis to verify the gene expression levels in the AMPK/SREBP1c pathway. According to transcriptome analysis, gene expression signatures were profoundly distinguished among the experimental groups. Considering the degree and diversity of gene expression changes, only genes associated with the target pathway were screened in this study. *AMPK*, a key molecule in the regulation of biological energy metabolism, is involved in diabetes and metabolism-related diseases (42). Peroxisome proliferator activated receptor (*PPARα*) and peroxisome proliferator-activated receptor gamma coactivator-1α (*PGC-1*) play an important role in regulating the homeostasis of adipose tissue by jointly regulating the balance between fatty acid synthesis and oxidation (43). The expression of *PPARα*, which is negatively correlated with the severity of NASH, is significantly reduced in NAFLD (44). ATX alleviated the gene expression associated with EIF-2 signaling in NASH rather than improved the expression of gene related to mitochondrial dysfunction (45). In present study, the results revealed that dietary 0.75% ATX significantly decreased the expression levels of *AMPK*, *SREBP1c*, *ACC*, *FAS*, *PPARγ*, and *SCD-1* while increasing the expression levels of *PPARα*. As our previous manuscript shown, the interaction between *PPARα* and *PGC-1α* promoted the oxidation of fatty acids and inhibited the expression of *SREBP1c* to a certain extent (18). During lipid metabolism, *CPT-1* is a key rate-limiting enzyme that accelerates the entry and β-oxidation of long-chain fatty acids into mitochondria (46). A high-fat diet suppresses the expression of *PGC-1α*, and the mitochondrial respiration rate decreases in the absence of *PGC-1α*, ultimately leading to a decrease in fatty acid oxidation capacity. In present study, our results found 0.75% ATX effectively up-regulated the expression level of *PGC-1α* and further stimulated the expression of its downstream gene *CPT-1α*, indicating that ATX reduced intracellular lipid content by promoting fatty acid oxidation. A previous study confirmed that the suppression of *SCD-1* could effectively attenuate HFD-induced insulin resistance and hepatic steatosis (47). However, we did not examine the effects of *SCD-1* knockdown or overexpression on liver lipid metabolism in mice, which should be addressed in future studies. Cholesterol 7α-hydroxylase (*CYP7A1*) and cytochrome P450 27A1 (*CYP27A1*), two important rate-limiting enzymes, play major roles in maintaining the balance of cholesterol and bile acid in the bile acid biosynthetic pathway in the liver (48). The decrease in serum cholesterol is due to a decrease in its de novo synthesis in the liver and an increase in the conversion to bile acids. *LXRα*, as nuclear receptors, regulates the transcription of *CYP7A1,* which is related to regulation of cholesterol and bile acids metabolisms (49). Our data showed that a HFD could downregulate *LXRα*, *CYP7A1*, and *CYP27A1* expression, while high-dose ATX supplementation could upregulate them, indicating that ATX could eliminate excess cholesterol in liver tissue by stimulating the conversion of cholesterol to bile acids. Besides, the expression of *CYP7A1* and *CYP27A1* is regulated by the intestinal flora (50). In summary, our study provides evidence to support the hypothesis that ATX may mediate cholesterol metabolism, fatty acid oxidation and synthesis via the AMPK/SREBP1c pathway to prevent obesity and fatty liver.

The characteristic role of diet in obesity and metabolic disorders is that diet has become an important factor in regulating the gut environment. Both long-term and short-term dietary interventions will induce changes in the structure and function of intestinal microbes (51). Briefly, liver metabolites mainly affect the composition of gut microbes and the integrity of the intestinal barrier, while gut microbiota regulate the synthesis of bile acids, glucose and lipid metabolism in the liver (52). Noticeably, many recent studies have shown that functional foods and natural health products, directly or indirectly, prevent obesity and metabolic diseases by improving intestinal diversity (25, 53). In the current study, mice fed a HFD exhibited lower diversity and gut microbiota disturbance; however, ATX had a salutary effect on promoting gut microbiota and improving diversity. ATX significantly reduced the values of *Firmicutes/Bacteroidetes* (F/B), indicating that the reduction in weight gain might be partly due to changes in F/B. Moreover, the increase in *Actinobacteria* and *Verrucomicrobia* at the phylum level indicated that ATX effectively activated functional bacteria.

Astaxanthin treatment had the greatest impact on *Allobaculum* and *Akkermansia* at the genus level. The relative abundance of *Allobaculum* is associated with hormone secretion, SCFA production, serum HDL-C concentration, and intestinal barrier integrity, which is usually found in higher relative abundances in healthy individuals in prior studies (54, 55). In addition, *Akkermansia*, an intestinal symbiont colonizing the mucosal layer, is considered to be a functional probiotic that is closely related to fat increase, secondary bile acid biosynthesis and IR (56). In this study, the relative abundance of *Allobaculum* and *Akkermansia* in the 0.75% ATX group was even higher than that in the ND group. In addition, ATX significantly decreased the abundance of *Desulfovibrio*, a pathogenic bacterium that induces lipopolysaccharide (57). *Lactobacillus*, *Clostridum*, and *Bifidobacterium* are closely associated with cholesterol metabolism, and the abundance of *Bifidobacterium* is positively correlated with the level of high-density lipoprotein (HDL) (58). Surprisingly, further screening found that ATX, in contrast to chalk and cheese from our previous research, promoted *Butyricimonas*, *Lactobacillus*, *Clostridum*, and *Bifidobacterium* in the current results. As the results shown, 0.75% ATX significantly increased the abundance levels of *Lactobacillus*, *Clostridum*, and *Bifidobacterium*, implying that these probiotics may directly or indirectly regulate the expression of genes related to bile acid synthesis, which was consistent with previous report (49). Another interesting finding in this study was the promotion of *Butyricimonas*, a probiotic that produces butyric acid metabolites, after ATX supplementation, which contributed to

alleviating systemic obesity and gut inflammation. Moreover, butyrate can restore intestinal mucosal injury induced by a high-fat diet and reduce nonalcoholic steatohepatitis (59). Thus, according to the increase in these functional probiotics, ATX supplementation could effectively prevent the microbial dysbiosis induced by HFD. All in all, when compared to our previous study, we found that the preventive effect of ATX is better than its therapeutic effect whether from the physiological and biochemical level, from the metabolic level or from the multi-omics and pathological level.

In conclusion, the current study shows that ATX has a better preventive effect on the development of obesity and NAFLD induced by HFD when compared with prognosis treatment. Both physiological and biochemical profiles demonstrate that long-term consumption of ATX effectively prevents body weight gain, dyslipidaemia and abnormal liver function. Subsequently, pathological analysis indicated that ATX relieves liver steatosis, as well as oxidative stress and apoptosis caused by excessive fatty acids. In addition, we also confirmed that ATX regulates lipid metabolism by mediating the expression of genes in the AMPK/SREBP1c pathway. Moreover, ATX improves hepatic lipid metabolism and increases gut probiotics, confirming that some metabolites might be positively correlated with specific bacteria to maintain body health through the liver-gut axis. This study provides scientific evidence for the functional effects of ATX on obesity prevention. However, our research still has some limitations. Future studies should focus on verifying the role of different pathways in the regulation of lipid metabolism at the protein level and exploring the molecular mechanism of liver oxidative stress and apoptosis through fatty acids mediated by ATX.

DATA AVAILABILITY STATEMENT

The data presented in the study are deposited in the DRYAD repository, accession number: doi: 10.5061/dryad.dz08kprzs.

ETHICS STATEMENT

The animal study was reviewed and approved by Institutional Animal Care and Use Committee of Shanxi Agricultural University.

AUTHOR CONTRIBUTIONS

MW and WX: conceptualization and methodology. MW, WX, JY, YL, CJ, CZ, JX, and RL: validation and investigation. MW: formal analysis, writing—original draft preparation, visualization, and project administration. HC: resources, writing—review, editing, supervision, and funding acquisition. All authors have read and agreed to the published version of the manuscript.

FUNDING

This work was supported by National Natural Science Foundation of China (31902394), the Scientific and Technological Innovation Programs of Higher Education Institutions in Shanxi (2021L119), Outstanding Doctor to Work in Shanxi Province Research Project (SXYBKY2019036), the State Key Laboratory of Integrative Sustainable Dryland Agriculture (in preparation), Shanxi Agricultural University (202105D121008-3-6), the Specialized Scientific Project of Shanxi Agricultural Valley Construction (SXNGJSKYZX201906), the Science and Technology Innovation Planning Project of Shanxi Agricultural University (2018YJ16).

ACKNOWLEDGMENTS

We thank HM from Xi'an Jiaotong University for helping to polish the language.

SUPPLEMENTARY MATERIAL

The Supplementary Material for this article can be found online at: https://www.frontiersin.org/articles/10.3389/fnut.2022.840648/full#supplementary-material

Supplementary Figure 1 | Evaluation of TUNEL reagent on cell apoptosis. (A) The positive result of is indicated by the green marked spots in the sample. (B) Apoptosis rate of each treatment. Values are expressed as mean ± SD of triplicate. The different letters (a–d) indicate significant differences ($P < 0.05$) according to Duncan's multiple range test in ANOVA.

Supplementary Figure 2 | The screened genes and Volcano plot of ND vs. HFD and HFD vs. HFD + 0.75% ATX by RNA-seq results.

Supplementary Figure 3 | Cluster heatmap of metabolites in all samples.

REFERENCES

1. Piche ME, Tchernof A, Despres JP. Obesity phenotypes, diabetes, and cardiovascular diseases. *Circ Res.* (2020) 126:1477–500. doi: 10.1161/CIRCRESAHA.120.316101
2. Hall KD, Guo J, Courville AB, Boring J, Brychta R, Chen KY, et al. Effect of a plant-based, low-fat diet versus an animal-based, ketogenic diet on ad libitum energy intake. *Nat Med.* (2021) 27:344–53. doi: 10.1038/s41591-020-01209-1
3. Ipsen DH, Lykkesfeldt J, Tveden-Nyborg P. Molecular mechanisms of hepatic lipid accumulation in non-alcoholic fatty liver disease. *Cell Mol Life Sci.* (2018) 75:3313–27. doi: 10.1007/s00018-018-2860-6
4. Eo H, Jeon YJ, Lee M, Lim Y. Brown alga *Ecklonia cava* polyphenol extract ameliorates hepatic lipogenesis, oxidative stress, and inflammation by activation of AMPK and SIRT1 in high-fat diet-induced obese mice. *J Agric Food Chem.* (2015) 63:349–59. doi: 10.1021/jf502830b
5. Hagstrom H, Nasr P, Ekstedt M, Hammar U, Stal P, Hultcrantz R, et al. Risk for development of severe liver disease in lean patients with nonalcoholic fatty liver disease: a long-term follow-up study. *Hepatol Commun.* (2018) 2:48–57. doi: 10.1002/hep4.1124
6. Hu L, Huang X, You C, Li J, Hong K, Li P, et al. Prevalence of overweight, obesity, abdominal obesity and obesity-related risk factors in southern China. *PLoS One.* (2017) 12:e0183934. doi: 10.1371/journal.pone.0183934
7. Mazidi M, Ofori-Asenso R, Kengne AP. Dietary patterns are associated with likelihood of hepatic steatosis among US adults. *J Gastroen Hepatol.* (2020) 35:1916–22. doi: 10.1111/jgh.15076

8. Hsiao YH, Wang YH, Lin WS, Cheng YC, Nagabhushanam K, Ho CT, et al. Molecular mechanisms of the anti-obesity properties of *Agardhiella subulata* in mice fed a high-fat diet. *J Agric Food Chem.* (2021) 69:4745–54. doi: 10.1021/acs.jafc.1c01117
9. Rani V, Deep G, Singh RK, Palle K, Yadav UC. Oxidative stress and metabolic disorders: pathogenesis and therapeutic strategies. *Life Sci.* (2016) 148:183–93. doi: 10.1016/j.lfs.2016.02.002
10. Carrier A. Metabolic syndrome and oxidative stress: a complex relationship. *Antioxid Redox Signal.* (2017) 26:429–31. doi: 10.1089/ars.2016.6929
11. Wharton S, Bonder R, Jeffery A, Christensen RAG. The safety and effectiveness of commonly-marketed natural supplements for weight loss in populations with obesity: a critical review of the literature from 2006 to 2016. *Crit Rev Food Sci Nutr.* (2020) 60:1614–30. doi: 10.1080/10408398.2019.1584873
12. Srivastava G, Apovian CM. Current pharmacotherapy for obesity. *Nat Rev Endocrinol.* (2018) 14:12–24. doi: 10.1038/nrendo.2017.122
13. Clugston RD. Carotenoids and fatty liver disease: current knowledge and research gaps. *Biochim Biophys Acta Mol Cell Biol Lipids.* (2020) 1865:158597. doi: 10.1016/j.bbalip.2019.158597
14. Lee Y, Hu S, Park YK, Lee JY. Health benefits of carotenoids: a role of carotenoids in the prevention of non-alcoholic fatty liver disease. *Prev Nutr Food Sci.* (2019) 24:103–13. doi: 10.3746/pnf.2019.24.2.103
15. Mounien L, Tourniaire F, Landrier JF. Anti-Obesity effect of carotenoids: direct impact on adipose tissue and adipose tissue-driven indirect effects. *Nutrients.* (2019) 11:1562. doi: 10.3390/nu11071562
16. Ambati RR, Phang SM, Ravi S, Aswathanarayana RG. Astaxanthin: sources, extraction, stability, biological activities and its commercial applications–a review. *Mar Drugs.* (2014) 12:128–52. doi: 10.3390/md12010128
17. Wu D, Xu H, Chen J, Zhang L. Effects of astaxanthin supplementation on oxidative stress. *Int J Vitam Nutr Res.* (2020) 90:179–94. doi: 10.1024/0300-9831/a000497
18. Wang M, Ma H, Guan S, Luo T, Zhao C, Cai G, et al. Astaxanthin from *Haematococcus pluvialis* alleviates obesity by modulating lipid metabolism and gut microbiota in mice fed a high-fat diet. *Food Funct.* (2021) 12:9719–38. doi: 10.1039/d1fo01495a
19. Haotian M, Chen SH, Xiong HY, Wang M, Hang W, Zhu X, et al. Astaxanthin from *Haematococcus pluvialis* ameliorates the chemotherapeutic drug (doxorubicin) induced liver injury through the Keap1/Nrf2/HO-1 pathway in mice. *Food Funct.* (2020) 11:4659–71. doi: 10.1039/c9fo02429h
20. Mashhadi NS, Zakerkish M, Mohammadiasl J, Zarei M, Mohammadshahi M, Haghighizadeh MH. Astaxanthin improves glucose metabolism and reduces blood pressure in patients with type 2 diabetes mellitus. *Asia Pac J Clin Nutr.* (2018) 27:341–6. doi: 10.6133/apjcn.052017.11
21. Boursier J, Mueller O, Barret M, Machado M, Fizanne L, Araujo-Perez F, et al. The severity of nonalcoholic fatty liver disease is associated with gut dysbiosis and shift in the metabolic function of the gut microbiota. *Hepatology.* (2016) 63:764–75. doi: 10.1002/hep.28356
22. Wang Z, Gerstein M, Snyder MRNA-. Seq: a revolutionary tool for transcriptomics. *Nat Rev Genet.* (2009) 10:57–63. doi: 10.1038/nrg2484
23. Conesa A, Madrigal P, Tarazona S, Gomez-Cabrero D, Cervera A, McPherson A, et al. A survey of best practices for RNA-seq data analysis. *Genome Biol.* (2016) 17:13. doi: 10.1186/s13059-016-0881-8
24. Ling Z, Liu X, Jia X, Cheng Y, Luo Y, Yuan L, et al. Impacts of infection with different toxigenic *Clostridium difficile* strains on faecal microbiota in children. *Sci Rep.* (2014) 4:7485. doi: 10.1038/srep07485
25. Jiang X, Hao J, Liu ZJ, Ma XT, Feng YX, Teng LR, et al. Anti-obesity effects of *Grifola frondosa* through the modulation of lipid metabolism via ceramide in mice fed a high-fat diet. *Food Funct.* (2021) 12:6725–39. doi: 10.1039/d1fo00666e
26. Kayser B, Verges S. Hypoxia, energy balance, and obesity: an update. *Obes Rev.* (2021) 2:e13192. doi: 10.1111/obr.13192
27. Rinella ME, Siddiqui MS, Gardikiotes K, Gottstein J, Elias M, Green RM. Dysregulation of the unfolded protein response in db/db mice with diet-induced steatohepatitis. *Hepatology.* (2011) 5:1600–9. doi: 10.1002/hep.24553
28. Bieghs V, van Gorp PJ, Walenbergh SM, Gijbels MJ, Verheyen F, Buurman WA, et al. Specific immunization strategies against oxidized low-density lipoprotein: a novel way to reduce nonalcoholic steatohepatitis in mice. *Hepatology.* (2012) 3:894–903. doi: 10.1002/hep.25660
29. Li JJ, Guo CY, Wu JY. Astaxanthin in liver health and disease: a potential therapeutic agent. *Drug Des Dev Ther.* (2020) 14:2275–85. doi: 10.2147/DDDT.S230749
30. Ni Y, Nagashimada M, Zhuge F, Zhan L, Nagata N, Tsutsui A, et al. Astaxanthin prevents and reverses diet-induced insulin resistance and steatohepatitis in mice: a comparison with vitamin E. *Sci Rep.* (2015) 5:17192. doi: 10.1038/srep17192
31. Mohammadi AA, Jazayeri S, Khosravi-Darani K, Solati Z, Mohammadpour N, Asemi Z, et al. Effects of probiotics on biomarkers of oxidative stress and inflammatory factors in petrochemical workers: a randomized, double-blind, placebo-controlled trial. *Int J Prev Med.* (2015) 6:82. doi: 10.4103/2008-7802.164146
32. Lasker S, Rahman MM, Parvez F, Zamila M, Miah P, Nahar K, et al. High-fat diet-induced metabolic syndrome and oxidative stress in obese rats are ameliorated by yogurt supplementation. *Sci Rep.* (2019) 9:20026. doi: 10.1038/s41598-019-56538-0
33. Zhang XQ, Xu CF, Yu CH, Chen WX, Li YM. Role of endoplasmic reticulum stress in the pathogenesis of nonalcoholic fatty liver disease. *World J Gastroenterol.* (2014) 7:1768–76. doi: 10.3748/wjg.v20.i7.1768
34. Cao SS, Kaufman RJ. Endoplasmic reticulum stress and oxidative stress in cell fate decision and human disease. *Antioxid Redox Signal.* (2014) 3:396–413. doi: 10.1089/ars.2014.5851
35. Ulla A, Alam MA, Sikder B, Sumi FA, Rahman MM, Habib ZF, et al. Supplementation of *Syzygium cumini* seed powder prevented obesity, glucose intolerance, hyperlipidemia and oxidative stress in high carbohydrate high fat diet induced obese rats. *BMC Complement Altern Med.* (2017) 17:289. doi: 10.1186/s12906-017-1799-8
36. Li KQ, Deng Y, Deng GM, Chen PY, Wang YT, Wu HT, et al. High cholesterol induces apoptosis and autophagy through the ROS-activated AKT/FOXO1 pathway in tendon-derived stem cells. *Stem Cell Res Ther.* (2020) 11:131. doi: 10.1186/s13287-020-01643-5
37. Liu J, Xian G, Li M, Zhang Y, Yang M, Yu Y, et al. Cholesterol oxidase from *Bordetella* species promotes irreversible cell apoptosis in lung adenocarcinoma by cholesterol oxidation. *Cell Death Dis.* (2014) 5:e1372. doi: 10.1038/cddis.2014.324
38. Feng KL, Zhu XA, Liu G, Kan QX, Chen T, Chen YJ, et al. Dietary citrus peel essential oil ameliorates hypercholesterolemia and hepatic steatosis by modulating lipid and cholesterol homeostasis. *Food Funct.* (2020) 11:7217–30. doi: 10.1039/d0fo00810a
39. Lin H, An Y, Tang H, Wang Y. Alterations of bile acids and gut microbiota in obesity induced by high fat diet in rat model. *J Agric Food Chem.* (2019) 67:3624–32. doi: 10.1021/acs.jafc.9b00249
40. Den Hartogh DJ, Vlavcheski F, Giacca A, Tsiani E. Attenuation of free fatty acid (FFA)-induced skeletal muscle cell insulin resistance by resveratrol is linked to activation of AMPK and inhibition of mTOR and p70 S6K. *Int J Mol Sci.* (2020) 21:4900. doi: 10.3390/ijms21144900
41. Zhu XP, Bian H, Wang L, Sun XY, Xu X, Yan HM, et al. Berberine attenuates nonalcoholic hepatic steatosis through the AMPK-SREBP-1c-SCD1 pathway. *Free Radical Bio Med.* (2019) 141:192–204. doi: 10.1016/j.freeradbiomed.2019.06.019
42. Carling D. AMPK signalling in health and disease. *Curr Opin Cell Biol.* (2017) 45:31–7. doi: 10.1016/j.ceb.2017.01.005
43. Mazzucotelli A, Viguerie N, Tiraby C, Annicotte JS, Mairal A, Klimcakova E, et al. The transcriptional coactivator peroxisome proliferator activated receptor (PPAR)gamma coactivator-1 alpha and the nuclear receptor PPAR alpha control the expression of glycerol kinase and metabolism genes independently of PPAR gamma activation in human white adipocytes. *Diabetes.* (2007) 56:2467–75. doi: 10.2337/db06-1465
44. Francque S, Verrijken A, Caron S, Prawitt J, Paumelle R, Derudas B, et al. PPARα gene expression correlates with severity and histological treatment response in patients with non-alcoholic steatohepatitis. *J Hepatol.* (2015) 1:164–73. doi: 10.1016/j.jhep.2015.02.019
45. Kobori M, Takahashi Y, Sakurai M, Ni Y, Chen G, Nagashimada M, et al. Hepatic transcriptome profiles of mice with diet-induced nonalcoholic steatohepatitis treated with astaxanthin and vitamin E. *Int J Mol Sci.* (2017) 3:593. doi: 10.3390/ijms18030593
46. Hatori M, Vollmers C, Zarrinpar A, DiTacchio L, Bushong EA, Gill S, et al. Time-restricted feeding without reducing caloric intake prevents metabolic

diseases in mice fed a high-fat diet. *Cell Metab.* (2012) 15:848–60. doi: 10.1016/j.cmet.2012.04.019
47. Chen M, Xu JG, Wang Y, Wang Z, Guo LP, Li XP, et al. *Arctium lappa* L. polysaccharide can regulate lipid metabolism in type 2 diabetic rats through the SREBP-1/SCD-1 axis. *Carbohyd Res.* (2020) 494:108055.
48. Qi Y, Jiang C, Cheng J, Krausz KW, Li T, Ferrell JM, et al. Bile acid signaling in lipid metabolism: metabolomic and lipidomic analysis of lipid and bile acid markers linked to anti-obesity and anti-diabetes in mice. *Biochim Biophys Acta.* (2015) 1851:19–29. doi: 10.1016/j.bbalip.2014.04.008
49. Chambers KF, Day PE, Aboufarrag HT, Kroon PA, et al. Polyphenol effects on cholesterol metabolism via bile acid biosynthesis, CYP7A1: a review. *Nutrients.* (2019) 11:2588. doi: 10.3390/nu11112588
50. Sayin SI, Wahlström A, Felin J, Jäntti S, Marschall HU, Bamberg K, et al. Gut microbiota regulates bile acid metabolism by reducing the levels of tauro-beta-muricholic acid, a naturally occurring FXR antagonist. *Cell Metab.* (2013) 17:225–35. doi: 10.1016/j.cmet.2013.01.003
51. Porras D, Nistal E, Martinez-Florez S, Pisonero-Vaquero S, Olcoz JL, Jover R, et al. Protective effect of quercetin on high-fat diet-induced non-alcoholic fatty liver disease in mice is mediated by modulating intestinal microbiota imbalance and related gut-liver axis activation. *Free Radical Bio Med.* (2017) 102:188–202. doi: 10.1016/j.freeradbiomed.2016.11.037
52. Tripathi A, Debelius J, Brenner DA, Karin M, Loomba R, Schnabl B, et al. The gut-liver axis and the intersection with the microbiome. *Nat Rev Gastroenterol Hepatol.* (2018) 15:397–411. doi: 10.1038/s41575-018-0011-z
53. Park YH, Lee JJ, Son HK, Kim BH, Byun J, Ha JH. Antiobesity effects of extract from *Spergularia marina* Griseb in adipocytes and high-fat diet-induced obese rats. *Nutrients.* (2020) 12:336. doi: 10.3390/nu12020336
54. Collins B, Hoffman J, Martinez K, Grace M, Lila MA, Cockrell C, et al. A polyphenol-rich fraction obtained from table grapes decreases adiposity, insulin resistance and markers of inflammation and impacts gut microbiota in high-fat-fed mice. *J Nutr Biochem.* (2016) 31:150–65. doi: 10.1016/j.jnutbio.2015.12.021
55. Zhang M, Zhu JY, Zhang X, Zhao DG, Ma YY, Li DL, et al. Aged citrus peel (chenpi) extract causes dynamic alteration of colonic microbiota in high-fat diet induced obese mice. *Food Funct.* (2020) 11:2667–78. doi: 10.1039/c9fo02907a
56. Barcena C, Valdes-Mas R, Mayoral P, Garabaya C, Durand S, Rodriguez F, et al. Healthspan and lifespan extension by fecal microbiota transplantation into progeroid mice. *Nature Medicine.* (2019) 25:1234–42. doi: 10.1038/s41591-019-0504-5
57. Xie G, Wang X, Liu P, Wei R, Chen W, Rajani C, et al. Distinctly altered gut microbiota in the progression of liver disease. *Oncotarget.* (2016) 7:19355–66. doi: 10.18632/oncotarget.8466
58. Ivey KL, Hodgson JM, Kerr DA, Thompson PL, Stojceski B, Prince RL. The effect of yoghurt and its probiotics on blood pressure and serum lipid profile; a randomised controlled trial. *Nutr Metab Cardiovasc Dis.* (2015) 25:46–51. doi: 10.1016/j.numecd.2014.07.012
59. Liang YJ, Lin CL, Zhang YP, Deng YJ, Liu C, Yang QH. Probiotic mixture of *Lactobacillus* and *Bifidobacterium alleviates* systemic adiposity and inflammation in non-alcoholic fatty liver disease rats through Gpr109a and the commensal metabolite butyrate. *Inflammopharmacology.* (2018) 26:1051–5. doi: 10.1007/s10787-018-0479-8

Conflict of Interest: The authors declare that the research was conducted in the absence of any commercial or financial relationships that could be construed as a potential conflict of interest.

Publisher's Note: All claims expressed in this article are solely those of the authors and do not necessarily represent those of their affiliated organizations, or those of the publisher, the editors and the reviewers. Any product that may be evaluated in this article, or claim that may be made by its manufacturer, is not guaranteed or endorsed by the publisher.

frontiers | Frontiers in Nutrition

ORIGINAL RESEARCH
published: 12 April 2022
doi: 10.3389/fnut.2022.849767

Amino Acid and Fatty Acid Metabolism Disorders Trigger Oxidative Stress and Inflammatory Response in Excessive Dietary Valine-Induced NAFLD of Laying Hens

Huafeng Jian[1,2,3,4,5], *Qianqian Xu*[1,2,3,4,5], *Xiaoming Wang*[1,2,3,4,5], *Yating Liu*[1,2,3,4,5], *Sasa Miao*[1,2,3,4,5], *Yan Li*[1,2,3,4,5], *Tianming Mou*[1,2,3,4,5], *Xinyang Dong*[1,2,3,4,5] *and Xiaoting Zou*[1,2,3,4,5]*

[1] *Institute of Feed Science, College of Animal Sciences, Zhejiang University, Hangzhou, China,* [2] *The National Engineering Laboratory for Feed Safety and Pollution Prevention and Controlling, National Development and Reform Commission, Zhejiang University, Hangzhou, China,* [3] *Key Laboratory of Molecular Animal Nutrition, Ministry of Education, Zhejiang University, Hangzhou, China,* [4] *Key Laboratory of Animal Nutrition and Feed Science, Ministry of Agriculture and Rural Affairs, Zhejiang University, Hangzhou, China,* [5] *Key Laboratory of Animal Feed and Nutrition of Zhejiang Province, Zhejiang University, Hangzhou, China*

OPEN ACCESS

Edited by:
Gratiela Gradisteanu Pircalabioru, University of Bucharest, Romania

Reviewed by:
Martina Wallace, University College Dublin, Ireland
Yuying Li, Institute of Subtropical Agriculture (CAS), China

***Correspondence:**
Xiaoting Zou
xtzou@zju.edu.cn

Specialty section:
This article was submitted to Nutrition and Metabolism, a section of the journal Frontiers in Nutrition

Received: *06 January 2022*
Accepted: *24 February 2022*
Published: *12 April 2022*

Citation:
Jian H, Xu Q, Wang X, Liu Y, Miao S, Li Y, Mou T, Dong X and Zou X (2022) Amino Acid and Fatty Acid Metabolism Disorders Trigger Oxidative Stress and Inflammatory Response in Excessive Dietary Valine-Induced NAFLD of Laying Hens. Front. Nutr. 9:849767. doi: 10.3389/fnut.2022.849767

Non-alcoholic fatty liver disease (NAFLD) is a chronic and metabolic liver disease and commonly occurs in humans with obesity and type 2 diabetes mellitus (T2DM); such a condition also exists in animals such as rodents and laying hens. Since the pathogenesis of fatty liver hemorrhagic syndrome (FLHS) of laying hens is similar to human NAFLD, hen's FLHS is commonly selected as a study model of NAFLD. Altered circulating amino acids, particularly elevated branched-chain amino acids (BCAAs) and aromatic amino acids (AAAs), are consistently reported in patients with NAFLD and T2DM. How long-term dietary individual BCAA, such as valine, impacts amino acid and fatty acid metabolism remains unknown. In this study, we demonstrated that when laying hens are fed with dietary valine at different levels (59, 0.64, 0.69, 0.74, and 0.79%) in a feeding trial that lasted for 8 weeks, long-term exposure to excessive valine diets at 0.74 and 0.79% levels could induce amino acid imbalance, impair amino acid metabolism, increase fatty acid synthesis, and inhibit fatty acid utilization. Long-term intake of excessive dietary valine could result in impaired amino acid metabolism *via* inhibiting C/EBP-β/asparagine synthetase (Asns). This process is mediated by downregulating the general control nonderepressible-eukaryotic initiation factor 2α- activating transcription factor (GCN2-eIF2α-ATF4) pathway and elevating corresponding circulating BCAAs and AAAs levels, which could ultimately result in amino acid imbalance. High levels of dietary valine stimulated lipid deposition by suppressing the GCN2-eIF2α-ATF4-fibroblast growth factor-19 (FGF19)-target of rapamycin complex 1 (TORC1) signaling pathway to promote fatty acid synthesis, repress fatty acid utilization, and eventually accelerate the development of NAFLD. The Spearman correlation analysis revealed that circulating amino acid imbalance is significantly associated with fatty acid metabolism disorder

and enhanced oxidative stress. The inhibition of the GCN2-TORC1 pathway induced autophagy suppression to trigger liver oxidative stress and inflammatory response. In conclusion, our results revealed the adverse metabolic response to excessive dietary valine mediated by amino acid and fatty acid metabolism disorders. This study also suggested reducing dietary valine as a novel approach to preventing and treating NAFLD in humans and FLHS in laying hens.

Keywords: amino acid imbalance, fatty acid metabolism, TORC1, autophagy, NAFLD, laying hens

INTRODUCTION

Non-alcoholic fatty liver disease (NAFLD) is one of the most common metabolic and chronic liver. Its prevalence and incidence are increasing and affect one-fourth of the population worldwide (1). The characteristics of NAFLD include a series of liver pathologies ranging from simple hepatic steatosis, non-alcoholic steatohepatitis (NASH), fibrosis, and cirrhosis (2). Hepatic lipid deposition [including elevated free fatty acids (FFAs) and triglycerides (TGs)], steatosis, insulin resistance, oxidative stress, inflammatory response, endoplasmic reticulum (ER) stress, and autophagy inhibition are the main characters of NAFLD. The mechanisms of NAFLD which favor the development of hepatic steatosis and transition to NASH, cirrhosis, and hepatocellular carcinoma (HCC) are still not fully understood (2–4). The original model of NASH pathogenesis was the "two-hit" hypothesis which dictated that hepatic lipid accumulation provides a "first hit" that sensitized the liver to a "second hit" of oxidative stress due to increased lipotoxicity and subsequent necro-inflammation that precipitated NASH (5, 6). The chronic metabolic challenge of hepatocytes with oxidative and ER stress caused by lipotoxicity and necro-inflammation leads to cellular damage or cell death and disease progression resulting in immune cell infiltration, fibrogenesis, and activation of hepatic progenitor cells (7–9). Lipotoxicity induced by excessive lipids such as FFAs and TGs involves ER stress, oxidative stress, mitochondrial dysfunction, impaired autophagy, and inflammation (10). Lipid-induced autophagy, for instance, lipid overload facilitates autophagy of lipid droplets (LDs, lipophagy) (11). To date, there is an increasing burden of NAFLD due to the pathogenesis complexity of NAFLD and the lack of available therapies.

In addition to altered lipid metabolism in the progression of NAFLD, several reports have indicated that amino acid metabolism imbalance has been associated with an increased risk and disease severity of NAFLD (12–15). For instance, elevated serum or plasma concentrations of BCAAs, such as leucine, isoleucine, valine, and aromatic amino acids (AAAs, e.g., tyrosine, phenylalanine, and tryptophan), are found in the T2DM and NAFLD in humans and are associated with increased severity of liver diseases (16–19). Apart from increased BCAAs and AAAs, glutamine, glutamate, alanine, and aspartate are positively associated with increased hepatic insulin resistance, whereas decreased glycine and serine are found in humans with NAFLD (20–23). The BCAAs leucine, isoleucine, and valine have assumed particular prominence, both because of their role in affecting mammalian target of rapamycin (mTOR)-key pathways linking nutrition with health and aging (24) and also because their circulating levels are positively associated with obesity, insulin resistance, and metabolic dysfunction in rodents and humans (16, 25, 26). As an important nutrition sensor, mTOR consists of mTORC1 and mTORC2, and the mTORC1 can be activated by branched-chain amino acids (BCAAs) which subsequently inhibit autophagy (27). During amino acid sufficiency, mTORC1 is activated and resulting in dissociation of the UNC-like autophagy-activating kinase 1 (ULK1) active complex and inhibition of autophagy (11, 27). In addition to mTOR, eukaryotic initiation factor 2α (eIF2α) kinase general control nonderepressible (GCN2) can also function as an amino acid sensor to promote transcription of autophagy genes (11). During amino acid starvation, GCN2 suppressed intestinal inflammation by inhibiting inflammasome activation and triggering autophagy in mice, and eventually decreased the production of pro-inflammatory cytokines interleukin (IL)-1β and IL-17 (28). GCN2 might detect a paucity of one or more essential amino acids to inhibit mTORC1, resulting in autophagy induction (29).

In poultry, specifically the laying hens, fatty liver hemorrhagic syndrome (FLHS) resulting from NAFLD has been a significant cause of death in commercial layers (30). The pathogenesis of FLHS is similar to NAFLD in humans, which is characterized by increased hepatic TG content accompanied by liver hemorrhage and large amounts of lipid accumulation in the abdominal cavity, which usually causes considerable mortality of laying hens during the peak laying period owing to liver rupture resulting in internal bleeding (31). Our recent reports demonstrated that diet-supplemented valine has significantly altered the serum-free amino acid profile of laying hens. Additionally, long-term exposure to high levels of dietary valine at 0.74 and 0.79% has accelerated the development of NAFLD of laying hens by promoting lipogenesis and inhibiting fatty acid oxidation mediated by GCN2-eIF2α-activating transcription factor 4 (ATF4) (32, 33). NAFLD induced by excessive dietary valine resulted in strengthening oxidative stress, ER stress, and inflammatory response (32, 33). Nevertheless, a comprehensive investigation of the roles of dietary valine in the change of amino acid profile and fatty acid metabolism in NAFLD has not been fully pursued.

In the current study, we sought to determine whether and how dietary valine manipulation impacts serum amino

TABLE 1 | Composition and nutrient levels of the basal diet (air-dry basis).

Ingredients	Dietary valine levels (%)[a]				
	0.59	0.64	0.69	0.74	0.79
Corn	66.6	66.6	66.6	66.6	66.6
Soybean meal	10.5	10.65	11.2	11.55	11.8
Wheat bran	2.9	2.9	2.91	2.92	2.92
Peanut meal	8.7	8.5	7.9	7.5	7.2
Limestone	9.3	9.3	9.3	9.3	9.3
Soybean oil	0.3	0.3	0.3	0.3	0.3
DL-Methionine (98%)	0.16	0.16	0.15	0.15	0.15
Lysine (78%)	0.11	0.11	0.11	0.1	0.1
Valine (98%)	0	0.0508	0.1016	0.1523	0.2031
CaHPO4	0.6	0.6	0.6	0.6	0.6
Salt	0.36	0.36	0.36	0.36	0.36
Choline chloride, 60%	0.2	0.2	0.2	0.2	0.2
Mineral and vitamin premix[b]	0.27	0.27	0.27	0.27	0.27
Calculated nutritional level, %					
Crude protein (CP) (kcal/g)	14.7 (58.8)	14.7 (58.8)	14.7 (58.8)	14.7 (58.8)	14.7 (58.8)
ME, MJ/Kg (kcal/g)	2.68 (2.70)	2.68 (2.70)	2.68 (2.70)	2.68 (2.70)	2.68 (2.70)
Weight Fat/Carbohydrate	37.04	37.04	37.04	37.04	37.04
Fat, kcal/g	9	9	9	9	9
Carbohydrate, kcal/g	10.8	10.8	10.8	10.8	10.8
Analyzed nutritional level, %					
Crude protein (CP)	14.65	14.72	14.75	14.74	14.78
Calcium (calculated)	3.58	3.58	3.59	3.59	3.59
Total phosphorus	0.46	0.46	0.46	0.46	0.46
Methionine	0.36	0.36	0.36	0.37	0.37
Lysine	0.66	0.66	0.66	0.67	0.67
Threonine	0.48	0.48	0.48	0.49	0.49
Tryptophan	0.14	0.14	0.14	0.14	0.14
Arginine	1.05	1.04	1.03	1.03	1.02
Leucine	0.82	0.82	0.82	0.82	0.82
Isoleucine	0.65	0.65	0.65	0.65	0.65
Valine	0.59	0.64	0.69	0.74	0.79

[a] *Analyzed value of pooled experimental diets 0.59, 0.64, 0.69, 0.74, and 0.79% valine.*

[b] *The premix provided following per kilogram of diet: vitamin A, 7,500 IU; vitamin D3, 2500 IU; vitamin E, 49.5 mg; vitamin K3, 2.5 mg; vitamin B1, 1.5 mg; vitamin B2, 4 mg; vitamin B6, 2 mg; vitamin B12, 0.02 mg; niacin, 30 mg; folic acid, 1.1 mg; pantothenic acid, 10 mg; biotin,0.16 mg; chloride choline, 400 mg; Sodium chloride, 2,500 mg; Fe, 80 mg; Cu, 20 mg; Mn, 60 mg; Zn, 80 mg; I, 0.8 mg.*

acid balance, amino acid metabolism, fatty acid metabolism, and the relationship between dietary valine and amino acid and fatty acid metabolism. We further analyzed whether strengthening oxidative stress and inflammatory response was mediated by the mTORC1-autophagy pathway. To test this hypothesis, we used adult laying hens as a model fed with different levels of dietary valine for 8 weeks and examined the impacts of dietary valine supplementation on serum-free amino acid profile and fatty acid metabolism. We also examined whether enhanced oxidative stress and inflammatory response are mediated by a mTORC1-autophagy pathway, which is a downstream signaling pathway of GCN2-eIF2α-ATF4.

MATERIALS AND METHODS

Diets, Birds, and Management

Corn and soybean meals were selected as major ingredients to make up a corn-soybean-type basal diet and prepared according to NRC (1994) and China's "Chicken Feeding Standard (NY/T33-2004)" (34, 35). Synthetic L-Val (98% purity, Specom Biochemical Co. Ltd, Zhangjiagang, China) was supplemented to the basal diet in 0, 0.0508, 0.1016, 0.1523, and 0.2031% increments, resulting in experimental diets containing 0.59, 0.64, 0.69, 0.74, and 0.79% valine, respectively (**Table 1**). In addition, the ratio of other amino acids of the diet was corrected to be consistent with each group by dietary protein.

A total of 960 healthy 33-weeks-old Fengda No. 1 laying hens with similar body weight and laying rate were randomly allocated into 5 experimental groups, and each group included 6 replicates of 32 laying hens (8 birds/cage). This study lasted 9 weeks, including a 1-week acclimation period and an 8-week experimental period. All hens were housed in an environmentally controlled room where the temperature was maintained at approximately 23°C. The hens were exposed to a 16 h photoperiod throughout the experiment by the use of artificial lighting. Hens were supplied with water and fed a complete feeding mixture twice daily. All animal works in this experiment were conducted by following the Chinese Guidelines for Animal Welfare and approved by the Zhejiang University Institutional Animal Care and Use Committee (No. ZJU2013105002) (Hangzhou, China).

Sample Collection and Processing

At the end of the 8-week experiment, 2 hens were randomly selected from each replication (12 hens in each group; a total of 60 hens) and fasted for 12 h. A blood sample (5 ml; bird-1) was collected from the vein under the wing. After centrifugation at 3,000 × *g* for 10 min, serum was separated. After blood sampling, hens were euthanized with pentobarbital sodium and sacrificed. The liver was collected for the determination of liver lipid metabolism parameters and mRNA expression.

Liver Parameter Measurements

One gram liver was homogenized in 9 ml of 0.9% (w/v) sterile normal saline on ice and centrifuged at 3,500 × *g* at 4°C for 15 min. Total protein in the tissue supernatant was measured with a BCA protein assay kit (Nanjing Jiancheng Bioengineering Institute, Nanjing, China) according to the manufacturer's protocol and stored at −80°C storage. The concentrations of non-esterified fatty acid (NEFA), high-density lipoprotein cholesterol (HDL), and low-density lipoprotein cholesterol (LDL) were determined using commercial kits (Nanjing Jiancheng Bioengineering Institute, Nanjing, China). All assays were performed according to the manufacturer's instructions.

ELISA Determination

The concentrations of fatty acid synthase (FASN), acetyl-CoA carboxylase (ACC), ATP citrate lyase (ACLY), and very-low-density lipoprotein cholesterol (VLDL) in the liver were determined using chicken-specific ELISA quantitation kits (Nanjing Jiancheng Bioengineering Institute, Nanjing, China). All assays were performed according to the manufacturer's instructions.

Total RNA Isolation and Relative Quantitative RT-PCR

The liver mRNA expression level was determined using real time-PCR. Total RNA was extracted using TRIzol reagent (Takara code: 9109, Shiga, Japan). RNA quality and quantity were determined using a NanoDrop 2000 spectrophotometer (Thermo Fisher Scientific, Massachusetts, USA). cDNA was synthesized with a HiScriptIIqRT SuperMix Reverse Transcriptase (Vazyme Biotechnology, Nanjing, Jiangsu, China). Real-time PCR was conducted with a SYBR Premix PCR kit (Vazyme Biotechnology, Nanjing, Jiangsu, China) *via* the CFX96TM Real-Time System (Bio-Rad, Hercules, CA, USA). **Table 2** shows gene-specific primers for RT-PCR. The reference gene β-actin was used as an internal control. Each sample was run in triplicate, and the $2^{-\Delta\Delta Ct}$ method was employed for evaluating the relative mRNA expression level of the target gene.

Spearman Correlation Analysis

The Spearman correlation analysis was analyzed on the free online platform of LC-Bio Cloud Platform (https://www.omicstudio.cn/). In brief, Spearman correlation analysis was conducted to examine the association between dietary valine levels and serum-free amino acids, serum-free amino acids and lipid metabolism parameters, serum-free amino acids, and anti-oxidase parameters using LC-Bio Cloud Platform (https://www.omicstudio.cn/). The sample size and sample individual of the Spearman correlation analysis in the current research was a one-to-one correspondence between serum free amino acids and lipid metabolism parameters and anti-oxidase parameters ($n = 4$). The results of the Spearman correlation analysis were shown in a heatmap and * represents $P < 0.05$ and ** represents $P < 0.01$.

Statistical Analysis

The Gaussian distribution of data was analyzed by the Kolmogorov–Smirnov test using SPSS 20 (Chicago, IL, USA). The variance of the data was analyzed by the homogeneity of variance test (SPSS 20). Statistical analysis was performed with one-way ANOVA followed by LSD's multiple comparison tests with SPSS 20. The linear or quadratic verification was performed by SPSS 20. Data presented in the article are shown as means ± SEM and are considered significant at $P < 0.05$.

RESULTS

NAFLD Driven by Excessive Dietary Valine-Altered Serum Free Amino Acid Profile and Liver Amino Acid Metabolism Mediated by GCN2-EIF2α-ATF4

Our previous results demonstrated that dietary valine treatment significantly elevated serum-free Isoleucine (Ile), Lysine (Lys), Phenylalanine (Phe), Valine (Val), and Tyrosine (Tyr) with increasing of dietary valine levels, whereas decreased serum free Arginine (Arg), Histidine (His), Methionine (Met), Threonine (Thr), Alanine (Ala), Aspartic acid (Asp), Glutamic acid (Glu), Glycine (Gly), Leucine (Leu), and Serine (Ser) (32). In addition, there is no difference was observed in serum-free Proline (Pro) and Cystine (Cys) among all treatments (32). Elevated circulating levels of BCAAs and AAAs have been reported in patients with NAFLD (16–19). Based on significantly changed serum free amino acid profile, we further sought to determine the relationship of dietary valine levels and altered serum free amino acids by Spearman correlation analysis. The Spearman correlation analysis heatmap revealed that serum free His was

TABLE 2 | Primers used for quantitative real-time PCR.

Gene	Primer	Primer sequence (5'-3')	GenBank number
β-Actin	Forward	TCCCTGGAGAAGAGCTATGAA	NM_205518.1
	Reverse	CAGGACTCCATACCCAAGAAAG	
FABP1	Forward	GCAGAATGGGAATAAGTT	NM_204192.4
	Reverse	TTGTATGGGTGATGGTGT	
FATP1	Forward	TACAATGTGCTCCAGAAGGG	NM_001039602.2
	Reverse	GTCTGGTTGAGGATGTGACTC	
CD36	Forward	ACTGCGCTTCTTCTCCTCTGA	NM_001030731.1
	Reverse	TCACGGTCTTACTGGTCTGGTAAA	
apoA1	Forward	GTGACCCTCGCTGTGCTCTT	NM_205525.5
	Reverse	CACTCAGCGTGTCCAGGTTGT	
apoB	Forward	ATGTTCAAAAGATGCGGCCC	NM_001044633.2
	Reverse	GCATGGCTCTTCTCTCACTG	
C/EBP-β	Forward	ACGAGGCGGACTGTTTGG	NM_205253.3
	Reverse	GCTGCTGGGATGCTGCTAA	
Asns	Forward	ACCACTCCATGCTGCTTGTG	NM_001030977.2
	Reverse	ATCCAAGCCCCCTGACAAAA	
LC3I	Forward	ATGGCAGAGGTGTACAGGGACTAC	XM_419549.6
	Reverse	GGGTGAGTGAGCAGCATCCAAAC	
LC3II	Forward	AGTGAAGTGTAGCAGGATGA	NM_001031461.1
	Reverse	AAGCCTTGTGAACGAGAT	
ULK1	Forward	GAGCAAGAGCACACCGACATCC	XM_015275648.2
	Reverse	TTTCAGGGCAGCAATCTCCATCAC	
Atg5	Forward	GCCTTCAGTGGGGTTTCAGTTCC	XM_015284517.2
	Reverse	TATGCGTCCAAACCACACATCTCG	
Atg7	Forward	TCAGATTCAAGCACTTCAGA	NM_001030592.1
	Reverse	GAGGAGATACAACCACAGAG	
FGF19	Forward	CCCGCTGTCTCACTTCTTACCCA	NM_204674.3
	Reverse	GGATCCATGCTGTCCGTTTCG	
UCP3	Forward	ACTCTGTGAAGCAGCTCTACACC	NM_204107.1
	Reverse	ATGTACCGCGTCTTCACCACATC	
TORC1	Forward	GGACTCTTCCCTGCTGGCTAA	XM_417614.5
	Reverse	TACGGGTGCCCTGGTTCTG	

positively associated with Ala, Ser, and Met, while was negatively associated with Val, Ile, and Lys ($P < 0.01$); Met was positively associated with Gly, Ala, Leu, Ser, and His, but was negatively associated with Phe, Val, Ile, and Lys ($P < 0.05$); Ser was positively associated with Gly, Ala, Leu, Met, and His, whereas was negatively associated with Val, Ile, and Lys ($P < 0.05$); Cys was positively associated with Phe, Thr, Gly, and Leu ($P < 0.01$); Leu was positively associated with Thr, Gly, Cys, Ser, and Met, yet was negatively associated with Val, Ile, and Lys ($P < 0.05$); Ala was positively associated with Thr, Gly, Ser, Met, and His, whereas was negatively associated with Val, Ile, Lys, and Arg ($P < 0.05$); Gly was positively associated with Thr, Ala, Leu, Cys, Ser, and Met, whereas was negatively associated with Val, Ile, and Lys ($P < 0.05$); Thr was positively associated with Asp, Gly, Ala, Leu, and Cys ($P < 0.01$); Glu was negatively associated with Tyr, Asp, and Lys ($P < 0.05$); Arg was negatively associated with Ala ($P < 0.05$); Lys was positively associated with Val and Ile, but was negatively associated with Glu, Gly, Ala, Leu, Ser, Met, and His ($P < 0.05$); Ile was positively associated with Phe, Val, and Lys, yet was negatively associated with Gly, Ala, Leu, Ser, Met, and His ($P < 0.05$); Val was positively associated with Phe, Ile, and Lys, whereas was negatively associated with Gly, Ala, Leu, Ser, Met, and His ($P < 0.05$); Phe was positively associated with Val, Ile, and Cys, but was negatively associated with Met ($P < 0.05$); Asp was positively associated with Tyr and Thr, yet was negatively associated with Glu ($P < 0.01$); Tyr was positively associated with Asp, whereas was negatively associated with Glu ($P < 0.01$) (**Figure 1A**). The correlation network further revealed dietary valine treatment dramatically influencing the components of serum-free Gly, Met, Ile, Ala, Ser, Val, His, Lys, and Thr (**Figure 1B**). Taken together, the above results may indicate that NAFLD induced by excessive dietary valine changed amino acid profile by elevating BCAAs and AAAs, in particular, Ile, Val, Phe, and Tyr, and reducing

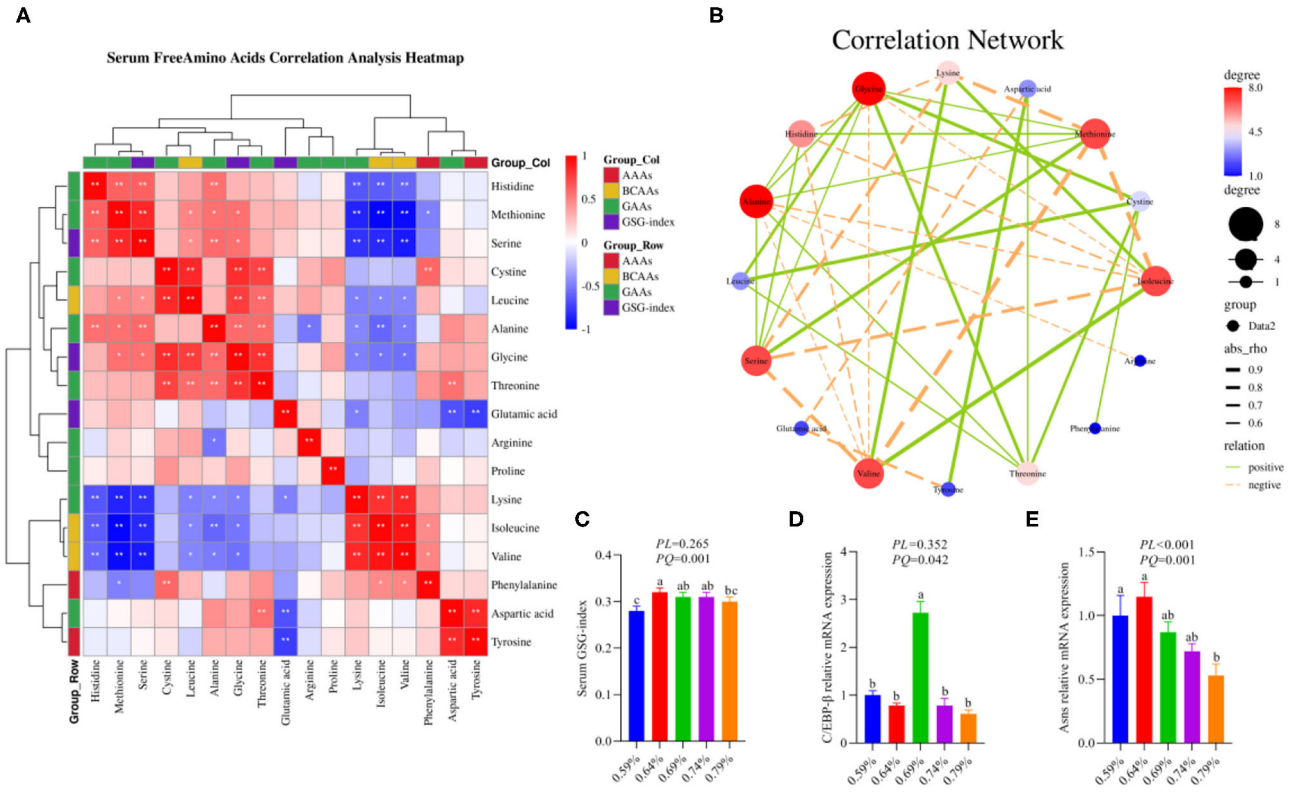

FIGURE 1 | Dietary valine changed serum free amino acid profile and liver amino acid metabolism ($n = 6$–8). **(A)** Serum-free amino acids correlation analysis heatmap. **(B)** Correlation network. **(C)** Serum GSG-index. **(D)** C/EBP-β relative mRNA expression level. **(E)** Asns relative mRNA expression level. $^{*}P < 0.05$ and $^{**}P < 0.01$. $^{a-c}$Means with different superscripts within a column differ significantly ($P < 0.05$). GSG index, Glutamate–serine–glycine (GSG) index [glutamate/(serine1glycine)]; AAAs, aromatic amino acids; BCAAs, branched-chain amino acids; GAAs, glycogenous amino acids.

Gly, Met, Ala, Ser, His, and Thr, and eventually lead to amino acid imbalance.

As shown in the correlation analysis heatmap and network, dietary valine supplementation significantly correlated with elevated concentrations of BCAAs (e.g., Ile and Val) and AAAs such as Phe and Tyr (**Figure 1B**), which has been confirmed that was associated with the development and progression of NAFLD (16–19). The glutamate–serine–glycine (GSG) index [glutamate/(serine1glycine)], a new marker of severity of liver disease independent of body mass index (12), showed a quadratic decrease with increasing dietary valine concentrations ($P < 0.01$) (**Figure 1C**). Compared with 0.59% dietary treatment (not supplement L-Val), the GSG-index of other four treatments were higher ($P < 0.05$) (**Figure 1C**). The changed serum-free amino acid profile may reflect altered amino acid metabolism in the NAFLD of laying hens. The mRNA expression levels of C/EBP-β and asparagine synthetase (Asns) revealed that dietary treatment significantly downregulated the mRNA expression levels of C/EBP-β and Asns, which is consistent with decreased serum free Arg, His, Met, Thr, Ala, Asp, Glu, Gly, Leu, and Ser, indicating NAFLD induced by excessive dietary valine dramatically impaired liver amino acid metabolism of laying hens (**Figures 1D,E**). In combination with the above results, these results clearly demonstrated that NAFLD induced by excessive dietary valine are both sufficient to alter serum free amino acid profile and damage liver amino acid metabolism, and eventually lead to amino acid imbalance.

Excessive Dietary Valine Treatment Trigger NAFLD by Stimulating Liver Fatty Acid Synthesis

As a substrate for the synthesis of TG, fatty acids can be esterified with glycerol sterol backbones, generating TGs or sterol esters (SEs), respectively, and then stored in LDs (36). Our recent report indicated dietary valine treatment dramatically increased the concentration of TG in the serum and liver with increasing dietary levels (33). We first investigated the effects of dietary valine on liver fatty acid synthesis, and we found that dietary valine supplementation dramatically improved the contents of liver ACLY, NEFA, HDL, and VLDL ($P < 0.05$) (**Figures 2C,D,E,G**), whereas the content of liver FASN showed an increase first and then decreased with the increase of dietary valine levels ($P < 0.05$) (**Figure 2A**). Dietary valine treatment did not affect the contents of liver ACC and LDL among all groups ($P > 0.05$) (**Figures 2B,F**). Consistent with our previous

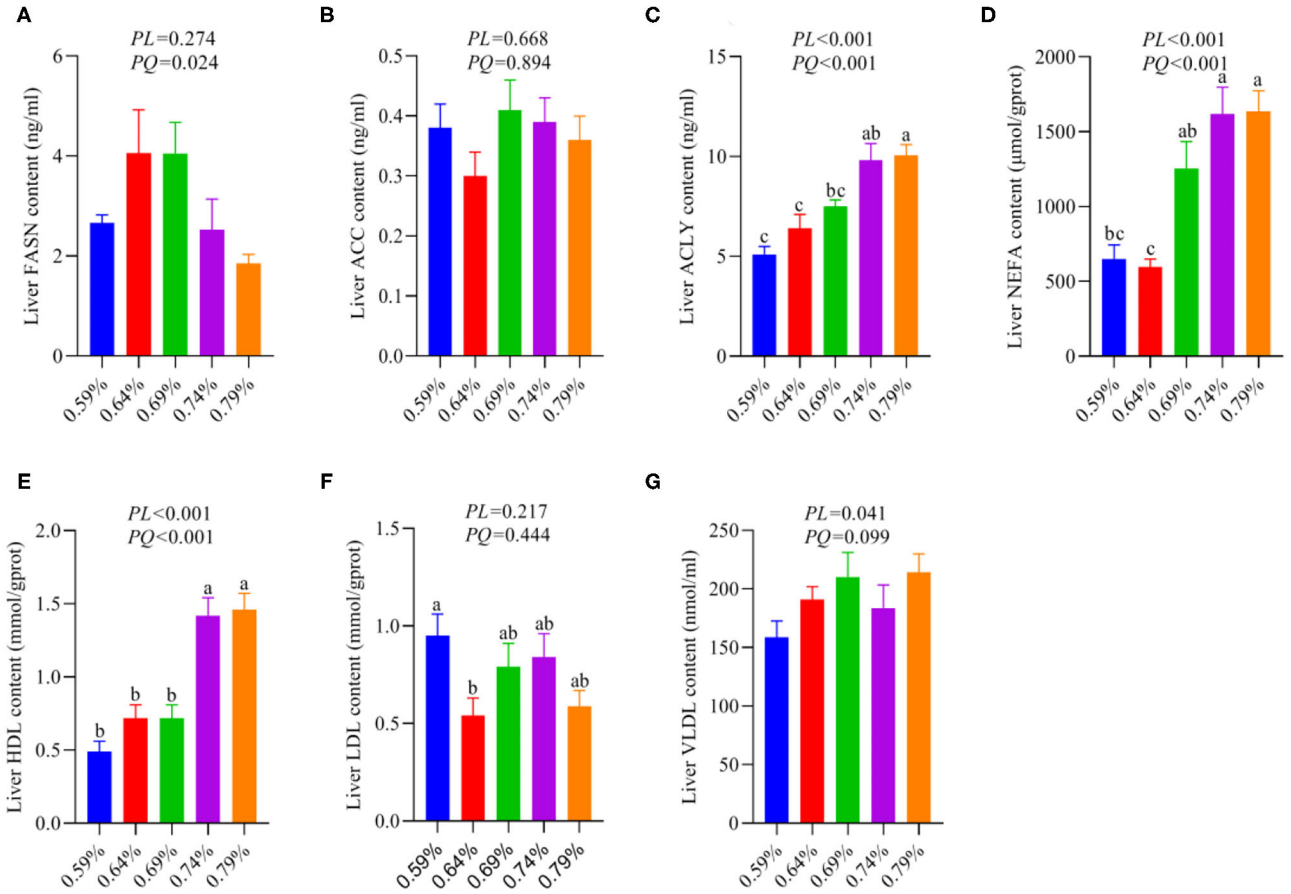

FIGURE 2 | Effects of dietary valine levels on liver lipid parameters (n = 6–8). **(A)** FASN. **(B)** ACC. **(C)** ACLY. **(D)** NEFA. **(E)** HDL. **(F)** LDL. **(G)** VLDL. $^{a-c}$Means with different superscripts within a column differ significantly ($P < 0.05$).

results that dietary valine significantly upregulated the mRNA expression levels of FASN and ACLY yet did not affect the mRNA expression level of ACC (33). Taken together with our previous results, we can conclude that excessive dietary valine treatment drives NAFLD by promoting fatty acid synthesis.

Dietary Valine Treatment Promoted Lipid Deposition Drive NAFLD by Suppressing Liver Fatty Acid Utilization

The metabolism and utilization of hepatocyte fatty acid involving fatty acid synthesis, fatty acid uptake, fatty acid transportation, including import and export, and fatty acid oxidation. Our previous results suggested dietary valine supplementation significantly inhibited fatty acid β-oxidation *via* downregulating the mRNA expression levels of CPT1, ACOX1, and PPARα (33). Thus, we further investigated whether dietary valine treatment impact hepatocyte fatty acid metabolisms such as fatty acid uptake, fatty acid transportation, including import and export. As shown in **Figure 3**, dietary valine supplementation dramatically downregulated the mRNA expression levels of fatty acid export associated genes including apolipoproteinA1 (apoA1) and apoB (**Figures 3D,E**), whereas the mRNA expression level of fatty acid-binding protein (FABP1) showed first decreased and then increased in a quadratic manner ($P < 0.05$) (**Figure 3C**). However, dietary valine treatment did not affect the mRNA expression levels of fatty acid uptake and fatty acid transportation associated genes such as fatty acid translocase (CD36) and fatty acid transport protein 1 (FATP1) ($P > 0.05$) (**Figures 3A,B**). In combination with previous results, we can conclude that dietary valine treatment promoted lipid deposition trigger NAFLD *via* suppressing fatty acid export and β-oxidation associated genes mRNA expression levels.

Elevated Serum Free Amino Acid Val, Ile, and Lys Are Correlated With Serum TG, Liver NEFA, TG, HDL, and ACLY

Amino acids as substrate or precursor generate acetyl-coenzyme A (CoA) *via* tricarboxylic acid (TCA) cycle participate in fatty acid metabolism, thus we sought to elaborate the relationship between serum free amino acids and fatty acid metabolism by the Spearman correlation analysis. The Spearman correlation analysis heatmap demonstrated serum free amino acids were significantly associated with serum and liver lipid metabolism parameters. As shown in **Figure 4A**, serum free Met was

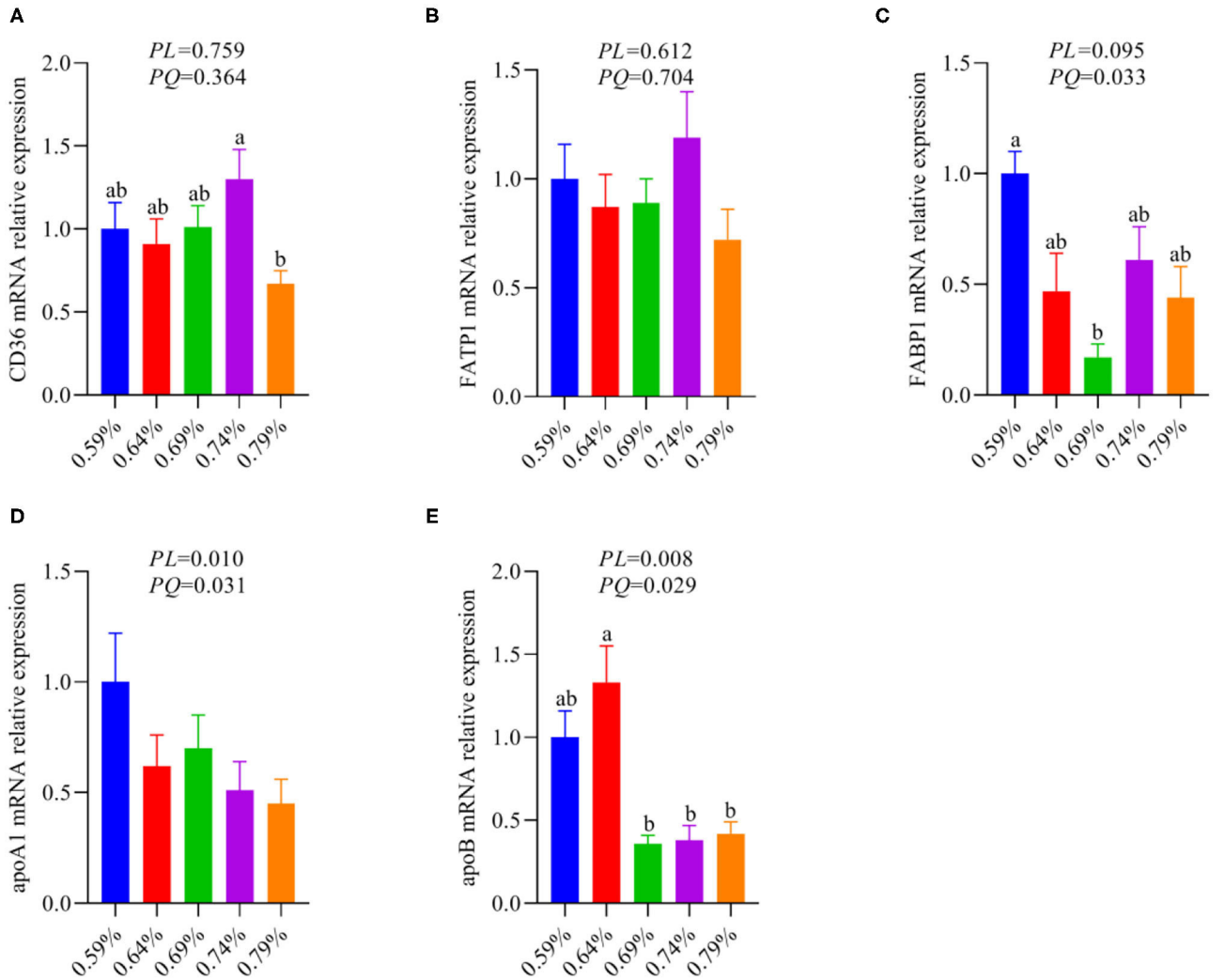

FIGURE 3 | The relative mRNA expression levels of fatty acid metabolism associated genes in the liver of laying hens (n = 6–8). **(A)** CD36. **(B)** FATP1. **(C)** FABP1. **(D)** apoA1. **(E)** apoB. [a,b]Means with different superscripts within a column differ significantly ($P < 0.05$).

negatively associated with serum TG, liver NEFA, ACLY, and HDL ($P < 0.01$); Ser was negatively associated with liver NEFA, ACLY, HDL, ALT, and AST ($P < 0.05$); Ala was negatively associated with liver ACLY, TG, and HDL ($P < 0.05$); His was negatively associated with liver NEFA, ACLY, TG, and HDL ($P < 0.05$); Arg was negatively associated with serum TG, whereas was positively associated with liver FASN ($P < 0.05$); Glu was negatively associated with liver NEFA and AST ($P < 0.05$); Leu was negatively associated with liver ACLY, TG, HDL, and AST ($P < 0.05$); Gly was negatively associated with liver TG and HDL ($P < 0.05$); Thr was negatively associated with liver TG and HDL ($P < 0.05$); Yet, Lys was positively associated with serum T-CHO, liver NEFA, ACLY, HDL, and AST ($P < 0.05$); Ile was positively associated with serum TG and T-CHO, liver NEFA, ACLY, TG, and HDL ($P < 0.05$); Val was positively associated with serum TG, liver NEFA, ACLY, HDL, ALT, and AST ($P < 0.05$); Tyr was positively associated with liver AST ($P < 0.05$); Phe was positively associated with liver NEFA ($P < 0.05$). The correlation network analysis further revealed serum free amino acids dramatically influenced liver NEFA, ACLY, and HDL, serum-free Val, Ile, and Lys play a positive role, yet Met, Ser, His, Leu, and Ala plays a negative role (**Figure 4B**). Overall, these results suggested that circulating amino acid quantity—and in particular, the elevated concentrations of Val, Ile, and Lys in serum circulation—may be an important accelerant of fatty acid synthesis.

Dietary Valine Promoted Lipogenesis Trigger NAFLD *via* Repressing FGF19-TORC1 Signaling Pathway Mediated by GCN2-EIF2α-ATF4

Our recent report indicated that low levels of dietary valine activated the GCN2-eIF2α-ATF4 pathway, while high levels of dietary valine inhibited it (33). Fibroblast growth factor

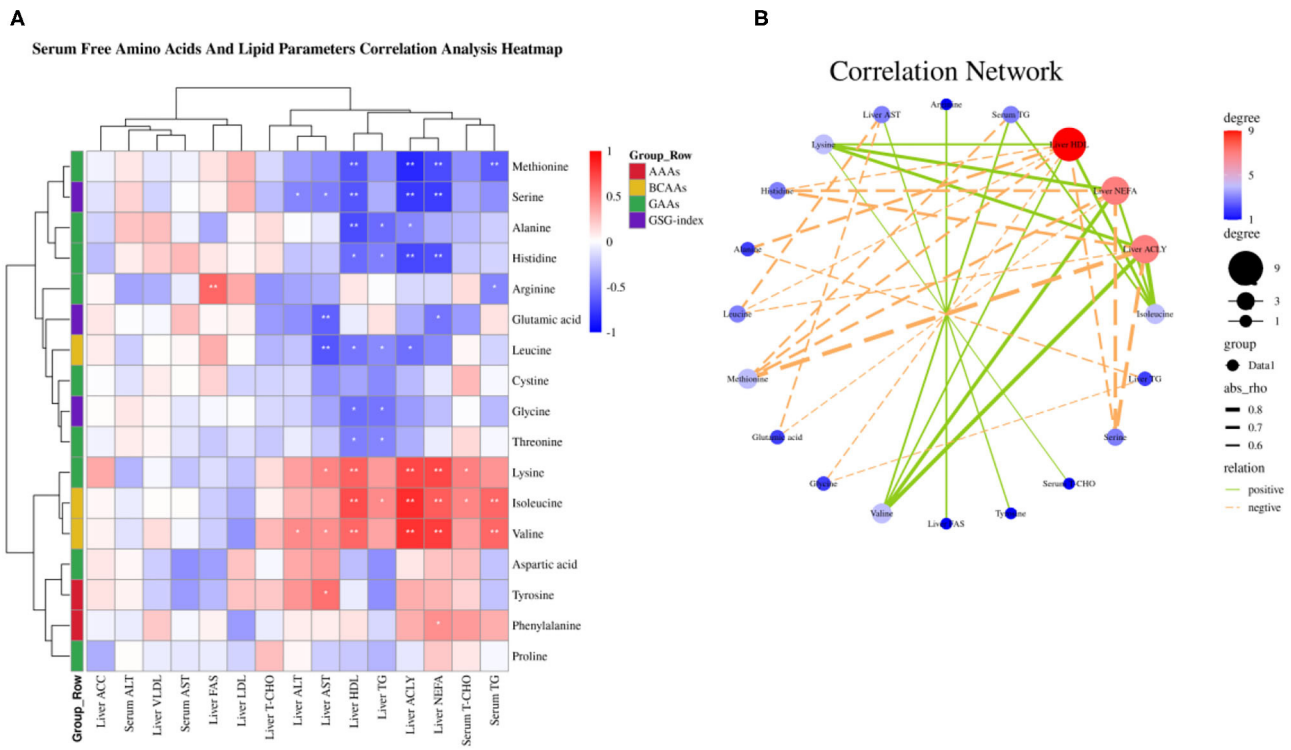

FIGURE 4 | Serum-free amino acids and lipid parameters correlation analysis. **(A)** Serum-free amino acids and lipid parameters correlation analysis heatmap. **(B)** Correlation network. *$P < 0.05$ and **$P < 0.01$.

family (FGF), for instance, FGF21 and FGF19 (37). FGF21 is a target gene of ATF4 and is critical to the adaptive metabolic response to amino acid deprivation (37–39). FGF19 is a late-fed-state gut hormone that is induced by the bile acid nuclear receptor which can inhibit lipogenesis (39). GCN2 has also been connected to mTORC1 activation and activation of the GCN2-ATF4 signaling pathway in amino acid-deprived cells results in mTORC1 inhibition (40). In addition, FGF21 can repress insulin- or nutrient-stimulated activation of mTORC1 in the liver (41). Last research suggested that each BCAA has distinct metabolic effects, and a low isoleucine diet reprograms liver and adipose metabolism *via* activating the FGF21-uncoupling protein 1 (UCP1) axis (42). Reducing valine induces similar but more modest metabolic effects, whereas these effects are absent with low leucine (42). Therefore, we further investigated whether dietary valine influences the FGF19-TORC1 or UCP3 axis and whether it is mediated by the GCN2-eIF2α-ATF4 pathway, while the FGF21 and UCP1 are not detected due to the chicken genome lack of them. With increasing dietary valine levels, our RT-PCR revealed that dietary valine supplementation dramatically downregulated the mRNA expression levels of FGF19 and TORC1 (**Figures 5A,B**), yet the UCP3 showed first downregulated and then upregulated in a quadratic manner ($P < 0.05$) (**Figure 5C**). Taken together with our previous results, we found that excessive dietary valine stimulated lipogenesis drives NAFLD by inhibiting the FGF19-TORC1 pathway in a GCN2-eIF2α-ATF4 dependent manner.

NAFLD Induced by Excessive Dietary Valine Repressed Autophagy *via* GCN2-FGF19-TORC1 Results in Enhanced Inflammatory Response

As an amino acid sensor, GCN2 is sensitive to a paucity of one or more essential amino acids to inhibit mTORC1, resulting in autophagy induction (29). The mTORC1 activation promotes phosphorylation of ULK1, an upstream regulator of autophagosome biogenesis, thereby inhibiting autophagy (11, 27). Based on the results of **Figure 5**, thus, we further analyze whether inhibition of the GCN2-FGF19-TORC1 signaling pathway affects autophagy. We found that dietary valine treatment significantly downregulated the mRNA expression levels of ULK1, LC3I, Atg5, and Atg7 in a linear or quadratic manner with the increase of dietary valine levels ($P < 0.05$) (**Figures 6A,B,D,E**), whereas did not impact LC3II mRNA expression level ($P > 0.05$) (**Figure 6C**). Lipotoxicity induced by excessive lipids commonly triggers inflammation reaction and eventually induces NASH (5, 6). GCN2-autophagy defect can trigger the production of pro-inflammatory cytokines such as IL-β and IL-17 (28). Our previous results confirmed that NAFLD induced by high levels of dietary valine significantly increased the liver concentrations of IL-β and IL-17 in a quadratic manner (33). Given both the inhibition of the GCN2-FGF19-TORC1-autophagy signaling pathway and enhanced liver inflammatory response, we concluded that NAFLD induced by high levels of

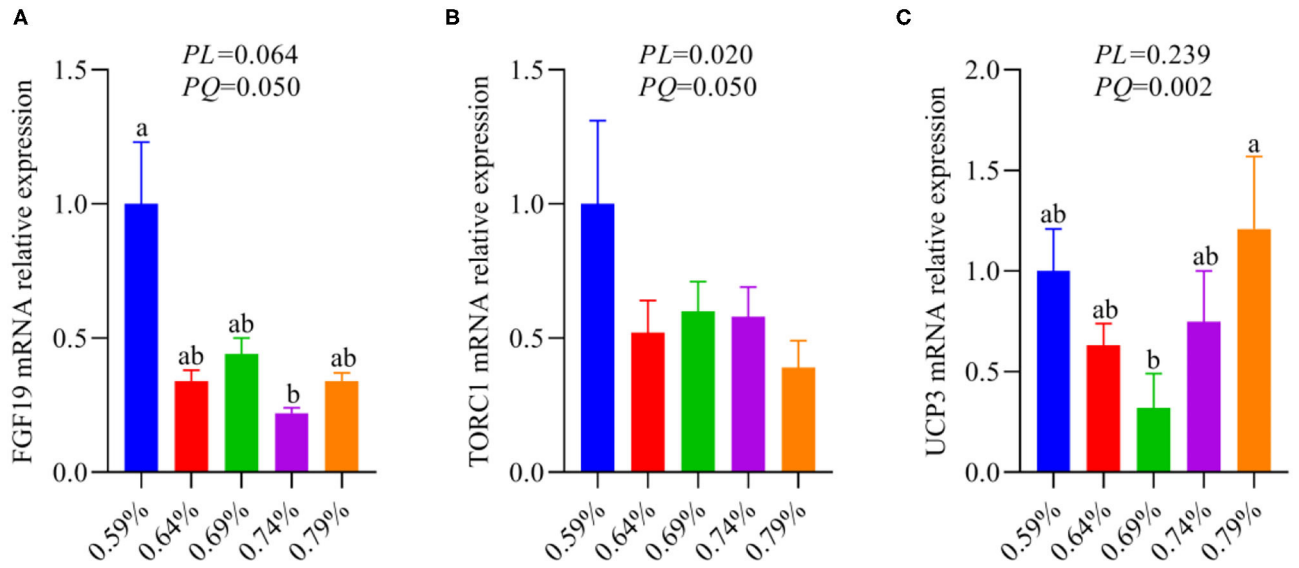

FIGURE 5 | The relative mRNA expression levels of an FGF19-TORC1 signaling pathway ($n = 6$–8). **(A)** FGF19. **(B)** TORC1. **(C)** UCP3. [a,b]Means with different superscripts within a column differ significantly ($P < 0.05$).

dietary valine trigger liver inflammatory response *via* suppressing the GCN2-FGF19-TORC1-autophagy signaling pathway.

Amino Acid Imbalance and NAFLD Synergistically Trigger Oxidative Stress

A "second hit" of oxidative stress induced by lipid toxicity leads to the generation of high levels of reactive oxygen species (ROS), which further accelerate the NAFLD transform to NASH (5, 6). Inhibition of autophagy accelerates the production of ROS and decreased amino acids including glutamine, glutamate, cysteine, glycine, threonine, and serine, which suppress the production of GSH synergistically promote the severity of oxidative stress (15, 20–23). Based on our previous research that dietary valine treatment significantly inhibited the production of anti-oxidases and the concentrations of serum and liver GSH and GSSG (32, 33). Therefore, here we attempt to analyze the relationship between changed serum free amino acid profile and body anti-oxidases by correlation analysis. As shown in **Figure 7A**, the Spearman correlation analysis revealed that changed serum free amino acid profile dramatically associated with altered body anti-oxidases. Correlation heatmap indicated that serum free Lys was positively associated with liver GSH, but was negatively associated with serum GSH and GSSG, and liver GSH-Px, CAT, T-SOD, and GSSG ($P < 0.05$); Ile and Val were positively associated with liver T-AOC, while were negatively associated with serum GSH and GSSG, and liver GSH-Px, CAT, T-SOD, and GSSG ($P < 0.05$); Phe was positively associated with serum GSH-Px ($P < 0.05$); Leu was positively associated with serum T-SOD, CAT, GSH, and GSSG, and liver GSH-Px and T-SOD, yet was negatively associated with serum MDA ($P < 0.05$); Cys was positively associated with serum GSH and liver CAT ($P < 0.05$); Gly was positively associated with serum GSH and GSSG, and liver CAT ($P < 0.05$); Arg was positively associated with serum CAT and liver GSH-Px and CAT, whereas was negatively associated with serum T-AOC and MDA ($P < 0.05$); Ala was positively associated with serum GSSG, while was negatively associated with liver T-AOC ($P < 0.05$); Met was positively associated with serum GSH and GSSG, and liver CAT, T-SOD, and GSSG, but was negatively associated with liver T-AOC ($P < 0.05$); Ser was positively associated with serum GSSG, and liver GSH-Px, CAT, T-SOD, and GSSG, yet was negatively associated with liver T-AOC ($P < 0.05$); Glu was positively associated with liver CAT ($P < 0.05$); His was positively associated with serum GSH, and liver GSH-Px and T-SOD, while was negatively associated with liver GSH ($P < 0.05$). Furthermore, the correlation network analysis found that serum-free amino acids significantly affected serum GSH and GSSG, and liver CAT, T-SOD, and GSSG, serum-free Leu, Met, Gly, His, Cys, and Ser plays a positive role, whereas serum-free Val, Lys, and Ile play a negative role (**Figure 7B**). Together with previous results, we concluded that amino acid imbalance and NAFLD synergistically accelerated oxidative stress.

DISCUSSION

Non-alcoholic fatty liver disease commonly occurs in humans with obesity and T2DM, as well as in animals including rodents and laying hens. This condition is often accompanied by systemic metabolic disorders, such as excessive lipids deposition, steatosis, insulin resistance, oxidative stress, inflammatory response, ER stress, and autophagy inhibition (2–4). Perturbations in amino acid metabolism were suggested to be implicated in the pathogenesis of NAFLD and progression to NASH (23, 43, 44). In particular, elevated circulating BCAAs and AAAs and lower circulating glutamine, glutamate, alanine, aspartate, and glycine

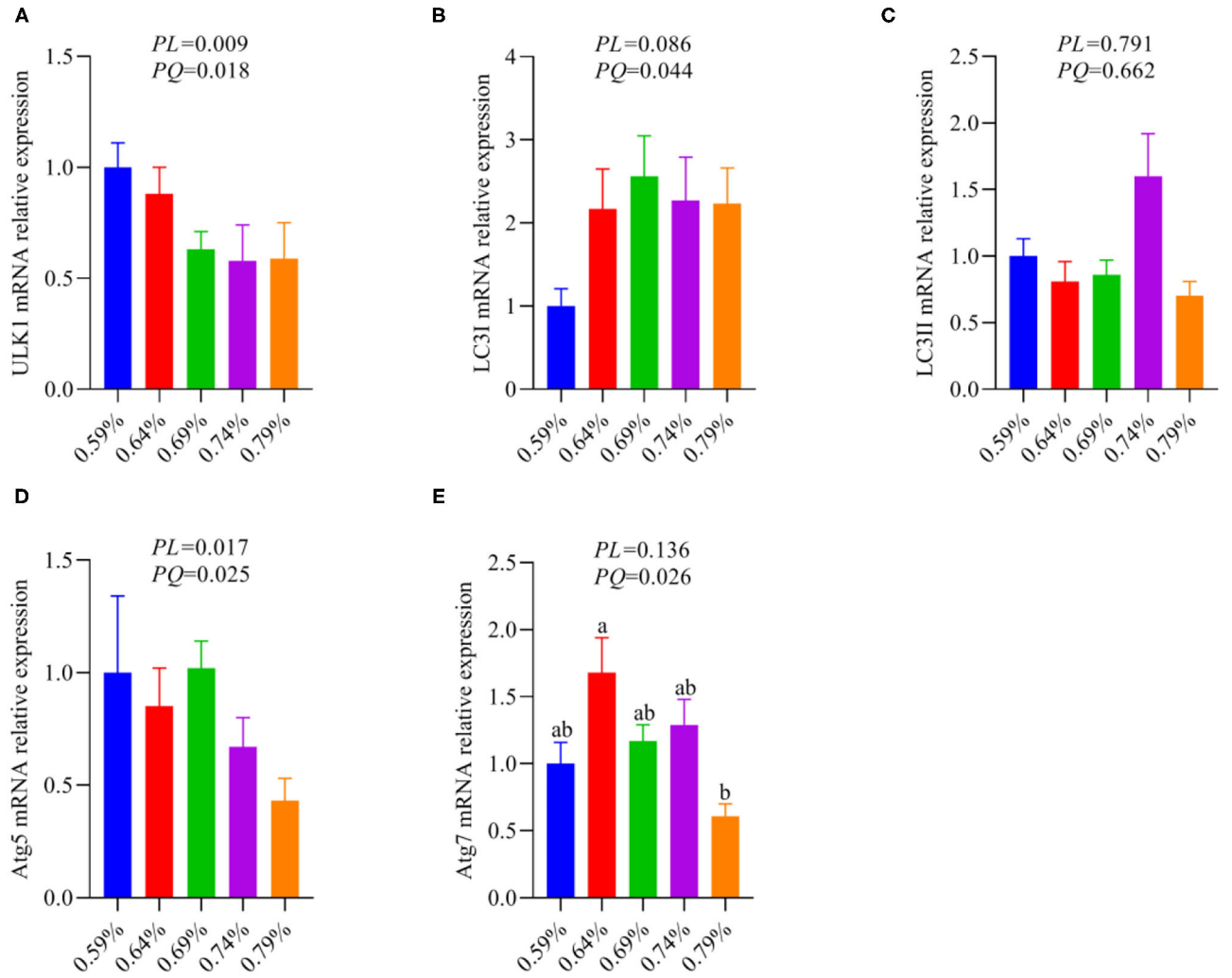

FIGURE 6 | The relative mRNA expression levels of an autophagy signaling pathway (n = 6–8). **(A)** ULK1. **(B)** LC3I. **(C)** LC3II. **(D)** Atg5. **(E)** Atg7. [a,b]Means with different superscripts within a column differ significantly ($P < 0.05$).

have been consistently reported in patients with NAFLD (12, 16–23), whereas single BCAA such as valine how to affect the development of NAFLD has not been systematically addressed so far. Here, we integrated our previous results and further identified that changed serum amino acid profile and impaired amino acid metabolism were significantly associated with fatty acid metabolism, oxidative stress, and inflammatory response mediated by the GCN2-FGF19-TORC1-autophagy signaling pathway. Using the Spearman correlation analysis and dietary intervention approaches to change dietary valine levels, we provide evidence for a causative role of valine in NAFLD of laying hens.

Based on our previous results that dietary valine supplementation dramatically influenced serum amino acid profile (32). For instance, dietary valine treatment significantly elevated serum BCAAs including valine and isoleucine, and AAAs such as phenylalanine and tyrosine (32). It has been demonstrated that increased concentrations of BCAAs contribute to insulin resistance in obese and T2DM humans and were associated with an increased risk of NAFLD (16–18). However, Solon-Biet and colleagues found that long-term exposure to high BCAA diets leads to hyperphagia and obesity and promotes hepatosteatosis and *de novo* lipogenesis (14). These effects are not due to elevated BCAA *per se* or hepatic mammalian target of rapamycin activation but instead are due to a shift in the relative quantity of dietary BCAAs and other amino acids, in particular, tryptophan and threonine (14). Consistent with our previous results that dietary valine feed significantly decreased the serum concentration of threonine, whereas we did not determine tryptophan due to the limitation of the detection method (32). Furthermore, our Spearman correlation analysis revealed that serum-free threonine was positively associated with Asp, Gly, Ala, Cys, and Leu, which was further confirmed by decreased contents of Asp, Gly, Ala, Cys,

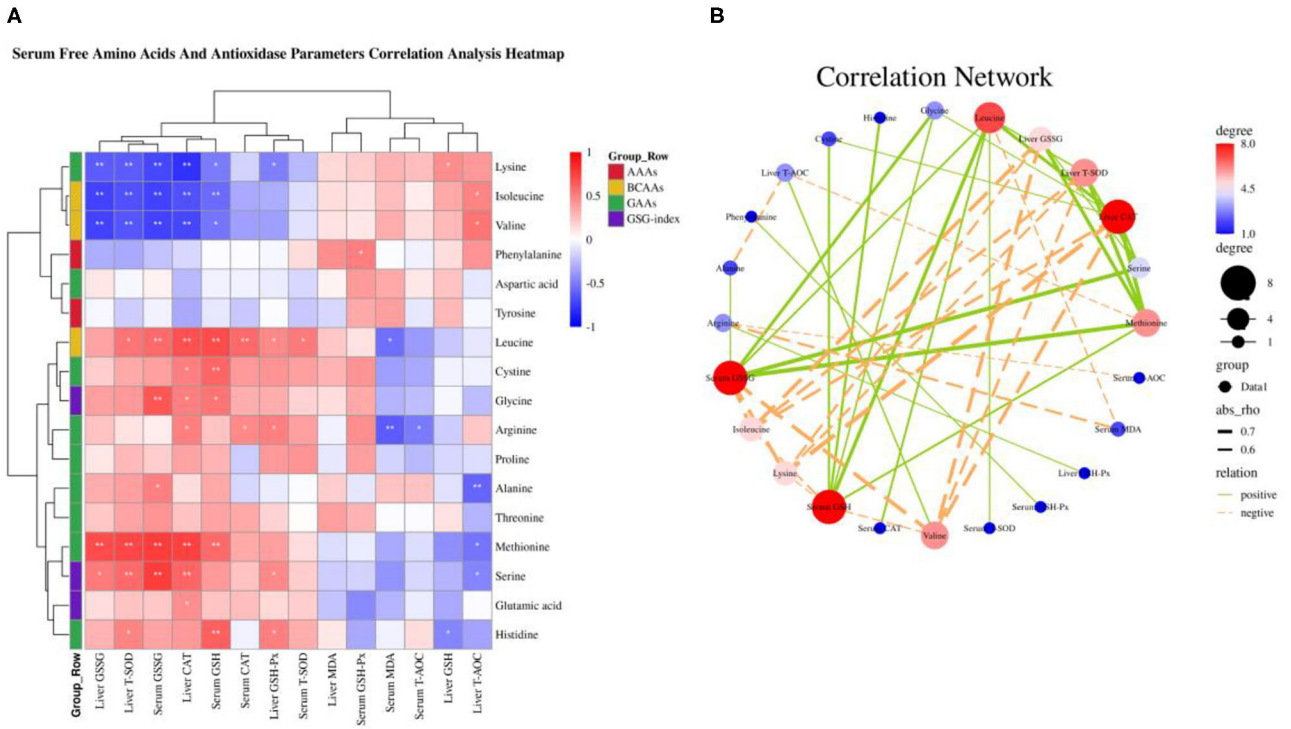

FIGURE 7 | Serum-free amino acids and anti-oxidase parameters correlation analysis. **(A)** Serum-free amino acids and anti-oxidase parameters correlation analysis heatmap. **(B)** Correlation network. *$P < 0.05$ and **$P < 0.01$.

and Leu in our recent research (32). The latest research indicated each BCAA has distinct metabolic effects in a low protein diet and the isoleucine and valine have similar metabolic effects, but the leucine does not have similar metabolic effects (42). It is interesting that we also found similar results that dietary valine treatment dramatically increased the concentrations of serum-free valine and isoleucine, whereas decreased the content of serum-free leucine (32). Our Spearman correlation analysis further demonstrated the serum-free leucine was positively associated with Gly, Thr, and Cys, yet was negatively associated with Lys, Ile, and Val. In combination with our results and the findings of other studies, these pieces of research may again indicate the unique metabolic effects of each individual BCAA, and future research should consider whether decreasing the ratio of Ile and Val and increasing the ratio of Leu will contribute to inhibiting the development of NAFLD. The AAAs including tryptophan, phenylalanine, and tyrosine, were found to increase with increased severity of liver diseases (19). Elevated circulating levels of AAAs contributed to promoting hepatic and adipose tissue lipids deposition and eventually accelerate the development and progress of NAFLD (4). In addition, AAAs can be degraded by the gut microbiota into phenylacetic acid (PAA), which can increase BCAA utilization and enhance hepatic lipid accumulation (45). Similarly, our previous results also revealed that dietary valine supplementation significantly increased the levels of serum-free phenylalanine and tyrosine (32), which is confirmed by Spearman correlation analysis that indicated serum-free phenylalanine was positively correlated with serum-free valine, isoleucine, and cysteine, but was negatively correlated with serum-free methionine.

Apart from increased circulating levels of BCAAs and AAAs, we also reported that serum-free arginine, histidine, methionine, threonine, alanine, aspartic acid, glutamic acid, glycine, and serine showed significantly decreased upon dietary valine treatment (32). Many pieces of research have indicated that glutamine, glutamate, alanine, and aspartate are positively associated with increased hepatic insulin resistance, whereas decreased glycine and serine were found in NAFLD humans (20–23), which is partly consistent with our results. Lower circulating glycine in the patients with NAFLD was associated with impaired glycine metabolism primarily mediated by alanine-glyoxylate aminotransferase 1 (AGXT1), glycine metabolism disorder plays a causative role in the development of NAFLD (15). As a new marker of severity of liver disease independent of body mass index, glutamate–serine–glycine (GSG) index [glutamate/(serine1glycine)] is reported to correlate with hepatic insulin resistance (12). Our results suggested that dietary valine supplementation elevated serum GSG-index and showed a quadratic decrease with increasing dietary levels, which may be revealed as enhanced hepatic insulin resistance in NAFLD induced by high levels of dietary valine. The correlation network analysis revealed that dietary valine supplementation dramatically influenced the components of serum-free amino acids such as valine, isoleucine, methionine, glycine, alanine,

serine, threonine, histidine, and lysine. The above mentioned results suggested that dietary valine treatment significantly altered serum-free amino acid profile and led to an amino acid imbalance. Amino acid composition imbalance may imply damage to amino acid metabolism which has been confirmed in a previous study (15). Our RT-PCR results demonstrated dietary valine treatment dramatically downregulated amino acid biosynthetic genes mRNA relative expression levels, e.g., C/EBP-β and Asns. C/EBP-β can be activated by induced translationally ATF4 (46), which has been found downregulated by high levels of dietary valine in our previous report (33). As an amino acid metabolism and transport gene, asparagine synthetase (Asns) mRNA expression is dependent upon both GCN2 and ATF4 (47), which is further confirmed by our current and previous results (33). In combination with changed serum free amino acid profile and impaired amino acid metabolism, we can conclude that dietary valine supplementation resulted in amino acid imbalance and damaged amino acid metabolism mediated by GCN2-eIF2α-ATF4.

The first step of lipid deposition is synthesizing fatty acids *via* stimulating liver FASN, ACLY, and ACC secretions, and then, the fatty acids are esterified to generate TGs, eventually to store in lipid droplets (36). We found that dietary valine supplementation dramatically elevated the contents of liver ACLY, whereas the content of liver FASN first increased and then decreased with the increase of dietary valine levels. However, dietary valine treatment did not affect the contents of liver ACC. Consistently, our previous study confirmed this result, wherein dietary valine significantly upregulated the mRNA relative expression levels of FASN and ACLY yet did not affect the mRNA expression level of ACC (33). Our data of elevated NEFA further proved that dietary valine promoted fatty acid synthesis by stimulating the secretion of FASN and ACLY. Previous results have demonstrated that excess BCAAs directly contributed to *de novo* lipogenesis or *via* increased ACLY phosphorylation mediated by the branched-chain ketoacid dehydrogenase kinase (BCKDK) (48, 49). The decreased concentration and downregulated mRNA expression level of FASN at the 0.74 or 0.79% level may be due to excessive fatty acid secretion feedback inhibiting it or resulting from the downregulation of GCN2-eIF2α-ATF4 mRNA expression levels (33). ACC carboxylates acetyl-CoA to form malonyl-CoA, dietary valine did not affect the concentration and mRNA expression level of ACC may be contributing to the metabolism of valine mainly produce propionyl-CoA (18). The elevation of fatty acid contributes to *de novo* lipogenesis by synthesizing TG, which has been certificated by significantly increased serum and liver TG (33). Under conditions of excess nutrients, liver fatty acid can be esterified to produce TG, which can then be secreted as VLDL-TG or stored within lipid droplets (50). Consistently, we found dietary valine treatment effectively elevated the content of VLDL but did not affect LDL. The net retention of intrahepatic TG is a prerequisite for the development of NAFLD, which encompasses a spectrum of diseases, starting with simple steatosis, through to the development of cirrhosis and hepatocellular carcinoma (51). Patients with T2DM and those with NAFLD have been reported to have an overproduction of VLDL particles (52). Interestingly, we found dietary valine also elevated the content of HDL, although the exact mechanism is not fully understood.

In addition to the increased synthesis of fatty acids, lipids can be brought into cells *via* passive diffusion and fatty acid transport or translocase proteins, including FATPs and CD36 (53). CD36 is a transporter that plays an important role in facilitating intracellular FFA uptake and trafficking, which dysfunction has been implicated in lipophagy reduction and NAFLD development (54). As the most common fatty acid transport protein in the liver, FATP1 can function both to promote fatty acid uptake and to facilitate the import of long-chain fatty acids (LCFAs) (53). However, we found dietary valine did not affect the mRNA expression levels of FATP1 and CD36, which revealed that lipids accumulation induced by excessive dietary valine has not resulted in enhanced fatty acid uptake. We found dietary valine treatment significantly upregulated FABP1 mRNA expression level, which is a liver-specific FABP and mainly expressed in intracellular and its upregulation contributes to lipid droplets formation (55). In addition, we found dietary valine dramatically downregulated the mRNA expression levels of apolipoprotein A1 and B, which plays vital roles in lipids transport out of the liver and the utilization of lipids (56). Combining upregulated FABP1 and downregulated apoA1 and apoB, our current results may imply that dietary valine promotes lipid accumulation *via* accelerating lipid droplets formation and inhibiting lipids utilization. Our previous report suggested that dietary valine significantly inhibited fatty acids β-oxidation by downregulating the mRNA expression levels of fatty acid oxidation-related genes such as CPT1, ACOX1, and PPARα (33). Taken together with our previous and current results, we can conclude that dietary valine accelerated the development of NAFLD by promoting lipogenesis (including fatty acids, TG, and VLDL), inhibiting lipids export and utilization, and fatty acid oxidation mediated by GCN2-eIF2α-ATF4.

The role of amino acids in lipid metabolism has been well-demonstrated and understood, for instance, BCAAs, AAAs, and glycine (14, 15, 33, 42, 47–49). It has been clarified that amino acid imbalance and impaired amino acid metabolism contribute to lipid accumulation and the occurrence and development of NAFLD (14, 15). Thus, we sought to elaborate on the relationship between imbalanced amino acids and fatty acid metabolism by Spearman correlation analysis. Our correlation analysis revealed imbalanced amino acids are dramatically correlated with fatty acid metabolism. Serum-free valine, isoleucine, and lysine, in particular, were positively associated with liver NEFA, ACLY, and HDL, whereas serum-free methionine, serine, and histidine were negatively associated with liver NEFA, ACLY, and HDL. The correlation network further confirmed dietary valine supplementation mainly contributes to elevating liver HDL, NEFA, and ACLY mediated by elevating valine, isoleucine, and lysine levels. Long-term exposure to excessive valine diets led to amino acid imbalance, impaired amino acid metabolism, and enhanced NAFLD, which were maybe induced by a shift in the relative quantity of dietary valine, isoleucine, and lysine and other amino acids, notably methionine, serine, and histidine. For example, imbalanced amino acids drive hyperphagia and shorten lifespan due to a shift in the relative quantity of dietary

BCAAs and tryptophan and threonine (14). However, there are no more reports about dietary lysine, methionine, serine, and histidine how to influence lipid metabolism. Further research will be required to fully define the mechanisms by which dietary lysine, methionine, serine, and histidine regulate the amino acid and lipid metabolism, and whether is mediated by GCN2-eIF2α-ATF4.

As a target gene of ATF4, FGF21 is critical to the adaptive metabolic response to amino acid deprivation, while the chicken genome lacks FGF21 (37). FGF19 is a late-fed-state gut hormone that is induced by the bile acid nuclear receptor which can inhibit lipogenesis (37). Our results suggested that dietary valine significantly downregulated liver FGF19 mRNA expression level, which is consistent with a previous report (39). The report found that GCN2 can connect to mTORC1 activation and activation of the GCN2-ATF4 signaling pathway in amino acid-deprived cells results in mTORC1 inhibition (40). In addition, FGF21 can repress insulin-or nutrient-stimulated activation of mTORC1 in the liver (41). Consistent with the mRNA expression level of FGF19, we found dietary valine also dramatically downregulated liver TORC1 expression level. Together with our previous results that high levels of dietary valine significantly inhibited GCN2-eIF2α-ATF4 expression levels, which may indicate the FGF19-TORC1 is the downstream target genes of GCN2-eIF2α-ATF4. Recent research suggested that a low isoleucine diet reprograms liver and adipose metabolism by increasing hepatic insulin sensitivity and ketogenesis, increasing energy expenditure, and activating the FGF21-UCP1 axis (42). Reducing valine induces similar but more modest metabolic effects, whereas these effects are absent with low leucine (42). Herein, we found the mRNA expression level of UCP3 is in contrast to GCN2-eIF2α-ATF4, which were maybe induced by the inhibition of GCN2-eIF2α-ATF4, and eventually result in the activation of UCP3.

General control non-derepressible 2 is a classic amino acid sensor and is sensitive to a paucity of one or more essential amino acids to inhibit mTORC1, resulting in autophagy induction (29). The activation of mTORC1 promotes phosphorylation of ULK1, an upstream regulator of autophagosome biogenesis, thereby inhibiting autophagy (11, 27). Based on inhibited expression levels of GCN2-eIF2α-ATF4-FGF19-TORC1, we further analyze the effects of dietary valine levels on the autophagy signaling pathway. We found dietary valine significantly downregulated the mRNA expression levels of ULK1, LC3I, and autophagy-associated proteins such as Atg5 and Atg7 yet did not impact the LC3II expression level. In NAFLD, the excess of triglycerides and FFAs suppresses the initiation of autophagy through activation of mammalian target of rapamycin (mTOR) and the suppression of serine/threonine-protein kinase ULK1 activity, leading to increased hepatic oxidative stress (57, 58). Consistent with our results that dietary valine significantly downregulated the mRNA expression levels of TORC1 and ULK1. Mice with a hepatocyte-specific knockout of Atg7 or cultured mouse hepatocytes with knock-down of Atg7 or Atg5 expression have revealed that inhibition of autophagy increases triglyceride storage in lipid droplets (59). Herein, we found dietary valine treatment dramatically inhibited the mRNA expression levels of Atg5 and Atg7, which may be induced by the inhibition of GCN2-eIF2α-ATF4-FGF19-TORC1. It has been demonstrated that LC3 was localized on the surface of LDs and the LC3 conjugation system is essential for lipid metabolism mediated by macroautophagy *via* LD formation (60). We found dietary valine significantly downregulated the mRNA expression level of LC3I, whereas did not affect LC3II. The mTORC1-ULK1 plays a vital role in autophagy by regulating autophagolyosome formation. LC3 is cleaved by ATG4 to form LC3I, and LC3I then conjugates with phosphatidylethanolamine *via* ATG7 and ATG3 to form LC3II (61). The ATG12 complex promotes LC3II formation and its conjugation to the phagosome (61, 62). NAFLD induced by excessive dietary valine did not affect the expression level of LC3II may be associated with the formation of the ATG12 complex. Future research should consider the effect of the excessive individual BCAAs on the autophagic flux and the formation of ATG12 complex *in vitro* hepatocytes. Inhibition of autophagy trigger hepatic inflammation and liver injury, which has been our previous report proved that NAFLD induced by excessive dietary valine showed enhanced inflammatory response mediated by the production of IL-1β and IL-17 *via* inhibiting GCN2 (33). In the presence of NASH, inflammation and oxidative stress are increased. Defects in macrophage autophagy induced by Atg5 knockout promoted hepatic inflammation and pro-inflammatory M1 macrophage polarization and decreased anti-inflammatory M2 macrophage polarization, resulting in the onset of liver injury in mice (63). In combination with autophagy inhibition and enhanced inflammatory response, we conclude that NAFLD induced by excessive dietary valine accelerated liver inflammation by inhibiting GCN2-TORC1-autophagy signaling pathways.

In addition to enhanced inflammatory response, lipids excess also inhibits autophagy mediated by mTORC1 and autophagy-associated proteins, resulting in increased hepatic oxidative stress (57, 58), which has been our and others reports confirmed (33, 57, 58). Our report suggested dietary valine treatment accelerated oxidative stress induced by NAFLD *via* inhibiting anti-oxidase production (33). Apart from increased hepatic oxidative stress induced by autophagy inhibition, amino acid imbalance and impaired amino acid metabolism also promote oxidative stress by increasing ROS levels. As an anti-oxidant molecule, GSH is produced by several tissues in response to oxidative stress and increased production of ROS (64). ROS stimulates the synthesis of GSH from cysteine, glycine, and glutamate, which are produced from the transamination of alanine and aspartate (12). Our previous report indicated dietary valine treatment significantly decreased serum free cysteine, glycine, glutamate, alanine, and aspartate, which is consistent with recent reports (12). Here, we revealed serum increased free valine, isoleucine, and lysine are dramatic negatively associated with decreased serum GSH and GSSG, and liver CAT, T-SOD, and GSSG by Spearman correlation analysis. In contrast, serum decreased free leucine, cysteine, glycine, arginine, methionine, serine, and histidine were significantly positively correlated with decreased serum and liver anti-oxidases. Studies have shown that metabolic dysregulation is often associated with a reduction in glycine and serine concentrations and an increase in the levels of valine

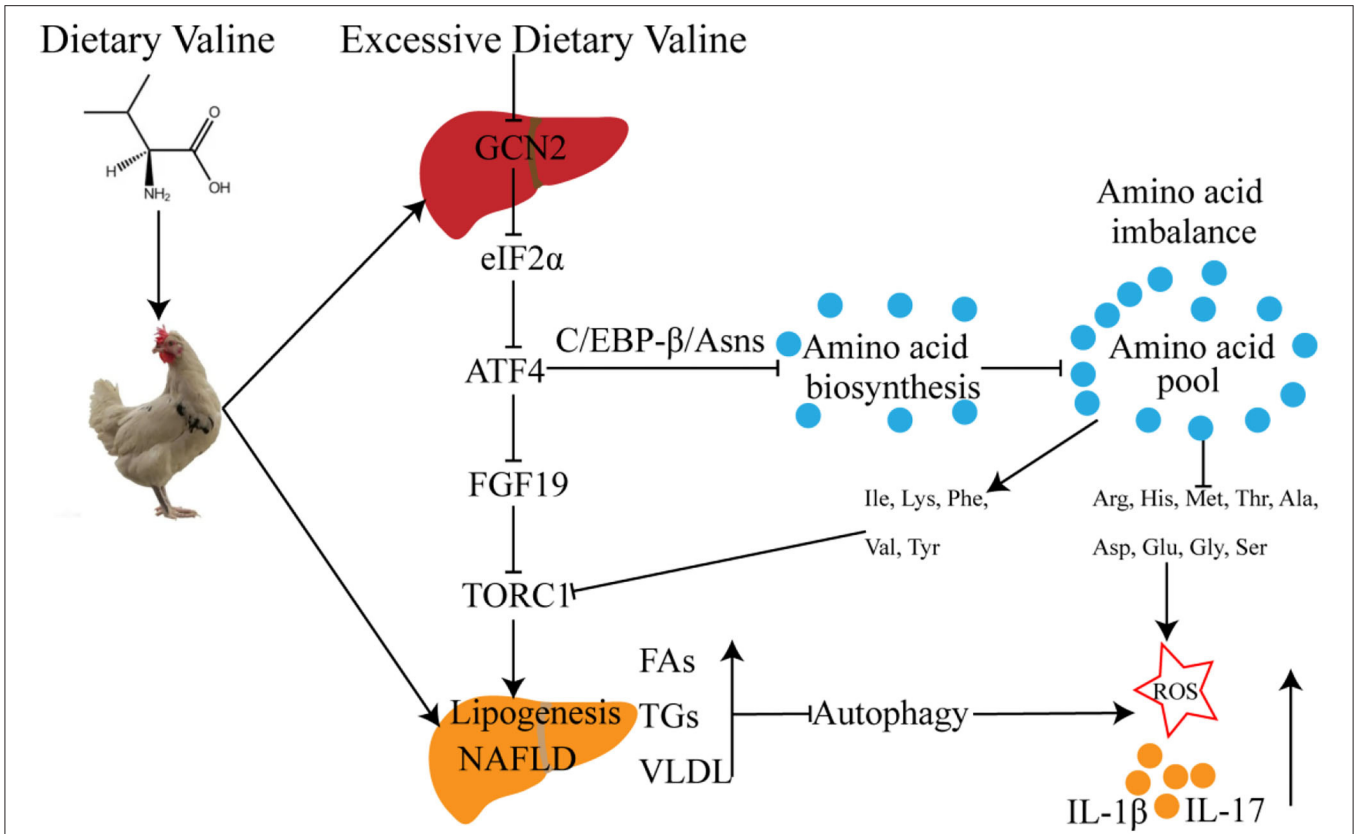

FIGURE 8 | The possible molecular mechanism of dietary valine regulates amino acid and fatty acid metabolism mediated by the GCN2-TORC1-Autophagy pathway in NAFLD of laying hens.

and leucine (23, 65, 66), which is similar to our results (33). A recent cohort of subjects with NAFLD but without diabetes found reduced concentrations of glycine and serine (a precursor of cysteine) (12). In addition, as the limiting step for GSH synthesis (22), Glycine also plays an important role in metabolic regulation and intracellular redox balance (64), and decreased glycine has been found in NAFLD subjects (15). Correlation network analysis demonstrated dietary valine supplementation mainly contributes to promoting the production of anti-oxidases such as GSH, GSSG, CAT, and T-SOD by decreasing leucine, cysteine, glycine, arginine, methionine, serine, and histidine, whereas valine, isoleucine, and lysine suppress it. Oxidative stress usually results in liver damage and is characterized by mitochondrial dysfunction, impaired oxidation, and the production of ROS (65, 66). This process increases the demand for GSH synthesis to counteract the production of ROS by increasing intracellular GSH turnover (64). Amino acids, including glycine, serine, and glutamate, are used for the synthesis of GSH. Our results showed decreased serum free glycine, serine, and glutamate is consistent with decreased GSH and GSSG in the serum and liver (32, 33). An additional question is that decreased serum leucine was distinct from increased isoleucine and valine, which has been demonstrated in recent research that leucine has distinct metabolic effects from isoleucine and valine (42). In addition, we also surprisingly found serum lysine is dramatically increased and was positively associated with isoleucine, valine, liver NEFA, ACLY, HDL, and AST, whereas was negatively correlated with serum GSH and GSSG, and liver CAT, T-SOD, GSSG, and GSH-Px. Future research should focus on the effects of the individual BCAAs on the occurrence and development of NAFLD and its adverse metabolic impact whether is mediated by lysine.

In summary, we further demonstrated that long-term exposure to excessive dietary valine influenced amino acid and fatty acid metabolism in laying hens by inducing amino acid imbalance, impairing amino acid metabolism, promoting fatty acid synthesis, and inhibiting fatty acid utilization mediated by GCN2-FGF19-TORC1 signaling pathways. These results further lead to the occurrence and development of NAFLD, which triggers oxidative stress and inflammatory response *via* repressing autophagy pathway (**Figure 8**). Our results revealed the adverse metabolic effects of excessive dietary valine in laying hens, highlighting the critical importance of dietary levels of valine for the adverse metabolic function of NAFLD, which is due to the inhibition of GCN2-TORC1-autophagy signaling pathways. Finally, we suggest that reducing dietary valine may be a novel preventive and therapeutic strategy to combat the twin epidemics of NAFLD and FLHS in laying hens.

DATA AVAILABILITY STATEMENT

The original contributions presented in the study are included in the article/supplementary material, further inquiries can be directed to the corresponding author.

ETHICS STATEMENT

The animal study was reviewed and approved by No. ZJU2013105002.

AUTHOR CONTRIBUTIONS

HJ: conceptualization, data curation, investigation, writing the original draft, reviewing, and editing. QX: data curation, methodology, writing, reviewing, and editing. XW: conceptualization, data curation, and methodology. YLiu: data curation and investigation. SM: methodology and investigation. YLi: data curation. TM: investigation. XD: investigation and writing, reviewing, and editing. XZ: project administration, conceptualization, funding acquisition, writing, reviewing, and editing. All authors have read and agreed to the published version of the manuscript.

FUNDING

This study was supported by the Earmarked Fund for Modern Agro-Industry Technology Research System of China (CARS-40-K10).

REFERENCES

1. Younossi ZM, Koenig AB, Abdelatif D, Fazel Y, Henry L, Wymer M. Global epidemiology of nonalcoholic fatty liver disease-meta-analytic assessment of prevalence, incidence, and outcomes. *Hepatology.* (2016) 64:73–84. doi: 10.1002/hep.28431
2. Friedman SL, Neuschwander-Tetri BA, Rinella M, Sanyal AJ. Mechanisms of NAFLD development and therapeutic strategies. *Nat Med.* (2018) 24:908–22. doi: 10.1038/s41591-018-0104-9
3. Bedossa P, Poitou C, Veyrie N, Bouillot JL, Basdevant A, Paradis V, et al. Histopathological algorithm and scoring system for evaluation of liver lesions in morbidly obese patients. *Hepatology.* (2012) 56:1751–9. doi: 10.1002/hep.25889
4. Loomba R, Friedman SL, Shulman GI. Mechanisms and disease consequences of nonalcoholic fatty liver disease. *Cell.* (2021) 184:2537–64. doi: 10.1016/j.cell.2021.04.015
5. Day CP, James OF. Steatohepatitis: a tale of two "hits"? *Gastroenterology.* (1998) 114:842–5. doi: 10.1016/S0016-5085(98)70599-2
6. Day CP, Saksena S. Non-alcoholic steatohepatitis: definitions and pathogenesis. *J Gastroenterol Hepatol.* (2002) 17(Suppl. 3):S377–84. doi: 10.1046/j.1440-1746.17.s3.31.x
7. Krenkel O, Puengel T, Govaere O, Abdallah AT, Mossanen JC, Kohlhepp M, et al. Therapeutic inhibition of inflammatory monocyte recruitment reduces steatohepatitis and liver fibrosis. *Hepatology.* (2018) 67:1270–83. doi: 10.1002/hep.29544
8. Gadd VL, Skoien R, Powell EE, Fagan KJ, Winterford C, Horsfall L, et al. The portal inflammatory infiltrate and ductular reaction in human nonalcoholic fatty liver disease. *Hepatology.* (2014) 59:1393–405. doi: 10.1002/hep.26937
9. Moylan CA, Pang H, Dellinger A, Suzuki A, Garrett ME, Guy CD, et al. Hepatic gene expression profiles differentiate presymptomatic patients with mild versus severe nonalcoholic fatty liver disease. *Hepatology.* (2014) 59:471–82. doi: 10.1002/hep.26661
10. Lytrivi M, Castell AL, Poitout V, Cnop M. Recent insights into mechanisms of β-Cell lipo- and glucolipotoxicity in type 2 diabetes. *J Mol Biol.* (2020) 432:1514–34. doi: 10.1016/j.jmb.2019.09.016
11. Kim KH, Lee MS. Autophagy–a key player in cellular and body metabolism. *Nat Rev Endocrinol.* (2014) 10:322–37. doi: 10.1038/nrendo.2014.35
12. Gaggini M, Carli F, Rosso C, Buzzigoli E, Marietti M, Della Latta V, et al. Altered amino acid concentrations in NAFLD: impact of obesity and insulin resistance. *Hepatology.* (2018) 67:145–58. doi: 10.1002/hep.29465
13. Hasegawa T, Iino C, Endo T, Mikami K, Kimura M, Sawada N, et al. Changed amino acids in NAFLD and liver fibrosis: a large cross-sectional study without influence of insulin resistance. *Nutrients.* (2020) 12:1450. doi: 10.3390/nu12051450
14. Solon-Biet SM, Cogger VC, Pulpitel T, Wahl D, Clark X, Bagley E, et al. Branched chain amino acids impact health and lifespan indirectly via amino acid balance and appetite control. *Nat Metab.* (2019) 1:532–45. doi: 10.1038/s42255-019-0059-2
15. Rom O, Liu Y, Liu Z, Zhao Y, Wu J, Ghrayeb A, et al. Glycine-based treatment ameliorates NAFLD by modulating fatty acid oxidation, glutathione synthesis, and the gut microbiome. *Sci Transl Med.* (2020) 12:eaaz2841. doi: 10.1126/scitranslmed.aaz2841
16. Newgard CB, An J, Bain JR, Muehlbauer MJ, Stevens RD, Lien LF, et al. A branched-chain amino acid-related metabolic signature that differentiates obese and lean humans and contributes to insulin resistance. *Cell Metab.* (2009) 9:311–26. doi: 10.1016/j.cmet.2009.02.002
17. Adeva MM, Calviño J, Souto G, Donapetry C. Insulin resistance and the metabolism of branched-chain amino acids in humans. *Amino Acids.* (2012) 43:171–81. doi: 10.1007/s00726-011-1088-7
18. Lynch CJ, Adams SH. Branched-chain amino acids in metabolic signalling and insulin resistance. *Nat Rev Endocrinol.* (2014) 10:723–36. doi: 10.1038/nrendo.2014.171
19. Morgan MY, Marshall AW, Milsom JP, Sherlock S. Plasma amino-acid patterns in liver disease. *Gut.* (1982) 23:362–70. doi: 10.1136/gut.23.5.362
20. Bianchi G, Marchesini G, Brunetti N, Manicardi E, Montuschi F, Chianese R, et al. Impaired insulin-mediated amino acid plasma disappearance in non-alcoholic fatty liver disease: a feature of insulin resistance. *Dig Liver Dis.* (2003) 35:722–7. doi: 10.1016/S1590-8658(03)00416-X
21. Sookoian S, Pirola CJ. Alanine and aspartate aminotransferase and glutamine-cycling pathway: their roles in pathogenesis of metabolic syndrome. *World J Gastroenterol.* (2012) 18:3775–81. doi: 10.3748/wjg.v18.i29.3775
22. Mardinoglu A, Bjornson E, Zhang C, Klevstig M, Söderlund S, Ståhlman M, et al. Personal model-assisted identification of NAD^+ and glutathione metabolism as intervention target in NAFLD. *Mol Syst Biol.* (2017) 13:916. doi: 10.15252/msb.20167422
23. Mardinoglu A, Agren R, Kampf C, Asplund A, Uhlen M, Nielsen J. Genome-scale metabolic modelling of hepatocytes reveals serine deficiency in patients with non-alcoholic fatty liver disease. *Nat Commun.* (2014) 5:3083. doi: 10.1038/ncomms4083
24. Soultoukis GA, Partridge L. Dietary protein, metabolism, and aging. *Annu Rev Biochem.* (2016) 85:5–34. doi: 10.1146/annurev-biochem-060815-014422
25. Maida A, Chan JSK, Sjøberg KA, Zota A, Schmoll D, Kiens B, et al. Repletion of branched chain amino acids reverses mTORC1 signaling but not improved metabolism during dietary protein dilution. *Mol Metab.* (2017) 6:873–81. doi: 10.1016/j.molmet.2017.06.009
26. Lackey DE, Lynch CJ, Olson KC, Mostaedi R, Ali M, Smith WH, et al. Regulation of adipose branched-chain amino acid catabolism enzyme expression and cross-adipose amino acid flux in human obesity. *Am J Physiol Endocrinol Metab.* (2013) 304:E1175–87. doi: 10.1152/ajpendo.00630.2012
27. Nicklin P, Bergman P, Zhang B, Triantafellow E, Wang H, Nyfeler B, et al. Bidirectional transport of amino acids regulates mTOR and autophagy. *Cell.* (2009) 136:521–34. doi: 10.1016/j.cell.2008.11.044

28. Ravindran R, Loebbermann J, Nakaya HI, Khan N, Ma H, Gama L, et al. The amino acid sensor GCN2 controls gut inflammation by inhibiting inflammasome activation. *Nature.* (2016) 531:523–7. doi: 10.1038/nature17186
29. Yuan W, Guo S, Gao J, Zhong M, Yan G, Wu W, et al. General control nonderepressible 2 (GCN2) kinase inhibits target of rapamycin complex 1 in response to amino acid starvation in saccharomyces cerevisiae. *J Biol Chem.* (2017) 292:2660–9. doi: 10.1074/jbc.M116.772194
30. Shini A, Shini S, Bryden WL. Fatty liver haemorrhagic syndrome occurrence in laying hens: impact of production system. *Avian Pathol.* (2019) 48:25–34. doi: 10.1080/03079457.2018.1538550
31. Lee BK, Kim JS, Ahn HJ, Hwang JH, Kim JM, Lee HT, et al. Changes in hepatic lipid parameters and hepatic messenger ribonucleic acid expression following estradiol administration in laying hens (Gallus domesticus). *Poult Sci.* (2010) 89:2660–7. doi: 10.3382/ps.2010-00686
32. Jian H, Miao S, Liu Y, Li H, Zhou W, Wang X, et al. Effects of dietary valine levels on production performance, egg quality, antioxidant capacity, immunity, and intestinal amino acid absorption of laying hens during the peak lay period. *Animals.* (2021) 11:1972. doi: 10.3390/ani11071972
33. Jian H, Miao S, Liu Y, Wang X, Xu Q, Zhou W, et al. Dietary valine ameliorated gut health and accelerated the development of nonalcoholic fatty liver disease of laying hens. *Oxid Med Cell Longev.* (2021) 2021:4704771. doi: 10.1155/2021/4704771
34. National Research Council. *Nutrient Requirements of Poultry*. Washington, DC; National Academic Press. 9th edition (1994).
35. *The Agricultural Industry Standard of the People's Republic of China-Chicken Feeding Standard (NY/T33-2004).* Beijing; Ministry of Agriculture of the PRC (2006).
36. Currie E, Schulze A, Zechner R, Walther TC, Farese RV Jr. Cellular fatty acid metabolism and cancer. *Cell Metab.* (2013) 18:153–61. doi: 10.1016/j.cmet.2013.05.017
37. De Sousa-Coelho AL, Marrero PF, Haro D. Activating transcription factor 4-dependent induction of FGF21 during amino acid deprivation. *Biochem J.* (2012) 443:165–71. doi: 10.1042/BJ20111748
38. De Sousa-Coelho AL, Relat J, Hondares E, Pérez-Martí A, Ribas F, Villarroya F, et al. FGF21 mediates the lipid metabolism response to amino acid starvation. *J Lipid Res.* (2013) 54:1786–97. doi: 10.1194/jlr.M033415
39. Kim YC, Seok S, Zhang Y, Ma J, Kong B, Guo G, et al. Intestinal FGF15/19 physiologically repress hepatic lipogenesis in the late fed-state by activating SHP and DNMT3A. *Nat Commun.* (2020) 11:5969. doi: 10.1038/s41467-020-19803-9
40. Ye J, Palm W, Peng M, King B, Lindsten T, Li MO, et al. GCN2 sustains mTORC1 suppression upon amino acid deprivation by inducing Sestrin2. *Genes Dev.* (2015) 29:2331–6. doi: 10.1101/gad.269324.115
41. Gong Q, Hu Z, Zhang F, Cui A, Chen X, Jiang H, et al. Fibroblast growth factor 21 improves hepatic insulin sensitivity by inhibiting mammalian target of rapamycin complex 1 in mice. *Hepatology.* (2016) 64:425–38. doi: 10.1002/hep.28523
42. Yu D, Richardson NE, Green CL, Spicer AB, Murphy ME, Flores V, et al. The adverse metabolic effects of branched-chain amino acids are mediated by isoleucine and valine. *Cell Metab.* (2021) 33:905–22.e6. doi: 10.1016/j.cmet.2021.03.025
43. Hoyles L, Fernández-Real JM, Federici M, Serino M, Abbott J, Charpentier J, et al. Molecular phenomics and metagenomics of hepatic steatosis in non-diabetic obese women. *Nat Med.* (2018) 24:1070–80. doi: 10.1038/s41591-018-0061-3
44. Sookoian S, Pirola C. Metabolic make-up of NASH: from fat and sugar to amino acids. *Nat Rev Gastroenterol Hepatol.* (2014) 11:205–7. doi: 10.1038/nrgastro.2014.25
45. Han H, Jiang Y, Wang M, Melaku M, Liu L, Zhao Y, et al. Intestinal dysbiosis in nonalcoholic fatty liver disease (NAFLD): focusing on the gut-liver axis. *Crit Rev Food Sci Nutr.* (2021) 18:1–18. doi: 10.1080/10408398.2021.1966738
46. Chen C, Dudenhausen E, Chen H, Pan YX, Gjymishka A, Kilberg MS. Amino-acid limitation induces transcription from the human C/EBPbeta gene via an enhancer activity located downstream of the protein coding sequence. *Biochem J.* (2005) 391:649–58. doi: 10.1042/BJ20050882
47. Guo F, Cavener DR. The GCN2 eIF2alpha kinase regulates fatty-acid homeostasis in the liver during deprivation of an essential amino acid. *Cell Metab.* (2007) 5:103–14. doi: 10.1016/j.cmet.2007.01.001
48. Green CR, Wallace M, Divakaruni AS, Phillips SA, Murphy AN, Ciaraldi TP, et al. Branched-chain amino acid catabolism fuels adipocyte differentiation and lipogenesis. *Nat Chem Biol.* (2016) 12:15–21. doi: 10.1038/nchembio.1961
49. White PJ, McGarrah RW, Grimsrud PA, Tso SC, Yang WH, Haldeman JM, et al. The BCKDH kinase and phosphatase integrate BCAA and lipid metabolism via regulation of ATP-citrate Lyase. *Cell Metab.* (2018) 27:1281–93.e7. doi: 10.1016/j.cmet.2018.04.015
50. Ontko JA. Metabolism of free fatty acids in isolated liver cells. Factors affecting the partition between esterification and oxidation. *J Biol Chem.* (1972) 247:1788–800. doi: 10.1016/S0021-9258(19)45544-0
51. Hodson L, Gunn PJ. The regulation of hepatic fatty acid synthesis and partitioning: the effect of nutritional state. *Nat Rev Endocrinol.* (2019) 15:689–700. doi: 10.1038/s41574-019-0256-9
52. Adiels M, Borén J, Caslake MJ, Stewart P, Soro A, Westerbacka J, et al. Overproduction of VLDL1 driven by hyperglycemia is a dominant feature of diabetic dyslipidemia. *Arterioscler Thromb Vasc Biol.* (2005) 25:1697–703. doi: 10.1161/01.ATV.0000172689.53992.25
53. Broadfield LA, Pane AA, Talebi A, Swinnen JV, Fendt SM. Lipid metabolism in cancer: New perspectives and emerging mechanisms. *Dev Cell.* (2021) 56:1363–93. doi: 10.1016/j.devcel.2021.04.013
54. Li Y, Yang P, Zhao L, Chen Y, Zhang X, Zeng S, et al. CD36 plays a negative role in the regulation of lipophagy in hepatocytes through an AMPK-dependent pathway. *J Lipid Res.* (2019) 60:844–55. doi: 10.1194/jlr.M090969
55. Mukai T, Egawa M, Takeuchi T, Yamashita H, Kusudo T. Silencing of FABP1 ameliorates hepatic steatosis, inflammation, and oxidative stress in mice with nonalcoholic fatty liver disease. *FEBS Open Bio.* (2017) 7:1009–16. doi: 10.1002/2211-5463.12240
56. Khodja Y, Samuels ME. Ethanol-mediated upregulation of APOA1 gene expression in HepG2 cells is independent of de novo lipid biosynthesis. *Lipids Health Dis.* (2020) 19:144. doi: 10.1186/s12944-020-01309-4
57. Reeves HL, Zaki MY, Day CP. Hepatocellular carcinoma in obesity, type 2 diabetes, and NAFLD. *Dig Dis Sci.* (2016) 61:1234–45. doi: 10.1007/s10620-016-4085-6
58. Kim J, Kundu M, Viollet B, Guan KL. AMPK and mTOR regulate autophagy through direct phosphorylation of Ulk1. *Nat Cell Biol.* (2011) 13:132–41. doi: 10.1038/ncb2152
59. Singh R, Kaushik S, Wang Y, Xiang Y, Novak I, Komatsu M, et al. Autophagy regulates lipid metabolism. *Nature.* (2009) 458:1131–5. doi: 10.1038/nature07976
60. Shibata M, Yoshimura K, Furuya N, Koike M, Ueno T, Komatsu M, et al. The MAP1-LC3 conjugation system is involved in lipid droplet formation. *Biochem Biophys Res Commun.* (2009) 382:419–23. doi: 10.1016/j.bbrc.2009.03.039
61. Zhang Y, Sowers JR, Ren J. Targeting autophagy in obesity: from pathophysiology to management. *Nat Rev Endocrinol.* (2018) 14:356–76. doi: 10.1038/s41574-018-0009-1
62. Kitada M, Koya D. Autophagy in metabolic disease and ageing. *Nat Rev Endocrinol.* (2021) 17:647–61. doi: 10.1038/s41574-021-00551-9
63. Liu K, Zhao E, Ilyas G, Lalazar G, Lin Y, Haseeb M, et al. Impaired macrophage autophagy increases the immune response in obese mice by promoting proinflammatory macrophage polarization. *Autophagy.* (2015) 11:271–84. doi: 10.1080/15548627.2015.1009787
64. Wang W, Ballatori N. Endogenous glutathione conjugates: occurrence and biological functions. *Pharmacol Rev.* (1998) 50:335–56.
65. Floegel A, Stefan N, Yu Z, Mühlenbruch K, Drogan D, Joost HG, et al. Identification of serum metabolites associated with risk of type 2 diabetes using a targeted metabolomic approach. *Diabetes.* (2013) 62:639–48. doi: 10.2337/db12-0495
66. Palmer ND, Stevens RD, Antinozzi PA, Anderson A, Bergman RN, Wagenknecht LE, et al. Metabolomic profile associated with insulin resistance

and conversion to diabetes in the insulin resistance atherosclerosis study. *J Clin Endocrinol Metab.* (2015) 100:E463–8. doi: 10.1210/jc.2014-2357

Conflict of Interest: The authors declare that the research was conducted in the absence of any commercial or financial relationships that could be construed as a potential conflict of interest.

Publisher's Note: All claims expressed in this article are solely those of the authors and do not necessarily represent those of their affiliated organizations, or those of the publisher, the editors and the reviewers. Any product that may be evaluated in this article, or claim that may be made by its manufacturer, is not guaranteed or endorsed by the publisher.

frontiers | Frontiers in Nutrition

CLINICAL TRIAL
published: 02 May 2022
doi: 10.3389/fnut.2022.861880

Beneficial Effects of a Low-Glycemic Diet on Serum Metabolites and Gut Microbiota in Obese Women With *Prevotella* and *Bacteriodes* Enterotypes: A Randomized Clinical Trial

Haeng Jeon Hur[1†], Xuangao Wu[2†], Hye Jeong Yang[1], Min Jung Kim[1], Kyun-Hee Lee[1,3], Moonju Hong[1,3], Sunmin Park[2] and Myung-Sunny Kim[1,3*]*

[1] Food Functionality Research Division, Korea Food Research Institute, Wanju, South Korea, [2] Obesity/Diabetes Research Center, Department of Food and Nutrition, Hoseo University, Asan, South Korea, [3] Department of Food Biotechnology, Korea University of Science and Technology, Wanju, South Korea

OPEN ACCESS

Edited by:
Gratiela Gradisteanu Pircalabioru, University of Bucharest, Romania

Reviewed by:
Julio Plaza-Diaz, Children's Hospital of Eastern Ontario (CHEO), Canada
Lars Christensen, University of Copenhagen, Denmark

***Correspondence:**
Sunmin Park
smpark@hoseo.edu
Myung-Sunny Kim
truka@kfri.re.kr

[†] These authors have contributed equally to this work and share first authorship

Specialty section:
This article was submitted to Nutrition and Metabolism, a section of the journal Frontiers in Nutrition

Received: 25 January 2022
Accepted: 31 March 2022
Published: 02 May 2022

Citation:
Hur HJ, Wu X, Yang HJ, Kim MJ, Lee K-H, Hong M, Park S and Kim M-S (2022) Beneficial Effects of a Low-Glycemic Diet on Serum Metabolites and Gut Microbiota in Obese Women With Prevotella and Bacteriodes Enterotypes: A Randomized Clinical Trial. Front. Nutr. 9:861880. doi: 10.3389/fnut.2022.861880

Generalized healthy eating patterns may not benefit everyone due to different genetics and enterotypes. We aimed to compare the effects of a low-glycemic diet representing the Korean traditional balanced diet (Low-GID) and westernized diet as a control diet (CD) on anthropometry, serum metabolites, and fecal bacteria in a randomized clinical trial according to enterotypes. We recruited 52 obese women aged 30–50 years, and they consumed Low-GID and CD meals for 1 month, with a 1-month washout period, in a crossover randomized clinical trial. The Low-GID was mainly composed of whole grains with fish, vegetables, seaweeds, and perilla oil, whereas CD contained refined rice, bread, noodles, meats, and processed foods. Serum lipid profiles, metabolomics, serum short-chain fatty acids, and fecal bacteria were analyzed. The important variables influenced by Low-GID and CD were determined by SHAP value in the XGBoost algorithm according to *Bacteroides* (ET-B) and *Prevotella* (ET-P). Low-GID and CD interventions did not change the enterotypes, but they modified serum metabolites and some fecal bacterial species differently according to enterotypes. The 10-fold cross-validation of the XGBoost classifier in the ET-P and ET-B clusters was 0.91 ± 0.04 and 0.8 ± 0.07, respectively. In the ET-P cluster, serum L-homocysteine, glutamate, leucine concentrations, and muscle mass were higher in the CD group than in the Low-GID group, whereas serum 3-hydroxybutyric acid concentration was significantly higher in the Low-GID group than in the CD group ($p < 0.05$). In fecal bacteria, *Gemmiger formicilis, Collinsella aerofaciens*, and *Escherichia coli* were higher in the CD group than in the Low-GID group. In the ET-B cohort, serum tryptophan and total cholesterol concentrations were higher in the CD group than in the Low-GID group, whereas serum glutathione and 3-hydroxybutyric acid concentrations were significantly higher in the Low-GID group than in the CD group ($p < 0.05$). However, *Bifidobacterium longum* was higher in CD than Low-GID in the ET-B cluster, but serum butyric acid levels were higher

in the Low-GID than in the CD group. In conclusion, Low-GID can be recommended in obese women with both ET-P and ET-B enterotypes, although its efficacy was more effective in ET-P.

Clinical Trial Registration: [https://cris.nih.go.kr/cris/search/detailSearch.do/17398], identifier [KCT0005340].

Keywords: low-glycemic diet, fecal bacteria, insulin resistance, metabolites, enterotypes, low-cholesterol diet, 3-hydroxybutyric acid

INTRODUCTION

Various microorganisms exist in all human body parts, including the intestines, mouth, and skin. Most of these microorganisms are located in the large intestines with more than 4,000–10,000 different microorganisms, representing 3.5 million genes, much greater than human genes (1). The gut microbiota bidirectionally interact with humans as a host to influence human health (2). Age, gender, diet, nutrient intake, and lifestyles in the host modulate the gut microbiota community (2). Gut microbiota affect the host's aging, immunity, food digestion, and drug functions and produce various metabolites that affect the host's metabolism (1). Gut dysbiosis has been reported to be related to obesity, type 2 diabetes, dyslipidemia, Alzheimer's disease, autism, depression, and other diseases (3, 4). Dietary modification can maintain gut eubiosis to prevent metabolic diseases.

South Korea has developed its own characteristic diet for a long period (5). Like the Mediterranean diet, the health benefits of the Korean traditional balanced diet have also been paid attention to in promoting healthy diets in various countries. The Korean diet is characterized by a high proportion of whole grains, cooked vegetables, beans, seaweeds, fish, fermented beans, and vegetables (5). The health benefits of the Korean traditional balanced diet are potentially related to its cooking methods, diverse foods, and cooking oil, including sesame and perilla oil (5). According to the previous studies, the Korean traditional balanced diet has low glycemic, antioxidant, and anti-inflammatory properties (6, 7). With socioeconomic growth in South Korea, this traditional diet pattern has undergone a rapid transformation toward westernized diets (8), which are mainly composed of animal meat, processed foods, refined rice, flour, and sugar and are generally considered unhealthy, leading to metabolic diseases, such as obesity, diabetes, and atherosclerosis (9, 10).

People with different ethnicities have major enterotypes because they share similar long-term lifestyles, mainly diet patterns (11). Since changes in individual gut microbiota are challenging to study, human enterotypes need to be divided into three categories: *Prevotella*, *Bacteroides*, and *Ruminococcus* (12). According to the previous studies, the *Prevotella* enterotype is related to a high intake of carbohydrates, especially sugar, whereas the *Bacteroides* enterotype is involved in high meat intake (11). There are a few studies on the connection between the *Ruminococcus* enterotype and diet, where some have pointed out that *Ruminococcus* and *Bacteroides* enterotypes are not the discrete clusters but continuums (13). The Mediterranean diet is one of the world's recognized healthy diets with antioxidant and anti-inflammatory properties (14). However, Huttenhower et al. showed that the Mediterranean diet has a better effect on reducing the risk of cardiometabolic diseases in individuals without *Prevotella copri* in the gut, supporting the need for a personalized diet based on gut microbiota (15).

Obesity is growing in Asians, and it is related to modifying the dietary patterns to consume more refined rice, processed foods, meats, and less vegetables with economic growth. The dietary changes of diet may alter the gut microbiota related to increasing obesity incidence. The traditional Korean balanced diet may have a protective effect on obesity, but there is no randomized clinical study about its impact on weight loss by modulating gut microbiota according to the enterotypes. Therefore, we aimed to determine the weight loss effect of the traditional Korean diet, representing a low-glycemic and low-cholesterol diet, and westernized Korean diet on gut microbiota and metabolomics in obese women aged 30–50 years according to enterotypes, such as *Bacteroides* and *Prevotella*.

MATERIALS AND METHODS

Participants and Experimental Design

The Institutional Review Board approved the study protocol at CHA University (1044308-201801-HR-033-04), and the study was conducted under the Declaration of Helsinki. All participants provided written informed consent, and it was registered at the Korean Clinical Trial Registry (CRIS; trial number KCT0005340). We voluntarily recruited 54 obese women aged 30–50 with a body mass index (BMI) of $23 \leq$ body mass index ≤ 30. They did not take diabetes, hyperlipidemia, hypertension, or hyperlipidemia medications, and they did not have a food allergy. The study started on 4 November 2019 and ended on 28 May 2020, and this clinical study was conducted using a crossover design study.

The sample size was calculated based on a previous human study (16): a difference in the inflammatory index ≥ 1.3 was clinically significant at a level of $\alpha = 0.05$, power of 0.80, and standard deviation of 0.80. The sample size was 48 for each group in the crossover design trial, and participants were added considering a 10% dropout rate. The initial sample size was 54 participants in each group, and one participant from each group dropped out due to not signing for the informed content form.

In the first trial, 52 participants were randomly divided into two groups (each group $n = 26$) with random numbers generated

by a computer, and they were randomly and blindly allocated into westernized diet (control diet, CD) and Korean traditional balanced diet representing low-glycemic and low-cholesterol diet (Low-GID) groups with random numbers. They consumed the assigned diet for 4 weeks and then had a 4-week washout period. In the second trial, the diet was switched to the other diet, and the participants consumed their newly assigned diet (either CD or Low-GID) for 4 weeks, followed by a 4-week washout period. Low-GID and CD were prepared for 1,900 kcal/day, an estimated energy requirement for 30–50 women. According to the Low-GID and CD meal plans, meals with beverages and snacks were delivered to each participant's home. Participants were encouraged to maintain their lifestyle, physical activity level, and diet throughout the study period. However, alcohol consumption was restricted.

Experimental Diet

Each Low-GID and CD meal was cooked under the supervision of a dietician. The composition of the Low-GID and CD is presented in **Table 1** and complies with the Koreans' dietary reference intake. The calorie intake for each participant was approximately 1,900 kcal per day, the estimated energy requirement for one Korean woman aged 30–49 years. Both diet patterns were based on Korean meal types, including staple food, soup, kimchi, and three side dishes in each meal (5). The Low-GID included two servings of whole grains as a staple food, 1–2 servings of fish or poultry, two servings of cooked vegetables, one serving of kimchi, and one serving of fruits. They were cooked using traditional Korean cooking methods, such as boiling, steaming, blanching, and pickling. CD consisted of two servings of refined rice, bread, or noodles as staple foods, one to two servings of meats, two servings of uncooked vegetables, one serving of kimchi, and one serving of fruits. The Low-GID had tea, fruit tea, and soymilk while CD had coffee, juice, and milk. They were cooked fried, stir-fried, sautéed, or baked, and uncooked vegetables were served with salad dressing.

The glycemic index (GI) of foods in the Low-GID and CD was extracted from the International GI Table in 2021 (17). GI values of foods from Asian countries were used to calculate the GI of the meals. GI of the daily meal was calculated by the following equation: GI for daily intake = $\sum_{k=1}^{n}$(each food of GI × carbohydrate intake from the food)$_k$/total carbohydrate intake for one day) (18). K indicated the number of foods consumed for a day. Means and standard deviations were calculated for 28-day meals. A computer-assisted nutritional analysis program (CAN-pro-3.0; Korean Nutrition Society, Seoul, South Korea) was used to calculate the energy and nutritional intake of the 24-h intervention meal. The Low-GID was characterized by 65–68% carbohydrates (energy), 15% protein, and 17–20% fat. The CD was composed of 60–63% carbohydrates, 15% protein, and 24–26% fat. **Table 1** lists the two diets and their calorie intake.

TABLE 1 | Food and nutrient intake during the intervention.

Food group	Low-GID (n = 52)	CD (n = 52)	p-value[1]
Total grains (g)	240 ± 2.6[1]	195 ± 8.73	<0.0001
Whole grains (g)	196.8 ± 2.2	1.7 ± 0.72	<0.0001
Vegetables (g)	380 ± 2.9	261 ± 12.3	<0.0001
Fruits (g)	90.4 ± 0.9	86.9 ± 5.05	NS
Kimchi (g)	171 ± 4.2	109 ± 13.0	<0.0001
Fermented soybeans (g)	22.2 ± 0.2	12 ± 0.72	<0.0001
Soybeans and tofu (g)	76.8 ± 0.6	16.8 ± 1.44	<0.0001
Fishes and seafood (g)	57.8 ± 0.7	26.1 ± 1.44	<0.0001
Meats (g)	12.9 ± 0.1	30.9 ± 1.44	<0.0001
Seaweeds (g)	7.4 ± 0.1	4.8 ± 0.72	<0.0001
Nuts (g)	7.4 ± 0.1	2.3 ± 0.72	<0.0001
Perilla oil (g)	5.7 ± 0.1	0.3 ± 0.72	<0.0001
Glycemic index of meal	50.3 ± 3.55	68.1 ± 2.89	<0.0001
Energy (kcal)	1834 ± 106	1859 ± 60.5[1]	0.1385
Carbohydrates (En %)	67.2 ± 0.50	62.4 ± 0.40	<0.0001
Dietary fiber (g)	36.7 ± 2.22	21.3 ± 0.83	<0.0001
Protein (En %)	13.0 ± 0.17	14.0 ± 0.10	<0.0001
Fat (En %)	19.5 ± 0.36	24.1 ± 0.33	<0.0001
Saturated fatty acids (En %)	2.45 ± 0	6.3 ± 0.48	<0.0001
MUFA (En %)	2.94 ± 0	5.3 ± 0.48	<0.0001
PUFA (En %)	4.91 ± 0.49	5.3 ± 0.48	NS
Cholesterol (mg)	146 ± 9.32	272 ± 7.84	<0.0001

Values are presented as means ± standard deviations.
[1]Statistical analysis with a two-sample t-test.
Low-GID, a low-glycemic diet representing Korean traditional balanced diet; CD, westernized diet; En %, energy percent; MUFAs, monounsaturated fatty acids; PUFAs, polyunsaturated fatty acids.

Primary Outcome Measurements

The measurements were taken in the Metabolic Research Unit of the Korea Food Research Institute. Primary outcome measurements included anthropometry and metabolites, including lipid profiles in the circulation. BMI was calculated by dividing body weight by height squared (kg/m^2). Muscle mass and fat mass were measured using InBody 4.0 (Cheonan, South Korea). Blood pressure was assessed using an automatic blood pressure monitor on the left arm. Total cholesterol, high-density lipoprotein (HDL), low-density lipoprotein (LDL), triglycerides, and plasma glucose levels were measured using a Hitachi 7600 Autoanalyzer (Hitachi Ltd., Tokyo, Japan). Serum high-sensitive C-reactive protein (CRP) and insulin concentrations were analyzed using an ELISA kit (Thermo Fisher Scientific, Waltham, MA, United States).

For metabolomic analysis, pretreated serum was mixed with cold acetonitrile and shaken for 30 min at 4°C. The supernatants were separated after centrifugation at 6,000 × g for 10 min. The supernatant was collected, and 20% caffeine methanol solution was added. The metabolites of the mixture were measured using ultraperformance liquid chromatography and quadrupole time-of-flight (UPLC-Q-TOF) method using an Acquity UPLC System (Waters, Milford, MA, United States). The stationary phase was Acquity UPLC BEH C18 (2.1 mm × 100 mm, 1.7 μm) chromatographic column, and the mobile phase was an aqueous solution and acetonitrile solution containing 0.1% formic acid. The separation program temperature was 40°C, and the flow rate was 0.35 ml/min (19).

Serum short-chain fatty acid (SCFA) measurement was based on adding a solvent mixture of n-butanol, tetrahydrofuran, and acetonitrile (Duksan, Ansan, South Korea) to the serum. The

serum was completely vortexed and mixed for 1 min, separated at the top of the supernatant after centrifugation at 7,500 × *g*, 15 min, and 4°C, and the separated upper layer was filtered with a 0.45-μm microporous filter. After filtration, it was injected into a PerkinElmer Clarus 680 GAS Chromatograph (Waltham, MA, United States). The stationary phase was an Elite-FFAP 30 m × 0.25 mm × 0.25 μm capillary column, and the mobile phase was high-purity helium. The column temperature program was established by increasing from 100 to 180°C at 10°C/min and then by elevating from 180 to 220°C at 20°C/min. The hydrogen, air, and helium flow rates were 45 ml/min, 450 ml/min, and 20 ml/min, respectively (20).

Secondary Outcomes

The fecal bacteria community was measured by next-generation sequencing (NGS). We used the QIAamp Power Fecal DNA Kit (12830-50; QIAGEN, Germany) to extract total DNA from feces. Using the KAPA HiFi HotStart Ready Mix PCR Kit (KK2602; Kapa Biosystems, United States), amplification was performed under the following conditions of PCR: 94°C for 3 min; 35 cycles at 94°C for 15 s, 55°C for 45 s, and 72°C for 1 min; and then extended at 72°C for 8 min. The 16S rRNA universal amplification primers used were rRNA genes B341F (5′-CCTACGGGNGGCWGCAG-3′) and B805R (5′-GACTACHVGGGTATCTAATCC-3′) (20). Electrophoresis was conducted on an agarose gel to confirm amplification. The amplified 16S rRNA was purified using AMPure beads (Beckman Coulter, Brea, CA, United States), and its head and tail were labeled using the Nextera XT Index Kit (Illumina, San Diego, CA, United States). The sample was subjected to the following PCR conditions: 95°C for 3 min; 8 cycles at 95°C for 30 s, 55°C for 30 s, and 72°C for 30 s; 72°C for 5 min; and then kept at 4°C. The labeled DNA was purified and sent to Macrogen Inc. (Seoul, South Korea) for sequencing.

Fecal Bacterial Community Analysis

After running MiSeq, 204 pairs of paired-end sequencing files were obtained, with 5,000,352 paired-end original sequences. Using the Mothur program (version 1.43.0) (21), 2,500,176 sequences were obtained after merging the double-ended sequences with the make.contigs command, the sequences were aligned with the SILVA v 1381 database, and non-target sequences, such as mitochondria, archaea, fungi, and unknown sequences, were removed. The remaining sequences were preclustered, and chimeras were eliminated using the chimera.vsearch command. The sequences were then clustered, with 97% similarity. The generated FASTA files were annotated according to the Greengenes reference taxonomy (22). Finally, 40,289 representative sequences were obtained for the subsequent analyses.

The correlation between serum concentration of SCFA (acetic acid, propionic acid, and butyric acid) and normalized fecal bacteria at the genus level was assessed using the Hmice package in the R program according to the Low-GID and CD.

Safety Outcome Measurements

Clinical conditions, including adverse reactions, were evaluated before and after interventions. Serum alanine aminotransferase (ALT), aspartate aminotransferase (AST), white blood cells (WBCs), and platelet concentrations were measured.

XGBoost Classifier Training and Shapley Additive Explanations Interpreter

To study the difference between the Low-GID and the CD effects according to enterotypes *Bacteroides* (ET-B) and *Prevotella* (ET-P), we used the Python-based XGBoost (version 1.3.3) package to train the characteristic features of the Low-GID and CD as classification devices in the ET-P and ET-B clusters (23). The characteristic features included the relative abundance of fecal bacteria at the species level, anthropometric variables, serum biochemical, and metabolic variables. A random grid search was used to find the best hyperparameter settings, and the number of search times was 1,000 in the XGBoost algorithm (24). We first trained the XGBoost algorithm with all variables to find the top 10 most important variables and then used these ten variables to retrain the XGBoost algorithm. Because the sample size was small, we used all of them to train the classifiers (Low-GID and CD) and then used 10-fold cross-validation to evaluate the accuracy of the selected model. The 10-fold cross-validation was calculated using the cross_val_score function in the sklearn package. The function splits the original training data into ten subsets and alternately used nine of them as training data and one as test data for iterating ten times. Finally, ten sets of data were generated to obtain the mean and variance, which were used as the final accuracy result of the model. Then, 0.9 of 10-fold cross-validation indicated that the accuracy of the selected model was 90%.

Shapley Additive exPlanations is a method used to explain the output of the XGBoost model (25). We used the SHAP (0.39.0) package to calculate the SHAP value of each variable relative to the classifier (diet types) and observed the importance of the variable and its impact on the classification.

The separation of Low-GID and CD groups in the included variable of the XGBoost model was determined by principal component analysis (PCA) in total participants, ET-B, and ET-B using FactoMineR and Factoextra packages in the R program.

Statistical Analysis

Mothur was used to perform downstream analysis of fecal bacteria; for β-diversity measurement, clearcut command in Mothur was used to construct a phylogenetic tree, unifrac.unweighted command was applied to calculate the unweighted UniFrac distance matrix, and then principal coordinate analysis (PCoA) was used for visualization. Analysis of molecular variance (AMOVA) command was conducted to compare a significant difference among β-diversity groups. The α-diversity metric was calculated with a summary.single command in the Mothur, and the Chao1 and Shannon indices were obtained. The enterotype analysis of each participant was acquired from the website[1] (12). Linear mixed model analysis

[1]https://enterotype.embl.de/enterotypes.html

was performed to analyze the differences between the Low-GID and CD in a crossover design study using the LME function of the NLE package of R-studio, and the ggplot2 package was used for visualization. The data are expressed as the mean ± standard deviation (SD), and statistical significance was set at $p < 0.05$.

RESULTS

General Characteristics of the Participants According to Enterotypes

Age was significantly different by enterotypes of the participants but not by dietary types (**Table 2**). Anthropometric measurements, such as body weight, BMI, waist circumferences, lean body mass, and fat mass, were not significantly different from the dietary types and enterotypes of the participants (**Table 2**). Metabolic parameters that include blood pressure, white blood cell counts, serum triglyceride, total cholesterol, HDL, LDL, glucose, insulin, and CRP concentrations did not differ by dietary types and enterotypes of the participants (**Table 2**). Also, the Homeostatic model assessment for insulin resistance (HOMA-IR) and HOMA for β-cell function (HOMA-B) were not different.

Primary Outcomes According to Enterotypes

Body mass index was lower in the Low-GID group than in the CD group in both enterotypes. However, muscle mass was lower in the Low-GID group than in the CD group. In the ET-P cluster, muscle mass was significantly higher in the Low-GID group than in the CD group ($p < 0.05$) (**Table 3**).

In both ET-P and ET-B clusters, serum total cholesterol and triglyceride concentrations were lower in the Low-GID group than in the CD group. However, serum LDL cholesterol concentrations in the Low-GID group were lower than those in the CD group in ET-B, but not in the ET-P group ($p < 0.05$) (**Table 3**). The atherogenic index calculated by serum HDL and LDL cholesterols did not differ between the Low-GID and CD in both enterotypes. Furthermore, there was no significant difference in serum CRP concentrations, HOMA-IR, HOMA-B, and quantitative insulin-sensitivity check index (QUICKI) between the Low-GID and CD in both enterotypes (**Table 3**). However, HOMA-IR tended to be lower in the Low-GID group than in the CD group in the *Prevotella* enterotype ($p = 0.08$).

In the ET-P cluster, serum concentrations of leucine, branched-chain amino acids (BCAAs), γ-glutamylisoleucine, tryptophan, tyrosine, glycine, L-homocysteine, and uric acid were lower in the Low-GID group than in the CD group (**Table 4**). In contrast, serum isoleucine and 3-hydroxybutyric acid concentrations in the Low-GID group were higher than those in the CD group ($p < 0.05$) (**Table 4**). In the ET-B cluster, serum BCAA, tryptophan, and uridine concentrations were significantly lower in the Low-GID group than in the CD group, whereas serum glutathione and 3-hydroxybutyric acid concentrations in the Low-GID group were higher than those in the CD group ($p < 0.05$). Serum SCFA concentrations did not differ between the Low-GID and CD in both enterotypes, but serum butyric acid concentrations were higher in the Low-GID than in the CD only in the ET-B cluster (**Table 4**).

Secondary Outcomes: Changes of Enterotypes

We used the relative abundance at the genus level to distinguish enterotypes. The fecal bacteria were separated into two enterotypes, ET-1 and ET-2 (**Figure 1A**). The dominant bacteria in the ET-1 group were *Bacteroides* enterotype (ET-B). *Bacteroides* mainly included *Bacteroides uniformis* and unclassified *Bacteroides*, which included various *Bacteroides* species but were not identified. The most abundant dominant bacteria at the genus level in the ET-2 group were *Prevotella* (ET-P). In ET-P, the most dominant *Prevotella* was *P. copri*, and only a small amount of *Prevotella stercorea* was included at the species level (**Figures 1B,C**). To explore the effect of dietary intervention on enterotype, we compared individual enterotype changes before and after diet intervention. After the Low-GID intervention, the ET-P proportion among 52 patients increased from 43.4 to 54.7%, and the ET-B proportion decreased from 56.6 to 45.3%. After the CD diet, the ET-B proportion decreased from 61.5 to 51.9%, whereas the ET-P proportion increased from 38.5 to 48.1% (**Figure 1D**). The results indicated that both diets increased the *Prevotella* enterotype.

Secondary Outcomes: Changes in α-Diversity, β-Diversity, and Fecal Bacteria

There was no significant difference between the Chao and Shannon indices of α-diversity in the participants with Low-GID and CD in all participants (**Figure 2A**; $p > 0.05$). The Chao and Shannon indices that represent α-diversity did not significantly differ between the Low-GID and CD in each ET-P and ET-B cluster. The PCoA chart for β-diversity calculated from the weighted-UniFrac distance method showed significant differences in fecal bacteria between Low-GID and CD in the AMOVA in all participants ($p < 0.05$; **Figure 2B**). However, there was no significant difference in β-diversity between the Low-GID and CD in the ET-P and ET-B clusters ($p > 0.05$; **Figure. 2B**).

To compare the fecal bacterial differences between the Low-GID and CD at the genus level, we intercepted the total counts of more than 400 bacterial genera. In all participants, the Low-GID exhibited a higher abundance of *Prevotella* and *Faecalibacterium* than CD, whereas CD intervention showed a higher abundance of *Bifidobacterium* and *Parabacteroides* than the Low-GID (**Figure 2C**). However, the differences in fecal bacteria at the genus level were not significantly different between the Low-GID and CD groups. It was due to the interaction of the participants' enterotypes with the dietary intervention to modulate fecal bacteria differently. In the ET-P cluster, the Low-GID intervention exhibited a higher abundance of *Prevotella*, whereas the CD group had a higher relative abundance of *Bacteroides* and *Bifidobacterium* (**Figure 2C**). However, there were no

TABLE 2 | Baseline characteristics in a low-glycemic diet (Low-GID) representing Korean traditional balanced diet and westernized diet as a control diet (CD) according to enterotypes.

	***Prevotella* enterotype**		***Bacteroides* enterotype**	
Variable	**Low-GID (*n* = 27)**	**Control-diet (*n* = 26)**	**Low-GID (*n* = 25)**	**Control-diet (*n* = 26)**
Age (years)	40.3 ± 1.04[a]	40.4 ± 1.01[a]	37 ± 1.08[b]	37 ± 1.11[b]**
Weight (kg)	65.3 ± 1.16	64.7 ± 0.97	65.6 ± 1.35	65.9 ± 1.5
Body mass index (kg/m^2)	25.4 ± 0.36	25.2 ± 0.32	25.5 ± 0.32	25.6 ± 0.38
Waist circumferences (cm)	79.6 ± 1.26	78.9 ± 1.07	81.2 ± 1.16	81.7 ± 1.09
Lean body mass (kg)	21.8 ± 0.43	21.7 ± 0.38	22 ± 0.5	22.4 ± 0.53
Fat mass (%)	38 ± 0.72	38.2 ± 0.71	38.4 ± 0.75	38.2 ± 0.85
Systolic blood pressure (mmHg)	118 ± 2.34	112 ± 2.46	116 ± 2	116 ± 1.98
Diastolic blood pressure (mmHg)	72.5 ± 1.27	73.2 ± 1.82	75 ± 1.24	74.9 ± 1.29
White blood cell ($\times 10^3/\mu$l)	5.85 ± 0.31	5.69 ± 0.23	5.86 ± 0.24	5.62 ± 0.28
Platelet ($\times 10^3/\mu$l)	24.6 ± 0.9	23.9 ± 0.77	25.6 ± 1.05	26.8 ± 0.97
Serum triglyceride (mg/dL)	90.3 ± 9	93.9 ± 9.47	111 ± 12.3	99 ± 11.7
Serum total cholesterol (mg/dL)	188 ± 6.25	187 ± 6.39	183 ± 5.81	178 ± 6.15
Serum HDL-C (mg/dL)	61.2 ± 2.88	61.7 ± 3.2	59.7 ± 2.64	60.5 ± 3.28
Serum LDL-C (mg/dL)	109 ± 5.82	106 ± 5.41	101 ± 5.95	98.3 ± 5.77
Fasting plasma glucose (mg/dL)	97 ± 1.21	97.2 ± 1.65	98.7 ± 1.62	97.9 ± 1.52
Fasting plasma Insulin (mU/L)	10.2 ± 0.72	9.37 ± 0.75	10.6 ± 0.72	10.3 ± 0.69
HOMA-IR	2.46 ± 0.18	2.26 ± 0.19	2.58 ± 0.21	2.54 ± 0.19
HOMA-B	110 ± 7.48	100 ± 6.99	112 ± 7.43	108 ± 7.33
Serum CRP (mg/dL)	1.13 ± 0.12	1.25 ± 0.23	2.82 ± 1.89	2.16 ± 0.62

Values are presented as means ± standard deviation.
HDL-C, high-density lipoprotein cholesterol; LDL-C, low-density lipoprotein cholesterol; HOMA-IR, homeostatic model assessment for insulin resistance; HOMA-B, HOMA for β-cell function; CRP, high-sensitive C-reactive protein.
***Significantly different by enterotype using two-way ANOVA with an interaction term at $p < 0.01$.*
[a,b]Means in the same row with different superscript letters were significantly different by Tukey's test at $p < 0.05$.

TABLE 3 | Anthropometric and serum biochemical index of the participants according to *Prevotella* and *Bacteroides* enterotypes after the intervention of a low-glycemic diet (Low-GID) representing Korean traditional balanced diet and westernized diet as control diet (CD).

	***Prevotella* enterotype**			***Bacteroides* enterotype**		
	Low-GID (*n* = 27)	**CD (*n* = 26)**	***p*-value[1]**	**Low-GID (*n* = 25)**	**CD (*n* = 26)**	***p*-value[2]**
Body mass index	24.7 ± 0.33	25.1 ± 0.33	<0.0001	25.0 ± 0.37	25.3 ± 0.37	0.04
Waist circumferences (cm)	77.6 ± 1.04	79.1 ± 1.05	0.16	78.6 ± 1.02	79.8 ± 1.01	0.16
Muscle mass (%)	21.5 ± 0.38	21.9 ± 0.38	<0.0001	21.9 ± 0.48	22.0 ± 0.48	0.58
Body fat (%)	37.6 ± 0.66	37.3 ± 0.66	0.17	37.2 ± 0.88	37.6 ± 0.87	0.49
Serum total cholesterol (mg/dL)	160 ± 5.25	173 ± 5.29	0.001	153.8 ± 5.80	169.4 ± 5.76	0.007
Serum triglyceride (mg/dL)	74.9 ± 7.76	90.93 ± 7.84	0.018	71.8 ± 7.44	87.0 ± 7.35	0.04
Serum HDL (mg/dL)	52.0 ± 2.60	56.9 ± 2.62	0.005	51.2 ± 1.77	55.1 ± 1.75	0.005
Serum LDL (mg/dL)	92.8 ± 4.48	97.8 ± 4.53	0.16	88.3 ± 5.42	96.9 ± 5.39	0.02
Atherogenic index[1]	2.20 ± 0.141	2.19 ± 0.142	0.87	2.07 ± 0.15	2.18 ± 0.15	0.29
Serum CRP (mg/dL)	1.11 ± 0.03	1.18 ± 0.16	0.36	1.71 ± 0.40	1.20 ± 0.40	0.37
HOMA-IR	1.58 ± 0.14	1.85 ± 0.12	0.08	1.78 ± 0.21	1.79 ± 0.20	0.97
HOMA-B	82.2 ± 6.88	95.7 ± 7.00	0.11	81.6 ± 6.85	88.7 ± 6.73	0.47
QUICKI	0.36 ± 0.005	0.35 ± 0.005	0.12	0.36 ± 0.005	0.36 ± 0.004	0.40

Values are presented as means standard deviation.
HDL, high-density lipoprotein cholesterol; LDL, low-density lipoprotein cholesterol; CRP, C-reactive protein; HOMA-IR, homeostatic model assessment for insulin resistance; HOMA-B, HOMA for β-cell function; QUICKI, quantitative insulin-sensitivity check index; atherogenic index: the ratio of HDL and LDL.
[1,2]Statistical difference between K-diet and CD in Prevotella enterotype[1] and Bacteroides enterotype[2] using a linear mixed model for crossover design.

changes in the relative abundance of *Prevotella* between Low-GID and CD groups in the ET-B cluster, whereas Low-GID increased the relative abundance of *Bacteroides* and *Faecalibacterium* but decreased that of *Bifidobacterium* (**Figure 2C**). Therefore, Low-GID and CD modulate the fecal bacterial community differently, whereas Low-GID increases *Bacteroides* and *Faecalibacterium* but suppresses *Bifidobacterium*.

TABLE 4 | Serum metabolites of the participants according to *Prevotella* and *Bacteroides* enterotypes after a low-glycemic diet (Low-GID) representing Korean traditional balanced diet and westernized diet as a control diet (CD).

		***Prevotella* enterotype**			***Bacteroides* enterotype**		
		Low-GID (*n* = 27)	**CD (*n* = 26)**	***P*-value[1]**	**Low-GID (*n* = 25)**	**CD (*n* = 26)**	***P*-value[2]**
Amino acid	Valine	42.2 ± 5.99	53.1 ± 6.11	0.08	37.2 ± 5.29	47.5 ± 5.21	0.08
	Leucine	279 ± 12.4	316 ± 12.6	0.01	262 ± 11.5	284 ± 11.3	0.10
	Isoleucine	14.9 ± 1.67	13.7 ± 0.47	0.02	13.0 ± 0.42	12.4 ± 0.42	0.16
	BCAA[a]	337 ± 13.5	381 ± 13.8	0.01	313 ± 12.4	343 ± 12.3	0.03
	γ-glutamylisoleucine	45 ± 6.41	65 ± 6.58	0.34	43.5 ± 6.99	52.0 ± 6.87	0.36
	Glutamate	9.00 ± 2.65	16.3 ± 2.71	0.07	7.82 ± 3.03	14.8 ± 2.98	0.07
	Glutamine	227 ± 7.32	236 ± 7.44	0.23	226 ± 8.99	222 ± 8.87	0.66
	Arginine	415 ± 57.8	531 ± 59.0	0.16	344 ± 49.0	391 ± 48.0	0.46
	Tryptophan	7,526 ± 253	8,607 ± 257	0.001	7,359 ± 215	7,849 ± 212	0.02
	Tyrosine	823 ± 29.9	971 ± 30.4	0.001	892 ± 34.8	911 ± 34.2	0.64
	Glycine	19.4 ± 0.78	23.1 ± 0.80	0.0003	19.0 ± 1.06	20.2 ± 0.91	0.30
	L-homocysteine	21.6 ± 16.8	73.3 ± 17.0	0.003	31.5 ± 16.8	43.2 ± 16.6	0.41
	Creatine	2187 ± 112	2331 ± 114	0.31	2071 ± 206	2381 ± 202	0.30
	Glutathione	43.6 ± 5.36	29.5 ± 5.47	0.08	39.8 ± 5.25	23.9 ± 5.16	0.04
Carnitines	Carnitine	9,572 ± 841	11,694 ± 857	0.09	9,637 ± 848	10,685 ± 832	0.35
	Short acylcarnitine[b]	1,796 ± 198	1,979 ± 202	0.52	1,684 ± 180	1,729 ± 176	0.83
	Long acylcarnitine[c]	38,716 ± 3390	37,184 ± 3428	0.75	36,333 ± 3824	37,388 ± 3757	0.23
Nucleosides	Uric acid	11,601 ± 424	12,986 ± 432	0.03	11,690 ± 518	12,071 ± 512	0.40
	Uridine	110 ± 5.45	119 ± 5.57	0.25	107 ± 4.24	121 ± 4.19	0.003
Organic acid	2-ketobutyric acid	199 ± 16.9	238 ± 16.9	0.12	202 ± 16.4	221 ± 16.2	0.39
	Pyruvic acid	218 ± 7.66	230 ± 7.75	0.08	214 ± 8.28	227 ± 8.17	0.15
	3-hydroxybutyric acid	15.0 ± 2.78	5.51 ± 2.82	0.002	17.4 ± 2.66	8.20 ± 2.62	0.02
	Isocitric acid	5,876 ± 213	5,983 ± 216	0.54	5,720 ± 226	5,979 ± 223	0.24
SCFA	Acetic acid	137 ± 12.9	145 ± 12.9	0.49	141 ± 8.9	135 ± 16.3	0.69
	Propionic acid	14.3 ± 0.8	14.7 ± 1.07	0.74	13.5 ± 0.63	13.4 ± 1.18	0.94
	Butyric acid	11.1 ± 0.52	10.8 ± 0.55	0.57	12.4 ± 0.64	10.6 ± 0.68	0.06

[a] *BCAA is obtained by adding valine, leucine and isoleucine.*
[b] *Short is obtained by adding propionyl carnitine, isobutyryl carnitine, isovaleryl carnitine, valeryl carnitine, and hexanoyl carnitine.*
[c] *Long is obtained by adding palmitoyl carnitine and oleoyl carnitine.*
BCAA, branched-chain amino acids; short: acylcarnitines of short-chain fatty acid; long: acylcarnitines with long-chain fatty acid.
[1,2] *Statistical difference between K-diet and CD in Prevotella enterotype[1] and Bacteroides enterotype[2] using a linear mixed model for crossover design.*

The correlation between serum concentrations of SCFA and fecal bacteria in the genus level is shown in **Supplementary Figure 1**. Although serum butyric acid concentration was higher in CD, the Low-GID showed a higher positive association of fecal bacteria with serum butyric acid concentration and lower serum acetic acid concentration.

A Novel Model for Low-Glycemic Diet and Control Diet From Biochemical and Anthropometric Parameters, Serum Metabolites, and Gut Microbiota Using Machine-Learning Classifier

We used the relative abundance of intestinal microbes at the species level, anthropometric and biochemical parameters, and serum metabolomics as the features to train the XGBoost classification models to find a novel model to compare Low-GID and CD diet according to ET-P, ET-B, and total participants. The variables were sorted from top to bottom with the relative importance of the SHAP value to explain the Low-GID and CD effects in the novel model. After a random grid search of the features in the XGBoost algorithm, the classifiers set at max_depth = 23, n_estimators = 840, and learning_rate = 1.16. The 10-fold cross-validation accuracy was 0.81 ± 0.03, suggesting that the model had an accuracy of approximately 81% to explain the comparison of Low-GID and CD in all participants. According to the relative importance of the feature using SHAP, the model included serum L-homocysteine, *Bifidobacterium longum*, serum tryptophan, serum glutathione, serum 3-hydroxybutyric acid, serum BCAA, muscle mass, *Gemmiger formicilis*, *Blautia obeum,* and serum uric acid in total participants (**Figure 3A**). CD increased serum tryptophan, serum BCAA concentrations, muscle mass, and *Gemmiger formicilis* compared to Low-GID, whereas serum L-homocysteine concentrations, *Bifidobacterium longum,* and *Gemmiger formicilis* were lower than in Low-GID. However, serum glutathione and 3-hydroxybutyrate concentrations were higher in the Low-GID than the CD in all participants using the SHAP model (**Figure 3A**). The PCA showed the well-separation of Low-GID and CD in the SHAP model of total participants:

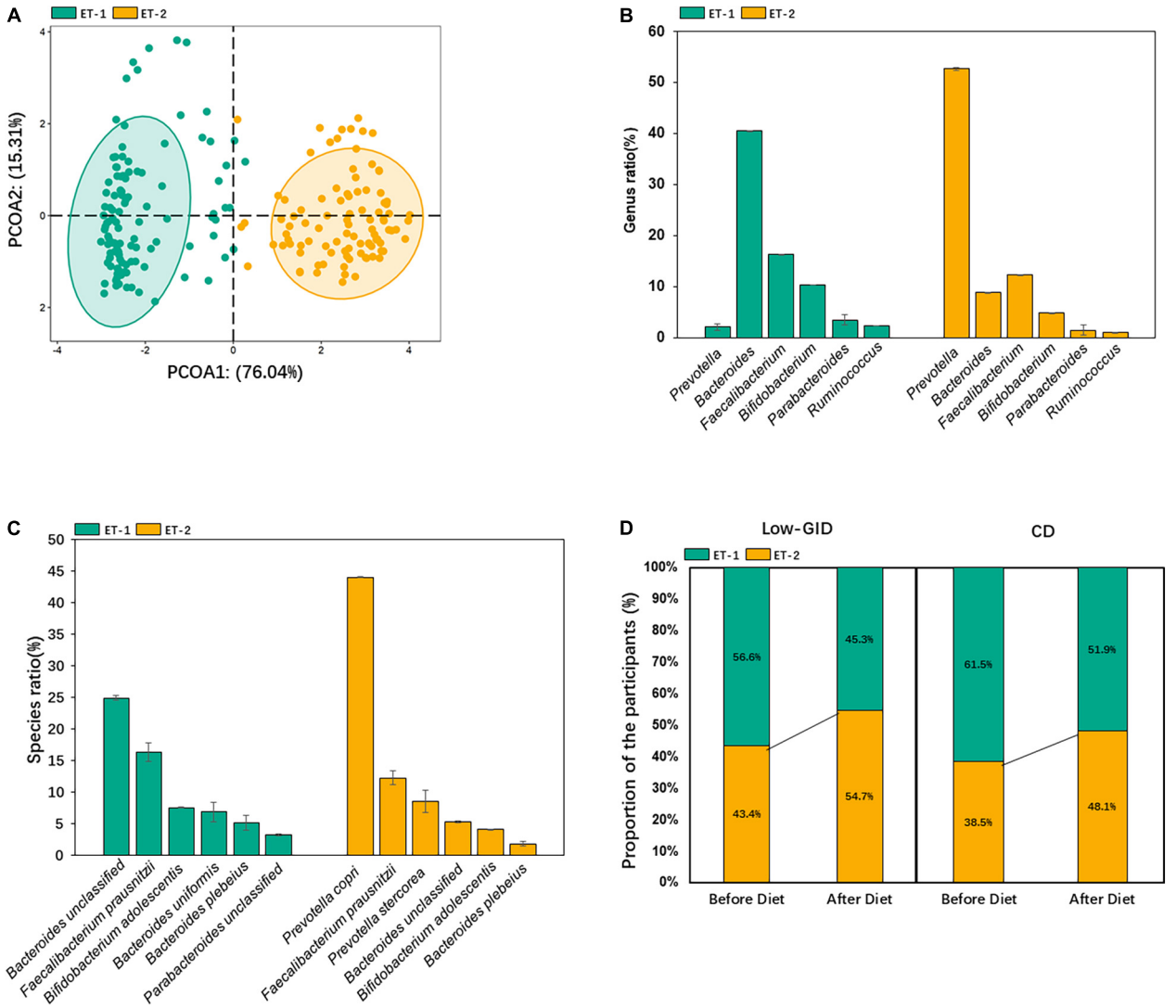

FIGURE 1 | Classification of enterotypes in the participants. **(A)** Classification map based on the principal coordinates of enterotype classification at the genus level. **(B)** The relative abundance of dominant bacteria at the genus level of each enterotype. **(C)** The relative abundance of dominant bacteria at the species level of each enterotype. **(D)** Changes of enterotype after the intervention of host diet.

PCA1 and PCA2 explained the variance of Low-GID and CD by 22.5 and 14.9%, respectively (**Figure 3B**).

The XGBoost classifier settings of the ET-P queue from the random grid search were as follows: max_depth = 84, n_estimators = 680, and learning_rate = 0.32. The 10-fold cross-validation accuracy was 0.91 ± 0.04, indicating approximately 91% accuracy of the SHAP model in the ET-P cluster. According to the relative importance of the feature using SHAP, the model included *Gemmiger formicilis,* serum L-homocysteine, *Collinsella aerofaciens,* serum 3-hydroxybutyric acid, serum glycine, serum glutamate, muscle mass, serum leucine concentrat*ions, Escherichia coli*, and *Bifidobacterium longum* in the ET-P cluster (**Figure 3C**). Among the ET-P cluster, CD increased *Gemmiger formicilis, Collinsella aerofaciens,* serum glycine, and muscle mass compared to the Low-GID, whereas serum L-homocysteine and serum glutamate levels decreased and serum 3-hydroxybutyric acid levels increased in the Low-GID compared to the CD using the SHAP model (**Figure 3C**). In the SHAP model of ET-P, Low-GID and CD showed better separation by the PCA than in the total participants: PCA1 and PCA2 explained the variance of Low-GID and CD by 24.5 and 18.3%, respectively (**Figure 3D**).

From the random grid search, the XGBoost classifier settings of the ET-B cluster included max_depth = 78, n_estimators = 580, and learning_rate = 0.01. The 10-fold cross-validation accuracy was 0.8 ± 0.07, suggesting that the model had approximately 80% accuracy in distinguishing the metabolic effects between the Low-GID and CD. Based on the relative importance of SHAP, the model contained serum L-homocysteine, serum butyric acid, serum 3-hydroxybutyric acid, *Bifidobacterium*

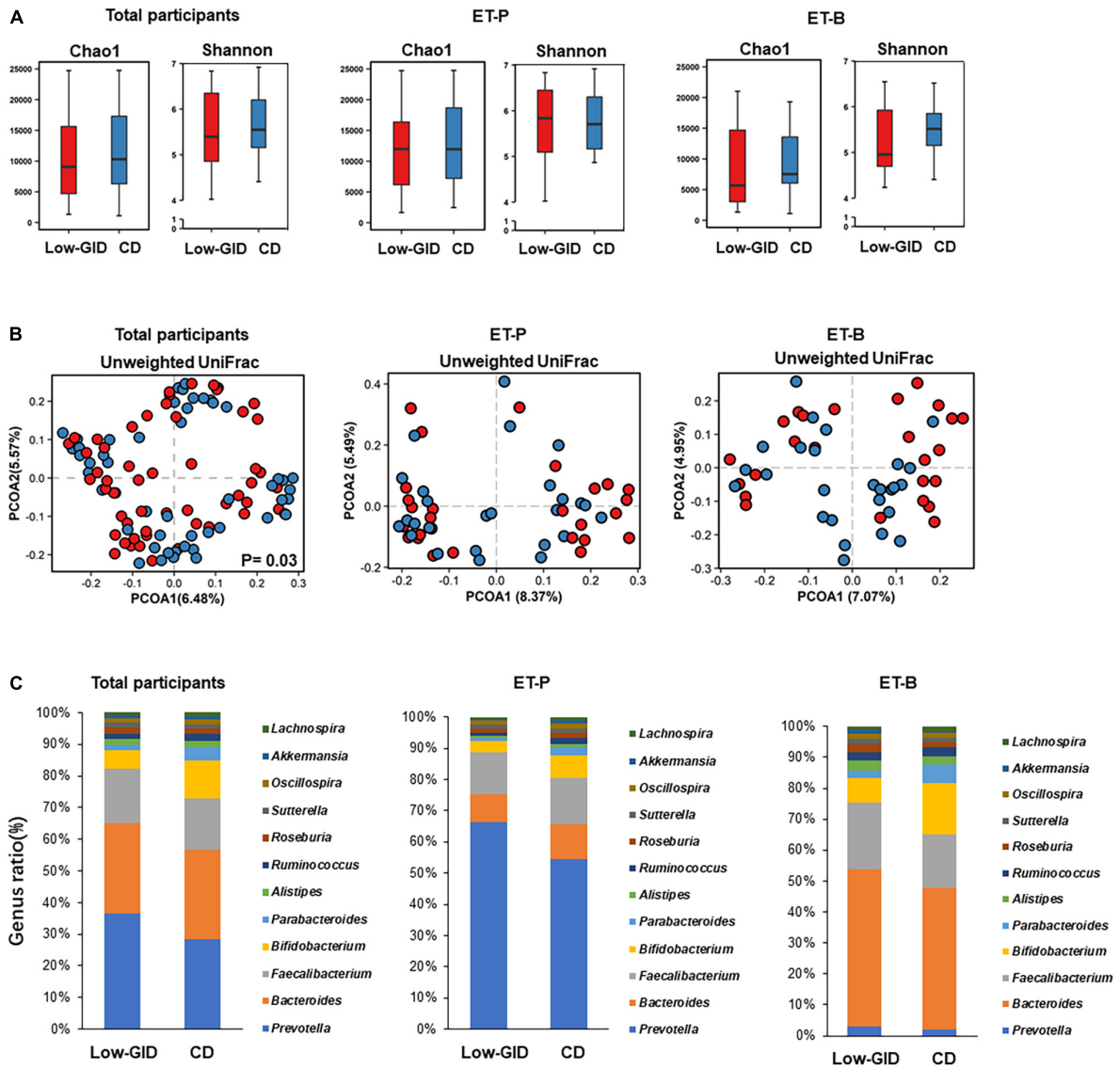

FIGURE 2 | The overall difference of intestinal microbes in the *Prevotella* and *Bacteroides* intestinal clusters after the Korean traditional balanced diet (Low-GID) and the westernized Korean diet, the control diet (CD), interventions. **(A)** The α-diversity difference between Chao and Shannon indices. **(B)** PCOA based on unweighted UniFrac. **(C)** Differences in the relative abundance of intestinal microbes at the genus level. Gut microbes with a total count of less than 400 and unclassified ones were truncated. A linear mixed model for α-diversity was used for statistical analysis; a significant difference is represented by $p < 0.05$. Using AMOVA for α-diversity's statistical analysis, there is a significant difference when $p < 0.05$.

longum, serum valine, serum isocitric acid, serum glutathione, serum isoleucine, serum total cholesterol concentrations, and *Escherichia coli* (**Figure 3E**). In the ET-B cluster, CD increased serum L-homocysteine, *Bifidobacterium longum*, serum valine, serum isocitric acid, serum total cholesterol concentrations, and *Escherichia coli* compared to the Low-GID. In contrast, serum butyric acid, serum 3-hydroxybutyric acid, serum glutathione, and serum isoleucine concentrations were higher in the Low-GID group than in the CD group (**Figure 3E**). In the SHAP model of ET-B, Low-GID and CD were closely clustered by the PCA: PCA1 and PCA2 explained the variance of Low-GID and CD by 18.5 and 15.8%, respectively (**Figure 3F**).

DISCUSSION

Based on community-based intestinal microbiota, extensive research has been conducted on enterotypes of different populations in different countries (26). Although most populations exhibit three enterotypes, the dominant intestinal microbial species differ due to diet and environmental reasons. *Prevotella* and *Bacteroides* are the discrete enterotypes that have been consistently identified in various studies (25–27). However, the *Ruminococcus* enterotype is not separated from the *Bacteroides* one (13). In this study, the *Ruminococcus* enterotype was not clustered as one enterotype, and all participants were

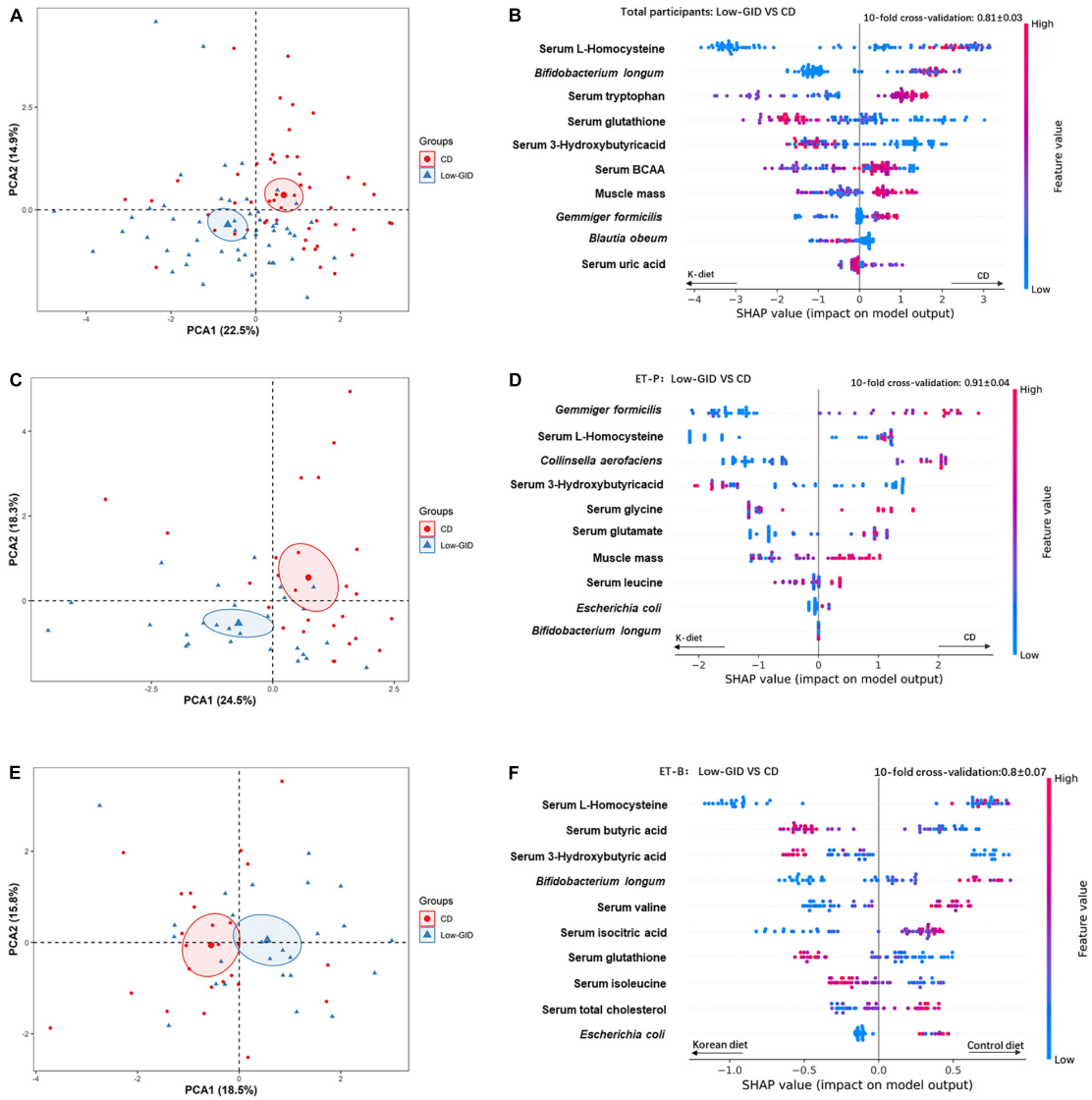

FIGURE 3 | XGBoost classification model variable interpretation of Korean traditional balanced diet (Low-GID) and control diet (CD) based on the overall SHAP, *Prevotella*, and *Bacteroides* clusters. The 10-fold cross-validation is expressed in terms of mean ± SD. In the figure, the left side of the scattered dots to the 0-scale line is the Korean traditional diet classification, and the right side is the control diet classification. The height of the color represents the size of the variable. **(A)** PCA analysis of CD and Low-GID in the overall cohort. **(B)** XGBoost categorical variable interpretation, in the overall cohort. **(C)** PCA analysis of CD and Low-GID in the Prevotella enterotype cohort. **(D)** XGBoost categorical variable interpretation, in the *Prevotella* intestinal cohort. **(E)** PCA analysis of CD and Low-GID in the Bacteriodes enterotype cohort. **(F)** XGBoost categorical variable interpretation, in the *Bacteroides* intestinal cohort. BCAA, branched-chain amino acid; TG, triglyceride.

divided into two discrete enterotypes, ET-B and ET-P. According to the previous studies, ET-B is related to long-term protein and animal fat intake, whereas ET-P is related to carbohydrates (11). In this study, the ET-B proportion was higher before the intervention, but the ET-P proportion increased after the intervention, which indicated that some participants changed during the intervention. The gut microbiota of adults are stabilized with age and are not easily modified (28). The participants who changed the enterotype after the intervention might have gut microbiota at the boundary of ET-P and ET-B before intervention. Previous studies have pointed out that typical long-term diet patterns do not change in adults, but only extreme dietary changes will moderate the gut microbiota (29). Therefore, short-term traditional diet interventions may not change enterotypes.

Prevotella is composed mainly of *Prevotella copri* (30), present in 39.1% of healthy people, especially in Asian populations (30). If present, *Prevotella copri* occupies a large part of the gut microbiota. In this study, *Prevotella copri*, at the species level of ET-P, accounted for approximately 45% of the total bacteria. In this study, the Low-GID increased *Prevotella* compared to the CD in ET-P but not ET-B, whereas the Low-GID elevated

Bacteroides in ET-B. According to the diet, a recent study has shown that *Prevotella copri* also affects the host's health response; the Mediterranean diet better impacts the risk of cardiometabolic diseases in people without *Prevotella.* It supports a personalized diet based on intestinal microbes (15, 31). This study also showed different impacts on fecal bacterial species and metabolism. The Low-GID reduced body weight in both ET-P and ET-B, but its decrease was related to muscle mass loss in ET-P, but not in ET-B. The Low-GID reduced serum lipid and amino acid concentrations compared to CD in both enterotypes, but the decrease was higher in ET-P than in ET-B. However, the Low-GID decreased *Bifidobacterium* compared to CD in both enterotypes. Therefore, this study showed some discrepancies in the dietary effects of ET-B and ET-P, but according to enterotypes, it is not clear which diet is better for health benefits. Therefore, further studies are needed to consider different enterotypes for personalized nutrition.

In the body composition and blood biochemical analysis, compared with CD in the two enterotypes, the Low-GID lowered BMI and maintained low serum total cholesterol and blood lipids in this study. The Low-GID and CD in the ET-P cohort showed more substantial differences in amino acids in the blood circulation than those in the ET-B group. The Low-GID group had lower serum leucine, BCAA, tryptophan, tyrosine, glycine, and L-homocysteine concentrations. According to recent studies, it has been found that there is a strong association between the chronic elevation of BCAA in serum and insulin resistance (32, 33). In a study of serum metabolites based on non-diabetic middle-aged people (34), serum tryptophan and tyrosine concentrations are found to be related to glucose intolerance and insulin resistance, and these two amino acids are also higher in patients with diabetics with decreased insulin secretion (34, 35). Serum L-homocysteine concentrations are also associated with insulin resistance and diabetes. Homocysteine interferes with the phosphorylation of insulin receptors to attenuate insulin signal transduction (36). Contrary to other serum amino acids, serum glycine concentration can reduce the accumulation of free fatty acids in the serum and is associated with a lower risk of type 2 diabetes (37). Therefore, this study suggested that the Low-GID reduced insulin resistance based on serum amino acids and their derivative concentrations compared to CD.

In addition to serum amino acids, the Low-GID group exhibited higher serum 3-hydroxybutyric acid concentrations; 3-hydroxybutyric acid is a primary ketone body produced from fatty acids, mainly under calorie restriction, a low-carbohydrate diet, and an intermittent diet. It acts as a regulatory molecule to inhibit gene expression involved in DNA methylation, oxidative stress, and inflammation (38). It contributes to increased longevity (38). The Low-GID increased serum 3-hydroxybutyrate concentrations in both enterotypes, but serum glutathione concentration increased with the Low-GID only in ET-B. This study suggests that a low-glycemic diet may have similar activity to a low-carbohydrate diet in both enterotypes. The CD group had higher serum uric acid levels than the control group. Uric acid is a product of purine metabolism in humans and other primates, and joint and soft tissue deposits can cause gout (39). The research found that serum uric acid levels are positively correlated with hyperinsulinemia and insulin resistance (40). Compared with CD, the Low-GID of the ET-B cohort had lower serum BCAA, tryptophan, and uridine levels in the serum. Uridine is associated with glucose homeostasis. Plasma uridine is a marker of insulin resistance in patients with type 2 diabetics. Animal experiments have shown that long-term or short-term uridine supplementation impairs glucose tolerance and insulin sensitivity (41). Therefore, the Low-GID could improve insulin sensitivity in both enterotypes, but its effect was more profound in ET-P than in CD.

According to the XGBoost machine learning model results, ET-P has a higher classification accuracy than ET-B. It shows the influence of the Low-GID and CD on energy and lipid metabolism in both ET-P and ET-B. In the Low-GID and CD classification, SHAP importance in all participants showed that *Blautia obeum* was positively correlated with Low-GID classification, whereas *Bifidobacterium longum* was positively linked to CD classification. *Blautia*, belonging to *Lachnospiraceae*, can reduce inflammatory and metabolic diseases, similar to probiotics (42). The classification of SHAP importance in the ET-P cohort showed that the levels of *Gemmiger formicilis*, *Collinsella aerofaciens*, and *Escherichia coli* were positively correlated with the CD classification. However, less is known about *Gemmiger formicilis*. In previous studies, *Collinsella aerofaciens* has shown a positive correlation between waist circumference and BMI (43). It corresponds to a higher BMI in the CD group. *Escherichia coli* is a widely recognized pathogenic strain (44). The SHAP importance of the ET-B cohort showed that the level of butyric acid was positively correlated with the Low-GID classification, whereas the CD group was positively correlated with serum isocitric acid concentrations. Butyric acid is an essential metabolite of intestinal microbes. Previous research has shown that butyric acid protects against obesity and obesity-related conditions and critically contributes to the diet–gut microbiota–host health axis (45). Thus, the Low-GID improved the gut microbiota community to prevent obesity and insulin resistance in ET-B. However, Low-GID decreased *Bifidobacterium,* which might be associated with milk intake.

With the advancement of nutrition and medical research, one healthy diet may not fit everyone, and it needs to be personalized according to genetics and/or gut microbiota. Each person's response to the diet may be affected by the characteristics of the microorganisms. For instance, on the one hand, *Prevotella* is generally related to many inflammatory diseases, although it is known to be high in lean Asians who consume high amounts of vegetables and grains (30). Studies have shown that *Prevotella* is a risk factor for glucose tolerance and type 2 diabetes because it synthesizes branched-chain fatty acids (46), and it corresponds to a marked increase in type 2 diabetes in Asians. *P. copri* was also identified as the most potent driving species for the positive correlation between microbial BCAA synthesis in the gut and increased insulin resistance traits in a cohort of non-diabetic men (47). On the other hand, research supports that *P. copri* benefits glucose and insulin resistance metabolism under a diet rich in fiber (48). However, this remains controversial. In this study, Low-GID showed a metabolic benefit compared to CD, and its benefit was more evident in the ET-P in reducing many possible

causes of insulin resistance and improving glucose homeostasis. For enterotypes, further large-scale clinical studies are needed to determine the effect of Low-GID on energy, glucose, and lipid metabolism.

Our study has some limitations. The experimental sample size is small for studying metabolism according to enterotypes, although the machine-learning model is especially needed for large sample sizes. By applying a machine-learning approach to large samples, we may be able to understand more precise and in-depth connections among the gut microbiota, metabolic changes, and diet. At the same time, the CD meal represents a modern western-style Korean meal, and its difference was not large enough to show the differences between diet patterns.

CONCLUSION

Our results show that the Low-GID was beneficial for energy and lipid metabolism in both ET-P and ET-B clusters, but it was more pronounced in ET-P. The Low-GID improved lipid metabolism and serum metabolites related to insulin resistance in ET-P more effectively, although the Low-GID reduced muscle mass compared to CD. Low-GID can be recommended to overweight and obese women with both enterotypes, although its efficacy was more profound in ET-P. This study suggested that diet patterns could influence metabolic traits differently in obese women with different enterotypes, and the results support the possibility of a personalized diet based on enterotypes. Further studies are needed to find appropriate diets for each enterotype.

DATA AVAILABILITY STATEMENT

The datasets presented in this study can be found in online repositories. The names of the repository/repositories and accession number(s) can be found below: NCBI; PRJNA801359.

ETHICS STATEMENT

The Institutional Review Board approved the study protocol at CHA University (1044308-201801-HR-033-04), and the study was conducted under the Helsinki Declaration. All participants provided written informed consent. The patients/participants provided their written informed consent to participate in this study.

AUTHOR CONTRIBUTIONS

M-SK and SP conceptualized the study. XW and SP contributed to methodology, investigation, and writing the original draft. XW, HH, and K-HL contributed to formal analysis. HY, MH, and MK contributed to validation. M-SK contributed to funding acquisition. All authors contributed to supervision, writing, reviewing, and editing the manuscript, and approved the submitted version.

FUNDING

This research was supported by the Research Program of the Korea Food Research Institute (KFRI) and funded by the Ministry of Science and ICT.

SUPPLEMENTARY MATERIAL

The Supplementary Material for this article can be found online at: https://www.frontiersin.org/articles/10.3389/fnut.2022.861880/full#supplementary-material

REFERENCES

1. Lynch SV, Pedersen O. The human intestinal microbiome in health and disease. *N Engl J Med.* (2016) 375:2369–79.
2. Tuddenham S, Sears CL. The intestinal microbiome and health. *Curr Opin Infect Dis.* (2015) 28:464.
3. Luca M, Di Mauro M, Perry G. Neuropsychiatric disturbances and diabetes mellitus: the role of oxidative stress. *Oxid Med Cell Longev.* (2019) 2019:5698132. doi: 10.1155/2019/5698132
4. Stephens RW, Arhire L, Covasa M. Gut microbiota: from microorganisms to metabolic organ influencing obesity. *Obesity.* (2018) 26:801–9. doi: 10.1002/oby.22179
5. Kim SH, Kim MS, Lee MS, Park YS, Lee HJ, Kang S-A, et al. Korean diet: characteristics and historical background. *J Ethnic Foods.* (2016) 3:26–31. doi: 10.1016/j.healthplace.2019.102147
6. Ham D, Jun S, Kang M, Paik H-Y, Joung H, Shin S. Consumption of Korean foods with high flavonoid contents reduces the likelihood of having elevated C-reactive protein levels: data from the 2015–2017 Korea national health and nutrition examination survey. *Nutrients.* (2019) 11:2370. doi: 10.3390/nu11102370
7. Jun S, Chun OK, Quansah DY, Hei Y, Joung H. Estimation of Dietary Total Antioxidant Capacity of Korean Adults. *FASEB J.* (2016) 30:lb362. doi: 10.1007/s00394-017-1447-6
8. Linando AY, Lee S-K. Socioeconomic, dietary, nutrition, body weight and epidemiologic transitions: three nations at different stage of development. *Progr Nutr.* (2018) 20:602–15. doi: 10.1038/sj.ejcn.1602727
9. Mozaffarian D. Dietary and policy priorities for cardiovascular disease, diabetes, and obesity: a comprehensive review. *Circulation.* (2016) 133:187–225. doi: 10.1161/CIRCULATIONAHA.115.018585
10. Liu B, Zhang Y, Wang R, An Y, Gao W, Bai L, et al. Western diet feeding influences gut microbiota profiles in apoE knockout mice. *Lipids Health Dis.* (2018) 17:1–8. doi: 10.1186/s12944-018-0811-8
11. Wu GD, Chen J, Hoffmann C, Bittinger K, Chen Y-Y, Keilbaugh SA, et al. Linking long-term dietary patterns with gut microbial enterotypes. *Science.* (2011) 334:105–8. doi: 10.1126/science.1208344
12. Mobeen F, Sharma V, Tulika P. Enterotype variations of the healthy human gut microbiome in different geographical regions. *Bioinformation.* (2018) 14:560–73. doi: 10.6026/97320630014560
13. Gorvitovskaia A, Holmes SP, Huse SM. Interpreting *Prevotella* and *Bacteroides* as biomarkers of diet and lifestyle. *Microbiome.* (2016) 4:1–12. doi: 10.1007/978-3-319-23534-9_1
14. Mentella MC, Scaldaferri F, Ricci C, Gasbarrini A, Miggiano GAD. Cancer and Mediterranean diet: a review. *Nutrients.* (2019) 11:2059. doi: 10.3390/nu11092059
15. Wang DD, Nguyen LH, Li Y, Yan Y, Ma W, Rinott E, et al. The gut microbiome modulates the protective association between a Mediterranean

diet and cardiometabolic disease risk. *Nat Med.* (2021) 27:333–43. doi: 10.1038/s41591-020-01223-3
16. Shin P-K, Park S-J, Kim MS, Kwon DY, Kim MJ, Kim K, et al. A traditional Korean diet with a low dietary inflammatory index increases anti-inflammatory IL-10 and decreases pro-inflammatory NF-κB in a small dietary intervention study. *Nutrients.* (2020) 12:2468. doi: 10.3390/nu12082468
17. Atkinson FS, Brand-Miller JC, Foster-Powell K, Buyken AE, Goletzke J. International tables of glycemic index and glycemic load values 2021: a systematic review. *Am J Clin Nutr.* (2021) 114:1625–32. doi: 10.1093/ajcn/nqab233
18. Song S, Choi H, Lee S, Park J, Kim B, Paik HY, et al. Establishing a table of glycemic index values for common Korean foods and an evaluation of the dietary glycemic index among the Korean adult population. *Korean J Nutr.* (2012) 45:80–93. doi: 10.4163/kjn.2012.45.1.80
19. Kim MJ, Lee D-H, Ahn J, Ha T-Y, Jang YJ, Do E, et al. A pilot study on characteristics of metabolomics and lipidomics according to Sasang constitution. *Evid Based Complem Alternat Med.* (2018) 2018:9214960. doi: 10.1155/2018/9214960
20. Ribeiro WR, Vinolo MAR, Calixto LA, Ferreira CM. Use of gas chromatography to quantify short chain fatty acids in the serum, colonic luminal content and feces of mice. *Bio Protocol.* (2018) 8:e3089. doi: 10.21769/BioProtoc.3089
21. Schloss PD, Westcott SL, Ryabin T, Hall JR, Hartmann M, Hollister EB, et al. Introducing mothur: open-source, platform-independent, community-supported software for describing and comparing microbial communities. *Appl Environ Microbiol.* (2009) 75:7537–41. doi: 10.1128/AEM.01541-09
22. Desantis TZ, Hugenholtz P, Larsen N, Rojas M, Brodie EL, Keller K, et al. Greengenes, a chimera-checked 16S rRNA gene database and workbench compatible with ARB. *Appl Environ Microbiol.* (2006) 72:5069–72. doi: 10.1128/AEM.03006-05
23. Chen T, Guestrin C. Xgboost: a scalable tree boosting system. *Proceedings of the 22nd ACM SIGKDD International Conference on Knowledge Discovery and Data Mining*. New York, NY (2016). p. 785–94.
24. Bergstra J, Bengio Y. Random search for hyper-parameter optimization. *J Mach Learn Res.* (2012) 13:281–305.
25. Lundberg SM, Erion G, Chen H, Degrave A, Prutkin JM, Nair B, et al. From local explanations to global understanding with explainable AI for trees. *Nat Mach Intell.* (2020) 2:56–67. doi: 10.1038/s42256-019-0138-9
26. Costea PI, Hildebrand F, Arumugam M, Bäckhed F, Blaser MJ, Bushman FD, et al. Enterotypes in the landscape of gut microbial community composition. *Nat Microbiol.* (2018) 3:8–16. doi: 10.1038/s41564-017-0072-8
27. Couch CE, Stagaman K, Spaan RS, Combrink HJ, Sharpton TJ, Beechler BR, et al. Diet and gut microbiome enterotype are associated at the population level in African buffalo. *Nat Commun.* (2021) 12:2267. doi: 10.1038/s41467-021-22510-8
28. Xiao L, Wang J, Zheng J, Li X, Zhao F. Deterministic transition of enterotypes shapes the infant gut microbiome at an early age. *Genome Biol.* (2021) 22:1–21. doi: 10.1186/s13059-021-02463-3
29. David LA, Maurice CF, Carmody RN, Gootenberg DB, Button JE, Wolfe BE, et al. Diet rapidly and reproducibly alters the human gut microbiome. *Nature.* (2014) 505:559–63. doi: 10.1038/nature12820
30. Tett A, Huang KD, Asnicar F, Fehlner-Peach H, Pasolli E, Karcher N, et al. The *Prevotella copri* complex comprises four distinct clades underrepresented in westernized populations. *Cell Host Microbe.* (2019) 26:666–79.e7. doi: 10.1016/j.chom.2019.08.018
31. Christensen L, Roager HM, Astrup A, Hjorth MF. Microbial enterotypes in personalized nutrition and obesity management. *Am J Clin Nutr.* (2018) 108:645–51. doi: 10.1093/ajcn/nqy175
32. Arany Z, Neinast M. Branched chain amino acids in metabolic disease. *Curr Diab Rep.* (2018) 18:1–8. doi: 10.1159/000410880
33. Zhou M, Shao J, Wu C-Y, Shu L, Dong W, Liu Y, et al. Targeting BCAA catabolism to treat obesity-associated insulin resistance. *Diabetes.* (2019) 68:1730–46. doi: 10.2337/db18-0927
34. Bos MM, Noordam R, Bennett K, Beekman M, Mook-Kanamori DO, Van Dijk KW, et al. Metabolomics analyses in non-diabetic middle-aged individuals reveal metabolites impacting early glucose disturbances and insulin sensitivity. *Metabolomics.* (2020) 16:1–10. doi: 10.1007/s11306-020-01653-7
35. Vangipurapu J, Stancáková A, Smith U, Kuusisto J, Laakso M. Nine amino acids are associated with decreased insulin secretion and elevated glucose levels in a 7.4-year follow-up study of 5,181 Finnish men. *Diabetes.* (2019) 68:1353–8. doi: 10.2337/db18-1076
36. Kumar A, Palfrey HA, Pathak R, Kadowitz PJ, Gettys TW, Murthy SN. The metabolism and significance of homocysteine in nutrition and health. *Nutr Metab.* (2017) 14:1–12. doi: 10.1186/s12986-017-0233-z
37. Adeva-Andany M, Souto-Adeva G, Ameneiros-Rodriguez E, Fernandez-Fernandez C, Donapetry-Garcia C, Dominguez-Montero A. Insulin resistance and glycine metabolism in humans. *Amino Acids.* (2018) 50:11–27. doi: 10.1007/s00726-017-2508-0
38. Møller N. Ketone body, 3-hydroxybutyrate: minor metabolite-major medical manifestations. *J Clin Endocrinol Metab.* (2020) 105:2884–92. doi: 10.1210/clinem/dgaa370
39. Kim S-K. Interrelationship of uric acid, gout, and metabolic syndrome: focus on hypertension, cardiovascular disease, and insulin resistance. *J Rheum Dis.* (2018) 25:19–27. doi: 10.4078/jrd.2018.25.1.19
40. Wu Y, He H, Yu K, Zhang M, An Z, Huang H. The association between serum uric acid levels and insulin resistance and secretion in prediabetes mellitus: a cross-sectional study. *Ann Clin Lab Sci.* (2019) 49:218–23.
41. Zhang Y, Guo S, Xie C, Fang J. Uridine metabolism and its role in glucose, lipid, and amino acid homeostasis. *Biomed Res Int.* (2020) 2020:7091718. doi: 10.1155/2020/7091718
42. Liu X, Mao B, Gu J, Wu J, Cui S, Wang G, et al. Blautia—a new functional genus with potential probiotic properties? *Gut Microbes.* (2021) 13:1–21. doi: 10.1080/19490976.2021.1875796
43. Gallardo-Becerra L, Cornejo-Granados F, García-López R, Valdez-Lara A, Bikel S, Canizales-Quinteros S, et al. Metatranscriptomic analysis to define the Secrebiome, and 16S rRNA profiling of the gut microbiome in obesity and metabolic syndrome of Mexican children. *Microb Cell Fact.* (2020) 19:1–18. doi: 10.1186/s12934-020-01319-y
44. Manges AR, Geum HM, Guo A, Edens TJ, Fibke CD, Pitout JD. Global extraintestinal pathogenic *Escherichia coli* (ExPEC) lineages. *Clin Microbiol Rev.* (2019) 32: e00135–18. doi: 10.1128/CMR.00135-18
45. Coppola S, Avagliano C, Calignano A, Berni Canani R. The protective role of butyrate against obesity and obesity-related diseases. *Molecules.* (2021) 26:682. doi: 10.3390/molecules26030682
46. De Filippis F, Pasolli E, Tett A, Tarallo S, Naccarati A, De Angelis M, et al. Distinct genetic and functional traits of human intestinal *Prevotella copri* strains are associated with different habitual diets. *Cell Host Microbe.* (2019) 25:444–53.e3. doi: 10.1016/j.chom.2019.01.004
47. Pedersen HK, Gudmundsdottir V, Nielsen HB, Hyotylainen T, Nielsen T, Jensen BA, et al. Human gut microbes impact host serum metabolome and insulin sensitivity. *Nature.* (2016) 535:376–81. doi: 10.1038/nature18646
48. De Vadder F, Kovatcheva-Datchary P, Zitoun C, Duchampt A, Bäckhed F, Mithieux G. Microbiota-produced succinate improves glucose homeostasis *via* intestinal gluconeogenesis. *Cell Metab.* (2016) 24:151–7. doi: 10.1016/j.cmet.2016.06.013

Conflict of Interest: The authors declare that the research was conducted in the absence of any commercial or financial relationships that could be construed as a potential conflict of interest.

Publisher's Note: All claims expressed in this article are solely those of the authors and do not necessarily represent those of their affiliated organizations, or those of the publisher, the editors and the reviewers. Any product that may be evaluated in this article, or claim that may be made by its manufacturer, is not guaranteed or endorsed by the publisher.

frontiers | Frontiers in Nutrition

ORIGINAL RESEARCH
published: 12 May 2022
doi: 10.3389/fnut.2022.852767

Acidic Activated Charcoal Prevents Obesity and Insulin Resistance in High-Fat Diet-Fed Mice

*Xuguang Zhang[1], Pan Diao[1], Hiroaki Yokoyama[2], Yoshiki Inoue[3], Kazuhiro Tanabe[4], Xiaojing Wang[1,5], Chihiro Hayashi[4], Tomoki Yokoyama[2], Zhe Zhang[1], Xiao Hu[1,6], Takero Nakajima[1], Takefumi Kimura[7], Jun Nakayama[8], Makoto Nakamuta[9] and Naoki Tanaka[10,11,12]**

[1] Department of Metabolic Regulation, Shinshu University School of Medicine, Matsumoto, Japan, [2] Sumi Plus Lab Co., Ltd., Yokohama, Japan, [3] Ina Carbonization Laboratory Co., Ltd., Ina, Japan, [4] Medical Solution Promotion Department, Medical Solution Segment, LSI Medience Corporation, Tokyo, Japan, [5] Department of Gastroenterology, Lishui Hospital, Zhejiang University School of Medicine, Lishui, China, [6] Department of Pathophysiology, Hebei Medical University, Shijiazhuang, China, [7] Department of Gastroenterology, Shinshu University School of Medicine, Matsumoto, Japan, [8] Department of Molecular Pathology, Shinshu University School of Medicine, Matsumoto, Japan, [9] Department of Gastroenterology, Kyushu Medical Center, Fukuoka, Japan, [10] Department of Global Medical Research Promotion, Shinshu University Graduate School of Medicine, Matsumoto, Japan, [11] International Relations Office, Shinshu University School of Medicine, Matsumoto, Japan, [12] Research Center for Social Systems, Shinshu University, Matsumoto, Japan

OPEN ACCESS

Edited by:
Gratiela Gradisteanu Pircalabioru, University of Bucharest, Romania

Reviewed by:
Shunxing Rong, University of Texas Southwestern Medical Center, United States
Christine Feillet-Coudray, Institut National de Recherche pour l'Agriculture, l'Alimentation et l'Environnement (INRAE), France

***Correspondence:**
Naoki Tanaka
naopi@shinshu-u.ac.jp

Specialty section:
This article was submitted to Nutrition and Metabolism, a section of the journal Frontiers in Nutrition

Received: *11 January 2022*
Accepted: *11 April 2022*
Published: *12 May 2022*

Citation:
Zhang X, Diao P, Yokoyama H, Inoue Y, Tanabe K, Wang X, Hayashi C, Yokoyama T, Zhang Z, Hu X, Nakajima T, Kimura T, Nakayama J, Nakamuta M and Tanaka N (2022) Acidic Activated Charcoal Prevents Obesity and Insulin Resistance in High-Fat Diet-Fed Mice. Front. Nutr. 9:852767. doi: 10.3389/fnut.2022.852767

Obesity is becoming a major public health problem worldwide. Making charcoal from wood ("Sumi-yaki") has been a traditional activity in the southern part of Nagano Prefecture for centuries, with activated charcoal having reported detoxifying effects. However, it is unclear whether activated charcoal also possesses anti-obesity properties. Additionally, since activated charcoal is usually alkaline and might be affected by gastric juice, we evaluated the effect of acidic activated charcoal on high-fat diet (HFD)-induced obesity. This study demonstrated that co-treatment of acidic activated charcoal with a HFD significantly improved obesity and insulin resistance in mice in a dose-dependent manner. Metabolomic analysis of cecal contents revealed that neutral lipids, cholesterol, and bile acids were excreted at markedly higher levels in feces with charcoal treatment. Moreover, the hepatic expressions of genes encoding cholesterol 7 alpha-hydroxylase and hydroxymethylglutaryl-CoA reductase/synthase 1 were up-regulated by activated charcoal, likely reflecting the enhanced excretions from the intestine and the enterohepatic circulation of cholesterol and bile acids. No damage or abnormalities were detected in the gastrointestinal tract, liver, pancreas, and lung. In conclusion, acidic activated charcoal may be able to attenuate HFD-induced weight gain and insulin resistance without serious adverse effects. These findings indicate a novel function of charcoal to prevent obesity, metabolic syndrome, and related diseases.

Keywords: obesity, acidic activated charcoal, insulin resistance, metabolic syndrome, metabolomic analysis, bile acid, intestine, enterohepatic circulation

Abbreviations: Acta2, actin alpha 2; ALT, alanine aminotransferase; Asbt, apical sodium-bile acid transporter; AST, aspartate aminotransferase; AUC, area under the receiver operating characteristic curve; BA, bile acid; BAT, brown adipose tissue; BW, body weight; Ccl2, chemokine (C-C motif) ligand 2; Cd68, cluster of differentiation 68; Col1a1, collagen, type I, alpha 1; Cyp7a1, cholesterol 7 alpha-hydroxylase; DCA, deoxycholic acid; eWAT, epididymal white adipose tissue; FA, fatty acid; Fabp6, fatty acid-binding protein 6; Fgf15, fibroblast growth factor 15; FXR, farnesoid X receptor; GTT, glucose tolerance test; HFD, high-fat diet; Hmgcr, hydroxymethylglutaryl-CoA reductase; Hmgcs1, hydroxymethylglutaryl-CoA synthase 1; HOMA-IR, homeostatic model assessment for insulin resistance; Il1b, interleukin 1 beta; ITT, insulin tolerance test; NEFA, non-esterified fatty acid; PL, phospholipid; qPCR, quantitative polymerase chain reaction; SEM, standard error of the mean; Shp, small heterodimer partner; TBA, total bile acid; T-Chol, total cholesterol; TG, triglyceride; Tgfb1, transforming growth factor beta 1; TGR5, Takeda G protein-coupled receptor 5; Tnf, tumor necrosis factor alpha; TSH, thyroid-stimulating hormone.

INTRODUCTION

Obesity has reached pandemic levels worldwide. Since 1980, the prevalence of obesity has doubled in more than 70 countries/regions and has continued to increase in most other countries. Obesity is a disease caused by excessive fat accumulation. It increases the risk of other diseases, such as cardiovascular disease, type 2 diabetes, hypertension, non-alcoholic fatty liver disease, chronic kidney disease, sleep apnea syndrome, and mood disorders. In recent years, obesity has become a major public health concern in South Asia. In some Asian countries, obesity and its related metabolic diseases is widespread in more than one-third of the population (1–3).

Making charcoal from wood ("Sumi-yaki") has been a traditional activity in the southern part of Nagano Prefecture for centuries, with "Ina Akamatsu" charcoal was made into activated charcoal for deodorant and water purification. Previous studies have revealed detoxifying effects for activated charcoal. Meinita et al. reported that the material could remove 5-hydroxymethylfurfural, levulinic acid, and other toxic substances within 30 min (4). Elsewhere, recommendations given by poison control centers in Germany state that activated charcoal is suitable for primary toxin clearance in cases of moderate-to-severe poisoning; charcoal is especially suitable for poisons that remain for long periods in the stomach and poisons circulating between the intestine and liver (5). Neuvonen et al. also demonstrated the ability of activated charcoal to effectively bind bile acids (BAs) *in vitro* (6). The above observations corroborate the biological action of activated charcoal as an absorber of toxins and lipid derivatives.

It is well known that dietary composition, including fat and contaminants, as well as microbiota-produced BAs affect adiposity through multiple pathways. To date, however, the anti-obesity effect of activated charcoal has not been addressed. In a preliminary experiment, the anti-obesity effect of alkaline activated charcoal was not significant in high-fat diet (HFD)-treated mice. Additionally, the mice consuming alkaline activated charcoal looked irritable (unpublished data). We speculated that acidic activated charcoal may avoid interference of gastric juice and be more suitable than regular alkaline charcoal. Therefore, we originally developed acidic activated charcoal with a pH of approximately 5 and treated C57BL/6J mice with the acidic activated charcoal powder-containing HFD, in order to investigate whether the acidic charcoal exerts an anti-obesity effect.

MATERIALS AND METHODS

Mice and Treatment

All animal experiments were conducted in adherence to the animal research methods outlined in the "Guidelines for the Care and Use of Laboratory Animals" approved by the ethics committee of Shinshu University School of Medicine. Male 6-week-old mice on a C57BL/6J genetic background were purchased from CLEA Japan, Inc. (Tokyo, Japan) and maintained in a controlled and clean environment (25°C, 12-h light/dark cycle). The control diet was purchased from ORIENTAL YEAST Co., Ltd (Tokyo, Japan). The HFD (D12492M) containing 60% kcal of fat was purchased from Research Diet (New Brunswick, NJ). The ingredients of these diets were shown in **Supplementary Tables 1**, **2**, respectively. Acidic activated charcoal was provided from Sumi Plus Lab Co., Ltd. (Yokohama, Kanagawa, Japan), with dextrin (Pinedex#2, Matsutani Chemical Industry Co., Ltd., Itami, Hyogo, Japan) used as a vehicle. The acidic charcoal was prepared by carbonizing plants and trees at constant atmospheric pressure and temperature above 700°C after soaking acidic deep seawater (pH 5.5). The activated charcoal powder was completely mixed with HFD and then administered to mice. Inulin (Fuji FF, Fuji Nihon Seito Corporation, Tokyo, Japan) and raffinose (Nitten Raffinose FP, Nippon Beet Sugar Manufacturing Co., Ltd., Tokyo, Japan) were added to prevent charcoal-induced constipation. In the first experiment, mice (n = 21) weighing 22–26 grams were randomly divided into three groups after acclimatization for at least 2 weeks into (1) a control diet group (Con, n = 5), (2) a HFD with 5% dextrin and 5% inulin raffinose group (HFD + Veh, n = 8), and (3) a HFD with 5% acidic activated charcoal and 5% inulin raffinose group (HFD + 5%C, n = 8). As an additional dose-dependency experiment, mice (n = 28) weighing 23–28 grams were randomly divided into five groups fed (1) a control diet (Con, n = 4), (2) a HFD with 5% dextrin and 5% inulin raffinose (HFD + Veh, n = 6), (3) a HFD with 1.5% acidic activated charcoal and 1.5% inulin raffinose (HFD + 1.5%C, n = 6), (4) a HFD with 3% acidic activated charcoal and 3% inulin raffinose (HFD + 3%C, n = 6), and (5) a HFD with 4.5% acidic activated charcoal and 4.5% inulin raffinose (HFD + 4.5%C, n = 6). During the experiments, the animals' body weight (BW) and food intake were measured weekly. At 12 weeks of treatment, the mice were sacrificed by CO_2 asphyxiation after 6-h fasting for collecting blood and tissues. Blood samples were centrifuged twice at 3,000 rpm for 15 min to obtain serum and stored at −80°C until use. The organs were harvested, washed with 0.9% sterile saline, and weighed, and the length of the small intestine was measured. The tissues were preserved either by immediate fixation in 10% neutral formalin or immediate freezing with dry ice and storage at −80°C. The feces during 6-h fasting before killing were collected manually, weighted, and stored at −80°C until use.

Glucose/Insulin Tolerance Tests

For the glucose tolerance test (GTT), the mice were injected intraperitoneally with 1 g/kg BW of glucose dissolved in 0.9% sterile saline using a 26-gauge needle after 18-h fasting. For the insulin tolerance test (ITT), the mice were injected intraperitoneally with 0.6 unit/kg BW of insulin (Humulin R; Eli Lilly, Indianapolis, IN) in the same manner after 6-h fasting. Blood glucose concentrations were determined at 0, 15, 30, 60, 90, and 120 min after injection using a FreeStyle Freedom Lite glucose meter (NIPRO, Osaka, Japan).

Biochemical Analysis

Serum levels of aspartate aminotransferase (AST) (#431-30901), alanine aminotransferase (ALT) (#431-30901), triglycerides (TGs) (#632-50991), total cholesterol (T-Chol) (#294-65801),

non-esterified fatty acids (NEFAs) (#279-75401), phospholipids (PLs) (#433-36201), total bile acid (TBA) (#431-15001), and glucose (#298-65701) were measured with commercially available enzyme assay kits (Wako Pure Chemical Industries Co., Ltd., Osaka, Japan). Serum insulin, leptin, and high-molecular-weight adiponectin were determined by ELISA kits (AKRIN-011T, AKRLP-011, and AKMAN-011, respectively, FUJIFILM Wako Shibayagi, Gunma, Japan). Homeostatic model assessment for insulin resistance (HOMA-IR) was calculated using the equations published by Matthews et al. (7). Serum thyroid-stimulating hormone (TSH) was determined by ELISA kits (KT-29922, KAMIYA BIOMEDICAL COMPANY, Seattle, WA) (8).

Total liver lipids and fecal lipids were extracted according to the hexane:isopropanol method (9) with a slight modification and quantified using the abovementioned kit (Wako Pure Chemical Industries Co., Ltd.). For extracting liver lipids, approximately 50 mg of liver tissues were disrupted and sonicated in 5–10 volumes of sodium phosphate buffer (NaPi, 50 mM). The lysate (50 μL) was drawn into a new tube, and 900 μL of hexane/isopropanol (3:2, vol/vol) (HIP) was added. The tube was vigorously vortexed for 1 min and centrifuged at 2,500 rpm for 5 min at 4°C, and the upper layer was transferred to a new tube and centrifuged under vacuum at 40–50°C. After evaporation, the lipid extracts were dissolved in 100 μL of HIP containing 1% (wt/vol) Triton X-100 and evaporated again by vacuum centrifuge. Then, 100 μL of distilled water was added to the sample, incubated at 37°C for 30 min, and vortexed. Finally, the lipid extracts were solubilized in 1% Triton X-100/water as described previously (10), and 10 μL of the lipid extracts (corresponding to 0.25 mg of livers) were used for measuring TG, PL, T-Chol, and NEFAs (11).

For extracting fecal lipids, 20–30 mg of dry feces were collected and placed in 19 volumes of 50 mM NaPi. The tube was kept on ice for 30–60 min until the feces become swollen, and then sonicated on ice until the feces were completely dispersed in the solution. The total lipids in feces were extracted in a similar manner as those in the liver and finally solubilized in 1% Triton X-100/water at a concentration of 0.025 mg feces eq./μL. Ten μL of the lipid extracts (corresponding to 0.25 mg of feces) were used for measuring TBA, TG, T-Chol, PL, and NEFAs.

Histological Analysis

Formalin-fixed liver tissues were embedded in paraffin, cut into 3 μm sections, and stained with hematoxylin and eosin (12). To quantify the size of adipocytes and the relative area of islets, 10 independent sections of epididymal white adipose tissue (eWAT) and pancreas were photomicrographed (×200 magnification) in each group, and the size of each adipocyte and the area of each islet were quantified using the 1.52V version of Image J (National Institutes of Health, Bethesda, MD). Values were expressed as the percentage of adipocytes of the corresponding size. The total islet area was also expressed as the percentage of the total area of pancreatic parenchyma in the sections.

Quantification of mRNA Levels

Total RNA was isolated from frozen liver tissues using a NucleoSpin RNA Plus Kit (QiagenMACHEREY-NAGEL Gmbh & Co., KG, Neumann, Germany). Total RNA from the stomach, upper small intestine, lower small intestine, large intestine, brown adipose tissue (BAT), and eWAT were extracted using TRI reagent (MOR Molecular Research Center, Inc., Cincinnati, OH). Tissues (50 mg) were disrupted and sonicated in 500 μL of TRI reagent. The homogenate was incubated at room temperature for 5 min, 100 μL of chloroform was added, and the homogenate was shaken vigorously for 15 sec. The homogenate was then incubated at room temperature for 2–3 min and centrifuged at 12,000 × *g* for 15 min at 4°C. The upper layer was transferred to a new tube and 1 volume of 70% ethanol was added and vortexed. The mixture was transferred to a column with a silica membrane and centrifuged at 12,000 × *g* for 1 min at room temperature. The silica membrane was washed and dried, and RNA was eluted and collected using RNase-free water. The RNA samples were reverse transcribed to cDNA using ReverTra Ace qPCR RT Master Mix (Toyobo Co., Ltd., Osaka, Japan). All mRNA levels were determined by the real-time quantitative polymerase chain reaction (qPCR) using a SYBR qPCR mix (Toyobo Co., Ltd.) on a Thermo Fisher QuantStudio 3 Real-Time PCR Instrument (Thermo Fisher Scientific, Waltham, MA). The mRNA levels were normalized to 18S ribosomal RNA (18S rRNA) levels and expressed as fold changes relative to those of C57BL/6J mice fed the control diet. The primer sequences were listed in **Supplementary Table 3**.

Metabolomic Analysis

The detailed method of metabolomic analysis is described in **Supplementary Information**.

Statistical Analysis

Results were expressed as the mean ± standard error of the mean (SEM). Two-tailed Student's *t*-tests and a one-way analysis of variance (ANOVA) with the Bonferroni's correction were conducted using SPSS statistics version 22 (IBM, Armonk, NY). A *P*-value of less than 0.05 was considered statistically significant.

RESULTS

Acidic Activated Charcoal Prevents High-Fat Diet-Induced Obesity

In the first experiment, test mice were given the three different diets for 12 weeks. In the HFD + 5%C group, the limbs, fur and tail turned black from the charcoal (**Supplementary Figure 1A**). Weight gain in the HFD + 5%C group was significantly suppressed as compared with the HFD + Veh group and was similar to the Con group (**Figure 1A** and **Supplementary Table 4**). There were no significant differences in food intake between the HFD + Veh and HFD + 5%C groups (**Figure 1B**), nor were remarkable differences seen for the gross appearance of the liver, lungs, or subscapular BAT among the three groups (**Figures 1C,D**). We observed that eWAT became larger, the cecum became smaller, and the small intestine became shorter by HFD treatment, which were all mitigated by the charcoal-containing HFD (**Figures 1C,D** and **Supplementary Table 4**). Since thyroid dysfunction can lead to darker fur and weight loss, we measured serum levels of TSH, a sensitive indicator of primary hypothyroidism. The TSH levels were not changed by

charcoal treatment (**Supplementary Figure 1B**). These results demonstrated that acidic activated charcoal prevented HFD-induced obesity.

Acidic Activated Charcoal Improves High-Fat Diet-Induced Insulin Resistance

Since obesity has been found to impair glucose metabolism, the GTT was conducted in the tenth week of HFD treatment. The blood glucose levels of the HFD + 5%C group were consistently lower than those of the HFD + Veh group (**Figure 2A**). Accordingly, the area under the receiver operating characteristic curve (AUC) was significantly smaller in the HFD + 5%C group than in the HFD + Veh group (**Figure 2A**).

To assess whether the improved glucose intolerance stemmed from enhanced insulin sensitivity, the ITT was performed in the twelfth week of HFD treatment. After insulin injection, glucose levels in the HFD + 5%C group fell faster than in the HFD + Veh group (**Figure 2B**). The blood glucose initial ratio in the HFD + 5%C group was consistently lower than in the HFD + Veh group. Consequently, the AUC was also significantly smaller in the HFD + 5%C group (**Figure 2B**). These results indicated that acidic activated charcoal intake could reverse HFD-induced insulin resistance.

In agreement with the GTT/ITT results, serum insulin levels and HOMA-IR were significantly lower in the HFD + 5%C group than in the HFD + Veh group, while serum leptin and high-molecular-weight adiponectin were comparable between the HFD + Veh and HFD + 5%C groups (**Figure 2C**). To exclude the possibility that decreased serum insulin levels were due to impaired pancreatic function, we assessed the histology of pancreas. There were no significant abnormalities, such as atrophy, inflammation, and fibrosis, in pancreatic parenchyma of charcoal-containing HFD-fed mice. Quantification of the relative islet area and pancreatic expression levels of *Ins2* (insulin 2) revealed no significant differences between the groups (**Supplementary Figures 2A,B**).

In the determination of serum lipid profiles, while serum TBA levels were significantly decreased in the HFD + 5%C group, no significant differences in the other parameters were observed between the HFD + Veh and HFD + 5%C groups (**Figure 2C**).

Acidic Activated Charcoal Has No Obvious Effect on the Liver

In both the HFD + Veh and HFD + 5%C groups, the serum levels of AST and ALT, which are conventional indices of liver damage, were within the reference values, and no abnormal morphologies were found in the liver tissue (**Figure 2C** and **Supplementary Figure 3A**). In the latter group, no charcoal deposition was observed in the liver. Quantification of mRNA in the liver demonstrated no significant differences in gene expression related to fatty acid (FA)/TG metabolism, inflammation, or fibrosis (**Supplementary Figures 3B–F**). Quantitative analysis of hepatic lipids showed that TGs in the HFD + 5%C group were increased, while PL, T-Chol, and NEFA levels were comparable among the groups (**Supplementary Figure 3G**). Taken together, it appeared that the liver was not a primary target of acidic activated charcoal for preventing HFD-induced BW gain and insulin resistance.

Acidic Activated Charcoal Improves Epididymal White Adipose Tissue Hypertrophy and Inflammation Caused by High-Fat Diet

The finding that acidic activated charcoal prevented eWAT weight gain prompted us to assess the phenotypic changes in white adipocytes. Microscopic examination of eWAT revealed marked adipocyte hypertrophy and inflammatory cell infiltration around adipocytes in the HFD + Veh group, and the proportion of larger adipocytes (4,001–12,000 μm^2) in this group was significantly increased. These alterations were prevented by 5% charcoal intake (**Figures 3A,D**).

We next evaluated whether eWAT mRNA levels were associated with adipocyte enlargement and inflammation. Compared with the HFD + Veh group, the expression levels of the genes related to inflammation and fibrosis, including interleukin 1 beta (*Il1b*), chemokine (C-C motif) ligand 2 (*Ccl2*), transforming growth factor beta 1 (*Tgfb1*), and actin alpha 2 (*Acta2*), were significantly decreased in the HFD + 5%C group (**Figures 3B,C**). The mRNA levels of other inflammation-related genes, such as cluster of differentiation 68 (*Cd68*) and tumor necrosis factor alpha (*Tnf*), were decreased as well but did not reach statistical significance (**Figures 3B,C**).

The improvement of adipocyte hypertrophy in the HFD + 5%C group may have been associated with increased FA catabolism, browning of white adipocytes, and decreased FA uptake and TG synthesis. Among several genes related to FA/TG metabolism, the mRNA levels of the cluster of differentiation 36 (*Cd36*) and FA-binding protein 4 (*Fabp4*) genes, both responsible for FA uptake into adipocytes, tended to be decreased in the HFD + 5%C group (**Supplementary Figure 4**). No browning of white adipocytes was detected in the HFD + 5%C group (**Supplementary Figure 4**).

Acidic Activated Charcoal Improves Whitening of Brown Adipose Tissue Caused by High-Fat Diet, but Does Not Enhance Browning

BAT plays an important role in the maintenance of whole-body energy/fuel metabolism through the promotion of fat burning. To evaluate whether the anti-obesity effect of charcoal stemmed from enhanced fat burning in BAT, we assessed for phenotypic changes in this tissue. Histological analysis revealed that the HFD + Veh group had increased unilocular lipid droplets and white adipocytes (i.e., whitening), with slight inflammatory cell infiltration around adipocytes, while such changes were absent in the HFD + 5%C group (**Supplementary Figure 5A**). In mRNA quantifications of BAT, compared with the HFD + Veh group, the expression levels of the inflammation-related genes *Cd68* and *Ccl2* tended to be decreased in the HFD + 5%C group. The mRNA levels

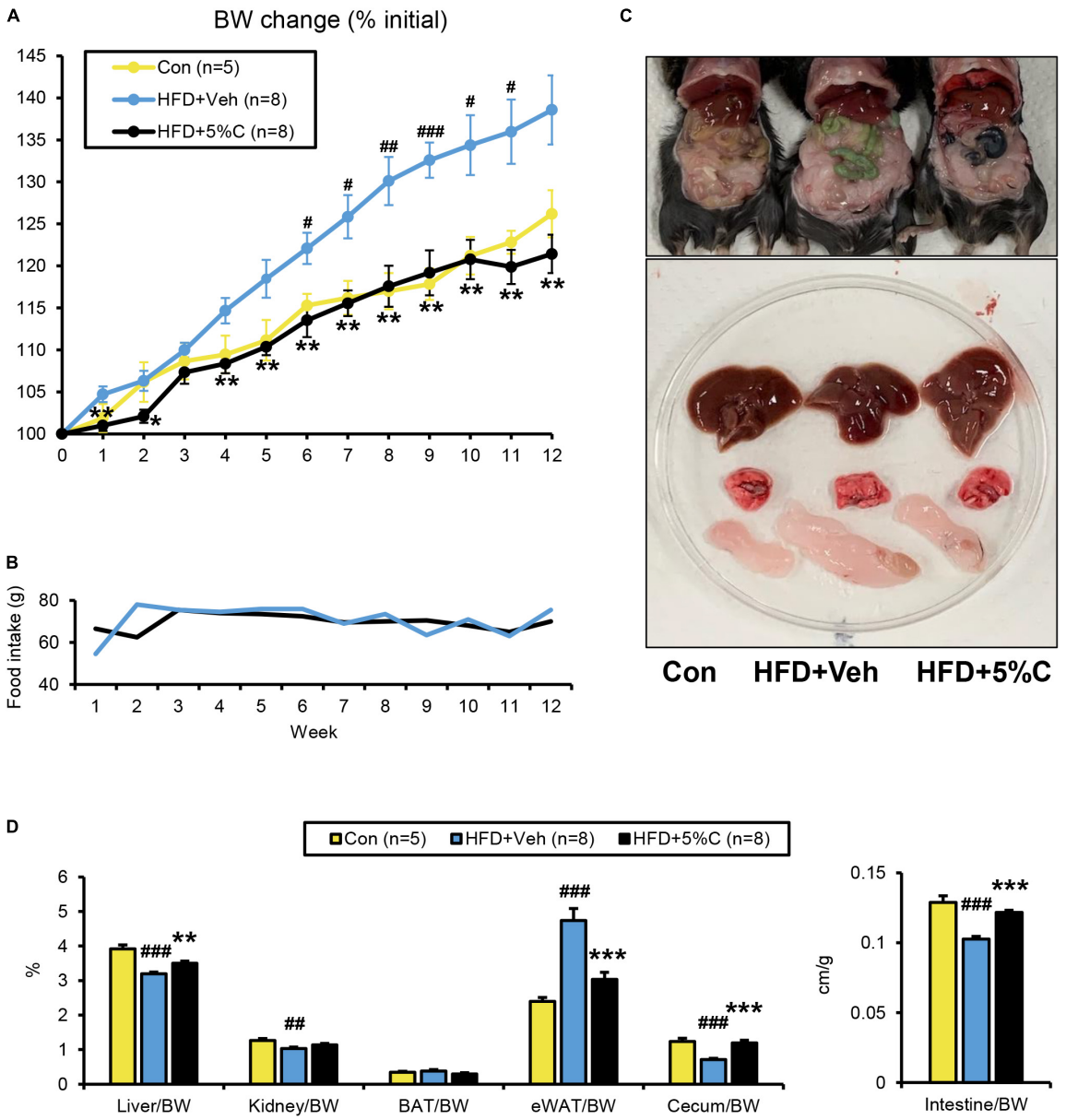

FIGURE 1 | A diet containing acidic activated charcoal can improve obesity in mice fed HFD after 12 weeks of treatment. **(A)** Changes in BW. **(B)** Food intake. **(C)** Gross appearance of representative mice from the three groups. From top to bottom, the liver, lung and epididymal white adipose tissue (eWAT) are shown. **(D)** The weights of the liver, kidney, BAT, eWAT, and cecum along with the length of the small intestine. Values were corrected by body weight (BW). Data are expressed as the mean ± SEM. Statistical analysis was performed using two-tailed Student's *t*-tests. $^{*}P < 0.05$, $^{**}P < 0.01$, and $^{***}P < 0.001$ between the HFD + Veh group and the HFD + 5%C group. $^{\#}P < 0.05$, $^{\#\#}P < 0.01$, and $^{\#\#\#}P < 0.001$ between the HFD + Veh group and the Con group.

associated with fat burning, including uncoupling protein 1 (*Ucp1*), cell death-inducing DNA fragmentation factor alpha-like effector A (*Cidea*), type 2 iodothyronine deiodinase (*Dio2*), peroxisome proliferator-activated receptor gamma coactivator 1 alpha (*Ppargc1a*), and cytochrome c oxidase subunit 5B (*Cox5b*) and 8B (*Cox8b*), were not increased by the co-administration of charcoal (**Supplementary Figure 5B**). Cell death-inducing DNA fragmentation factor alpha-like effector C (*Cidec*) as a gene related to lipid storage was decreased but did not reach statistical significance. The above results indicated that although activated charcoal could improve whitening in BAT, it was not due to enhanced fat oxidation.

Acidic Activated Charcoal Does Not Damage the Lungs and Digestive Tract

Since acidic activated charcoal powder was not digested or absorbed into the body and charcoal was excreted into the feces and mouse bedding in the cage turned black by the charcoal treatment (**Supplementary Figure 6A**), we next examined for possible pulmonary and gastrointestinal toxicity. To assess the

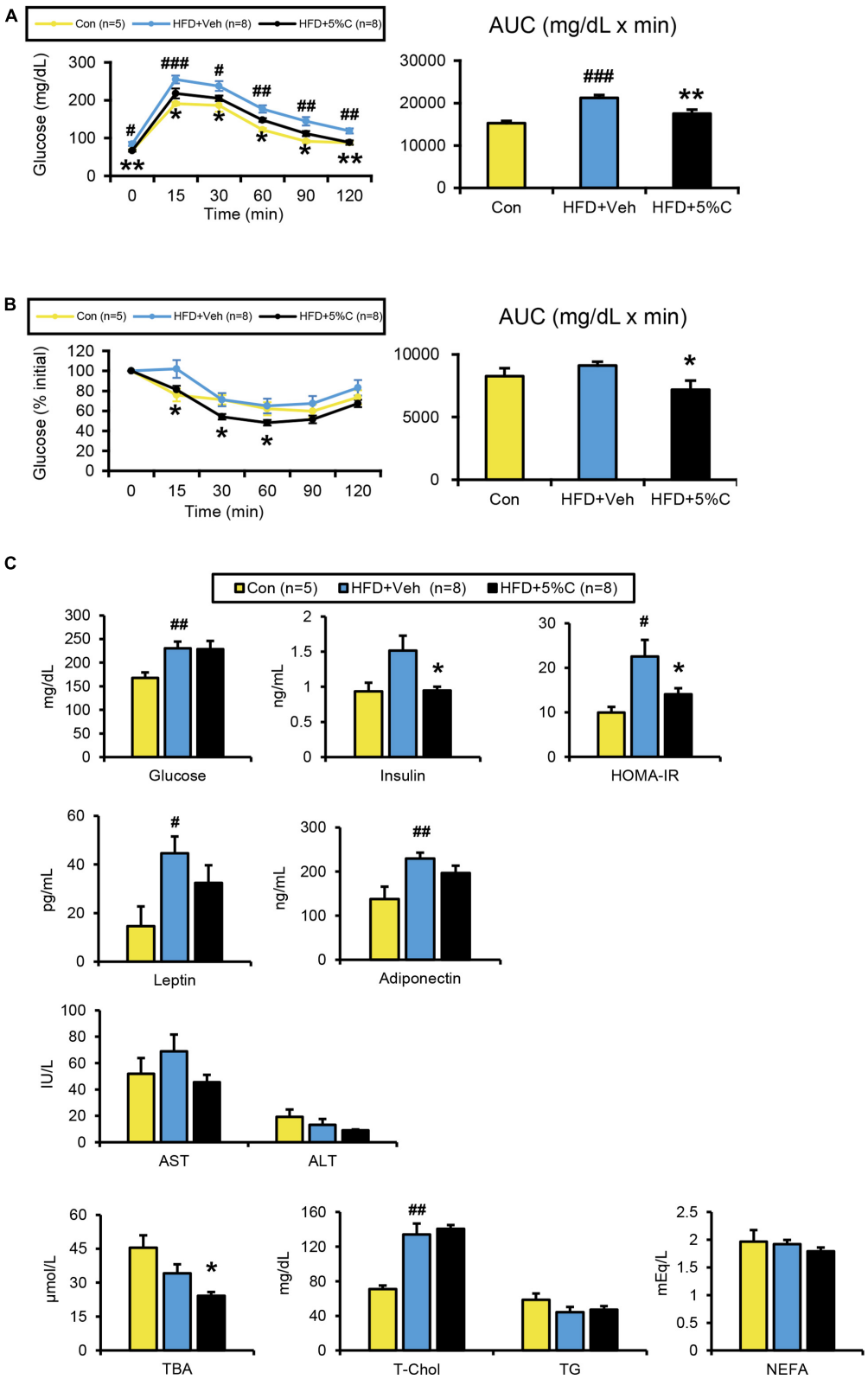

FIGURE 2 | Changes in metabolic parameters of mice treated with acidic activated charcoal. **(A)** GTT at 10 weeks of HFD feeding. **(B)** ITT at 12 weeks of HFD feeding. **(C)** Serum levels of glucose, insulin, HOMA-IR, leptin, high-molecular-weight adiponectin, AST, ALT, TBA, T-Chol, TG, and NEFA. Data are expressed as the mean ± SEM. Statistical analysis was performed using two-tailed Student's *t*-tests. $^{*}P < 0.05$ and $^{**}P < 0.01$ between the HFD + Veh group and the HFD + 5%C group. $^{\#}P < 0.05$, $^{\#\#}P < 0.01$, and $^{\#\#\#}P < 0.001$ between the HFD + Veh group and the Con group.

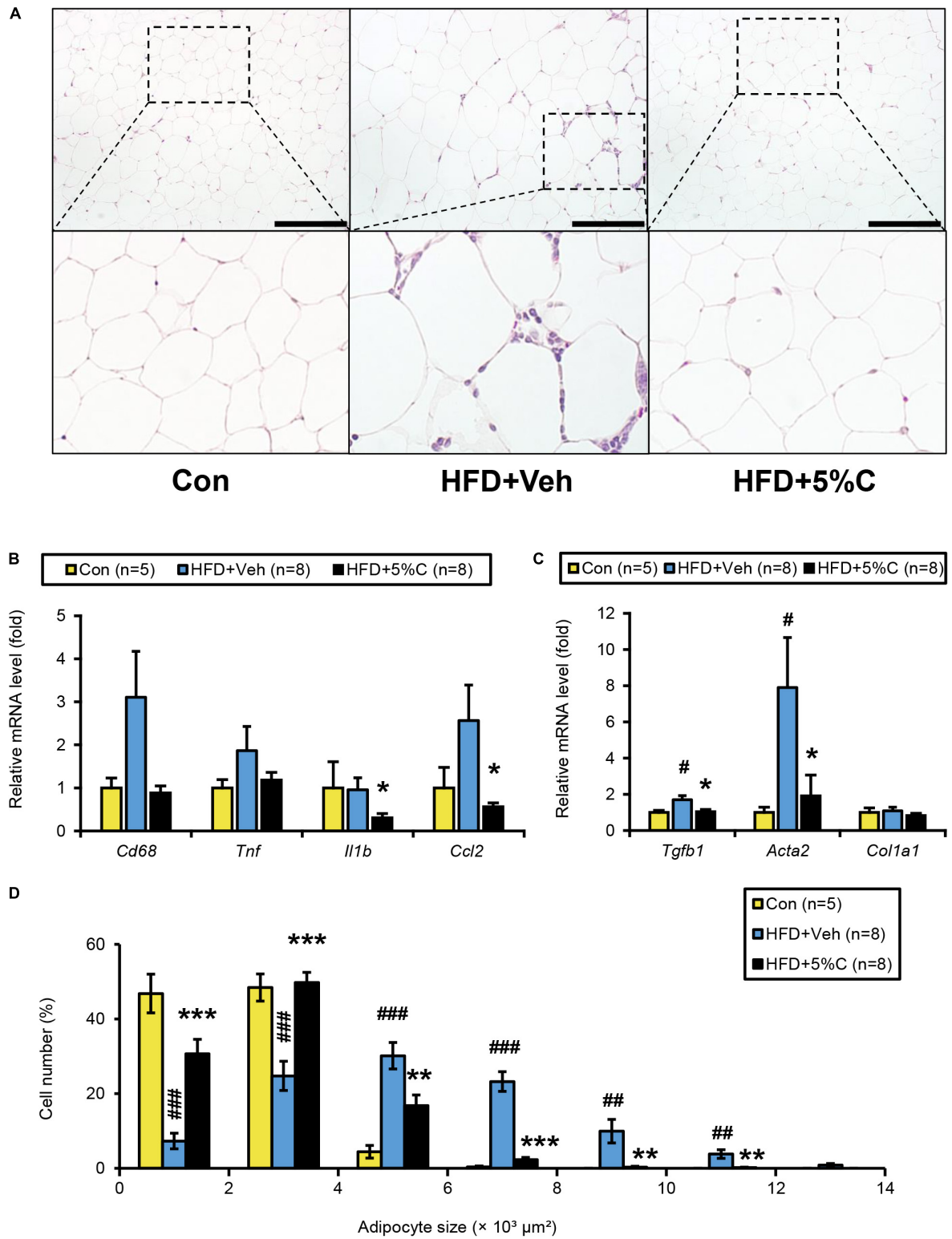

FIGURE 3 | Changes in eWAT after activated charcoal treatment. **(A)** Histological appearance of eWAT. The sections were stained with hematoxylin and eosin. Scale bars = 150 μm (x200 magnification). **(B)** The mRNA levels of genes related to inflammation (*Cd68, Tnf, Il1b,* and *Ccl2*) in the liver. **(C)** The mRNA levels of genes related to fibrosis (*Tgfb1, Acta2,* and *Col1a1*) in the liver. **(D)** Proportions of adipocytes of different sizes. Data are expressed as the mean ± SEM. Statistical analysis was performed using two-tailed Student's *t*-tests. $^{*}P < 0.05$, $^{**}P < 0.01$, and $^{***}P < 0.001$ between the HFD + Veh group and the HFD + 5%C group. $^{\#}P < 0.05$, $^{\#\#}P < 0.01$, and $^{\#\#\#}P < 0.001$ between the HFD + Veh group and the Con group.

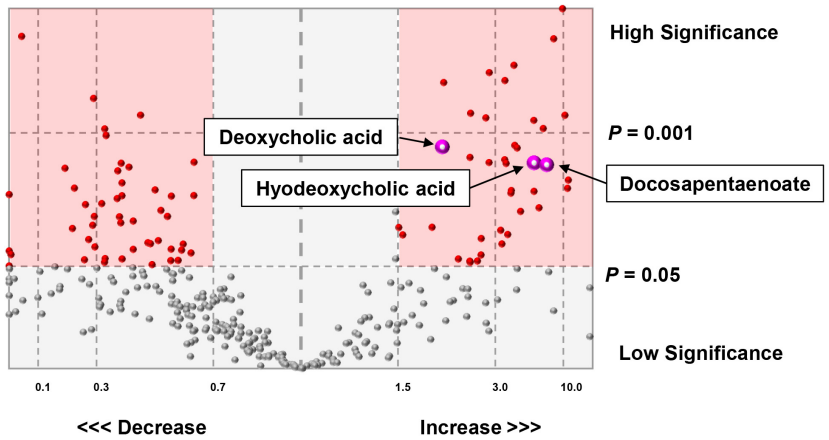

FIGURE 4 | Metabolomic analysis of cecal contents. A volcano plot identified 42 metabolites, including deoxycholic acid, hyodeoxycholic acid, and docosapentaenoate, that were significantly increased in the HFD + 5%C group as compared with the HFD + Veh group (right pink square).

presence of inflammation in the lungs and gastrointestinal tract, we determined mRNA levels in the lung (**Supplementary Figure 6B**), stomach (**Supplementary Figure 6C**), upper small intestine (**Supplementary Figure 6D**), lower small intestine (**Supplementary Figure 6E**), and large intestine (**Supplementary Figure 6F**). The mRNA levels of genes related to inflammation [*Il1b*, *Ccl2*, and nitric oxide synthase 2 (*Nos2*)], fibrosis (*Tgfb1*), and neutrophil infiltration [myeloperoxidase (*Mpo*)] were not significantly different between the HFD + 5%C and HFD + Veh groups. The possibility that co-treatment with acidic activated charcoal could injure/irritate the respiratory and gastrointestinal mucosa was therefore considered low.

Acidic Activated Charcoal Affects Bile Acid Metabolism

Since shortening of the small intestine and a reduction in cecal contents were prevented by treatment with acidic activated charcoal, we tested the possibility that the intestinal environment was altered by such treatment by the metabolomic analysis of cecal contents. A volcano plot identified 42 metabolites that were significantly increased in the HFD + 5%C group as compared with the HFD + Veh group (**Figure 4**). The 20 most significantly increased metabolites are listed in **Supplementary Table 5**. Nine metabolites were neutral lipids, FAs, or BAs such as docosapentaenoate, deoxycholic acid (DCA), and hyodeoxycholic acid (**Figure 4**). To validate these metabolomic results, fecal lipids and BAs were quantified, revealing that the amounts of TGs, PLs, and TBA were significantly increased in the feces of all mice in the HFD + 5%C group (**Figure 5A**).

BA metabolism, including DCA, lithocholic acid, and taurocholic acid, is controlled by farnesoid X receptor (FXR). Analysis of the FXR signaling pathway in the lower small intestine and liver revealed that the mRNA levels of *Fxr* and its target genes, including small heterodimer partner (*Shp*), fibroblast growth factor 15 (*Fgf15*), apical sodium BA transporter (*Asbt*), and FA-binding protein 6 (*Fabp6*), were significantly down-regulated in the HFD + 5%C group vs. the HFD + Veh group in the intestine (**Figure 5B**) while those of *Fxr*-regulated genes were unchanged in the liver, indicating that intestinal FXR was specifically down-regulated by charcoal co-administration. BAs have also been shown to effectively activate Takeda G protein-coupled receptor 5 (TGR5), although the mRNA levels of *Tgr5* in the lower small intestine were not significantly increased in the HFD + 5%C group (**Figure 5B**).

The hepatic mRNA expression of cholesterol 7 alpha-hydroxylase (*Cyp7a1*), a rate-limiting enzyme of BA synthesis, as well as those of hydroxymethylglutaryl-CoA synthase 1 (*Hmgcs1*) and reductase (*Hmgcr*), both rate-limiting enzymes of *de novo* cholesterol synthesis, were significantly increased in the HFD + 5%C group as compared with the HFD + Veh group, while those of ATP-binding cassette sub-family B member 11 (*Abcb11*) and *Fxr* were comparable to the HFD + Veh group (**Figure 5C**). These changes were likely due to an adaptive response to decreased BA reabsorption in the intestine, i.e., increased BA excretion into the feces, by acidic activated charcoal.

Acidic Activated Charcoal Prevents High-Fat Diet-Induced Obesity and Insulin Resistance in a Dose-Dependent Manner

To evaluate the reproducibility and dose dependency of the anti-obesity effect of acidic activated charcoal, a second mouse cohort was given a HFD supplemented with different charcoal contents for 12 weeks. In the 1.5, 3, and 4.5% charcoal-containing HFD groups (HFD + 1.5%C, HFD + 3%C, and HFD + 4.5%C, respectively), weight gain was significantly suppressed vs. the HFD + Veh group, which was enhanced with charcoal dosage (**Figure 6A** and **Supplementary Table 6**). There were no significant differences in the gross appearance of the liver or the liver/body weight ratio among the five

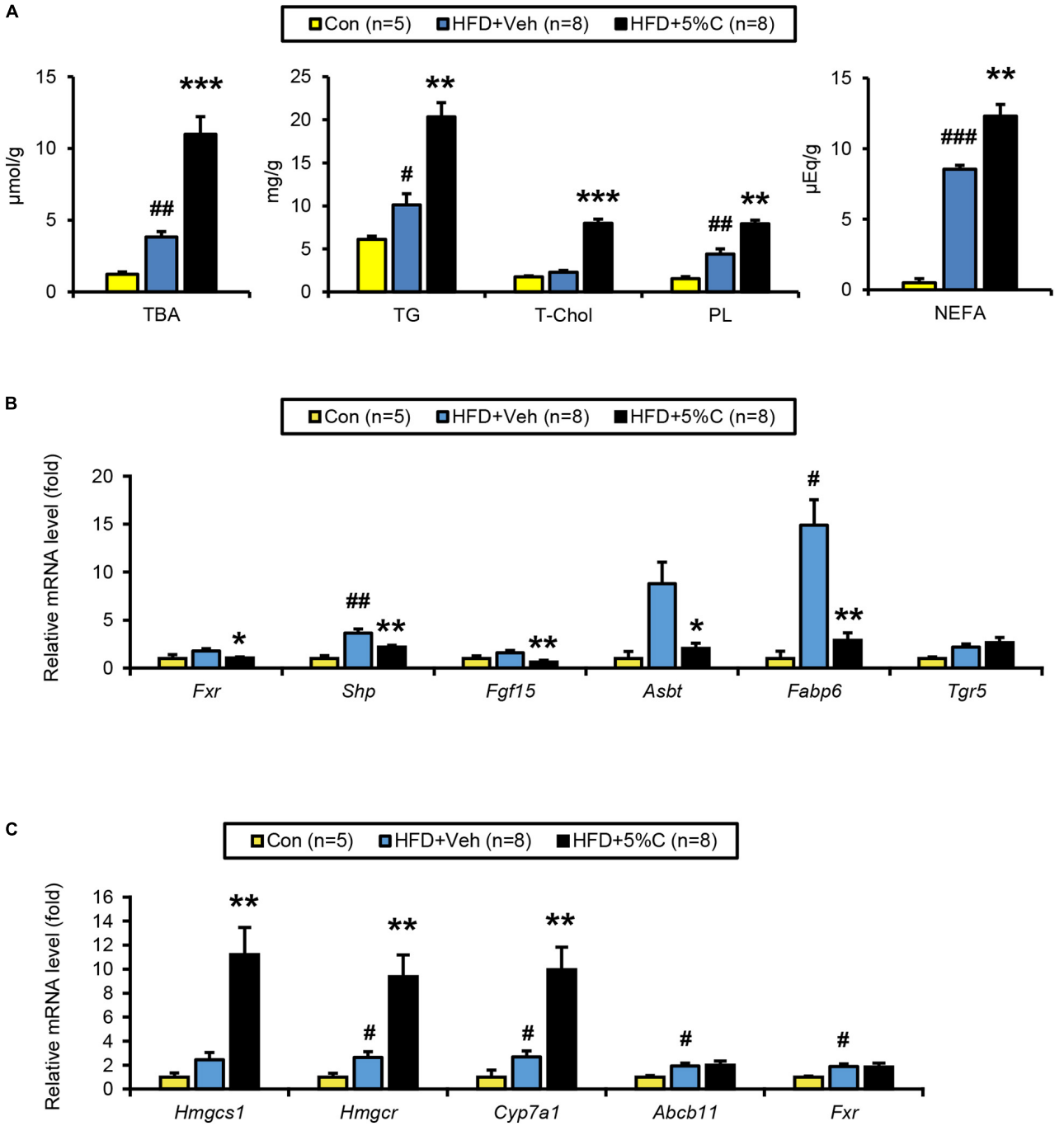

FIGURE 5 | BA metabolism is affected by activated charcoal treatment. **(A)** Quantitative analysis of TBA, TG, T-Chol, PL, and NEFA in cecal contents. **(B)** The mRNA levels of genes related to BA metabolism (*Fxr, Shp, Fgf15, Asbt*, *Fabp6*, and *Tgr5*) in the intestine. **(C)** The mRNA levels of genes related to BA/cholesterol metabolism (*Hmgcs1, Hmgcr*, *Cyp7a1, Abcb11*, and *Fxr*) in the liver. Data are expressed as the mean ± SEM. Statistical analysis was performed using two-tailed Student's *t*-tests. $^{*}P < 0.05$, $^{**}P < 0.01$, and $^{***}P < 0.001$ between the HFD + Veh group and the HFD + 5%C group. $^{\#}P < 0.05$, $^{\#\#}P < 0.01$, and $^{\#\#\#}P < 0.001$ between the HFD + Veh group and the Con group.

groups (**Figures 6B,C**). As in the first experiment, eWAT became larger and the cecum became smaller in the HFD + Veh group over the Con group. Acidic activated charcoal improved these changes in a dose-dependent manner without affecting thyroid function (**Figures 6B,C**, **Supplementary Figure 1B** and **Supplementary Table 6**).

The GTT was conducted in the ninth week of HFD treatment. The blood glucose levels of all HFD + C (1.5%C, 3%C, and 4.5%C)

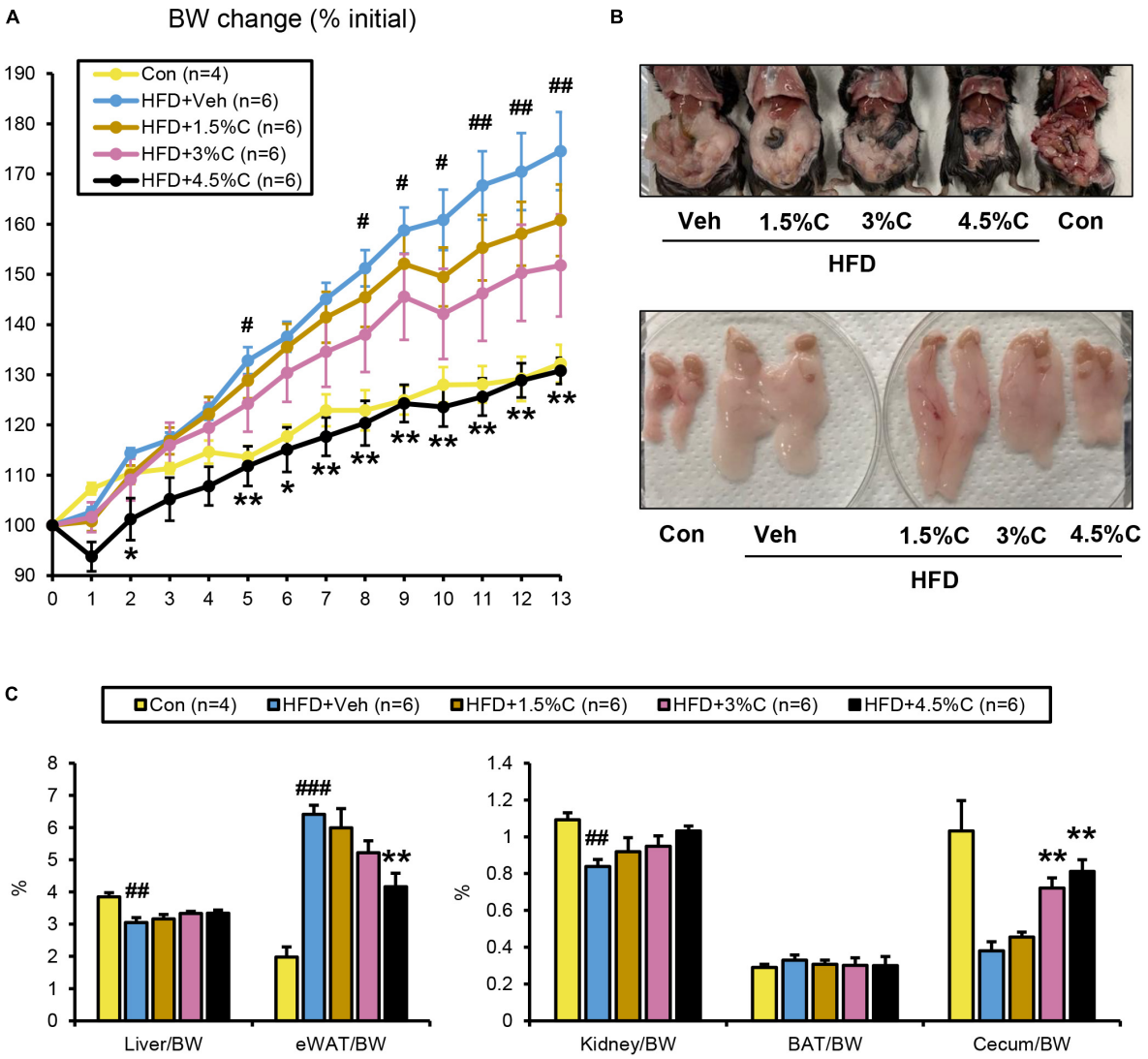

FIGURE 6 | HFD containing 4.5% acidic activated charcoal showed the strongest anti-obesity effect after 13 weeks of treatment. **(A)** Changes in BW. **(B)** Gross appearance of abdominal organs (upper panel) and epididymal white adipose tissue (eWAT) (lower panel) derived from five representative groups of mice. **(C)** Weights of the liver, eWAT, kidney, BAT, and cecum. Values were corrected by body weight (BW). Data are expressed as the mean ± SEM. Statistical analysis was performed using a one-way analysis of variance (ANOVA) with the Bonferroni's correction. $^{*}P < 0.05$, and $^{**}P < 0.01$ between the HFD + Veh group and the HFD + C group. $^{\#}P < 0.05$, $^{\#\#}P < 0.01$, and $^{\#\#\#}P < 0.001$ between the HFD + Veh group and the Con group.

groups were consistently lower than that of the HFD + Veh group, with the HFD + 4.5%C group exhibiting the lowest blood sugar level (**Figure 7A**). The AUC became smaller with increasing doses in the HFD + C groups vs. the HFD + Veh group (**Figure 7A**).

The ITT in the eleventh week of treatment showed that the glucose levels in all HFD + C groups fell faster than in the HFD + Veh group. The decrease in the HFD + 4.5%C group was especially larger than in the Con group (**Figure 7B**), which was reflected in the AUC results (**Figure 7B**). Serum insulin levels and HOMA-IR significantly decreased in the HFD + C groups with rising charcoal doses (**Figure 7C**). These findings indicated that 4.5%C exerted the strongest therapeutic effect on HFD-induced insulin resistance. Similarly to the results of the first experiment, there were no significant differences in serum and hepatic lipid profile parameters between the HFD + Veh and HFD + C groups (**Figure 7D** and **Supplementary Figure 7A**).

Acidic Activated Charcoal Improves High-Fat Diet-Induced Epididymal White Adipose Tissue Hypertrophy and Inflammation as Well as Brown Adipose Tissue Whitening in a Dose-Dependent Manner

Microscopic examination of eWAT revealed that the adipocyte hypertrophy and inflammatory cell infiltration around adipocytes in the HFD + Veh group were dose-dependently corrected by charcoal intake; as the charcoal doses increased, the proportion

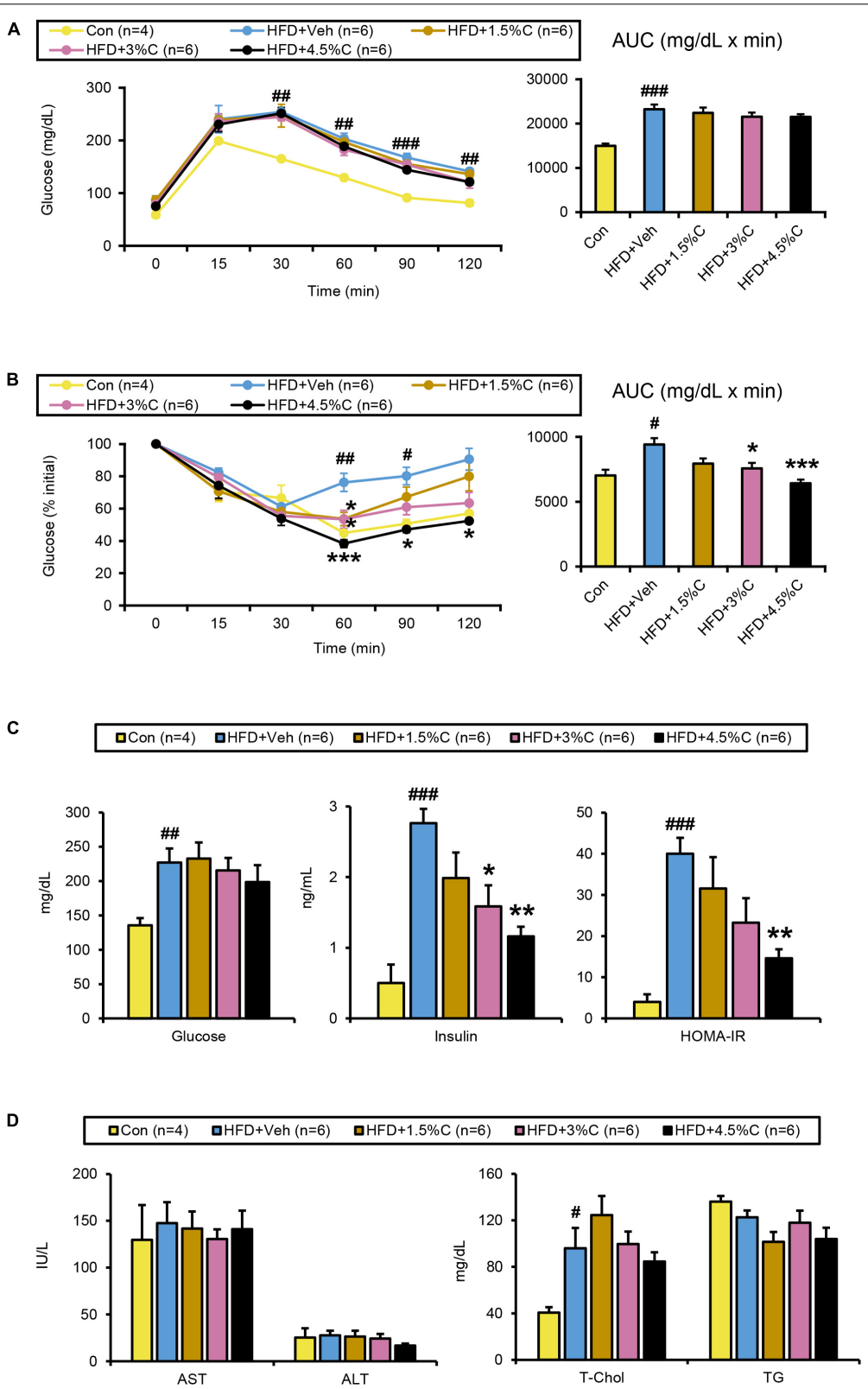

FIGURE 7 | Changes in metabolic parameters of mice treated with different dosages of acidic activated charcoal. **(A)** GTT at 9 weeks of HFD feeding. **(B)** ITT at 11 weeks of HFD feeding. **(C)** Serum levels of glucose, insulin and HOMA-IR. **(D)** Serum levels of AST, ALT, T-Chol, and TG. Data are expressed as the mean ± SEM. Statistical analysis was performed using a one-way analysis of variance (ANOVA) with the Bonferroni's correction. $^{*}P < 0.05$, $^{**}P < 0.01$, and $^{***}P < 0.001$ between the HFD + Veh group and the HFD + C group. $^{\#}P < 0.05$, $^{\#\#}P < 0.01$, and $^{\#\#\#}P < 0.001$ between the HFD + Veh group and the Con group.

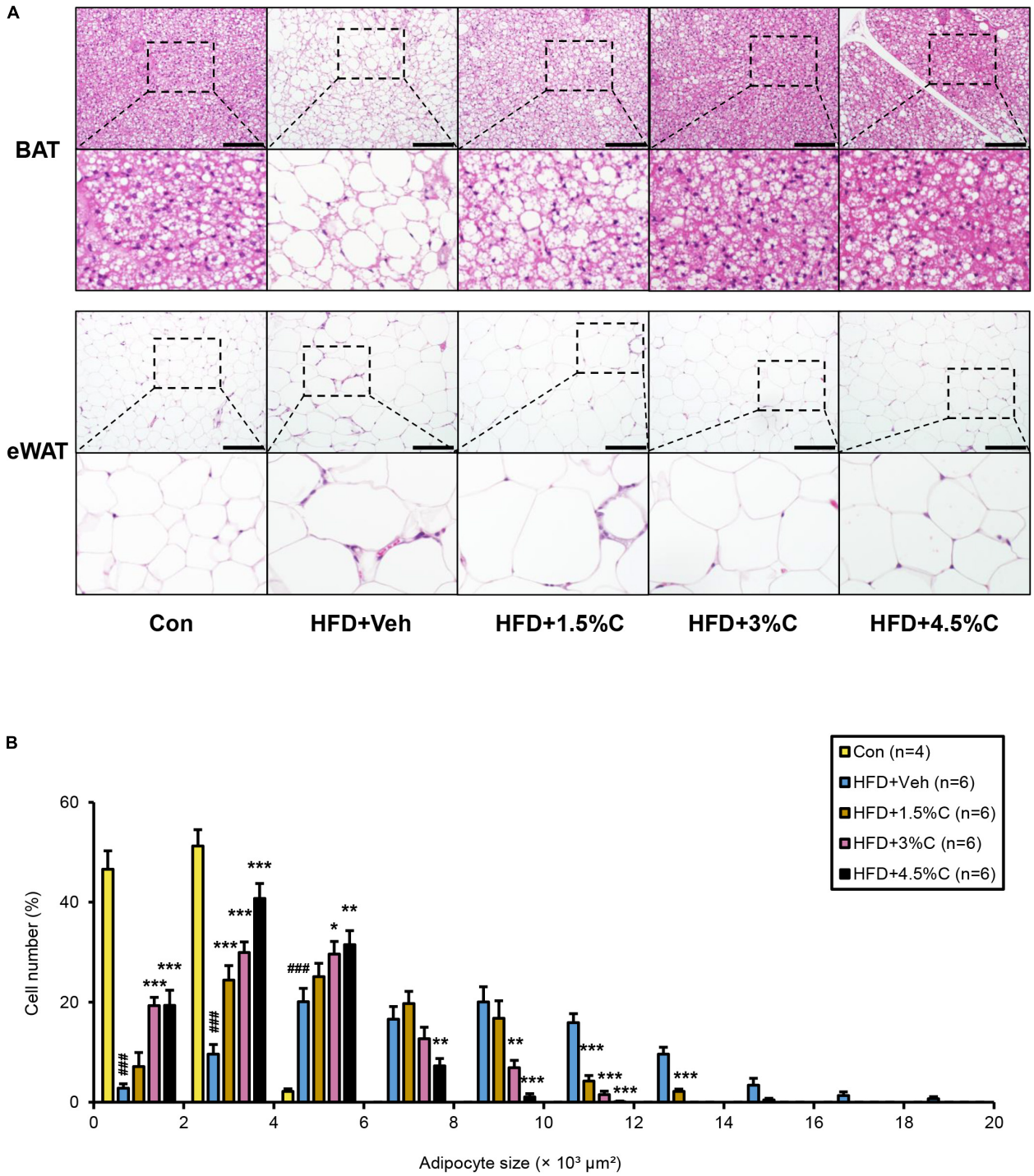

FIGURE 8 | Changes in histological appearance after treatment with different dosages of acidic activated charcoal. **(A)** Histological appearance of BAT and eWAT. The sections were stained with hematoxylin and eosin. Scale bars = 150 μm (x200 magnification). **(B)** Proportions of adipocytes of different sizes. Data are expressed as the mean ± SEM. Statistical analysis was performed using a one-way analysis of variance (ANOVA) with the Bonferroni's correction. $^{*}P < 0.05$, $^{**}P < 0.01$, and $^{***}P < 0.001$ between the HFD + Veh group and the HFD + C group. $^{###}P < 0.001$ between the HFD + Veh group and the Con group.

of larger adipocytes decreased significantly (**Figures 8A,B**). Compared with the HFD + Veh group, the expression levels of inflammation- and fibrosis-related genes, such as *Cd68*, *Il1b*, *Ccl2*, *Tgfb1*, *Acta2*, and *Col1a1*, were decreased in the HFD + C groups with rising charcoal doses (**Figure 9A**). Histological analysis of BAT revealed that the HFD-induced unilateral

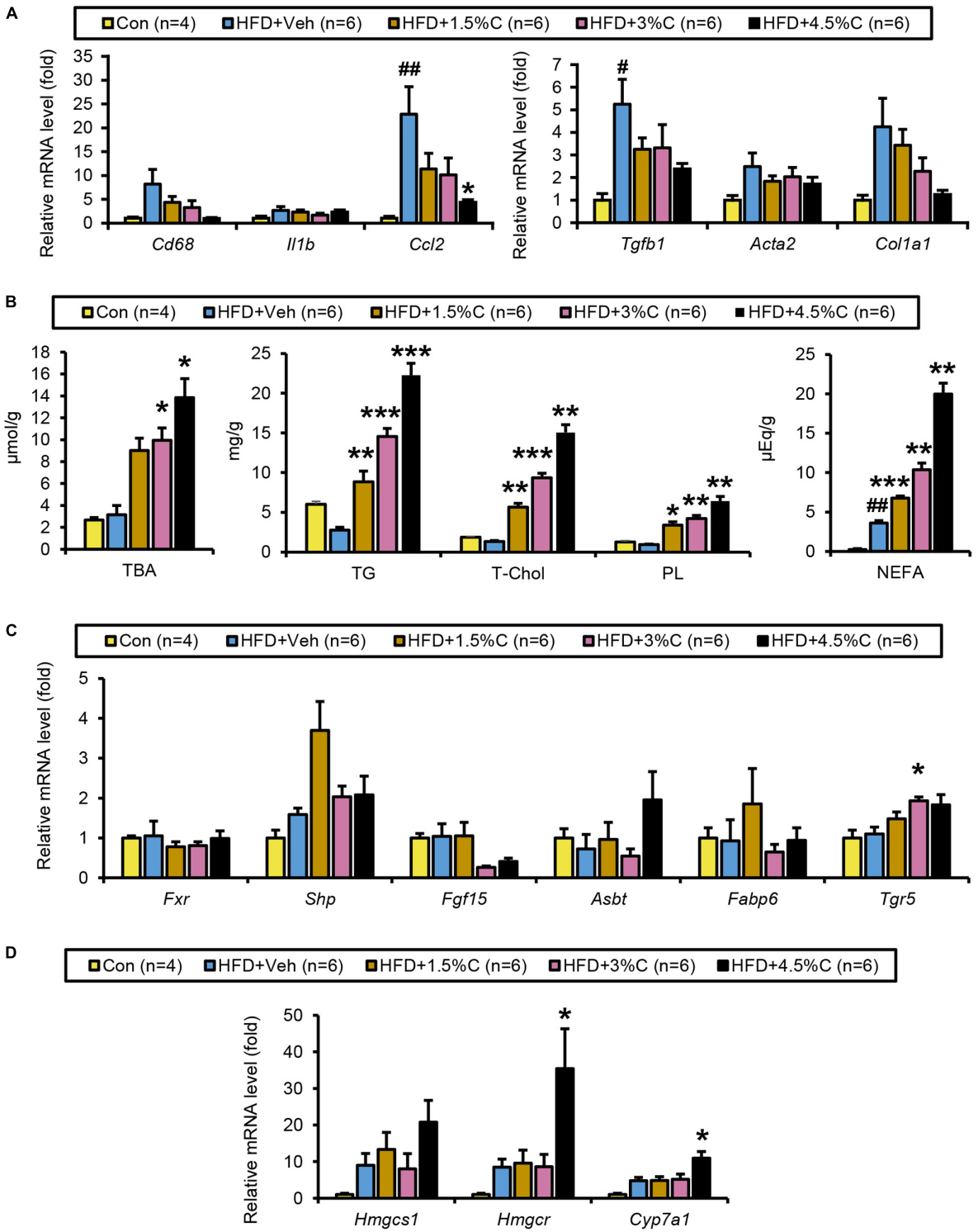

FIGURE 9 | Changes in lipid metabolism after treatment with different dosages of acidic activated charcoal. **(A)** The mRNA levels of genes related to inflammation (*Cd68, Il1b,* and *Ccl2*) and fibrosis (*Tgfb1, Acta2,* and *Col1a1*) in the liver. **(B)** Quantitative analysis of TBA, TG, T-Chol, PL, and NEFA in cecal contents. **(C)** The mRNA levels of genes related to BA metabolism (*Fxr, Shp, Fgf15, Asbt, Fabp6,* and *Tgr5*) in the intestine. **(D)** The mRNA levels of genes related to cholesterol metabolism (*Hmgcs1, Hmgcr,* and *Cyp7a1*) in the liver. Data are expressed as the mean ± SEM. Statistical analysis was performed using a one-way analysis of variance (ANOVA) with the Bonferroni's correction. $^{*}P < 0.05$, $^{**}P < 0.01$, and $^{***}P < 0.001$ between the HFD + Veh group and the HFD + C group. $^{\#}P < 0.05$, and $^{\#\#}P < 0.01$ between the HFD + Veh group and the Con group.

lipid droplets and slight inflammatory cell infiltration around adipocytes were ameliorated with increasing charcoal doses (**Figure 8A**). Overall, our results indicated that the improvement of HFD-induced eWAT hypertrophy and inflammation by acidic activated charcoal, as well as BAT whitening, were dose-dependent.

Acidic Activated Charcoal Increases Fecal Lipids and Bile Acids in a Dose-Dependent Manner

The amounts of TBA, TGs, T-Chol, PLs, and NEFAs all significantly increased with higher charcoal doses in feces samples collected from the HFD + C groups (**Figure 9B**). However, *Fxr* and its related genes (*Shp*, *Fgf15*, *Asbt*, and *Fabp6*) showed no remarkable differences between the HFD + Veh group and the HFD + C groups. Interestingly, the mRNA level of *Tgr5* increased with greater doses of charcoal, which was significant in the HFD + 3%C groups (**Figure 9C**).

The finding that the hepatic mRNA expressions of *Hmgcr* and *Cyp7a1* were significantly increased in the HFD + 4.5%C group indicated enhanced synthesis of cholesterol and BAs in the liver (**Figure 9D**), likely reflecting dose-dependent increases in cholesterol/BA excretion into the feces.

DISCUSSION

The current study showed that acidic activated charcoal could prevent HFD-induced obesity, insulin resistance, eWAT hypertrophy and inflammation, as well as enhance BAT whitening in a dose-dependent manner without any serious adverse effects. Metabolomic analysis of cecal contents revealed that neutral lipids, cholesterol, and BAs were markedly more excreted into the feces with charcoal supplementation. Consequently, the enterohepatic circulation of cholesterol/BA was promoted as evidenced by the up-regulated hepatic expression of *de novo* BA- and cholesterol-synthesizing enzymes (13). The current study proposes a novel function of acidic activated charcoal to prevent obesity, overnutrition, metabolic syndrome, and related diseases.

The most intriguing finding of the initial study was that the BW gain in the mice treated with activated charcoal was significantly lower than in the HFD + Veh group, which was similar to that in the Con group, with no difference in food intake or thyroid function between the HFD + 5%C and HFD + Veh groups. Moreover, acidic activated charcoal significantly improved HFD-induced hyperinsulinemia, insulin resistance, WAT hypertrophy and intestinal length shortening and could reduce cecum volume to levels comparable to the Con group.

In order to validate the findings of the first study and clarify which concentrations of activated charcoal exhibited the highest anti-obesity properties, we investigated progressively higher doses of the material. Our results showed that 4.5% activated charcoal was the most effective in improving the phenotypic changes induced by long-term HFD feeding without any detrimental effects. This information might be applicable to humans in future food additives to prevent obesity.

In the initial study and dose-dependent study, liver TG levels did not increase in the HFD + Veh group. In this study, inulin, dextrin, and raffinose were used as a vehicle to prevent constipation by charcoal. It was documented that inulin could attenuate hepatic TG accumulation in several mouse models, such as high-fat/high-sucrose treated mice and high-cholesterol treated mice (14, 15). Additionally, raffinose could ameliorate hepatic lipid accumulation in high cholic acid treated rats (16). The absence of marked TG accumulation may be associated with the action of inulin and raffinose to attenuate hepatic steatosis.

According to the metabolomic analysis, large amounts of BAs were excreted into the feces by inhibiting their reabsorption in the intestine, and so altered amounts of BAs in the enterohepatic circulation were detected in the liver. As a compensatory response, *Cyp7a1*, a rate-limiting enzyme for *de novo* BA synthesis from cholesterol, may have been increased by the charcoal; a sufficient supply of cholesterol is necessary to synthesize BAs. The intestinal absorption of dietary cholesterol requires emulsification by BAs (17). A large amount of BAs were combined with activated charcoal and excreted through the feces, which demonstrated altered digestion and absorption of cholesterol in the intestine. These changes may increase *Hmgcs1* and *Hmgcr*.

Prior studies have found that FXR disruption and activated TGR5 in the intestine, which are closely associated with intestinal BA signaling and nutrient homeostasis, produce an anti-obesity effect and improve glucose metabolism (18–22). The inconsistency of changes in intestinal FXR/TGR5 between the two independent experiments prompted us to conclude that FXR/TGR5 was not a primary reason explaining the anti-obesity effect of acidic activated charcoal. The charcoal also absorbed BAs, cholesterol, and neutral lipids in the small intestine, thereby enhancing the excretion of fat into the feces and preventing BW gain.

It was earlier reported that obese patients were in a state of persistent chronic inflammation, which mediated the development of obesity-related diseases, especially type 2 diabetes (23, 24). In particular, adipose expansion induces the adipose inflammation related to insulin resistance (25–27). Indeed, the expression levels of *Il1b* and *Ccl2* in the HFD + 5%C group were significantly decreased vs. the HFD + Veh group. Although no remarkable differences were observed for *Cd68* or *Tnf*, the HFD + 5%C group showed a decreasing trend. In the dose-dependency experiment, the mRNA levels of *Cd68*, *Ccl2*, *Tgfb1*, and *Col1a1* all decreased with increasing levels of acidic activated charcoal. This indicated that the charcoal alleviated the adipose microinflammation caused by obesity, with larger doses of the material being more effective.

Since the activated charcoal was a powder and was not digested by the animals, we were concerned about pneumoconiosis and damage to the digestive tract (28). However, there were no visible differences of the lungs and gastrointestinal tract, and inflammation-related gene levels were not increased in the

HFD + 5%C compared with HFD + Veh groups. Based on those findings, we consider the oral administration of acidic activated charcoal to be relatively safe, although further long-term studies are required to confirm its safety and applicability in humans. Moreover, because activated charcoal can absorb lipids, it may disrupt the absorption of fats, fat-soluble vitamins, and folic acid (29–31). As the next step, extended experiments will be mandatory to monitor for deficiencies in essential FAs and fat-soluble vitamins. Acidic activated charcoal can absorb not only lipids, but also toxic contaminants in foods, and metabolites from microbiota, such as indole acetate and lithocholic acid. These metabolites are ligands for the aryl hydrocarbon receptor and pregnane X receptor, which modulate intestinal mucosal immunity (32). It is of great interest whether acidic activated charcoal can modulate the crosstalk between metabolites, the microbiome, epithelial cells, and immune cells.

CONCLUSION

Acidic activated charcoal improved HFD-induced obesity and insulin resistance without any serious adverse effects. These beneficial effects were likely due to modulating lipid absorption and altered FA/BA metabolism.

DATA AVAILABILITY STATEMENT

The raw data supporting the conclusions of this article will be made available by the authors, without undue reservation.

ETHICS STATEMENT

The animal study was reviewed and approved by the Shinshu University School of Medicine.

AUTHOR CONTRIBUTIONS

NT contributed to conception and design of the study. HY, YI, and TY made activated charcoal and provided it. XZ, PD, XW, ZZ, XH, TN, TK, and NT conducted animal experiments, collected the data, and performed statistical analysis. KT, CH, and MN performed metabolomic analysis. JN supervised histological analysis. XZ, TK, and NT wrote the manuscript. All authors contributed to manuscript revision, read, and approved the submitted version.

FUNDING

This study was partially supported by the Shinshu Public Utility Foundation for Promotion of Medical Sciences 2021. The authors declare that this study received funding from Sumi Plus Lab Co., Ltd. and Ina Carbonization Laboratory Co., Ltd. The funders were not involved in the study design, collection, analysis, interpretation of data, the writing of this article or the decision to submit it for publication.

ACKNOWLEDGMENTS

We thank Trevor Ralph for editing the manuscript and Nobuhiro Okubo of LSI Medience for assistance with the metabolomic analysis.

SUPPLEMENTARY MATERIAL

The Supplementary Material for this article can be found online at: https://www.frontiersin.org/articles/10.3389/fnut.2022.852767/full#supplementary-material

REFERENCES

1. Collaborators GBDO, Afshin A, Forouzanfar MH, Reitsma MB, Sur P, Estep K, et al. Health effects of overweight and obesity in 195 Countries over 25 years. *N Engl J Med.* (2017) 377:13–27. doi: 10.1056/NEJMoa1614362
2. Kapoor N, Furler J, Paul TV, Thomas N, Oldenburg B. Normal weight obesity: an underrecognized problem in individuals of South Asian descent. *Clin Ther.* (2019) 41:1638–42. doi: 10.1016/j.clinthera.2019.05.016
3. Schetz M, De Jong A, Deane AM, Druml W, Hemelaar P, Pelosi P, et al. Obesity in the critically ill: a narrative review. *Intensive Care Med.* (2019) 45:757–69. doi: 10.1007/s00134-019-05594-1
4. Meinita MD, Hong YK, Jeong GT. Detoxification of acidic catalyzed hydrolysate of *Kappaphycus alvarezii* (cottonii). *Bioprocess Biosyst Eng.* (2012) 35:93–8. doi: 10.1007/s00449-011-0608-x
5. Zellner T, Prasa D, Farber E, Hoffmann-Walbeck P, Genser D, Eyer F. The use of activated charcoal to treat intoxications. *Dtsch Arztebl Int.* (2019) 116:311–7. doi: 10.3238/arztebl.2019.0311
6. Neuvonen PJ, Kuusisto P, Manninen V, Vapaatalo H, Miettinen TA. The mechanism of the hypocholesterolaemic effect of activated charcoal. *Eur J Clin Invest.* (1989) 19:251–4. doi: 10.1111/j.1365-2362.1989.tb00226.x
7. Matthews DR, Hosker JP, Rudenski AS, Naylor BA, Treacher DF, Turner RC. Homeostasis model assessment: insulin resistance and beta-cell function from fasting plasma glucose and insulin concentrations in man. *Diabetologia.* (1985) 28:412–9. doi: 10.1007/BF00280883
8. Tanaka N, Matsubara T, Krausz KW, Patterson AD, Gonzalez FJ. Disruption of phospholipid and bile acid homeostasis in mice with nonalcoholic steatohepatitis. *Hepatology.* (2012) 56:118–29. doi: 10.1002/hep.25630
9. Hara A, Radin NS. Lipid extraction of tissues with a low-toxicity solvent. *Anal Biochem.* (1978) 90:420–6. doi: 10.1016/0003-2697(78)90046-5
10. Carr TP, Andresen CJ, Rudel LL. Enzymatic determination of triglyceride, free cholesterol, and total cholesterol in tissue lipid extracts. *Clin Biochem.* (1993) 26:39–42. doi: 10.1016/0009-9120(93)90015-x
11. Hu X, Tanaka N, Guo R, Lu Y, Nakajima T, Gonzalez FJ, et al. PPARalpha protects against trans-fatty-acid-containing diet-induced steatohepatitis. *J Nutr Biochem.* (2017) 39:77–85. doi: 10.1016/j.jnutbio.2016.09.015
12. Tanaka N, Takahashi S, Fang ZZ, Matsubara T, Krausz KW, Qu A, et al. Role of white adipose lipolysis in the development of NASH induced by methionine- and choline-deficient diet. *Biochim Biophys Acta.* (2014) 1841:1596–607. doi: 10.1016/j.bbalip.2014.08.015
13. Vicens M, Macias RI, Briz O, Rodriguez A, El-Mir MY, Medarde M, et al. Inhibition of the intestinal absorption of bile acids using cationic derivatives: mechanism and repercussions. *Biochem Pharmacol.* (2007) 73:394–404. doi: 10.1016/j.bcp.2006.10.014
14. Yang J, Zhang S, Henning SM, Lee R, Hsu M, Grojean E, et al. Cholesterol-lowering effects of dietary pomegranate extract and inulin in mice fed an

obesogenic diet. *J Nutr Biochem.* (2018) 52:62–9. doi: 10.1016/j.jnutbio.2017.10.003
15. Huang WC, Lin CL, Hsu YJ, Chiu YS, Chen YM, Wu MF, et al. Inulin and fibersol-2 combined have hypolipidemic effects on high cholesterol diet-induced hyperlipidemia in Hamsters. *Molecules.* (2016) 21:313. doi: 10.3390/molecules21030313
16. Maegawa K, Koyama H, Fukiya S, Yokota A, Ueda K, Ishizuka S. Dietary raffinose ameliorates hepatic lipid accumulation induced by cholic acid *via* modulation of enterohepatic bile acid circulation in rats. *Br J Nutr.* (2021) 14:1–10. doi: 10.1017/S0007114521002610
17. Chen ML, Takeda K, Sundrud MS. Emerging roles of bile acids in mucosal immunity and inflammation. *Mucosal Immunol.* (2019) 12:851–61. doi: 10.1038/s41385-019-0162-4
18. Porez G, Prawitt J, Gross B, Staels B. Bile acid receptors as targets for the treatment of dyslipidemia and cardiovascular disease. *J Lipid Res.* (2012) 53:1723–37. doi: 10.1194/jlr.R024794
19. Zhang X, Huang S, Gao M, Liu J, Jia X, Han Q, et al. Farnesoid X receptor (FXR) gene deficiency impairs urine concentration in mice. *Proc Natl Acad Sci USA.* (2014) 111:2277–82. doi: 10.1073/pnas.1323977111
20. Jiang C, Xie C, Li F, Zhang L, Nichols RG, Krausz KW, et al. Intestinal farnesoid X receptor signaling promotes nonalcoholic fatty liver disease. *J Clin Invest.* (2015) 125:386–402. doi: 10.1172/JCI76738
21. de Aguiar Vallim TQ, Tarling EJ, Edwards PA. Pleiotropic roles of bile acids in metabolism. *Cell Metab.* (2013) 17:657–69. doi: 10.1016/j.cmet.2013.03.013
22. Albaugh VL, Banan B, Antoun J, Xiong Y, Guo Y, Ping J, et al. Role of bile acids and GLP-1 in mediating the metabolic improvements of bariatric surgery. *Gastroenterology.* (2019) 156:1041–1051e4. doi: 10.1053/j.gastro.2018.11.017
23. Magkos F, Hjorth MF, Astrup A. Diet and exercise in the prevention and treatment of type 2 diabetes mellitus. *Nat Rev Endocrinol.* (2020) 16:545–55. doi: 10.1038/s41574-020-0381-5
24. Malone JI, Hansen BC. Does obesity cause type 2 diabetes mellitus (T2DM)? Or is it the opposite? *Pediatr Diabetes.* (2019) 20:5–9. doi: 10.1111/pedi.12787
25. Winer DA, Luck H, Tsai S, Winer S. The intestinal immune system in obesity and insulin resistance. *Cell Metab.* (2016) 23:413–26. doi: 10.1016/j.cmet.2016.01.003
26. Olefsky JM, Glass CK. Macrophages, inflammation, and insulin resistance. *Annu Rev Physiol.* (2010) 72:219–46. doi: 10.1146/annurev-physiol-021909-135846
27. Tanaka N, Takahashi S, Matsubara T, Jiang C, Sakamoto W, Chanturiya T, et al. Adipocyte-specific disruption of fat-specific protein 27 causes hepatosteatosis and insulin resistance in high-fat diet-fed mice. *J Biol Chem.* (2015) 290:3092–105. doi: 10.1074/jbc.M114.605980
28. Huber M, Pohl W, Reinisch G, Attems J, Pescosta S, Lintner F. Lung disease 35 years after aspiration of activated charcoal in combination with pulmonary lymphangioleiomyomatosis. a histological and clinicopathological study with scanning electron microscopic evaluation and element analysis. *Virchows Arch.* (2006) 449:225–9. doi: 10.1007/s00428-006-0236-z
29. Thomas-Valdes S, Tostes M, Anunciacao PC, da Silva BP, Sant'Ana HMP. Association between vitamin deficiency and metabolic disorders related to obesity. *Crit Rev Food Sci Nutr.* (2017) 57:3332–43. doi: 10.1080/10408398.2015.1117413
30. Borel P, Caillaud D, Cano NJ. Vitamin D bioavailability: state of the art. *Crit Rev Food Sci Nutr.* (2015) 55:1193–205. doi: 10.1080/10408398.2012.688897
31. Hale SE, Arp HP, Kupryianchyk D, Cornelissen G. A synthesis of parameters related to the binding of neutral organic compounds to charcoal. *Chemosphere.* (2016) 144:65–74. doi: 10.1016/j.chemosphere.2015.08.047
32. Tanaka N, Aoyama T, Kimura S, Gonzalez FJ. Targeting nuclear receptors for the treatment of fatty liver disease. *Pharmacol Ther.* (2017) 179:142–57. doi: 10.1016/j.pharmthera.2017.05.011

Conflict of Interest: HY and TY were employed by Sumi Plus Lab Co., Ltd. YI was employed by Ina Carbonization Laboratory Co., Ltd. KT and CH were employed by LSI Medience Corporation.

The remaining authors declare that the research was conducted in the absence of any commercial or financial relationships that could be construed as a potential conflict of interest.

Publisher's Note: All claims expressed in this article are solely those of the authors and do not necessarily represent those of their affiliated organizations, or those of the publisher, the editors and the reviewers. Any product that may be evaluated in this article, or claim that may be made by its manufacturer, is not guaranteed or endorsed by the publisher.

frontiers | Frontiers in Nutrition

ORIGINAL RESEARCH
published: 16 May 2022
doi: 10.3389/fnut.2022.857879

Polydatin, A Glycoside of Resveratrol, Is Better Than Resveratrol in Alleviating Non-alcoholic Fatty Liver Disease in Mice Fed a High-Fructose Diet

Guangshan Zhao[1,2,3,4,5,6†], Lian Yang[1†], Wenshen Zhong[1], Yuze Hu[2], Yu Tan[2], Zhe Ren[2,5,6], Qiuyan Ban[7*], Chung S. Yang[8*], Yifei Wang[2,5,6*] and Zhiping Wang[1*]*

[1] Guangdong Provincial Engineering Center of Topical Precise Drug Delivery System, School of Pharmacy, Guangdong Pharmaceutical University, Guangzhou, China, [2] Department of Cell Biology, College of Life Science and Technology, Jinan University, Guangzhou, China, [3] School of Food Science and Technology, Henan Agricultural University, Zhengzhou, China, [4] Guangdong Province Key Laboratory of Bioengineering Medicine, Guangzhou, China, [5] Guangdong Provincial Biotechnology Drug and Engineering Technology Research Center, Guangzhou, China, [6] Guangzhou Jinan Biomedicine Research and Development Center Co., Ltd., Guangzhou, China, [7] College of Horticulture, Henan Agricultural University, Zhengzhou, China, [8] Department of Chemical Biology, Ernest Mario School of Pharmacy, Rutgers, The State University of New Jersey, Piscataway, NJ, United States

Resveratrol (RES) is considered to be an activator of AMP-activated protein kinase (AMPK) with many reported health benefits. Polydatin (POD) is a natural precursor and glycosylated form of RES. The glycoside structure of POD alters the bioactivity. Overnutrition-stimulated reactive oxygen species (ROS) promote the AMPK suppression and metabolic dysregulation. The present work compared the effects of POD and RES in ameliorating energy homeostasis imbalance in mice fed a high-fructose diet and elucidated the underlying mechanisms of action. Our results showed that POD elevated the fecal levels of valeric acid and caproic acid *via* modification of gut microbiota, while RES did not significantly influence the levels of fecal short-chain fatty acids (SCFAs). Both POD and RES markedly decreased the oxidative stress and activated the AMPK signaling pathways in the liver. POD and RES exerted a similar effect in alleviating glucose dysmetabolism, but POD was more effective in ameliorating lipid dysmetabolism than RES. Furthermore, valeric acid and caproic acid alone can activate the AMPK and ameliorate hypercholesterolemia, and enhance the effects of POD on improving lipid metabolism in mice. Overall, for the first time, we demonstrated that POD administration elevated the fecal levels of valeric acid and caproic acid by modifying gut microbiota, thus promoting AMPK activation may be the underlying mechanism that POD is superior to RES in alleviating the lipid dysmetabolism. Our results suggest that POD may be an alternative for RES as an AMPK activator.

Keywords: polydatin, resveratrol, non-alcoholic fatty liver disease, 5′-aMP-activated protein kinase, gut microbiota, short-chain fatty acids

OPEN ACCESS

Edited by:
Gratiela Gradisteanu Pircalabioru, University of Bucharest, Romania

Reviewed by:
Guanglin Zhang, University of California, Los Angeles, United States
Liang Zhao, Beijing Technology and Business University, China
Kang Sun, Southwest University, China

***Correspondence:**
Qiuyan Ban
banqiuyan717@163.com
Chung S. Yang
csyang@pharmacy.rutgers.edu
Yifei Wang
twang-yf@163.com
Zhiping Wang
wzping_jshb@126.com

† These authors have contributed equally to this work

Specialty section:
This article was submitted to Nutrition and Metabolism, a section of the journal Frontiers in Nutrition

Received: *19 January 2022*
Accepted: *04 March 2022*
Published: *16 May 2022*

Citation:
Zhao G, Yang L, Zhong W, Hu Y, Tan Y, Ren Z, Ban Q, Yang CS, Wang Y and Wang Z (2022) Polydatin, A Glycoside of Resveratrol, Is Better Than Resveratrol in Alleviating Non-alcoholic Fatty Liver Disease in Mice Fed a High-Fructose Diet. Front. Nutr. 9:857879. doi: 10.3389/fnut.2022.857879

INTRODUCTION

As the glycosylated form of resveratrol (RES, 3,4′,5-trihydroxystilbene) (**Figure 1D**), polydatin (POD, 3,4′,5-trihydroxystilbene-3-β-D-glucoside) (**Figure 1A**), also called piceid, is an interesting bioactive compound of Polygonum cuspidatum (2% of dry weight) (1). For a long time, POD was considered to be a lower bioavailability than RES, because the glycoside with a large molecular size and just can be better absorbed when the glycosides are hydrolyzed to their bioactive aglycones RES by β-glucosidases in the small intestine (2–6). *Polygonum cuspidatum* plants, grapes, berries, and peanuts contain RES only approximately 0.2% of dry weight (5), but RES possesses well-known health benefits and is widely applied in medicines, foods, and cosmetic products. RES mainly exists as the glycoside POD in plants (5, 6), hence, to increase the production of RES, POD should be converted into RES by deglycosylation technique (3–6), which is difficult and expensive. In the last decade, accumulated evidence suggests gut microbiota, such as *Lactobacillus* spp., *Bacteroides* spp., and *Bifidobacterium* spp, involves in the absorption, metabolism, and bioavailability of polyphenols glycosides (7–9). For instance, glycosides can be hydrolyzed to bioactive aglycones by β-glucosidases that secreted by bacterial in colon and enable the absorption of polyphenols glycosides (8, 9). *Bifidobacterium* strains show the capacity to enhance the bioavailability of daidzein under dysbiosis conditions (8). In addition, antibiotics treatment caused gut dysbiosis was involved in poor bioconversion of daidzin glycoside and polyphenols (8, 10). These reports indicated that gut microbiota-derived β-glucosidases in the colon play a role in improving the absorption and bioavailability of polyphenols glycosides, especially under the condition that a large amount of ingested but unabsorbed polyphenols glycosides can reach and persist to the colon. Moreover, Wang et al. recently found that POD and RES keep balance through mutual transformation after oral administration and ultimately POD is the main substance in serum (∼70%) (11). Thus, the actual bioactivity of POD and RES *in vivo* needs further comparative investigations.

The prevalence of metabolic disease is a serious public health challenge, as recognized by the World Health Organization in 2000 (12, 13). Fructose consumption increased pronouncedly in recent decades because the use of sucrose and high-fructose corn syrup in processed foods and beverages, and it has markedly contributed to the incidence rate of metabolic disease, such as non-alcoholic fatty liver disease, obesity and type 2 diabetes mellitus (T2DM) (14–16). Mammalian 5′-AMP-activated protein kinase (AMPK) is a regulator of cellular energy homeostasis and a sensor of adenine nucleotides that is activated in states of energy deficiency but suppressed in the overnutrition conditions (17, 18).

Extensive studies have demonstrated that the specific activation of AMPK in liver is beneficial to metabolic syndrome control; thus, AMPK is considered a crucial target for prevention and treatment of overnutrition-associated disease (19–21). Putative AMPK activators, such as the first-line and most prescribed drug metformin, have been identified and developed for the treatment of T2DM (20, 21). SCFAs mainly produced from the catabolism of carbohydrates by gut microbiota (22, 23), and may play an important role in regulating energy homeostasis. Acetate, butyrate, and propionate participate glucolipid neogenesis in liver (24), facilitate fat storage and fatty acid oxidation by browning of fat tissues (25, 26) or restrict energy intake *via* promoting the release of glucagon-like peptide 1 and peptide YY in colon (26, 27). Overnutrition-stimulated ROS promotes the AMPK deactivation by the suppression of phosphorylation of AMPKa at Thr172 (p-AMPKα [Thr172]) is one of the major inducements of metabolic disorders (18, 28, 29).

In addition, numerous studies have shown that nutrient overload could cause the gut microbiota dysbiosis and alter the levels of SCFAs in gut (30–32), and enhance the systemic oxidative stress level (18, 33, 34). All these alterations are consistently associated with the accumulated adipose tissue, elevated body weight, blood glucose level, systemic inflammation, and metabolic complications (30, 35).

Resveratrol is the most widely studied plant-derived natural product that can activate AMPK by multiple mechanisms such as the activation of SIRT1 (36) and the inhibition of mitochondrial function (37) and phosphodiesterases (38). Recent years, several studies suggest that POD possesses higher ability than RES on ameliorating oxidative stress by increasing the levels of total superoxide dismutase (SOD), catalase, glutathione peroxidase, and glutathione and decreasing the level of malondialdehyde (MDA) in mice (11), and has stronger anti-inflammatory effect on reducing the production of proinflammatory cytokine interleukin-17 in human peripheral blood mononuclear cells (39). In addition, POD can prevent fructose-induced liver lipid deposition by activating nuclear factor (erythroid-derived 2)-like 2 antioxidant pathway and scavenging ROS in rats (40), inhibit adipose tissue inflammation and improve the lipid metabolism in high-fat-fed mice (41), and ameliorate glucolipid dysmetabolisms *via* activating AMPK signaling pathway in human hepatoma HepG2 cells (42). Of important is that gut microbiota participates in enhancing the absorption, metabolism, and bioconversion of glycosides by promoting the activity and secretion of β-glucosidases in colon (2, 8, 32). Considering the contribution of accumulated ROS, gut microbiota dysbiosis, and deactivation or suppression of AMPK to energy homeostasis imbalance in the condition of nutrient overload, the above-mentioned reports indicate that POD may possess stronger bioactivity than RES on regulating glucolipid metabolism. Herein, we hypothesized that POD is stronger than RES on ameliorating energy homeostasis imbalance. This study aimed to compare the alleviating effects of POD and RES on glucolipid dysmetabolism and non-alcoholic fatty liver disease and investigate the underlying mechanisms of action in high-fructose diet-fed mice.

MATERIALS AND METHODS

Chemicals and Materials

The primary antibodies AMPKα, p-AMPKα (Thr172), insulin receptor substrate (IRS), p-IRS (Ser307), phosphatidylinositol 3-kinases (PI3K), p-PI3Kp85 (Tyr458)/p55 (Tyr199), protein kinase B (AKT), p-AKT(Ser473), acetyl-CoA carboxylase

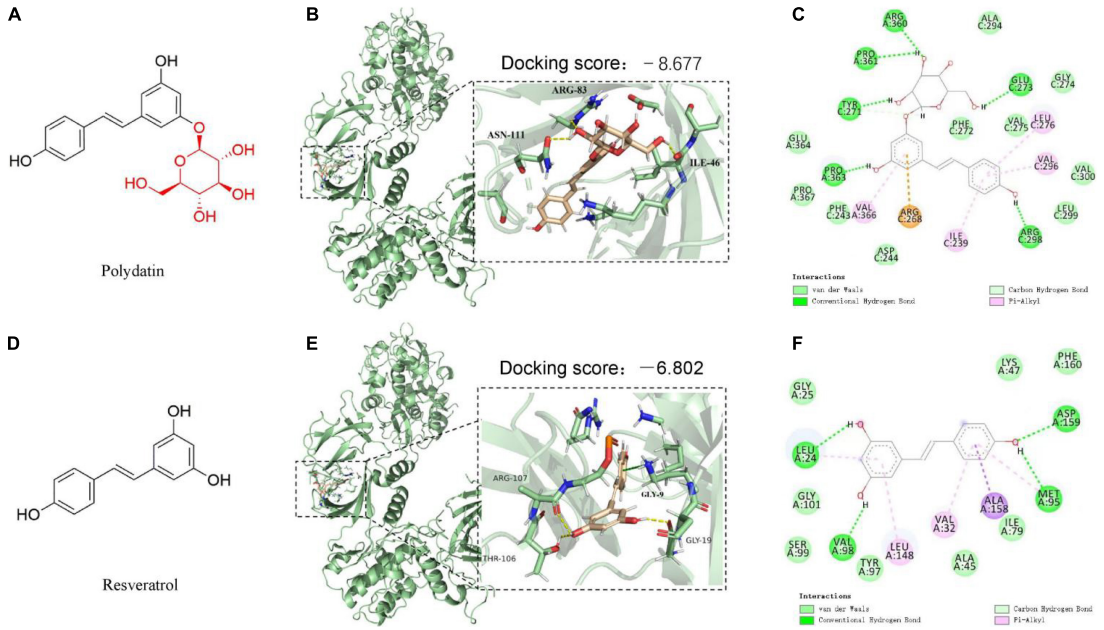

FIGURE 1 | The predicted binding modes of polydatin (POD) and resveratrol (RES) docked into AMP-activated protein kinase (APMK). **(A,D)** Chemical structures of POD and RES, respectively. The binding location of AMPK (black box area) interacting with POD and RES were shown as molecular surface structures in 3D docking model **(B,E)**; H-bonds and hydrophobic interactions between POD or RES and AMPK in a 2D docking model **(C,F)**.

(ACC), p-ACC (Ser79), thioredoxin-interacting protein (TXNIP) and the second antibodies anti-mouse IgG and anti-rabbit IgG were purchased form the Cell Signaling Technology Inc. (Boston, MA, United States). The primary antibodies peroxisome proliferator-activated receptor-alpha (PPAR-α) and PPAR-β were purchased from the Santa Cruz Biotechnology Co., Ltd. (Dallas, United States) and carnitine palmitoyltransferase-1 alpha (CPT-1α) was obtained from the Abcam (Cambridge, United Kingdom). POD (purity above 95%) and RES (purity above 99%) were obtained from the Aladdin Biochemical Technology Co., Ltd. (Shanghai, China). Fructose, valeric acid sodium and caproic acid sodium were purchased from the Maclin Biochemical Technology Co., Ltd. (Shanghai, China). Recombinant human insulin was bought from Tonghua Dongbao Pharmaceutical Co., Ltd. (Tonghua, China). N-acetylcysteine (NAC) was purchased from the Sigma-Aldrich (St. Louis, MO, United States). Other chemicals and drugs were of the highest grade available.

Molecular Docking

The isoform and binding site of AMPK (α1β1γ1) was confirmed according to the previously reported AMPK direct activator A-769662 (43–45). The three-dimensional (3D) structure of AMPK was downloaded from the Protein Data Bank (ID: 4ZHX), and the ligand 2D and 3D structures of POD and RES were constructed by Chem3D Ultra (Version 8.0), respectively. The ligand (POD or RES) was docked into the active site of the prepared AMPK crystal structure by Schrodinger (Version 12.5). The binding ability of POD or RES with AMPK was evaluated by docking scores.

Animal Care Experimental Design for Drug Ddministration

Male C57BL/6J mice, 5 weeks old and weighing 20 ± 2 g, were purchased from the Guangdong Provincial Laboratory Animal Center Co., Ltd. (Guangzhou, China). Mice were housed in a room with controlled temperature (23 ± 2°C, 40 ± 10% relative humidity, and 12-h light–dark cycle), and were allowed free access to water *ad libitum* and food.

Experiment 1: The animal model of non-alcoholic fatty liver disease was induced by 10% (w/v) fructose for 3 weeks and 30% fructose for 5 weeks in drinking water. The mice were randomly divided into four groups based on body weight ($n = 5$–8): Mice in Control group were given *ad libitum* access to drinking water, mice in Model group were given 30% fructose-containing drinking water, and mice in POD or RES group were given 30% fructose-containing drinking water and 50 mg/kg/day POD or RES by oral gavage, respectively, for another 10 weeks (**Figure 2**). After that all mice were fasted overnight, peripheral blood was collected from the ophthalmic vein after anesthetized and then the mice were sacrificed by cervical dislocation. Serum was obtained by centrifugation (5,000 round/min, 10 min, 4°C) and stored at −80°C. Livers were collected and stored at −80°C. The fresh fecal samples of each mouse were collected and stored at −80°C during the final week of the animal experiment. POD and RES (5 mg/mL) were suspended sufficiently in the carboxymethylcellulose sodium aqueous solution (0.5%, w/v).

Experiment 2: The animal model of non-alcoholic fatty liver disease was induced by fructose (30%, w/v) in drinking water for 5 weeks. The mice were randomly divided into eight groups based on the body weight ($n = 5$–7): Mice in Control group were

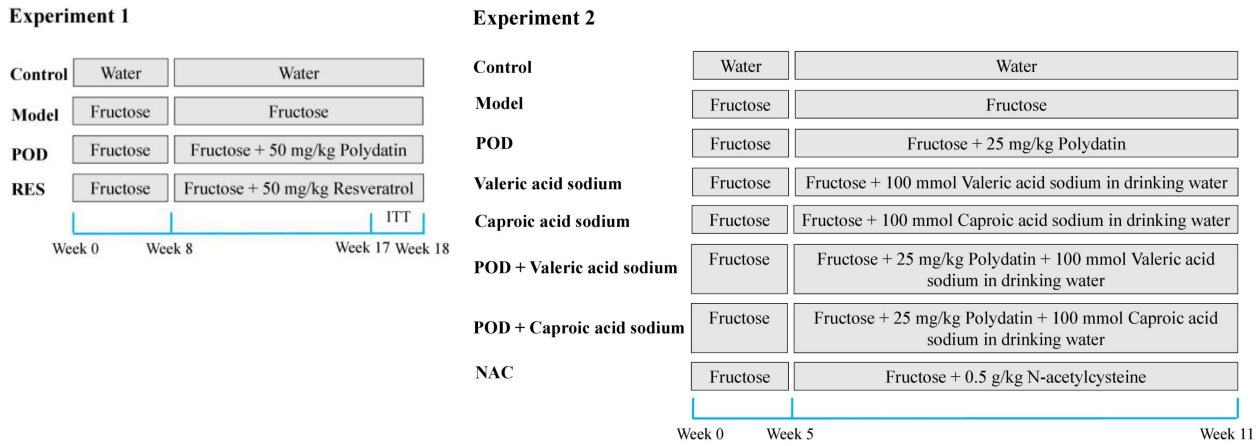

FIGURE 2 | Experimental design for drug administration.

given *ad libitum* access to drinking water, mice in Model group were given 30% fructose-containing drinking water, mice in POD group were given 30% fructose-containing drinking water and 25 mg/kg/day POD by oral gavage, mice in valeric acid sodium group were given 30% fructose and 100 mmol/L valeric acid sodium-containing drinking water, mice in caproic acid sodium group were given 30% fructose and 100 mmol/L caproic acid sodium-containing drinking water, mice in POD plus Valeric acid sodium group were given 30% fructose and 100 mmol/L valeric acid sodium-containing drinking water and 25 mg/kg/day POD by oral gavage, mice in POD plus caproic acid sodium group were given 30% fructose and 100 mmol/L caproic acid sodium-containing drinking water and 25 mg/kg/day POD by oral gavage, and the mice in NAC group were given 30% fructose-containing drinking water and 0.5 g/kg/day NAC by oral gavage, for another 6 weeks (**Figure 2**). After that all mice were fasted overnight and sacrificed by cervical dislocation after anesthetized. Liver and serum were harvested and stored at −80°C. The drinking fluid was exchanged daily.

Fasting Blood Glucose Measurement and Insulin Tolerance Tests

One touch glucometer (Roche Diagnostics, Mannheim, Germany) was used to measure the fasting blood glucose (FBG) levels on tail vein blood of mice after overnight fasting. For the insulin tolerance tests (ITT), after overnight fasting, insulin (0.3 unit) was administered by the intraperitoneal injection, and the blood glucose was measured at 0.5, 1.0, 1.5, and 2.0 h after the injection with the glucometer.

Serum Parameters Assay

Serum aspartate aminotransferase (AST), alanine aminotransferase (ALT), creatinine (Cr), and blood urea nitrogen (BUN) levels were measured with an automatic biochemical analyzer (HITACHI 7020, Japan). Kits for triglyceride (TG), total cholesterol (TC), free fatty acid (FFA), LDL-cholesterol (LDL-C), MDA, and SOD obtained from Nanjing Jiancheng Bioengineering Institute (Nanjing, China). The levels of serum insulin and HbA1c were measured using the commercial ELISA kits from Jiangsu Meimian industrial Co., Ltd. (Yancheng, China) and Jiangsu Boshen Biotechnology Co., Ltd. (Nanjing, China). Homeostasis model assessment-insulin resistance (HOMA-IR) index was calculated by the following formula:

$$HOMA - IR = Glucose\ (mmol/L) \times Insulin\ (mU/L) \div 22.5$$

Quantitation of Total Cholesterol, Triglyceride, and Free Fatty Acid in Liver

Livers (0.1 g) were homogenized in ice-cold tissue extraction buffer (1 ml) and then the lysates were clarified by centrifugation (12,000 *g*, 4°C, 15 min), after that the supernatant was collected for analysis. The levels of TC, TG, and FFA were measured according the corresponding protocols in the commercial kits provided by manufacturers.

Histology Assay

Harvested liver specimens were fixed in paraformaldehyde solution at room temperature, dehydrated, embedded in paraffin, after that a fully automated rotary microtome (LEICA RM2255, Shanghai, China) was used to cut the paraffin into 5 μm thickness serially. Periodic acid-schiff (PAS), hematoxylin-eosin (HE), MASSON, and oil red O stains were performed according to the standard protocols of the corresponding commercial kits, respectively, and then the slices were pictured with electron microscope (Nikon eclipse ti, Japan). All the assays were performed in a blinded manner.

Quantitative Real-Time Polymerase Chain Reaction

Total RNA was extracted from liver tissues of mouse using TRIzol reagent, obtained from Takara Biotechnology, according to the manufacturer's protocol. The cDNA was prepared using 50 ng of total RNA by the reverse transcription according to

the manufacturer's instructions. SYBR Green qPCR SuperMix was performed on a CFX System (Bio-Rad, Hercules, CA, United States) according to the manufacturer's instructions. Real-time PCR of cDNA was performed using standard PCR cycling condition. Relative expression level of target gene was normalized against control group β-actin and presented as a ratio to the expression level in other groups with the formula $2^{-(\Delta\Delta Ct)}$. The primer sequence of each tested gene is shown in **Supplementary Table 1**.

Western Blot

Livers (0.1 g) were homogenized in 0.1 mg/ml phenylmethylsulfonyl fluoride-containing ice-cold RIPA buffer (1 ml) and then the lysates were clarified by centrifugation (12,000 *g*, 4°C, 15 min), after that the supernatant was collected and stored at −80°C. The samples were denatured with loading buffer (99°C, 10 min), then the equal protein were separated by SDS-PAGE gel electrophoresis and transferred onto a polyvinylidene fluoride (PVDF) membrane. The membrane was probed with primary antibody according to the dilution ratio provided by manufacturers overnight at 4°C, and then incubated with secondary antibody according to the dilution ratio provided by manufacturers at room temperature for 60 min. The immunoreactivity was detected using the ChemiDoc XRS + detection system (ECL, Bio-Rad, United States). The densitometric analysis was performed with Quantity One® Image Analyzer software program (Bio-Rad). Glyceraldehyde-3-phosphate dehydrogenase (GAPDH) was used for normalization.

Gut Microbiota Profiling

Total genome DNA of bacterial was extracted from frozen feces with QIAamp DNA stool Mini Kit (Qiagen, Hilden, Germany) according to the manufacturer's guideline. The specific primer with the barcode (16S V3 + V4) was used to amplify the 16S rDNA gene. TruSeq® DNA PCR-Free Sample Preparation Kit (Suzhou RENOLD Biological Technology Co., Ltd., Suzhou, China) was used to construct the DNA sequencing libraries. Fast Hifidelity Polymerase and Phusion® High-Fidelity PCR Master Mix with GC Buffer (New England Biolabs Co., Ltd., Beijing, China) were used for The PCR amplification under the standard thermal cycling and extension conditions. Paired-end sequencing of the PCR products was performed on the NovaSeq6000 at Suzhou Bionovogene Co., Ltd. (Suzhou, China).

Short-Chain Fatty Acids Measurement

Gas chromatography-mass spectrometer method (Thermo TRACE 1310-ISQ LT instrument, Agilent HP-INNOWAX column with 30 m × 0.25 mm ID × 0.25 μm particle size) (Suzhou Bionovogene Co., Ltd., China) was used to measure the fecal levels of acetic acid, propionic acid, butyrate, isobutyric acid, caproic acid, valerate and isovaleric acid. 50 μL phosphoric acid (15%), 100 μL internal standard (isohexic acid) solution (125 μg/mL) and 400 μL ether were homogenated with 50 mg fresh feces for 1 min, then the mix were centrifuged at 12000 rpm and 4°C for 10 min. After that the supernatant was collected for measurement.

Statistical Analysis

Data were expressed as mean ± SEM, and compared using the Student's *t*-test or two-way ANOVA *post hoc* Bonferroni test, as appropriate (GraphPad Prism 5 Software, Inc., La Jolla, CA, United States). The correlation coefficient between the fecal levels of SCFAs and the relative abundance of gut microbiota at the genus level were performed with Pearson correlation analysis (SPSS software, version 20, IBM, Armonk, NY, United States). The significance levels were established at a p-value of <0.05.

RESULTS

Binding Interactions of Polydatin and Resveratrol With Activated Protein Kinase

To better understand the interactions of POD and RES with AMPK, molecular docking study was performed to analyze the binding abilities of POD and RES with AMPK. The molecular docking results between the ligands (POD and RES) and the receptor (AMPK) suggest POD displayed a higher predicted binding score than RES (−8.677 *vs.* −6.802) (**Figures 1B,E**). This indicates that POD possesses a stronger interaction with AMPK than RES. Conventional hydrogen bond and van der Waals are the mainly binding bonds between POD and RES with AMPK. POD exerts higher binding ability with AMPK than RES may involve there are more hydroxyl groups in POD (**Figure 1**) because hydroxyl groups formed H-bonds to AMPK (**Figure 1C**) are important for stable binding. The more residues of AMPK units or binding pocket involved in the H-bond interaction or the binding of POD and AMPK by van der Waals also contributed to its binding (**Figure 1C**).

Polydatin Is More Active Than Resveratrol in Alleviating Lipid Dysmetabolism Than Resveratrol in Mice Fed a High-Fructose Diet

Body weight (**Supplementary Figure 1A**) and serum parameters, such as ALT, AST, Cr, and BUN (**Supplementary Table 2**), showed that the doses of POD and RES employed did not possess toxicity in mice. Since the intake of extra calories from fructose in drinking fluid (**Supplementary Figure 1B**), the food intake was lowered (**Figure 3A**). Both the POD and RES administrations did not significantly influence the fluid intake (**Supplementary Figure 1A**), but, interestingly, elevated the food intake of the mice (**Figure 3A**). High-fructose diet enhanced the insulin tolerance (**Figures 3B,C**), elevated the levels of serum insulin, FBG, and serum HbA1c (**Figures 3D–F**) and caused the hepatic glycogen accumulation and fibrogenesis (**Figures 3G,H**). POD and RES alleviated these lesions with a similar effect (**Figures 3D–H**). In addition, serious lipid accumulation (**Figure 3I**), fatty infiltration and amyloidosis (**Figure 3J**) of liver were also observed in the model mice. POD showed a better effect on preventing these lesions than RES (**Figures 3I,J**). This was also validated by the higher capacity of POD in reducing the levels of TC and TG in liver (**Figures 3K,L**) and serum (**Figures 3M,N**). These

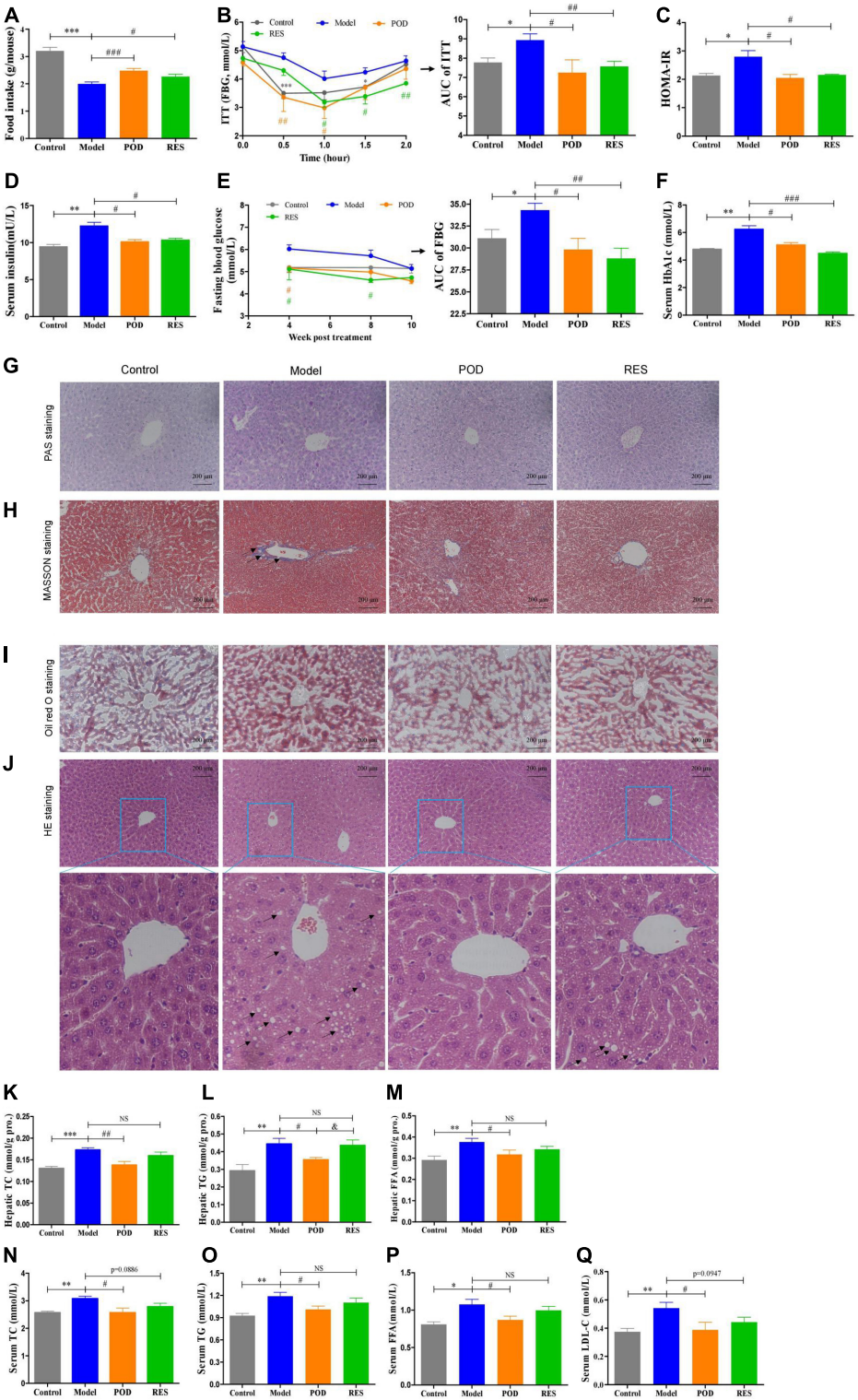

FIGURE 3 | Effects of POD and RES on glucolipid metabolism and fatty liver. **(A)** Food intake. **(B)** Insulin tolerance test (ITT) and the area under the curve (AUC). **(C)** Homeostasis model assessment -insulin resistance (HOMR-IR, HOMA-IR = Glucose [mmol/L] × Insulin [mU/L] ÷ 22.5). **(D)** Serum insulin level. **(E)** Fasting blood glucose level (FBG) and AUC of FBG. **(F)** Serum HbA1c level. **(G–J)** Hepatic periodic acid-schiff (PAS) (200×), MASSON (200×), Oil red O (200×), and HE stainings (200×), respectively. **(K–M)** Total cholesterol (TC), triglycerides (TG), and free fatty acid (FFA) in liver, respectively. **(N–Q)** Serum levels of TC, TG, FFA, and low-density lipoprotein-cholesterol (LDL-C), respectively. Data are presented as mean ± SEM. * $p < 0.05$, ** $p < 0.01$, *** $p < 0.001$. # $p < 0.05$, ## $p < 0.01$, ### $p < 0.001$, compared to model group. & $p < 0.05$, compared to POD group. NS, $p > 0.05$.

results suggest that POD and RES can alleviate the glucolipid dysmetabolism, and POD is superior to RES on ameliorating non-alcoholic fatty liver disease than RES in mice fed a high-fructose diet.

At the molecular level, fructose consumption suppressed the AMPK signaling pathway, such as downregulation of p-AMPK (Thr172), CPT-1α, PPAR-α, PPAR-γ, p-ACC (Ser79), p-AKT (Ser473), -PI3Kp85 (Tyr485), and p-IRS1 (Ser307) and upregulation of TXNIP, in liver (**Figures 4A,B**). POD significantly prevented these alterations (**Figures 4A,B**), and RES displayed a preventing effect on the downregulation of p-AMPKα (Thr172) (**Figure 4A**), but without affecting the levels of the downstream proteins PPAR-γ, p-ACC (Ser79), p-AKT (Ser473), and p-PI3Kp85 (Tyr485) (**Figures 4A,B**). In addition, long-term fructose consumption caused elevation of oxidative stress level in liver indicated by the pronouncedly increase of TXNIP (**Figure 4A**) and MDA (**Figure 4E**) and decrease of SOD (**Figure 4F**), both POD and RES administrations effectively prevented these alterations (**Figures 4E,F**). However, neither POD nor RES affected the mRNA levels of GPR41 and GPR43 in liver (**Figures 4C,D**).

Polydatin Increases the Fecal Levels of Caproic Acid and Valeric Acid by Modification of the Gut Microbiota

The α-diversity analysis of the gut microbiomes showed frcutose consumption lowered the diversity of microbiota (**Figures 5A,B**). POD and RES administrations markedly increased the microbiota diversity evidenced by the elevated Shannon and Simpson indexes (**Figures 5A,B**). The β-diversity analysis evaluated the overall differences in groups, results showed a distinct clustering of gut microbial community structure in control and model groups (**Figure 5C**), POD and RES administrations altered the structure in a similar trend (**Figure 5C**). The Venn diagrams were used to show the over lapping operational taxonomic units (OTUs), which displayed the similarity and consistency of samples. There are 313 OTUs shared in all groups (**Figure 5D**). Three hundred and 68 OTUs were identified in control group, and fructose consumption increased the OTUs numbers to 509 (**Figure 5D**). Interestingly, POD administration lowered the OTUs numbers to 398 and RES increased the OTUs numbers to 511 (**Figure 5D**). These results indicated long-term intake of fructose markedly affected the community structure and relative abundance of gut microbiomes (**Figures 5A–E**), and POD has a higher regulating effect on gut microbiomes than RES (**Figure 5D**). The function of the significantly altered gut microbiota (**Figures 5F–K**) post POD or RES treatment will be discussed in the discussion section.

Our results showed the levels of fecal SCFAs of mice in the model group without a significant alteration compared to control (**Figures 5L–N**), POD treatment markedly elevated the levels of valeric acid and caproic acid (**Figures 5M,N**), but RES did not pronouncedly affect the levels of SCFAs (**Figures 5L–N**). Correlation analyses between SCFAs levels and relative abundance of gut microbiota indicated the valeric acid level was significantly negative correlated with the abundance of *Parasutterella* (**Figure 5O**) and positive correlated with the abundance of *Acetitomaculum*, *Anaerotruncus*, *Candidatus_Soleaferrea*, *Colidextribacter*, *Harryflintia*, *Mucispirillum*, *Negativibacillus*, *Butyricimonas*, *[Eubacterium]_ventriosum_group*, *Candidatus_Soleaferrea*, *Bifidobacterium*, *Monoglobus*, *Lactococcus*, *Allobaculum*, *Intestinimonas*, *Lachnoclostridium*, *[Eubacterium]_nodatum_group*, *Streptococcus*, *Romboutsia*, *Anaerovorax*, and *unidentified_Ruminococcace* at the genus level (**Figure 5O**). However, the caproic acid level was significantly negative correlated with the abundance of *Escherichia-Shigella*, *NK4A214_group*, *Roseburia* and *Colidextribacter*, and positive correlated with the abundance of *Anaerofustis* and *[Eubacterium]_ventriosum_group* (**Figure 5O**).

Caproic Acid and Valeric Acid Activate Activated Protein Kinase and Enhance the Effects of Polydatin on Alleviating Lipid Dysmetabolism in Mice Fed a High-Fructose Diet

The markedly elevated levels of fecal valeric acid and caproic acid *via* modifying gut microbiomes by POD administration may be the main reason that POD exerted a higher property on ameliorating lipid dysmetabolism than RES. Thereby, we next investigated the regulating effects of valeric acid and caproic acid on AMPK and lipid metabolism in mice fed a high-fructose diet. Results showed that both caproic acid sodium and valeric acid sodium reduced the lipid accumulation, and the levels of TG and FFA in liver (**Figures 6A,C,D**). In addition, caproic acid sodium decreased the levels of TC, TG, FFA, and LDL-C in serum (**Figures 6E–H**). Importantly, we found when the low dose of POD (25 mg/kg) without a pronouncedly improvement on non-alcoholic fatty liver disease, caproic acid sodium and/or valeric acid sodium can enhance the effects of POD on preventing lipid dysmetabolism (**Figures 6A,B,F–H**). Consistently with these improving effects of SCFAs (caproic acid sodium and valeric acid sodium) or SCFA plus POD on lipid metabolism, AMPK was activated post the treatment indicated by the significantly upregulation of p-AMPK α (Thr172) and p-ACC (Ser79) (**Figure 7**). Neither caproic acid sodium nor valeric acid sodium affected the mRNA levels of GPR41 and GPR43 in liver.

DISCUSSION

In this work, we firstly demonstrated that POD shows higher ameliorating effect on non-alcoholic fatty liver disease than RES in mice fed a high-fructose diet. The mechanism of action may involve POD administration promoted the elevation of valeric acid and caproic acid in feces by modifying gut microbiota thus activating the AMPK signaling pathway. Since nutrition overload and overnutrition-stimulated ROS promoted the AMPK deactivation or suppression which is the major pathological mechanism of metabolic disorders (17, 18, 28, 29) (**Figures 4A**, **7A**), considering POD has been proved with the property of activating AMPK *in vitro* (42) and scavenging ROS

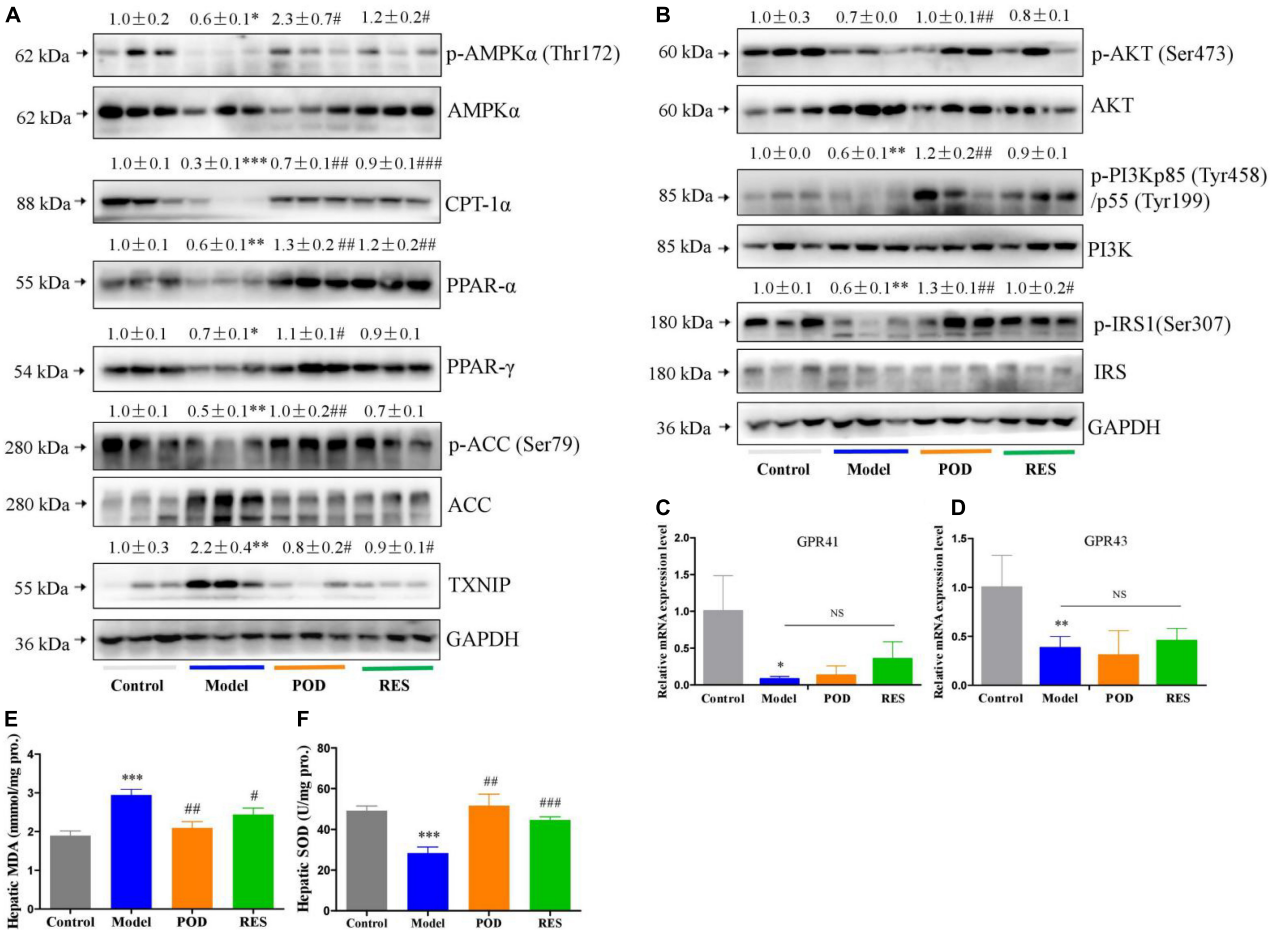

FIGURE 4 | Effects of POD and RES on AMPK signaling pathway and biomarkers of oxidative stress in liver. **(A)** AMPK signaling pathway proteins. **(B)** Insulin signaling pathway proteins. **(C,D)** The mRNA levels of GPR41 and GPR43. **(E)** MDA level. **(F)** SOD enzyme activity level. Data are presented as mean ± SEM. * $p < 0.05$, ** $p < 0.01$, *** $p < 0.001$, compared to control group. # $p < 0.05$, ## $p < 0.01$, ### $p < 0.001$, compared to model group. NS, $p > 0.05$.

in vivo (40, 46, 47), and exerts stronger anti-oxidant capacity *in vivo* (11) and anti-inflammatory effect *in vitro* than RES (39). Our results suggest that POD displayed a higher effects than RES on improving the overnutrition-related diseases by activating the AMPK signaling pathway *via* modification of the gut microbiota *in vivo*.

Gut microbiota and its metabolites SCFAs and oxidative stress state play an important role in maintaining energy homeostasis through regulating AMPK. *Butyricimonas* is a SCFA-producing bacteria (48–52) and participates in driving the reduction of body mass index (BMI) in response to insulin (50, 52). POD treatment pronouncedly increased the abundance of *Butyricimonas* (**Figure 5F**) though the fructose intake without significant decreasing the abundance of *Butyricimonas* at the genus level. *Bifidobacterium* is considered a probiotics that participates SCFAs production (8, 9, 53). Both POD and RES markedly increased the abundance of *Bifidobacterium* at the genus level (**Figure 5G**). *Lactobacillus* involves in the absorption and metabolism of polyphenols glycosides by enhancing the activity and secretion of β-glucosidase (7–9). POD did not compromise the abundance of Lactobacillus, but RES exerted a suppression effect on *Lactobacillus* when fructose consumption increased the abundance of *Lactobacillus* at the genus level (**Figure 5H**). *Desulfovibrio*, *Muribaculum*, and *Rikenella* are probiotics that beneficial for the energy homeostasis (8, 54, 55). Both POD and RES significantly increased the abundance of the genera *Desulfovibrio* and *Muribaculum* (**Figures 5I,J**), and RES increased the genera *Rikenella* (**Figure 5K**). In addition, correlation analyses between SCFAs levels and gut microbiota abundance indicated that the valeric acid level was significantly positive correlated with the abundance of *Butyricimonas*, *[Eubacterium]_ventriosum_group* and *Bifidobacterium* (**Figure 5O**). And the caproic acid level was significantly positive correlated with the abundance of [Eubacterium]_ventriosum_group (**Figure 5O**). These results suggest that *Butyricimonas*, *[Eubacterium]_ventriosum_group* and *Bifidobacterium* may involve in the elevation of fecal levels of valeric acid and caproic acid (**Figures 5M,N**). Of interest is that POD displayed a higher regulating effect on the gut microbiomes and its metabolites SCFAs than RES, which is indicated by

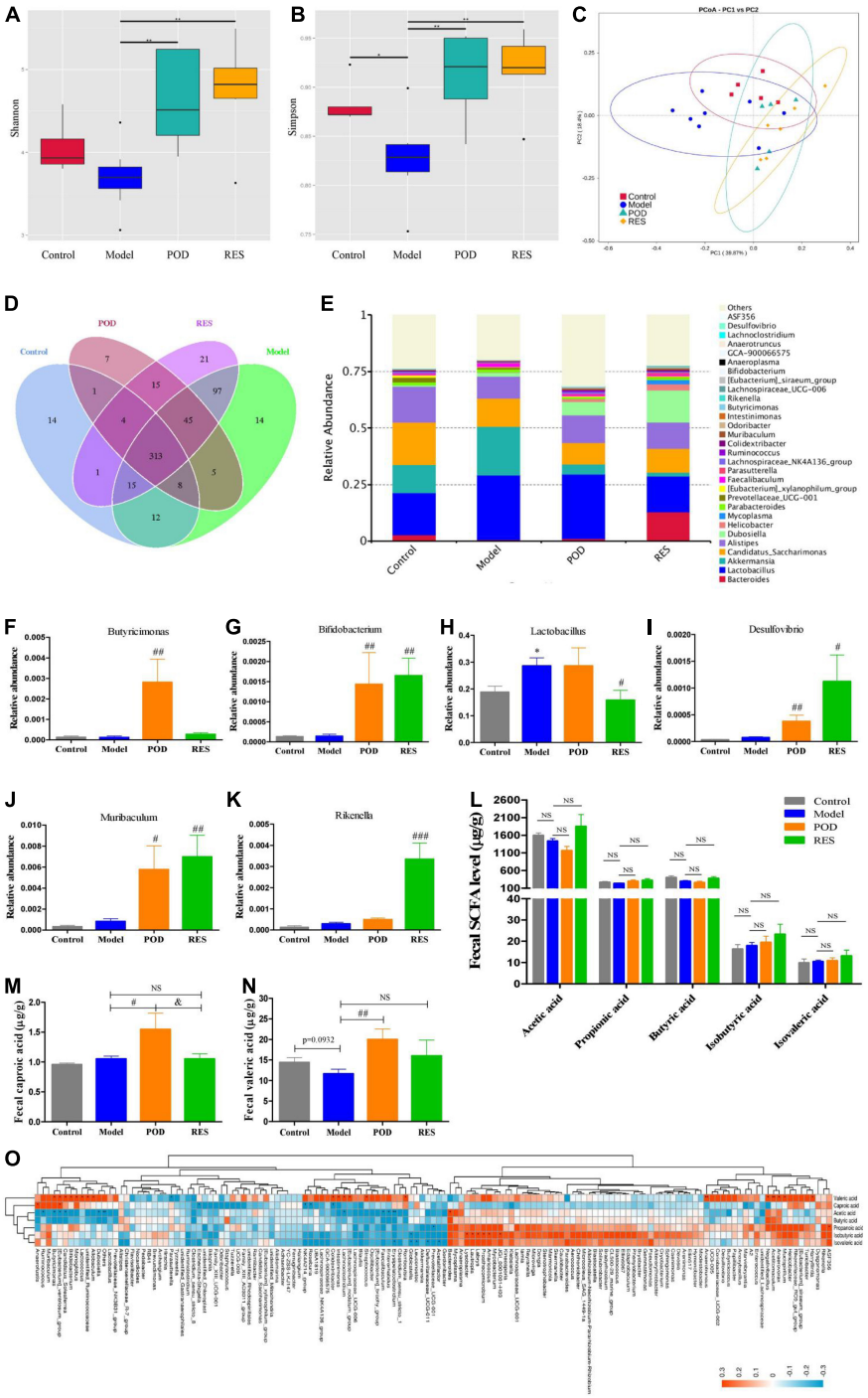

FIGURE 5 | Microbiome and SCFAs of the fecal samples. Alpha-Diversity was presented by a box plot of the Shannon **(A)** and Simpson **(B)**. **(C)** Principal coordinate analysis (PCoA) plot analysis. **(D)** Petal analysis of OTU. **(E)** Relative abundance of gut microbiota at the genus level (top 30). **(F–K)** Relative abundance of the altered microbiota. **(L–N)** Levels of SCFAs. **(O)** Correlation analysis of SCFAs level and gut microbiota abundance at the genus level. Data are presented as mean ± SEM. Orange, positive correlation. Blue, negative correlation. * $p < 0.05$, ** $p < 0.01$, compared to control group. # $p < 0.05$, ## $p < 0.01$, ### $p < 0.001$, compared to model group. & $p < 0.05$, compared to POD group. NS, $p > 0.05$.

the reversed OTUs (**Figure 5D**) and pronouncedly elevated the valeric acid and caproic acid levels in feces (**Figures 5M,N**) by POD administration. This is in line with the reports that since the ingested glycosides are poorly absorbed by the small intestine, a significant fraction of POD can persist to the colon, where they encounter the gut microbiota and play a better modifying effect

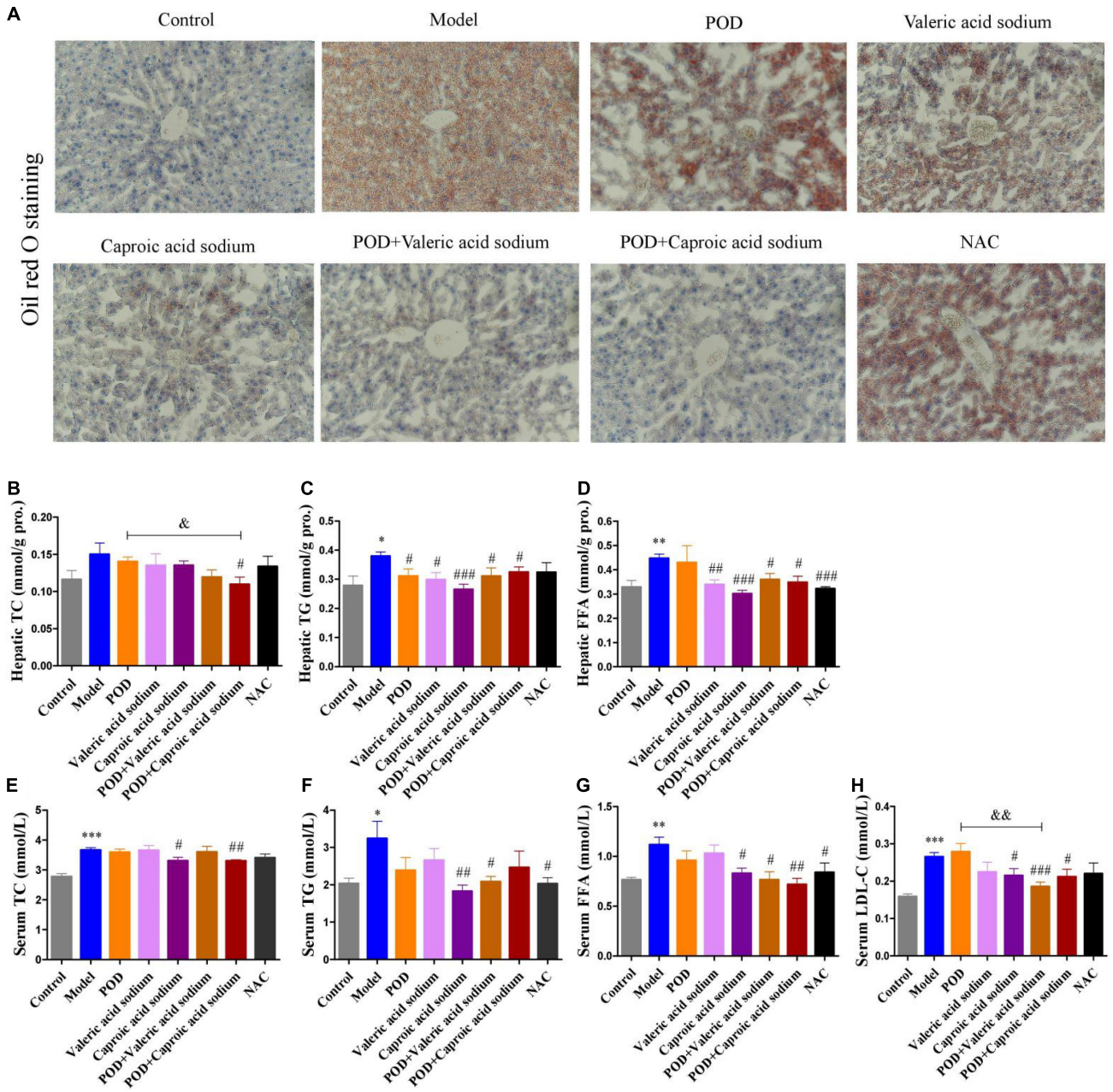

FIGURE 6 | Effects of valeric acid and caproic acid on lipid metabolism in mice fed a high-fructose diet. **(A)** Oil red O staining (200 ×). **(B–D)** Levels of TC, TG, and FFA in liver. **(E–H)** Levels of TC, TG, FFA, and LDL-C in serum. Data are presented as mean ± SEM. * $p < 0.05$, ** $p < 0.01$, *** $p < 0.001$, compared to control group. $^{\#}$ $p < 0.05$, $^{\#\#}$ $p < 0.01$, $^{\#\#\#}$ $p < 0.001$, compared to model group. $^{\&}$ $p < 0.05$, $^{\&\&}$ $p < 0.01$, compared to POD group. NS, $p > 0.05$.

on the structure and composition of microbiota and ultimately affecting its metabolites (2, 8, 32).

Emerging evidence indicates that intestinal microbial metabolites influence the host and contribute to the development of metabolic syndrome and T2DM (24, 56). SCFA formed from the result of a complex interplay between the gut microbiota and dietary fiber. As the signaling molecules between the gut microbiota and the host, SCFAs play a regulatory role on human metabolism in local, intermediary, and peripheral metabolism (56). As the endogenous receptors for SCFAs, G protein-coupled receptor free fatty acid receptor 2 (FFAR2, GPR43), and FFAR3 (GPR41) have already been identified. Acetate, propionate, and butyrate are the most abundant SCFAs produced by microbiota and presented in the gut lumen at high levels (57–59). Meanwhile, the shorter acetate preferentially activates GPR43, the longer butyrate preferentially activates GPR41, and propionate displays similar agonism on GPR43 and GPR41 (60). However, several reports have clarified and discussed that SCFAs can activate

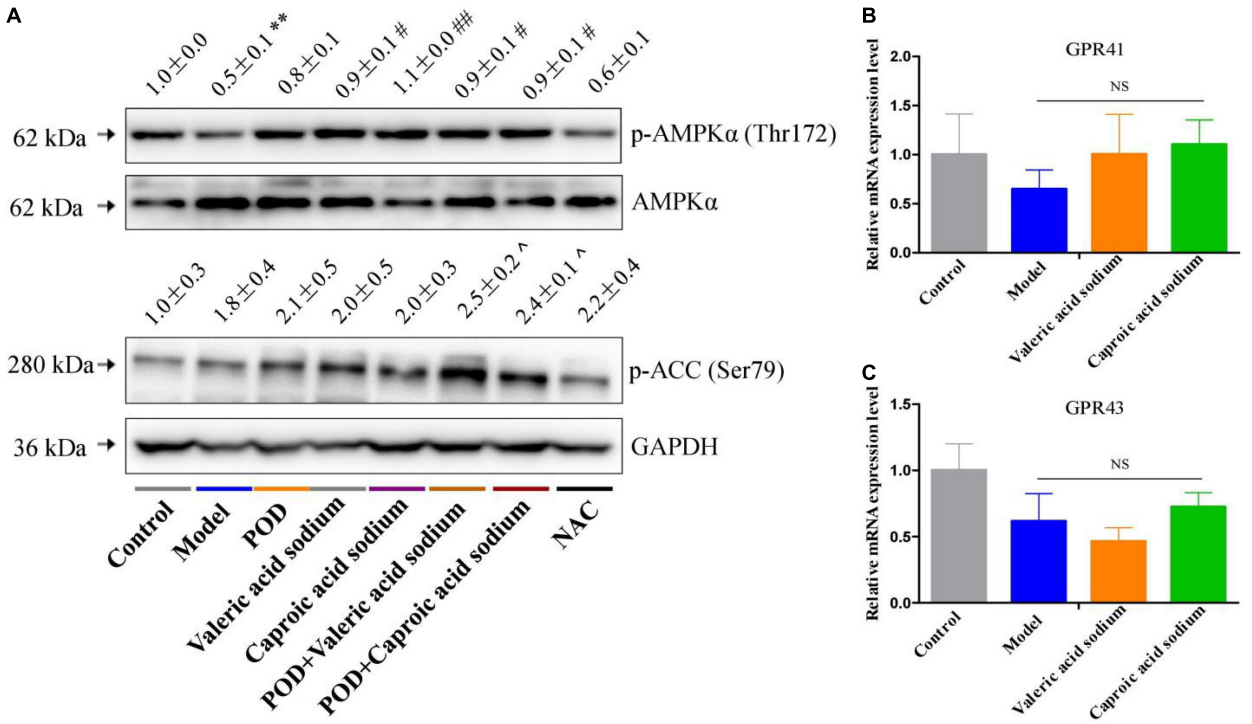

FIGURE 7 | Effects of valeric acid and caproic acid on p-AMPK α (Thr172) and p-ACC (Ser79) proteins and GPR41 and GPR43 mRNA levels in liver. **(A)** The protein levels of p-AMPK α (Thr172) and p-ACC (Ser79). **(B,C)** The mRNA levels of GPR41 and GPR43. Data are presented as mean ± SEM. ** $p < 0.01$, compared to control group. # $p < 0.05$, ## $p < 0.01$, compared to model group. ^ $p < 0.05$, compared to control group. NS, $p > 0.05$.

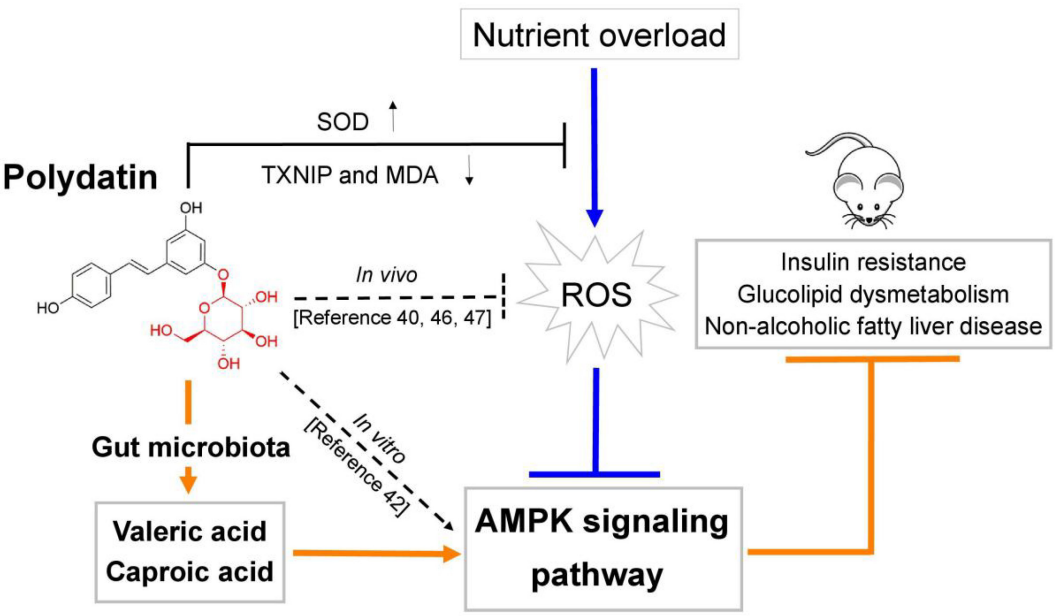

FIGURE 8 | Schematic diagram showing the underlying mechanisms of polydatin administration on ameliorating energy homeostasis imbalance.

the AMPK and maintain the energy homeostasis (61–63) in a GPR43 or GPR41 dependent (64–66) or independent (63, 67) mechanism, and the independent mechanism is consistent with the finding that butyrate and propionate still ameliorated insulin resistance and body weight gain in GPR41-deficient mice (67). In this study, we found the markedly elevated fecal levels of valeric

acid and caproic acid by modification of gut microbiota by POD administration can activate the AMPK (**Figures 4A**, **7A**) and promote the effects of POD on ameliorating lipid dysmetabolism (**Figures 6A,B,F–H**) without affecting the mRNA levels of GPR43 and GPR41 in liver (**Figures 4C,D**, **7B,C**). Our results firstly demonstrated the activation of valeric acid and caproic acid on AMPK *in vivo*, and reinforced the concept that SCFAs activate AMPK is likely the common mechanism (61, 63, 67) for alleviating the energy homeostasis imbalance in a GPR43 or GPR41 independent manner.

The NAC, recognized as a ROS scavenger, is widely employed as a tool for explaining the consequences of oxidative stress and as a clinical drug for antioxidant therapy (68, 69). Scavenging of ROS is beneficial for alleviating metabolic disorders in high glucose conditions (18, 70). Indeed, in the present work, we found NAC administration significantly reduced the levels of FFA in liver (**Figure 6D**) and TG and FFA in serum (**Figures 6F,G**) in mice fed a high-fructose diet. However, NAC treatment without preventing the downregulation of p-AMPK α (Thr172) (**Figure 6A**), and the elevation of lipid accumulation, TC and TG in liver (**Figures 6A–C**), and TC and LDL-C in serum (**Figures 6E,H**). This indicates that reducing the level of oxidative stress alone by NAC cannot reverse the lipid dysmetabolism induced by high-fructose diet. POD administration alleviated oxidative stress by reducing ROS-driven TXNIP over-expression (**Figure 5A**) (40) and lipid peroxide MDA (**Figure 4E**), and enhancing the antioxidant enzyme SOD in liver (**Figure 4F**); and activated hepatic AMPK signaling pathway (**Figures 4A**, **7A**) by elevating the fecal levels of valeric acid and caproic acid *via* modifying gut microbiota (**Figures 5M,N**). As a consequence of the improved oxidative stress state and activated AMPK signaling pathway, POD ameliorated the lipid dysmetabolism more effectively (**Figure 3**). Furthermore, the crucial role of valeric acid and caproic acid in activation of AMPK and improvement of lipid metabolism were confirmed by the upregulation of p-AMPK upalpha (Thr172) (**Figure 7A**) and the reduction of lipid accumulation, TC, TG, FFA, or LDL-C in liver and serum (**Figure 6**) by valeric acid sodium and/or caproic acid sodium treatment and valeric acid sodium or caproic acid sodium plus POD administration in mice fed a high-fructose diet.

CONCLUSION

In summary, this study investigated the ameliorating effects of POD and RES on insulin resistance, glucolipid dysmetabolism and non-alcoholic fatty liver disease by reducing the oxidative stress and preventing AMPK suppression induced by high-frcutose diet in mice (**Figure 8**). For the first time, we found POD possesses a higher improvement effect on non-alcoholic fatty liver disease than RES (**Figures 3I–Q**) in mice, the mechanism of action may involve the pronouncedly elevated fecal levels of valeric acid and caproic acid *via* modification of gut microbiota by POD administration can activate AMPK signaling pathway and enhance the effects of POD on alleviating lipid dysmetabolism (**Figures 4A**, **7A**, **6A,B,F–H**). RES is considered to be an AMPK activator (71–73) with well-known health benefits and widely applied in medicines, foods, and cosmetic products. As a natural precursor of RES, POD is superior to RES in anti-oxidant (11), anti-inflammatory (39), modification of gut microbiota (**Figures 5D,M,N**), and improvement of lipid metabolism (**Figures 3I–Q**). Thus, POD may be an alternative of RES as AMPK activator and for industrial and medical applications.

DATA AVAILABILITY STATEMENT

The datasets presented in this study can be found in online repositories. The names of the repository/repositories and accession number(s) can be found below: NCBI; PRJNA799661.

ETHICS STATEMENT

The animal study was reviewed and approved by Institutional Animal Care and Use Committee at Jinan University (IACUC Issue No: 20200329-22).

AUTHOR CONTRIBUTIONS

GZ: conceptualization. GZ, LY, QB, and YH: methodology. GZ, LY, WZ, and YT: investigation. GZ, ZW, and YW: validation, project administration, and funding acquisition. GZ, QB, and LY: writing—original draft preparation. GZ, CY, and QB: writing—review and editing. GZ, ZW, YW, and ZR: supervision. All authors contributed to the article and approved the submitted version.

FUNDING

This work was supported by the Open Fund of State Key Laboratory of Tea Plant Biology and Utilization (SKLTOF20200127 and SKLT0F20200108), Guangdong Modern Agricultural Industrial Technology System Innovation Team Project (2019KJ142 and 2020KJ142), Guangdong Province ordinary universities characteristic innovation project (2020KTSCX060), and Undergraduate Innovation and Entrepreneurship Training Program of Guangdong Pharmaceutical University (S202010573044).

ACKNOWLEDGMENTS

We wish to express our appreciation to Suzhou Bionovogene Co., Ltd., for technical assistance.

SUPPLEMENTARY MATERIAL

The Supplementary Material for this article can be found online at: https://www.frontiersin.org/articles/10.3389/fnut.2022.857879/full#supplementary-material

REFERENCES

1. Kirino A, Takasuka Y, Nishi A, Kawabe S, Yamashita H, Kimoto M, et al. Analysis and functionality of major polyphenolic components of Polygonum cuspidatum (itadori). *J Nutr Sci Vitaminol.* (2012) 58:278–86. doi: 10.3177/jnsv.58.278
2. Scalbert A, Williamson G. Dietary intake and bioavailability of polyphenols. *J Nutr.* (2000) 130:2073S–85S. doi: 10.1093/jn/130.8.2073S
3. Wang H, Liu L, Guo YX, Dong YS, Zhang DJ, Xiu ZL. Biotransformation of piceid in Polygonum cuspidatum to resveratrol by Aspergillus oryzae. *Appl Microbiol Biotechnol.* (2007) 75:763–8. doi: 10.1007/s00253-007-0874-3
4. Chen M, Li D, Gao ZQ, Zhang CZ. Enzymatic transformation of polydatin to resveratrol by piceid-β-D-glucosidase from Aspergillus oryzae. *Bioprocess Biosyst Eng.* (2014) 37:1411–6. doi: 10.1007/s00449-013-1113-1
5. Wang CQ, Liu XL, Zhang ML, Shao HY, Zhang MM, Wang XM, et al. Efficient enzyme-assisted extraction and conversion of polydatin to resveratrol from polygonum cuspidatum using thermostable cellulase and immobilized β-glucosidase. *Front Microbiol.* (2019) 10:445. doi: 10.3389/fmicb.2019.00445
6. Averilla JN, Oh J, Wu ZX, Liu KH, Jang CH, Kim HJ, et al. Improved extraction of resveratrol and antioxidants from grape peel using heat and enzymatic treatments. *J Sci Food Agric.* (2019) 99:4043–53. doi: 10.1002/jsfa.9632
7. Roncaglia L, Amaretti A, Raimondi S, Leonardi A, Rossi M. Role of bifidobacteria in the activation of the lignan secoisolariciresinol diglucoside. *Appl Microbiol Biotechnol.* (2011) 92:159–68. doi: 10.1007/s00253-011-3338-8
8. Yao R, Wong CB, Nakamura K, Mitsuyama E, Tanaka A, Kuhara T, et al. Bifidobacterium breve MCC1274 with glycosidic activity enhances in vivo isoflavone bioavailability. *Benef Microbes.* (2019) 10:521–31. doi: 10.3920/BM2018.0179
9. Marín L, Miguélez EM, Villar CJ, Lombó F. Bioavailability of dietary polyphenols and gut microbiota metabolism: antimicrobial properties. *Biomed Res Int.* (2015) 2015:905215. doi: 10.1155/2015/905215
10. Gott DM, Griffiths LA. Effects of antibiotic pretreatments on the metabolism and excretion of [U14C](+)-catechin [(U14C](+)-cyanidanol-3) and its metabolite, 3′-0-methyl-(+)-catechin. *Xenobiotica.* (1987) 17:423–34. doi: 10.3109/00498258709043949
11. Wang HL, Gao JP, Han YL, Xu X, Wu R, Gao Y, et al. Comparative studies of polydatin and resveratrol on mutual transformation and antioxidative effect in vivo. *Phytomedicine.* (2015) 22:53–9. doi: 10.1016/j.phymed.2015.03.014
12. Isolauri E. Microbiota and obesity. *Nestle Nutr Inst Workshop Ser.* (2017) 88:95–105. doi: 10.1159/000455217
13. World Health Organization [WHO]. *Obesity: Preventing and Managing the Global Epidemic Report of a WHO Consultation (WHO Technical Report Series 894)*. Geneva: World Health Organization (2000).
14. Jensen T, Abdelmalek MF, Sullivan S, Nadeau KJ, Green M, Roncal C, et al. Fructose and sugar: a major mediator of non-alcoholic fatty liver disease. *J Hepatol.* (2018) 68:1063–75. doi: 10.1016/j.jhep.2018.01.019
15. Hannou SA, Haslam DE, McKeown NM, Herman MA. Fructose metabolism and metabolic disease. *J Clin Invest.* (2018) 128:545–55. doi: 10.1172/JCI96702
16. Lambert JE, Ramos-Roman MA, Browning JD, Parks EJ. Increased de novo lipogenesis is a distinct characteristic of individuals with nonalcoholic fatty liver disease. *Gastroenterology.* (2014) 146:726–35. doi: 10.1053/j.gastro.2013.11.049
17. Lin SC, Hardie DG. AMPK: sensing glucose as well as cellular energy status. *Cell Metab.* (2018) 27:299–313. doi: 10.1016/j.cmet.2017.10.009
18. Jiang P, Ren LJ, Zhi L, Yu Z, Lv FX, Xu FL, et al. Negative regulation of AMPK signaling by high glucose via E3 ubiquitin ligase MG53. *Mol Cell.* (2021) 81:629–37.e5. doi: 10.1016/j.molcel.2020.12.008
19. Woods A, Williams JR, Muckett PJ, Mayer FV, Liljevald M, Bohlooly-Y M, et al. Liver-specific activation of AMPK prevents steatosis on a high-fructose diet. *Cell Rep.* (2017) 18:3043–51. doi: 10.1016/j.celrep.2017.03.011
20. Steinberg GR, Carling D. AMP-activated protein kinase: the current landscape for drug development. *Nat Rev Drug Discov.* (2019) 18:527–51. doi: 10.1038/s41573-019-0019-2
21. Rena G, Hardie DG, Pearson ER. The mechanisms of action of metformin. *Diabetologia.* (2017) 60:1577–85. doi: 10.1007/s00125-017-4342-z
22. Koh A, Vadder FD, Kovatcheva-Datchary P, Bäckhed F. From dietary fiber to host physiology: short-chain fatty acids as key bacterial metabolites. *Cell.* (2016) 165:1332–45. doi: 10.1016/j.cell.2016.05.041
23. Lau WL, Savoj J, Nakata MB, Vaziri ND. Altered microbiome in chronic kidney disease: systemic effects of gut-derived uremic toxins. *Clin Sci.* (2018) 132:509–22. doi: 10.1042/CS20171107
24. Herrema H, Niess JH. Intestinal microbial metabolites in human metabolism and type 2 diabetes. *Diabetologia.* (2020) 63:2533–47. doi: 10.1007/s00125-020-05268-4
25. Beek CMVD, Canfora EE, Lenaerts K, Troost FJ, Damink SWMO, Holst JJ, et al. Distal, not proximal, colonic acetate infusions promote fat oxidation and improve metabolic markers in overweight/obese men. *Clin Sci.* (2016) 130:2073–82. doi: 10.1042/CS20160263
26. Tolhurst G, Heffron H, Lam YS, Parker HE, Habib AM, Diakogiannaki E, et al. Short-chain fatty acids stimulate glucagon-like peptide-1 secretion via the G-protein-coupled receptor FFAR2. *Diabetes.* (2012) 61:364–71. doi: 10.2337/db11-1019
27. Chambers ES, Viardot A, Psichas A, Morrison DJ, Murphy KG, Zac-Varghese SEK, et al. Effects of targeted delivery of propionate to the human colon on appetite regulation, body weight maintenance and adiposity in overweight adults. *Gut.* (2015) 64:1744–54. doi: 10.1136/gutjnl-2014-307913
28. Coughlan KA, Valentine RJ, Ruderman NB, Saha AK. Nutrient excess in AMPK downregulation and insulin resistance. *J Endocrinol Diabetes Obes.* (2013) 1:1008.
29. Viollet B, Horman S, Leclerc J, Lantier L, Foretz M, Billaud M, et al. AMPK inhibition in health and disease. *Crit Rev Biochem Mol Biol.* (2010) 45:276–95. doi: 10.3109/10409238.2010.488215
30. Sittipo P, Lobionda S, Lee YK, Maynard CL. Intestinal microbiota and the immune system in metabolic diseases. *J Microbiol.* (2018) 56:154–62. doi: 10.1007/s12275-018-7548-y
31. Li SQ, Qi C, Zhu HL, Yu RQ, Xie CL, Peng YD, et al. Lactobacillus reuteri improves gut barrier function and affects diurnal variation of the gut microbiota in mice fed a high-fat diet. *Food Funct.* (2019) 10:4705–15. doi: 10.1039/c9fo00417c
32. Zhang XY, Chen J, Yi K, Peng L, Xie J, Gou X, et al. Phlorizin ameliorates obesity-associated endotoxemia and insulin resistance in high-fat diet-fed mice by targeting the gut microbiota and intestinal barrier integrity. *Gut Microbes.* (2020) 12:1–18. doi: 10.1080/19490976.2020.1842990
33. Ding Y, Fang HQ, Shang W, Xiao Y, Sun T, Hou N, et al. Mitoflash altered by metabolic stress in insulin-resistant skeletal muscle. *J Mol Med.* (2015) 93:1119–30. doi: 10.1007/s00109-015-1278-y
34. Wang XH, Zhang X, Wu D, Huang ZL, Hou TT, Jian CS, et al. Mitochondrial flashes regulate ATP homeostasis in the heart. *Elife.* (2017) 6:e23908. doi: 10.7554/eLife.23908
35. Cani PD, Amar J, Iglesias MA, Poggi M, Knauf C, Bastelica D, et al. Metabolic endotoxemia initiates obesity and insulin resistance. *Diabetes.* (2007) 56:1761–72. doi: 10.2337/db06-1491
36. Price NL, Gomes AP, Ling AJY, Duarte FV, Martin-Montalvo A, North BJ, et al. SIRT1 is required for AMPK activation and the beneficial effects of resveratrol on mitochondrial function. *Cell Metab.* (2012) 15:675–90. doi: 10.1016/j.cmet.2012.04.003
37. Hawley SA, Ross FA, Chevtzoff C, Green KA, Evans A, Fogarty S, et al. Use of cells expressing gamma subunit variants to identify diverse mechanisms of AMPK activation. *Cell Metab.* (2010) 11:554–65. doi: 10.1016/j.cmet.2010.04.001
38. Park SJ, Ahmad F, Philp A, Baar K, Williams T, Luo HB, et al. Resveratrol ameliorates aging-related metabolic phenotypes by inhibiting cAMP phosphodiesterases. *Cell.* (2012) 148:421–33. doi: 10.1016/j.cell.2012.01.017
39. Lanzilli G, Cottarelli A, Nicotera G, Guida S, Ravagnan G, Fuggetta MP. Anti-inflammatory effect of resveratrol and polydatin by in vitro IL-17 modulation. *Inflammation.* (2012) 35:240–8. doi: 10.1007/s10753-011-9310-z
40. Zhao XJ, Yu HW, Yang YZ, Wu WY, Chen TY, Jia KK, et al. Polydatin prevents fructose-induced liver inflammation and lipid deposition through increasing miR-200a to regulate Keap1/Nrf2 pathway. *Redox Biol.* (2018) 18:124–37. doi: 10.1016/j.redox.2018.07.002
41. Zheng L, Wu JY, Mo JF, Guo L, Wu XY, Bao Y. Polydatin inhibits adipose tissue inflammation and ameliorates lipid metabolism in high-fat-fed mice. *Biomed Res Int.* (2019) 2019:7196535. doi: 10.1155/2019/7196535
42. Hao J, Huang KP, Chen C, Liang Y, Wang Y, Zhang XJ, et al. Polydatin improves glucose and lipid metabolisms in insulin-resistant HepG2 Cells

through the AMPK Pathway. *Biol Pharm Bull.* (2018) 41:891–8. doi: 10.1248/bpb.b17-01027
43. Cameron KO, Kung DW, Kalgutkar AS, Kurumbail RG, Miller R, Salatto CT, et al. Discovery and preclinical characterization of 6-Chloro-5-[4-(1-hydroxycyclobutyl)phenyl]-1H-indole-3-carboxylic acid (PF-06409577), a direct activator of adenosine monophosphate-activated protein kinase (AMPK), for the potential treatment of diabetic nephropathy. *J Med Chem.* (2016) 59:8068–81. doi: 10.1021/acs.jmedchem.6b00866
44. Liu RJ, Zhang Y, Yao X, Wu Q, Wei MG, Yan ZW. ε-Viniferin, a promising natural oligostilbene, ameliorates hyperglycemia and hyperlipidemia by activating AMPK in vivo. *Food Funct.* (2020) 11:10084–93. doi: 10.1039/d0fo01932a
45. Li YY, Peng JL, Li PH, Du HB, Li YP, Liu XY, et al. Identification of potential AMPK activator by pharmacophore modeling, molecular docking and QSAR study. *Comput Biol Chem.* (2019) 79:165–76. doi: 10.1016/j.compbiolchem.2019.02.007
46. Ma Y, Jia XJ. Polydatin alleviates radiation-induced testes injury by scavenging ROS and inhibiting apoptosis pathways. *Med Sci Monit.* (2018) 24:8993–9000. doi: 10.12659/MSM.913725
47. Liao P, He Y, Yang FY, Luo GH, Zhuang J, Zhai ZQ, et al. Polydatin effectively attenuates disease activity in lupus-prone mouse models by blocking ROS-mediated NET formation. *Arthritis Res Ther.* (2018) 20:254. doi: 10.1186/s13075-018-1749-y
48. Zhang W, Xu JH, Yu T, Chen QK. Effects of berberine and metformin on intestinal inflammation and gut microbiome composition in db/db mice. *Biomed Pharmacother.* (2019) 118:109131. doi: 10.1016/j.biopha.2019.109131
49. Lee H, Lee Y, Kim J, An J, Lee S, Kong H, et al. Modulation of the gut microbiota by metformin improves metabolic profiles in aged obese mice. *Gut Microbes.* (2018) 9:155–65. doi: 10.1080/19490976.2017.1405209
50. Garcia-Mantrana I, Selma-Royo M, Alcantara C, Collado MC. Shifts on gut microbiota associated to mediterranean diet adherence and specific dietary intakes on general adult population. *Front Microbiol.* (2018) 9:890. doi: 10.3389/fmicb.2018.00890
51. Jang JH, Yeom MJ, Ahn S, Oh JY, Ji S, Kim TH, et al. Acupuncture inhibits neuroinflammation and gut microbial dysbiosis in a mouse model of Parkinson's disease. *Brain Behav Immun.* (2020) 89:641–55. doi: 10.1016/j.bbi.2020.08.015
52. Rodriguez J, Hiel S, Neyrinck AM, Roy TL, Pötgens SA, Leyrolle Q, et al. Discovery of the gut microbial signature driving the efficacy of prebiotic intervention in obese patients. *Gut.* (2020) 69:1975–87. doi: 10.1136/gutjnl-2019-319726
53. Lee J, d'Aigle J, Atadja L, Quaicoe V, Honarpisheh P, Ganesh BP, et al. Gut microbiota-derived short-chain fatty acids promote poststroke recovery in aged mice. *Circ Res.* (2020) 127:453–65. doi: 10.1161/CIRCRESAHA.119.316448
54. Marion S, Desharnais L, Studer N, Dong Y, Notter MD, Poudel S, et al. Biogeography of microbial bile acid transformations along the murine gut. *J Lipid Res.* (2020) 61:1450–63. doi: 10.1194/jlr.RA120001021
55. Cai TT, Ye XL, Li RR, Chen H, Wang YY, Yong HJ, et al. Resveratrol modulates the gut microbiota and inflammation to protect against diabetic nephropathy in mice. *Front Pharmacol.* (2020) 11:1249. doi: 10.3389/fphar.2020.01249
56. Morrison DJ, Preston T. Formation of short chain fatty acids by the gut microbiota and their impact on human metabolism. *Gut Microbes.* (2016) 7:189–200. doi: 10.1080/19490976.2015.1134082
57. Nicholson JK, Holmes E, Kinross J, Burcelin R, Gibson G, Jia W, et al. Host-gut microbiota metabolic interactions. *Science.* (2012) 336:1262–7. doi: 10.1126/science.1223813
58. Kau AL, Ahern PP, Griffin NW, Goodman AL, Gordon JI. Human nutrition, the gut microbiome and the immune system. *Nature.* (2011) 474:327–36. doi: 10.1038/nature10213
59. Bergman EN. Energy contributions of volatile fatty acids from the gastrointestinal tract in various species. *Physiol Rev.* (1990) 70:567–90. doi: 10.1152/physrev.1990.70.2.567
60. Brown AJ, Goldsworthy SM, Barnes AA, Eilert MM, Tcheang L, Daniels D, et al. The orphan G protein-coupled receptors GPR41 and GPR43 are activated by propionate and other short chain carboxylic acids. *J Biol Chem.* (2003) 278:11312–9. doi: 10.1074/jbc.M211609200
61. Gao ZG, Yin J, Zhang J, Ward RE, Martin RJ, Lefevre M, et al. Butyrate improves insulin sensitivity and increases energy expenditure in mice. *Diabetes.* (2009) 58:1509–17. doi: 10.2337/db08-1637
62. Sakakibara S, Yamauchi T, Oshima Y, Tsukamoto Y, Kadowaki T. Acetic acid activates hepatic AMPK and reduces hyperglycemia in diabetic KK-A(y) mice. *Biochem Biophys Res Commun.* (2006) 344:597–604. doi: 10.1016/j.bbrc.2006.03.176
63. Besten GD, Bleeker A, Gerding A, Eunen KV, Havinga R, Dijk THV, et al. Short-chain fatty acids protect against high- fat diet-induced obesity via a PPARγ-dependent switch from lipogenesis to fat oxidation. *Diabetes.* (2015) 64:2398–408. doi: 10.2337/db14-1213
64. Stoddart LA, Smith NJ, Jenkins L, Brown AJ, Milligan G. Conserved polar residues in transmembrane domains V, VI, and VII of free fatty acid receptor 2 and free fatty acid receptor 3 are required for the binding and function of short chain fatty acids. *J Biol Chem.* (2008) 283:32913–24. doi: 10.1074/jbc.M805601200
65. Milligan G, Stoddart LA, Smith NJ. Agonism and allosterism: the pharmacology of the free fatty acid receptors FFA2 and FFA3. *Br J Pharmacol.* (2009) 158:146–53. doi: 10.1111/j.1476-5381.2009.00421.x
66. Kimura I, Ozawa K, Inoue D, Imamura T, Kimura K, Maeda T, et al. The gut microbiota suppresses insulin-mediated fat accumulation via the short-chain fatty acid receptor GPR43. *Nat Commun.* (2013) 4:1829. doi: 10.1038/ncomms2852
67. Lin HV, Frassetto A, Kowalik EJ Jr., Nawrocki AR, Lu MM, Kosinski JR, et al. Butyrate and propionate protect against diet-induced obesity and regulate gut hormones via free fatty acid receptor 3-independent mechanisms. *PLoS One.* (2012) 7:e35240. doi: 10.1371/journal.pone.0035240
68. Dodd S, Dean O, Copolov DL, Malhi GS, Berk M. N-acetylcysteine for antioxidant therapy: pharmacology and clinical utility. *Expert Opin Biol Ther.* (2008) 8:1955–62. doi: 10.1517/14728220802517901
69. Cotgreave IA. N-acetylcysteine: pharmacological considerations and experimental and clinical applications. *Adv Pharmacol.* (1997) 38:205–27. doi: 10.1016/s1054-3589(08)60985-0
70. Rizwan H, Pal S, Sabnam S, Pal A. High glucose augments ROS generation regulates mitochondrial dysfunction and apoptosis via stress signalling cascades in keratinocytes. *Life Sci.* (2020) 241:117148. doi: 10.1016/j.lfs.2019.117148
71. Fullerton MD, Steinberg GR. SIRT1 takes a backseat to AMPK in the regulation of insulin sensitivity by resveratrol. *Diabetes.* (2010) 59:551–3. doi: 10.2337/db09-1732
72. Jeon BT, Jeong EA, Shin HJ, Lee Y, Lee DH, Kim HJ, et al. Resveratrol attenuates obesity-associated peripheral and central inflammation and improves memory deficit in mice fed a high-fat diet. *Diabetes.* (2012) 61:1444–54. doi: 10.2337/db11-1498
73. Um JH, Park SJ, Kang H, Yang ST, Foretz M, McBurney MW, et al. AMP-activated protein kinase-deficient mice are resistant to the metabolic effects of resveratrol. *Diabetes.* (2010) 59:554–63. doi: 10.2337/db09-0482

Conflict of Interest: GZ, ZR, and YW were employed by the company Guangzhou Jinan Biomedicine Research and Development Center Co., Ltd.

The remaining authors declare that the research was conducted in the absence of any commercial or financial relationships that could be construed as a potential conflict of interest.

Publisher's Note: All claims expressed in this article are solely those of the authors and do not necessarily represent those of their affiliated organizations, or those of the publisher, the editors and the reviewers. Any product that may be evaluated in this article, or claim that may be made by its manufacturer, is not guaranteed or endorsed by the publisher.

frontiers | Frontiers in Nutrition

REVIEW
published: 17 May 2022
doi: 10.3389/fnut.2022.886902

The Therapeutic Effect of SCFA-Mediated Regulation of the Intestinal Environment on Obesity

Huimin You[1,2], Yue Tan[1,2], Dawei Yu[1,2], Shuting Qiu[1,2], Yan Bai[3], Jincan He[3], Hua Cao[4], Qishi Che[5], Jiao Guo[2] and Zhengquan Su[1,2]**

[1] Guangdong Engineering Research Center of Natural Products and New Drugs, Guangdong Provincial University Engineering Technology Research Center of Natural Products and Drugs, Guangdong Pharmaceutical University, Guangzhou, China, [2] Key Laboratory of Glucolipid Metabolic Disorder, Guangdong TCM Key Laboratory for Metabolic Diseases, Guangdong Metabolic Disease Research Center of Integrated Chinese and Western Medicine, Ministry of Education of China, Guangdong Pharmaceutical University, Guangzhou, China, [3] School of Public Health, Guangdong Pharmaceutical University, Guangzhou, China, [4] School of Chemistry and Chemical Engineering, Guangdong Pharmaceutical University, Guangzhou, China, [5] Guangzhou Rainhome Pharm & Tech Co., Ltd, Guangzhou, China

Intestinal environment disorder is a potential pathological mechanism of obesity. There is increasing evidence that disorders in the homeostasis of the intestinal environment can affect various metabolic organs, such as fat and liver, and lead to metabolic diseases. However, there are few therapeutic approaches for obesity targeting the intestinal environment. In this review, on the one hand, we discuss how intestinal microbial metabolites SCFA regulate intestinal function to improve obesity and the possible mechanisms and pathways related to obesity-related pathological processes (depending on SCFA-related receptors such as GPCRs, MCT and SMCT, and through epigenetic processes). On the other hand, we discuss dietary management strategies to enrich SCFA-producing bacteria and target specific SCFA-producing bacteria and whether fecal bacteria transplantation therapy to restore the composition of the gut microbiota to regulate SCFA can help prevent or improve obesity. Finally, we believe that it will be of great significance to establish a working model of gut– SCFA– metabolic disease development in the future for the improvement this human health concern.

Keywords: SCFA, gut microbiota, intestinal environment, obesity, metabolism

OPEN ACCESS

Edited by:
Gratiela Gradisteanu Pircalabioru, University of Bucharest, Romania

Reviewed by:
Yu-Anne Yap, Monash University, Australia
Tiancun Xiao, University of Oxford, United Kingdom

****Correspondence:***
Jiao Guo
gyguoyz@163.com
Zhengquan Su
suzhq@scnu.edu.cn

Specialty section:
This article was submitted to Nutrition and Metabolism, a section of the journal Frontiers in Nutrition

Received: *01 March 2022*
Accepted: *20 April 2022*
Published: *17 May 2022*

Citation:
You H, Tan Y, Yu D, Qiu S, Bai Y, He J, Cao H, Che Q, Guo J and Su Z (2022) The Therapeutic Effect of SCFA-Mediated Regulation of the Intestinal Environment on Obesity. Front. Nutr. 9:886902. doi: 10.3389/fnut.2022.886902

INTRODUCTION

Obesity is among the largest health epidemics of the twenty first century, with a prevalence of ∼13% in the world's adult population, and it is a major contributor to global diseases such as diabetes, cardiovascular disease and cancer and premature death (1, 2). Obesity is strongly associated with intestinal health, and the intestinal environment of obese patients is obviously disturbed (3, 4). On the one hand, because the intestine is continuously exposed to antigens from food, the microbiota and metabolites, intestinal inflammation is considered the origin of metabolic diseases. However, until recently, the relationship between intestinal inflammation and immune cell changes and obesity and insulin resistance has not been thoroughly studied (5–8). Increasing evidence shows that a high-fat diet (HFD) is related to low-grade intestinal inflammation. The intestinal immune system changes during HFD feeding. Therefore, inhibiting intestinal inflammation may be a treatment for obesity (6, 9, 10). In addition, intestinal hormones produced by intestinal epithelial

cells (IECs), which are related to affect nutrient absorption rate, enteric environment composition and epithelial barrier integrity, are also thought to be associated with obesity. Regulating the release of endogenous glucagon-like peptide-1 (GLP-1) and other intestinal hormones is considered a promising strategy for obesity treatment, and may even mimic bariatric surgery (11, 12). In addition, intestinal function is closely related to the body's energy metabolism. IECs can absorb lipids and package them into chylomicrons for delivery to peripheral tissues. In performing this function, intestinal cells consume up to 20% of all incoming energy and therefore represent the primary cell type utilizing energy in these tissues (13). However, there are few in-depth therapeutic studies on obesity-induced changes in the intestinal epithelial barrier, microbiota, and innate and adaptive immune cells.

To date, there is growing evidence that the gut microbiota regulates the effects of diet and alters host metabolism and the incidence of metabolic disorders. The gut microbiota produces a wide range of metabolites that act as messengers between microorganisms and their hosts. Microorganisms produce these metabolites as intermediates in their constituent metabolic pathways to chemically modify specific dietary components through enzymatic reactions unrelated to normal metabolism. Most of these metabolites have beneficial effects on the host (14, 15). Short-chain fatty acids (SCFA) are produced by bacterial fermentation of non-digestible carbohydrates (NDCs) (16, 17). The main SCFA in the intestinal tract are acetate, propionate and butyrate, which account for more than 95% of all SCFA. They are usually present in the gut at a concentration ratio of 3:1:1 (18, 19). SCFA have long been proven to affect different cell processes and functions in the intestine, such as cell differentiation, cell apoptosis, colon motility and electrolyte absorption (20–22). Therefore, to take advantage of gut bacterial metabolites such as SCFA and improve the intestinal environment by adjusting metabolism via SCFA-based treatment of obesity and related metabolic diseases, this review focuses on two aspects: first, the use of SCFA to regulate intestinal homeostasis to treat obesity and second, treatment based on targeting the role of gut microbes in SCFA production as obesity-related treatment.

SCFA MEDIATE THE INTERPLAY BETWEEN INTESTINAL HOMEOSTASIS AND OBESITY

Evidence from nearly a decade of studies has shown that obesity is associated with gut dysfunction (**Figure 1**). First, intestinal dysfunction in obese patients is associated with intestinal dysbiosis, which has been found in HFD-fed animals. When dysbiosis occurs, the intestinal tract may gradually leak, allowing lipopolysaccharide (LPS) produced by gram-negative bacteria to enter the hepatoenteric circulation (3). Low levels of LPS in the blood may then activate signaling in various Toll-like receptor 4 (TLR4) cells, leading to systemic and local inflammation in HFD-fed mice. Overproduction of proinflammatory cytokines such as tumor necrosis factor-α (TNF-α), interleukin-1β (IL-1β), and interferon-γ (IFN-γ) in obese animals may be responsible for chronic inflammation and insulin resistance, in part through the nuclear factor kappa-B (NF-κB) pathway (7, 23–28). Second, intestinal immune function is also reduced in obese people. Researchers have found an increased number of white blood cells in the intestinal mucosal barrier, a shift to proinflammatory cell types (such as Th1 cells, total macrophages, dendritic cells, and natural killer (NK) cells) in obese people, and an increased incidence of colitis (6, 29, 30). Finally, it is well-known that an important feature of intestinal microbiota disorder is the decreased bacterial abundance of SCFA in the intestinal microbiota of obese patients, which leads to a decrease in SCFA levels and the occurrence of intestinal inflammation (31). SCFA, as key microbial metabolites that maintain the function of the intestinal epithelium, have been deeply studied regarding their ability to support intestinal barrier function (**Table 1**). On the one hand, SCFA can provide energy for the host epithelium. SCFA epithelial metabolism is a major determinant of hypoxia in the mucous membrane, and bacteria producing butyrate affect the oxygen consumption of epithelial cells and lead to the stabilization of hypoxia-inducible factor (HIF), a transcription factor that coordinates barrier protection and thus plays a key role in the maintenance of epithelial barrier function (53, 54). On the other hand, SCFA have been shown to increase the expression of the intestinal barrier-related genes tight junction protein 1 (TJP1), occludin (OCLN) and zonula occludens 1 (ZO-1) and inhibit the expression of Claudin 2 to repair the intestinal barrier (55–61). In obesity and related metabolic diseases, SCFA mainly inhibit histone deacetylases (HDACs) and activate SCFA-related receptors to maintain the intestinal environment. Based on this background, the following two aspects are focused on in the discussion below. First, we discuss SCFA-dependent receptor pathways in and out of cells and second, we discuss the SCFA receptor-independent pathways that repair intestinal barrier function in the course of obesity treatment, providing new ideas and potential targets for obesity treatment in the future.

SCFA-Associated Receptor-Dependent Pathways

Extracellular SCFA Receptor Pathway and Obesity

SCFA-sensing G protein-coupled receptors (GPCRs), also known as free fatty acid receptors (FFARs), including GPR41 (FFAR3), GPR43 (FFAR2), and GPR109A, are mainly expressed by IECs, especially intestinal endocrine cells (31, 62, 63). They can be activated by SCFA and are highly expressed in the human intestinal mucosa, playing a key role in maintaining the homeostasis of intestinal barrier function. These receptors are present in the apical membrane of the colon epithelium, and luminal SCFA activate these receptors to function outside the cell without entering the cell (26, 64, 65). Activation of these receptors can stimulate the Gαs and Gβγ subunit signaling pathways to activate ERK, reduce the cellular level of cyclic adenosine monophosphate (cAMP) and increase intracellular Ca^{2+} levels, which act as a secondary messenger to initiate biological effects and activate various downstream signaling events, such as protein phosphorylation and changes in cellular behavior (66–68). The binding of GPCRs to β-inhibitory protein (β-ARR)

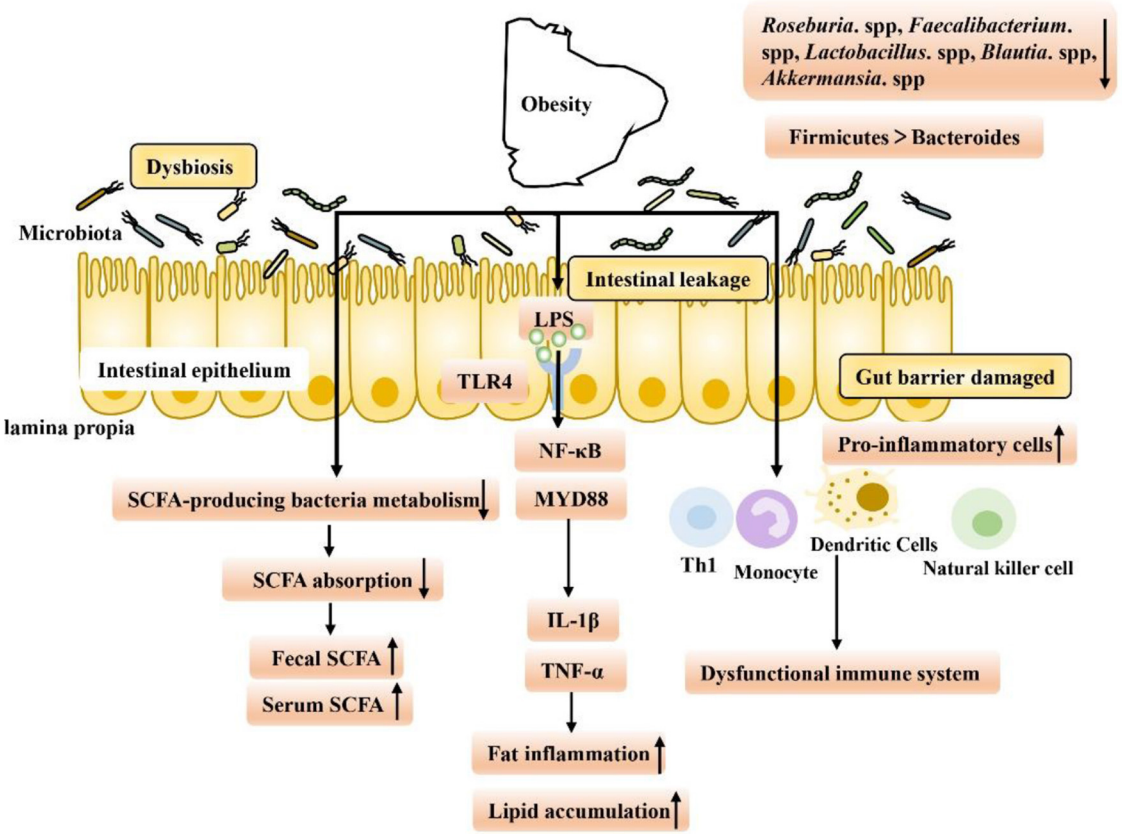

FIGURE 1 | Gut microbiome disorders in obese patients are caused by intestinal environment disorders, which have the following characteristics: (1) Intestinal leakage and low levels of LPS in the blood may activate signal transduction in various TLR4-expressing cells, leading to the occurrence of fat inflammation and lipid accumulation. (2) Intestinal immune function decreased, and levels of proinflammatory Th1 cells, total macrophages, dendritic cells and NK cells increased, exacerbating inflammation. (3) The abundance of SCFA-producing bacteria decreased, leading to a decrease in the intestinal absorption capacity of SCFA and an increase in fecal SCFA concentration. Increased nutrient intake is associated with increased levels of gastrointestinal leakage, and through passive ingestion, increased serum SCFA concentration.

also stimulates and promotes the activation of the Gαs and Gβγ subunits, thereby regulating *in vivo* physiological activities such as chemotaxis, apoptosis, proliferation, differentiation and gene expression (69–71).

Based on the response mechanism of SCFA receptor activation, many studies have proven that the activation/damage of SCFA receptors produces a significant response, especially in the intestinal tract, in early life (72) (**Figure 2**). HFD intake before and during pregnancy can change the composition of the maternal intestinal microbiota and ultimately lead to an increase in maternal circulating LPS levels. Reduction in maternal SCFA levels and inhibition of their receptor, GPR41, impairs the integrity of the intestinal barrier and may ultimately lead to changes in placental vasculogenesis and fetal intestinal development (73, 74). In a recent study, investigation of the SCFA-GPR41 and SCFA-GPR43 axes confirmed that offspring of germ-free maternal mice were more prone to obesity and glucose intolerance than offspring of non-specific pathogen-free female mice. SCFA produced by the gut microbiota of pregnant mice can enter the embryo through the blood. SCFA act on the sympathetic nerve receptor GPR41 and intestinal epithelial and pancreatic GPR43, promoting the expression of GLP-1 in nerve cells and intestinal endocrine cells and the differentiation of islet β cells. Other studies have shown that maternal supplementation with butyrate can increase the expression level of GPR43 in maternal adipose tissue, promote the decomposition of maternal white adipose tissue, reduce the liver lipid deposition of offspring, and play an important role in alleviating fetal malnutrition caused by metabolic disorders in maternal and fetal offspring. These results suggest that during pregnancy, intestinal microbiota and maternal microbiota SCFA promote a good environment for shaping the metabolic system development of embryos and energy homeostasis of offspring (75, 76). In addition, some researchers have attempted to establish that the SCFA-GPR43-GLP-1 pathway in the intestinal tract relieves hyperglycemia and found that activating this pathway had a good effect on the gut microbiota disturbance induced by tacrolimus and glucose metabolism disorder caused

TABLE 1 | Location, signaling molecules and mechanisms of SCFA-associated receptor pathways in maintaining intestinal homeostasis.

Types	Localization	Associated signal molecule	Mechanism	References
SCFA-associated receptor (GPCRs)				
GPR 43	Intestinal epithelial cells, Dendritic cells (DCs), Human intestinal lamina propria (LP) CD4 T cells	RegIIIγ, β-defensins, IgA ↑	• Activate mTOR and STAT3 in IECs and induce AMP production, promote IEC RegIIIc and b-defensins in a GPR43-dependent manner. • SCFA(acetate) promoted intestinal IgA responses, which was mediated by "metabolite-sensing" GPR43.	(32, 33)
	Human intestinal LP CD4 T cells	IFNγ, IL-17↓	• GPR43 signaling enhances histone acetylation • Decrease the activation and proliferation of Human intestinal LP CD4 T cells and the production of inflammatory cytokines *in vitro*.	(34)
	Colon epithelial cells	IL-18↑	• GPR43 activates NLRP3 through Ca^{2+} mobilization and membrane hyperpolarization, and the activated Caspase 1 cleaves IL-18 and IL-18 is released	(35)
GPR 41	Colon endocrine cells, Intestinal L-cell	PYY, GLP-1, Cholecystokinin, GIP ↑	• Promote sympathetic outflow, promote resistance to obesity and improve insulin sensitivity • Inhibits gastric empties and food intake • Stimulates insulin secretion of β-cells of the islets of Langerhans	(36–40)
	Paneth cell	α-defense↑	• Paneth cells recognize GPR 41 and increase the secretion of α -defencin	(41)
GPR 109A	Colon epithelial cell	Claudin-3↑	• Butyrate acts on the Akt signaling pathway in a GPR109A-dependent manner to promote Claudin-3 expression	(42)
		IL-18, IL-10↑	• Promotes anti-inflammatory properties of colon macrophages and DCs • Induced differentiation of Treg and Tr1 cells • By stimulating GPR109A to induce MCT-1 to recruit to the parietal membrane, the anti-inflammatory effect of SCFA in intestinal tract was enhanced	(43, 44)
	Intestinal tumor cell	Cyclin D1, C-Myc↓	• Activation of GPR109A inhibited NF-κB, down-regulated cyclin D1 and up-regulated death receptor pathway	(45)
SCFA transport receptor				
MCT 1	Colon epithelial cells, Human colon cancer cells	TGF-β, IL-10 ↑ TNFα, IFN-γ, IL-8, IL-6, NF-κB, ERK1/2, Syk, JNK1/2, p38 MAPK ↓	• Down-regulated MCT 1 expression affects butyrate uptake and oxidation pathways as well as cellular regulation • Up-regulation of MCT1 promotes the transport of butyrate to IECs • Hyperhistone acetylation of butyrate upregulates Foxp3 expression in T cells and enhances the production of anti-inflammatory cytokines TGF-β and IL-10 • MCT-1 mediated SCFA inhibits TNF-α -induced IL-8 and IL-6 expression	(44, 46–49)
SMCT 1	Rat IECs, Human colon cancer cells	TNF-α ↓	• The transport function of SMCT1 is stimulated to mediate Na^+ dependent absorption of luminal butyrate	(50)
	Non-tumor rat IECs	ROS↑	• Oxidative stress can inhibit SMCT1-mediated butyric acid uptake and stimulate butyric acid uptake and outflow through passive diffusion	(51)
	Human colon adenocarcinoma cells	COX-2, HIF-1α↓	• SMCT-1 mediates butyrate uptake followed by activation of cAMP response element-binding protein-binding protein/p300	(52)

by ecological disorders; it also reversed the change in butyrate concentration in the cecum and increased the expression level of GPR43 in intestinal crypts. Moreover, this approach promoted GLP-1 secretion by L cells of the intestinal endocrine mucosa and restored fasting blood glucose (FBG), glycosylated hemoglobin (HbA1c) and oral glucose tolerance test (OGTT) values to normal levels (77). Therefore, SCFA, as an important regulator of body metabolism, play a key role in affecting adipose tissue metabolism, lipid oxidation capacity, β cell function and insulin secretion, suggesting that there is a mutual relationship among the microbiota, SCFA, and metabolism and that they may be potential targets for the treatment of obesity and related metabolic diseases (**Figure 3**). Therefore, we believe that targeting the gut microbiota to adjust SCFA levels to improve the intestinal environment and adjust glucose-regulating hormones in colonic L cells will in turn stimulate insulin secretion to improve glucose homeostasis, and if this approach is used particularly to intervene early in life, we can improve metabolism in adulthood. This strategy has great potential for treating metabolic diseases such as obesity.

Intracellular SCFA Transporter [MCT (SLC16A) and SMCT (SLC5A)] Expression

In addition to the extracellular functions described above, SCFA can also function intracellularly, which obviously requires their entry into colon epithelial cells. SCFA must pass through the epithelium to reach the serosa side to act on immune cells in the lamina propria (78, 79). Transport mechanisms are needed for intraluminal entry and transcellular transport; otherwise, SCFA cannot produce intracellular effects in colon epithelial cells and

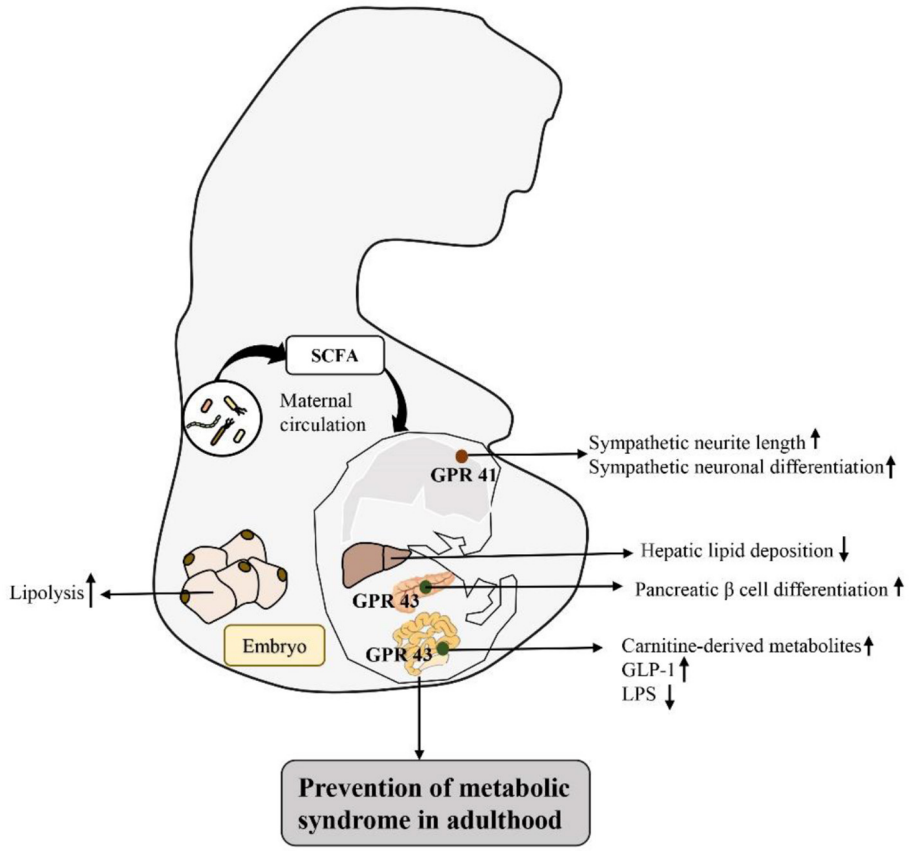

FIGURE 2 | Activation of SCFA-associated receptors in early life intestinal response mechanisms to prevent metabolic diseases in adulthood: by regulating the intestinal flora matrix, increased maternal SCFA flows into the embryo to activate embryonic sympathetic nerve receptor GPR41 and intestinal epithelium and pancreas GPR43, promotes the development of the baby's nerve and bowel, improves embryo glucolipid metabolism, and improves the fetal malnutrition caused by maternal metabolic disorders, preventing metabolic diseases in adulthood.

cannot act on mucosal immune cells. Moreover, at physiological colonic pH (5.6–6.6), the main form of SCFA is anionic and they cannot undergo simple diffusion. At the junction of the lumen, ionization of most SCFA is expected at physiological pH. In this regard, many studies have reported evidence for carrier-mediated absorption pathways for ionized SCFA (79, 80). Therefore, SCFA transporters expressed in the colon epithelium are also major determinants of the beneficial effects of SCFA on the host (78, 81–84). For example, H^+-coupled transporters [monocarboxylate transporter (MCT)1/4] and Na^+-coupled transporters [sodium-coupled monocarboxylate transporter (SMCT)1/2] transfer SCFA to colon epithelial cells and play specific roles in the absorption and utilization of SCFA in the intestine (**Figure 3**).

Recent studies have shown that the expression of SCFA transporters is effective in the treatment of obesity and related metabolic diseases. On the one hand, MCT1 is one of the main routes of butyrate transport in Caco-2 cells (85); when MCT1 expression is eliminated by siRNA, secretion of angiopoietin-like protein 4 (ANGPTL4) induced by *Clostridium butyricum* producing butyrate is greatly affected, thus affecting fat generation (86). In addition, it is worth noting that MCT1 has been proven to have certain effects on heat production and energy homeostasis. Inhibition of MCT1 can block the effect of butyrate in adipocytes. After inhibition of MCT1 expression, the effect of butyrate on LSD1 and UCP1 is completely blocked, and MCT1 has been proven to be a lactate transporter in adipocytes. It plays an important role in adipocyte function by mediating lactate flux (87). In addition, the Irving team first reported the relationship among SCFA, body mass index (BMI), and jejunum transporters in a cohort of morbidly obese patients undergoing bariatric surgery. The results showed that BMI was positively correlated with SMCT1 mRNA levels and that BMI was positively correlated with serum butyrate, valeric acid, and isocaproic acid concentrations. The increase in serum SCFA concentration may be due to increased uptake of SCFA in the colon, in part due to increased nutrient intake and the association of obesity with increased levels of gastrointestinal leakage, resulting in a complete bypass of SCFA transporters and increased passive uptake of SCFA. Interestingly, a new finding in this study is that although the jejunum was not a major site of SCFA uptake, increased serum SCFA concentrations were positively associated with the mRNA levels of the SCFA

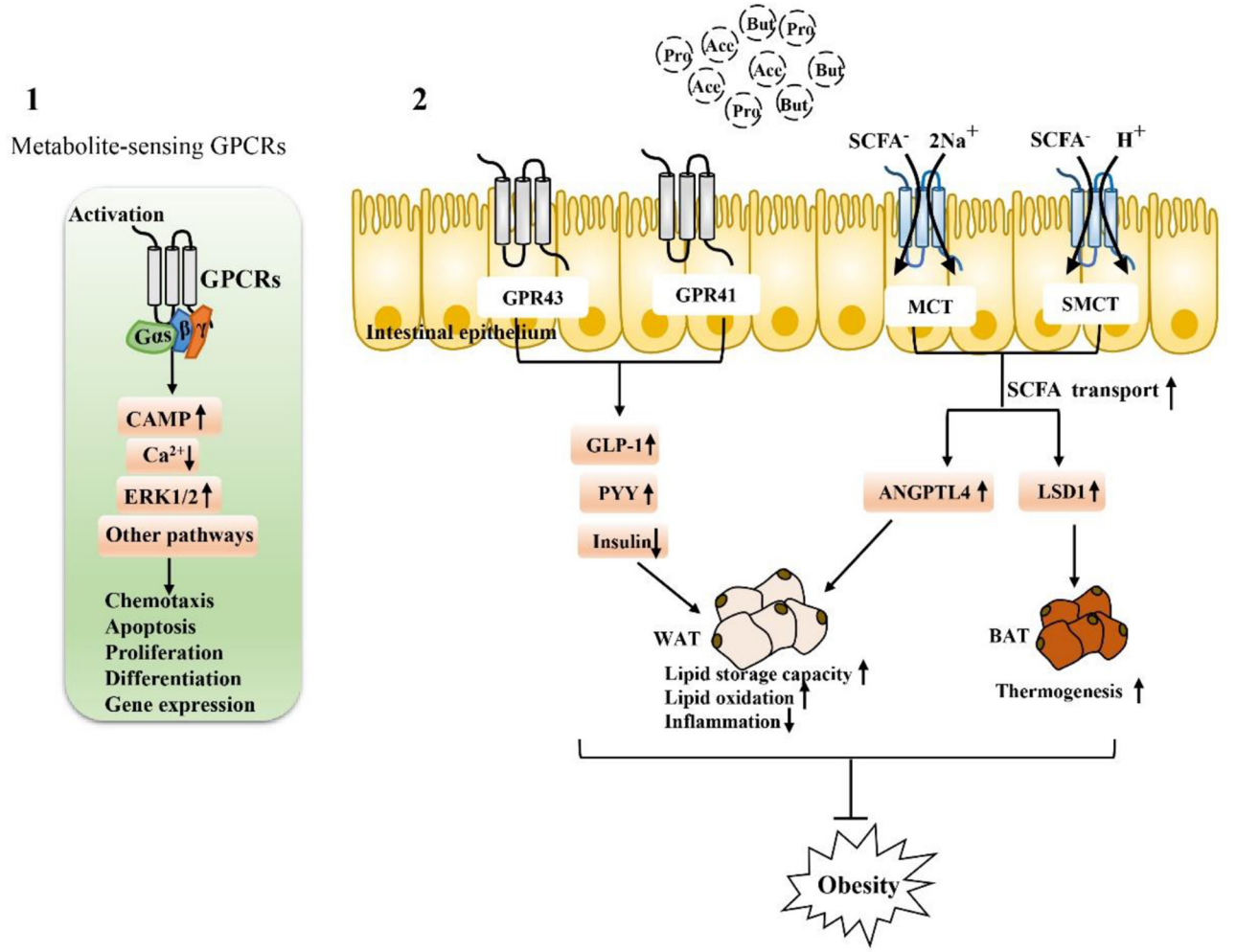

FIGURE 3 | Activation depends on SCFA-associated receptors to maintain intestinal function and alleviate metabolic disorders: (1) Extracellular, SCFA-sensing G-protein-coupled receptors (GPCRs) are activated to recruit and bind downstream effector proteins (e.g., G proteins, β-arrestin, etc.), which then function *in vivo* through the cAMP signaling pathway, ERK signaling pathway 1/2, and calcium ion signaling pathway. (2) The activation of GPR43 and GPR41 receptors on intestinal endocrine cells is closely related to the regulation of metabolic disorders. After activation, GLP-1 can be stimulated, the secretion of PPY maintains glucose homeostasis, and the activation of SCFA transporters MCT and SMCT can promote the entry of SCFA into intestinal epithelial cells and regulate genes related to fat metabolism. Activation of these SCFA-dependent receptors is particularly important for fat storage, oxidation, inflammation, and thermogenesis.

transporter SMCT1 in the jejunum (88). In summary, SCFA are essential for optimal colonic health. Transporters responsible for the entry and cross-cell transfer of these bacterial products into the intestinal epithelium are key determinants of maintaining intestinal function under physiological and disease conditions. By influencing the expression of SCFA transporters to regulate the intestinal tract, extraintestinal tissues and serum SCFA concentration can be used as a future therapeutic target to reduce the intestinal dysfunction caused by obesity.

SCFA Receptor-Independent Pathway

SCFA also function by inhibiting the receptor-independent pathway of histone deacetylases (HDACs) (**Figure 4**). HDACs are groups of deacetylases that remove acetyl groups from histone and non-histone complexes that regulate gene expression, and HDAC inhibitors have been shown to exhibit potent anti-inflammatory activity in inflammatory diseases (89–91). SCFA produced by intestinal microorganisms inhibit HDAC activity, which increases histone acetylation, relaxes chromatin structure and increases the accessibility of certain genes to transcription factors, thereby increasing their expression (92–95). SCFA-mediated HDAC inhibition is accelerated during intestinal barrier repair and plays a major role in the regulation of metabolic diseases. There is tremendous potential particularly for the use of the SCFA butyrate, which is a recognized HDAC inhibitor, in the treatment of obesity-related metabolic diseases (96–100). In IECs, a specific HDAC, HDAC3, can regulate histone acetylation in IECs, integrate microbiological signals to regulate intestinal homeostasis, and regulate lipid metabolism genes in a variety of tissues. HDAC3 expression in the small

intestine in children is positively correlated with body weight, which was specifically observed with HDAC3 knockout in mouse IECs. The lack of HDAC3 changed the expression of genes (Chka, Mttp, Apoa1, and Pck1) that respond to the regulation of metabolism in IECs, increased the expression of β-oxidation-related genes in mitochondria and peroxisomes, and increased the oxidation rate of fatty acids. HDAC3 has also been found to inhibit genes involved in fatty acid oxidation in intestinal cells by inhibiting transcriptional targets in the peroxisome proliferator-activated receptor (PPAR) nuclear receptor family, which play a central role in coordinating PPAR regulation of lipid oxidation in the intestinal epithelium. In addition to artificially reversing the reduced weight loss in obese mice, fibroblast growth factor 21 (FGF21) gene expression in the liver and hepatocytes can be induced by inhibiting HDACs, thus stimulating the β-oxidation of long-chain fatty acids and the production of ketone bodies, which may be a treatment for obesity (13, 99, 101). Thus, SCFA (mainly butyrate) prevent diet-induced obesity by inhibiting HDAC3 activity in IECs, and attempts to regulate the butyrate-HDAC3 pathway may be used to prevent and ameliorate obesity-related diseases. Changes in the gut microbiota have been thought to affect intestinal inflammation and obesity. Antibiotic treatment can affect weight gain by eliminating microbes that produce HDAC inhibitors, which have anti-inflammatory effects by increasing regulatory T (Treg) cell counts, but a new study found that mice without HDAC6 did not show resistance to obesity but rather showed accelerated weight gain. HDAC6 deficiency may lead to enhanced activation of CD4+ and CD8+ T cells and imbalance of the gut microbiota; accordingly, the representation of the S24–7 family and Lactobacillus decreases, Bacteroides and Parabacteroides abundances increase, which promotes obesity (102). In summary, the microbial communities of obese individuals and the inhibition of HDACs exhibit a strong relationship. In conclusion, there is a strong correlation between the microbiome of obese people and the inhibition of HDAC, and the relationship between obesity and HADC needs to be further explored. SCFA, especially butyrate, as HDAC inhibitors, play a beneficial role in sustained low-grade inflammation in obesity and especially in balancing pro-inflammatory and anti-inflammatory immune responses, which has great research significance for the treatment of obesity.

SCFA-BASED MICROBIAL THERAPY

As mentioned above, SCFA have a strong relationship with intestinal microbial metabolites in the treatment of obesity and the repair of intestinal function. The role of SCFA is closely related to intestinal microbes. The microbiota of the human gut affects the metabolism of the host in various ways and may play a role in the development of obesity. Some species of microbes can play specific roles (26, 103). For example, at the genus level, *Blautia* is the only bacterium for which its abundance is negatively correlated with visceral fat area, which may be related to its ability to produce SCFA to regulate GPR41 and GPR43, promote fat decomposition and reduce fat accumulation (104, 105). In addition, it is recognized that the Firmicutes/Bacteroidetes ratio is increased in obese animals and humans, but acetate and propionate are mainly produced by Bacteroidetes, while butyrate is mainly produced by Firmicutes (18, 106, 107). The increased Firmicutes/Bacteroidetes ratio in obese individuals implies higher butyrate and lower propionate and acetate production in these subjects, a finding partially contradicted by the respective anti-obesogenic and obesogenic effects of these SCFA. According to the literature, there may be fewer SCFA-producing bacteria in obese individuals, and these bacteria are gradually replaced by other bacteria belonging to the same phylum, resulting in reduced production of SCFA in the colon (108). For example, the abundance of *Faecalibacterium prausnitzii* (Firmicutes), which is thought to be associated with obesity, has been shown to be significantly reduced in obese children (109, 110). Therefore, it is necessary to maintain the abundance and diversity of SCFA-producing bacteria, and attempts to regulate the species of SCFA-producing bacteria may have a beneficial effect on the treatment of obesity. In addition, it is worth mentioning that in the feces, the SCFA (butyrate, propionate, and isovaleric acid) concentration gradually increased with the increase in body weight and the increase in the level of microbial metabolism associated with obesity, but by adding SCFA, the host intake of SCFA triggered by the increase in the gut microbiota can cause the fecal SCFA concentration to be further reduced (26). In summary, certain drugs and microbe-oriented therapies can be used to help obese adults lose weight, triggering the metabolism of gut microbes in the body. In particular, some bacteria can increase SCFA production, thereby increasing the integrity of IECs, which can become one of the means for the treatment of obesity and related metabolic diseases (**Figure 5**).

Diet Therapy

It is well-known that dietary and microbiota interactions may activate bacterial metabolic pathways and functional metabolites associated with fat deposition in humans (111–114). Recent studies indicate that SCFA produced by carbohydrate fermentation are necessary for maintaining human health from an ecological perspective and can be considered an ecosystem service provided by the gut microbiota to human hosts. Restoring or enhancing lost or missing functions by re-establishing functional active ecological populations as ecosystem service providers (ESPs) is key to building a healthier microbiome, which helps mitigate disease. Targeted promotion of SCFA producers as ESPs through personalized nutrition may provide a new ecological approach for controlling gut microbiota to manage dysbiosis-related diseases (115). Therefore, dietary interventions to regulate the gut microbiota and increase the level of SCFA in the intestinal tract to repair the intestinal barrier, reduce inflammation caused by obesity and inhibit the occurrence of obesity and related diseases have become current hot spots. For example, dietary supplementation with sodium butyrate can inhibit histone deacetylation and activate signal transducer and activator of transcription 3 (STAT3), and induction of α-defensin expression in Paneth cells reduces intestinal barrier dysfunction in obese mice induced by HFD and corrects the intestinal microbiota imbalance in mice induced by HFD. In addition,

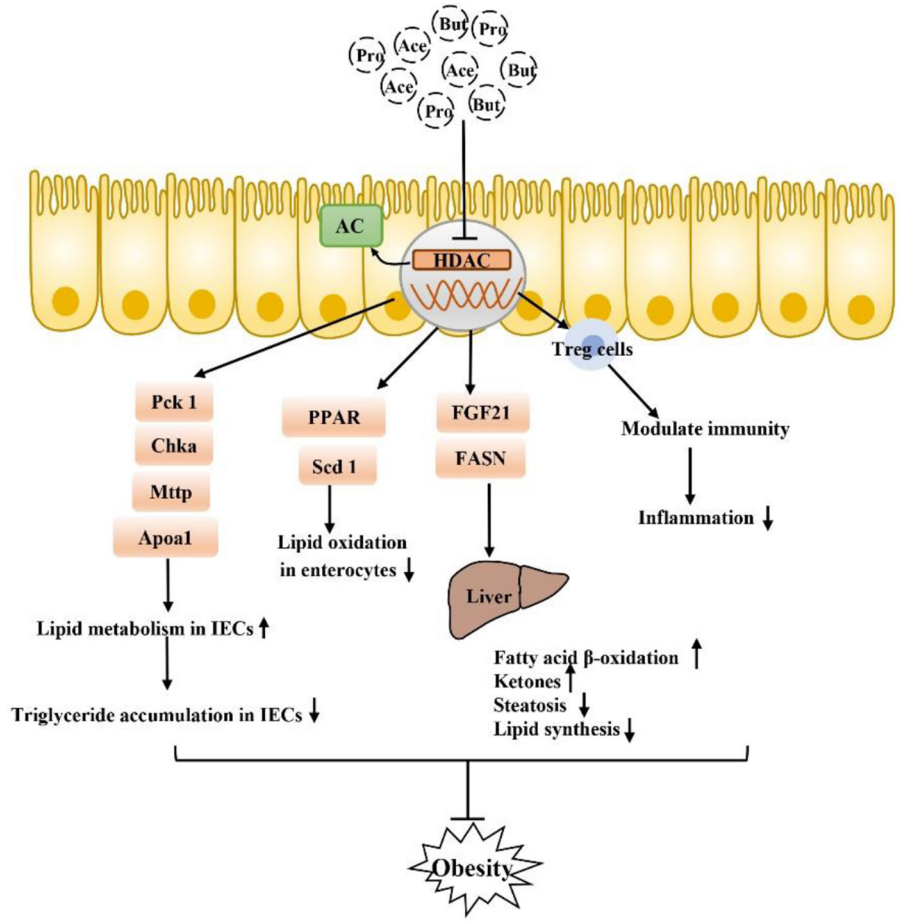

FIGURE 4 | SCFA can also inhibit obesity by inhibiting the HDAC receptor-independent pathway: after inhibiting HDAC, SCFA play a core role in PPAR-regulated lipid oxidation in the intestinal epithelium and can regulate a variety of genes that respond to microflora regulation of metabolism to improve lipid accumulation in intestinal epithelial cells. Moreover, inhibition of HADA has been found to play a beneficial role in lipid metabolism in the liver, in addition to the regulation of Tregs in immune cells. Inhibition of inflammation is also closely related to the occurrence and development of obesity.

butyrate increased the abundances of beneficial bacteria such as *Christensenellaceae*, *Blautia* and *Lactobacillus* that produce butyrate in a seemingly virtuous cycle. Thus, butyrate repaired intestinal mucosal damage, improved tight junction structure, reduced intestinal endotoxin entry into the liver, and alleviated liver inflammation and lipid accumulation caused by HFD consumption (116, 117). In addition, SCFA-producing bacteria such as *Ruminococcaceae*, *Muribaculaceae* and *Akkermansia* can also be enriched directly through diet to increase the level of SCFA to increase the expression levels of intestinal tight junction mRNA and protein and reduce intestinal permeability, improving intestinal barrier function in obese mice (118). Finding specific SCFA-producing bacteria and using diet or drugs to target certain bacteria is also a new therapeutic approach. For example, studies have found that strains of *Anaerostipes* and *Dysosmobacter welbionis* can metabolize inositol into propionate and butyrate to regulate the intestinal homeostasis of the body, which is associated with higher heat production of the body and may be beneficial to patients with obesity and diabetes (119–121). In a randomized clinical study of a specifically designed isoenergy diet, Zhao et al. used a bacteria-level, microbiome association approach to characterize the dynamics of the gut microbiome and its effect on glycemic homeostasis in patients with type II diabetes and identified a group of bacterial strains that produce acetate and butyrate. These strains are selectively promoted by increasing the availability of a variety of fermentable carbohydrates in the form of dietary fiber. These SCFA producers may be key players in maintaining a mutually beneficial relationship between the gut microbiome and the human host, playing a key role in maintaining a healthy gut environment (115). Additionally, a new strain of *Akkermansia muciniphila* isolated from healthy human feces plays a critical role in maintaining mucin layer integrity, thereby reducing proinflammatory lipopolysaccharide translocation and controlling fat storage, adipose tissue metabolism and glucose homeostasis (122–124) (**Figure 6**). Researchers also established a cAMP-responsive binding protein H (CREBH)-deficient mouse model to demonstrate that the use of *A. muciniphila*

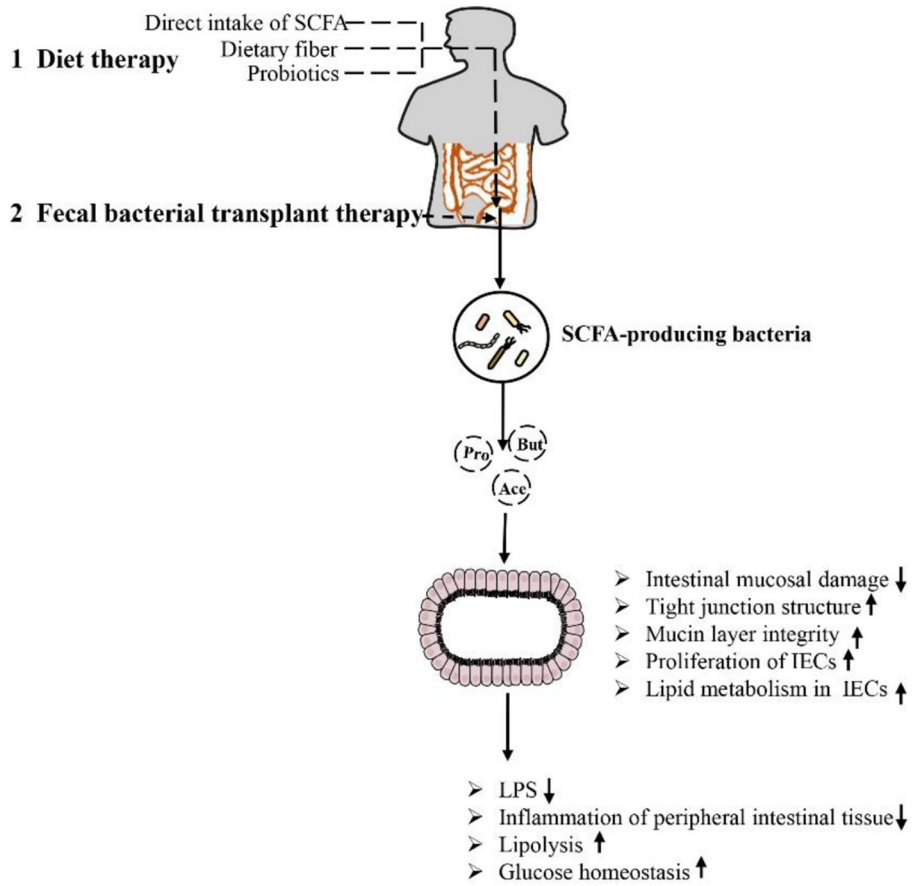

FIGURE 5 | Methods and approaches to improve obesity-related metabolic diseases by regulating the intestinal environment through SCFA: Dietary therapy (direct supplementation of SCFA, dietary fiber and prebiotics) and microbiological therapy (fecal bacteria transplantation) concentrate/target SCFA-producing bacteria, increase SCFA production, repair intestinal barrier damage, reduce inflammation in intestinal and periintestinal tissues, enhance lipolysis, and improve glucose homeostasis. This approach results in inhibition of the occurrence of obesity and related metabolic diseases.

administration ameliorated chronic hypertriglyceridemia caused by deletion of the CREBH gene in mice. This effect is mediated by upregulation of hepatic LDL receptor expression to facilitate clearance of triglyceride-rich lipoprotein residues from circulation. Moreover, such treatment improved glucose intolerance and reduced hepatic inflammatory stress caused by CREBH depletion (125). The role of *A. muciniphila* is closely related to SCFA. *A. muciniphila* has been proven to use mucin as an energy source and transform it into SCFA (acetate and propionate); on the other hand, SCFA production was increased by altering the abundance of Bacteroidetes, which produce acetate and propionate. Moreover, SCFA play a key role in supporting the differentiation of mucus-secreting goblet cells, promoting the maturation of Wnt3- and defensin-secreting Paneth cells, and promoting the proliferation of IECs in a GPR43/41-dependent manner (117, 123). In addition, *A. muciniphila* can degrade human milk oligosaccharides (HMO) to produce acetate and propionate to maintain a healthy mucosal layer and metabolic state under *in vitro* culture conditions containing breast milk (126). Based on its regulation of intestinal homeostasis, *A. muciniphila* has also been proven to have potential effects for the treatment of lipid metabolism disorders. Some researchers have observed that *A. muciniphila* has potential effects on lipid metabolism in host IECs. Several key transcription factors and genes involved in fatty acid, cholesterol and bile acid metabolism have been identified. For example, genes encoding liver x receptor (Lxr), carnitine palmitoyltransferase 1 (Cpt1), and hydroxymethylglutarate coenzyme A (HMG-CoA) synthase are all affected by *A. muciniphila.* In addition, Fiaf has been found to be related to obesity and can regulate lipid metabolism in different tissues, while *A. muciniphila* and its related SCFA metabolites can induce the expression of Fiaf, inhibit the generation of low-density lipoprotein (LDL), and maintain lipid homeostasis and metabolism in intestinal and peripheral tissues (127). The association between the gut microbiota and metabolic disease can be altered by diet. For example, metformin, commonly used in patients with type II diabetes, has recently been shown to alter the composition of the gut microbiota by enriching *A. muciniphila*, which degrades mucin, as well as several SCFA-producing microbiota constituents. Metformin's

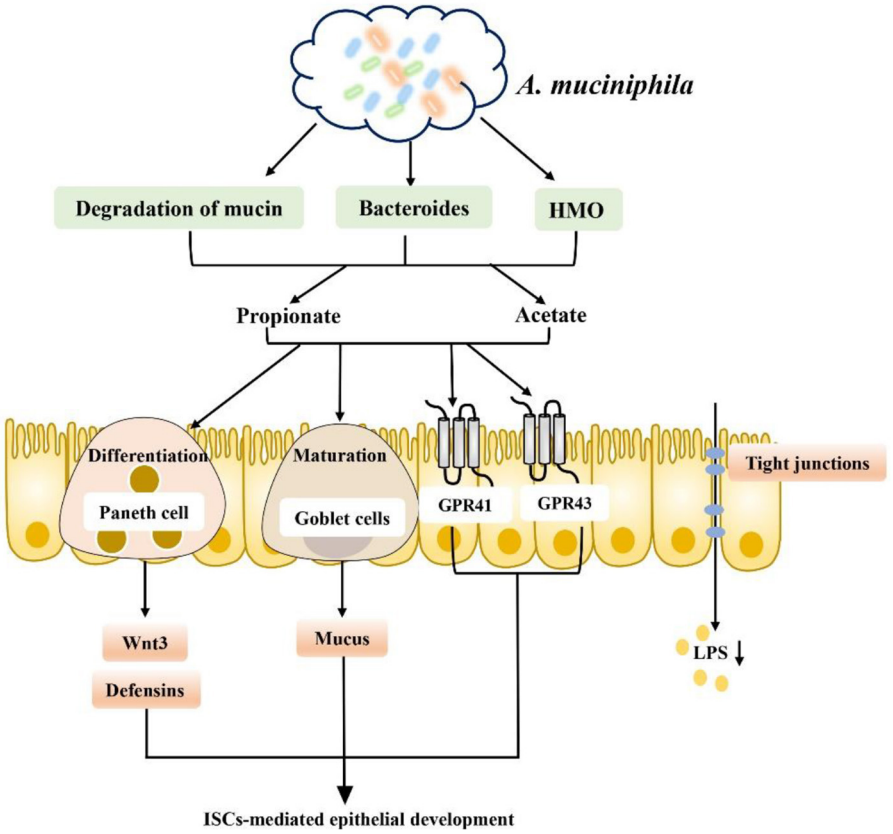

FIGURE 6 | *A. muciniphila* promotes SCFA metabolism and improves the intestinal environment to improve metabolic abnormalities: (1) *A. muciniphila* can increase the production of SCFA (such as propionate and acetate) by degrading mucin, increasing the abundance of Bacteroidetes and degrading HMO. (2) Promoting intestinal epithelial cell proliferation by supporting mucus-secreting goblet cell differentiation, promoting the maturation of Wnt3- and defensin-secreting Paneth cells in a GPR43/41-dependent manner. (3) Promoting the secretion of GLP-1 and PYY in a GPR43/41-dependent manner. (4) Inducing Fiaf expression and inhibiting LDL production. (5) Inhibiting LPS production and inflammation.

effect on the gut microbiota alters gut metabolomics, increasing the ability to produce butyric and propionic acids, with beneficial effects on glucose metabolism (128). In conclusion, intestinal barrier dysfunction is one of the key pathogenic factors of obesity, and SCFA generated by intestinal microbial metabolism play an obvious role in reducing intestinal leakage and inflammation of peripheral intestinal tissues, such as liver and adipose tissues, caused by obesity. Based on the level of intestinal microbial control of SCFA production, prevention of obesity-induced systemic inflammation may be a potential treatment for obesity and its related metabolic diseases in the future by using dietary interventions to enrich beneficial SCFA-producing bacteria or by directly targeting certain SCFA-producing bacteria to correct obesity-induced intestinal microbiome dysregulation.

Fecal Bacterial Transplant Therapy

The composition of gut microbes can be changed by diet and prebiotics or probiotics, but a new and unexplored method altering the gastrointestinal microbiota called fecal microbiota transplantation (FMT) has become a hot research topic (129–131). In theory, FMT increases the diversity of the gut microbiota, alters microbial metabolism, limits intestinal permeability and reduces local and systemic inflammation. FMT has also been shown to be durable, to be mostly safe, and to have relatively few side effects (132–136). Recently, the treatment of obesity by FMT has attracted the attention of many researchers and is considered a potential treatment option for obese patients in the future (137–140). In a previously published study, Ridaura et al. (131) transplanted fecal flora from obese or lean identical twins into germ-free mice. The mice transplanted with the lean-associated microflora were reared with the mice transplanted with the corresponding obese-associated microflora, which inhibited weight gain and obesity-related metabolic phenotypes in the mice transplanted with the obese-associated microflora. The inhibition of obesity development was found to be associated with specific members of Bacteroidetes in the lean-associated microflora. Clinically, researchers have attempted to evaluate the efficacy of oral coated FMT plus supplementary fiber supplementation in a representative population with severe obesity and metabolic syndrome in North America and found that oral FMT can alter the microbial ecology of the recipient, thereby improving insulin sensitivity. Dietary fiber supplementation can enhance

or maintain these effects, demonstrating that FMT can be an effective microbiological therapy (141). In addition, a recent preliminary clinical trial reported for the first time the short-term efficacy and safety of FMT in obese patients without metabolic disorders. Although FMT effectively and continuously changed the composition of the gut microbiota and bile acid metabolism of the subjects, making them more similar to those of lean donors, the BMI and SCFA and GLP-1 levels did not change significantly in the short term. However, during the experiment, it was observed that the butyrate-producing bacterium *F. prausnitzii* was implanted, and the gene level of butyrate-producing bacteria increased. Since it was not found in the obese microbiota, the researchers hypothesized that butyrate may be rapidly metabolized by colon cells, leaving no measurable content behind (142). In addition, it is worth mentioning that studies have found that although FMT can change the gut microbiota of obese subjects, it produces no significant improvement in body weight or most metabolic indicators. It seems unlikely that the changes in the composition of the microbiota induced by FMT alone can be sufficient to treat or prevent metabolic disorders in humans. It has been suggested that in the future, whether preselected or specifically designed microbial compositions of donors or recipients can optimize changes in beneficial microbiota constituents should be explored (143). This information indicates the inconsistent response rates and occasional adverse events of fecal bacterial transplantation, which illustrate the complexity of the treatment regimen. Attempts have also been made to find potential alternatives by using specific bacterial lysates (dissolved products of bacteria), specific components of bacteria or inactivated bacteria to treat diet-induced obesity in mice fed lysates of *Methylococcus capsulatus Bath.* Increased SCFA levels indirectly promoted Treg cell polarization after treatment, significantly enriched the abundance of Parabacteroides, increased FoxP3+RORγT+IL-17+ Treg cell levels, enhanced intestinal barrier function, and significantly improved diet-induced obesity (144). All these results suggest that FMT is effective in the treatment of obesity, but it is still necessary to determine the effect of the microbiota and its metabolites, such as SCFA, to develop more effective microbiota-based treatments for obesity in the future.

CONCLUSION AND FUTURE PERSPECTIVE

Obesity is a major global health problem, and its incidence is increasing each year. It is a chronic disease that affects various physiological systems, among which the intestinal tract has become the main target of study. In recent years, increasing evidence has shown that obesity is related to intestinal health. Studies have shown that the characteristics of the gut environment in obese individuals are related to the following aspects: intestinal immune responses promoting intestinal inflammation, reduction in intestinal microbial diversity and changes in intestinal microbial composition, damage to the integrity of the intestinal epithelial barrier, bacterial translocation, and increased LPS levels, decreased levels of intestinal hormones released by intestinal endocrine cells (GLP-1, GIP), and abnormalities in intestinal fat absorption and metabolism. These findings suggest that intestinal intervention is a promising target for the treatment of obesity and related metabolic diseases.

In the past decade, biological studies combining animal models and human studies have shown that gut microbes produce a large number of metabolites that regulate host responses and play an important role in human health. As one of the important metabolites of intestinal microorganisms, SCFA have a variety of beneficial effects on host energy metabolism regulation, especially in obesity and related metabolic diseases. As a bridge between obesity and intestinal homeostasis, SCFA are closely related to the pathogenesis of obesity and related metabolic diseases. SCFA are thought to be ligands that activate cellular signaling cascades. Specific cell signaling receptors, such as GPCRs, MCT and SMCT, and the epigenetic process, and, namely, the inhibition of HDACs, regulates the intestinal environment in obesity. Based on this knowledge, the first part of this review summarized the dependent pathways through which SCFA activate SCFA-associated receptors: (1) The establishment of the SCFA-GPR43/41-GLP-1 axis induces the release of endogenous GLP-1 and other intestinal hormones by intestinal epithelial cells (Colon L cells) to stimulate insulin secretion to improve glucose homeostasis, especially in the early stages of life. (2) By activating SCFA transporters (MCT and SMCT), which are responsible for the entry and transcellular transfer of SCFA into the intestinal epithelium, these receptors are closely associated with higher concentrations of SCFA in serum and feces *in vivo*, as well as intestinal permeability, markers of metabolic disorders, obesity and hypertension. Activation of SCFA transporter receptors can promote the transport of SCFA, increase the absorption and utilization of SCFA in the intestinal tract, regulate the concentration of SCFA in intestinal and extraintestinal tissues, reduce tissue inflammation caused by obesity, and regulate energy metabolism. (3) The SCFA non-receptor-dependent pathway inhibits the HDAC receptor-independent pathway. Interestingly, HDAC3, a specific HDAC, plays a significant role in integrating microbial signals to regulate intestinal homeostasis and regulate the expression of genes involved in lipid metabolism in a variety of tissues, especially through inhibiting transcription of the PPAR nuclear receptor family and inhibiting lipid oxidation. In addition, SCFA play a role in regulating gut microbes. The use of microbiome regulation has become an attractive strategy reported in several clinical studies. In this regard, the second part of this review summarized the use of microbial-oriented therapies to trigger the metabolism of intestinal microorganisms in the body, especially the enrichment of some SCFA-producing bacteria or the targeting of specific SCFA-producing bacteria, such as the representative *A. muciniphila* strain, to improve the intestinal environment to help obese adults lose weight. This is mainly done using the following two methods for enriching/targeting SCFA-producing bacteria to intervene in

the occurrence and development of obesity. The first is the most common strategy: dietary management. SCFA-producing bacteria can be enriched/targeted by the use of certain dietary treatments or certain drugs to promote the production and transformation of SCFA by intestinal microorganisms. The second is a microbe-based therapy—FMT therapy—continuous FMT treatment improved the metabolic disorder of obese people, and could produce the effect mainly due to its effects on the metabolism of the gut microbes, and especially through the increase in microbial SCFA gene expression levels. However, it is worth noting that the microbiome is a complex ecosystem, and whether SCFA play a role directly or by regulating gut microbes remains to be explored. However, the clinical therapeutic effects of dietary management, drug therapy and fecal bacteria transplantation are still controversial and complicated, and there are inconsistent data on response rates and adverse events. Therefore, the physiological and pathophysiological functions of SCFA should be fully investigated, and we think in the future, further study of SCFA in obesity and related metabolic diseases and the mechanisms through which they affect the intestinal environment is required, and how to better apply the regulation of SCFA produced by gut microbes to treat diseases await exploration.

AUTHOR CONTRIBUTIONS

HY participated in the production, creation, and drawing of the manuscript. JG and QC participated in the revision, conception, and drafting of the manuscript. YT, DY, SQ, YB, JH, HC, and QC participated in the review and revision of the manuscript. All authors contributed to the article and approved the submitted version.

FUNDING

This work was financially supported by the Science and Technology Program of Guangzhou, China (NO.202103000089), the Guangdong Demonstration Base for Joint Cultivation of Postgraduates (2019), the Science Foundation for Distinguished Young Scholars of Guangdong (2020B1515020026), and the National Natural Science Foundation of China (21804025).

REFERENCES

1. Luo YN, Huang WZ, Liu XX, Markevych I, Bloom MS, Zhao T, et al. Greenspace with overweight and obesity: a systematic review and meta-analysis of epidemiological studies up to 2020. *Obes Rev.* (2020) 21:e13078. doi: 10.1111/obr.13078
2. Fauchier G, Bisson A, Bodin A, Herbert J, Semaan C, Angoulvant D, et al. Metabolically healthy obesity and cardiovascular events: a nationwide cohort study. *Diabetes Obes Metab.* (2021) 23:2492–501. doi: 10.1111/dom.14492
3. Wang Y, Yang J, Wang W, Sanidad KZ, Cinelli MA, Wan D, et al. Soluble epoxide hydrolase is an endogenous regulator of obesity-induced intestinal barrier dysfunction and bacterial translocation. *Proc Natl Acad Sci USA.* (2020) 117:8431–6. doi: 10.1073/pnas.1916189117
4. Meijnikman AS, Aydin O, Prodan A, Tremaroli V, Herrema H, Levin E, et al. Distinct differences in gut microbial composition and functional potential from lean to morbidly obese subjects. *J Intern Med.* (2020) 288:699–710. doi: 10.1111/joim.13137
5. Winer DA, Luck H, Tsai S, Winer S. the intestinal immune system in obesity and insulin resistance. *Cell Metab.* (2016) 23:413–26. doi: 10.1016/j.cmet.2016.01.003
6. Lécuyer E, Le Roy T, Gestin A, Lacombe A, Philippe C, Ponnaiah M, et al. Tolerogenic dendritic cells shape a transmissible gut microbiota that protects from metabolic diseases. *Diabetes.* (2021) 70:2067–80. doi: 10.2337/db20-1177
7. Nakanishi T, Fukui H, Wang X, Nishiumi S, Yokota H, Makizaki Y, et al. Effect of a high-fat diet on the small-intestinal environment and mucosal integrity in the gut-liver axis. *Cells.* (2021) 10:3168. doi: 10.3390/cells10113168
8. Liu T, Kern J, Jain U, Sonnek N, Xiong S, Simpson K, et al. Western diet induces paneth cell defects through microbiome alterations and farnesoid x receptor and type I interferon activation. *Cell Host Microbe.* (2021) 29:988–1001.e6. doi: 10.1016/j.chom.2021.04.004
9. Luck H, Tsai S, Chung J, Clemente-Casares X, Ghazarian M, Revelo XS, et al. Regulation of obesity-related insulin resistance with gut anti-inflammatory agents. *Cell Metab.* (2015) 21:527–42. doi: 10.1016/j.cmet.2015.03.001
10. A high-fat diet controls MHC class II on ISCS via the microbiome. *Cancer Discov.* (2021) 11:2672. doi: 10.1158/2159-8290.Cd-rw2021-134
11. Shi Q, Wang Y, Hao Q, Vandvik P, Guyatt G, Li J, et al. Pharmacotherapy for adults with overweight and obesity: a systematic review and network meta-analysis of randomised controlled trials. *Lancet.* (2021) 399:P259–69. doi: 10.1016/S0140-6736(21)01640-8
12. Park B, Kim G, Lee H, Ryu J, Kim D, Seong J, et al. Anti-obesity therapeutics with complementary dual-agonist activities at glucagon and glucagon-like peptide 1 receptors. *Diabetes Obes Metab.* (2021) 24:50–60. doi: 10.1111/dom.14546
13. Davalos-Salas M, Montgomery MK, Reehorst CM, Nightingale R, Ng I, Anderton H, et al. Deletion of intestinal Hdac3 remodels the lipidome of enterocytes and protects mice from diet-induced obesity. *Nat Commun.* (2019) 10:5291. doi: 10.1038/s41467-019-13180-8
14. Jackson DN, Theiss AL. Gut bacteria signaling to mitochondria in intestinal inflammation and cancer. *Gut Microbes.* (2020) 11:285–304. doi: 10.1080/19490976.2019.1592421
15. Wargo J. Modulating Gut Microbes. *Science.* (2020) 369:1302–3. doi: 10.1126/science.abc3965
16. Tsukuda N, Yahagi K, Hara T, Watanabe Y, Matsumoto H, Mori H, et al. Key bacterial taxa and metabolic pathways affecting gut short-chain fatty acid profiles in early life. *ISME J.* (2021) 15:2574–90. doi: 10.1038/s41396-021-00937-7
17. Harris HC, Morrison DJ, Edwards CA. Impact of the source of fermentable carbohydrate on SCFA production by human gut microbiota *in vitro* - a systematic scoping review and secondary analysis. *Crit Rev Food Sci Nutr.* (2020) 61:3892–903. doi: 10.1080/10408398.2020.1809991
18. Sun M, Wu W, Liu Z, Cong Y. Microbiota metabolite short chain fatty acids, Gpcr, and inflammatory bowel diseases. *J Gastroenterol.* (2017) 52:1–8. doi: 10.1007/s00535-016-1242-9
19. Faits T, Walker M, Rodriguez-Morato J, Meng H, Gervis J, Galluccio J, et al. Exploring changes in the human gut microbiota and microbial-derived metabolites in response to diets enriched in simple, refined, or unrefined carbohydrate-containing foods: a *post hoc* analysis of a randomized clinical trial. *Am J Clin Nutr.* (2020) 112:1631–41. doi: 10.1093/ajcn/nqaa254
20. Gill PA, van Zelm MC, Muir JG, Gibson PR. Review article: short chain fatty acids as potential therapeutic agents in human gastrointestinal and inflammatory disorders. *Aliment Pharmacol Ther.* (2018) 48:15–34. doi: 10.1111/apt.14689
21. Peng M, Biswas D. Short chain and polyunsaturated fatty acids in host gut health and foodborne bacterial pathogen inhibition. *Crit Rev Food Sci Nutr.* (2017) 57:3987–4002. doi: 10.1080/10408398.2016.1203286

22. Sanna S, van Zuydam NR, Mahajan A, Kurilshikov A, Vich Vila A, Vosa U, et al. Causal relationships among the gut microbiome, short-chain fatty acids and metabolic diseases. *Nat Genet.* (2019) 51:600–5. doi: 10.1038/s41588-019-0350-x
23. Cani P, Jordan B. Gut microbiota-mediated inflammation in obesity: a link with gastrointestinal cancer. *Nat Rev Gastroenterol Hepatol.* (2018) 15:671–82. doi: 10.1038/s41575-018-0025-6
24. Ying W, Fu W, Lee Y, Olefsky J. The role of macrophages in obesity-associated islet inflammation and B-cell abnormalities. *Nat Rev Endocrinol.* (2020) 16:81–90. doi: 10.1038/s41574-019-0286-3
25. Konner AC, Bruning JC. Toll-like receptors: linking inflammation to metabolism. *Trends Endocrinol Metab.* (2011) 22:16–23. doi: 10.1016/j.tem.2010.08.007
26. Holmes Z, Silverman J, Dressman H, Wei Z, Dallow E, Armstrong S, et al. Short-chain fatty acid production by gut microbiota from children with obesity differs according to prebiotic choice and bacterial community composition. *mBio.* (2020) 11:e00914-20. doi: 10.1128/mBio.00914-20
27. Kang Y, Kang X, Yang H, Liu H, Yang X, Liu Q, et al. *Lactobacillus acidophilus* ameliorates obesity in mice through modulation of gut microbiota dysbiosis and intestinal permeability. *Pharmacol Res.* (2021) 175:106020. doi: 10.1016/j.phrs.2021.106020
28. Emara NA, Mahmoud MF, El Fayoumi HM, Mahmoud AAA. The renoprotective effect of glycyrrhizic acid in insulin-resistant rats exposed to aluminum involves the inhibition of Tlr4/Nf-kappa B signaling pathway. *Naunyn Schmiedebergs Arch Pharmacol.* (2021) 394:863–72. doi: 10.1007/s00210-020-02012-y
29. Rohm TV, Fuchs R, Muller RL, Keller L, Baumann Z, Bosch AJT, et al. Obesity in humans is characterized by gut inflammation as shown by pro-inflammatory intestinal macrophage accumulation. *Front Immunol.* (2021) 12:668654. doi: 10.3389/fimmu.2021.668654
30. Liu P-H, Burke KE, Ananthakrishnan AN, Lochhead P, Olen O, Ludvigsson JF, et al. Obesity and weight gain since early adulthood are associated with a lower risk of microscopic colitis. *Clin Gastroenterol Hepatol.* (2019) 17:2523–32.e1. doi: 10.1016/j.cgh.2018.11.057
31. Pérez-Reytor D, Puebla C, Karahanian E, García K. Use of short-chain fatty acids for the recovery of the intestinal epithelial barrier affected by bacterial toxins. *Front Physiol.* (2021) 12:650313. doi: 10.3389/fphys.2021.650313
32. Zhao Y, Chen F, Wu W, Sun M, Bilotta AJ, Yao S, et al. Gpr43 mediates microbiota metabolite Scfa regulation of antimicrobial peptide expression in intestinal epithelial cells via activation of Mtor and Stat3. *Mucosal Immunol.* (2018) 11:752–62. doi: 10.1038/mi.2017.118
33. Wu W, Sun M, Chen F, Cao AT, Liu H, Zhao Y, et al. Microbiota metabolite short-chain fatty acid acetate promotes intestinal Iga response to microbiota which is mediated by Gpr43. *Mucosal Immunol.* (2017) 10:946–56. doi: 10.1038/mi.2016.114
34. Kibbie JJ, Dillon SM, Thompson TA, Purba CM, McCarter MD, Wilson CC. Butyrate directly decreases human gut lamina propria Cd4 T cell function through Histone Deacetylase (Hdac) inhibition and Gpr43 signaling. *Immunobiology.* (2021) 226:152126. doi: 10.1016/j.imbio.2021.152126
35. Macia L, Tan J, Vieira AT, Leach K, Stanley D, Luong S, et al. Metabolite-sensing receptors Gpr43 and Gpr109a facilitate dietary fibre-induced gut homeostasis through regulation of the inflammasome. *Nat Commun.* (2015) 6:6734. doi: 10.1038/ncomms7734
36. Bellahcene M, O'Dowd JF, Wargent ET, Zaibi MS, Hislop DC, Ngala RA, et al. Male mice that lack the G-protein-coupled receptor Gpr41 have low energy expenditure and increased body fat content. *Br J Nutr.* (2013) 109:1755–64. doi: 10.1017/S0007114512003923
37. Petersen N, Frimurer TM, Terndrup Pedersen M, Egerod KL, Wewer Albrechtsen NJ, Holst JJ, et al. Inhibiting Rhoa signaling in mice increases glucose tolerance and numbers of enteroendocrine and other secretory cells in the intestine. *Gastroenterology.* (2018) 155:1164–76 e2. doi: 10.1053/j.gastro.2018.06.039
38. Samuel B, Shaito A, Motoike T, Rey F, Backhed F, Manchester J, et al. Effects of the gut microbiota on host adiposity are modulated by the short-chain fatty-acid binding G protein-coupled receptor, Gpr41. *Proc Natl Acad Sci USA.* (2008) 105:16767–72. doi: 10.1073/pnas.0808567105
39. Schwartz TW, Offermanns S, Jones RM, Han S, Seier Poulsen S, Grunddal KV, et al. Gpr41/Ffar3 and Gpr43/Ffar2 as cosensors for short-chain fatty acids in enteroendocrine cells Vs Ffar3 in enteric neurons and Ffar2 in enteric leukocytes. *Endocrinology.* (2013) 154:3552–64. doi: 10.1210/en.2013-1142
40. Arora T, Rudenko O, Egerod K, Husted A, Kovatcheva-Datchary P, Akrami R, et al. Microbial fermentation of flaxseed fibers modulates the transcriptome of Gpr41-expressing enteroendocrine cells and protects mice against diet-induced obesity. *Am J Physiol Endocrinol Metab.* (2019) 316:E453–63. doi: 10.1152/ajpendo.00391.2018
41. Takakuwa A, Nakamura K, Kikuchi M, Sugimoto R, Ohira S, Yokoi Y, et al. Butyric acid and leucine induce alpha-defensin secretion from small intestinal paneth cells. *Nutrients.* (2019) 11:2817. doi: 10.3390/nu11112817
42. Feng W, Wu Y, Chen G, Fu S, Li B, Huang B, et al. Sodium butyrate attenuates diarrhea in weaned piglets and promotes tight junction protein expression in colon in a Gpr109a-dependent manner. *Cell Physiol Biochem.* (2018) 47:1617–29. doi: 10.1159/000490981
43. Singh N, Gurav A, Sivaprakasam S, Brady E, Padia R, Shi H, et al. Activation of Gpr109a, receptor for niacin and the commensal metabolite butyrate, suppresses colonic inflammation and carcinogenesis. *Immunity.* (2014) 40:128–39. doi: 10.1016/j.immuni.2013.12.007
44. Hung TV, Suzuki T. Short-chain fatty acids suppress inflammatory reactions in caco-2 cells and mouse colons. *J Agric Food Chem.* (2018) 66:108–17. doi: 10.1021/acs.jafc.7b04233
45. Chen D, Jin D, Huang S, Wu J, Xu M, Liu T, et al. *Clostridium butyricum*, a butyrate-producing probiotic, inhibits intestinal tumor development through modulating Wnt signaling and gut microbiota. *Cancer Lett.* (2020) 469:456–67. doi: 10.1016/j.canlet.2019.11.019
46. Ferrer-Picon E, Dotti I, Corraliza AM, Mayorgas A, Esteller M, Perales JC, et al. Intestinal inflammation modulates the epithelial response to butyrate in patients with inflammatory bowel disease. *Inflamm Bowel Dis.* (2020) 26:43–55. doi: 10.1093/ibd/izz119
47. Thibault R, De Coppet P, Daly K, Bourreille A, Cuff M, Bonnet C, et al. Down-regulation of the monocarboxylate transporter 1 is involved in butyrate deficiency during intestinal inflammation. *Gastroenterology.* (2007) 133:1916–27. doi: 10.1053/j.gastro.2007.08.041
48. Ota S, Sakuraba H, Hiraga H, Yoshida S, Satake M, Akemoto Y, et al. Cyclosporine protects from intestinal epithelial injury by modulating butyrate uptake via upregulation of membrane monocarboxylate transporter 1 levels. *Biochem Biophys Rep.* (2020) 24:100811. doi: 10.1016/j.bbrep.2020.100811
49. De Preter V, Arijs I, Windey K, Vanhove W, Vermeire S, Schuit F, et al. Impaired butyrate oxidation in ulcerative colitis is due to decreased butyrate uptake and a defect in the oxidation pathway*. *Inflamm Bowel Dis.* (2012) 18:1127–36. doi: 10.1002/ibd.21894
50. Borthakur A, Anbazhagan A, Kumar A, Raheja G, Singh V, Ramaswamy K, et al. The probiotic *Lactobacillus plantarum* counteracts tnf-{alpha}-induced downregulation of Smct1 expression and function. *Am J Physiol Gastrointest Liver Physiol.* (2010) 299:G928–34. doi: 10.1152/ajpgi.00279.2010
51. Goncalves P, Gregorio I, Catarino TA, Martel F. The effect of oxidative stress upon the intestinal epithelial uptake of butyrate. *Eur J Pharmacol.* (2013) 699:88–100. doi: 10.1016/j.ejphar.2012.11.029
52. Kurata N, Tokashiki N, Fukushima K, Misao T, Hasuoka N, Kitagawa K, et al. Short chain fatty acid butyrate uptake reduces expressions of prostanoid Ep4 receptors and their mediation of cyclooxygenase-2 induction in Hca-7 human colon cancer cells. *Eur J Pharmacol.* (2019) 853:308–15. doi: 10.1016/j.ejphar.2019.04.014
53. Kelly CJ, Zheng L, Campbell EL, Saeedi B, Scholz CC, Bayless AJ, et al. Crosstalk between microbiota-derived short-chain fatty acids and intestinal epithelial hif augments tissue barrier function. *Cell Host Microbe.* (2015) 17:662–71. doi: 10.1016/j.chom.2015.03.005
54. Fan S, Zhang Z, Zhong Y, Li C, Huang X, Geng F, et al. Microbiota-related effects of prebiotic fibres in lipopolysaccharide-induced endotoxemic mice: short chain fatty acid production and gut commensal translocation. *Food Funct.* (2021) 12:7343–57. doi: 10.1039/D1FO00410G
55. Devriese S, Eeckhaut V, Geirnaert A, Van den Bossche L, Hindryckx P, Van de Wiele T, et al. Reduced mucosa-associated butyricicoccus activity in patients with ulcerative colitis correlates with aberrant claudin-1 expression. *J Crohns Colitis.* (2017) 11:229–36. doi: 10.1093/ecco-jcc/jjw142
56. Zheng L, Kelly CJ, Battista KD, Schaefer R, Lanis JM, Alexeev EE, et al. Microbial-derived butyrate promotes epithelial barrier function

through il-10 receptor-dependent repression of claudin-2. *J Immunol.* (2017) 199:2976–84. doi: 10.4049/jimmunol.1700105
57. Tian P, Zhu H, Qian X, Chen Y, Wang Z, Zhao J, et al. Consumption of butylated starch alleviates the chronic restraint stress-induced neurobehavioral and gut barrier deficits through reshaping the gut microbiota. *Front Immunol.* (2021) 12:755481. doi: 10.3389/fimmu.2021.755481
58. Fang W, Xue H, Chen X, Chen K, Ling W. Supplementation with sodium butyrate modulates the composition of the gut microbiota and ameliorates high-fat diet-induced obesity in mice. *J Nutr.* (2019) 149:747–54. doi: 10.1093/jn/nxy324
59. Xia Z, Han Y, Wang K, Guo S, Wu D, Huang X, et al. Oral administration of propionic acid during lactation enhances the colonic barrier function. *Lipids Health Dis.* (2017) 16:62. doi: 10.1186/s12944-017-0452-3
60. Pearce S, Weber G, van Sambeek D, Soares J, Racicot K, Breault D. Intestinal enteroids recapitulate the effects of short-chain fatty acids on the intestinal epithelium. *PloS ONE.* (2020) 15:e0230231. doi: 10.1371/journal.pone.0230231
61. Huang X, Oshima T, Tomita T, Fukui H, Miwa H. Butyrate alleviates cytokine-induced barrier dysfunction by modifying claudin-2 levels. *Biology.* (2021) 10:205. doi: 10.3390/biology10030205
62. Docampo M, Burgos da Silva M, Lazrak A, Nichols K, Lieberman S, Slingerland A, et al. Alloreactive T cells deficient of the short-chain fatty acid receptor Gpr109a induce less graft-versus-host disease. *Blood.* (2021) 139:2392–405. doi: 10.1182/blood.2021010719
63. Baumard L, Weerts Z, Masclee A, Keszthelyi D, Michael-Titus A, Peiris M. Effect of obesity on the expression of nutrient receptors and satiety hormones in the human colon. *Nutrients.* (2021) 13:1271. doi: 10.3390/nu13041271
64. Smith PM, Howitt MR, Panikov N, Michaud M, Gallini CA, Bohlooly YM, et al. The microbial metabolites, short-chain fatty acids, regulate colonic treg cell homeostasis. *Science.* (2013) 341:569–73. doi: 10.1126/science.1241165
65. McKenzie C, Tan J, Macia L, Mackay C. The nutrition-gut microbiome-physiology axis and allergic diseases. *Immunol Rev.* (2017) 278:277–95. doi: 10.1111/imr.12556
66. Le Poul E, Loison C, Struyf S, Springael J, Lannoy V, Decobecq M, et al. Functional characterization of human receptors for short chain fatty acids and their role in polymorphonuclear cell activation. *J Biol Chem.* (2003) 278:25481–9. doi: 10.1074/jbc.M301403200
67. Gaidarov I, Chen X, Anthony T, Maciejewski-Lenoir D, Liaw C, Unett D. Differential tissue and ligand-dependent signaling of Gpr109a receptor: implications for anti-atherosclerotic therapeutic potential. *Cell Signal.* (2013) 25:2003–16. doi: 10.1016/j.cellsig.2013.06.008
68. Park B, Kim S, Kim J, Kim S, Park B, Han S, et al. The short-chain fatty acid receptor Gpr43 modulates Yap/Taz via rhoa. *Mol Cells.* (2021) 44:458–67. doi: 10.14348/molcells.2021.0021
69. Bottke T, Ernicke S, Serfling R, Ihling C, Burda E, Gurevich VV, et al. Exploring Gpcr-arrestin interfaces with genetically encoded crosslinkers. *EMBO Rep.* (2020) 21:e50437. doi: 10.15252/embr.202050437
70. O'Hayre M, Eichel K, Avino S, Zhao X, Steffen DJ, Feng X, et al. Genetic evidence that beta-arrestins are dispensable for the initiation of Beta2-adrenergic receptor signaling to Erk. *Sci Signal.* (2017) 10:eaal3395. doi: 10.1126/scisignal.aal3395
71. Schlatterer K, Peschel A, Kretschmer D. Short-chain fatty acid and Ffar2 activation - a new option for treating infections? *Front Cell Infect Microbiol.* (2021) 11:785833. doi: 10.3389/fcimb.2021.785833
72. Dai X, Guo Z, Chen D, Li L, Song X, Liu T, et al. Maternal sucralose intake alters gut microbiota of offspring and exacerbates hepatic steatosis in adulthood. *Gut Microbes.* (2020) 11:1043–63. doi: 10.1080/19490976.2020.1738187
73. Gohir W, Kennedy KM, Wallace JG, Saoi M, Bellissimo CJ, Britz-McKibbin P, et al. High-fat diet intake modulates maternal intestinal adaptations to pregnancy and results in placental hypoxia, as well as altered fetal gut barrier proteins and immune markers. *J Physiol.* (2019) 597:3029–51. doi: 10.1113/JP277353
74. Stinson LF, Gay MCL, Koleva PT, Eggesbo M, Johnson CC, Wegienka G, et al. Human milk from atopic mothers has lower levels of short chain fatty acids. *Front Immunol.* (2020) 11:1427. doi: 10.3389/fimmu.2020.01427
75. Kimura I, Miyamoto J, Ohue-Kitano R, Watanabe K, Yamada T, Onuki M, et al. Maternal gut microbiota in pregnancy influences offspring metabolic phenotype in mice. *Science.* (2020) 367:eaaw8429. doi: 10.1126/science.aaw8429
76. Zhou J, Gao S, Chen J, Zhao R, Yang X. Maternal sodium butyrate supplement elevates the lipolysis in adipose tissue and leads to lipid accumulation in offspring liver of weaning-age rats. *Lipids Health Dis.* (2016) 15:119. doi: 10.1186/s12944-016-0289-1
77. Jiao W, Zhang Z, Xu Y, Gong L, Zhang W, Tang H, et al. Butyric acid normalizes hyperglycemia caused by the tacrolimus-induced gut microbiota. *Am J Transpl.* (2020) 20:2413–24. doi: 10.1111/ajt.15880
78. Stumpff F. A look at the smelly side of physiology: transport of short chain fatty acids. *Pflugers Arch.* (2018) 470:571–98. doi: 10.1007/s00424-017-2105-9
79. Kaji I, Iwanaga T, Watanabe M, Guth PH, Engel E, Kaunitz JD, et al. Scfa transport in rat duodenum. *Am J Physiol Gastrointest Liver Physiol.* (2015) 308:G188–97. doi: 10.1152/ajpgi.00298.2014
80. Binder HJ. Role of colonic short-chain fatty acid transport in diarrhea. *Annu Rev Physiol.* (2010) 72:297–313. doi: 10.1146/annurev-physiol-021909-135817
81. Holota Y, Dovbynchuk T, Kaji I, Vareniuk I, Dzyubenko N, Chervinska T, et al. The long-term consequences of antibiotic therapy: role of colonic Short-Chain Fatty Acids (Scfa) system and intestinal barrier integrity. *PLoS ONE.* (2019) 14:e0220642. doi: 10.1371/journal.pone.0220642
82. Sivaprakasam S, Bhutia YD, Yang S, Ganapathy V. Short-chain fatty acid transporters: role in colonic homeostasis. *Compr Physiol.* (2017) 8:299–314. doi: 10.1002/cphy.c170014
83. Moschen I, Bröer A, Galić S, Lang F, Bröer S. Significance of short chain fatty acid transport by members of the Monocarboxylate Transporter Family (Mct). *Neurochem Res.* (2012) 37:2562–8. doi: 10.1007/s11064-012-0857-3
84. Binder H, Rajendran V, Sadasivan V, Geibel J. Bicarbonate secretion: a neglected aspect of colonic ion transport. *J Clin Gastroenterol.* (2005) 39:S53–8. doi: 10.1097/01.mcg.0000155521.81382.3a
85. Borthakur A, Saksena S, Gill R, Alrefai W, Ramaswamy K, Dudeja P. Regulation of Monocarboxylate Transporter 1 (Mct1) promoter by butyrate in human intestinal epithelial cells: involvement of Nf-Kappab pathway. *J Cell Biochem.* (2008) 103:1452–63. doi: 10.1002/jcb.21532
86. Zhao X, Guo Y, Liu H, Gao J, Nie W. *Clostridium butyricum* reduce lipogenesis through bacterial wall components and butyrate. *Appl Microbiol Biotechnol.* (2014) 98:7549–57. doi: 10.1007/s00253-014-5829-x
87. Wang D, Liu CD, Li HF, Tian ML, Pan JQ, Shu G, et al. Lsd1 mediates microbial metabolite butyrate-induced thermogenesis in brown and white adipose tissue. *Metabolism.* (2020) 102:154011. doi: 10.1016/j.metabol.2019.154011
88. Irving B, Wood G, Bennotti P, Babu E, Deshpande A, Lent M, et al. Nutrient transporter expression in the jejunum in relation to body mass index in patients undergoing bariatric surgery. *Nutrients.* (2016) 8:683. doi: 10.3390/nu8110683
89. Friedrich M, Gerbeth L, Gerling M, Rosenthal R, Steiger K, Weidinger C, et al. Hdac inhibitors promote intestinal epithelial regeneration via autocrine Tgfβ1 signalling in inflammation. *Mucosal Immunol.* (2019) 12:656–67. doi: 10.1038/s41385-019-0135-7
90. Elfiky A, Ghiboub M, Li Yim A, Hageman I, Verhoeff J, de Krijger M, et al. Carboxylesterase-1 assisted targeting of HDAC inhibitors to mononuclear myeloid cells in inflammatory bowel disease. *J Crohns Colitis.* (2021) 15:jjab176. doi: 10.1093/ecco-jcc/jjab176
91. Vizioli M, Liu T, Miller K, Robertson N, Gilroy K, Lagnado A, et al. Mitochondria-to-nucleus retrograde signaling drives formation of cytoplasmic chromatin and inflammation in senescence. *Genes Dev.* (2020) 34:428–45. doi: 10.1101/gad.331272.119
92. Li M, van Esch B, Henricks PAJ, Folkerts G, Garssen J. The anti-inflammatory effects of short chain fatty acids on lipopolysaccharide- or tumor necrosis factor alpha-stimulated endothelial cells via activation of Gpr41/43 and inhibition of Hdacs. *Front Pharmacol.* (2018) 9:533. doi: 10.3389/fphar.2018.00533

93. Bose P, Dai Y, Grant S. Histone deacetylase inhibitor (Hdaci) mechanisms of action: emerging insights. *Pharmacol Ther.* (2014) 143:323–36. doi: 10.1016/j.pharmthera.2014.04.004
94. Zhang J, Peng J, Huang Y, Meng L, Li Q, Xiong F, et al. Identification of Histone Deacetylase (Hdac)-associated proteins with DNA-programmed affinity labeling. *Angew Chem.* (2020) 59:17525–32. doi: 10.1002/anie.202001205
95. Zhou Y, Xu H, Xu J, Guo X, Zhao H, Chen Y, et al. Prausnitzii F, and its supernatant increase Scfas-producing bacteria to restore gut dysbiosis in Tnbs-induced colitis. *AMB Express.* (2021) 11:33. doi: 10.1186/s13568-021-01197-6
96. Yang W, Yu T, Huang X, Bilotta AJ, Xu L, Lu Y, et al. Intestinal microbiota-derived short-chain fatty acids regulation of immune cell Il-22 production and gut immunity. *Nat Commun.* (2020) 11:4457. doi: 10.1038/s41467-020-18262-6
97. Wang RX, Lee JS, Campbell EL, Colgan SP. Microbiota-derived butyrate dynamically regulates intestinal homeostasis through regulation of actin-associated protein synaptopodin. *Proc Natl Acad Sci USA.* (2020) 117:11648–57. doi: 10.1073/pnas.1917597117
98. Dupraz L, Magniez A, Rolhion N, Richard ML, Da Costa G, Touch S, et al. Gut microbiota-derived short-chain fatty acids regulate Il-17 production by mouse and human intestinal gammadelta T cells. *Cell Rep.* (2021) 36:109332. doi: 10.1016/j.celrep.2021.109332
99. Whitt J, Woo V, Lee P, Moncivaiz J, Haberman Y, Denson L, et al. Disruption of epithelial Hdac3 in intestine prevents diet-induced obesity in mice. *Gastroenterology.* (2018) 155:501–13. doi: 10.1053/j.gastro.2018.04.017
100. Waldecker M, Kautenburger T, Daumann H, Busch C, Schrenk D. Inhibition of histone-deacetylase activity by short-chain fatty acids and some polyphenol metabolites formed in the colon. *J Nutr Biochem.* (2008) 19:587–93. doi: 10.1016/j.jnutbio.2007.08.002
101. Li H, Gao Z, Zhang J, Ye X, Xu A, Ye J, et al. Sodium butyrate stimulates expression of fibroblast growth factor 21 in liver by inhibition of histone deacetylase 3. *Diabetes.* (2012) 61:797–806. doi: 10.2337/db11-0846
102. Lieber AD, Beier UH, Xiao H, Wilkins BJ, Jiao J, Li XS, et al. Loss of Hdac6 alters gut microbiota and worsens obesity. *FASEB J.* (2019) 33:1098–109. doi: 10.1096/fj.201701586R
103. de la Cuesta-Zuluaga J, Mueller N, Álvarez-Quintero R, Velásquez-Mejía E, Sierra J, Corrales-Agudelo V, et al. Higher fecal short-chain fatty acid levels are associated with gut microbiome dysbiosis, obesity, hypertension and cardiometabolic disease risk factors. *Nutrients.* (2018) 11:51. doi: 10.3390/nu11010051
104. Ozato N, Saito S, Yamaguchi T, Katashima M, Tokuda I, Sawada K, et al. Blautia genus associated with visceral fat accumulation in adults 20-76 years of age. *NPJ Biofilms Microbiomes.* (2019) 5:28. doi: 10.1038/s41522-019-0101-x
105. Wang P, Gao J, Ke W, Wang J, Li D, Liu R, et al. Resveratrol reduces obesity in high-fat diet-fed mice via modulating the composition and metabolic function of the gut microbiota. *Free Radic Biol Med.* (2020) 156:83–98. doi: 10.1016/j.freeradbiomed.2020.04.013
106. Vemuri R, Gundamaraju R, Shinde T, Perera A, Basheer W, Southam B, et al. Lactobacillus acidophilus Dds-1 modulates intestinal-specific microbiota, short-chain fatty acid and immunological profiles in aging mice. *Nutrients.* (2019) 11:1297. doi: 10.3390/nu11061297
107. Koh A, De Vadder F, Kovatcheva-Datchary P, Bäckhed F. From dietary fiber to host physiology: short-chain fatty acids as key bacterial metabolites. *Cell.* (2016) 165:1332–45. doi: 10.1016/j.cell.2016.05.041
108. Murphy E, Cotter P, Healy S, Marques T, O'Sullivan O, Fouhy F, et al. Composition and energy harvesting capacity of the gut microbiota: relationship to diet, obesity and time in mouse models. *Gut.* (2010) 59:1635–42. doi: 10.1136/gut.2010.215665
109. Indiani C, Rizzardi KF, Castelo PM, Ferraz LFC, Darrieux M, Parisotto TM. Childhood obesity and firmicutes/bacteroidetes ratio in the gut microbiota: a systematic review. *Child Obes.* (2018) 14:501–9. doi: 10.1089/chi.2018.0040
110. Furet J, Kong L, Tap J, Poitou C, Basdevant A, Bouillot J, et al. Differential adaptation of human gut microbiota to bariatric surgery-induced weight loss: links with metabolic and low-grade inflammation markers. *Diabetes.* (2010) 59:3049–57. doi: 10.2337/db10-0253
111. Zhao S, Jang C, Liu J, Uehara K, Gilbert M, Izzo L, et al. Dietary fructose feeds hepatic lipogenesis via microbiota-derived acetate. *Nature.* (2020) 579:586–91. doi: 10.1038/s41586-020-2101-7
112. Li R, Huang X, Liang X, Su M, Lai KP, Chen J. Integrated omics analysis reveals the alteration of gut microbe-metabolites in obese adults. *Brief Bioinform.* (2021) 22:bbaa165. doi: 10.1093/bib/bbaa165
113. Murphy E, Cotter P, Hogan A, O'Sullivan O, Joyce A, Fouhy F, et al. Divergent metabolic outcomes arising from targeted manipulation of the gut microbiota in diet-induced obesity. *Gut.* (2013) 62:220–6. doi: 10.1136/gutjnl-2011-300705
114. Beyaz S, Chung C, Mou H, Bauer-Rowe K, Xifaras M, Ergin I, et al. Dietary suppression of Mhc class Ii expression in intestinal epithelial cells enhances intestinal tumorigenesis. *Cell Stem Cell.* (2021) 28:1922–35.e5. doi: 10.1016/j.stem.2021.08.007
115. Zhao L, Zhang F, Ding X, Wu G, Lam YY, Wang X, et al. Gut bacteria selectively promoted by dietary fibers alleviate type 2 diabetes. *Science.* (2018) 359:1151–56. doi: 10.1126/science.aao5774
116. Zhou D, Pan Q, Xin FZ, Zhang RN, He CX, Chen GY, et al. Sodium butyrate attenuates high-fat diet-induced steatohepatitis in mice by improving gut microbiota and gastrointestinal barrier. *World J Gastroenterol.* (2017) 23:60–75. doi: 10.3748/wjg.v23.i1.60
117. Beisner J, Filipe Rosa L, Kaden-Volynets V, Stolzer I, Gunther C, Bischoff SC. Prebiotic inulin and sodium butyrate attenuate obesity-induced intestinal barrier dysfunction by induction of antimicrobial peptides. *Front Immunol.* (2021) 12:678360. doi: 10.3389/fimmu.2021.678360
118. Tian B, Zhao J, Zhang M, Chen Z, Ma Q, Liu H, et al. *Lycium ruthenicum* anthocyanins attenuate high-fat diet-induced colonic barrier dysfunction and inflammation in mice by modulating the gut microbiota. *Mol Nutr Food Res.* (2021) 65:e2000745. doi: 10.1002/mnfr.202000745
119. Bui T, Mannerås-Holm L, Puschmann R, Wu H, Troise A, Nijsse B, et al. Conversion of dietary inositol into propionate and acetate by commensal anaerostipes associates with host health. *Nat Commun.* (2021) 12:4798. doi: 10.1038/s41467-021-25081-w
120. Le Roy T, Moens de Hase E, Van Hul M, Paquot A, Pelicaen R, Regnier M, et al. *Dysosmobacter welbionis* is a newly isolated human commensal bacterium preventing diet-induced obesity and metabolic disorders in mice. *Gut.* (2021) 71:534–43. doi: 10.1136/gutjnl-2020-323778
121. Zeevi D, Korem T, Godneva A, Bar N, Kurilshikov A, Lotan-Pompan M, et al. Structural variation in the gut microbiome associates with host health. *Nature.* (2019) 568:43–8. doi: 10.1038/s41586-019-1065-y
122. Depommier C, Everard A, Druart C, Plovier H, Van Hul M, Vieira-Silva S, et al. Supplementation with *Akkermansia muciniphila* in overweight and obese human volunteers: a proof-of-concept exploratory study. *Nat Med.* (2019) 25:1096–103. doi: 10.1038/s41591-019-0495-2
123. Kim S, Shin Y-C, Kim T-Y, Kim Y, Lee Y-S, Lee S-H, et al. Mucin degrader *Akkermansia muciniphila* accelerates intestinal stem cell-mediated epithelial development. *Gut Microbes.* (2021) 13:1–20. doi: 10.1080/19490976.2021.1892441
124. Lee J, Song W, Lim J, Choi T, Jo S, Jeon H, et al. An integrative multiomics approach to characterize anti-adipogenic and anti-lipogenic effects of *Akkermansia muciniphila* in adipocytes. *Biotechnol J.* (2021) 17:e2100397. doi: 10.1002/biot.202100397
125. Shen J, Tong X, Sud N, Khound R, Song Y, Maldonado-Gomez MX, et al. Low-density lipoprotein receptor signaling mediates the triglyceride-lowering action of *Akkermansia muciniphila* in genetic-induced hyperlipidemia. *Arterioscler Thromb Vasc Biol.* (2016) 36:1448–56. doi: 10.1161/ATVBAHA.116.307597
126. Kostopoulos I, Elzinga J, Ottman N, Klievink JT, Blijenberg B, Aalvink S, et al. *Akkermansia muciniphila* uses human milk oligosaccharides to thrive in the early life conditions *in vitro*. *Sci Rep.* (2020) 10:14330. doi: 10.1038/s41598-020-71113-8
127. Lukovac S, Belzer C, Pellis L, Keijser BJ, de Vos WM, Montijn RC, et al. Differential modulation by *Akkermansia muciniphila* and *Faecalibacterium prausnitzii* of host peripheral lipid metabolism and histone acetylation in mouse gut organoids. *mBio.* (2014) 5:e01438-14. doi: 10.1128/mBio.01438-14

128. Vallianou NG, Stratigou T, Tsagarakis S. Metformin and gut microbiota: their interactions and their impact on diabetes. *Hormones.* (2019) 18:141–4. doi: 10.1007/s42000-019-00093-w
129. Olesen SW, Leier MM, Alm EJ, Kahn SA. Searching for superstool: maximizing the therapeutic potential of Fmt. *Nat Rev Gastroenterol Hepatol.* (2018) 15:387–8. doi: 10.1038/s41575-018-0019-4
130. Dickson I. Therapy: oral capsule Fmt effective for *C. difficile* infection. *Nat Rev Gastroenterol Hepatol.* (2018) 15:68. doi: 10.1038/nrgastro.2017.188
131. Ridaura VK, Faith JJ, Rey FE, Cheng J, Duncan AE, Kau AL, et al. Gut microbiota from twins discordant for obesity modulate metabolism in mice. *Science.* (2013) 341:1241214. doi: 10.1126/science.1241214
132. Rizzetto L, Fava F, Tuohy KM, Selmi C. Connecting the immune system, systemic chronic inflammation and the gut microbiome: the role of sex. *J Autoimmun.* (2018) 92:12–34. doi: 10.1016/j.jaut.2018.05.008
133. Bajaj JS, Kakiyama G, Savidge T, Takei H, Kassam ZA, Fagan A, et al. Antibiotic-associated disruption of microbiota composition and function in cirrhosis is restored by fecal transplant. *Hepatology.* (2018) 68:1549–58. doi: 10.1002/hep.30037
134. Paramsothy S, Nielsen S, Kamm MA, Deshpande NP, Faith JJ, Clemente JC, et al. Specific bacteria and metabolites associated with response to fecal microbiota transplantation in patients with ulcerative colitis. *Gastroenterology.* (2019) 156:1440–54 e2. doi: 10.1053/j.gastro.2018.12.001
135. de Groot P, Scheithauer T, Bakker G, Prodan A, Levin E, Khan M, et al. Donor metabolic characteristics drive effects of faecal microbiota transplantation on recipient insulin sensitivity, energy expenditure and intestinal transit time. *Gut.* (2020) 69:502–12. doi: 10.1136/gutjnl-2019-318320
136. Bajaj J, Salzman N, Acharya C, Sterling R, White M, Gavis E, et al. Fecal microbial transplant capsules are safe in hepatic encephalopathy: a phase 1, randomized, placebo-controlled trial. *Hepatology.* (2019) 70:1690–703. doi: 10.1002/hep.30690
137. Gundling F, Roggenbrod S, Schleifer S, Sohn M, Schepp W. Patient perception and approval of Faecal Microbiota Transplantation (Fmt) as an alternative treatment option for obesity. *Obes Sci Pract.* (2019) 5:68–74. doi: 10.1002/osp4.302
138. Zhu L, Fu J, Xiao X, Wang F, Jin M, Fang W, et al. Faecal microbiota transplantation-mediated jejunal microbiota changes halt high-fat diet-induced obesity in mice via retarding intestinal fat absorption. *Microbial Biotechnol.* (2021) 10:1663–76. doi: 10.1111/1751-7915.13951
139. Wilson B, Vatanen T, Jayasinghe T, Leong K, Derraik J, Albert B, et al. Strain engraftment competition and functional augmentation in a multi-donor fecal microbiota transplantation trial for obesity. *Microbiome.* (2021) 9:107. doi: 10.1186/s40168-021-01060-7
140. Fuhri Snethlage C, Nieuwdorp M, Hanssen N. Faecal microbiota transplantation in endocrine diseases and obesity. *Best Pract Res Clin Endocrinol Metab.* (2021) 35:101483. doi: 10.1016/j.beem.2020.101483
141. Mocanu V, Zhang Z, Deehan EC, Kao DH, Hotte N, Karmali S, et al. Fecal microbial transplantation and fiber supplementation in patients with severe obesity and metabolic syndrome: a randomized double-blind, placebo-controlled phase 2 trial. *Nat Med.* (2021) 27:1272–9. doi: 10.1038/s41591-021-01399-2
142. Allegretti JR, Kassam Z, Mullish BH, Chiang A, Carrellas M, Hurtado J, et al. Effects of fecal microbiota transplantation with oral capsules in obese patients. *Clin Gastroenterol Hepatol.* (2020) 18:855–63 e2. doi: 10.1016/j.cgh.2019.07.006
143. Yu EW, Gao L, Stastka P, Cheney MC, Mahabamunuge J, Torres Soto M, et al. Fecal microbiota transplantation for the improvement of metabolism in obesity: the Fmt-trim double-blind placebo-controlled pilot trial. *PLoS Med.* (2020) 17:e1003051. doi: 10.1371/journal.pmed.1003051
144. Jensen BAH, Holm JB, Larsen IS, von Burg N, Derer S, Sonne SB, et al. Lysates of *Methylococcus capsulatus* bath induce a lean-like microbiota, intestinal Foxp3+Rorγt+Il-17+ tregs and improve metabolism. *Nat Commun.* (2021) 12:1093. doi: 10.1038/s41467-021-21408-9

Conflict of Interest: QC was employed by Guangzhou Rainhome Pharm & Tech Co., Ltd.

The remaining authors declare that the research was conducted in the absence of any commercial or financial relationships that could be construed as a potential conflict of interest.

frontiers | Frontiers in Nutrition

ORIGINAL RESEARCH
published: 15 June 2022
doi: 10.3389/fnut.2022.823756

Metabolic and Microbiome Alterations Following the Enrichment of a High-Fat Diet With High Oleic Acid Peanuts Versus the Traditional Peanuts Cultivar in Mice

Sarit Anavi-Cohen[1], Gil Zandani[2], Nina Tsybina-Shimshilashvili[2], Ran Hovav[3], Noa Sela[4], Abraham Nyska[5] and Zecharia Madar[2]**

[1] Peres Academic Center, Rehovot, Israel, [2] Faculty of Agriculture, Food and Environment, The Hebrew University of Jerusalem, Rehovot, Israel, [3] Department of Field Crops and Vegetables Research, Plant Sciences Institute, Agricultural Research Organization, Beit Dagan, Israel, [4] Department of Plant Pathology and Weed Research, The Volcani Center, Rishon LeZion, Israel, [5] Sackler School of Medicine, Tel Aviv University, Tel Aviv, Israel

OPEN ACCESS

Edited by:
Gratiela Gradisteanu Pircalabioru, University of Bucharest, Romania

Reviewed by:
Karuna Rasineni, University of Nebraska Medical Center, United States
Julio Plaza-Diaz, Children's Hospital of Eastern Ontario (CHEO), Canada

***Correspondence:**
Sarit Anavi-Cohen
saritanavi@pac.ac.il
Zecharia Madar
zecharia.madar@mail.huji.ac.il

Specialty section:
This article was submitted to Nutrition and Metabolism, a section of the journal Frontiers in Nutrition

Received: *28 November 2021*
Accepted: *09 May 2022*
Published: *15 June 2022*

Citation:
Anavi-Cohen S, Zandani G, Tsybina-Shimshilashvili N, Hovav R, Sela N, Nyska A and Madar Z (2022) Metabolic and Microbiome Alterations Following the Enrichment of a High-Fat Diet With High Oleic Acid Peanuts Versus the Traditional Peanuts Cultivar in Mice. Front. Nutr. 9:823756. doi: 10.3389/fnut.2022.823756

A new Israeli-developed peanut cultivar, "Hanoch-Oleic" (HO), uniquely contains enlarged oleic acid contents and was designed to confer additional beneficial effects over the traditional cultivar, "Hanoch" (HN). This work elucidates metabolic changes and microbiota adaptations elicited by HO addition to a high-fat diet (HFD). Male C57BL/6 mice were fed for 18 weeks with a normal diet or a HFD with/without the addition of HN (HFDh) or HO (HFDo). Body-weight did not differ between HFD-fed mice groups, while liver and adipose weight were elevated in the HFDh and HFD groups, respectively. Insulin-sensitivity (IS) was also decreased in these groups, though to a much greater extent in the traditional peanuts-fed group. Modifications in lipids metabolism were evident by the addition of peanuts to a HFD. Liver inflammation seems to return to normal only in HFDh. Peanuts promoted an increase in α-diversity, with HFDo exhibiting changes in the abundance of microbiota that is primarily associated with ameliorated gut health and barrier capacity. In conclusion, the HO cultivar appears to be metabolically superior to the traditional peanut cultivar and was associated with an improved inflammatory state and microbial profile. Nevertheless, IS-negative effects reinforced by peanuts addition, predominantly NH, need to be comprehensively defined.

Keywords: peanuts, inflammation, NAFLD, gut microbiome, oleic acid

INTRODUCTION

The World Health Organization defines obesity (and overweight) as an "abnormal or excessive fat accumulation that presents a risk to health" (1). Non-alcoholic fatty liver disease (NAFLD) is a comorbidity usually, though not always, associated with obesity. NAFLD is currently considered one of the most common forms of chronic liver disease worldwide and encompasses a wide spectrum of pathologies starting from simple steatosis through non-alcoholic steatohepatitis which may further progress to comprehensive fibrosis, cirrhosis, and hepatocellular carcinoma. NAFLD is

prominently related to other metabolic alterations such as insulin resistance (IR), and a reciprocal relationship has been demonstrated between this disease and type 2 diabetes (2).

Obesity is also often manifested by IR and chronic low-grade inflammation. Adipose tissue has been implicated as an imperative participant in the establishment of systemic inflammation in the setting of obesity. Pro-inflammatory cytokines, other adipokines, along free fatty acids (FFA) secreted from adipose tissue may trigger and/or aggravate the development of IR and other pathological repercussions (2).

Peanuts are a dietary source of many nutrients and other compounds including proteins, fibers, vitamins (E, riboflavin, and folate), minerals (niacin, magnesium, selenium, manganese), and the well-acknowledged antioxidant polyphenols (3, 4). Fat constitutes the foremost macronutrient in peanuts and peanuts products, e.g., peanut butter and peanut oil. Unsaturated fatty acids comprise the vast majority of this fat, accounting for about 80% of all fats with half consisting of monounsaturated fatty acids (MUFAs) and the rest ∼30% of polyunsaturated fatty acids (PUFA). Hanoch (HN) is the traditional cultivar, also referred to as the conventional peanut, being used for industrial purposes. Given the encouraging metabolic and health-promoting effects attributed to oleic acid (5) a new peanut type was developed by the Israeli Agricultural Research Organization back in 2020 and was called "Hanoch-Oleic" (HO). With the goal of promoting human health, this improved cultivar is particularly characterized by augmented amounts of oleic acid which represents 82.7% of all fatty acids, compared to 55% in HN cultivar.

The profound influence exerted by the gut microbiome on human health is well recognized and has been established by numerous data. Diet and the metabolic state of the individual are interlinked with changes in the composition and activity of the gut microbiome. Compelling evidence has highlighted the mutuality that exists between diet, microbiome, and health, and this area has become the center of attention and a subject of ongoing research (6–8). Several studies demonstrated nut consumption affects gut microbiota composition is several taxonomical levels (9–11). However, the influence of peanuts specifically is largely obscure, with only a few studies conducted on this subject (12, 13). Moreover, the impact of HO peanuts cultivar consumption on the gut microbiome is yet to be tested. Thus, estimation of peanuts' effects, especially those with a high oleic acid content, on the bacterial population in the gut is extremely desired.

The present work aimed to define the effects of habitual consumption of the traditional peanut cultivar, HN, and the new high-oleic peanut cultivar, HO, as an integral part of diet-induced obesity. Specifically, their role on the liver, adipose tissue, and gut microbiota was evaluated.

MATERIALS AND METHODS

Experimental Animals and Diets

All animal experiments were done according to the rules of ethics of the Hebrew University of Jerusalem, Israel, and were approved by Institutional Animal Care Ethics Committee. All mice were maintained at 22 ± 2°C, controlled moisture of 60%, and in a 12 h light/12 h dark cycle with *ad libitum* access to food and water. After a 3-day acclimation period of standard rodent food, the food was replaced by the experimental diets. Thirty-two male 7–8 week old mice (C57BL/6J), were randomly divided into four groups (n = 8 per group). Experimental groups were as follows: (1) normal-diet (ND), (2) HFD, (3) HFD with "Hanoch" peanuts (HFDh), w/w 4%, (4) HFD with high oleic acid "Hanoch-Oleic" peanuts (HFDo), w/w 4%. Peanuts and diet composition are elaborated in **Tables 1**, **2**. Diets were given for 18 weeks. Bodyweight was recorded once a week, and food intake was measured three times a week.

Oral Glucose Tolerance Test

On the 16th week, an oral glucose tolerance test (OGTT) was performed in overnight (12 h) fasted mice as previously described (14).

Animal Sacrifice and Organ Collection

At the end of the 18th week, the mice were fasted for 12 h, weighted, and randomly eliminated by isoflurane USP inhalation. Blood was drawn from the vena cava. Liver and adipose tissues were removed, weighed, placed in liquid nitrogen, and stored at −80°C. A small liver sample was also embedded in 4% formaldehyde. The cecum content was collected and stored at −80°C for microbiota analysis.

Plasma Analysis

Blood liver enzymes and lipid profile analysis were conducted by American Laboratory (Herzliya, Israel). Plasma insulin levels were determined using an Insulin Rat/Mouse ELISA Kit (Cat. #EZRMI−13K). Homeostatic model assessment for insulin resistance (HOMA-IR) index was calculated as previously described (14). Plasma FFA was determined using an Abcam Free Fatty Acids Quantification Assay Kit (ab65341) according to the manufacturer's instructions.

Hepatic Triglyceride Levels and Histological Examination

Liver triglyceride levels were measured using the Triglyceride Quantification Assay Kit (Abcam, ab-65336), according to the

TABLE 1 | Seeds composition of the two peanut varieties.

	Peanut variety	
Compounds	**Hanoch (HN)***	**Hanoch-Oleic (HO)***
Carbohydrates %	20.9	21.5
Protein %	23.5	22.6
Fat %	49.5	48.7
C16:0 (palmitic acid) %	8.4	4.99
C18:0 (stearic acid) %	3.23	2.03
C18:1n9 *cis* (oleic acid) %	55.28	82.68
C18:2n6 (linoleic acid) %	25.01	2.08

**HN, conventional peanut strain; HO, high oleic peanut strain.*

TABLE 2 | Diet consumption.

	Experiment 1			
Ingredients	**ND***	**HFD**	**HFDh**	**HFDo**
Casein (gr)	21	26,5	25,48	25,48
L-Methionine (gr)	0,3	0,4	0,38	0,38
Corn starch (gr)	50	–	–	–
Maltodextrin (gr)	10	16	15,38	15,38
Anhydrous milkfat (gr)	2	–	–	–
Sucrose (gr)	3,9	9	8,65	8,65
Cellulose (gr)	3,5	6,6	6,35	6,35
Soybean oil (gr)	2	3	2,88	2,88
Lard (gr)	2	31	29,81	29,81
Peanut (gr)	–	–	3,85	3,85
Mineral mix (gr)	3,5	5,1	5,1	5,1
Vitamin mix (gr)	1,5	2,1	2,1	2,1
Choline chloride (gr)	0,3	0,3	0,3	0,3
BHT (gr)	0,014	0,014	0,014	0,014
Total (gr)	100	100	100	100
Total (kcal)	394,89	514	518,2	517,9
Protein (%)	21,58	21	21,13	21,08
Carbohydrate (%)	64,75	19,46	19,52	19,55
Fat (%)	13,68	59,53	59,07	59,04

**ND, normal diet; HFD, high fat diet; HFDh, high fat diet plus 4% (w/w) of Hanoch; HFDo, high fat diet plus 4% (w/w) of Hanoch-Oleic.*

manufacturer's instructions. Histological slides were prepared by Patholab (Rehovot, Israel). The tissues were embedded in paraffin, and serial sections (3–5 μm thick) were cut from each block and stained with hematoxylin and eosin (H&E) as previously described (12).

Western Blot Analysis

Tissues were extracted with lysis buffer, and the protein concentration was determined by the Bradford method followed by western blot. Blots were incubated at 4°C overnight with the primary antibodies: anti–adenosine monophosphate–activated protein kinase (AMPK) #2532; pAMPK, #2531; acetyl-CoA carboxylase (ACC), #3662; pACC #3661; CREB, p-CREB, inducible nitric oxide synthase (iNOS); and cluster of differentiation 36 (CD36), ab124515 ABCAM. The membranes were washed and then incubated with secondary goat antibodies (Jackson ImmunoResearch Laboratories, West Grove, PA, United States). The immune reaction was detected by enhanced chemiluminescence, with bands being quantified by densitometry and expressed as arbitrary units. An unspecific band out of the total protein (Ponceau) was used as housekeeping protein.

Quantitative Real-Time Polymerase Chain Reaction

Total RNA was isolated from tissues using TRI Reagent (Sigma-Aldrich, Rehovot, Israel) according to the manufacturer's protocol. Complementary DNA was prepared with the High-Capacity cDNA Reverse Transcription Kit (Quanta, BioSciences, Gaithersburg, MD, United States). Real-time polymerase chain reaction (PCR) was performed using the 7300 Real-Time PCR System (Applied Biosystems, Foster City, CA, United States), with specific primers. Quantitative changes in gene expression were determined by normalizing to 18S. Primer sequences are listed in **Table 3**.

Gut Microbiota Analysis

The effects of each diet on the bacterial population in the gut microbiome were examined with the analysis of the prokaryotic 16S ribosomal RNA gene (16S rRNA), using a two-step PCR-based method for preparing samples for sequencing the variable V3 and V4 regions of the 16S rRNA gene (12). The paired-end sequences were processed, paired, and trimmed, and low-quality reads were removed using the "QIIME2" software package. Chimeric sequences were filtered using the chimera-removal function of UCHIME (15), implemented within "QIIME2." Illumina sequence denoising was done *via* DADA2 implemented in QIIME2 (16). Sequences with 97% similarity were assigned to the same operational taxonomic units (OTU). Chloroplast and mitochondrial 16S rRNA sequences, as well as all OTUs represented by fewer than 10 sequences, were

TABLE 3 | Primers sequences.

Name	Reverse	Forward
18s	5′-CCTCAGTTCCGAAAACCAAC-3′	5′-ACCGCAGCTAGGAATAATGG-3′
Fasn	5′-GGTCGTTTCTCCATTAAATTCTCAT-3′	5′-CTAGAAACTTTCCCAGAAATCTTCC-3′
SREBP-1c	5′-TAGATGGTGGCTGCTGAGTG-3′	5′-GATCAAAGAGGAGCCAGTGC-3′
TNFα	5′-CCACAAGCAGGAATGAGAAGA-3′	5′-ACGTGGAACTGGCAGAAGAG-3′
HSL	5′-TGCCCAGGAGTGTGTCTGAG-3′	5′-AGGACACCTTGGCTTGAGCG-3′
ATGL	5′-GGTTCAGTAGGCCATTCCTC-3′	5′-GTGCAAACAGGGCTACAGAG-3′
CPT-1	5′-CAGCGAGTAGCGCATAGTCA-3′	5′-TGAGTGGCGTCCTCTTTGG-3′
IL-6	5′-TGCAAGTGCATCATCGTTGT-3′	5′-ACTTCACAAGTCGGAGGCTTAAT-3′
PPARγ	5′-CAGCTTCTCCTTCTCGGCCT-3′	5′-CACAATGCCATCAGGTTTGG-3′
PGC-1α	5′-AGAGCAAGAAGGCGACACAT-3′	5′-AACAAGCACTTCGGTCATCC-3′
PPAR α	5′-CTGCGCATGCTCCGTG-3′	5′-CTTCCCAAAGCTCCTTCAAAAA-3′

18S, 18S ribosomal RNA; Fasn, fatty acid synthase gene; SREBP-1c, sterol regulatory element-binding transcription factor 1; TNFα, tumor necrosis factor alpha; HSL, hormone sensitive lipase; ATGl, adipose triglyceride lipase; CPT-1, carnitine palmitoyl transferase I; IL-6, interleukin 6; PPARγ, peroxisome proliferator-activated receptor gamma; PGC-1 α, peroxisome proliferator-activated receptor gamma coactivator 1-alpha; PPAR α, peroxisome proliferator-activated receptor alpha.

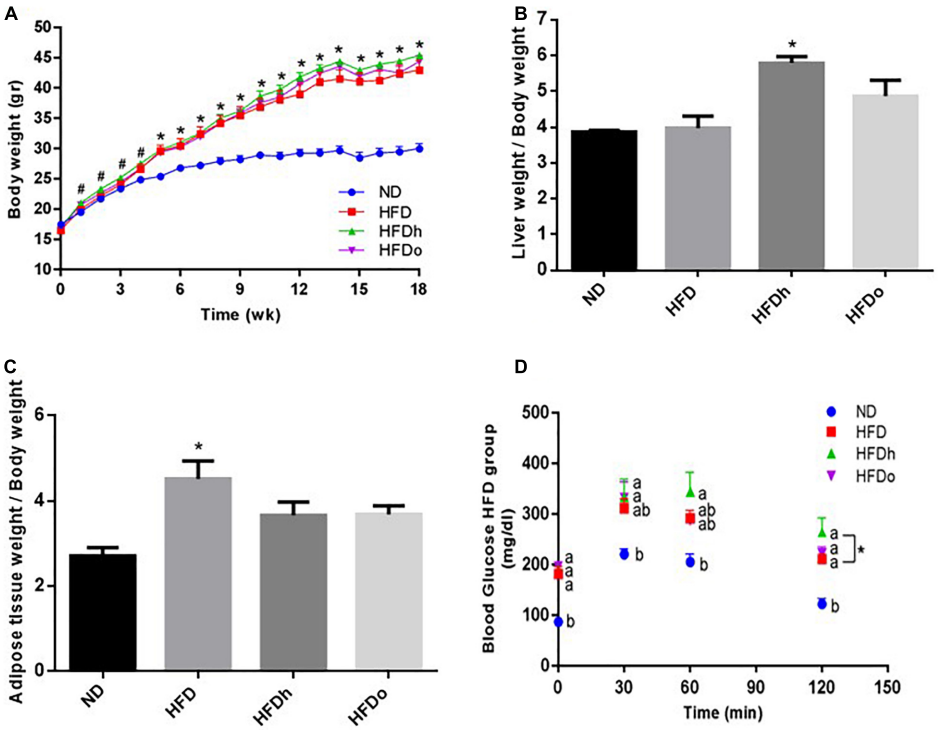

FIGURE 1 | The effect of diets on body, liver and adipose tissue weight and glucose tolerance. Mice consumed either a normal diet (ND), a high-fat diet (HFD), a high-fat diet plus 4% (w/w) of HN (HFDh) or HO (HFDo) peanuts for 18 weeks. Body weight **(A)**, liver weight to body weight **(B)**, and adipose tissue weight to body weight **(C)** ratios were measured. Two weeks before the end of the experimental period, an oral glucose tolerance test (OGTT) was carried out **(D)**. A Tukey-Kramer HSD post hoc test and the Student's *T*-test were performed. The values presented are mean ± SE ($n = 8$). Different letters indicate statistical variance at a significance level of $p < 0.05$.

removed from the OTU count table. The count data were rarefied to avoid variable library size bias (17). OTUs of representative sequences at a similarity of 97% and their relative abundances were used to calculate and analyze rarefaction curves. Bacterial richness and diversity within samples were classified by alpha diversity (Pielou's index, observed-species indices, and Shannon index).

Statistical Analysis

Statistical analysis was performed using a one-way analysis of variance (one-way ANOVA) followed by the Tukey–Kramer HSD *post hoc* test. The results are presented as means ± standard error (SEM). For all analyses, the JMP 14 Pro Software Suites (SAS Institute, Cary, NC, United States) was used. All p values were calculated using these two tests. p Values less than 0.05 were considered statistically significant.

RESULTS

Effect of Peanuts Addition to a High-Fat Diet on Mice Weight, Food Intake, and Liver and Adipose Tissue Weight

As shown in **Figure 1A**, at the end of the experiment, body weight was profoundly higher in all HFD-fed groups compared with the control (ND). In comparison with the control group, liver-to- body weight ratio was elevated only in the group that was supplemented with the regular peanut cultivar whereas a significant increase in adipose tissue weight-to-body weight ratio was found merely in the HFD group (**Figures 1B,C**). Measurement of hepatic TG levels and histological staining further corroborated similar TG/lipid accumulation in the livers of all HFD-fed groups, with solely the HFDh group demonstrating significantly increased values above those of the control in the former analysis (**Supplementary Figures 1A,B**).

Effects of Peanuts Addition to a High-Fat Diet on Blood Biochemistry Profile

Blood TG levels were lower in the HFDh and HFDo groups compared to the ND group, while no significant differences were found between the HFD-fed groups. Total blood cholesterol levels were significantly elevated in all HFD-groups, with the HFDo group exhibiting higher levels compared to HFD alone. HDL cholesterol was markedly augmented in all HFD groups. FFA blood levels only differed between HFD and HFDh groups, with levels being lower in the former. Compared with the control, blood levels of the liver enzymes AST and ALT were elevated in the HFD groups that were supplemented with peanuts, while those of ALT were significantly and similarly

TABLE 4 | Blood biochemistry profile.

	Groups			
Parameters	**ND**	**HFD**	**HFDh**	**HFDo**
Triglycerides (mg/dl)	101.67 ± 9.89^{a}	80.75 ± 5.31^{ab}	72.38 ± 2.22^{b}	65.29 ± 4.89^{b}
Total cholesterol (mg/dl)	124.5 ± 5.94^{c}	197.38 ± 15.02^{b}	229 ± 11.15^{ab}	245 ± 8.79^{a}
HDL cholesterol (mg/dl)	99.77 ± 3.97^{b}	147.64 ± 10.38^{a}	163.79 ± 6.37^{a}	175.84 ± 5.87^{a}
FFA (nmol/μl)	0.29 ± 0.01^{ab}	0.24 ± 0.01^{b}	0.30 ± 0.02^{a}	0.27 ± 0.01^{ab}
AST (IU/L)	52.6 ± 5.18^{c}	88.71 ± 10.86^{bc}	101 ± 8.79^{ab}	134.86 ± 11.17^{a}
ALT (IU/L)	31.2 ± 7.56^{b}	112.13 ± 19.44^{a}	114.25 ± 13.52^{a}	158.38 ± 11.73^{a}
ALP (IU/L)	69.67 ± 4.18	70.88 ± 7.07	76.88 ± 4.51	76.25 ± 4.5
Insulin (mmol/l)	6.97 ± 0.65^{b}	10.51 ± 0.34^{b}	14.52 ± 0.99^{a}	14.92 ± 1.29^{a}
HOMA-IR index	0.51 ± 0.07^{c}	4.04 ± 0.68^{c}	15.74 ± 1.61^{a}	9.42 ± 1.65^{b}

The effect of diets on lipid profiles, free fatty acid (FFA) blood levels, liver enzymes, insulin level, and HOMA-IR Index. Mice consumed either a normal diet (ND), a high-fat diet (HFD), a high-fat diet plus 4% (w/w) of HN (HFDh) or HO (HFDo) peanuts for 18 weeks. At the end of the experiment, plasma triglycerides, cholesterol, HDL-cholesterol (high-density lipoprotein cholesterol), alkaline phosphatase (AST), glutamic-pyruvic transaminase (ALT), glutamic oxaloacetic transaminase (ALP), FFA levels, and insulin levels were measured in the plasma (n = 8). HOMA-IR index was calculated by using the formula: [Fasting insulin concentration (microU/ml) × Glucose concentration (mg/dl)/405]. A Tukey–Kramer HSD post hoc statistical test was performed. The value presented are mean ± SE (n = 8). Different letters indicate statistical variance at a significant level of $p < 0.05$.

elevated in all HFD-fed groups. No change was observed in ALP levels (**Table 4**).

Effects of Peanuts Addition to a High-Fat Diet on the Glycemic Response, Homeostatic Model Assessment for Insulin Resistance Index, and Liver Gluconeogenesis

Oral glucose tolerance test was carried out to assess the effect of the diets on the glycemic response. The ND group had the lowest blood glucose levels throughout the test (**Figure 1D**). At the last time point (120 min), a noteworthy difference was observed between the HFDh and HFD groups, with blood glucose being greater in the former. No significant changes were found between the groups in ΔOGTT or AUC analyses (data not shown).

Fasting plasma insulin concentrations at the end of the experiment were higher in the HFDh and HFDo groups than in the HFD and ND groups. Consequently, HOMA-IR Index, a surrogate measure of insulin resistance, was profoundly greater in those HFD groups that were supplemented with peanuts (**Table 4**).

The effect of diets on liver gluconeogenesis was assessed by measuring the expression of key players in this metabolic pathway. The rate of CREB activation, measured as phosphorylated CREB at Ser133/total CREB ratio, was markedly and significantly increased by the consumption of HFD supplemented with peanuts (**Figure 2A**). However, this increase was not paralleled to a similar gene expression pattern, in which PGC-1α, G6Pase, and PEPCK mRNA levels were unaffected or even downregulated by HFD with or without peanuts addition (**Figures 2B–D**).

Effects of Peanuts Addition to a High-Fat Diet on Liver Lipid Metabolism and Related Regulators

Liver lipid metabolism was examined by measuring the expression of factors participating in *de novo* lipogenesis as well as lipid oxidation. SREBP-1c and Fasn gene expression was significantly elevated in the HFDh group compared to the other groups (**Figures 3A,B**). PPARα and CPT-1 gene expression was attenuated merely in the HFDo group, compared to the control. Furthermore, whereas HFD and HFDh exhibited a significant increase in PPARγ expression levels, HFDo was also the only group whose this parameter was similar to that of the control (**Figures 3C–E**). Additional analyses were carried out to clarify whether the AMPK pathway was affected by the diets combination. While AMPK activation was amplified in the HFD group, as assessed by phospho-to-total AMPK and ACC ratios, this activation was significantly abolished by the addition of peanuts to HFD (**Figures 3F,G**). Despite being an important activator of the AMPK pathway, adiponectin receptors expression did not correspond with AMPK activation. Characterization of these receptors revealed an inverse expression pattern between AdipoR1 and AdipoR2. Whereas AdipoR1 expression was significantly higher in HFDh relatively to HFDo, the complete opposite result was registered in AdipoR2 expression, i.e., greater levels in the HFDo group compared to the HFDh group (**Figures 3H,I**). Finally, under the HFD regime, FFA uptake into liver cells appears to be diminished as reflected by the profound decrease observed in CD36 protein levels in all HFD-fed groups (**Figure 3J**).

The Effect of Peanuts Addition to a High-Fat Diet on Liver Inflammation

iNOS appears to be induced in the liver by the consumption of HFD, as seen by the increase in this enzyme protein levels. Although iNOS expression was not significantly altered by this diet, a similar trend was found. Importantly, the addition of the oleic-rich peanut to HFD prevented iNOS induction at both, protein and expression, levels (**Figures 4A,B**). A similar pattern was found in SAA-1. Accordingly, whereas HFD promoted this gene expression, the increase was insignificant by the addition of oleic-rich peanuts (**Figure 4C**). Interestingly, HFD supplemented with the other, "traditional" peanut strain, not only failed to

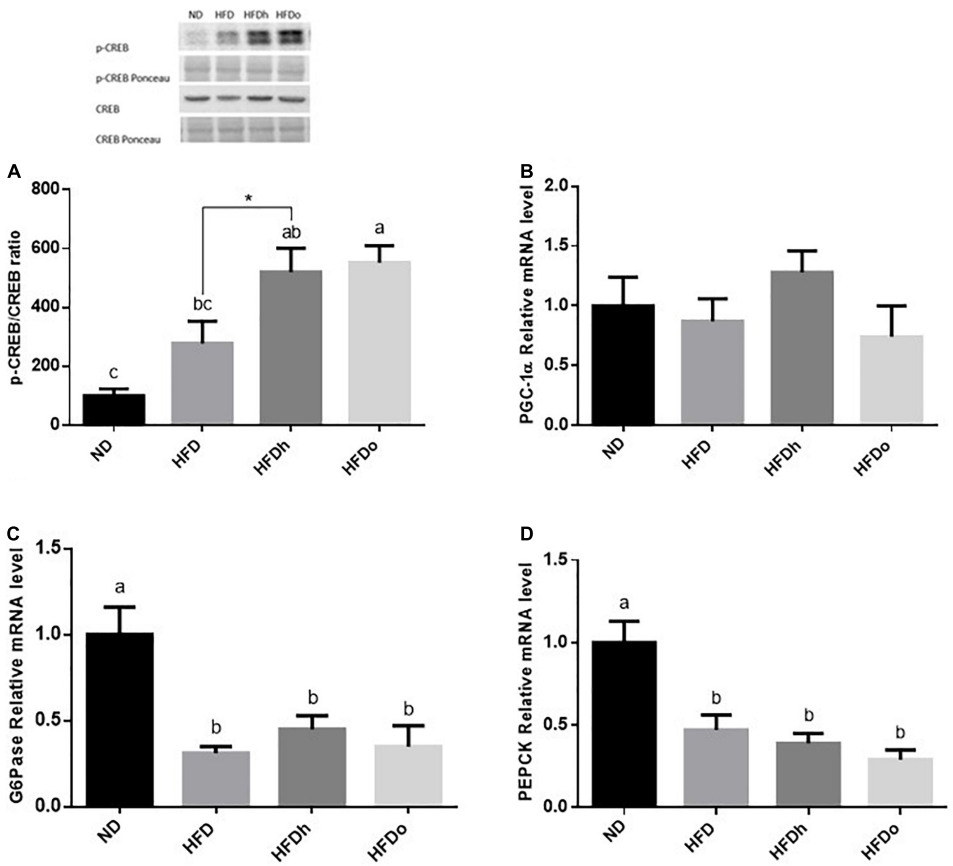

FIGURE 2 | The effect of diets on key players that participate in carbohydrate metabolism in the liver. Mice consumed either a normal diet (ND), a high-fat diet (HFD), a high-fat diet plus 4% (w/w) HN (HFDh) or HO (HFDo) peanuts for 18 weeks. The p-CREB/CREB protein ratio **(A)** was measured using Western blot where an unspecific band of total protein (Ponceau) was used as a control protein. The PGC-1α **(B)**, G6Pase **(C)**, and PEPCK **(D)** gene expressions were measured at the transcription level (RT-PCR), and the results normalized to the 18S gene expression. A Tukey's Kramer post-hos test and Student's *T*-test were performed. The values displayed are mean ± standard error. Columns marked with different letters indicate statistically significant variances at $p < 0.05$.

decrease the inflammatory state of the liver but rather seems to further enhance it. Indeed, the HFDh group exhibited the highest SSA-1 expression levels, greater than the levels found following the consumption of HFD alone. Consistently, whereas HFD did not affect TNFα nor IL-6 expression, the expression of the former was induced in the HFDh group (**Figures 4D,E**).

Effects of Peanuts Addition to a High-Fat Diet on Adipose Lipid Metabolism and Inflammation in Adipose Tissue

High-fat diet insignificantly tended to increase the expression of the lipolytic enzymes, ATGL and HSL. However, while the expression of both genes was further increased by the addition of regular peanuts to HFD, changes were completely blunted by the addition of oleic-rich peanuts to the HFD (**Figures 5A,B**). To examine the effect of HFD with or without peanuts addition on adipose tissue lipogenesis, PPARγ, SREBP-1c, and Fasn gene expression were measured. Whereas only SREBP-1c expression was positively induced by HFD, the expression of all tested genes was significantly upregulated in the HFDh group, compared to the ND control. Conversely, the HFDo group did not exhibit any alteration in the expression of these genes and displayed equal levels as those of the ND group (**Figures 5C–E**).

The expression pattern of PPARα and CPT-1, which participate in FFA oxidation, was similar. While the consumption of HFD and HFDo enhanced the expression of these genes, no marked change was found following the consumption of HFDh (**Figures 5F,G**). Compared to the ND group, AMPK activation was significantly increased in the HFDh group whereas a trend toward higher levels was noticed in HFD and HFDo groups (**Figure 5H**). A rather similar pattern was observed with PGC-1α gene expression. However, this measure significantly differed between HFDh and HFDo groups, with PGC-1α being greater in the former (**Figure 5I**). CD36 protein levels were profoundly decreased by the consumption of HFD regardless of the addition of peanuts to this diet (**Figure 5J**).

Adipose tissue inflammatory state is known to impact the whole-body metabolism. Thus, to further gain insight into the effects of the different peanut strains, key inflammatory markers were assessed. Consumption of HFD considerably elevated the

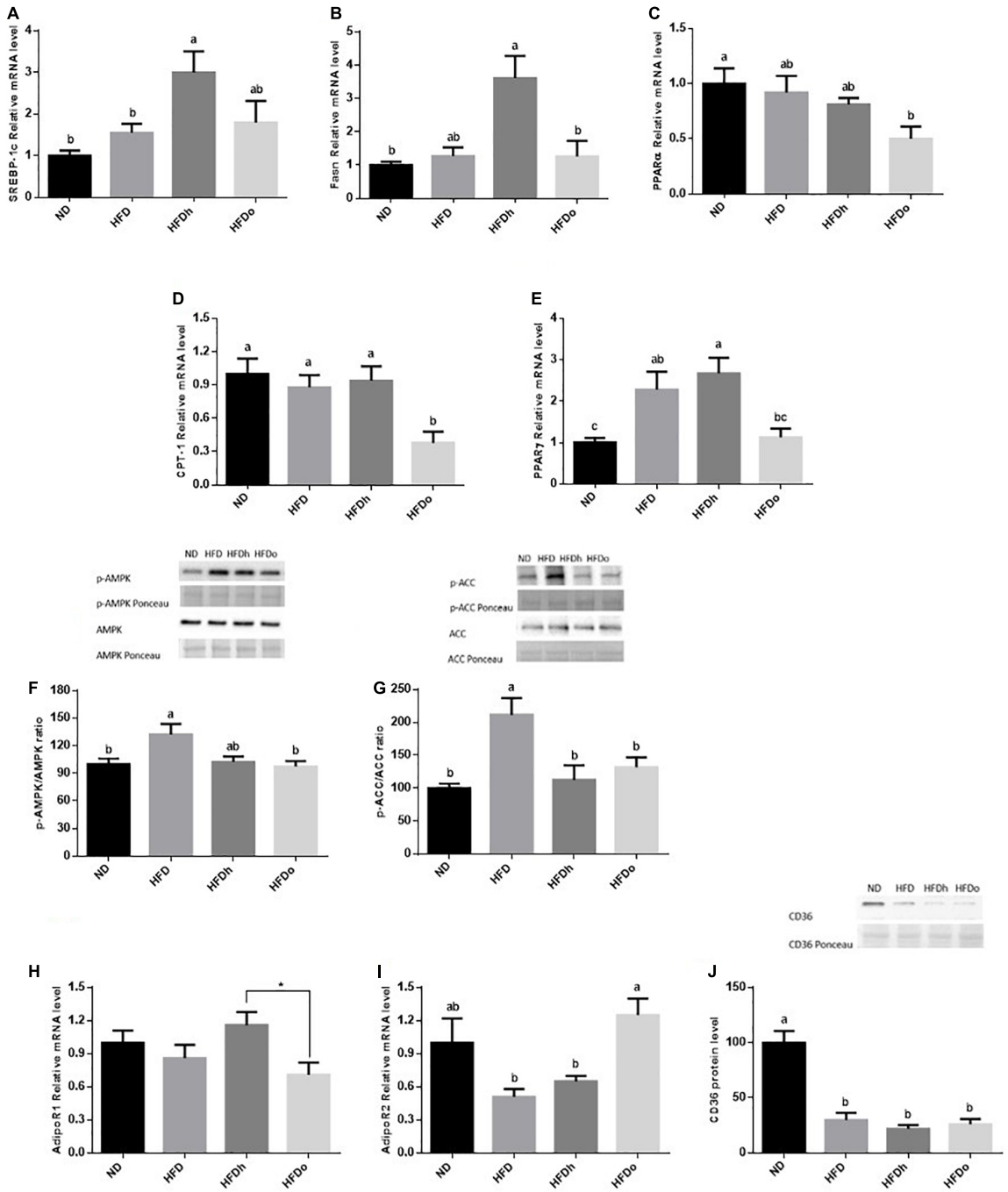

FIGURE 3 | The effect of diets on key players that participate and/or regulate lipid metabolism in the liver. Mice consumed either a normal diet (ND), a high-fat diet (HFD), a high-fat diet plus 4% (w/w) HN (HFDh) or HO (HFDo) peanuts for 18 weeks. The SREBP-1c **(A)**, Fasn **(B)**, PPARα **(C)**, CPT-1 **(D)**, PPARγ **(E)**, AdipoR1 **(H)** and AdipoR2 **(I)** gene expressions were measured at the transcription level (RT-PCR), and the results normalized to the 18S gene expression. The p-AMPK/AMPK protein ratio **(F)**, p-ACC/ACC protein ratio **(G)**, and CD36 protein levels **(J)** were measured using Western blots where an unspecific band of total protein (Ponceau) was used as a control protein. A Tukey's Kramer post-hos test and Student's *T*-test were performed. The values displayed are mean ± standard error. Columns marked with different letters indicate statistically significant variances at $p < 0.05$.

pro-inflammatory cytokines TNFα and IL-6 expression. TNFα and IL-6 expression was significantly or tended to further increase in the HFDh group, respectively. Conversely, these gene expression levels were not significantly induced by the addition of high-oleic peanuts to HFD compared to the ND control (**Figures 5K,L**).

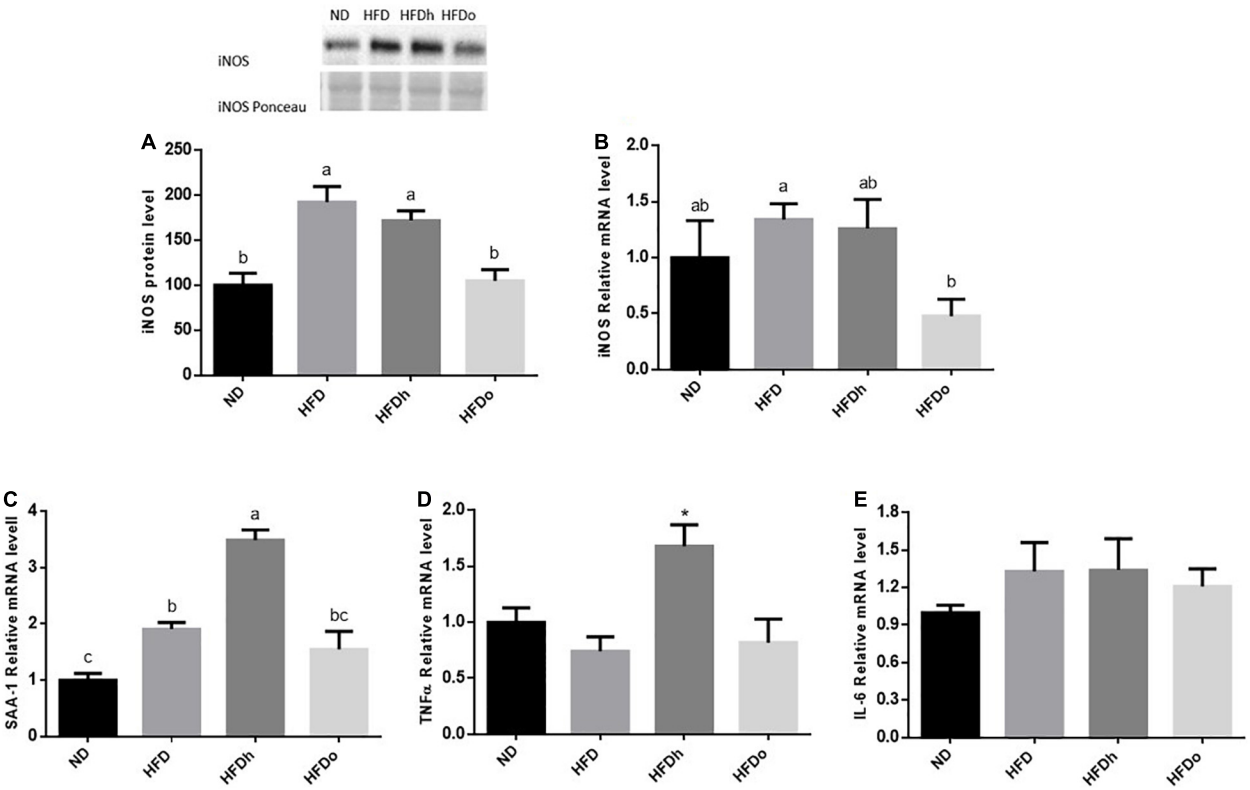

FIGURE 4 | The effect of diets on protein and inflammatory genes expression in the liver. Mice consumed either a normal diet (ND), a high-fat diet (HFD), a high-fat diet plus 4% (w/w) HN (HFDh) or HO (HFDo) peanuts for 18 weeks. The protein expression of iNOS **(A)** was measured using Western blot where an unspecific band of total protein (Ponceau) was used as a control protein. The gene expressions of iNOS **(B)**, SAA-1 **(C)**, TNFα **(D)**, and IL-6 **(E)** were measured at the transcription level (RT-PCR), and the results were normalized to the 18S gene expression. A Tukey's Kramer post-hos test and ANOVA (Dunnett's) statistical test were performed. The values displayed are mean ± standard error. Columns marked with different letters indicate statistically significant variances at $p < 0.05$.

Effect of Peanuts Addition to a High-Fat Diet on Intestinal Microbiota

The effects of diets on microbiota species richness and diversity (observed OUT's and Shannon Index, respectively) were evaluated as well. Diversity, which explicitly represents the integration of species richness with evenness into a distinct value (18), was found to be upraised by peanuts consumption, regardless of the cultivar been used. Species abundance *per se*, the evenness component of diversity, as measured by the Pielou's index, was marginally increased by HFD consumption with additional effect being observed only in the HFDh group (**Table 5**).

Significant alterations in gut microbiota composition are elaborated in **Table 5**. At the phylum level, peanuts addition, as well as HFD, elicited profound changes in the two most dominant bacterial phyla, Bacteroidetes and Firmicutes, leading to decreased and decreased levels, respectively. Consequently, the F/B ratio was elevated by these treatments. Actinobacteria levels were decreased whereas those of Proteobacteria were elevated or tended to be higher in the HFD-fed group with or without peanuts addition. Deferribacteres presence was diminished in the groups where peanuts were added to HFD, regardless of the cultivar. Finally, Tenericutes abundance was abolished following the consumption of the HFD or HFDo group while no change was noted in the HFDh group. At the family level, Bifidobacteriales, Bacteroidales, RF32, and Verrucomicrobiales abundance was lower in all HFD-fed groups, except for the RF32 family in the HFDo group and Verrucomicrobiales family in the HFDh group. Conversely, greater quantities of Clostridiales and Desulfovibrionales were found in all HFD-fed groups. A marked decrease in the Erysipelotrichales family was observed in the group fed with HFD with the addition of high-oleic peanuts, compared with the rest of the groups. On the other hand, Anaeroplasmatales levels were higher in the HFDh group, compared to HFD and HFDo groups, with levels comparable to the control.

DISCUSSION

The present work elucidated several metabolic consequences driven by the incorporation of the new, predominantly oleic-rich, peanut cultivar HO to a HFD and further compared them to those obtained by the addition of the traditional cultivar, HN, to the same diet. This study further characterized the alterations in gut resident microbiota implemented

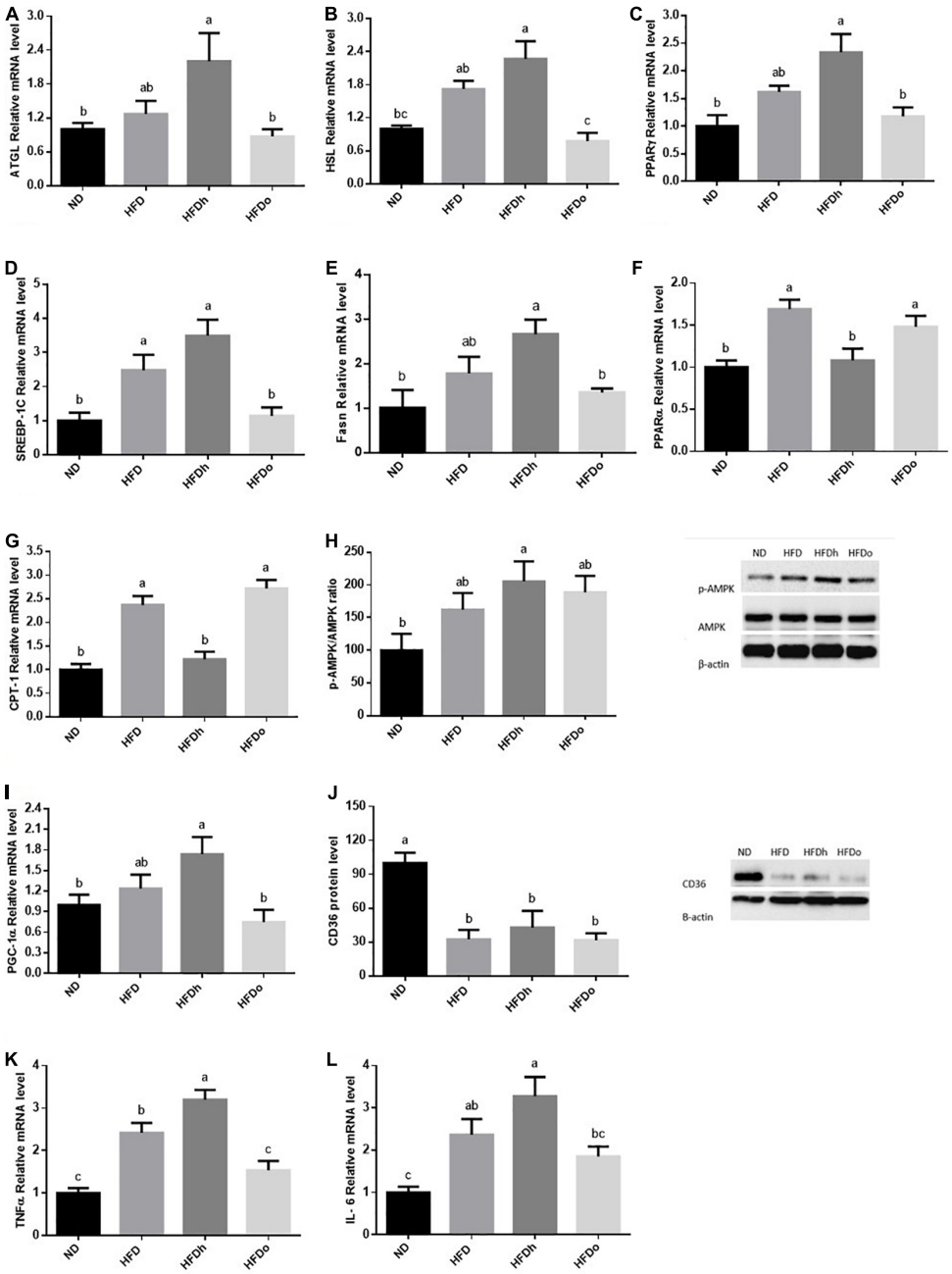

FIGURE 5 | The effect of diets on key players that participate in fat metabolism and inflammation in adipose tissue. Mice consumed either a normal diet (ND), a high-fat diet (HFD), a high-fat diet plus 4% (w/w) of HN (HFDh) or HO (HFDo) peanuts for 18 weeks. The ATGL **(A)**, HSL **(B)**, PPARγ **(C)**, SREBP-1c **(D)**, Fasn **(E)**, PPARα **(F)**, CPT-1 **(G)**, PGC-1α **(I)**, Il-6 **(K)** and TNFα **(L)** genes expressions were measured at the transcription level (RT-PCR), and the results normalized to the 18S gene expression. The p-AMPK/AMPK ratio **(H)** and CD36 **(J)** protein levels were measured using Western blots where β-actin was used as a control protein. A Tukey's Kramer post-hos test was performed. The values displayed are mean ± standard error. Columns marked with different letters indicate statistically significant variances at $p < 0.05$.

by these dietary manipulations. Although the addition of peanuts did not abolish the irregularities emanating from the obesogenic diet, results posit HO constitutes the preferred type in metabolic terms and plausibly in microbiota adaptation.

Peanut addition, regardless of the type, under the setting of diet-induced obesity failed to mitigate the increase in body weight. However, under obesogenic conditions, not only is the amount of weight-gain important but also where it is stored. Under a HFD regime, the liver-to-bodyweight ratio was

significantly elevated only in the group that was supplemented with the conventional peanut "Hanoch," indicating ectopic fat accumulation in this group. The ratio between epididymal adipose tissue, a representative of the visceral fat pad in rodents (12–19) to-total body weight was comparable between ND and HFD-supplemented with peanuts but was markedly increased in the HFD alone, suggesting more fat stored as visceral fat. The lack of profound changes in the ratio between liver and epididymal fat pad to body weight in the HFDo group, despite an increase in body weight, may infer that this peanut cultivar is associated with a "healthier" pattern of weight gain.

Analysis of insulin regulation revealed enhanced IR when the conventional peanut cultivar was added to the HFD. When the high-oleic cultivar was added to the HFD, though IR in this group was higher than that of the HFD-fed group, IR was much less profound in this group than in the regular cultivar-supplemented group. Consist with this, in a previous study, the addition of traditional peanuts to a HFD ameliorated the AUC obtained from OGTT, though was associated with increased fasting insulin concentrations compared to HFD alone. Conversely, the addition of a different high-oleic cultivar used in that study did not elicit any extra deleterious effect on those of the HFD *per se* (12). The clinical outcomes attributed to long-term peanuts consumption have been investigated by several works (4). Concerning glycemic factors, results are conflicting. Although no change in fasting blood glucose was found in several works, others have reported a decrease or, alternatively, an increase in this parameter by incorporating peanuts into the diet (4). Similarly, blood insulin was either unchanged or increased following peanuts consumption (12). Regarding high-oleic peanuts specifically, Moreira et al. investigated the metabolic consequences of such a peanut cultivar during the consumption of HFD. These researchers found no advantage for the high-oleic peanuts on fasting blood glucose and insulin levels over the conventional cultivar. Yet, a moderated glycemic response following meal intake was observed (20, 21). These, along with the current findings, do not support the notion that peanuts with high-oleic content convey fundamental benefits and effects on blood glucose and/or insulin levels though they may be advantageous to/over the conventional cultivar under specific circumstances.

The mechanism by which the addition of peanuts negatively affected insulin sensitivity in the present work is not understood. However, under conditions of elevated oxidative stress, double-bond/s containing FA might be oxidized to yield harmful products (22). Supporting this notion, AST levels were significantly augmented in the peanuts-enriched groups. These findings may argue for the essential need for additional antioxidant compounds when obesogenic diets are fortified with unsaturated FA (23).

Abnormally activated GNG is well acknowledged as one of the processes that pathologically influence fasting blood glucose. GNG is controlled, among other mechanisms, at the transcriptional level through the transcription factor CREB, which is activated through its phosphorylation at ser133 residue. Activated CREB subsequently potentiates GNG by upregulating the expression of the key GNG enzymes PEPCK and G6Pase and the expression of the co-activator PGC-1α (24). Surprisingly, in the current study, CREB activation was not concomitant with a similar increase in the expression of pro/GNG genes. In fact, the mRNA levels of both GNG enzymes were downregulated in mice that were fed with HFDh, and HFDo despite a significant induction of CREB. Likewise, the tendency toward CREB activation in the HFD group was accompanied by a decrease rather than an increase in PEPCK and G6Pse gene expression. This lack of coherency is obscure. Yet, several mechanisms may be accounted for this phenomenon, including the disruption of the CREB/CRTC2 complex by insulin. Insulin is a robust negative regulator of GNG at several levels, including by mediating the interaction between activated CREB and small heterodimer partner–interacting leucine zipper protein (SMILE) instead of with CRTC2. CREB-SMILE complex is unable to induce PEPCK and G6Pase nor PGC-1alpha gene expression (25). Given that Insulin levels were or tended to be increased in the same mentioned groups and the ability of IR to be selective in the liver, it is posited that insulin can be the cause of the discrepancy between CREB activation and GNG-gene expression. Nevertheless, since the outcome of GNG, i.e., fasting blood glucose specifically, remained unaltered, it is presumed levels were counterbalanced by enhanced glycogenolysis or increased peripheral IR in HFD-fed groups.

Much attention has also been drawn to the impact of peanuts intake on lipidemia. Although not well established, it is consensually believed a reduction in TG and LDL cholesterol levels is among the health-promoting effects peanuts intake may carry out (3). In the present study, TG levels were lower while those of HDL were greater in all HFD-fed groups without any significant impact on peanuts addition. In accord, a recent meta-analysis failed to demonstrate a positive effect of peanuts consumption on blood TG levels.

Over the years, several works have appraised the usefulness of nuts, including peanuts, on liver fat concentration with the results being controversial (3). The results presented here demonstrate diverse outcomes can be derived depending on the dietary regime applied and/or peanut cultivar being used. As stated, under an obesogenic diet, the development of NAFLD was further promoted by the addition of conventional peanuts to HFD, as manifested by the liver to body weight ratio in this group. Inline, this group exhibited augmented expression of key players required for the implementation of *de novo* lipogenesis while those that govern fatty acids oxidation were unaffected. Altered adipose tissue lipid metabolism, lipolysis specifically, is among the salient factors contributing to the establishment of liver steatosis. ATGL and HSL expression in adipose tissue was significantly upregulated by the addition of traditional peanuts to this diet, suggesting enhanced adipocyte lipolytic capacity in this group which may subsequently contribute to ectopic fat accumulation in the liver. On the contrary, liver steatosis was more constrained in the group fed with the alternate, high-oleic peanuts cultivar, as seen by the insignificantly increased liver to body-weight ratio and hepatic TG contents. Lower hepatic and adipocytes lipogenic capacity concomitantly to lower adipocytes lipolysis and enhanced FFA oxidation may

TABLE 5 | Taxonomical levels and diversity indexes.

	ND	HFD	HFDh	HFDo
α diversity				
Observed OUT's	141.80 ± 3.20	133.75 ± 4.67	162.80 ± 7.69$^{\#}$	168.00 ± 12.63$^{\#}$
Shannon index	6.00 ± 0.07	6.15 ± 0.06	6.61 ± 0.12$^{*,\#}$	6.55 ± 0.15$^{*,\#}$
Pielou's index	0.84 ± 0.01	0.87 ± 0.01*	0.90 ± 0.01$^{*,\#}$	0.89 ± 0.01*
Phylum level				
Actinobacteria	1.30 ± 0.21	0.49 ± 0.12*	0.67 ± 0.20*	0.25 ± 0.06*
Bacteroidetes	51.70 ± 2.69	34.21 ± 2.24*	30.03 ± 1.89*	32.03 ± 2.14*
Deferribacteres	1.16 ± 0.09	1.56 ± 0.28	0.93 ± 0.13$^{\#}$	0.95 ± 0.25$^{\#}$
Firmicutes	39.75 ± 2.86	52.83 ± 1.93*	58.30 ± 2.29*	58.82 ± 3.85*
Proteobacteria	4.36 ± 0.52	10.10 ± 1.70*	8.50 ± 0.94	8.63 ± 1.30*
Tenericutes	0.34 ± 0.11	0.23 ± 0.08	0.74 ± 0.18$^{*,\#}$	0.41 ± 0.06
Verrucomicrobia	0.96 ± 0.03	0.00 ± 0.00$^{\#}$	0.48 ± 0.36	0.00 ± 0.00$^{\#}$
F/B ratio	0.79 ± 0.10	1.57 ± 0.16*	1.98 ± 0.19*	1.90 ± 0.26*
Class level				
Coriobacteriia	0.65 ± 0.12	0.50 ± 0.12	0.58 ± 0.18$^{\$}$	0.20 ± 0.03*
Bacteroidia	51.69 ± 2.69	34.21 ± 2.24*	30.03 ± 1.89*	32.03 ± 2.14*
Deferribacteres	1.16 ± 0.10	1.56 ± 0.28	0.93 ± 0.13$^{\#}$	0.95 ± 0.25$^{\#}$
Clostridia	36.84 ± 2.93	50.43 ± 2.29*	54.69 ± 2.09*	56.98 ± 3.78*
Erysipelotrichi	1.64 ± 0.11	1.48 ± 0.53	1.96 ± 0.51$^{\$}$	0.26 ± 0.15$^{*,\#}$
Alphaproteobacteria	0.56 ± 0.18	0.16 ± 0.03*	0.10 ± 0.06*	0.45 ± 0.13
Deltaproteobacteria	3.55 ± 0.46	9.70 ± 1.65*	8.15 ± 0.85*	9.28 ± 1.41*
Mollicutes	0.34 ± 0.11	0.23 ± 0.08	0.75 ± 0.18$^{*,\#}$	0.41 ± 0.06
Verrucomicrobiae	3.21 ± 0.51	0.00 ± 0.00*	0.48 ± 0.36	0.00 ± 0.00*
Order level				
Bifidobacteriales	0.65 ± 0.17	0.00 ± 0.00*	0.08 ± 0.05*	0.05 ± 0.05*
Coriobacteriales	0.65 ± 0.12	0.5 ± 0.12	0.58 ± 0.18$^{\$}$	0.20 ± 0.03*
Bacteroidales	51.69 ± 2.69	34.21 ± 2.24*	30.03 ± 1.89*	32.03 ± 2.14*
Deferribacterales	1.16 ± 0.10	1.56 ± 0.28	0.93 ± 0.13$^{\#}$	0.95 ± 0.25$^{\#}$
Clostridiales	36.84 ± 2.93	50.43 ± 2.29*	54.69 ± 2.09*	56.98 ± 3.77*
Erysipelotrichales	1.64 ± 0.11	1.48 ± 0.53	1.96 ± 0.51$^{\$}$	0.26 ± 0.15$^{*,\#}$
RF32	0.56 ± 0.18	0.16 ± 0.03*	0.10 ± 0.06*	0.45 ± 0.13
Desulfovibrionales	3.55 ± 0.46	9.70 ± 1.65*	8.15 ± 0.85*	9.28 ± 1.41*
Anaeroplasmatales	0.27 ± 0.09	0.03 ± 0.03	0.32 ± 0.14$^{\#,\$}$	0.04 ± 0.03
RF39	0.07 ± 0.03	0.20 ± 0.08	0.43 ± 0.12*	0.37 ± 0.06*
Verrucomicrobiales	0.96 ± 0.31	0.00 ± 0.00*	0.48 ± 0.36	0.00 ± 0.00*
Family level				
Bifidobacteriaceae	0.65 ± 0.17	0.00 ± 0.00*	0.08 ± 0.05*	0.05 ± 0.05*
Coriobacteriaceae	0.65 ± 0.12	0.5 ± 0.12	0.58 ± 0.18$^{\$}$	0.20 ± 0.03*
Bacteroidaceae	6.98 ± 1.02	5.57 ± 1.09	2.10 ± 0.45$^{*,\#}$	3.48 ± 0.45*
Porphyromonadaceae	0.62 ± 0.13	0.45 ± 0.16	4.56 ± 1.63$^{*,\#}$	3.74 ± 1.83
Prevotellaceae	0.00 ± 0.00	0.01 ± 0.01	0.02 ± 0.01$^{\$}$	0.23 ± 0.08$^{*,\#}$
Rikenellaceae	5.32 ± 0.42	5.42 ± 0.26	7.69 ± 0.86$^{*,\#}$	7.73 ± 0.75$^{*,\#}$
S24-7	14.77 ± 1.23	7.31 ± 1.45*	8.43 ± 0.64*	7.74 ± 0.94*
Deferribacteraceae	1.16 ± 0.10	1.56 ± 0.28	0.93 ± 0.13$^{\#}$	0.95 ± 0.25$^{\#}$
Clostridiaceae	0.54 ± 0.09$^{\#}$	0.00 ± 0.00	0.59 ± 0.06$^{\#}$	0.41 ± 0.11$^{\#}$
Dehalobacteriaceae	0.26 ± 0.08	0.41 ± 0.07	0.55 ± 0.07*	0.48 ± 0.05*
Lachnospiraceae	4.47 ± 0.57	9.88 ± 0.96*	9.09 ± 0.45*	9.43 ± 0.56*
Peptococcaceae	0.18 ± 0.03	0.49 ± 0.08	0.43 ± 0.04	0.55 ± 0.13
Peptostreptococcaceae	0.00 ± 0.00	0.34 ± 0.13*	0.57 ± 0.04*	0.53 ± 0.11*
Ruminococcaceae	10.63 ± 0.97	14.59 ± 1.98	13.48 ± 0.99	16.94 ± 2.12*
Erysipelotrichaceae	1.64 ± 0.11	1.48 ± 0.53	1.96 ± 0.51$^{\$}$	0.26 ± 0.15$^{*,\#}$
Desulfovibrionaceae	3.55 ± 0.46	9.70 ± 1.65*	8.15 ± 0.85*	9.28 ± 1.41*
Anaeroplasmataceae	0.27 ± 0.09	0.03 ± 0.03	0.32 ± 0.14$^{\#,\$}$	0.04 ± 0.03
Verrucomicrobiaceae	0.96 ± 0.31	0.00 ± 0.00*	0.48 ± 0.36	0.00 ± 0.00*

(Continued)

TABLE 5 | (Continued)

	ND	HFD	HFDh	HFDo
Genus level				
Bifidobacterium	0.65 ± 0.17	0.00 ± 0.00*	0.08 ± 0.05*	0.05 ± 0.05*
Adlercreutzia	0.31 ± 0.05	0.26 ± 0.05	0.18 ± 0.04*	0.19 ± 0.03
Bacteroides	6.98 ± 1.02	5.57 ± 1.09	2.10 ± 0.45*,#	3.48 ± 0.45*
Parabacteroides	0.62 ± 0.13	0.45 ± 0.16	4.56 ± 1.63*,#	3.74 ± 1.83
Prevotella	0.00 ± 0.00	0.01 ± 0.01	0.02 ± 0.01$	0.23 ± 0.08*,#
AF12	1.20 ± 0.22	1.17 ± 0.25	2.51 ± 0.56*,#	2.25 ± 0.36
Mucispirillum	1.16 ± 0.10	1.56 ± 0.28	0.93 ± 0.13#	0.95 ± 0.25#
Dehalobacterium	0.26 ± 0.08	0.41 ± 0.07	0.55 ± 0.07*	0.48 ± 0.05*
Coprococcus	0.38 ± 0.20	0.52 ± 0.20	0.79 ± 0.10	1.08 ± 0.21*
Ruminococcus	1.49 ± 0.12	2.28 ± 0.48*	1.97 ± 0.17	1.65 ± 0.16
Oscillospira	3.97 ± 0.43	6.42 ± 1.12*	4.38 ± 0.33	5.91 ± 0.77
Allobaculum	1.62 ± 0.11	1.45 ± 0.51	1.96 ± 0.51$	0.26 ± 0.15*,#
Bilophila	1.87 ± 0.47	7.09 ± 1.30*	3.52 ± 0.56#	5.61 ± 1.41*
Desulfovibrio	1.26 ± 0.14	1.90 ± 0.35	4.02 ± 0.74*,#	2.78 ± 0.30*
Anaeroplasma	0.27 ± 0.09	0.03 ± 0.03	0.32 ± 0.14#,$	0.04 ± 0.03
Akkermansia	0.96 ± 0.31	0.00 ± 0.00*	0.48 ± 0.36	0.00 ± 0.00*
Species level				
Acidifaciens	1.43 ± 0.24	0.91 ± 0.13	0.93 ± 0.17	0.66 ± 0.18*
Schaedleri	1.16 ± 0.10	1.56 ± 0.28	0.93 ± 0.13#	0.95 ± 0.25#
Gnavus	1.49 ± 0.12	2.28 ± 0.48*	1.97 ± 0.17	1.65 ± 0.16
Flavefaciens	0.45 ± 0.10	0.00 ± 0.00*	0.03 ± 0.02*	0.19 ± 0.09*
Muciniphila	0.96 ± 0.31	0.00 ± 0.00*	0.48 ± 0.36	0.00 ± 0.00*

*The effect of diets on gut microbiota richness and diversity as well as microbiota composition at all taxonomic levels. Mice were fed with normal diet (ND), high fat diet (HFD), high fat diet plus 4% (w/w) of Hanoch (HFDh) or high fat diet plus 4% (w/w) of Hanoch-Oleic (HFDo) for 18 weeks. Values are expressed as mean ± SEM (n = 5). *$p < 0.05$ versus ND group; #$p < 0.05$ versus HFD; $$p < 0.05$ versus HFDo group.*

facilitate the discrepancy in liver-fat deposition between the two peanuts cultivars.

Anti–adenosine monophosphate–activated protein kinase is a crucial regulator known to orchestrate numerous signaling pathways involved in glucose and lipid metabolism. AMPK directs the cellular adjustment and facilitates the transition from anabolic to catabolic pathways, intending to restore energy homeostasis. A previous study has found enhanced AMPK activation following the exposure of myotube cells to oleate (26), purporting similar induction may be accountable for the advantages metabolic impact of high-oleic peanuts over the regular cultivar. However, in contradiction to this surmise, in the liver AMPK was upregulated merely by HFD and in adipose tissue by the combination of HFD and the traditional peanuts, while such induction was failed to be achieved by the addition of HO peanuts to HFD. Although the mechanism responsible for these AMPK activations is not comprehended it is tempting to suggest such activation, at least in the liver, is a consequence of energy shortage subsequent to mitochondrial damage due to fat accumulation. In such context, the absence of AMPK activation in the group supplemented with high-oleate peanuts represents a positive rather than a negative finding with the deduction of adequate energy metabolism in those groups. More studies are needed of course to corroborate this speculation.

Prolonged nuts consumption was also implicated in ameliorating oxidative stress (27). Minor liver inflammation was present in the HFD and HFDh groups, as evident by increased iNOS protein levels and SAA-1 expression in both groups as well as TNFα expression in the latter. A similar expression pattern of pro-inflammatory cytokines was found in adipose tissue. Essentially, in both tissues, HFD-induced inflammation was diminished by the incorporation of high-oleic peanuts into this diet. A recent work conducted on overweight men evaluated the ability of high-oleic peanuts daily consumption (56 gr/day for 4 weeks) combined with a hypocaloric diet to suppress inflammation and oxidative stress. Results fall short of expectation with no identification of such beneficial influences (28). Likewise, controversial results were also obtained from studies that investigated the mitigating effects of diverse nuts on oxidative stress and inflammation. These rebuttals appear to be derived from differences in fundamental parameters including, nut type and cultivar, nut dosage, and population feature of study design (e.g., study duration).

Intense, ongoing research effort is devoted to comprehensively defining the effects of diet on gut microbiota diversity and composition and the consequences of these interoceptive changes on human health. At the phylum level, the current study found a vigorous decrease and increase in Bacteroidetes and Firmicutes phyla, respectively, and consequently elevated Firmicutes/Bacteroidetes (F/B) ratio in all HFD-fed groups.

Alterations in those phyla in response to HFD feeding are well documented in the literature. A greater F/B ratio was measured

in humans and rodents with obesity and related metabolic conditions, giving rise to the posit that this elevation represents a feature of obesity. Yet, this corollary is not compellingly supported by current data, and more research is required to elucidate the metabolic results driven by this increment or what accompanies it (29). Moreover, differences in this ratio between human and animal models of NAFLD were also elucidated (8), further questioning whether a general conclusion regarding its repercussion can be driven. Finally, whether and which of these modifications precede or proceed with metabolic and/or dysbiosis changes are yet to be utterly determined. Consist with this notion, the shift in F/B ratio appears to be, in the main part, attributed to the rise in the Clostridia class of the Firmicutes phyla. A recent study conducted by Petersen et al. (30) suggested Clostridia species diminishes lipid absorption and renders protection from obesity. Thus, the registered elevation in this class may represent a protecting or compensating mechanism aimed to tone down weight gain.

Concerning the observed increase in Proteobacteria in the groups that were fed with HFD with or without peanuts, although the augmented proliferation of this phyla is putative as pathogenic, its role here is hard to define. Several classes of Proteobacteria were found to be associated with intestinal and extra-intestinal diseases (31). Yet, except for Deltaproteobacteria, none of the other families were found to be significantly altered in the present study. Recent work by Apollo et al. suggested enriched levels of Deltaproteobacteria may constitute a part of the gut microbiota alignment to facilitate colonization resistance, a process that aims to impede infection, in previously infected mice. The corollary that arises from Apollo et al., work is that taurine utilization by Deltaproteobacteria alleviates their expansion and sulfide production by these bacteria to subsequently hamper pathogen respiration (32). Accordingly, the expansion of Deltaproteobacteria appears to confer beneficial outcomes under different conditions associated with "leaky-gut" like those occasionally documented in metabolic diseases (33). However, it should be stressed that colonic mucosal damage was also attributed to increased sulfide in individuals with ulcerative colitis (31).

At the family level, peanuts supplementation failed to restore or hinder the negative effect of HFD on the enrichment of the beneficial bacteria Bifidobacteriaceae, s24-7, and Verrucomicrobiaceae. Likewise, these additions were incompetent to inhibit the aberrant robust growth of metabolic diseases/alterations-associated bacteria of Lachnospiraceae and Desulfovibrionaceae families (34). Yet, interesting modifications were indeed registered in the gut microbiota of those groups that should be considered.

Both peanuts added groups demonstrated an adequate Deferribacteraceae and Clostridiaceae abundance despite the propensity increase and the profound decrease, respectively, detected in those families in the HFD-fed group. The enhanced presence of Deferribacteraceae (the only described family of the phylum Deferribacteres) was noted in animal models of obesity or diabetes (35). Data obtained from work conducted in rodents have implicated this phylum as being a part of the pathogenesis in inflammatory circumstances, conjecturing it encourages gut colonization during these conditions (35–37). Of great interest, a flourishment of the mucin-degrader Mucispirillum genus of this phylum was previously associated with gut pathology (36, 37). In the present study, Mucispirillum was the foremost genus of this phylum. Although the Mucispirillum genus did not portentously overgrow following the consumption of HFD, a tendency was disclosed. Essentially, the addition of peanuts to this diet efficaciously resulted in a marked reduction in the Mucispirillum genus.

The notion of imbuing gut barrier capacity following habitual peanuts addition to a HFD is further supported by differences in the levels of families with butyrate-producing/promoting bacteria (directly or indirectly),(38, 39) of Clostridiaceae, Prevotellaceae, Lachnospiraceae, and Ruminococcaceae (34). Whereas the levels of the last two families increased or tended to increase in all HFD treated groups, those of the first were downregulated in HFD-fed mice while remaining unaffected in those that were also supplemented with peanuts. Prevotellaceae presence was enriched merely in the HFDo group, which may imply an additional capacity for butyrogenesis in those mice. The role of butyrate in the gut is decidedly imperative and was shown to promote favorable metabolic and physiological effects, comprising enhanced insulin sensitivity and gut-wall integrity among others (7, 8, 40).

Although it is very tempting to propose these results are representative of a healthier gut in terms of mucus layer integrity in peanuts-fed mice, such an inference cannot yet to be made. Nonetheless, it appears that lower Mucispirillum genus (Schaedleri sp.) abundance along with enhanced butyrate-generation aptitude, observed in the groups that were fed with peanuts-added HFD, represents a consequential attempt to accommodate better barrier capacity under an obesogenic diet.

Two families, namely, Coriobacteriaceae and Erysipelotrichaceae of the Actinobacteria and Firmicutes phyla, respectively, were distinctively altered in the HFDo group where they displayed reduced relative amounts. Coriobacteriaceae can be considered as "pathobiont," a term used to define symbiont who may potentially promote pathology, though only under specific circumstances (41–43). Previous evidence has demonstrated the existence of positive correlations between Coriobacteriaceae and hepatic TG concentrations in C3H/Orl female mice and plasma non-HDL levels in hamsters (43), converging with the notion that this family participates in the host bile acid and lipid metabolism (44). Notably, the role of diminished amounts of Coriobacteriaceae in the HFDo group is hard to determine. Of great interest, lower levels of Erysipelotrichaceaewere distinguished in the HFDo group. Accelerated levels of the Erysipelotrichaceae family were found in HFD-fed mice and humans as well as in mice models of liver injury and colitis-induced diabetes (44–46), thus arguing for the favorable effects of high-oleic peanuts addition to HFD.

CONCLUSION

In summary, data presented here suggest the new high oleic acid cultivar is metabolically superior to the traditional peanut type

and was associated with a better inflammatory state and microbial profile. Nevertheless, the glycemic response failed to be restored by peanuts addition and appeared to be negatively reinforced in those groups, predominantly in the traditional peanut type. Further research is essentially required to further define the impact of this new high-oleic cultivar and to gain a more in-depth insight into the precise underlying mechanisms.

DATA AVAILABILITY STATEMENT

The datasets presented in this study can be found in online repositories. The names of the repository/repositories and accession number(s) can be found below: https://www.ncbi.nlm.nih.gov/, All raw sequence data was uploaded to SRA under the BioProject accession number PRJNA784088.

ETHICS STATEMENT

The animal study was reviewed and approved by the Institutional Animal Care Ethics Committee, The Hebrew University of Jerusalem.

AUTHOR CONTRIBUTIONS

SA-C: data interpretation and original draft preparation. NT-S: performing experiments and acquiring data. NT-S, GZ, RH, NS, and AN: data processing and analyzing. ZM, RH, and GZ: providing support in the experiments. ZM and NT-S: conceptualization and designing. All authors have read and agreed to the published version of the manuscript.

FUNDING

This work was supported by the Israel Ground Nuts Production & Marketing Board.

SUPPLEMENTARY MATERIAL

The Supplementary Material for this article can be found online at: https://www.frontiersin.org/articles/10.3389/fnut.2022.823756/full#supplementary-material

REFERENCES

1. Fruh SM. Obesity: risk factors, complications, and strategies for sustainable long-term weight management. *J Am Assoc Nurse Pract.* (2017) 29:S3–14. doi: 10.1002/2327-6924.12510
2. Targher G, Corey KE, Byrne CD, Roden M. The complex link between NAFLD and type 2 diabetes mellitus — mechanisms and treatments. *Nat Rev Gastroenterol Hepatol.* (2021) 18:599–612. doi: 10.1038/s41575-021-00448-y
3. Torres MCP, Bodini G, Furnari M, Marabotto E, Zentilin P, Giannini EG. Nuts and non-alcoholic fatty liver disease: are nuts safe for patients with fatty liver disease? *Nutrients.* (2020) 12:1–15. doi: 10.3390/nu12113363
4. Azad JB, Daneshzad E, Azadbakht L. Peanut and cardiovascular disease risk factors: a systematic review and meta-analysis. *Crit Rev Food Sci Nutr.* (2020) 60:1123–40. doi: 10.1080/10408398.2018.1558395
5. Alves M, Moreira B, Macedo VS, Bressan J, de Cássia Gonçalves Alfenas R, Mattes R, et al. High-oleic peanuts: new perspective to attenuate glucose homeostasis disruption and inflammation related obesity. *Obesity (Silver Spring).* (2014) 22:1981–8. doi: 10.1002/oby.20825
6. Pd C. Human gut microbiome: hopes, threats and promises. *Gut.* (2018) 67:1716–25. doi: 10.1136/GUTJNL-2018-316723
7. Jasirwan COM, Lesmana CRA, Hasan I, Sulaiman AS, Gani RA. The role of gut microbiota in non-alcoholic fatty liver disease: pathways of mechanisms. *Biosci Microbiota Food Health.* (2019) 38:81. doi: 10.12938/BMFH.18-032
8. Quesada-Vázquez S, Aragonès G, Del Bas JM, Escoté X. Diet, gut microbiota and non-alcoholic fatty liver disease: three parts of the same axis. *Cells.* (2020) 9:176. doi: 10.3390/CELLS9010176
9. Fitzgerald E, Lambert K, Stanford J, Neale EP. The effect of nut consumption (tree nuts and peanuts) on the gut microbiota of humans: a systematic review. *Br J Nutr.* (2021) 125:508–20. doi: 10.1017/S0007114520002925
10. Lamuel-Raventos RM, Onge MPS. Prebiotic nut compounds and human microbiota. *Crit Rev Food Sci Nutr.* (2017) 57:3154–63. doi: 10.1080/10408398.2015.1096763
11. Creedon AC, Hung ES, Berry SE, Whelan K. Nuts and their effect on gut microbiota, gut function and symptoms in adults: a systematic review and meta-analysis of randomised controlled trials. *Nutrients.* (2020) 12:1–21. doi: 10.3390/nu12082347
12. Bimro ET, Hovav R, Nyska A, Glazer TA, Madar Z. High oleic peanuts improve parameters leading to fatty liver development and change the microbiota in mice intestine. *Food Nutr Res.* (2020) 64:1–21. doi: 10.29219/fnr.v64.4278
13. Wang S, Zhang L, Wang D, Huang M, Zhao J, Malik V, et al. Gut microbiota composition is associated with responses to peanut intervention in multiple parameters among adults with metabolic syndrome risk. *Mol Nutr Food Res.* (2021) 65:1–11. doi: 10.1002/mnfr.202001051
14. Zandani G, Anavi-cohen S, Tsybina-shimshilashvili N, Sela N. Broccoli florets supplementation improves insulin sensitivity and alters gut microbiome population — a steatosis mice model induced by high-fat diet. *Front Nutr.* (2021) 8:680241. doi: 10.3389/fnut.2021.680241
15. Zolti A, Green SJ, Ben E, Hadar Y, Minz D. Science of the total environment root microbiome response to treated wastewater irrigation. *Sci Total Environ.* (2019) 655:899–907. doi: 10.1016/j.scitotenv.2018.11.251
16. Callahan BJ, Mcmurdie PJ, Rosen MJ, Han AW, Johnson AJ, Holmes SP. DADA2: high-resolution sample inference from Illumina amplicon data. Nat Methods. (2016) 13:581–3. doi: 10.1038/nmeth.3869.DADA2
17. Gihring TM, Green SJ, Schadt CW. Correspondence massively parallel rRNA gene sequencing exacerbates the potential for biased community diversity comparisons due to variable library sizes. *Environ Microbiol.* (2012) 14:285–90. doi: 10.1111/j.1462-2920.2011.02550.x
18. Ph FID. Ecological diversity indices: any hope for one again? *J Environ Earth Sci.* (2012) 2:45–52.
19. Chusyd DE, Wang D, Huffman DM, Nagy TR. Relationships between rodent white adipose fat pads and human white adipose fat depots. *Front Nutr* (2016) 3:10. doi: 10.3389/fnut.2016.00010
20. Moreira Alves RD, Boroni Moreira AP, Macedo VS, Bressan J, De Cássia Gonçalves Alfenas R, Mattes R, et al. High-oleic peanuts: new perspective to attenuate glucose homeostasis disruption and inflammation related obesity. *Obesity.* (2014) 22:1981–8.
21. Moreira APB, Teixeira TFS, Alves RDM, Peluzio MCG, Costa NMB, Bressan J, et al. Effect of a high-fat meal containing conventional or high-oleic peanuts on post-prandial lipopolysaccharide concentrations in overweight/obese men. *J Hum Nutr Diet.* (2016) 29:95–104. doi: 10.1111/jhn.12284
22. Halvorsen BL, Blomhoff R. Determination of lipid oxidation products in vegetable oils and marine omega-3 supplements. *Food Nutr Res.* (2011) 55:5792. doi: 10.3402/fnr.v55i0.5792
23. Ayala A, Muñoz MF, Argüelles S. Lipid peroxidation: production, metabolism, and signaling mechanisms of malondialdehyde and 4-hydroxy-2-nonenal. *Oxid Med Cell Longev.* (2014) 2014:360438. doi: 10.1155/2014/360438

24. Herzig S, Long F, Jhala US, Hedrick S. CREB regulates hepatic gluconeogenesis through the coactivator PGC-1. *Nature.* (2001) 413:179–83. doi: 10.1038/35093131
25. Lee JM, Han HS, Jung YS, Harris RA, Koo SH, Choi HS. The SMILE transcriptional corepressor inhibits cAMP response element– binding protein (CREB)–mediated transactivation of gluconeogenic genes. *J Biol Chem.* (2018) 293:13125–33. doi: 10.1074/jbc.RA118.002196
26. Salvadó L, Coll T, Gómez-Foix AM, Salmerón E, Barroso E, Palomer X, et al. Oleate prevents saturated-fatty-acid-induced ER stress, inflammation and insulin resistance in skeletal muscle cells through an AMPK-dependent mechanism. *Diabetologia.* (2013) 56:1372–82. doi: 10.1007/s00125-013-2867-3
27. Silveira BKS, da Silva A, Hermsdorff HHM, Bressan J. Effect of chronic consumption of nuts on oxidative stress: a systematic review of clinical trials. *Crit Rev Food Sci Nutr.* (2020) 0:1–12. doi: 10.1080/10408398.2020.1828262
28. Caldas APS, Alves RDM, Hermsdorff HHM, De Oliveira LL, Bressan J. Effects of high-oleic peanuts within a hypoenergetic diet on inflammatory and oxidative status of overweight men: a randomised controlled trial. *Br J Nutr.* (2020) 123:673–80. doi: 10.1017/S0007114519003246
29. Magne F, Gotteland M, Gauthier L, Zazueta A, Pesoa S, Navarrete P, et al. The firmicutes/bacteroidetes ratio: a relevant marker of gut dysbiosis in obese patients? *Nutrients.* (2020) 12:1474. doi: 10.3390/nu12051474
30. Petersen C, Bell R, Klag KA, Lee SH, Soto R, Ghazaryan A, et al. T cell–mediated regulation of the microbiota protects against obesity. *Science.* (2019) 365:eaat9351. doi: 10.1126/science.aat9351
31. Mukhopadhya I, Hansen R, El-Omar EM, Hold GL. IBD-what role do *Proteobacteria* play? *Nat Rev Gastroenterol Hepatol.* (2012) 9:219–30. doi: 10.1038/nrgastro.2012.14
32. Stacy A, Andrade-Oliveira V, McCulloch JA, Hild B, Oh JH, Perez-Chaparro PJ, et al. Infection trains the host for microbiota-enhanced resistance to pathogens. *Cell.* (2021) 184:615.e–27.e. doi: 10.1016/j.cell.2020.12.011
33. Jensen BAH, Marette A. Microbial translocation in type 2 diabetes: when bacterial invaders overcome host defence in human obesity. *Gut.* (2020) 69:1724–6. doi: 10.1136/gutjnl-2020-321288
34. Vacca M, Celano G, Calabrese FM, Portincasa P, Gobbetti M, De Angelis M. The controversial role of human gut lachnospiraceae. *Microorganisms.* (2020) 8:1–25. doi: 10.3390/microorganisms8040573
35. Hoffmann C, Hill DA, Minkah N, Kirn T, Troy A, Artis D, et al. Community-wide response of the gut microbiota to enteropathogenic *Citrobacter rodentium* infection revealed by deep sequencing. *Infect Immun.* (2009) 77:4668–78. doi: 10.1128/IAI.00493-09
36. Albers SV, Siebers B. The family sulfolobaceae. In: Rosenberg E, DeLong EF, Lory S, Stackebrandt E, Thompson F editors. *The Prokaryotes*. (Berlin: Springer) (2014). p. 323–46. doi: 10.1007/978-3-642-38954-2_329
37. Berry D, Schwab C, Milinovich G, Reichert J, Ben Mahfoudh K, Decker T, et al. Phylotype-level 16S rRNA analysis reveals new bacterial indicators of health state in acute murine colitis. *ISME J.* (2012) 6:2091–106. doi: 10.1038/ismej.2012.39
38. Esquivel-Elizondo S, Ilhan ZE, Garcia-Peña EI, Krajmalnik-Brown R. Insights into butyrate production in a controlled fermentation system via. *mSystems.* (2017) 2:e00051–17. doi: 10.1128/mSystems.00051-17
39. Zhang HH, Liu J, Lv YJ, Jiang YL, Pan JX, Zhu YJ, et al. Changes in intestinal microbiota of type 2 diabetes in mice in response to dietary supplementation with instant tea or Matcha. *Can J Diabetes.* (2020) 44:44–52. doi: 10.1016/j.jcjd.2019.04.021
40. Miura K, Ohnishi H. Role of gut microbiota and toll-like receptors in nonalcoholic fatty liver disease. *World J Gastroenterol.* (2014) 20:7381–91. doi: 10.3748/wjg.v20.i23.7381
41. Clavel T, Desmarchelier C, Haller D, Gérard P, Rohn S, Lepage P, et al. Intestinal microbiota in metabolic diseases: from bacterial community structure and functions to species of pathophysiological relevance. *Gut Microbes.* (2014) 5:544–51. doi: 10.4161/gmic.29331
42. Claus SP, Ellero SL, Berger B, Krause L, Bruttin A, Molina J, et al. Colonization-induced host-gut microbial metabolic interaction. *mBio.* (2011) 2:e00271–10. doi: 10.1128/mBio.00271-10
43. Martínez I, Wallace G, Zhang C, Legge R, Benson AK, Carr TP, et al. Diet-induced metabolic improvements in a hamster model of hypercholesterolemia are strongly linked to alterations of the gut microbiota. *Appl Environ Microbiol.* (2009) 75:4175–84. doi: 10.1128/AEM.00380-09
44. Liu H, Zhang H, Wang X, Yu X, Hu C, Zhang X. The family Coriobacteriaceae is a potential contributor to the beneficial effects of roux-en-Y gastric bypass on type 2 diabetes. *Surg Obes Relat Dis.* (2018) 14:584–93. doi: 10.1016/j.soard.2018.01.012
45. Harris JK, El Kasmi KC, Anderson AL, Devereaux MW, Fillon SA, Robertson CE, et al. Specific microbiome changes in a mouse model of parenteral nutrition associated liver injury and intestinal inflammation. *PLoS One.* (2014) 9:e110396. doi: 10.1371/journal.pone.0110396
46. Sorini C, Cosorich I, Lo Conte M, De Giorgi L, Facciotti F, Lucianò R, et al. Loss of gut barrier integrity triggers activation of islet-reactive T cells and autoimmune diabetes. *Proc Natl Acad Sci USA.* (2019) 116:15140–9. doi: 10.1073/pnas.1814558116

Conflict of Interest: The authors declare that the research was conducted in the absence of any commercial or financial relationships that could be construed as a potential conflict of interest.

Publisher's Note: All claims expressed in this article are solely those of the authors and do not necessarily represent those of their affiliated organizations, or those of the publisher, the editors and the reviewers. Any product that may be evaluated in this article, or claim that may be made by its manufacturer, is not guaranteed or endorsed by the publisher.

frontiers | Frontiers in Nutrition

TYPE Original Research
PUBLISHED 04 August 2022
DOI 10.3389/fnut.2022.913729

OPEN ACCESS

EDITED BY
Mariana Carmen Chifiriuc,
University of Bucharest, Romania

REVIEWED BY
Jorge Sánchez-Burgos,
Instituto Tecnológico de Tepic, Mexico
Jacob Folz,
University of California, Davis, United States
Shuang Song,
Dalian Polytechnic University, China

*CORRESPONDENCE
Ai-dong Sun
adsun@bjfu.edu.cn

SPECIALTY SECTION
This article was submitted to Nutrition and Metabolism, a section of the journal Frontiers in Nutrition

RECEIVED 06 April 2022
ACCEPTED 17 June 2022
PUBLISHED 04 August 2022

CITATION
Zhu Y, Wei Y-l, Karras I, Cai P-j, Xiao Y-h, Jia C-l, Qian X-l, Zhu S-y, Zheng L-j, Hu X and Sun A-d (2022) Modulation of the gut microbiota and lipidomic profiles by black chokeberry (*Aronia melanocarpa* L.) polyphenols *via* the glycerophospholipid metabolism signaling pathway. *Front. Nutr.* 9:913729. doi: 10.3389/fnut.2022.913729

Modulation of the gut microbiota and lipidomic profiles by black chokeberry (*Aronia melanocarpa* L.) polyphenols *via* the glycerophospholipid metabolism signaling pathway

Yue Zhu[1,2], Yu-long Wei[1,2], Ioanna Karras[3], Peng-ju Cai[1,2], Yu-hang Xiao[1], Cheng-li Jia[2], Xiao-lin Qian[1,2], Shi-yu Zhu[1,2], Lu-jie Zheng[1,2], Xin Hu[1,2] and Ai-dong Sun[1,2]*

[1]College of Biological Sciences and Technology, Beijing Forestry University, Beijing, China, [2]Beijing Key Laboratory of Forest Food Processing and Safety, Beijing Forestry University, Beijing, China, [3]College of Agricultural, Consumer and Environmental Sciences, University of Illinois at Urbana-Champaign, Urbana, IL, United States

Black chokeberry (*Aronia melanocarpa* L.) is rich in polyphenols with various physiological and pharmacological activities. However, the relationship between the modulation effect of black chokeberry polyphenols on obesity and the alteration of lipid metabolism is not clearly understood. This study aimed to investigate the beneficial effects of the black chokeberry polyphenols (BCPs) treatment on the structure of gut microbiota, lipid metabolism, and associated mechanisms in high-fat diet (HFD)-induced obese rats. Here, we found that a high-fat diet promoted body weight gain and lipid accumulation in rats, while oral BCPs supplementation reduced body weight, liver, and white adipose tissue weight and alleviated dyslipidemia and hepatic steatosis in HFD-induced obese rats. In addition, BCPs supplementation prevented gut microbiota dysbiosis by increasing the relative abundance of *Bacteroides*, *Prevotella*, *Romboutsia*, and *Akkermansia* and decreasing the relative abundance of *Desulfovibrio* and *Clostridium*. Furthermore, 64 lipids were identified as potential lipid biomarkers through lipidomics analysis after BCPs supplementation, especially PE (16:0/22:6), PE (18:0/22:6), PC (20:3/19:0), LysoPE (24:0), LysoPE (24:1), and LysoPC (20:0). Moreover, our studies provided new evidence that composition of gut microbiota was closely related to the alteration of lipid profiles after BCPs supplementation. Additionally, BCPs treatment could ameliorate the disorder of lipid metabolism by regulating the mRNA and protein expression of genes related to the glycerophospholipid metabolism signaling pathway in HFD-induced obese rats. The mRNA and protein expression of PPARα, CPT1α, EPT1, and LCAT were significantly altered after BCPs treatment. In conclusion, the results of this study indicated that BCPs treatment alleviated HFD-induced

obesity by modulating the composition and function of gut microbiota and improving the lipid metabolism disorder *via* the glycerophospholipid metabolism signaling pathway.

KEYWORDS

obesity, high-fat diet, black chokeberry polyphenols extract, gut microbiota, glycerophospholipid metabolism

Introduction

Over the past 15 years, the gut microbiome has been considered an important regulator of host metabolism *via* the modulation of metabolites, including the bile acids, trimethylamine N-oxide, and short-chain fatty acids by mediating the interaction between the gastrointestinal system and other organs (1, 2). Changes in the composition of gut microbiota are associated with many diseases. Obesity, dyslipidemia, type 2 diabetes mellitus (T2DM), and other metabolic diseases are related to dysbiosis of gut microbiota profiles (2). Evidence suggest that obesity and associated metabolic disorders resulted in reduced intestinal microbial richness and diversity and increased the abundance of *Firmicutes* or the ratio of *Firmicutes* to *Bacteroidetes* (F/B ratio) in high-fat diet (HFD)-fed rats (3, 4). Diet is an important external factor affecting the gut microbiota, which is considered an important option for the management of the severity of obesity and related chronic diseases (5). Black chokeberry (*Aronia melanocarpa* L.), known as "superberries," belongs to the Rosaceae family, and originates from the eastern parts of North America and East Canada (6). Black chokeberry has been involved in numerous clinical and animal studies due to its antioxidant properties, which are in turn correlated to the high polyphenol content such as procyanidins, anthocyanins, and phenolic acids (4). In addition, polyphenols components from black chokeberry play a protective role against metabolic disorders, diabetes, and cardiovascular diseases because of

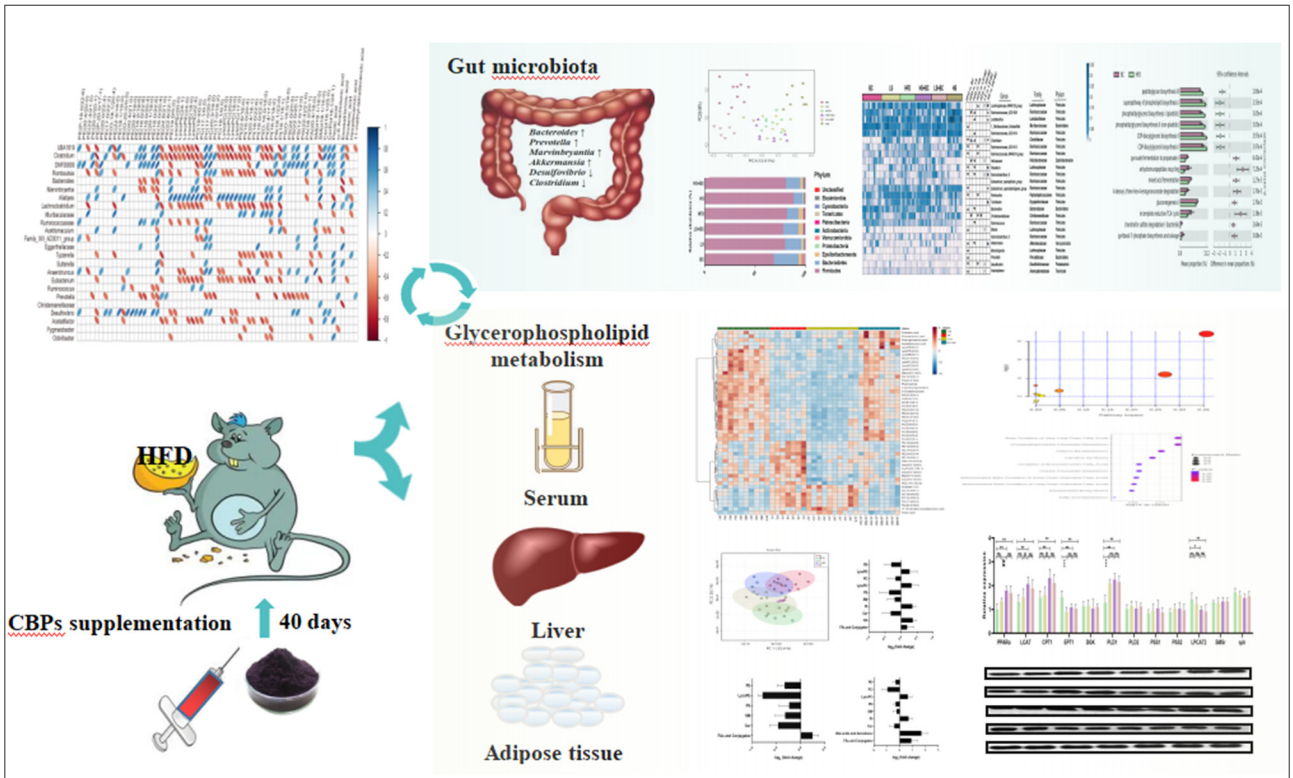

GRAPHICAL ABSTRACT | BCPs supplementation significantly ameliorated obesity and lipid metabolic dysfunctions through regulating gut microbial composition and glycerophospholipid metabolism signaling pathway in HFD-induced rats.

supportive impacts on lipid metabolism, fasting plasma glucose, and blood pressure levels (7, 8). Previous studies have revealed that black chokeberry polyphenols supplementation could decrease the total cholesterol (TC) and triglyceride (TG) levels by altering the related hepatic gene expression in HFD-induced mice (9, 10). Moreover, the fermented black chokeberry supplementation reduced body weight and weight gain in HFD-induced mice (11). However, the mechanism of BCPs in anti-obesity and alleviating lipid metabolism disorder has not been fully elucidated.

As an important subset of metabolomics, lipidomics can be defined as the systematic characterization of lipids and their interactions in the host. Previous studies have demonstrated that lipidomics is a powerful tool to investigate lipid profile changes in some tissues (12, 13). It has been suggested that the profiling of lipidomics is closer to the disease's phenotype than that of genetic, transcriptomic, and proteomic, which may help to identify the key disease-causing regulators and biomarkers for many diseases (14). Therefore, this study aims to investigate the anti-obesity effect of the black chokeberry polyphenols (BCPs) and evaluate the role of the gut microbiota, as well as to perform a comprehensive screen of serum lipidomics, and find potential therapeutic targets and biomarkers in the HFD-induced obese rats.

Materials and methods

Extraction of polyphenols from black chokeberry

The BCPs were extracted in accordance with our previous research (15). Supplementary Table 1 showed the polyphenols profile of the black chokeberry. Briefly, 10 kg frozen black chokeberry were crushed using a beater for 3 min. Then, 13:7 (v/v) ethanol/water solution was added to extract polyphenols. The extraction condition was 45°C for 90 min (simultaneous with 30 min ultrasonic extraction). The solution was centrifuged at 4,000 rpm for 20 min. The supernatant was collected, and ethanol was removed from the supernatant through rotatory evaporation under vacuum at 40°C. The BCPs were then freeze-dried and stored at −80°C.

Animals and experimental design

Wistar male rats, 6 weeks old (weighing 220 ± 20 g), were purchased from the Beijing Vital River Laboratory Animal Technology Co., Ltd. Rats were housed in specific pathogen-free (SPF) conditions and maintained in a temperature-controlled room (24°C, 60% humidity) under a 12 h-light/12 h-dark cycle. All rats were adaptively raised 1 week and randomly divided into two groups: (1) ND group (n = 10), fed with a control diet (10% kcal from fat, 20% kcal from proteins, 70% kcal from carbohydrates), (2) high-fat diet group, fed with a high-fat diet (45% kcal from fat, 20% kcal from proteins, 35% kcal from carbohydrates). After 2 months of continuous feeding, the obese rats model was successfully established. The high-fat diet group rats were randomly divided into five groups: (1) HFD group (n = 8), continually fed with HFD and administered intragastrically normal saline with 2 ml/kg body weight once daily. (2) BC group (n = 10), continually fed with HFD and administered intragastrically BCPs with 1,000 mg/kg body weight once daily. (3) LS group (n = 10), continually fed with HFD and administered intragastrically simvastatin with 5 mg/kg body weight once daily. (4) HS group (n = 8), continually fed with HFD and administered intragastrically simvastatin with 20 mg/kg body weight 1 time daily. (5) LS+BC group (n = 8), continually fed with HFD and administered intragastrically simvastatin with 5 mg/kg and BCPs with 1,000 mg/kg body weight once daily, respectively. (6) HS+BC group (n = 8), continually fed with HFD and administered intragastrically simvastatin with 20 mg/kg and BCPs with 1,000 mg/kg body weight 1 time daily, respectively. Animals had free access to food and water at all times. All of these treatments lasted for 6 weeks and the body weight of rats was measured weekly. At the end of the experimental period, fecal samples were collected and placed in liquid nitrogen and stored at −80°C immediately. Animals were sacrificed with carbon dioxide and blood samples were collected *via* posterior ophthalmic venous plexus. Serum was separated and stored at −80°C for biochemical analysis. The liver, kidney, spleen, heart, lung, pancreas, testicle, epididymal adipose tissue (eWAT), inguinal adipose tissue (iWAT), perirenal adipose tissue (pWAT), and mesentery adipose tissue (mWAT) were immediately removed and weighed using a precision balance. All samples were stored at −80°C for further assays.

Blood and liver biochemical analyses

The serum was melted at 4°C for 1 h. Serum TC, TG, high-density lipoproteincholesterol (HDL-C), low-density lipoproteincholesterol (LDL-C), leptin, alanine aminotransferase (ALT), aspartate aminotransferase (AST), hepatic TC and TG were analyzed using the commercially available kits from Nanjing Jiancheng Bioengineering Institute (Nanjing, China) according to the manufacturer's instructions.

Histopathological examinations

The method of histopathological examinations followed that of the previous study (16, 17). At room temperature, liver, eWAT, and iWAT were fixed in 4% paraformaldehyde for 24 h and then dehydrated with a sequence of ethanol solutions and

embedded in paraffin. Tissue sections (5–6 μm thick) were cut and stained with hematoxylin and eosin (H&E) staining. Hepatocyte and adipocyte sizes were examined under 400× magnification and 200× magnification by a Nikon Eclipse E100 microscope (Nikon, Japan).

Bacterial DNA extraction and 16S RRNA sequencing

Total genome DNA from 300 mg fecal samples was extracted using Magen Hipure Soil DNA Kit following the manufacturer's instructions. NGS library preparations and Illumina MiSeq sequencing were conducted by GENEWIZ, Inc. (Suzhou, China). About 20 ng DNA was used to generate amplification and V3 and V4 hypervariable regions of prokaryotic 16S rDNA were amplified. At the same time, indexed adapters were added to the ends of the 16S rDNA amplicons to generate indexed libraries ready for downstream NGS sequencing on Illumina Miseq. The PCR reactions condition are as follow: 2.5 μl of TransStart Buffer, 2 μl of dNTPs, 1 μl of each primer, and 20 ng of template DNA. Qubit 3.0 Fluorometer was used to confirm the DNA libraries concentration, which quantified the library to 10 nM. DNA libraries were multiplexed and loaded on an Illumina MiSeq instrument according to the manufacturer's instructions (Illumina, San Diego, CA, USA). Sequencing was performed using PE250/300 paired-end, image analysis and base calling were conducted by the MiSeq Control Software (MCS) embedded in the MiSeq instrument.

Lipidomics profiling analysis

Sample preparation

Serum samples (200 μl each) were precipitated by adding 3 volumes of IPA pre-cooled to −20°C and mixed for 1 min. Then, the samples were incubated at room temperature for 10 min and stored overnight at −20°C to improve protein precipitation. After that, the samples were centrifuged at 12,000 g for 20 min. The supernatant was collected and analyzed by HPLC-MS.

Untargeted analysis of serum samples using HPLC-MS

The sample analysis was performed on an ExionLC (SCIEX, USA) coupled with a TripleTOF 5,600+(SCIEX, USA) in both positive and negative ionization modes. The column was a 2.1 × 100 mm, 2.6 μm, C18 100Å column (Phenomenex, CHN), and the temperature was maintained at 45°C. Mobile phase A consisted of H_2O/ACN/MeOH (3:1:1, v:v:v) mixed with 5 mM ammonium acetate and mobile phase B consisted of IPA mixed with 5 mM ammonium acetate. The flow rate was 0.3 ml/min. The injection volume was 2 μl. The separation was conducted under the following gradient: 0 min 30% B; 0–1 min 30% B; 1–14 min 95% B; 14–17 min 95% B; 17–17.1 min 30% B; 17.1–20 min 30% B. The QTOFMS instrument was operated in electrospray ionization by using IDA high-sensitivity scanning mode with the following parameters: curtain gas, 35 psi; ion source gas 1, 60 psi; ion source gas 2, 60 psi; temperature, 600 °C for the positive mode and 550°C for the negative mode; ion spray voltage floating, 5.5 KV for the positive mode and 4.5 KV for the negative node. The scanning time was 20 min; scan range was from 100 to 1,200 m/z for MS scan and 50–1,200 m/z for MS/MS scans. Twelve ions from the MS scan were selected for MS/MS scan. The MS/MS accumulation time was 0.05 s, the collision energy was 40, and the collision energy range is the theoretical frequency ± 20.

Real-time PCR analysis

An RNeasy kit (SinoGene Biotech co., Ltd. China) was used to extract total RNA from the liver and eWAT. Thermo First cDNA Synthesis Kit (SinoGene Biotech co., Ltd. China) was used for reverse transcription. Gene expression was relatively quantified with SYBR green probe using a StepOnePLUS Real-Time PCR System (Thermo Fisher Scientific Inc. Waltham, MA USA). β-actin gene was applied as reference. Primer sequences were listed in Supplementary Table 2.

Western blot analysis

RIPA lysis buffer (P0013B, Beyotime, China) was used to extract the protein in liver tissues. Protein was separated on SDS-PAGE and then transferred to polyvinylidene fluoride (PVDF) membranes. The PVDF membranes were immersed in TBS-Tween containing 5% skimmed milk powder at room temperature on a shaker for 2 h and incubated overnight with primary antibodies at 4°C. The membrane was washed four times and incubated with secondary antibodies for 1 h. The membrane was washed 4 times and the protein bands were visualized using Western Chemiluminescent HRP Substrate (Millipore, USA).

Statistics analysis

Statistical analysis was performed by using SPSS 21 software and GraphPad Prism version 8.4. One-way ANOVA was employed to calculate the differences between multiple groups with Tukey's *post-hoc* test. $p < 0.05$ were considered statistically significant. All data are expressed as the mean ± SEM.

The QIIME data analysis package was used for 16S rRNA data analysis. The forward and reverse reads were joined and assigned to samples based on barcode and then truncated by

cutting off the barcode and primer sequence. Quality filtering on joined sequences was performed and sequences that did not fulfill the following criteria were discarded: sequence length > 200 bp, no ambiguous bases, mean quality score ≥ 20. Then the sequences were compared with the reference database (RDP Gold database) using the UCHIME algorithm to detect chimeric sequences, which were removed. Next, sequences were grouped into operational taxonomic units (OTUs) based on VSEARCH (1.9.6) against the Silva 132 database at a similarity of 97%. The Ribosomal Database Program (RDP) classifier was used to assign a taxonomic category to all OTUs at a confidence threshold of 0.8. α-diversity and β-diversity statistics were calculated in QIIME using the Shannon index, Simpson index, Chao1 index, and ACE. The abundance of annotated OTUs was performed to the linear discriminant analysis (LDA) effect size (LEfSe) online tool (http://huttenhower.sph.harvard.edu/galaxy/root?tool_id=lefse_upload).

The lipidomics raw data were imported to the Progenesis QI (Waters) for peak alignment to obtain a peak list containing the retention time, m/z, and peak area of each sample. Open database sources, including lipid maps, the Human Metabolome Database(HMDB), and the National Institute of Standards and Technology (NIST) were used to identify compounds.

Results

Effect of BCPs treatment on body weight, dyslipidemia, and liver steatosis of HFD-induced obese rats

As shown in Figure 1A, the body weight decreased gradually during BCPs treatment. Compared with the HFD group, weight gain was dramatically reduced in the BC group after 6 weeks ($p < 0.001$) (Figure 1B). The trend of body weight change in the LS+BC group was similar to that in the BC group. The body weight of the HS group and HS+BC group increased slowly and weight gain was 4.87 and 3.80%, respectively, which was not significantly altered compared to the HFD group (Figures 1A,B). However, there was a significant difference in weight gain between the HS group and the HS+BC group ($p < 0.05$). Similar results were also found between the LS group and LS+BC group ($p < 0.05$). Simultaneously, as shown in Table 1, compared to the HFD group, iWAT and pWAT weights were decreased in the six groups. Moreover, only the control group, BC group, and LS+BC group had a lower eWAT and mWAT weight than that of the HFD group. Except for the HS+BC group, the liver weight was reduced in all other groups compared to the HFD group. There were no significant differences in the weight of the heart, kidney, spleen, lung, pancreas, and testicles among these groups (Supplementary Figure 1). Furthermore, we next measured TC and TG concentration and observed H&E staining results in liver and adipose tissues. The TC levels in the liver were significantly reduced in the LS group, HS group, and HS+BC group compared to the HFD group ($p < 0.001$), whereas there was no significant difference in TG levels among the four groups. TC and TG levels were decreased in both the BC group and LS+BC group compared to the HFD group ($p = 0.01$ and $p < 0.05$, respectively) (Table 1). Similarly, H&E staining of liver and white adipose tissues also showed that obese rats treated with BCPs had significantly reduced hepatic fat droplets and adipocyte size (Figure 1C) in the liver, and improving liver steatosis was better than that of low-dose simvastatin treatment alone. Interestingly, increasing the simvastatin concentration did not significantly attenuate liver steatosis and lipid accumulation in white adipose tissues, which was not indicated dose-dependent manner in obese rats.

After 6 weeks of HFD treatment, the serum TC, TG, and LDL-C levels were observably increased and the serum HDL-C levels were decreased in the HFD group compared to the ND group. BCPs treatment significantly attenuated dyslipidemia in obese rats by decreasing the TC, TG, and LDL-C levels and increasing HDL-C levels (Table 1). Both high-dose simvastatin and low-dose simvastatin treatment could dramatically reduce TC and LDL-C levels in obese rats. As previously reported, statin therapy is associated with significantly lower TC and LDL-C levels, which is achieved through inhibiting HMG-CoA reductase activities. However, there was no significant difference in TG and HDL-C levels among the HFD group, LS group, and HS group. Furthermore, in terms of reducing serum TG and increasing HDL-C levels, the effect of low-dose simvastatin combined with BCPs treatment was better than high-dose simvastatin combined with BCPs treatment. In addition, there was no significant difference in serum leptin and ALT levels among these groups, whereas the serum AST level was observably increased in the HS group compared to the other groups.

Effect of BCPs treatment on the gut microbiota of HFD-induced obese rats

16S rRNA gene sequencing was performed to measure the structure and composition of gut microbiota in HFD-induced obese rats. As shown in Supplementary Figure 2, there were no significant differences in the ACE index, Chao1 index, Shannon index, and Simpson index among the six groups (BC group, LS group, HS group, HFD group, LS+BC group, and HS+BC group). To reveal the effect of BCPs treatment on gut microbial structure, principal coordinates analysis (PCoA) based on unweighted Unifrac distance was used to evaluate the structural changes among the six groups (Figure 2A). The PCoA analysis result indicated that gut microbiota structure of the BC group, LS+BC group, and HS group was separated from the HFD group. However, there was no significant

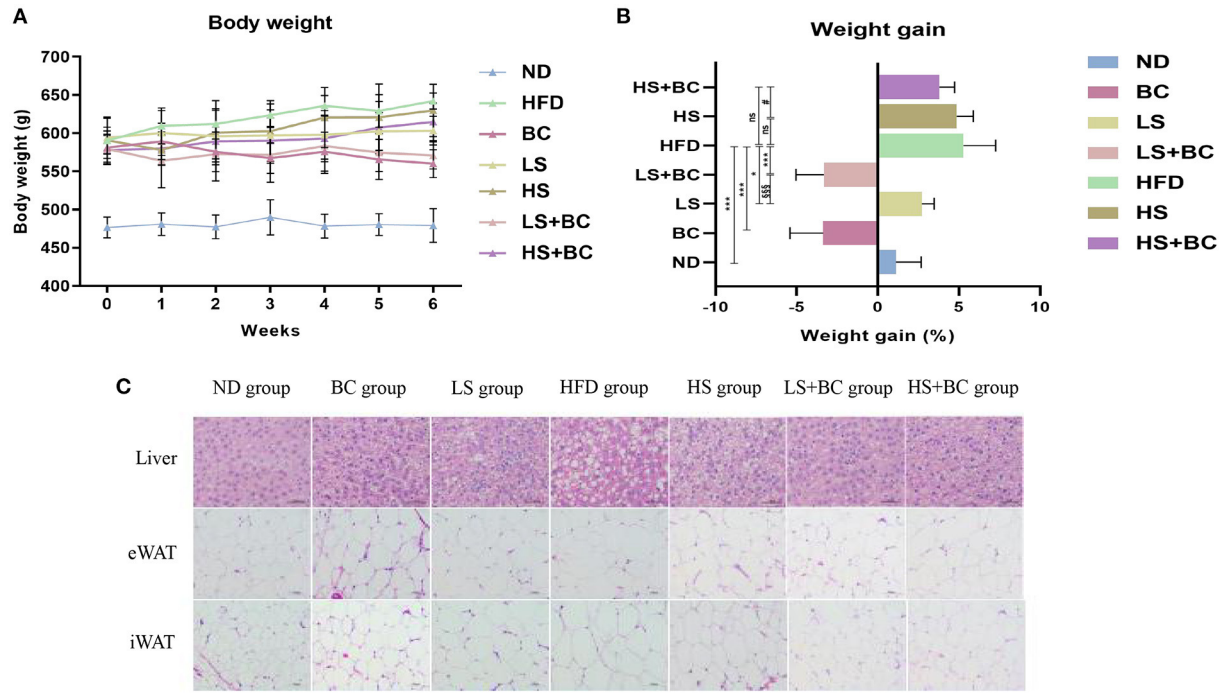

FIGURE 1
Effect of BCPs treatment on body weight and liver steatosis in HFD-induced obese rats. **(A)** body weight (g), **(B)** weight gain (%), **(C)** histological analysis for liver and adipose tissues. Values are means ± SEMs. $^{*}p < 0.05$, $^{**}p < 0.01$ and $^{***}p < 0.001$ when comparing other groups with HFD group, $^{\#}p < 0.05$, $^{\#\#}p < 0.01$, $^{\#\#\#}p < 0.001$ when comparing HS group with HS + BC group, $^{\S}p < 0.05$, $^{\S\S}p < 0.01$, $^{\S\S\S}p < 0.001$ when comparing LS group with LS+BC group.

TABLE 1 The liver weight, adipose tissues weight, liver and serum biochemical concentrations of TC, TG, HDL-C, LDL-C, leptin, AST and ALT in rats.

	ND	HFD	BC	LS	HS	LS+BC	HS+BC
Liver weight (g)	14.16 ± 1.73^{d}	25.75 ± 3.25^{a}	18.61 ± 1.52^{c}	21.29 ± 3.18^{b}	22.62 ± 4.34^{ab}	17.78 ± 2.17^{c}	19.56 ± 2.93^{bc}
eWAT weight (g)	11.75 ± 2.89^{c}	25.68 ± 7.48^{a}	19.48 ± 3.66^{b}	21.85 ± 3.01^{ab}	21.15 ± 5.57^{ab}	20.20 ± 2.33^{b}	20.92 ± 5.41^{ab}
iWAT weight (g)	8.71 ± 5.25^{d}	31.97 ± 6.43^{a}	14.27 ± 3.52^{c}	19.34 ± 4.07^{b}	18.57 ± 5.81^{b}	14.71 ± 2.98^{c}	16.50 ± 3.72^{bc}
pWAT weight (g)	11.91 ± 5.28^{d}	33.06 ± 4.27^{a}	22.84 ± 3.75^{c}	26.96 ± 3.32^{b}	25.81 ± 5.02^{bc}	20.93 ± 4.17^{c}	24.26 ± 5.05^{bc}
mWAT weight (g)	4.92 ± 1.33^{c}	13.30 ± 4.06^{a}	8.49 ± 2.62^{b}	11.35 ± 3.49^{ab}	10.30 ± 2.59^{ab}	8.68 ± 2.01^{b}	9.68 ± 4.39^{b}
Liver TC (mmol/gprot)	0.084 ± 0.02^{d}	0.20 ± 0.02^{a}	0.16 ± 0.02^{b}	0.15 ± 0.02^{b}	0.13 ± 0.01^{c}	0.14 ± 0.01^{bc}	0.13 ± 0.02^{c}
Liver TG (mmol/gprot)	0.25 ± 0.02^{c}	0.33 ± 0.04^{a}	0.26 ± 0.03^{a}	0.31 ± 0.02^{a}	0.34 ± 0.03^{b}	0.28 ± 0.03^{a}	0.31 ± 0.03^{bc}
Serum TC (mmoL/L)	3.19 ± 0.26^{c}	4.56 ± 0.56^{a}	3.67 ± 0.41^{b}	3.14 ± 0.57^{c}	3.32 ± 0.72bc	3.35 ± 0.53^{bc}	3.41 ± 0.62^{bc}
Serum TG (mmoL/L)	1.07 ± 0.22^{c}	1.58 ± 0.24^{a}	1.18 ± 0.21^{b}	1.28 ± 0.18^{ab}	1.60 ± 0.64^{a}	1.17 ± 0.28^{bc}	1.38 ± 0.49^{ab}
Serum HDL-C (mmoL/L)	3.20 ± 0.27^{a}	1.81 ± 0.38^{d}	2.86 ± 0.31^{b}	2.16 ± 0.22^{c}	2.24 ± 0.57^{c}	2.61 ± 0.24^{b}	2.35 ± 0.44^{c}
Serum LDL-C (mmoL/L)	0.72 ± 0.08^{c}	1.47 ± 0.41^{a}	0.88 ± 0.20^{b}	0.82 ± 0.14^{bc}	0.91 ± 0.21^{b}	0.68 ± 0.31^{c}	0.79 ± 0.17^{bc}
Serum leptin(ng/uL)	4.15 ± 0.75	4.90 ± 0.63	5.29 ± 1.02	4.99 ± 0.78	5.02 ± 0.55	4.59 ± 0.48	4.98 ± 0.51
Serum AST(mmoL/L)	426.12 ± 60.23^{b}	456.00 ± 55.14^{b}	470.22 ± 50.41^{b}	463.14 ± 69.17^{b}	568.50 ± 41.32^{a}	414.25 ± 33.57^{b}	396.38 ± 30.25^{b}
Serum ALT(mmoL/L)	44.25 ± 8.76	62.17 ± 7.17	54.25 ± 8.95	51.00 ± 10.89	63.14 ± 6.47	62.50 ± 6.25	68.63 ± 7.25

Data are shown as the mean ± SEM.
eWAT, epididymal adipose tissue; iWAT, inguinal adipose tissue; pWAT, perirenal adipose tissue; mWAT, mesentery adipose tissue.
One-way ANOVA was conducted to compare these groups. Different letters indicate difference between groups.

separation of gut microbiota structure among the LS group, HS+BC group, and HFD group. This result demonstrated that the BCPs treatment, high-dose simvastatin treatment alone, and low-dose simvastatin combined with BCPs treatment significantly influenced the gut microbiota structure in HFD-induced obese rats.

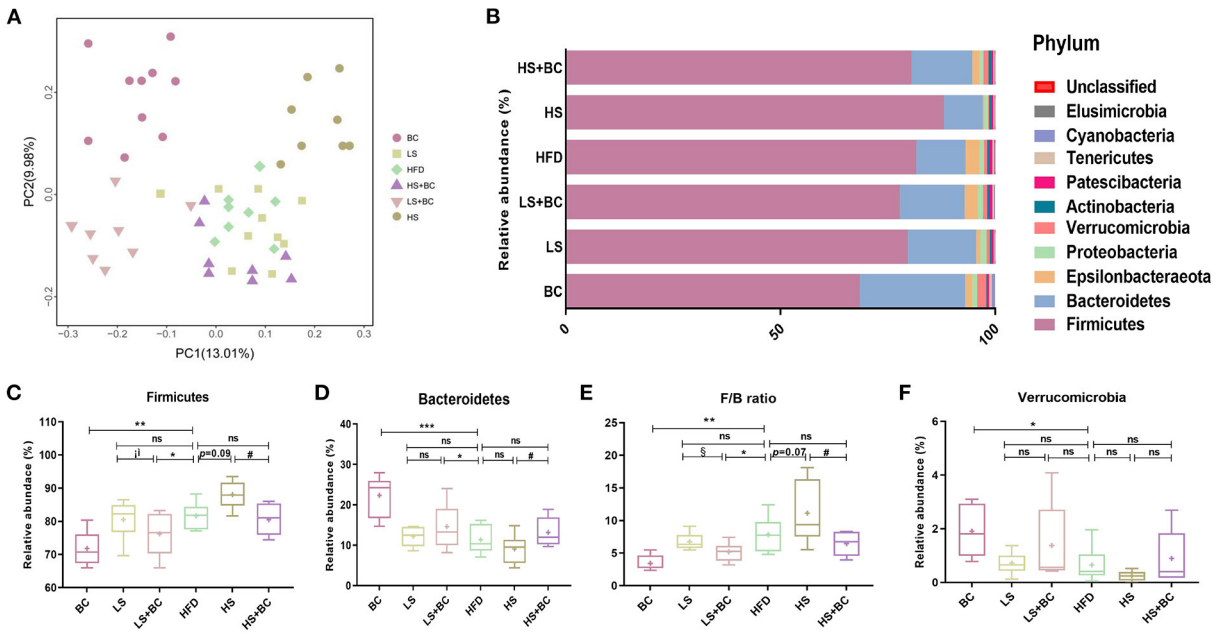

FIGURE 2
Effect of BCPs treatment on gut microbiota structure of phylum level in HFD-induced obese rats. **(A)** Principal coordinates analysis (PCoA) of gut microbiota between the six groups, **(B)** compositional change at the phylum level, **(C–F)** the relative abundance of *Firmicutes*, *Bacteroidetes*, *Verrucomicrobia* and F/B ratio in the six groups. Values are means ± SEMs. $^{*}p < 0.05$, $^{**}p < 0.01$ and $^{***}p < 0.001$ when comparing other groups with HFD group, $^{\#}p < 0.05$, $^{\#\#}p < 0.01$, $^{\#\#\#}p < 0.001$ when comparing HS group with HS+BC group, $^{\S}p < 0.05$, $^{\S\S}p < 0.01$, $^{\S\S\S}p < 0.001$ when comparing LS group with LS+BC group.

At the phylum level, the relative abundance of *Bacteroidetes* increased and the relative abundance of *Firmicutes* decreased in the BC group and LS+BC group compared to the HFD group (Figures 2B–D). Moreover, the F/B ratio markedly decreased in the BC group and LS+BC group compared to the HFD group ($p < 0.01$ and $p < 0.05$, respectively) (Figure 2E). Notably, the relative abundance of *Verrucomicrobia* in the BC group was higher than that of HFD group (Figure 2F). In addition, compared with the HFD group, the relative abundance of *Bacteroidetes, Firmicutes*, *Verrucomicrobia,* and F/B ratio did not change in the LS group, HS group, and HS+BC group (Figures 2C–F). At the genus level, the relative abundance of *Bacteroides*, *Romboutsia*, *Prevotella*, *Akkermansia*, *Marvinbryantia,* and *Anaerofilum* was sharply increased, whereas the relative abundance of *Clostridium*, *Ruminococcaceae_UCG-013*, *Ruminococcaceae_NK4A214_group*, *Roseburia*, *Desulfovibrio*, *Ruminiclostridium_6,* and *Eubacterium_coprostanollgenes_group* was decreased in the BC group compared to the HFD group (Figures 3A,B). Moreover, the relative abundance of *Lachnospiraceae_NK4A136_group*, *Bacteroides*, *Prevotella*, *Romboutsia,* and *Anaerofilum* was increased and the relative abundance of *Ruminococcaceae_UCG-013*, *Ruminococcaceae_NK4A214_group*, *Christensenellaceae,* and *Desulfovibrio* was lowered in LS+BC group compared to the HFD group. The relative abundance of *Ruminococcaceae_UCG-005*, *Clostridium*, *Helicobacter, Ruminiclostridium_6,* and *Christensenellaceae* was significantly changed in the LS group compared to the HFD group. However, there was no significant difference in the relative abundance of genera between the HS+BC group and the HFD group. Furthermore, the relative abundance of beneficial genus *Bacteroides* and *Akkermansia* was reduced and the relative abundance of the conditional pathogenic genus *Clostridium* was increased in the HS group compared to the HFD group.

The LEfSe analysis was used to identify the biomarkers with significant differences between the two groups. As shown in Figure 4A and Supplementary Figure 3A, compared with the BC group, the relative abundance of *Sutterella, Romboutsia*, *Ruminococcaceae_UCG-013*, *UBA1819*, *Anaerotruncus,* and *DNF00809* was altered significantly in the HFD group. However, the relative abundance of *Bacteroides*, *Prevotella,* and *Ruminococcus_1* had significant differences in the BC group compared to the HFD group. Similarly, there was a significant difference in the relative abundance of *Intestinimonas*, *Sutterella, Dubosiella*, *Ruminococcaceae_UCG-005,* and *Ruminococcaceae_NK4A214_group* between the LS+BC group and the HFD group (Figure 4C and Supplementary Figure 3C). In addition, the relative abundance of *Paenalcaligenes* and *Christensenellaceae_r_7_group* were changed between the LS group and HFD group (Figure 4B). Only one genus *Turicibacter* was significantly changed in the HS+BC group

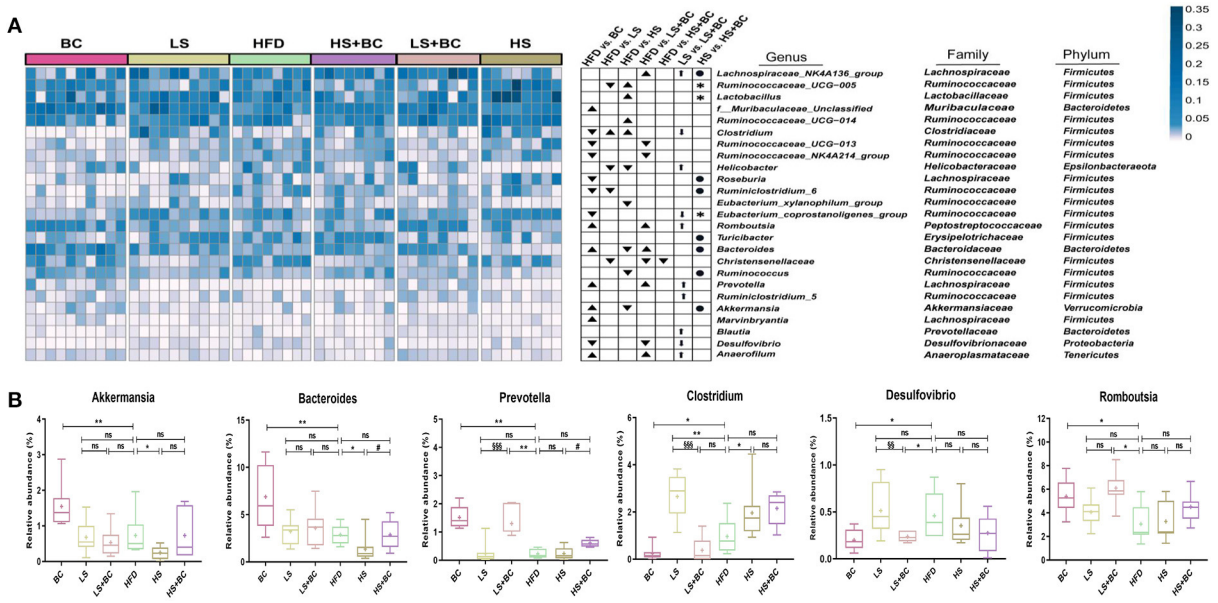

FIGURE 3
Effect of BCPs treatment on gut microbiota structure of genera level in HFD-induced obese rats. **(A)** Heatmap showing the abundance of 25 genera significantly altered after BC treatment; ▲ represent more abundant in BC group, LS group, HS group, LS+BC group and HS+BC group relative to HFD group; ▼ represent less abundant in BC group, LS group, HS group, LS+BC group and HS+BC group relative to HFD group; ↑ represent more abundant in LS+BC group relative to LS group; ↓ represent less abundant in LS+BC group relative to LS group; • represent more abundant in HS+BC group relative to HS group; ✻ represent less abundant in HS+BC group relative to HS group; **(B)** Changes in the relative abundance of representative genera. Values are means ± SEMs. $^{*}p<0.05$, $^{**}p<0.01$ and $^{***}p<0.001$ when comparing other groups with HFD group, $^{\#}p < 0.05$, $^{\#\#}p < 0.01$, $^{\#\#\#}p < 0.001$ when comparing HS group with HS+BC group, $^{\S}p < 0.05$, $^{\S\S}p < 0.01$, $^{\S\S\S}p < 0.001$ when comparing LS group with LS+BC group.

compared to the HFD group (Supplementary Figure 3D). Besides, compared with HFD group, there was no significant difference in the relative abundance of genus level in the HS group (Supplementary Figure 3E). The result was consistent with the above analysis of genus level. Therefore, the results indicated that BCPs combined with high-dose simvastatin treatment, as well as high-dose simvastatin treatment alone failed to alter the composition of beneficial bacteria in the intestine and inhibit obesity. Moreover, PICRUSt analysis was used to predict the function of microbial genes involved in the metabolism pathway in the HFD group, BC group, LS group, and LS+BC group. As shown in Figures 4D–F, the results of the PICRUSt analysis suggested that the CDP-diacylglycerol biosynthesis I pathway, CDP-diacylglycerol biosynthesis II pathway, phosphatidylglycerol biosynthesis I (plastidic) pathway, phosphatidylglycerol biosynthesis II (non-plastidic) pathway and super pathway of phospholipid biosynthesis I pathway were mainly changed in the BC group compared to the HFD group (Figure 4D). The similar result was found between LS+BC group and HFD group (Figure 4F). In the LS group, teichoic acid (poly-glycerol) biosynthesis pathway and peptidoglycan biosynthesis II (staphylococci) pathway were changed compared to the HFD group (Figure 4E). Hence, we assumed that BCPs treatment may improve the disorder of lipid metabolism by reshaping the structure and function of gut microbiota, and further inhibit obesity. Next, untargeted lipidomic analysis was used to explore the effect of BCPs treatment on lipid metabolism in HFD-induced obese rats.

Effect of BCPs treatment on lipid profiles in serum of HFD-induced obese rats

To study the effect of BCPs treatment on lipid profiles in HFD-induced obese rats, we performed untargeted lipidomics analysis in the BC group, LS group, LS+BC group, and HFD group. Based on the OPLS-DA models of lipid profiles in serum, the levels of R^2Y and Q^2 were 99 and 76%, respectively (Supplementary Figure 4A). There was a clear classification between the BC group and the HFD group, demonstrating that lipid profiles were significantly distinguished between the two groups. Similarly, the LS+BC group and HFD group were obviously clustered and the levels of R^2Y and Q^2 were 99 and 80%, respectively (Supplementary Figure 4C). However, the level of the OPLS-DA model in the LS group and HFD group were slightly lower and the values of R^2Y and Q^2 were 92 and 54%, respectively (Supplementary Figure 4B). In addition,

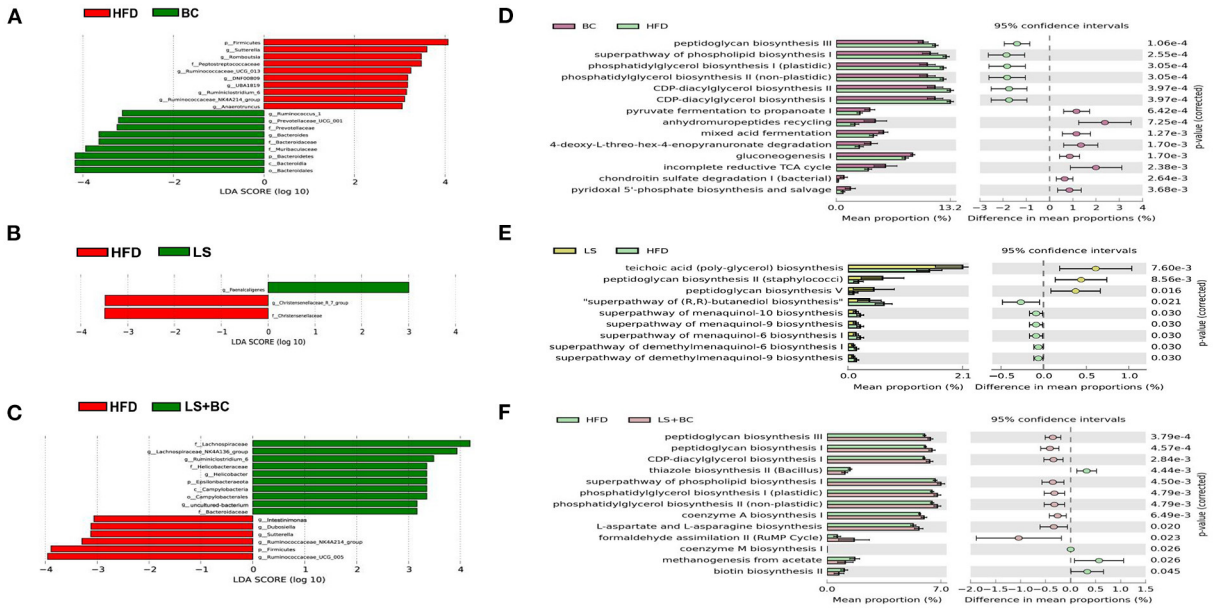

FIGURE 4
Different genera and metabolic pathways were found between BC group, LS group, and LS+BC group. **(A–C)** Linear discriminant analysis (LDA) scores derived from LEfSe analysis, showing the biomarker taxa, **(D–F)** prediction of the function of microbial genes involved in metabolism by PICRUSt analysis and based on the Welch's *t*-test ($p < 0.05$). The colored circles represent the 95% confidence intervals calculated by Welch's inverted method.

principle component analysis (PCA) was performed to analyze the lipidomics data (Figure 5A). The BC group and LS+BC group showed clear trends of separation from the HFD group.

Further, we analyzed the change in metabolites between the two groups using lipidomics analysis and selected metabolites with a VIP (variable importance of projection)>1 and $p < 0.05$. Sixty-four lipid species were significantly changed in the BC group compared to the HFD group and were listed in Supplementary Table 3. Generally, the levels of phosphatidylethanolamine (PE), phosphatidylcholine (PC), phosphatidylserine (PS), sphingomyelin (SM), and Ceramides (Cer) were decreased, whereas the levels of all phosphatidylinositols (PI), phosphatidic acid (PA), lysophosphatidylethanolamine (LysoPE), lysophosphatidylcholine (LysoPC), and fatty acids (FAs) and conjugates were enhanced in the BC group compared to the HFD group (Figure 5B). Furthermore, most of the individual PE species were obviously reduced in the BC group. The levels of PE(16:0/22:6) and PE(18:0/22:6) were significantly lower, while the levels of PE(22:4/19:0), PE(22:4/21:0), PE(22:6/21:0) and PE(22:6/22:1) were increased in the BC group compared to the HFD group (Figure 6A). In addition, seven PS species [PS(12:0/12:0), PS(18:1/20:0), PS(18:0/22:0), PS(20:4/20:0), PS(22:0/20:0), PS(22:0/20:0), and PS(O-16:0/19:0)] and 2 Cer species [Cer(d18:1/24:1) and Cer(d18:1/25:0)] were decreased in the BC group compared to the HFD group. Conversely, nine PI species [PI(16:0/18:1), PI(16:0/18:2), PI(16:0/20:4), PI(18:0/22:6), PI(18:1/18:1), PI(20:4/17:0), PI(20:4/18:1), PI(22:6/16:0) and PI(O-16:0/18:0)] and three PA species [PA(18:2/20:1), PA(20:4/18:0), and PA(22:4/20:1)] were increased after BCPs treatment. Besides, an elevation in serum levels of five LysoPE species [LysoPE(18:0), LysoPE(20:0), LysoPE(22:4), LysoPE(24:0) and LysoPE(24:1)] and four LysoPC species [LysoPC(15:0), LysoPC(17:0), LysoPC(18:0), and LysoPC(20:0)] was observed in the BC group compared to the HFD group. Interestingly, some PC and SM individual species were elevated, such as PC(17:1/0:0), PC(19:1/0:0), PC(19:3/0:0) and SM(d18:1/16:0), while some PC and SM individual species [PC(17:0/18:2), PC(17:0/20:3), PC(20:3/19:0), and SM(d19:1/18:0)] were reduced in the BC group compared to the HFD group. Additionally, eight FAs and conjugates were altered in the BC group. Among them, polyunsaturated fatty acids, octadecadienoic acid, ω-6 arachidonic acid, eicosatrienoic acid, and pinolenic acid, were increased in the BC group (Figure 6A). Notably, 52 individual lipid species in the LS group were notably distinguished compared to the HFD group's species (Supplementary Table 4). Compared to the HFD group, the level of Cer, PE, PS, SM, LysoPE, LysoPC, and FAs, and conjugates were significantly reduced in the LS group (Figure 5C). Specifically, the level of PE(16:0/18:1), PE(16:0/22:6), PE(18:0/22:6), PE(18:1/20:4), and PE(P-18:1/22:6) were obviously decreased in the LS group compared to the HFD group (Fold change (FC)>2) (Figure 6B). In addition, 60 individual lipid species were significantly changed

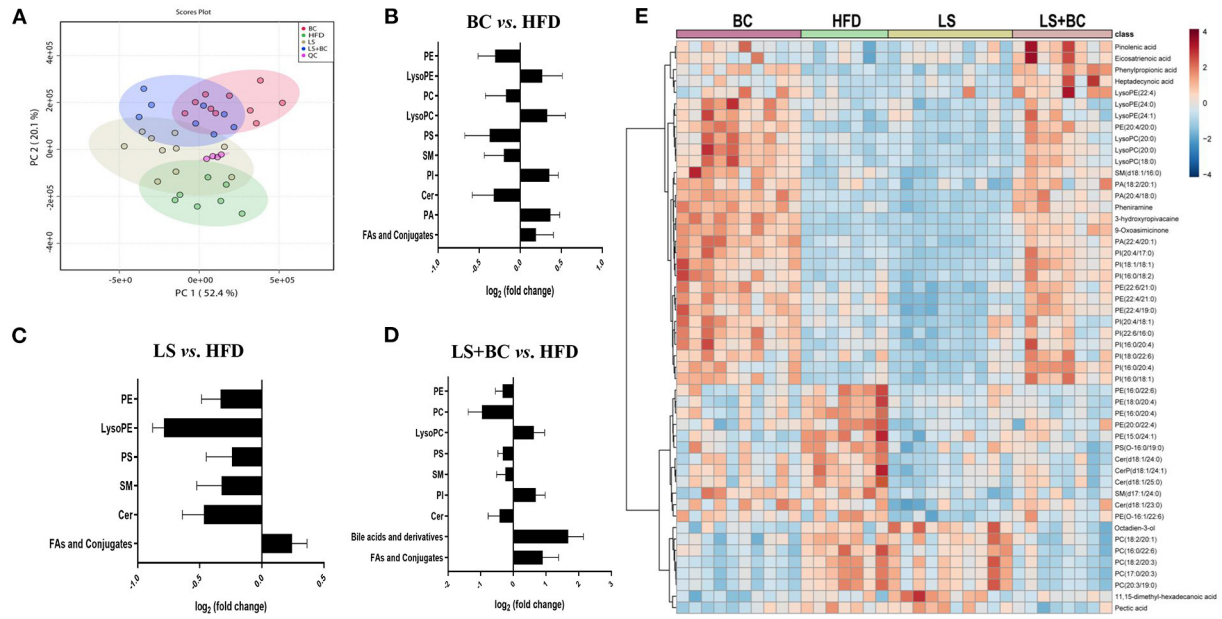

FIGURE 5
Effect of BCPs treatment on lipid profiles of serum in HFD-induced obese rats. **(A)** A two-dimensional principal component analysis (PCA) plot was generated with MetaboAnalyst 4.0 using the peak intensity data, **(B–D)** total lipids in the serum of BC group *vs.* HFD group, LS group *vs.* HFD group and LS+BC group *vs.* HFD group, respectively. The calculation of fold changes was based on the sum of all intensities of identified lipids of each class. **(E)** Heat map and hierarchical clustering of 50 identified differential lipids in the four groups.

in the LS+BC group (Supplementary Table 5). Among of them, PE, PC, PS, SM and Cer species were decreased in the LS+BC group (Figure 5D). In detail, the level of five PE species [PE(16:0/18:1), PE(16:0/20:4), PE(16:0/22:6), PE(18:1/20:4), PE(18:0/22:6)], two PC species [PC(17:0/20:3) and PC(20:3/19:0)] and 2 PS species [PS(12:0/12:0) and PS(O-16:0/19:0)] were significantly reduced (FC>2), whereas the level of 2 LysoPC species [LysoPC(18:0) and LysoPC(20:0)], six PI species [PI(16:0/18:1), PI(16:0/18:2), PI(16:0/20:4), PI(18:1/18:1), PI(20:4/17:0), and PI(22:6/18:1)] and 3 PA species [PA(18:2/20:1), PA(20:4/18:0) and PA(22:4/20:1)] were increased in the LS+BC group compared to the HFD group. Moreover, eight FAs and conjugates and three bile acids and derivatives were higher in the LS+BC group compared to the HFD group. In particular, heptadecanoic acid, eicosatrienoic acid, pinolenic acid, deoxycholic acid, ursodeoxycholic acid, and 12-ketodeoxycholic acid were sharply increased in the LS+BC group compared to the HFD group (FC>2) (Figure 6C).

To show the overall variation in the lipid profiles of the four groups, a heatmap was built and based on the 50 identified endogenous metabolites. As shown in Figure 5E, an obvious separation of the identified lipids was displayed between the four groups. Four FAs and conjugates species (pinolenic acid, eicosatrienoic acid, phenylpropionic acid, and heptadecynoic acid) were increased in the BC group and the LS+BC group. Moreover, a significant number of lipids were up-regulated in the BC group and LS+BC group in comparison with the HFD group and LS group, including three LysoPE species, three LysoPC species, nine PI species, and three PA species. In particular, PE species [(PE(20:4/20:0), PE(22:6/21:0), PE(22:4/21:0), and PE(22:4/19:0)] composed of long-chain high unsaturated fatty acids at the C-1 position were significantly increased in the BC group and LS+BC group, whereas the C-2 position consisting of long-chain high unsaturated fatty acids of six PE species [PE(16:0/22:6), PE(18:0/20:4), PE(16:0/20:4), and PE(20:0/22:4)] were elevated in the HFD group. Moreover, the level of 4 ceramides species [Cer(d18:1/24:0), CerP(d18:1/24:1), Cer(d18:1/25:0), and Cer(d18:1/23:0)] were positively associated with the HFD group. Besides, five PC species and two FAs and conjugates species were also higher in the LS group and BC group, including PC(18:2/20:1), PC(16:0/22:6), PC(18:2/20:3), PC(17:0/20:3), PC(20:3/19:0), 11,15-dimethyl-hexadecanoic acid and pectic acid (Figure 5E).

Furthermore, MetaboAnalyst 4.0 software was used for metabolic pathways analysis and enrichment analysis. The results were shown in Table 2 and Figure 7. Two main pathways, glycerophospholipid metabolism, and sphingolipid metabolism were identified in the BC group and LS+BC group as being associated with the effect on lipid metabolism (Figures 7A,C). Other impacted pathways included beta-oxidation of very long-chain fatty acids, phosphatidylinositol phosphate metabolism, vitamin B6 metabolism, carnitine synthesis, and oxidation of branched chain fatty acids in BC group and LS+BC group (Figures 7D,F). Meanwhile, three main

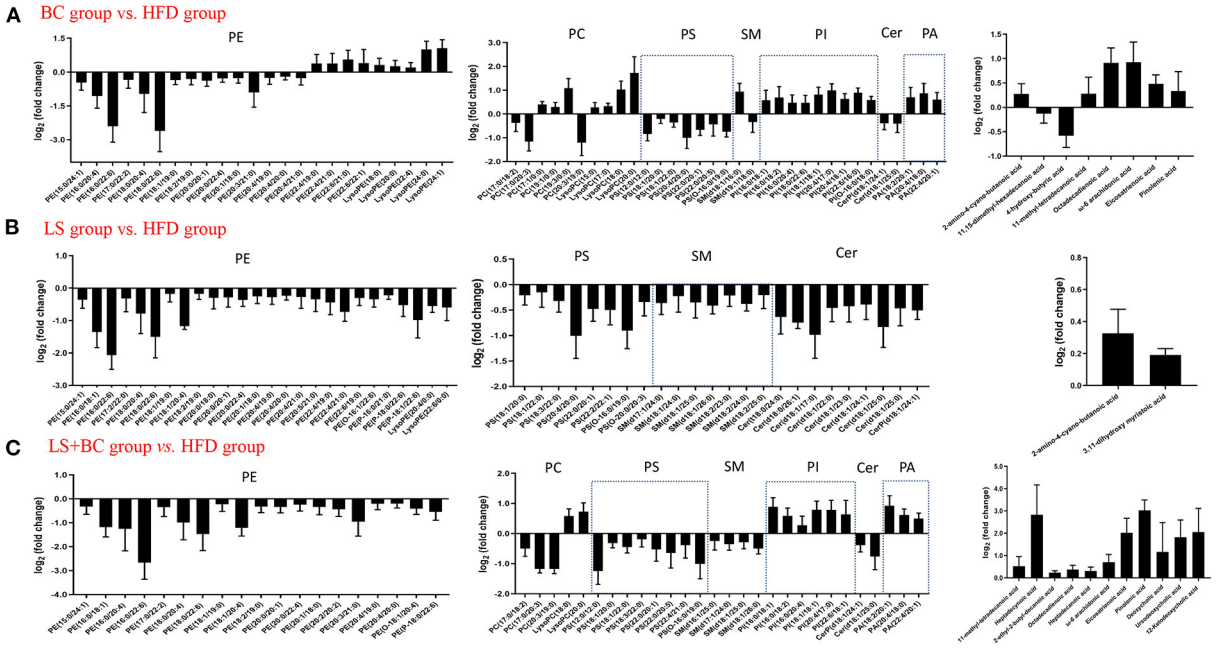

FIGURE 6
Subspecies level analysis of the potential lipid biomarkers responsible for anti-obesity and improving lipid profiling after CBPs treatment. **(A)** BC group *vs.* HFD group, **(B)** LS group *vs.* HFD group, **(C)** LS+BC group *vs.* HFD group. PE, phosphatidylethanolamines; PC, phosphatidylcholines; PS, phosphatidylserine; SM, sphingomyelin; PI, phosphatidylinositol; Cer, ceramides; PA, phosphatidic acids.

pathways were confirmed in the LS group compared to the HFD group, including sphingolipid metabolism, glycerophospholipid metabolism, and pentose and glucuronate interconversions (Figure 7B). The enrichment overview also highlighted the presence of malate-aspartate shuttle, gluconeogenesis, alpha linolenic acid, and linoleic acid metabolism and pentose phosphate pathway in LS group compared with the HFD group (Figure 7E).

The relationship of gut microbiota and serum lipid profiles in HFD-induced obese rats

In order to study the co-variation of the gut microbiota and serum lipid profiles, heatmap visualization of the microbiota-lipid correlations is shown in Figure 8. The statistical correlations were detected between 24 genera of gut microbiota and 64 lipid metabolites between the BC group and HFD group (Figure 8A). The decreased PE and PC species including PE(16:0/20:4), PE(16:0/22:6), PE(18:0/20:4), PE(18:0/22:6), PC(17:0/20:3), and PC(20:3/19:0) were positively correlated with *UBA1819*, *Clostridium*, *DNF00809*, *Ruminococcaceae*, *Desulfovibrio* and negatively correlated with *Bacteroides*, *Muribaculaceae*, and *Prevotella*. Inversely, a positive correlation was detected between five LysoPE species [LysoPE(18:0), LysoPE(20:0), LysoPE(22:4), LysoPE(24:0) and LysoPE(24:1)], 4 LysoPC species [LysoPC(15:0), LysoPC(17:0), LysoPC(18:0) and LysoPC(20:0)], PC(19:3/0:0), PI(20:4/17:0) and *UBA1819*, *Clostridium*, *Lachnoclostridium*, *Eubacterium* in the BC group. Moreover, PE(16:0/18:1), PE(16:0/20:4), PE(16:0/22:6), PE(18:0/22:6), PE(18:1/20:4), PC(17:0/20:3), PC(20:3/19:0) and PS(12:0/12:0) were positively associated with *Pygmaiobacter*, *Ruminococcaceae*, *Parabacteroides* and negatively associated with *Lachnoclostridium* and *Muribaculaceae* in the LS+BC group (Figure 8C). In the LS group, only eight genera were detected to be associated with lipid metabolites. Among them, *Christensenellaceae* and *Pygmaiobacter* were positively correlated with most PE, PS, and Cer species, especially PE(16:0/18:1), PE(16:0/22:6), PE(18:0/22:6), PE(18:0/20:4), and PE(P-18:1/22:6), which were significantly decreased in the LS group compared to the HFD group (Figure 8B).

Effect of BCPs treatment on glycerophospholipid metabolism and sphingolipid metabolism signaling pathway genes and protein expression in liver and adipose tissues of HFD-induced obese rats

To determine the role of BCPs treatment in mediating glycerophospholipid metabolism and sphingolipid metabolism signaling pathway, we evaluated the relative expression

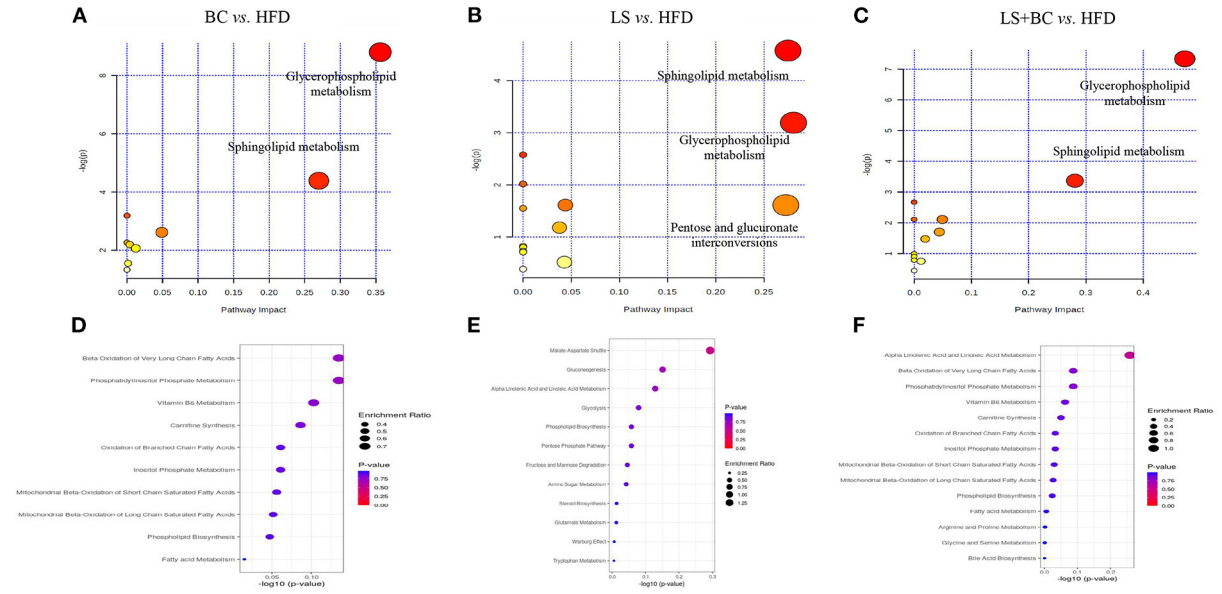

FIGURE 7
Lipid metabolic pathway analysis based on significantly differential lipid species in serum. **(A–C)** All matched pathways are plotted according to *p*-value from pathway enrichment analysis and pathway impact score from pathway topology analysis. The color and size of each circle represented the *p*-value and the pathway impact factor, respectively. **(D–F)** Over Representation Analysis (ORA) is performed and implemented using the hypergeometric test to evaluate whether a particular metabolite set is represented more than expected by chance within the lipid metabolite. One-tailed *p*-values are provided after adjusting for multiple testing. Enrichment ratio is computed by hits / expected. The color and size of each circle represented the *p*-value and the enrichment ratio, respectively.

levels of glycerophospholipid metabolism and sphingolipid metabolism-related genes. In the liver, the mRNA expression level of peroxisome proliferator-activated receptor alpha (PPARα), lecithin:cholesterol-acyl-transferase (LCAT), carnitine palmitoyltransferase 1 (CPT1), and phospholipase D1 (PLD1) were significantly up-regulated, whereas the mRNA expression of ethanolamine phosphotransferase 1 (EPT1) and lysophosphatidylcholine acyltransferase 2 (LPCAT2) was down-regulated in the BC group and LS+BC group compared to the HFD group (Figure 9A). There was no significant difference in the mRNA expression of diacylglycerol kinase (DGK), phospholipase D2 (PLD2), phosphatidylserine synthase 1 (PSS1), phosphatidylserine synthase 2 (PSS2), sphingomyelin synthase (SMS)-related protein (SMSr) and sphingomyelin phosphodiesterase (sph) among the four groups. In addition, after the simvastatin treatment, only PLD1 and EPT1 were significantly altered in HFD-induced obese rats. In eWAT, the mRNA expression of LCAT, DGK, and PLD2 were up-regulated, whereas the mRNA expression of EPT1 was down-regulated in the BC group and LS+BC group compared to the HFD group (Figure 9B). Moreover, BCPs supplementation increased the mRNA expression of PLD1 and reduced the mRNA expression of LPCAT2 and PPARα. After simvastatin treatment, the mRNA expression of EPT1 was lower and the mRNA expression of PPARα and PLD2 was increased in eWAT. Further, in the liver, the protein expression level of PPARα, CPT1, and LCAT was markedly increased and the protein expression level of EPT1 was decreased in the BC group and LS+BC group compared to the HFD group.

Discussion

Obesity is associated with increasing the risk of many metabolic syndromes, including dyslipidemia, hepatic steatosis, inflammation, and other chronic disease symptoms. In this study, we investigated the potential effects of BCPs treatment on obesity and lipid metabolic disorders in HFD-induced obese rats. In particular, our results indicated that BCPs supplementation reduced overall body weight, liver, and white adipose tissue weight, weight gain, and alleviated dyslipidemia and hepatic steatosis in HFD-induced obese rats. Moreover, BCPs supplementation altered the composition and structure of the gut microbiota, which was significantly associated with lipid metabolism in HFD-induced obese rats. Furthermore, lipid classes and individual species were also identified through unbiased lipidomic analysis. Differential lipid metabolites were mainly enriched in glycerophospholipid metabolism and sphingolipid metabolism signaling pathway. Finally, we demonstrated that BCPs treatment significantly changed the mRNA and protein levels of PPARα, LCAT, CPT1, and EPT1 in the glycerophospholipid metabolism signaling pathway, which

TABLE 2 The result of pathway enrichment analysis of plasma in BC group *vs.* HFD group, LS group *vs.* HFD group and LS+BC group *vs.* HFD group*.

Metabolic pathway	BC *vs.* HFD					LS *vs.* HFD					LS+BC *vs.* HFD				
	Total	Hits	Raw p	-log(p)	Impact	Total	Hits	Raw p	-log(p)	Impact	Total	Hits	Raw p	-log(p)	Impact
Glycerophospholipid metabolism	30	4	1.51E-04	8.80E+00	0.36	30	2	4.12E-02	3.19E+00	0.28	30	4	6.52E-04	7.34E+00	0.47
Sphingolipid metabolism	21	2	1.25E-02	4.38E+00	0.27	21	3	1.04E-02	4.57E+00	0.28	21	2	3.45E-02	3.37E+00	0.28
Linoleic acid metabolism	5	1	4.13E-02	3.19E+00	0.00	5	1	7.61E-02	2.58E+00	0.00	5	1	6.94E-02	2.67E+00	0.00
alpha-Linolenic acid metabolism	9	1	1.04E-01	2.26E+00	0.00	9	1	1.33E-01	2.02E+00	0.00	9	1	1.22E-01	2.11E+00	0.00
Glycosylphosphatidylinositol (GPI)- anchor biosynthesis	14	1	1.12E-01	2.19E+00	0.00	14	1	1.99E-01	1.61E+00	0.04	14	1	1.83E-01	1.70E+00	0.04
Arachidonic acid metabolism	36	1	2.64E-01	1.33E+00	0.00	36	1	4.38E-01	8.25E-01	0.00	36	1	4.08E-01	8.97E-01	0.00
Glycerolipid metabolism	16	1	1.27E-01	2.07E+00	0.01	-	-	-	-	-	16	1	2.29E-01	1.47E+00	0.02
Vitamin B6 metabolism	9	1	7.32E-02	2.61E+00	0.05	-	-	-	-	-	9	1	1.22E-01	2.11E+00	0.05
Phosphatidylinositol signaling system	28	1	2.12E-01	1.55E+00	0.00	-	-	-	-	-	-	-	-	-	-
Ascorbate and aldarate metabolism	-	-	-	-	-	9	1	7.61E-02	2.58E+00	0.00	-	-	-	-	-
Pentose and glucuronate interconversions	-	-	-	-	-	14	1	1.99E-01	1.61E+00	0.27	-	-	-	-	-
Terpenoid backbone biosynthesis	-	-	-	-	-	15	1	2.12E-01	1.55E+00	0.00	-	-	-	-	-
Starch and sucrose metabolism	-	-	-	-	-	23	1	3.07E-01	1.18E+00	0.04	-	-	-	-	-
Amino sugar and nucleotide sugar metabolism	-	-	-	-	-	37	1	4.47E-01	8.05E-01	0.00	-	-	-	-	-
Tryptophan metabolism	-	-	-	-	-	41	1	4.82E-01	7.30E-01	0.00	-	-	-	-	-
Drug metabolism - cytochrome P450	-	-	-	-	-	56	1	5.95E-01	5.19E-01	0.04	56	1	3.72E-01	9.89E-01	0.00
Biosynthesis of unsaturated fatty acids	-	-	-	-	-	42	1	4.90E-01	7.12E-01	0.00	42	1	4.58E-01	7.81E-01	0.00
Arginine and proline metabolism	-	-	-	-	-	-	-	-	-	-	44	1	4.74E-01	7.47E-01	0.01
Steroid hormone biosynthesis	-	-	-	-	-	-	-	-	-	-	70	1	6.44E-01	4.41E-01	0.00

*Total is the total number of compounds in the pathway; the Hits is the actually matched number from the user uploaded data; Raw p-value was calculated from the enrichment analysis; the Impact is the pathway impact value calculated from pathway topology analysis.

10.3389/fnut.2022.913729

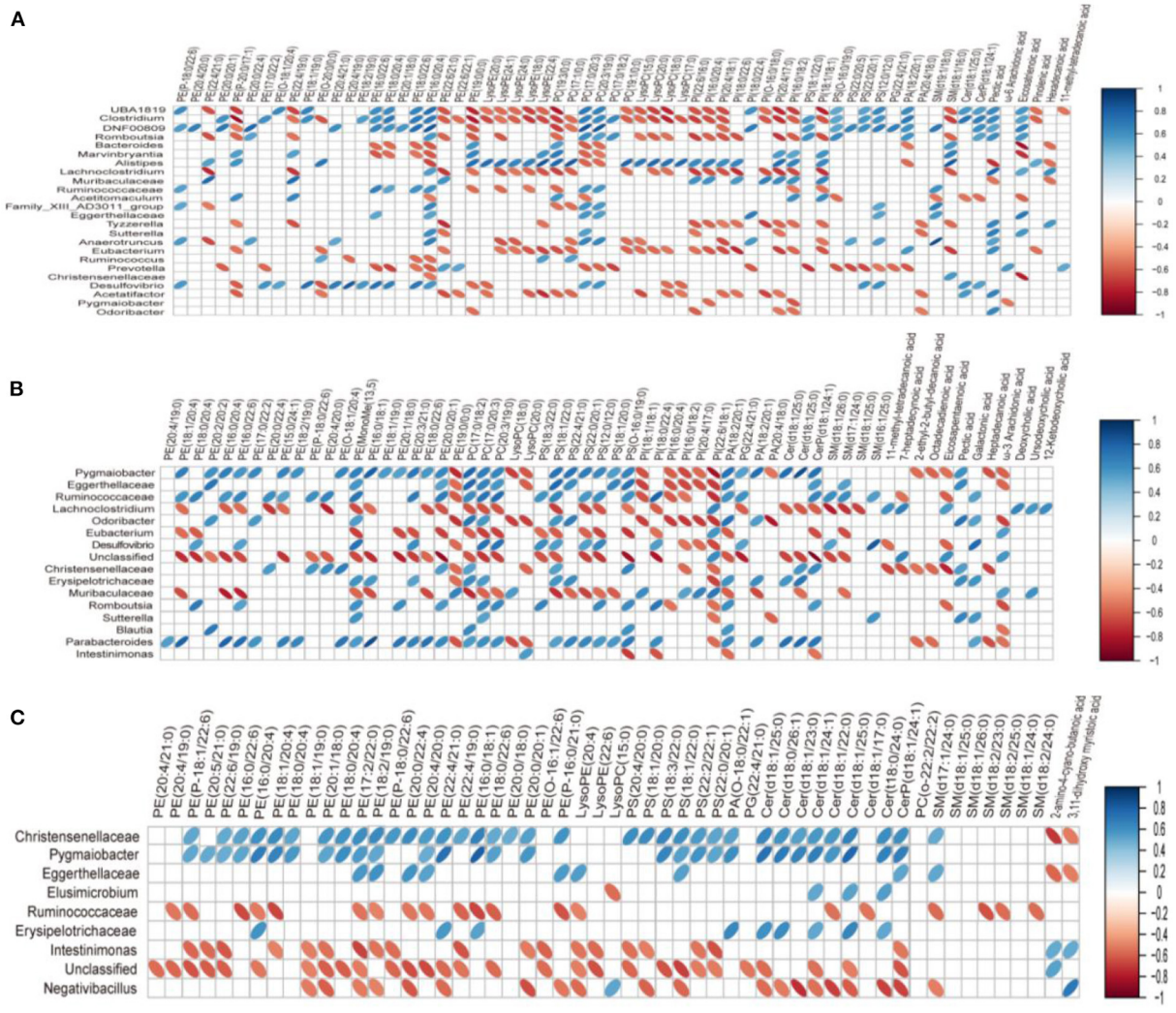

FIGURE 8
Correlation between lipid metabolism and gut microbiota in serum. **(A)** BC group *vs.* HFD group, **(B)** LS group *vs.* HFD group, **(C)** LS+BC group *vs.* HFD group. On the top of the graph is the name of metabolite, and on the left side is the name of association gut microbiota. Blue for positive correlation and red for negative correlation.

might be the underlying mechanisms involving BCPs treatment to alleviate obesity through reshaping gut microbiota and improving lipid metabolism disorders. Meanwhile, the results also indicated that both BCPs treatment alone and BCPs with low-dose simvastatin treatment have positive effects on obesity, which was better than low-dose simvastatin treatment alone.

Specifically, the body weight, liver weight, eWAT weight, iWAT weight, pWAT weight, and mWAT weight were observably decreased after BCPs treatment in HFD-induced obese rats (Figures 1A,B and Table 1). In the liver, BCPs treatment could reduce the TC and TG levels and reverse lipid accumulation. Meanwhile, the level of TC, TG, and LDL-C in serum was lower and the level of HDL-C was higher in the BC group compared to the HFD group (Table 1). Besides, simvastatin was applied as control and decreased the level of TC and LDL-C in serum by inhibiting the endogenous synthesis of cholesterol. Surprisingly, low-dose simvastatin treatment was better than high-dose simvastatin treatment in regard to reducing body weight and liver weight. Moreover, low-dose simvastatin treatment and high-dose simvastatin treatment failed to lower the level of TG and increase the level of HDL-C, which could not effectively alleviate obesity and hepatic steatosis in a dose-dependent manner. However, when BCPs were combined with low-dose simvastatin treatment, the effect of reducing body weight and serum TG level was superior to low-dose simvastatin treatment alone.

Lots of evidence has been gathered in support of the important role that the gut microbiota plays an important role

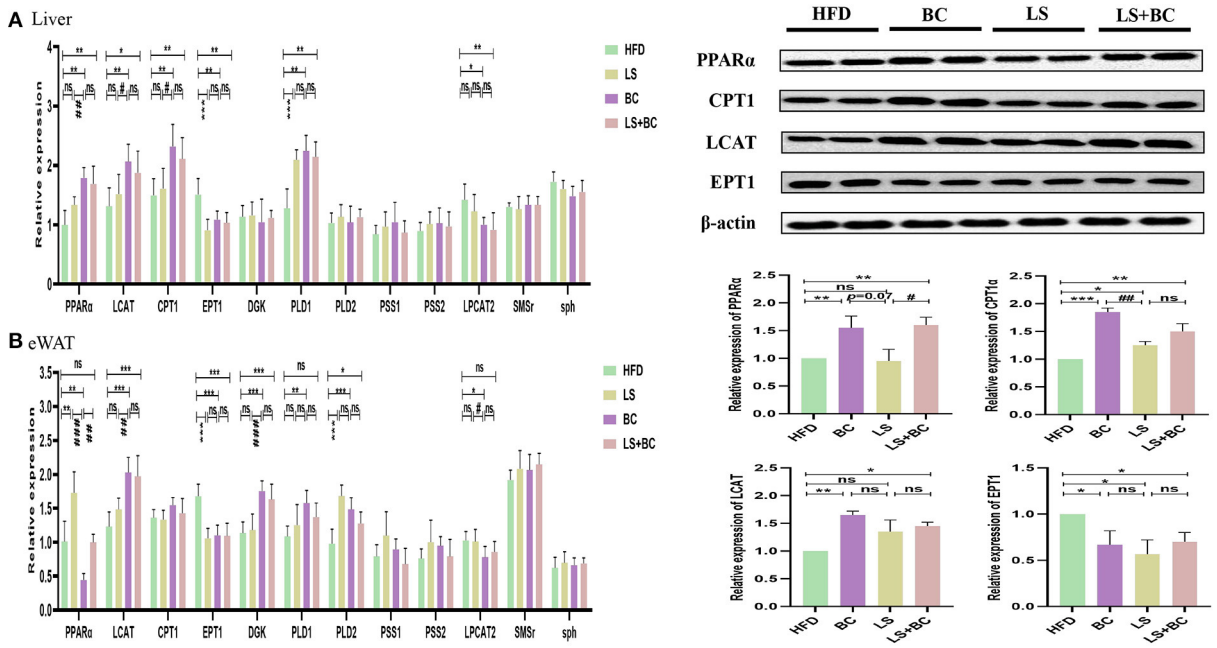

FIGURE 9
Effect of BCPs treatment on hepatic and eWAT gene expression linked to glycerophospholipid metabolism and sphingolipid metabolism in HFD-induced obese rats. The glycerophospholipid metabolism and sphingolipid metabolism pathway related genes were measured and β-actin gene was applied as a reference. **(A)** the mRNA expression in the liver; **(B)** the mRNA expression in the eWAT. The Values are means ± SEMs. $^{*}p < 0.05$, $^{**}p < 0.01$, and $^{***}p < 0.001$ compared with HFD group, $^{\#}p < 0.05$, $^{\#\#}p < 0.01$, $^{\#\#\#}p < 0.001$ compared with BC group.

in the pathogenesis of metabolic diseases such as obesity, insulin resistance, and type 2 diabetes (18). This study specifically evaluated the effect of BCPs treatment on gut microbiota in HFD-induced obese rats. There was no significant difference in the ACE index, Chao1 index, Shannon index, and Simpson index among these groups (Supplementary Figure 2). However, BCPs treatment observably reduced the F/B ratio in obese rats, which has been correlated with obesity and energy metabolic disorders (19). In particular, some reports have shown that several specific genera and/or species of gut microbiota could play a central role in the host's metabolism and obesity. The abundance of species *Bacteroides* and *Prevotella* was inversely associated with obesity and improved insulin sensitivity in mice (20). Furthermore, the fecal microbiota transplantation (FMT) from lean co-twins showed a higher abundance of the *Bacteroides* and *Prevotella*, as well as resulting in an increased level of short-chain fatty acids (2). *Akkermansia* had been identified to have a positive effect in reversing the metabolic disorders caused by a high-fat diet, including insulin resistance, diabetes, and adipose tissue inflammation (21). Henning et al. (22) have demonstrated that *Prevotella* and *Romboutsia* were significantly correlated with weight loss induced by tea extracts. However, the research results of Congying Chen et al. demonstrated that *Prevotella* activated host chronic inflammatory responses and increased host fat deposition significantly in pigs fed with commercial formula diets (23). In this study, the relative abundance of *Bacteroides*, *Prevotella*, *Romboutsia,* and *Akkermansia* were significantly decreased in the HFD group, whereas BCPs treatment could observably change these trends (Figure 3B). Besides, *Desulfovibrio* was one of the conditional pathogenic bacteria, which has been strongly correlated with hepatic inflammation and was enriched in samples of patients with T2DM (24). Compared with the HFD group, the relative abundance of *Desulfovibrio* and *Clostridium* in the BC group was significantly reduced (Figure 3B). The LEfSe results also demonstrated that BCPs treatment markedly improved the relative abundance of *Bacteroides* and *Prevotella* in HFD-induced obese rats (Figure 4A). Therefore, we concluded that alterations in the gut microbiota, especially the relative abundance of *Bacteroides, Prevotella, Romboutsia, and Akkermansia* play a crucial role in the overall beneficial effect of BCPs treatment in alleviating obesity, hepatic steatosis, and dyslipidemia. Additionally, the LEfSe results indicated that simvastatin treatment alone, whether low-dose or high-dose, could not significantly improve the structure of the gut microbiota in HFD-induced obese rats (Figure 4B and Supplementary Figure 3E). Furthermore, high-dose simvastatin treatment even reduced the relative abundance of some beneficial bacteria about inhibiting obesity (*Bacteroides* and *Akkermansia*) and increased the relative abundance of *Clostridium*, which have been positively correlated with obesity (25). We also found

that BCPs combined with low-dose simvastatin treatment were better than low-dose simvastatin treatment alone for improving the structure of gut microbiota. The relative abundance of *Desulfovibrio*, *Ruminococcaceae_UCG-013,* and *Ruminococcaceae_NK4A214_group* was decreased, while the relative abundance of *Bacteroides*, *Prevotella,* and *Romboutsia* was increased in the LS+BC group compared to HFD group (Figure 3B). Shi et al. found that *Ruminococcaceae* was were enriched in the HFD-induced mice (26). Due to the results that BCPs combined with high-dose simvastatin treatment, as well as high-dose simvastatin treatment alone failed to alter the composition of beneficial bacteria in the intestine, we continued to study the anti-obesity effect in the HFD group, BC group, LS group, and LS+BC group. Through the PICRUSt analysis of gut microbiota, we found that the relative abundance of microbial genes involved in lipid metabolism pathways (CDP-diacylglycerol biosynthesis I pathway, CDP-diacylglycerol biosynthesis II pathway, phosphatidylglycerol biosynthesis I (plastidic) pathway, phosphatidylglycerol biosynthesis II (non-plastidic) pathway and super pathway of phospholipid biosynthesis I pathway) was markedly altered in the BC group and LS+BC group compared to the HFD group. Therefore, the next step was to study the effect of BCPs treatment on lipid metabolism in obese rats.

Lipid metabolism pathways are greatly complicated and associated with numerous diseases such as diabetes type 2, hyperlipidemia, obesity, insulin resistance, cardiovascular diseases, and so on (27–29). As traditional lipid risk factors, TC, TG, HDL-C, and LDL-C could not specifically explain the pathogenic mechanism of these diseases. Lipidomics is a new frontier of "omics" research, which provides much promise for a new generation of biomarkers to expand our understanding of the complexity of lipid dysregulation in obesity and metabolic diseases (30). Through serum lipidomics analysis, PE, PC, PS, SM, PI, Cer, LysoPE, LysoPC, and FAs and their conjugates were mainly altered in our study. Among them, the total PE, PC, PS, SM, and Cer species were decreased, whereas the total LysoPC, PI, FAs and conjugates, and secosteroids were elevated in the BC group and LS+BC group compared to the HFD group (Figures 5B,D). Pathway enrichment analysis results showed that differential lipid species were mainly enriched in glycerophospholipid metabolism and sphingolipid metabolism pathway (Figures 7A,C and Table 2). The results indicated that BCPs treatment and BCPs combined with simvastatin treatment may share a similar lipid metabolic signaling pathway (glycerophospholipid metabolism and sphingolipid metabolism) to alleviate the lipid metabolic disorders in HFD-induced obese rats. Furthermore, PC and PE are the most abundant phospholipids in all mammalian cell membranes and are implicated in many metabolic diseases (31). Several studies have found an increased PE level in high-fat diet-induced obese mice and monkeys (32, 33). However, some reports indicated that PE was negatively associated with many diseases, such as hepatic steatosis and diabetes (34). In our study, when the length of the acyl chain at the *sn*-1 position <20 carbons, the level of PE species was decreased in the BC group and LS+BC group. In detail, PE containing polyunsaturated fatty acyl (PUFA) chains at the *sn*-2 position, such as PE(16:0/20:4), PE(16:0/22:6), PE(18:0/20:4), and PE(18:0/22:6), were dramatically decreased in the BC group, LS group, and LS+BC group compared to the HFD group. However, PE (22:4/19:0), PE (22:4/21:0), PE (22:6/21:0), and PE (22:6/22:1) containing 22 carbons at the *sn*-1 position were elevated in the BC group compared to the HFD group (Figure 6A). The results demonstrated that the length and saturation of acyl chains in PE species influenced their biological functions. Similarly, PC species only containing one acyl chain, such as PC(17:1/0:0), PC(19:1/0:0), and PC(19:3/0:0) increased and reduced the risk of obesity in the BC group, whereas PC(17:0/18:2), PC(17:0/20:3), and PC(20:3/19:0) were decreased in the BC group and LS+BC group compared to the HFD group (Figure 6C). Our findings were consistent with previous studies which have demonstrated that specific PE or PC species rather than the total PE or PC levels influence obesity (28).

Moreover, as the important signaling molecules, the LysoPE and LysoPC are derived from PC and PE, respectively. Previous research has demonstrated that LysoPE and LysoPC (LysoPC(18:0), especially) may be negatively associated with risks of hypercholesterolemia and obesity (35, 36). In our study, five LysoPE species and four LysoPC species were increased in the BC group compared to the HFD group. Furthermore, LysoPE(24:0), LysoPE(24:1), LysoPC(18:0), and LysoPC(20:0) were observably increased in the BC group (FC>2) (Figure 6A). Compared to the HFD group, LysoPE species were not significantly altered, while 2 LysoPC species, LysoPC(18:0) and LysoPC(20:0), were significantly higher in the LS+BC group (Figure 6C). Besides, the levels of all LysoPC and LysoPE species were not changed between the LS group and HFD group (Figure 6B). In fact, previous studies have shown that LysoPC in total plasma was primarily contained in HDL particles (37). So we speculated that enrichment in LysoPC species [LysoPC(15:0), LysoPC(17:0), LysoPC(18:0), and LysoPC(20:0)] could result in the increased HDL-C level after BCPs treatment, thereby reducing the risk of obesity and dyslipidemia. In addition, Cer was primarily contained in LDL-C, and inhibition of the Cer biosynthesis pathways has been proven to confer therapeutic benefits in lots of metabolic diseases (38, 39). SM could be synthesized through PC and Cer species and the level of SM in plasma membrane directly influences cholesterol homeostasis (40). The reduction of SM inhibited cholesterol biosynthesis and alleviated LDL-C present in atherosclerotic plaques (41). In our study, the levels of seven SM species, nine Cer species, TC, and LDL-C in serum were simultaneously decreased in the LS group compared to the HFD group (Figure 6B). Previous studies have proven that statin could inhibit the HMG-CoA reductase activities and then decreased the TC and LDL-C levels (42). Here, we present new

evidence for the correlation between simvastatin treatment and hypercholesteremia. Simvastatin treatment may decrease the levels of TC and LDL-C by regulating the SM and Cer metabolic pathways in HFD-induced obese rats. However, few SM and Cer species were altered in the BC group compared to the HFD group. In addition, the levels of PS species were decreased in the BC group, LS group, and LS+BC group compared to the HFD group. Some researchers have indicated that PS was synthesized by base exchange from PC or PE (Figure 10). In our study, most PC and PE species were reduced in the three groups, which may influence the PS synthesis. Interestingly, the levels of PI and PA species were increased in the BC group and LS+BC group compared to the HFD group. PA can be synthesized from 1,2-diacylglycerol (DAG) and converted to PI in two enzymatic steps (43). Shimizu et al. previously reported that body weight gain and the plasma levels of AST and cholesterol were suppressed after oral administration of PI suspension (44). However, serum-based PI exhibited a significant association with bipolar disorder risk and non-alcoholic fatty liver disease (45). Therefore, the effect of PI species on obesity and lipid metabolic disorders needs to be further investigated. Our results indicated that BCPs treatment has a great potential in the alleviation of lipid metabolic disorders in HFD-induced rats.

Furthermore, many studies have demonstrated the relationship between gut microbiota and the homeostasis of lipid metabolism in the host (3, 46). Here, our studies provided new evidence that the composition of gut microbiota was closely related to the lipid profiles after BCPs treatment. The increased relative abundance of *Clostridium*, *Ruminococcaceae_UCG-013,* and *Desulfovibrio* in HFD-induced obese rats were positively correlated with PE(16:0/20:4), PE(16:0/22:6), PE(18:0/20:4), PE(18:0/22:6), PC(17:0/20:3) and PC(20:3/19:0) in the BC group *vs.* HFD group (Figure 8A). However, *Bacteroides*, *Muribaculaceae,* and *Prevotella*, which have been reported to be reduced in obese individuals, were negatively correlated with PE(16:0/20:4), PE(16:0/22:6), PE(18:0/20:4), PE(18:0/22:6), PC(17:0/20:3) and PC(20:3/19:0) in BC group *vs.* HFD group. In addition, LysoPE(20:0), LysoPE(24:1), LysoPE(24:0), LysoPE(18:0), LysoPE(22:4), LysoPC(15:0), LysoPC(20:0), LysoPC(17:0), LysoPC(18:0), PC(19:3/0:0), PI(20:4/17:0) were negatively correlated with *UBA1819*, *Clostridium*, *Lachnoclostridium*, *Eubacterium* in the BC group *vs.* HFD group (Figure 8A). In the LS+BC group *vs.* HFD group, *Lachnoclostridium* and *Muribaculaceae*, which were beneficial to the inhibition of obesity, were negatively associated with PE(16:0/18:1), PE(16:0/20:4), PE(16:0/22:6), PE(18:0/22:6), PE(18:1/20:4), PC(17:0/20:3), PC(20:3/19:0), and PS(12:0/12:0). However, these lipids were positively associated with *Pygmaiobacter*, *Ruminococcaceae*, and *Parabacteroides* (Figure 8C).

To elucidate the underlying molecular mechanism of these effects, mRNA and protein expression levels of glycerophospholipid metabolism and sphingolipid metabolism signaling pathway related genes were measured in liver and adipose tissues. In the liver, the mRNA expression of PPARα and CPT1 were up-regulated in the BC group and LS+BC group compared to the HFD group (Figure 9A). PPARα has been shown to enhance free fatty acid β-oxidation and blunt the development of steatosis (47, 48). PPARα could be activated by natural and synthetic ligands such as PUFAs, eicosanoids, and so on (49). Through lipidomic analysis in serum, the long-chain unsaturated fatty acids (octadecadienoic acid, ω-6 arachidonic acid, eicosatrienoic acid and pinolenic acid) were significantly increased in the BC group and LS+BC group compared to the HFD group, which may induce the PPARα activation. CPT1, as a target gene of PPARα, is an essential enzyme in fatty acid ß-oxidation and is associated with hyperlipemia and obesity (48). Compared with the HFD group, the mRNA expression of PPARα and CPT1 was up-regulated in the BC group. We concluded that BCPs treatment could ameliorate hepatic steatosis *via* the PPARα/CPT1 pathway in HFD-induced obese rats.Moreover, the degradation of DAG occurs through the phosphorylation and cytidine diphosphate diacylglycerol (CDP-DAG) pathway by DGK and EPT1, generating PA and PE, respectively (50, 51). A previous study by Chibalin, A.V. et al. indicated that DAG content was increased and DGK activity was decreased, resulting in impaired insulin signaling and glucose metabolism in patients with type 2 diabetes (52). In our study, the mRNA expression of EPT1 was down-regulated, whereas the mRNA expression of DGK was not significantly altered in the BC group and LS+BC group compared to the HFD group. Besides, the levels of PC and LysoPC were regulated by LCAT and LPCAT2 genes through the "Lands Cycle" (Figure 10) (53). The up-regulated activity of LCAT in obese subjects potentially leads to an increase in circulating LysoPC levels. On the other hand, LPCAT2 is a key component of the Lands Cycle and catalyzes the esterification of LysoPC to form PC. After the BCPs treatment, the mRNA expression of LPCAT2 was inhibited and the mRNA expression of LCAT was increased in the liver, which indicated that more PC was converted to LysoPC. In addition, the available evidence has shown that PLD2 displays the same enzymatic activity as PLD1, catalyzing the hydrolysis of PC to produce free choline and PA. Jonathan Trujillo Viera et al. observed that $PLD1^{-/-}$ and $PLD2^{-/-}$ mice present elevated free fatty acids (FFAs) levels, which promote the development of overweight and diabetes (54). PSS1 and PSS2 catalyze the formation of PS from PE and PC, respectively (55). There was no significant difference in the mRNA expression of PLD1, PSS1, and PSS2 between the BC group and HFD group. Moreover, more DAG may be converted into PC rather than PE by upregulating the mRNA expression of CPT1 and downregulating the mRNA expression of EPT1, and then LysoPC was synthesized from PC through upregulation of the mRNA expression of LCAT and downregulation of the mRNA expression of LPCAT2 in the BC group and LS+BC group. As mentioned above, increased LysoPC content may be

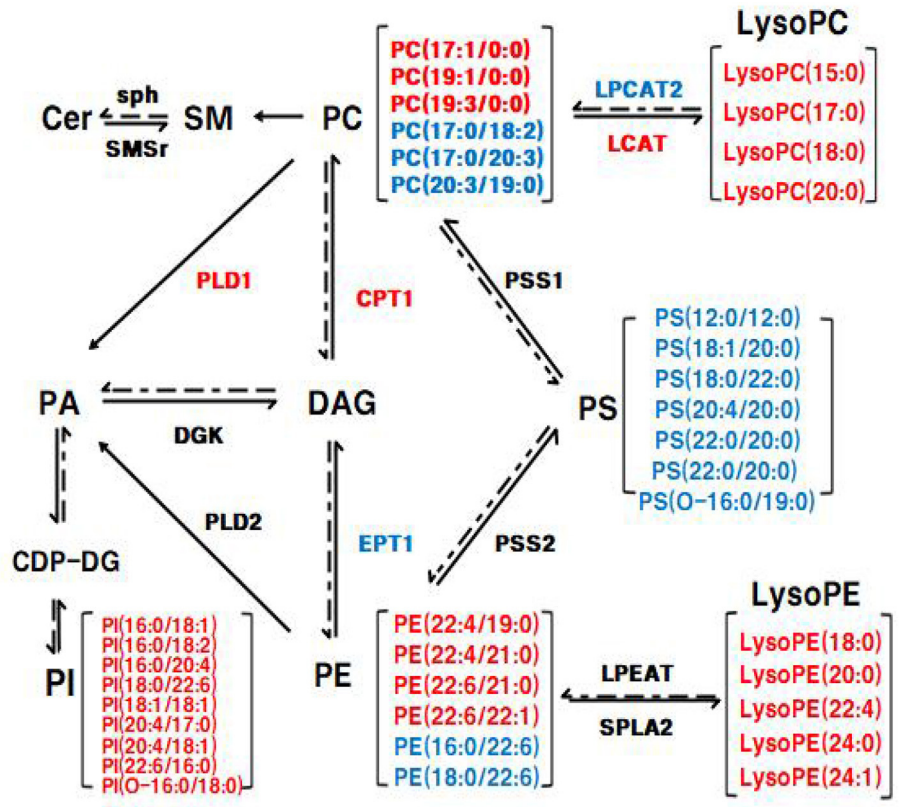

FIGURE 10
The Glycerophospholipid metabolism and sphingolipid metabolism in liver. The mRNA expression of genes in red was up-regulated and the mRNA expression of genes in blue was down-regulated in eWAT, respectively; the lipid level in red was up-regulated and the lipid level in blue was down-regulated in eWAT, respectively.

negatively associated with risks of hypercholesterolemia and obesity (35). In addition, activation of SMSr could increase levels of Cer and Cer were synthesized into SM by sph in the sphingolipid metabolism signaling pathway (56, 57). In our study, there was no significant difference in the mRNA expression of SMSr and sph among these groups. In eWAT, the mRNA expression of glycerophospholipid metabolism signaling pathway genes (LCAT, DGK, PLD1, PLD2) were up-regulated and EPT1 and LPCAT2 were down-regulated in the BC group compared to the HFD group. Furthermore, up-regulation mRNA expression of PLD1, PLD2, and DGK1 demonstrated that PA could be synthesized from PE, PC, and DAG in the BC group (Figure 9B). And then, PA is converted to PI at the endoplasmic reticulum for *De novo* PI synthesis (58). Therefore, in our study, three PA species and nine PI species were increased in the BC group compared to the HFD group (Figure 6A). Although the levels of PS species were decreased, the mRNA expression of PSS1 and PSS2 was not altered in the BC group and further investigation of this potential interaction is needed. Besides, we found that simvastatin treatment failed to change the mRNA expression of glycerophospholipid metabolism signaling pathway genes in the liver. In addition, the effect of BCPs combined with the simvastatin treatment was similar to that of BCPs treatment alone in HFD-induced obese rats, which could improve fat accumulation *via* the PPARα/CPT1 pathway in the liver. Meanwhile, BCPs combined with simvastatin treatment accelerated lipid transformation through up-regulation of the mRNA expression of LCAT, DGK, and PLD2 and down-regulation of the mRNA expression of EPT1 and LPCAT2 in eWAT. Regrettably, we did not identify the characteristic compounds and elucidate the bioconversion pathway after BCPs treatment in HFD-induced rats. It would further explain the anti-obesity mechanism of BCPs and their metabolites in HFD-induced rats.

Conclusion

In summary, these findings revealed that BCPs supplementation significantly alleviated obesity and lipid metabolic dysfunctions in a rats model of HFD-induced obesity. Meanwhile, BCPs supplementation in HFD-induced

obese rats increased the relative abundance of anti-obesity bacteria such as genera *Bacteroides*, *Prevotella, Romboutsia*, and *Akkermansia* and reduced the relative abundance of genera *Desulfovibrio* and *Clostridium*. Moreover, lipidomics analysis indicated that the total number of PE, PC, PS, SM, and Cer species decreased, whereas the total LysoPC, PI, FAs and conjugates, and secosteroids were elevated in the BC group compared to the HFD group. These lipid species, especially PE(16:0/22:6), PE(18:0/22:6), PC(20:3/19:0), LysoPE(24:0), LysoPE(24:1), and LysoPC(20:0), may be candidates for the diagnosis and study of obesity-related diseases. Furthermore, these dominant bacterial taxa altered by BCPs treatment were significantly associated with the lipid metabolic species in HFD-induced obese rats. In addition, the results indicated that BCPs treatment could ameliorate the disorder of lipid metabolism by regulating the mRNA and protein expression of genes related to the glycerophospholipid metabolism pathway in HFD-induced obese rats. The mRNA and protein expression of PPARα, CPT1, EPT1, and LCAT was significantly altered after BCPs treatment. Meanwhile, the effect of BCPs combined with simvastatin treatment on suppressing obesity and improving lipid metabolic disorders was similar to that of BCPs treatment, which was better than simvastatin treatment alone. Our findings provide evidence supporting the beneficial effects of BCPs intake on ameliorating functional disorders related to obesity and lipid metabolism.

Data availability statement

The data presented in the study are deposited in the NCBI Sequence Read Archive (SRA) repository, accession number PRJNA841446.

Ethics statement

The animal study experiments adhered to the China Institutional Animal Care Use Committee and were licensed by the Ethics Committee of Beijing Laboratory Animal Research Center (Qualified number: BLARC-2018-A033).

Author contributions

A-dS and YZ conceived and designed the experiments. YZ performed the experiments. Y-lW, P-jC, IK, X-lQ, L-jZ, S-yZ, and YZ analyzed the data. Y-hX, C-lJ, YZ, XH, and A-dS wrote the paper. All authors read and approved the final manuscript.

Funding

This present investigation was supported by the National Natural Science Foundation of China (31871817 and 32172222) and National Key R&D Plan (2016YFD0400302).

Acknowledgments

The authors wish to acknowledge all the people who participated in the experiment.

Conflict of interest

The authors declare that the research was conducted in the absence of any commercial or financial relationships that could be construed as a potential conflict of interest.

Publisher's note

Supplementary material

The Supplementary Material for this article can be found online at: https://www.frontiersin.org/articles/10.3389/fnut.2022.913729/full#supplementary-material

References

1. Canfora EE, Meex R, Venema K, Blaak EE. Gut microbial metabolites in obesity, NAFLD and T2DM. *Nat Rev Endocrinol.* (2019) 15:261–73. doi: 10.1038/s41574-019-0156-z

2. Tang WHW, Kitai T, Hazen SL. Gut microbiota in cardiovascular health and disease. *Circ Res.* (2017) 120:1183–96. doi: 10.1161/CIRCRESAHA.117.309715

3. Jardon KM, Canfora EE, Goossens GH, Blaak EE. Dietary macronutrients and the gut microbiome: a precision nutrition approach to improve cardiometabolic health. *Gut.* (2022) 71:1214–26. doi: 10.1136/gutjnl-2020-323715

4. Rufino AT, Costa VM, Carvalho F, Fernandes E. Flavonoids as antiobesity agents: a review. *Med Res Rev.* (2021) 41:556–85. doi: 10.1002/med.21740

5. Fernandez-Ruiz I. Modulating the gut microbiota with dietary interventions to protect against cardiometabolic disease. *Nat Rev Cardiol.* (2021) 18:305. doi: 10.1038/s41569-021-00537-0

6. Kulling S, Rawel H. Chokeberry (*Aronia melanocarpa*) - a review on the characteristic components and potential health effects. *Planta Med.* (2008) 74:1625–34. doi: 10.1055/s-0028-1088306

7. Jurikova T, Mlcek J, Skrovankova S, Sumczynski D, Sochor J, Hlavacova I, et al. Fruits of black chokeberry *aronia melanocarpa* in the prevention of chronic diseases. *Molecules.* (2017) 22:944. doi: 10.3390/molecules22060944

8. Cebova M, Klimentova J, Janega P, Pechanova O. Effect of bioactive compound of *Aronia melanocarpa* on cardiovascular system in experimental hypertension. *Oxid Med Cell Longev.* (2017) 2017:1–8. doi: 10.1155/2017/8156594

9. Park H, Liu Y, Kim H, Shin J. Chokeberry attenuates the expression of genes related to de novo lipogenesis in the hepatocytes of mice with nonalcoholic fatty liver disease. *Nutr Res.* (2016) 36:57–64. doi: 10.1016/j.nutres.2015.10.010

10. Jeong O, Kim H. Dietary chokeberry and dried jujube fruit attenuates high-fat and high-fructose diet-induced dyslipidemia and insulin resistance via activation of the IRS-1/PI3K/Akt pathway in C57BL/6 J mice. *Nutr Metab*. (2019) 16:38. doi: 10.1186/s12986-019-0364-5

11. Kim N, Jegal J, Kim YN, Chung D, Heo J, Rho J, et al. Antiobesity effect of fermented chokeberry extract in high-fat diet-induced obese mice. *J Med Food.* (2018) 21:1113–9. doi: 10.1089/jmf.2017.4124

12. Tham YK, Bernardo BC, Huynh K, Ooi JYY, Gao XM, Kiriazis H, et al. Lipidomic profiles of the heart and circulation in response to exercise versus cardiac pathology: A resource of potential biomarkers and drug targets. *Cell Rep.* (2018) 24:2757–72. doi: 10.1016/j.celrep.2018.08.017

13. Yang K, Han X. Lipidomics: techniques, applications, and outcomes related to biomedical sciences. *Trends Biochem Sci.* (2016) 41:954–69. doi: 10.1016/j.tibs.2016.08.010

14. Svati H. Shah WEKA: Related to common cardiovascular diseases: form and function metabolomic profiling for the identification of novel biomarkers and mechanisms. *Circulation.* (2012) 126:1110–20. doi: 10.1161/CIRCULATIONAHA.111.060368

15. Yue Zhu YWJZ. Isolation and identification of procyanidins in aronia melanocarpa using NMR, LC-IT-TOF/MS/MS and MALDI-TOF MS. *J Food Sci Technol.* (2019) 4:614–28. doi: 10.25177/JFST.4.1.RA.444

16. Naguib YM, Samaka RM, Rizk MS, Ameen O, Motawea SM. Countering adipose tissue dysfunction could underlie the superiority of telmisartan in the treatment of obesity-related hypertension. *Cardiovasc Diabetol.* (2021) 20:70. doi: 10.1186/s12933-021-01259-w

17. Ring C, Klopfleisch R, Dahlke K, Basic M, Bleich A, Blaut M. Akkermansia muciniphila strain ATCC BAA-835 does not promote short-term intestinal inflammation in gnotobiotic interleukin-10-deficient mice. *Gut Microbes.* (2019) 10:188–203. doi: 10.1080/19490976.2018.1511663

18. Fan Y, Pedersen O. Gut microbiota in human metabolic health and disease. *Nat Rev Microbiol.* (2020) 19:55–71. doi: 10.1038/s41579-020-0433-9

19. Liang D, Zhang L, Chen H, Zhang H, Hu H, Dai X. Potato resistant starch inhibits diet-induced obesity by modifying the composition of intestinal microbiota and their metabolites in obese mice. *Int J Biol Macromol.* (2021) 180:458–69. doi: 10.1016/j.ijbiomac.2021.02.209

20. Gil-Cardoso K, Ginés I, Pinent M, Ardévol A, Blay M, Terra X. Effects of flavonoids on intestinal inflammation, barrier integrity and changes in gut microbiota during diet-induced obesity. *Nutr Res Rev.* (2016) 29:234–48. doi: 10.1017/S0954422416000159

21. Schroeder BO, Birchenough GMH, Pradhan M, Nyström EEL, Henricsson M, Hansson GC, et al. Obesity-associated microbiota contributes to mucus layer defects in genetically obese mice. *J Biol Chem.* (2020) 295:15712–26. doi: 10.1074/jbc.RA120.015771

22. Henning SM, Yang J, Hsu M, Lee R, Grojean EM, Ly A, et al. Decaffeinated green and black tea polyphenols decrease weight gain and alter microbiome populations and function in diet-induced obese mice. *Eur J Nutr.* (2018) 57:2759–69. doi: 10.1007/s00394-017-1542-8

23. Chen C, Fang S, Wei H, He M, Fu H, Xiong X, et al. Prevotella copri increases fat accumulation in pigs fed with formula diets. *Microbiome.* (2021) 9:175. doi: 10.1186/s40168-021-01110-0

24. Olsson LM, Poitou C, Tremaroli V, Coupaye M, Aron-Wisnewsky J, Bäckhed F, et al. Gut microbiota of obese subjects with prader-willi syndrome is linked to metabolic health. *Gut.* (2020) 69:1229–38. doi: 10.1136/gutjnl-2019-319322

25. Man Zhang JZXZ. Aged citrus peel (chenpi) extract causes dynamic alteration of colonic microbiota in high-fat diet induced obese mice. *Food Funct.* (2020) 11:2667–78. doi: 10.1039/C9FO02907A

26. Shi H, Wang Q, Zheng M, Hao S, Lum JS, Chen X, et al. Supplement of microbiota-accessible carbohydrates prevents neuroinflammation and cognitive decline by improving the gut microbiota-brain axis in diet-induced obese mice. *J Neuroinflamm.* (2020) 17:77. doi: 10.1186/s12974-020-01760-1

27. Garcia-Jaramillo M, Spooner MH, Löhr CV, Wong CP, Zhang W, Jump DB. Lipidomic and transcriptomic analysis of western diet-induced nonalcoholic steatohepatitis (NASH) in female Ldlr $^{-/-}$ mice. *PLoS One.* (2019) 14:e214387. doi: 10.1371/journal.pone.0214387

28. Svegliati-Baroni G, Pierantonelli I, Torquato P, Marinelli R, Ferreri C, Chatgilialoglu C, et al. Lipidomic biomarkers and mechanisms of lipotoxicity in non-alcoholic fatty liver disease. *Free Radical Bio Med.* (2019) 144:293–309. doi: 10.1016/j.freeradbiomed.2019.05.029

29. Markgraf D, Al-Hasani H, Lehr S. Lipidomics—reshaping the analysis and perception of type 2 diabetes. *Int J Mol Sci.* (2016) 17:1841. doi: 10.3390/ijms17111841

30. Rai S, Bhatnagar S. Novel lipidomic biomarkers in hyperlipidemia and cardiovascular diseases: an integrative biology analysis. *J Integr Biol.* (2017) 21:132–42. doi: 10.1089/omi.2016.0178

31. van der Veen JN, Kennelly JP, Wan S, Vance JE, Vance DE, Jacobs RL. The critical role of phosphatidylcholine and phosphatidylethanolamine metabolism in health and disease. *Biochim Biophys Acta Biomembr.* (2017) 1859:1558–72. doi: 10.1016/j.bbamem.2017.04.006

32. Eisinger K, Liebisch G, Schmitz G, Aslanidis C, Krautbauer S, Buechler C. Lipidomic analysis of serum from high fat diet induced obese mice. *Int J Mol Sci.* (2014) 15:2991–3002. doi: 10.3390/ijms15022991

33. Wang J, Zhang L, Xiao R, Li Y, Liao S, Zhang Z, et al. Plasma lipidomic signatures of spontaneous obese rhesus monkeys. *Lipids Health Dis.* (2019) 18:8. doi: 10.1186/s12944-018-0952-9

34. Meikle PJ, Summers SA. Sphingolipids and phospholipids in insulin resistance and related metabolic disorders. *Nat Rev Endocrinol.* (2017) 13:79–91. doi: 10.1038/nrendo.2016.169

35. Nie Q, Xing M, Chen H, Hu J, Nie S. Metabolomics and lipidomics profiling reveals hypocholesterolemic and hypolipidemic effects of arabinoxylan on type 2 diabetic rats. *J Agr Food Chem.* (2019) 67:10614–23. doi: 10.1021/acs.jafc.9b03430

36. Cai X, Liang N, Wang H, Gao A, Xiao R, Yu H. Lipidomic profiles of maternal blood at the earlier stage of gestation and umbilical venous blood in response to supraphysiological hypercholesterolemia versus physiological hypercholesterolemia: An evidence of potential biomarkers and early intervention. *Biochim Biophys Acta Mol Cell Biol Lipids.* (2020) 1865:158587. doi: 10.1016/j.bbalip.2019.158587

37. Ding MRKM. A review of lipidomics of cardiovascular disease highlights the importance of isolating lipoproteins. *Metabolites.* (2020) 10:163–76. doi: 10.3390/metabo10040163

38. Dang VT, Huang A, Zhong LH, Shi Y, Werstuck GH. Comprehensive plasma metabolomic analyses of atherosclerotic progression reveal alterations in glycerophospholipid and sphingolipid metabolism in apolipoprotein e-deficient mice. *Sci Rep.* (2016) 6:35037. doi: 10.1038/srep35037

39. Bikman BT, Summers SA. Ceramides as modulators of cellular and whole-body metabolism. *J Clin Invest.* (2011) 121:4222–30. doi: 10.1172/JCI57144

40. Iqbal J, Walsh MT, Hammad SM, Hussain MM. Sphingolipids and lipoproteins in health and metabolic disorders. *Trends Endocrinol Metab.* (2017) 28:506–18. doi: 10.1016/j.tem.2017.03.005

41. Slotte JP. Biological functions of sphingomyelins. *Prog Lipid Res.* (2013) 52:424–37. doi: 10.1016/j.plipres.2013.05.001

42. Chait A, Ginsberg HN, Vaisar T, Heinecke JW, Goldberg IJ, Bornfeldt KE. Remnants of the triglyceride-rich lipoproteins, diabetes, and cardiovascular disease. *Diabetes.* (2020) 69:508–16. doi: 10.2337/dbi19-0007

43. Lutkewitte AJ, Finck BN. Regulation of signaling and metabolism by lipin-mediated phosphatidic acid phosphohydrolase activity. *Biomolecules.* (2020) 10:1386. doi: 10.3390/biom10101386

44. Shimizu K, Ida T, Tsutsui H, Asai T, Otsubo K, Oku N. Anti-obesity effect of phosphatidylinositol on diet-induced obesity in mice. *J Agr Food Chem.* (2010) 58:11218–25. doi: 10.1021/jf102075j

45. Knowles EE, Meikle PJ, Huynh K, Göring HH, Olvera RL, Mathias SR, et al. Serum phosphatidylinositol as a biomarker for bipolar disorder liability. *Bipolar Disord.* (2017) 19:107–15. doi: 10.1111/bdi.12468

46. Gao H, Wen J, Hu J, Nie Q, Chen H, Xiong T, et al. Fermented Momordica charantia L. juice modulates hyperglycemia, lipid profile, and gut microbiota in type 2 diabetic rats. *Food Res Int.* (2019) 121:367–78. doi: 10.1016/j.foodres.2019.03.055

47. Shi Y, Zou Y, Shen Z, Xiong Y, Zhang W, Liu C, et al. Trace elements, PPARs, and metabolic syndrome. *Int J Mol Sci.* (2020) 21:2612. doi: 10.3390/ijms21072612

48. Gross B, Pawlak M, Lefebvre P, Staels B. PPARs in obesity-induced T2DM, dyslipidaemia and NAFLD. *Nat Rev Endocrinol.* (2017) 13:36–49. doi: 10.1038/nrendo.2016.135

49. Montaigne D, Butruille L, Staels B. PPAR control of metabolism and cardiovascular functions. *Nat Rev Cardiol.* (2021) 18:809–23. doi: 10.1038/s41569-021-00569-6

50. Massart J, Zierath JR. Role of diacylglycerol kinases in glucose and energy homeostasis. *Trends Endocrinol Metab.* (2019) 30:603–17. doi: 10.1016/j.tem.2019.06.003

51. Yasuhiro Horibata OEAE. Ethanolamine phosphotransferase 1 (selenoprotein I) is critical for the neural development and maintenance of plasmalogen in human. *J Lipid Res.* (2018) 59:1015–26. doi: 10.1194/jlr.P081620

52. Chibalin AV, Leng Y, Vieira E, Krook A, Björnholm M, Long YC, et al. Downregulation of diacylglycerol kinase delta contributes to hyperglycemia-Induced insulin resistance. *Cell.* (2008) 132:375–86. doi: 10.1016/j.cell.2007.12.035

53. Wang B, Tontonoz P. Phospholipid remodeling in physiology and disease. *Annu Rev Physiol.* (2019) 81:165–88. doi: 10.1146/annurev-physiol-020518-114444

54. Trujillo Viera J, El-Merahbi R, Nieswandt B, Stegner D, Sumara G. Phospholipases D1 and D2 suppress appetite and protect against overweight. *PLoS ONE.* (2016) 11:e157607. doi: 10.1371/journal.pone.0157607

55. Hermansson M, Hokynar K, Somerharju P. Mechanisms of glycerophospholipid homeostasis in mammalian cells. *Prog Lipid Res.* (2011) 50:240–57. doi: 10.1016/j.plipres.2011.02.004

56. Jeśko H, Wencel PL, Wójtowicz S, Strosznajder J, Lukiw WJ, Strosznajder RP. Fingolimod affects transcription of genes encoding enzymes of ceramide metabolism in animal model of Alzheimer's disease. *Mol Neurobiol.* (2020) 57:2799–811. doi: 10.1007/s12035-020-01908-3

57. Zhang Y, Takagi N, Yuan B, Zhou Y, Si N, Wang H, et al. The protection of indolealkylamines from LPS-induced inflammation in zebrafish. *J Ethnopharmacol.* (2019) 243:112122. doi: 10.1016/j.jep.2019.112122

58. Gerald RV, Hammond EB. Novel roles of phosphoinositides in signaling, lipid transport, and disease. *Curr Opin Cell Biol.* (2020) 63:57–67. doi: 10.1016/j.ceb.2019.12.007

frontiers | Frontiers in Nutrition

TYPE Original Research
PUBLISHED 29 August 2022
DOI 10.3389/fnut.2022.929446

OPEN ACCESS

EDITED BY
Manfredi Rizzo,
University of Palermo, Italy

REVIEWED BY
Francesco Suriano,
University of Gothenburg, Sweden
Maomao Zeng,
Jiangnan University, China

*CORRESPONDENCE
Stephen A. Watts
sawatts@uab.edu

SPECIALTY SECTION
This article was submitted to Nutrition and Metabolism, a section of the journal Frontiers in Nutrition

RECEIVED 26 April 2022
ACCEPTED 26 July 2022
PUBLISHED 29 August 2022

CITATION
Chehade SB, Green GBH, Graham CD, Chakraborti A, Vashai B, Moon A, Williams MB, Vickers B, Berryhill T, Van Der Pol W, Wilson L, Powell ML, Smith DL Jr, Barnes S, Morrow C, Mukhtar MS, Kennedy GD, Bibb JA and Watts SA (2022) A modified standard American diet induces physiological parameters associated with metabolic syndrome in C57BL/6J mice. *Front. Nutr.* 9:929446. doi: 10.3389/fnut.2022.929446

A modified standard American diet induces physiological parameters associated with metabolic syndrome in C57BL/6J mice

Sophie B. Chehade[1], George B. H. Green[1], Christopher D. Graham[1], Ayanabha Chakraborti[2], Bijal Vashai[2], Amber Moon[2], Michael B. Williams[1], Benjamin Vickers[2], Taylor Berryhill[3], William Van Der Pol[4], Landon Wilson[5], Mickie L. Powell[1], Daniel L. Smith Jr.[6], Stephen Barnes[3], Casey Morrow[7], M. Shahid Mukhtar[1], Gregory D. Kennedy[2], James A. Bibb[2] and Stephen A. Watts[1]*

[1]Department of Biology, University of Alabama at Birmingham, Birmingham, AL, United States, [2]Department of Surgery, University of Alabama at Birmingham, Birmingham, AL, United States, [3]Comprehensive Cancer Center, University of Alabama at Birmingham, Birmingham, AL, United States, [4]Center for Clinical and Translational Science, University of Alabama at Birmingham, Birmingham, AL, United States, [5]Department of Pharmacology and Toxicology, University of Alabama at Birmingham, Birmingham, AL, United States, [6]Department of Nutrition Sciences, Nutrition Obesity Research Center, University of Alabama at Birmingham, Birmingham, AL, United States, [7]Department of Cell, Developmental, and Integrative Biology, University of Alabama at Birmingham, Birmingham, AL, United States

Investigations into the causative role that western dietary patterns have on obesity and disease pathogenesis have speculated that quality and quantity of dietary fats and/or carbohydrates have a predictive role in the development of these disorders. Standard reference diets such as the AIN-93 rodent diet have historically been used to promote animal health and reduce variation of results across experiments, rather than model modern human dietary habits or nutrition-related pathologies. In rodents high-fat diets (HFDs) became a classic tool to investigate diet-induced obesity (DIO). These murine diets often relied on a single fat source with the most DIO consistent HFDs containing levels of fat up to 45-60% (kcal), higher than the reported human intake of 33–35% (kcal). More recently, researchers are formulating experimental animal (pre-clinical) diets that reflect mean human macro- and micronutrient consumption levels described by the National Health and Nutrition Examination Survey (NHANES). These diets attempt to integrate relevant ingredient sources and levels of nutrients; however, they most often fail to include high-fructose corn syrup (HFCS) as a source of dietary carbohydrate. We have formulated a modified Standard American Diet (mSAD) that incorporates relevant levels and sources of nutrient classes, including dietary HFCS, to assess the basal physiologies associated with mSAD consumption. Mice proffered the mSAD for 15

weeks displayed a phenotype consistent with metabolic syndrome, exhibiting increased adiposity, fasting hyperglycemia with impaired glucose and insulin tolerance. Metabolic alterations were evidenced at the tissue level as crown-like structures (CLS) in adipose tissue and fatty acid deposition in the liver, and targeted 16S rRNA metagenomics revealed microbial compositional shifts between dietary groups. This study suggests diet quality significantly affects metabolic homeostasis, emphasizing the importance of developing relevant pre-clinical diets to investigate chronic diseases highly impacted by western dietary consumption patterns.

KEYWORDS

obesity, metabolic syndrome, Western Diet, high fructose corn syrup, high fat diet

Introduction

Obesity and related metabolic syndrome (MetS) are widespread in developed countries. Dietary consumption patterns generally referred to as the "Western Diet" (WD) have been scrutinized as possible causes of MetS (1, 2). The WD is characterized by increased consumption of processed foods, added sugars, saturated fat, sodium, and a high ratio of omega-6: omega-3 polyunsaturated fatty acids (PUFAs). The WD pattern is typically low in fibrous fruits and vegetables (3). From 1970 to 2003, the average daily calorie intake increased by 523 kcal with a concomitant 63% increase in consumption of animal fats and vegetable oils as well as a 19% increase of sugars (4). The quantity and quality of these dietary fats and sugars have been investigated as possible causes of diet-related health disorders (5, 6).

Understanding the etiology of MetS is paramount to identifying and treating at-risk populations. The strong association between WD patterns and the development of MetS highlights the importance of establishing a pre-clinical model that incorporates human-relevant dietary patterns (2). Currently, most researchers applying pre-clinical rodent models utilize standardized reference diets, such as AIN-93, in their studies (3). These semi-purified diets were originally created to address concerns of variation in results among experiments and are formulated to promote reproducible health and reproductive parameters of the model organism (7). Although these diets have been invaluable for standardizing murine research (8), they may not be adequate to model human nutrition-related pathologies. Historically, nutrition experiments utilizing rodent models employ experimental diets that are produced by modification of reference diets for specific ingredients or nutrient classes, such as protein, fat, or carbohydrate. Although useful for understanding disease pathologies induced by one specific nutrient change (over or under exposure), these altered diets are not representative of what is being consumed on average in the United States and have limited translatability to the average human population (2). For example, the classic high-fat diet (HFD) contains approximately 45–60% of kcal as fat derived from one or few dietary fat sources, typically lard and/or tallow, and has been successful in inducing MetS and associated pathologies (9). According to the CDC, however, the mean fat intake for men and women over 20 years old is approximately 34–35% of their caloric intake (10). Similar to the pitfalls of HFDs, choline-deficient diets are utilized to induce non-alcoholic fatty liver disease (NAFLD) associated with MetS, yet they fail to produce NAFLD that manifests in a physiologically relevant way to the human population (2). While of basic interest, these commonly used experimental diets may not accurately replicate the pathogenesis of metabolic disorders, resulting in poor translatability to human populations.

Recently, two groups of investigators designed WDs in accordance with survey responses reported by the National Health and Nutrition Examination Survey (NHANES) to reflect average human consumption patterns. Monsanto et aldeveloped the Total Western Diet (TWD) to address overestimations of fat intake as well as lack of inclusion of multiple sources of fat in previously established diets (3). Totsch et al. further modified the TWD to produce the Standard American Diet (SAD), incorporating multiple sources of dietary fat as well as human-relevant levels of omega-6: omega-3 PUFA (11). The primary source of carbohydrate in both the TWD and the SAD is sucrose; however, NHANES reports that sugar-sweetened beverages (SSBs) are primary contributors to added sugars being consumed across multiple age-groups in the United States (12). SSBs such as soft drinks are commonly sweetened with high fructose corn syrup (HFCS) and are associated with an increased risk for obesity (13).

There is increasing evidence that fructose consumption may be related to the development of metabolic disorders associated with obesity (2, 14–18). Following its introduction in the 1970s, HFCS consumption markedly increased until the early 2000s

(19). During this time, rates of obesity increased (20), leading many to hypothesize that fructose may be at least partially responsible (21). The HFCS contained in SSBs, HFCS-55, is an unequal mixture of glucose and fructose monosaccharides that are produced by a series of enzymatic reactions which convert extracted corn starch to glucose and fructose at levels of ca. 45 and 55%, respectively (22). In contrast, sucrose is a disaccharide composed of a 50:50 ratio of glucose: fructose.

To investigate the association of WD and the development of MetS, we have formulated a modified version of the SAD that reflects above-average macronutrient intakes as reported by NHANES. The modified SAD (mSAD) incorporates HFCS within the feed, an important distinction from diets that introduce HFCS in an *ad libitum* drinking solution (23). Beyond formulating the diet, we have characterized the basal physiologies of C57BL/6J mice consuming this diet. We hypothesize that a diet that represents above-average human intakes will produce metabolic phenotypes consistent with those seen in human populations with a greater incidence of obesity and MetS.

Materials and methods

Animals

All experiments were approved by the Institutional Animal Care and Use Committee at the University of Alabama at Birmingham (UAB), Birmingham, AL (IACUC-21005). Male C57BL/6J mice were obtained from Jackson Labs (000664) at 4 weeks of age and housed in AAALAC-approved facilities at UAB with a 12:12 h dark: light cycle (06:00–18:00). Mice were housed in groups of 3 in wire-top cages with *ad libitum* access to food and sterile water. Mice were acclimated for 7 days and then randomly assigned to the AIN93M control diet (CON) or the experimental diet (mSAD) at 5 weeks of age. Mice were proffered diets for 15 weeks. Food and water intake for each cage of mice were recorded weekly, and nutrient intake parameters were calculated from these records.

Diet

C57BL/6J male mice were assigned randomly to one of two groups (n = 12 total, n = 6/group, n = 3/cage, n = 2 cages/group) and proffered either the CON or the mSAD for a period of 15 weeks. The CON (AIN-93M, TD.94048, Envigo, Madison, WI, United States) is formulated for optimal health and is a common standard reference diet used in rodent research (7). AIN-93M consists of 12.4% protein (13.7% kcal), 68.3% carbohydrate (75.9% kcal), and 4.1% fat (10.3% kcal) (**Table 1**). The modified Standard American diet (mSAD, TD.180061, Envigo, Madison, WI, United States) was formulated to approximate 50th percentile macronutrient intakes from data reported by NHANES. Macro- and micronutrient levels are listed in **Table 1** and **Table 2**, respectively. The mSAD is composed of 12.3% protein dry matter (12.2% kcal), 49.5% carbohydrate (49.2% kcal), and 17.3% fat (38.6% kcal) (**Table 1**). The mSAD contains HFCS as the primary source of carbohydrate at a level of 26% of the diet (by weight). Multiple sources of saturated and unsaturated fat were incorporated in the mSAD, including palm oil, soybean oil, corn oil, cottonseed oil, lard, beef tallow, and anhydrous milkfat (**Table 1**). Moreover, the mSAD contains reduced levels of fiber and increased levels of sodium, which are supported by NHANES data (7).

Growth metrics and body composition

To assess body weight over time, individual body weights were measured weekly. Weight gain was calculated by subtracting the previous week's weight from the current week. Specific growth rate (SGR) was calculated using the following formula:

$$SGR = \left[\left(\frac{week\ 2\ weight}{week\ 1\ weight}\right)^{\frac{1}{\Delta t}} - 1\right] * 100\%.$$

Quantitative Magnetic Resonance (QMR) was performed according to previously published methods (24) on mice at weeks 4, 6, 7, 10, and 12 to measure *in vivo* fat and lean-tissue mass (EchoMRI^{TM} 3-in-1; Echo Medical Systems, Houston, TX, United States). Due to technical issues, QMR could not be performed at the termination of the study; however, QMR lean mass values for week 15 were predicted using a simple linear regression.

Glucose tolerance and insulin tolerance testing

Glucose tolerance tests (GTT) and insulin tolerance tests (ITT) were performed to evaluate glucose and insulin response, respectively. Tests were performed after 4, 6, 10, and 12 weeks of diet exposure. Mice were weighed and fasted prior to testing (5-h fast for GTT, 4-h fast for ITT). For GTTs, mice received i.p. injection of a 25% glucose solution in phosphate-buffered saline (PBS) at a concentration of 2 g/kg body weight and blood glucose was monitored at 0, 15, 30, 60, and 120 min post-injection. For ITTs, mice received i.p. injection of insulin at 0.5 U/kg body weight. Blood glucose was measured at 0, 15, 30, 45, 60, and 120 min following injection. All blood samples were collected via tail vein venipuncture and blood glucose was measured using a Contour glucose meter (Bayer 82486543).

Tissue collection and analysis

Following termination of the study, mice were euthanized by decapitation and trunk blood was collected for downstream analyses. Adipose depots (inguinal, dorsal, peri-renal, gonadal, mesenteric, and interscapular) and internal organs (kidney, liver, spleen, and alimentary canal) were dissected and weighed individually. Following overnight fixation in 10% Neutral Buffered Formalin (NBF), liver and adipose tissues were processed and embedded in paraffin by UAB's Molecular Detection Core Facility. Tissues were sectioned at 5 μm and mounted onto glass slides. To assess hepatic lipid deposition, liver sections were stained with Hematoxylin and Eosin (H&E). For CLS detection, adipose sections were stained with anti-Mac-2 antibody (1:2,800; Cedarlane Laboratories 61R-1589) followed by hematoxylin counterstaining. Slides were imaged using a Nikon stereomicroscope (Nikon SMZ1000N, Nikon, Melville, NY, United States). The total area occupied by CLS from the full field of each tissue section was quantified using NIS Elements imaging software (NIS Elements BR 3.2, Nikon, Melville, NY, United States).

Quantitative PCR

Total RNA was collected from proximal colon tissue using the RNeasy Plus Mini Kit (Qiagen 74134) per the manufacturer's instructions followed by quantification and purity assessment on a NanoDrop One (Thermo Fisher Scientific). RNA with a concentration >30 ng/μl and A260/280 > 2.00 was processed into complementary DNA (cDNA) using a High Capacity cDNA Reverse Transcription Kit (Applied Biosystems 4368814) per the manufacturer's instructions (200 ng RNA/reaction). cDNA was used in duplicate as a template for qRT-PCR using Taqman Fast Advanced

TABLE 1 AIN-93M control diet (CON) and modified Standard American Diet (mSAD) formulations.

AIN-93M		mSAD	
Ingredient	**g/kg**	**Ingredient**	**g/kg**
Casein	140	Casein	83
L-cysteine	1.8	L-cysteine	1.8
Corn starch	465.692	Whole wheat flour	374.77
Maltodextrin	155	High fructose corn syrup	264
Sucrose	100	Maltodextrin	60
Soybean oil	40	Palm oil	59.5
Cellulose	50	Soybean oil	17.3
Mineral mix	35	Corn oil	10.6
Vitamin mix	10	Cottonseed oil	20.9
Choline bitartrate	2.5	Lard	18
TBHQ, antioxidant	0.008	Beef tallow	16
		Anhydrous milkfat	23.3
		Cholesterol	0.4
		Sodium chloride	4.0
		Mineral Mix	35
		Vitamin Mix	10
		Choline bitartrate	1.4
		TBHQ, antioxidant	0.03
Macronutrient	**% kcal**	**Macronutrient**	**% kcal**
Protein	13.7	Protein	12.2
Fat	10.3	Fat	49.2
Carbohydrate	75.9	Carbohydrate	38.6
Kcal/g 3.6		**Kcal/g 4.0**	
Other Nutrients	**%**	**Other Nutrients**	**%**
Fiber*	5	Fiber*	3.75
Moisture	9.87	Moisture	10.4

*Fiber levels approximated by the addition of individual ingredient levels.

TABLE 2 AIN-93M control diet (CON) and modified Standard American Diet (mSAD) micronutrient profiles.

	AIN-93M	mSAD
Vitamins		
Vitamin A (IU/kg)	4000	3,951
Vitamin D (IU/kg)	1000	400
Vitamin E (IU/kg)	75	28
Vitamin K (mg/kg)	0.8	0.2
Biotin (mg/kg)	0.2	0.2
Choline (mg/kg)	1147.5	755
Folic Acid (mg/kg)	2	1.4
Niacin (mg/kg)	30	69.1
Pantothenate (mg/kg)	14.7	17
Riboflavin (mg/kg)	6	5
Thiamin (mg/kg)	4.9	5
Vitamin B6 (mg/kg)	5.8	5.4
Vitamin B12 (mg/kg)	0.03	0.01
Minerals		
Calcium (g/kg)	5	2.1
Phosphorus (g/kg)	3	3.3
Potassium (g/kg)	3.6	6.6
Sodium (g/kg)	1	7
Chlorine (g/kg)	1.6	10.8
Magnesium (g/kg)	0.5	1.1
Copper (mg/kg)	6.1	4.2
Iron (mg/kg)	36.9	45
Zinc (mg/kg)	39.8	36.8
Manganese (mg/kg)	10.5	25.5
Iodine (mg/kg)	0.21	0.21
Selenium (mg/kg)	0.15	0.44
Molybdenum (mg/kg)	0.15	0.15
Chromium (mg/kg)	1	1

Master Mix (Applied Biosystems 4444556) and the following primers on a QuantStudio 6 Flex (Applied Biosystems): Actin (Mm02619580_g1), TNFα (Mm00443258_m1), IL-1β (Mm00434228_m1), IL-6 (Mm00446190_m1). The 2ˆ(-delta Ct) method was used to calculate relative gene expression from raw cycle threshold (Ct) values and target gene expression was normalized to actin.

Microbiome analysis

Microbiome analysis was performed according to previously published methods (25). After 15 weeks of diet, feces were collected and fecal DNA was isolated using the Fecal DNA Isolation Kit (Zymo Research, Irvine, CA, United States, cat. no. 06010) and a 250 base pair amplicon library was generated via PCR with primers specific for the V4 region of the rRNA gene. PCR products were electrophoresed on agarose gel and subsequently excised from the gel and purified using the QIAquick Gel Extraction Kit (Qiagen, cat. no. 28704). Next-generation sequencing was accomplished using the Illumina MiSeq (Illumina, San Diego, CA, United States, cat. no. SY-410-1003) and microbiome analysis was performed using QIIME2 (Quantitative Insights Into Microbial Ecology) (25).

Taxonomic distribution

The taxonomic composition of the mouse fecal mSAD and control samples were determined utilizing QIIME2 (v.2021.11) bioinformatics tools (26). The samples raw sequence files was demultiplexed, via the Casava 1.8 paired-end demultiplexed fastq format, followed by denoising using DADA2 (q2-dada2) for quality filtering (27). The alignment of amplicon sequence variants (ASVs) was achieved using mafft (q2-alignment) (28), and the results were exported into fasttree2 (q2-phylogeny plugin) for phylogeny construction, using the FastTree building method (default setting) (29). The "Core-metrics-phylogenetic" command (q2-diversity plugin) generated Alpha-diversity metrics (Faith's Phylogenetic Diversity, and observed features) (30), Shannon (31), Simpson (32), chao1 (33), beta diversity metrics, un-weighted UniFrac, weighted UniFrac (34), Principle Coordinate Analysis (PCoA), Bray–Curtis dissimilarity, and Jaccard distance. The samples based off the minimum value of 15,411 sequences per sample were rarefied (subsampled without replacement). Taxonomic assignment to ASVs was achieved via q2-feature-classifier plugin (35), utilizing the "classify-sklearn" command against the silva-138-99-nb-classifier (36). The taxa were then collapsed into table format using the "qiime taxa collapse" command. Adonis and PERMANOVA beta-diversity metrics were determined via "qiime diversity beta-group-significance" plug-in (37).

Statistics

Statistical analysis was performed using Prism 9.0 software (GraphPad Software, San Diego, CA, United States) and R software (R Core Team (38)). Statistical significance was determined using Student's *t*-test (when comparing two groups), Welch's T-test (when comparing two groups with unequal variances), Wilcoxon T-test (when comparing two groups when data was not normally distributed), one-way analysis of variance (ANOVA) (when comparing more than two groups with one independent variable) or two-way ANOVA (when comparing more than two groups with two or more independent variables). When applicable, a Tukey–Kramer post-hoc test was used to calculate the Minimum Significant Difference (MSD) between any pair of means and statistical significance was assigned to groups with differences between the means greater than the MSD. A p-value < 0.05 was considered significant.

Results

Weight and body composition parameters recorded during the study revealed immediate and significant changes to the physical state of mice in response to mSAD feeding. After 15 weeks, mSAD-fed mice exhibited significantly more weight gain and a higher SGR than their CON counterparts (**Figures 1A–D**). Mice fed the mSAD accumulated higher absolute amounts of fat mass as well as a percentage of body weight than CON (**Figures 1E,F**). Both diets induced lean mass accumulation at a similar rate throughout the study (**Figure 1G**), but not as a percentage of total mass (**Figure 1H**).

Within the first week, water intake was higher in the mSAD diet compared to CON (**Figure 2A**). However, water intake in CON mice increased over the feeding period. Water intake values displayed high levels of variance, in some cases due to issues with leaky sippers that were noted at a few timepoints during the study. No change in weekly or overall food intake was observed between diet treatments (**Figures 2B–D**); however, because the mSAD had a higher caloric density, total energy intake in mSAD-fed mice was slightly higher (3,742 kcal) than in CON (3,314 kcal) (**Figure 2E**). Caloric efficiency, defined as total mg of weight gained/total kcal consumed, was significantly higher in mSAD-fed mice (**Figure 2F**). At the macronutrient level, mSAD-fed mice consumed more fat and less carbohydrate than CON mice, with no differences in protein intake (**Figures 2G–I**).

To assess whether the changes in body composition in response to mSAD intake are associated with metabolic alterations in glucose and insulin signaling, GTT and ITT were recorded during the study period. Prior to diet administration, mice showed no difference in fasting blood glucose or glucose tolerance (**Figure 3A**). However, mSAD-fed mice displayed fasting hyperglycemia and impaired glucose tolerance at every

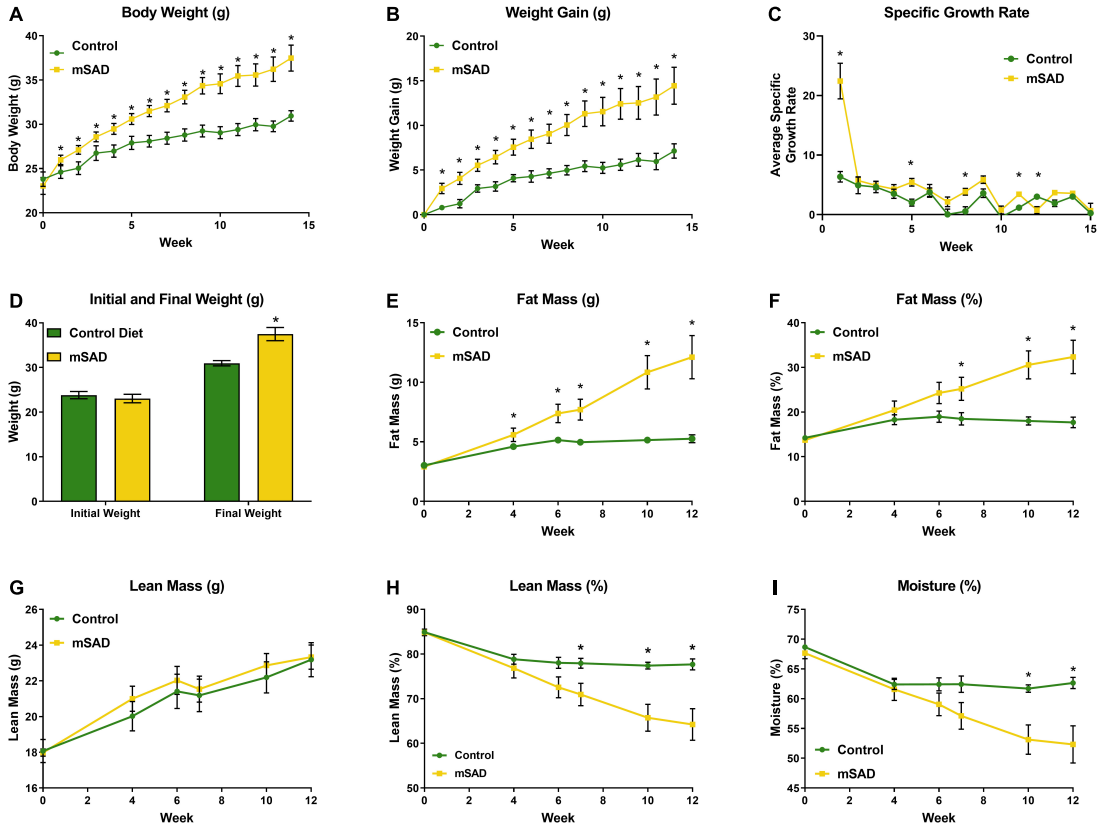

FIGURE 1
Effects of diet on weight and body composition. Male C57BL/6J mice were proffered the CON or the mSAD diet for a 15-week period. **(A)** Body weight was measured weekly (n = 12/diet). **(B)** Cumulative weight gain and **(C)** specific growth rate for each diet. **(D)** Initial and final weights for each diet. QMR analysis at 4, 6, 7, 10, and 12 weeks (n = 6/diet) includes **(E)** g fat mass, **(F)** % fat mass, **(G)** g lean mass, **(H)** % lean mass, and **(I)** percent water. Values are represented as mean ± SEM. Data were compared using Welch's t-test. *$p < 0.05$.

timepoint measured relative to CON mice (Figures 3B–E). Similarly, mSAD-fed mice display impaired insulin responsiveness at all time points measured (Figures 3F–H). At week 12, 4 of 6 control mice fell below the glucose threshold, forcing premature termination of the assay with no subsequent data collection.

Following termination of the study, mice were euthanized, and adipose depots, kidneys, liver, spleen, and alimentary canal were dissected and weighed for further assessment of mSAD alterations at the tissue-level. Inguinal, dorsal, perirenal, and gonadal depot weights of mSAD-fed mice were significantly heavier than CON mice (Figure 4A). Organ weights were evaluated by normalizing their absolute weight with regression-predicted lean matter weights at the 15-week timepoint. Although data cannot be statistically compared, organs of mSAD animals overall appeared larger than those in the control group (Figures 4B–E).

To understand cellular responses within the larger adipose mass with mSAD diets, adipocyte hyperplasia and hypertrophy were measured on gonadal tissue sections of CON- and mSAD-fed mice. Cell counts to evaluate adipocyte hyperplasia within equivalent areas of the tissue revealed significantly lower cell numbers in mSAD fat pads compared to CON (Figure 5A). Quantification of adipocyte cell area indicated a significantly larger average cell area in mSAD tissue sections compared to CON (Figure 5B).

The presence of CLS in gonadal adipose tissue sections of CON- and mSAD-fed mice was evaluated histologically (Figure 6A) followed by quantification of the percent area of CLS occupied in the total field of each tissue section (Figure 6B). mSAD-fed mice samples displayed a significantly higher percentage of CLS compared to CON mice.

FFPE liver sections of mice from both groups were stained with H&E to assess lipid deposition (Figures 7A,B). Gross increases in lipid deposits were observed in one of six CON mice and two of six mSAD-fed mice.

The presence of CLS within adipose tissue and hepatic steatosis in mSAD animals suggested that pro-inflammatory processes associated with mSAD feeding may affect multiple organ systems. To evaluate the role of inflammation in the colon, pro-inflammatory cytokine levels were measured. mSAD-fed mice exhibited significantly elevated gene expression levels of

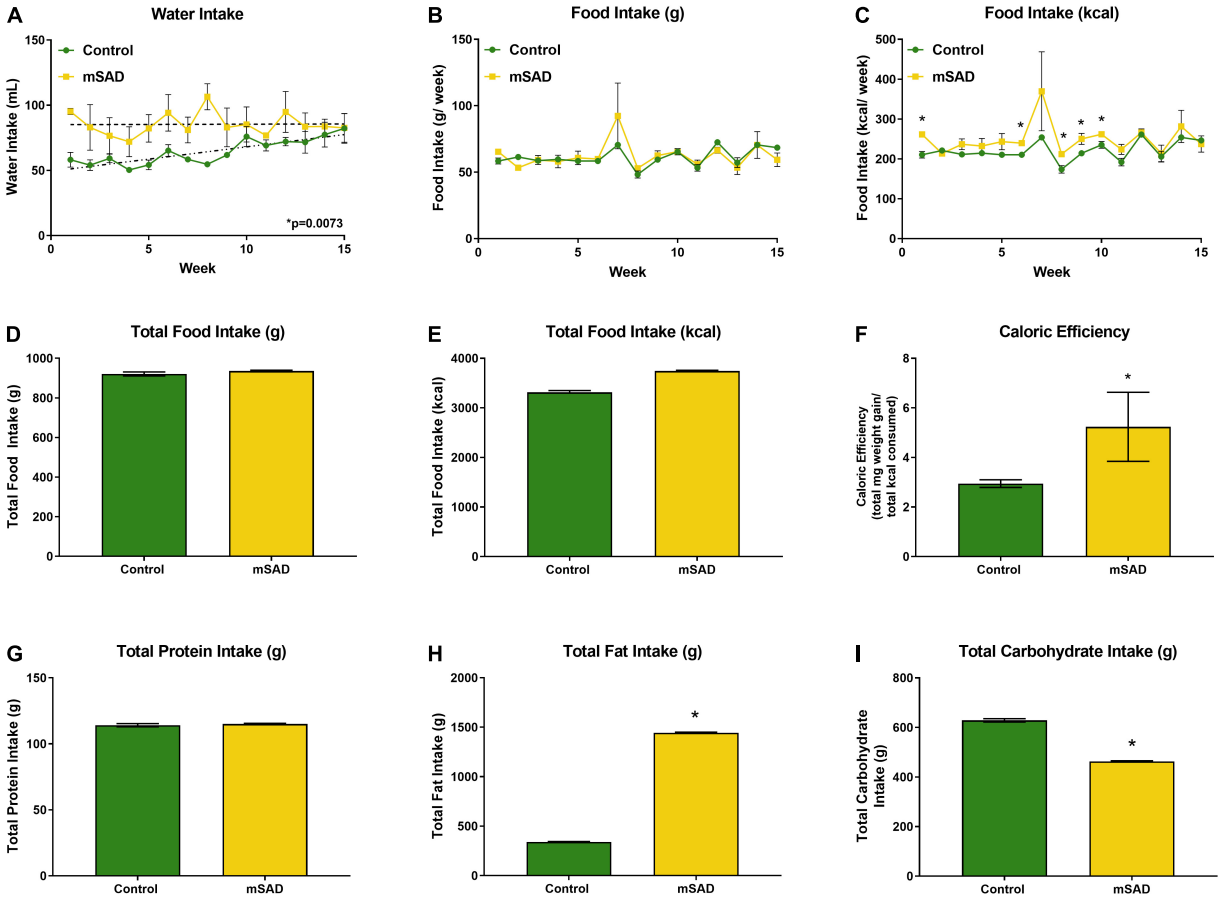

FIGURE 2
Water, food, and macronutrient intake. All values represent average cage intake (n = two cages, each containing three mice). Water intake was measured as mL per cage per week **(A)**. Food intake was measured as g per cage per week by a subtractive method of weekly provision minus weekly remnants **(B)** and kcal consumed per week **(C)**. Total food intake (g) **(D)** and kcal consumption **(E)** for the 15-week period. Caloric efficiency for each diet was calculated as total mg weight gain/total kcal consumed for the 15-week period **(F)**. Total protein **(G)**, lipid **(H)**, and carbohydrate intake **(I)** were calculated. Values are represented as mean ± SEM. Data were compared using Welch's t-test. *$p < 0.05$.

Tumor Necrosis Factor α (Tnfα), Interleukin 1 β (Il-1β), and Interleukin 6 (Il-6) relative to CON mice (Figures 8A–C) in colon tissues.

Increased levels of pro-inflammatory mediators prompted further analysis of the impact of the mSAD on the composition of the fecal microbe community. Using 16S rRNA sequencing and QIIME2 (v2021.11) analysis of pooled fecal samples, we assessed alpha and beta diversity metrics between CON and mSAD groups controlling for possible cage effects (Table 3 and Figures 9A,B, 10). Comparisons of alpha diversity in CON and mSAD samples measured by the Shannon index with cage input as a random effect produced a significant effect of diet ($p = 0.04$). Simpson and Chao1 comparisons with cage as a random effect produced nonsignificant results ($p = 0.11$, $p = 0.32$) (Table 3). Analysis of Bray-Curtis calculations (25) revealed significant differences between the microbe communities in the CON versus mSAD (BC < 0.001) indicating that exposure of mice to mSAD resulted in a re-structuring of the microbial community so that it was now distinct from that found in mice fed the CON diet. Visualization of changes in beta diversity of the sample groups can be seen in the principal coordinate analysis (PCOA) in Figure 10. Cluster separation seen in the PCOA plot between control cage 1 and control cage 2 was controlled for during analysis of beta diversity metrics with the Adonis test and resulted in a significant difference between diet groups ($p < 0.001$), and 83% ($R^2 = 0.826$) of the variation seen is due to the diet (Supplementary Table 2). Further evaluation of microbial composition within control cage 1 and control cage 2 was explored to assess the slight separation of the two cages seen in Figure 10. This assessment revealed that differences between these cages may be primarily influenced by two genera of microbes. In cage 1, genus *Romboutsia* represents approximately 9–25% of the microbiome, while in cage 2, genus *Faecalibaculum* represents ~10–30% of the microbiome. Across both cages and all six mice, all other genera are present in similar proportions (Supplementary Table 3). The pooled

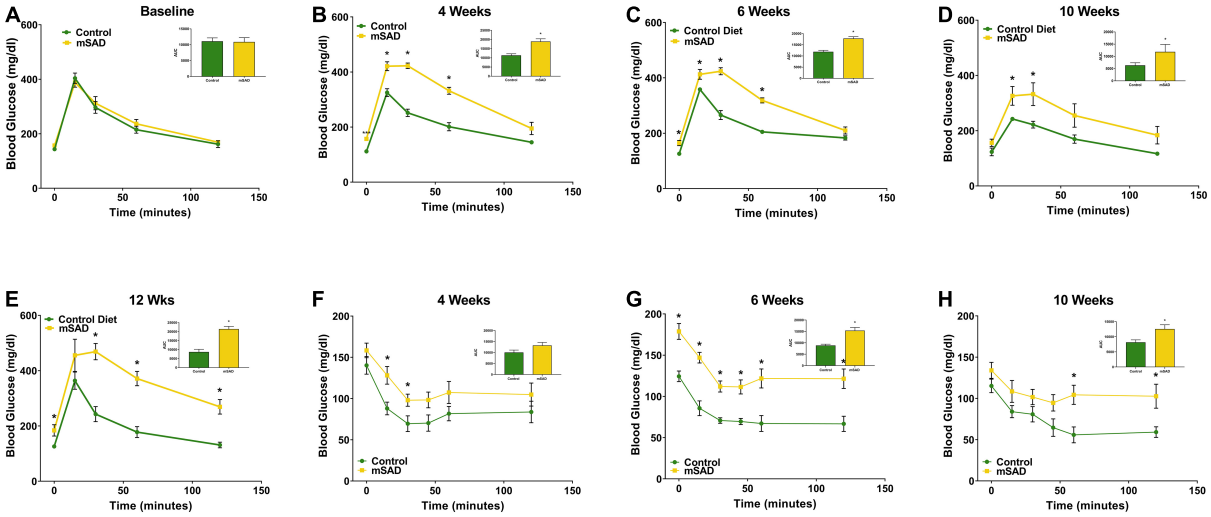

FIGURE 3
Effects of diet on glucose and insulin response. Glucose tolerance tests were performed prior to the feeding regimen **(A)** and after weeks 4 **(B)**, 6 **(C)**, 10 **(D)**, and 12 **(E)** weeks of diet. Insulin tolerance tests were performed after weeks 4, **(F)**, 6 **(G)**, and 10 **(H)** weeks of diet. Values are represented as mean ± SEM (n = 4–6/time point). Data were compared using Welch's t-test. *$p < 0.05$.

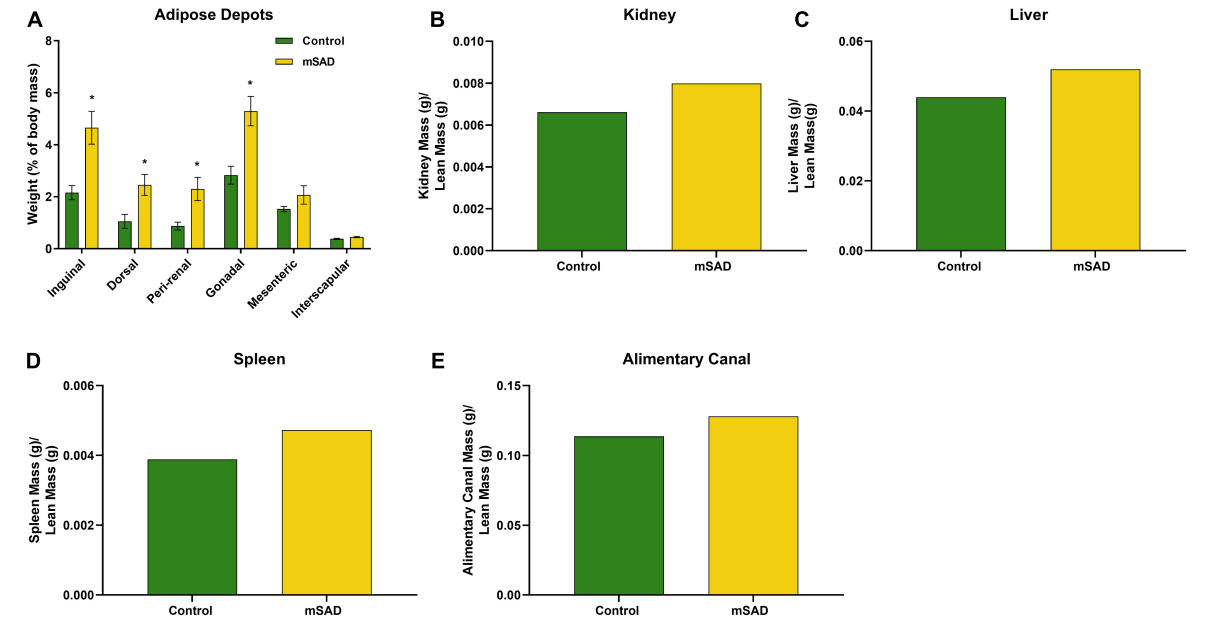

FIGURE 4
Effects of diet on an adipose depot and organ weights. Weights of the inguinal, dorsal, peri-renal, gonadal, mesenteric, and interscapular adipose depots were compared between CON- and mSAD-fed mice after 15 weeks of feeding **(A)**. Kidney **(B)**, liver **(C)**, spleen **(D)**, and alimentary canal **(E)** weights were also evaluated in both groups. Adipose depot values are represented as % of total body mass. Organ weight values are represented as absolute mass normalized by regression-predicted lean mass (g/g). When possible, data were compared using Student's t-tests. *$p < 0.05$.

fecal samples of mSAD and CON fed mice groups revealed taxa assigned to the *Firmicutes* phylum to be most abundant across groups (Figure 9A). *Ileibacterium*, and *Akkermansia* to be most abundant across diet groups. *Ileibacterium* was found to the more dominant taxon in the mSAD group (∼22–50%), compared to the control group (∼5–28%). The control group revealed a larger abundance of *Akkermansia* (∼7–57%), in contrast to the mSAD group (∼11–17%). A unique abundance of Lachnospiraceae family members (∼5–40%) were observed in the mSAD group, in contrast to the CON group (∼4–9%). The

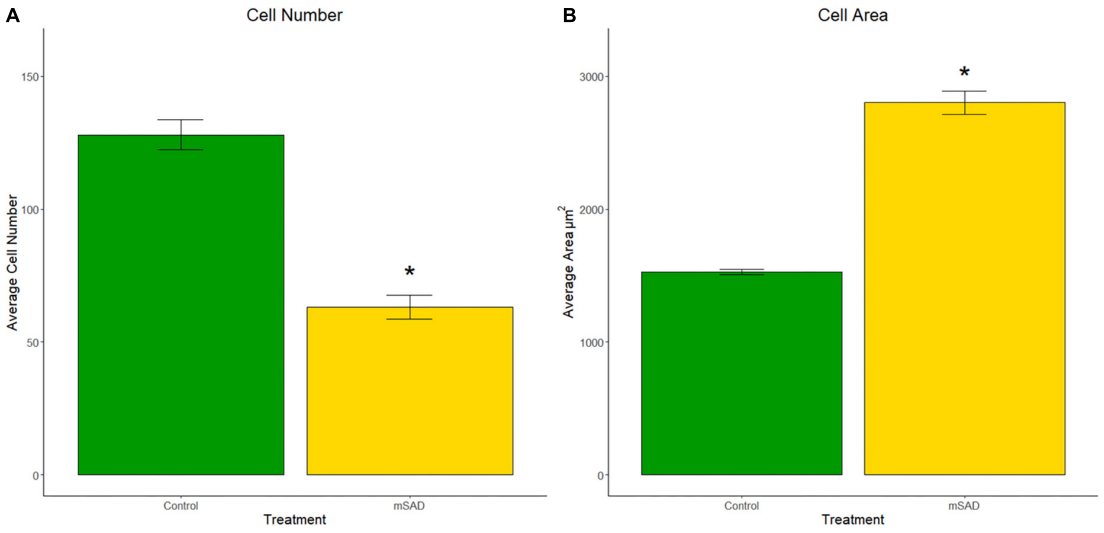

FIGURE 5
Effects of diet on gonadal adipocyte hyperplasia and hypertrophy. Cell counts and cell area measurements were performed on FFPE sections of gonadal fat pads stained with hematoxylin. Cell counts **(A)** and cell area measurements **(B)** were quantified. Values are representative of average cell count and average cell area (μm^2) of multiple regions of interest (CON, n = 6; mSAD, n = 3) each measuring 500 µm × 500 µm. Data were compared using the unpaired Wilcoxon rank-sum test. *$p < 0.001$.

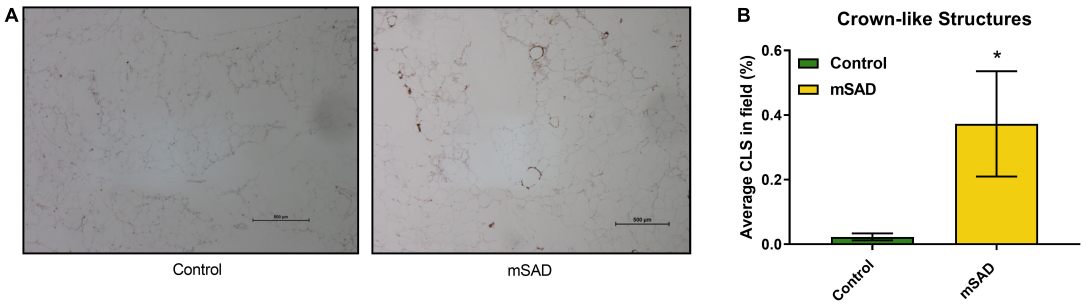

FIGURE 6
Effects of diet on gonadal fat pad inflammation. FFPE sections of gonadal fat pads from CON- or mSAD-fed mice were incubated with anti-MAC-2 followed by counter-staining with hematoxylin **(A)**. Quantification of CLS **(B)**. Values are represented as the average % area of CLS occupied in the total field of tissue sections. Data were compared using Student's t-test. *$p < 0.05$.

CON diet group showed distinct abundances of *Faecalibaculum* (0–31%) and *Romboutsia* (0–24%).

Discussion

Obesity is a defining characteristic of metabolic syndrome and is primarily classified by increased weight gain and adiposity (39). mSAD-fed mice exhibited significantly higher weight gain and adiposity relative to CON mice, even though overall dry matter, protein, and calorie intake were similar. These data emphasize that the nutrient content of the diet, not necessarily the energy content, is important in controlling energy storage and allocation, leading to weight gain and alterations in other physiological outcomes associated with MetS. These data further suggest that specific nutrients or combinations of nutrients, primarily carbohydrates or fats that are typically associated with the induction of obesity and MetS in humans, are inducing obesity and MetS related co-morbidities in male C57BL/6J mice. Since protein intake was similar between the diet treatments, we suggest protein was not directly an effector of obesity and MetS. Consequently, human-relevant diets can be formulated for C57BL/6J mice to emulate the physiological outcomes associated with obesity and MetS observed in humans (2).

Previous studies using NHANES-based diets that reflect western consumption patterns further demonstrate the effect of diet quality on metabolic outcomes. The TWD, although similar to the mSAD, is different in its formulation and includes lower n-6: n-3 and saturated fat levels. Interestingly, average weekly calorie intakes of mSAD and TWD mice were relatively

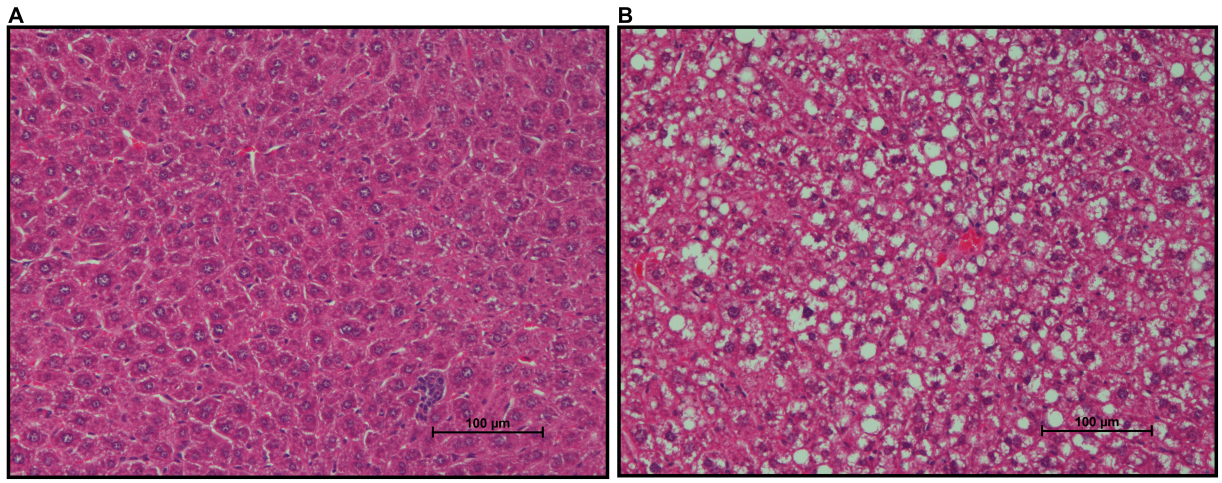

FIGURE 7
Effects of diet on hepatic lipid accumulation. Representative images of Formalin-fixed Paraffin-Embedded (FFPE) livers from six mice fed either CON diet with no lipid deposition **(A)** or mSAD with lipid deposition **(B)**. Tissue sections were stained with Hematoxylin and Eosin (H&E). Scale bars at the bottom right of images represent 100 µm.

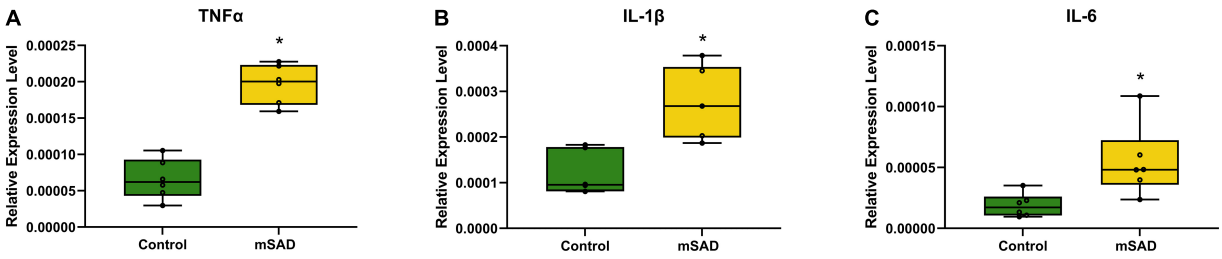

FIGURE 8
Effects of diet on colonic inflammation. Relative gene expression levels of *Tnfα* **(A)**, *Il-1β* **(B)**, and *Il-6* **(C)** in colon tissues of CON- and mSAD-fed mice. Values are represented as relative expression levels normalized to β-*actin*. Data were compared using one-way ANOVA. $*p < 0.05$.

similar, but weight-related outcomes were dramatically different at the end of each study (3). Comparatively, the SAD contains n-6: n-3 and saturated fat levels more similar to the mSAD and induced weight gain in a similar manner to the mSAD (11). Intake of both saturated fat and omega-6 PUFAs have been associated with an increased risk for obesity (40). In the current study, mice fed the mSAD exhibited equivalent food intake to the AIN93M-fed controls in terms of total dry matter, total protein, and total energy, but differed substantially in intake of fat and carbohydrate quantity and quality, leading to an obese phenotype. We hypothesize that specific lipids or carbohydrates in the diet, or a complex ratio therein, affect body mass outcomes leading to a MetS phenotype. Furthermore, the fact that significant differences in specific growth rates were observed in the first week of feeding suggests that the metabolic triggers and cell signaling cascades associated with MetS phenotypes are induced rapidly and persist as long as the diet is consumed.

Glucose dysregulation and HFD are both associated with the development of type 2 diabetes (T2D) in rodent models and humans (41–43). Within 4 weeks of diet intake, mSAD-fed mice developed hyperglycemia, glucose intolerance, and reduced insulin sensitivity relative to CON mice. Increased adiposity in obese individuals is linked to elevated secretion of adipokines and pro-inflammatory cytokines, which may provide a mechanistic basis for the development of insulin resistance (44). A high fat/high carbohydrate diet has been associated with increased levels of TNFα and was shown to activate downstream pathways (45). Interestingly, TWD-fed C57BL/6J mice did not exhibit metabolic effects of glucose metabolism seen in mSAD-fed mice. In comparison, mice fed the SAD displayed fasting hyperglycemia and reduced glucose tolerance after 20 weeks of diet (11). Moreover, SAD-fed rats exhibit increased gene expression levels of pro-inflammatory mediator TNFα (46). Altogether, these data suggest that mSAD promotes a more rapid induction of hyperglycemia and insulin resistance as compared to TWD or the SAD.

TABLE 3 Alpha diversity metrics were determined via QIIME2 diversity alpha plugin (QIIME_2, v2021.11), clustered according to cage_1_con (samples C1:C3, *n* = 3), cage_2_con (samples C4:C6, *n* = 3), cage_1_ex (samples mSAD1:mSAD3, *n* = 3), cage_2_ex (samples mSAD4:mSAD6, *n* = 3).

Sample_Name	Cage	chao1	Shannon	Simpson	Faith pd
C1	cage_1_con	87	3.41916094	0.77558052	8.09726054
C2	cage_1_con	95	3.90299357	0.84905891	7.87877218
C3	cage_1_con	82	2.96225955	0.65589128	9.11090517
C4	cage_2_con	68	4.24052121	0.90009793	5.93279296
C5	cage_2_con	55	3.31761141	0.82603949	5.53401411
C6	cage_2_con	51	3.44943346	0.82690652	5.09134285
mSAD1	cage_1_ex	63	3.68744323	0.82162558	5.86502142
mSAD2	cage_1_ex	103	4.65994564	0.88047728	8.83570895
mSAD3	cage_1_ex	67	3.4966321	0.77587981	7.03250057
mSAD4	cage_2_ex	80	4.35111254	0.89698438	7.18911116
mSAD5	cage_2_ex	88	4.23504497	0.89685054	6.88549864
mSAD6	cage_2_ex	99	4.6352924	0.90669609	8.04691229

Similarity metrics were determined via the ASV output table of QIIME2 (v2021.11), and chao1, Shannon, Simpson, and Faith –p-metric QIIME2 plug-ins. The table displays alpha diversity metrics for: chao1, Shannon, Simpson, and Faith_pd, clustered according to Cage column.

A notable difference in the mSAD and SAD is the inclusion of HFCS as a replacement for sucrose. HFCS is found in numerous consumer products, and dietary exposure to sucrose or HFCS may produce different metabolic and physiological effects, even when controlled for energy intake (17). Previous studies have investigated the effects of HFCS-infused drinking water; however, HFCS was included as an ingredient in the mSAD and not supplemented in the water to limit the direct effects of palatability on water consumption. Sweetened water may promote the consumption of liquid calories in place of dietary calories, thereby limiting the intake of the diet (23). Fructose has been implicated in the development of T2D (14), NALFD (47), and gut dysbiosis (48); however, conflicting studies (18) highlight the importance of further investigation into the source of fructose as an underlying factor in the development of these disorders.

Analysis of overall fat distribution revealed significant increases in visceral gonadal adipose tissue (VAT) depots. Accumulation of VAT is strongly linked to the development of T2D (36, 49) and may provide further insight into metabolic alterations induced by mSAD feeding. Expansion of VAT depots in murine DIO models results in enhanced recruitment of macrophages to adipose tissue that exhibit a pro-inflammatory M1 phenotype when compared to controls (50). During advanced obesity, these macrophages manifest histologically as rings of F4/80+ cells surrounding adipocytes called crown-like structures, and nearly all adipose-tissue derived TNFα is produced by macrophages (51). TNFα is well known to directly decrease insulin sensitivity (52) through proinflammatory signaling via the NF-κβ and JNK pathways. We suggest the presence of CLS in fat depots concomitant with increased levels of TNFα in the colon are related to alterations in glucose metabolism in mSAD-fed mice.

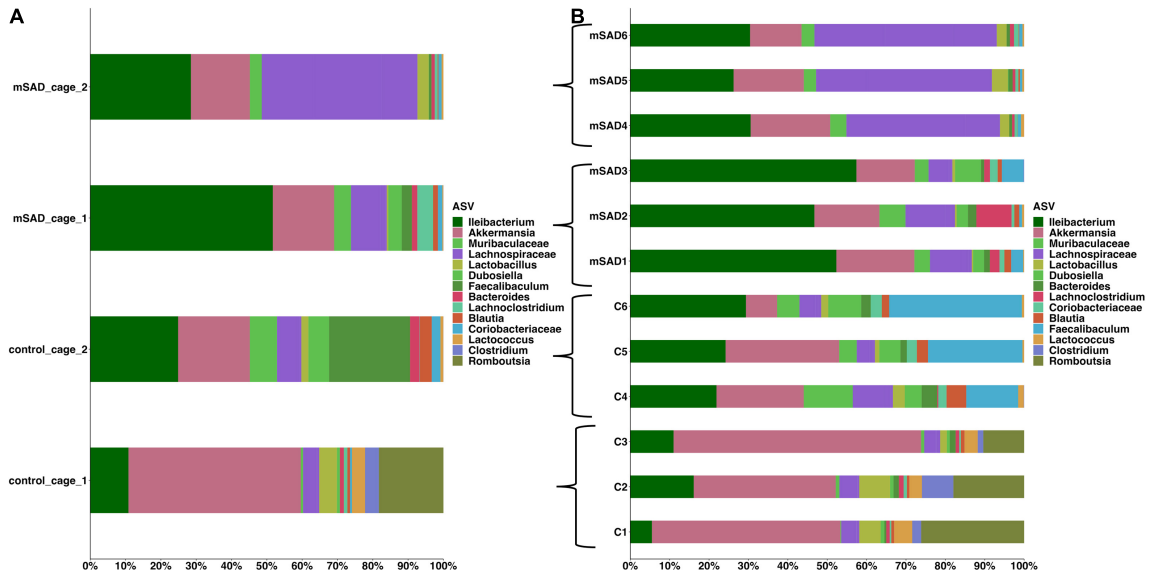

FIGURE 9
The mean of each sample group, according to cage was plotted for clarity, across sample groups **(A)**. Sample assignments are as follows: mSAD = mice fed the mSAD diet, control/con = mice feed the control diet, and cage represents their respective cage. Relative abundance stacked column bar graph showing top 15 taxa at the most resolved level across all samples (*n* = 3 for each sample) in the gut ecosystem of *mus musculus* **(B)**. Taxonomic identities were based on their assignment through the (SILVA v138) database as determined by the Quantitative Insights into Microbial Ecology (QIIME_2, v2021.11) and graphed using R (ggplot package).

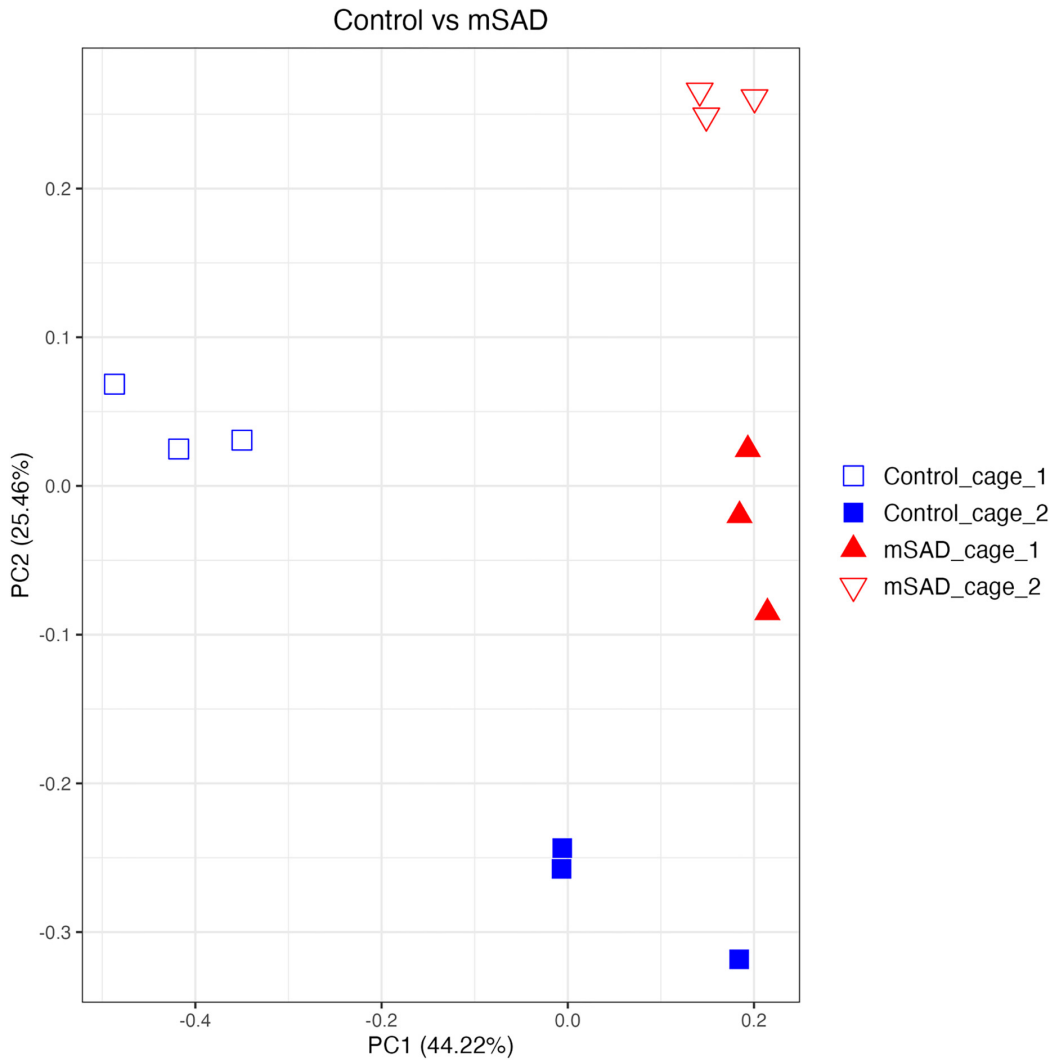

FIGURE 10
Beta diversity analysis of gut microbiota of mouse samples was observed across similarity metrics determined via QIIME2 (2021.11). A Bray–Curtis PCOA plot displays sample clustering patterns based on observed ASVs. plotted with R (ggplot package), and the q2-qiime diversity beta-group-significance. The group assignments are indicated as follows: control_cage_1 (blue open square; *n* = 3); control_cage_2 (blue square; *n* = 3); mSAD_cage_1 (red triangle; *n* = 3); mSAD_cage_2 (red open triangle; *n* = 3).

The development of insulin resistance is thought to play a significant role in the progression of NAFLD, a common manifestation of MetS. A high-fat, low-carbohydrate diet promotes increasing levels of liver fat when compared to an isocaloric low-fat, high-carbohydrate diet (53). Diets high in saturated fat with low PUFA levels have also been shown to promote increases in liver fat (54). In the present study, two of six mSAD-fed mice displayed hepatic steatosis. Interestingly, one CON mouse exhibited a similar phenotype. Although the AIN-93M control diet is formulated to support basic health and reproduction of murine models, there is one reported instance of liver steatosis formation in response to AIN-93M consumption (55), indicating that consumption of AIN-93 may, in some cases, induce NAFLD. Consumption of the SAD diet has been reported to increase liver triglycerides; however, the presence of NAFLD was not evaluated (11, 46). Liver steatosis may be an outcome that develops over longer periods and additional studies that focus on human-relevant dietary induction of NAFLD are warranted.

Reports of gut dysbiosis associated with WD consumption have led to increased interest in the role of the microbiome in the development of obesity and MetS. Several studies have linked WD-induced pathologies to altered populations of microbes (1, 24, 56) and reversion of gut dysbiosis has been shown to attenuate WD-induced dysfunction (57). The limited amount of microbiome data reported from previous NHANES-based WD studies prompted us to investigate the composition of the fecal microbiome of mSAD-fed mice. The separation between

control cage 1 and control cage 2 in the PCOA plot was of interest during the analyses. The two genera, *Romboutsia* and *Faecalibaculum* are shown to most likely be the primary components driving the separation of these cages. Interestingly, both of these genera of microbes belong the phylum Firmicutes and both have been identified in the gut of healthy patients and animals (58–61). Although these bacteria introduce variation between the control cages, we believe this variation does not represent an unhealthy population or that these animals have potential gut dysbiosis. Differences in microbial composition between diet groups were primarily of interest, as they may provide insight into physiological changes seen in mSAD mice. Similar to reported studies on diet-induced obesity, the fecal composition of mSAD mice was enriched with microbes from the Firmicutes phylum (62, 63). Increases in levels the Lachnospiraceae family were particularly interesting, as this family of microbes has been positively associated with multiple metabolic disorders, including alterations in glucose and lipid metabolism, onset of T2D, and diagnosis of NAFLD (64–68). Reduced levels of bacteria from the *Akkermansia* genus indicate a potential loss of protective microbes in the gut of mSAD mice. *Akkermansia mucinophilia,* the primary known species in this genus, is a mucin-degrading bacteria that has been documented to be altered under WD regimens (69). Levels of this species have shown to be inversely correlated with body weight in response to HFD (69) and reduced in models of type 2 diabetes, and administration of this species as a probiotic has shown to have protective effects on atherosclerosis, inflammation, and HFD-induced metabolic disorders (70, 71). Reduction of *Akkermansia* microbes in conjunction with altered glucose metabolism and increased body weight in mSAD mice agrees with existing reported data. The elevated presence of microbes from the *Ileibacterium* genus in the mSAD group may also be related to dietary intervention. This newly described genus was documented to be increased in response to HFD administration and positively correlated with serum lipid levels in a murine atherosclerosis model (72).

We recognize that microbial population dynamics observed alone cannot define the mechanism of action that resulted in increased weight gain, adiposity, and related co-morbidities. However, these trends lead us to hypothesize that shifts in microbial populations could result in a diet-dependent alteration of the metabolome. In fact, in a companion study, a metabolomic assessment of a Trp metabolite panel revealed diet-induced alterations in several Trp metabolites (24). Both nutrition and microbial populations are reported to be important in Trp metabolism and, as such, in maintaining systemic homeostasis including nutrient sensing, metabolic stress response, immunity (73), as well as neurological and behavioral interactions (24). Collectively, changes in diet, microbial populations and Trp metabolism could be important in the understanding progression of diet-induced metabolic disease and treatment options.

It is apparent that diet quality exerts pronounced effects on multiple physiological systems and signaling among these systems plays an integral role in the onset and development of metabolic disease (1, 41, 49, 74). The increased prevalence of obesity (75) and associated strain placed on the healthcare system (76) highlight the importance of developing research models that accurately reflect affected populations. Additionally, it is important to develop diets that initiate obesity and MetS to better understand the relation between diet and metabolic disease. Many previously established diets used to study DIO lacked relevant ingredients that reflect the consumption patterns that may ultimately induce and/or exacerbate metabolic disorders (1, 3, 77). The mSAD is formulated based upon the most recent data reflecting United States consumption patterns and induces pathologies consistent with MetS at a rate faster than SAD. We hypothesize the rapid development of MetS in C57BL/6J mice fed mSAD is due to either the inclusion of HFCS in the diets or interaction of carbohydrate and fat sources, leading to an aberrant metabolic cascade mediated by the gut-brain axis. We propose the mSAD diet induces the natural development of obesity-related pathologies and, therefore, becomes another important tool for improving rodent models of DIO and MetS. Moreover, this new diet can be reverse engineered to look for nutrient patterns and ratios contributing to disease outcomes, providing both a positive and negative control for future studies. This diet can also be used to address therapeutic targets and other interventions. We suggest that a new generation of diets can be developed in a variety of animal models, leading us to understand the basic universal cascades associated with consumption patterns leading to excessive weight gain and related co-morbidities.

Data availability statement

The datasets presented in this study can be found in online repositories. The names of the repository/repositories and accession number(s) can be found below: https://www.ncbi.nlm.nih.gov/, PRJNA718626.

Ethics statement

The animal study was reviewed and approved by Institutional Animal Care and Use Committee at the University of Alabama at Birmingham.

Author contributions

SW, GK, JB, CM, DS, MP, and MM conceived of, designed, and supervised the study. SC, CG, AC, GG, BVa, AM, MW, TB, WV, and LW assisted with data collection and interpretation.

SC, CG, GG, and WV assisted with statistical analyses, interpretation, and presentation under supervision of SW, CM, JB, DS, and GK. SC prepared initial versions of the manuscript with all authors providing input and final approval of the submitted and published versions. All authors contributed to the article and approved the submitted version.

Funding

This research was supported by the UAB Diabetes Research Center (NIH P30 DK079626), the National Center for Advancing Translational Sciences (NIH UL1TR001417), and the UAB Nutrition and Obesity Research Center Lab Animal Nutrition Core [(P30DK056336), NIH MH079710, and NIH MH116896].

Acknowledgments

We thank the UAB Diabetes Research Center (NIH P30 DK079626) for providing pilot grant funding, the UAB Small Animal Phenotyping Core for body composition and indirect calorimetry measures, and the UAB Microbiome Institutional Research Core for microbiome analysis. The National Center for Advancing Translational Sciences, (NIH) is acknowledged for Bioinformatics support. This work is also supported by the UAB Nutrition and Obesity Research Center, the Lab Animal Nutrition Core (P30DK056336).

Conflict of interest

The authors declare that the research was conducted in the absence of any commercial or financial relationships that could be construed as a potential conflict of interest.

Publisher's note

All claims expressed in this article are solely those of the authors and do not necessarily represent those of their affiliated organizations, or those of the publisher, the editors and the reviewers. Any product that may be evaluated in this article, or claim that may be made by its manufacturer, is not guaranteed or endorsed by the publisher.

Supplementary material

The Supplementary Material for this article can be found online at: https://www.frontiersin.org/articles/10.3389/fnut.2022.929446/full#supplementary-material

References

1. Bortolin RC, Vargas AR, Gasparotto J, Chaves PR, Schnorr CE, Martinello KB, et al. A new animal diet based on human Western diet is a robust diet-induced obesity model: comparison to high-fat and cafeteria diets in term of metabolic and gut microbiota disruption. *Int J Obes (Lond).* (2018) 42:525–34. doi: 10.1038/ijo.2017.225

2. Hintze KJ, Benninghoff AD, Cho CE, Ward RE. Modeling the western diet for preclinical investigations. *Adv Nutr.* (2018) 9:263–71. doi: 10.1093/advances/nmy002

3. Monsanto SP, Hintze KJ, Ward RE, Larson DP, Lefevre M, Benninghoff AD. The new total Western diet for rodents does not induce an overweight phenotype or alter parameters of metabolic syndrome in mice. *Nutr Res.* (2016) 36:1031–44. doi: 10.1016/j.nutres.2016.06.002

4. Lin BH, Tobenna DA, Buzby, JC, Bentley JT. *U.S. Food Commodity Availability by Food Source, 1994-2008, ERR–221*. Washington, DC: U.S. Department of Agriculture, Economic Research Service (2016).

5. Clifton P. Metabolic syndrome-role of dietary fat type and quantity. *Nutrients.* (2019) 11:1438. doi: 10.3390/nu11071438

6. Taskinen MR, Packard CJ, Borén J. Dietary fructose and the metabolic syndrome. *Nutrients.* (2019) 11:1987. doi: 10.3390/nu11091987

7. Reeves PG, Nielsen FH, Fahey GC Jr. AIN-93 purified diets for laboratory rodents: final report of the American institute of nutrition ad hoc writing committee on the reformulation of the AIN-76A rodent diet. *J Nutr.* (1993) 123:1939–51. doi: 10.1093/jn/123.11.1939

8. Nielsen FH. 90th anniversary commentary: the AIN-93 purified diets for laboratory rodents—the development of a landmark article in the journal of nutrition and its impact on health and disease research using rodent models. *J Nutr.* (2018) 148:1667–70. doi: 10.1093/jn/nxy121

9. Speakman JR. Use of high-fat diets to study rodent obesity as a model of human obesity. *Int J Obes (Lond).* (2019) 43:1491–2. doi: 10.1038/s41366-019-0363-7

10. National Center for Health Statistics. *Diet/ Nutrition*. (2019). Available online at: https://www.cdc.gov/nchs/fastats/diet.htm (accessed January 13, 2022).

11. Totsch SK, Meir RY, Quinn TL, Lopez SA, Gower BA, Sorge RE. Effects of a standard American diet and an anti-inflammatory diet in male and female mice. *Eur J Pain.* (2018) 22:1203–13. doi: 10.1002/ejp.1207

12. Bailey RL, Fulgoni VL, Cowan AE, Gaine PC. Sources of added sugars in young children, adolescents, and adults with low and high intakes of added sugars. *Nutrients.* (2018) 10:102. doi: 10.3390/nu10010102

13. Hu FB, Malik VS. Sugar-sweetened beverages and risk of obesity and type 2 diabetes: epidemiologic evidence. *Physiol Behav.* (2010) 100:47–54. doi: 10.1016/j.physbeh.2010.01.036

14. DiNicolantonio JJ, O'Keefe JH, Lucan SC. Added fructose: a principal driver of type 2 diabetes mellitus and its consequences. *Mayo Clin Proc.* (2015) 90:372–81. doi: 10.1016/j.mayocp.2014.12.019

15. Kisioglu B, Nergiz-Unal R. Potential effect of maternal dietary sucrose or fructose syrup on CD36, leptin, and ghrelin-mediated fetal programming of obesity. *Nutr Neurosci.* (2020) 23:210–20. doi: 10.1080/1028415X.2018.1491151

16. Ma X, Lin L, Yue J, Wu CS, Guo CA, Wang R, et al. Suppression of ghrelin exacerbates HFCS-induced adiposity and insulin resistance. *Int J Mol Sci.* (2017) 18:1302. doi: 10.3390/ijms18061302

17. Sadowska J, Bruszkowska M. Comparing the effects of sucrose and high-fructose corn syrup on lipid metabolism and the risk of cardiovascular disease in male rats. *Acta Sci Pol Technol Aliment.* (2017) 16:231–40.

18. Tsilas CS, de Souza RJ, Mejia SB, Mirrahimi A, Cozma AI, Jayalath VH, et al. Relation of total sugars, fructose and sucrose with incident type 2 diabetes:

a systematic review and meta-analysis of prospective cohort studies. *CMAJ.* (2017) 189:E711–20. doi: 10.1503/cmaj.160706

19. USDA. *Sugar and Sweeteners Yearbook Tables*. (2022). Available online at: https://www.ers.usda.gov/data-products/sugar-and-sweeteners-yearbook-tables.aspx (accessed January 13, 2022).

20. Centers for Disease Control and Prevention. *Health, United States*. (2018). Available online at: https://www.cdc.gov/nchs/data/hus/hus18.pdf (accessed January 13, 2022).

21. Bray GA, Nielsen SJ, Popkin BM. Consumption of high-fructose corn syrup in beverages may play a role in the epidemic of obesity. *Am J Clin Nutr.* (2004) 79:537–43. doi: 10.1093/ajcn/79.4.537

22. White JS. Sucrose, HFCS, and fructose: history, manufacture, composition, applications, and production. In: Rippe JM editor. *Fructose, High Fructose Corn Syrup, Sucrose and Health*. New York, NY: Springer (2014). p. 13–33. doi: 10.1007/978-1-4899-8077-9_2

23. Pan JH, Kim HS, Beane KE, Montalbano AM, Lee JH, Kim YJ, et al. IDH2 deficiency aggravates fructose-induced NAFLD by modulating hepatic fatty acid metabolism and activating inflammatory signaling in female mice. *Nutrients.* (2018) 10:679. doi: 10.3390/nu10060679

24. Chakraborti A, Graham C, Chehade S, Vashi B, Umfress A, Kurup P, et al. High fructose corn syrup-moderate fat diet potentiates anxio-depressive behavior and alters ventral striatal neuronal signaling. *Front Neurosci.* (2021) 15:669410. doi: 10.3389/fnins.2021.669410

25. Kumar R, Eipers P, Little RB, Crowley M, Crossman DK, Lefkowitz EJ, et al. Getting started with microbiome analysis: sample acquisition to bioinformatics. *Curr Protoc Hum Genet.* (2014) 82:18.8.1–29 doi: 10.1002/0471142905.hg1808s82

26. Bolyen E, Rideout JR, Dillon MR, Bokulich NA, Abnet CC, Al-Ghalith GA, et al. Reproducible, interactive, scalable and extensible microbiome data science using QIIME 2. *Nat Biotechnol.* (2019) 37:852–7.

27. Callahan BJ, McMurdie PJ, Rosen MJ, Han AW, Johnson AJ, Holmes SP. DADA2: high-resolution sample inference from illumina amplicon data. *Nat Methods.* (2016) 13:581–3. doi: 10.1038/nmeth.3869

28. Katoh K, Standley DM. MAFFT multiple sequence alignment software version 7: improvements in performance and usability. *Mol Biol Evol.* (2013) 30:772–80. doi: 10.1093/molbev/mst010

29. Price MN, Dehal PS, Arkin AP. FastTree 2–approximately maximum-likelihood trees for large alignments. *PLoS One.* (2010) 5:e9490. doi: 10.1371/journal.pone.0009490

30. Faith DP. Conservation evaluation and phylogenetic diversity. *Biol Conserv.* (1992) 61:1–10. doi: 10.1016/0006-3207(92)91201-3

31. Shannon CE. A mathematical theory of communication. *Bell Syst Tech J.* (1948) 27:379–423. doi: 10.1002/j.1538-7305.1948.tb01338.x

32. Simpson EH. Measurement of diversity. *Nature.* (1949) 163:688. doi: 10.1038/163688a0

33. Chao A. Nonparametric estimation of the number of classes in a population. *Scand J Stat.* (1984) 11:265–70.

34. Lozupone C, Lladser ME, Knights D, Stombaugh J, Knight R. UniFrac: an effective distance metric for microbial community comparison. *ISME J.* (2011) 5:169–72. doi: 10.1038/ismej.2010.133

35. Bokulich NA, Kaehler BD, Rideout JR, Dillon M, Bolyen E, Knight R, et al. Optimizing taxonomic classification of marker-gene amplicon sequences with QIIME 2's q2-feature-classifier plugin. *Microbiome.* (2018) 6:90. doi: 10.1186/s40168-018-0470-z

36. Yilmaz P, Parfrey LW, Yarza P, Gerken J, Pruesse E, Quast C, et al. The SILVA and "all-species living tree project (LTP)" taxonomic frameworks. *Nucleic Acids Res.* (2014) 42:D643–8. doi: 10.1093/nar/gkt1209

37. Anderson MJ. A new method for non-parametric multivariate analysis of variance. *Austr Ecol.* (2001) 26:32–46. doi: 10.1046/j.1442-9993.2001.01070.x

38. R Core Team. *R: A Language And Environment For Statistical Computing*. Vienna: R Foundation for Statistical Computing (2020).

39. Zafar U, Khaliq S, Ahmad HU, Manzoor S, Lone KP. Metabolic syndrome: an update on diagnostic criteria, pathogenesis, and genetic links. *Hormones (Athens).* (2018) 17:299–313. doi: 10.1007/s42000-018-0051-3

40. Simopoulos AP. The importance of the omega-6/omega-3 fatty acid ratio in cardiovascular disease and other chronic diseases. *Exp Biol Med (Maywood).* (2008) 233:674–88. doi: 10.3181/0711-MR-311

41. Heydemann A. An overview of murine high fat diet as a model for type 2 diabetes mellitus. *J Diabetes Res.* (2016) 2016:2902351. doi: 10.1155/2016/2902351

42. Kahn SE, Hull RL, Utzschneider KM. Mechanisms linking obesity to insulin resistance and type 2 diabetes. *Nature.* (2006) 444:840–6. doi: 10.1038/nature05482

43. Marshall JA, Hamman RF, Baxter J. High-fat, low-carbohydrate diet and the etiology of non-insulin-dependent diabetes mellitus: the San Luis valley diabetes study. *Am J Epidemiol.* (1991) 134:590–603. doi: 10.1093/oxfordjournals.aje.a116132

44. Dyck DJ, Heigenhauser GJ, Bruce CR. The role of adipokines as regulators of skeletal muscle fatty acid metabolism and insulin sensitivity. *Acta Physiol (Oxf).* (2006) 186:5–16. doi: 10.1111/j.1748-1716.2005.01502.x

45. Hirosumi J, Tuncman G, Chang L, Görgün CZ, Uysal KT, Maeda K, et al. A central role for JNK in obesity and insulin resistance. *Nature.* (2002) 420:333–6. doi: 10.1038/nature01137

46. Totsch SK, Quinn TL, Strath LJ, McMeekin LJ, Cowell RM, Gower BA, et al. The impact of the standard American diet in rats: effects on behavior, physiology and recovery from inflammatory injury. *Scand J Pain.* (2017) 17:316–24. doi: 10.1016/j.sjpain.2017.08.009

47. Tetri LH, Basaranoglu M, Brunt EM, Yerian LM, Neuschwander-Tetri BA. Severe NAFLD with hepatic necroinflammatory changes in mice fed trans fats and a high-fructose corn syrup equivalent. *Am J Physiol Gastrointest Liver Physiol.* (2008) 295:G987–95. doi: 10.1152/ajpgi.90272.2008

48. Volynets V, Louis S, Pretz D, Lang L, Ostaff MJ, Wehkamp J, et al. Intestinal barrier function and the gut microbiome are differentially affected in mice fed a western-style diet or drinking water supplemented with fructose. *J Nutr.* (2017) 147:770–80. doi: 10.3945/jn.116.242859

49. Després JP. Body fat distribution and risk of cardiovascular disease: an update. *Circulation.* (2012) 126:1301–13. doi: 10.1161/CIRCULATIONAHA.111.067264

50. Rocha VZ, Folco EJ, Sukhova G, Shimizu K, Gotsman I, Vernon AH, et al. Interferon-gamma, a Th1 cytokine, regulates fat inflammation: a role for adaptive immunity in obesity. *Circ Res.* (2008) 103:467–76. doi: 10.1161/CIRCRESAHA.108.177105

51. Weisberg SP, McCann D, Desai M, Rosenbaum M, Leibel RL, Ferrante AW Jr. Obesity is associated with macrophage accumulation in adipose tissue. *J Clin Invest.* (2003) 112:1796–808. doi: 10.1172/JCI200319246

52. Hotamisligil GS, Murray DL, Choy LN, Spiegelman BM. Tumor necrosis factor alpha inhibits signaling from the insulin receptor. *Proc Natl Acad Sci USA.* (1994) 91:4854–8. doi: 10.1073/pnas.91.11.4854

53. Westerbacka J, Lammi K, Häkkinen AM, Rissanen A, Salminen I, Aro A, et al. Dietary fat content modifies liver fat in overweight nondiabetic subjects. *J Clin Endocrinol Metab.* (2005) 90:2804–9. doi: 10.1210/jc.2004-1983

54. Rosqvist F, Iggman D, Kullberg J, Cedernaes J, Johansson HE, Larsson A, et al. Overfeeding polyunsaturated and saturated fat causes distinct effects on liver and visceral fat accumulation in humans. *Diabetes.* (2014) 63:2356–68. doi: 10.2337/db13-1622

55. Farias Santos J, Suruagy Amaral M, Lima Oliveira S, Porto Barbosa J, Rego Cabral C Jr., Sofia Melo I, et al. Dietary intake of ain-93 standard diet induces Fatty liver with altered hepatic fatty acid profile in Wistar rats. *Nutr Hosp.* (2015) 31:2140–6.

56. Martinez-Medina M, Denizot J, Dreux N, Robin F, Billard E, Bonnet R, et al. Western diet induces dysbiosis with increased *E coli* in CEABAC10 mice, alters host barrier function favouring AIEC colonisation. *Gut.* (2014) 63:116–24. doi: 10.1136/gutjnl-2012-304119

57. Battson ML, Lee DM, Jarrell DK, Hou S, Ecton KE, Weir TL, et al. Suppression of gut dysbiosis reverses Western diet-induced vascular dysfunction. *Am J Physiol Endocrinol Metab.* (2018) 314:E468–77. doi: 10.1152/ajpendo.00187.2017

58. Ferreira-Halder CV, Faria AVS, Andrade SS. Action and function of *Faecalibacterium prausnitzii* in health and disease. *Best Pract Res Clin Gastroenterol.* (2017) 31:643–8.

59. Martín R, Miquel S, Benevides L, Bridonneau C, Robert V, Hudault S, et al. Functional characterization of novel *Faecalibacterium prausnitzii* strains isolated from healthy volunteers: a step forward in the use of *F. prausnitzii* as a next-generation probiotic. *Front Microbiol.* (2017) 8:1226. doi: 10.3389/fmicb.2017.01226

60. Milani C, Ticinesi A, Gerritsen J, Nouvenne A, Lugli GA, Mancabelli L, et al. Gut microbiota composition and *Clostridium difficile* infection in hospitalized elderly individuals: a metagenomic study. *Sci Rep.* (2016) 6:25945. doi: 10.1038/srep25945

61. Ricaboni D, Mailhe M, Khelaifia S, Raoult D, Million M. *Romboutsia timonensis*, a new species isolated from human gut. *New Microbes New Infect.* (2016) 12:6–7. doi: 10.1016/j.nmni.2016.04.001

62. Ley RE, Bäckhed F, Turnbaugh P, Lozupone CA, Knight RD, Gordon JI. Obesity alters gut microbial ecology. *Proc Natl Acad Sci USA.* (2005) 102:11070–5. doi: 10.1073/pnas.0504978102

63. Zacarías MF, Collado MC, ómez-Gallego CG, Flinck H, Aittoniemi J, Isolauri E, et al. Pregestational overweight and obesity are associated with differences in gut microbiota composition and systemic inflammation in the third trimester. *PLoS One.* (2018) 13:e0200305. doi: 10.1371/journal.pone.0200305

64. Kameyama K, Itoh K. Intestinal colonization by a Lachnospiraceae bacterium contributes to the development of diabetes in obese mice. *Microbes Environ.* (2014) 29:427–30. doi: 10.1264/jsme2.ME14054

65. Lippert K, Kedenko L, Antonielli L, Kedenko I, Gemeier C, Leitner M, et al. Gut microbiota dysbiosis associated with glucose metabolism disorders and the metabolic syndrome in older adults. *Benef Microbes.* (2017) 8:545–56. doi: 10.3920/BM2016.0184

66. Qin J, Li Y, Cai Z, Li S, Zhu J, Zhang F, et al. A metagenome-wide association study of gut microbiota in type 2 diabetes. *Nature.* (2012) 490:55–60. doi: 10.1038/nature11450

67. Salonen A, Lahti L, Salojärvi J, Holtrop G, Korpela K, Duncan SH, et al. Impact of diet and individual variation on intestinal microbiota composition and fermentation products in obese men. *ISME J.* (2014) 8:2218–30. doi: 10.1038/ismej.2014.63

68. Shen F, Zheng RD, Sun XQ, Ding WJ, Wang XY, Fan JG. Gut microbiota dysbiosis in patients with non-alcoholic fatty liver disease. *Hepatobiliary Pancreat Dis Int.* (2017) 16:375–81.

69. Everard A, Belzer C, Geurts L, Ouwerkerk JP, Druart C, Bindels LB, et al. Cross-talk between *Akkermansia muciniphila* and intestinal epithelium controls diet-induced obesity. *Proc Natl Acad Sci USA.* (2013) 110:9066–71. doi: 10.1073/pnas.1219451110

70. Li J, Lin S, Vanhoutte PM, Woo CW, Xu A. *Akkermansia muciniphila* protects against atherosclerosis by preventing metabolic endotoxemia-induced inflammation in Apoe-/- mice. *Circulation.* (2016) 133:2434–46. doi: 10.1161/CIRCULATIONAHA.115.019645

71. Wu F, Guo X, Zhang M, Ou Z, Wu D, Deng L, et al. An *Akkermansia muciniphila* subtype alleviates high-fat diet-induced metabolic disorders and inhibits the neurodegenerative process in mice. *Anaerobe.* (2020) 61:102138. doi: 10.1016/j.anaerobe.2019.102138

72. Gu Y, Zhang Y, Li M, Huang Z, Jiang J, Chen Y, et al. Ferulic acid ameliorates atherosclerotic injury by modulating gut microbiota and lipid metabolism. *Front Pharmacol.* (2021) 12:621339. doi: 10.3389/fphar.2021.621339

73. Madison A, Kiecolt-Glaser JK. Stress, depression, diet, and the gut microbiota: human-bacteria interactions at the core of psychoneuroimmunology and nutrition. *Curr Opin Behav Sci.* (2019) 28:105–10. doi: 10.1016/j.cobeha.2019.01.011

74. Chalasani N, Younossi Z, Lavine JE, Diehl AM, Brunt EM, Cusi K, et al. The diagnosis and management of non-alcoholic fatty liver disease: practice guideline by the American association for the study of liver diseases, American college of gastroenterology, and the American gastroenterological association. *Hepatology.* (2012) 55:2005–23. doi: 10.1002/hep.25762

75. CDC. *Prevalence of Obesity Among Adults and Youth: United States, 2015-2016*. (2017). Available online at: https://www.cdc.gov/nchs/data/databriefs/db288.pdf (accessed January 13, 2022).

76. Lehnert T, Sonntag D, Konnopka A, Riedel-Heller S, König HH. Economic costs of overweight and obesity. *Best Pract Res Clin Endocrinol Metab.* (2013) 27:105–15. doi: 10.1016/j.beem.2013.01.002

77. Hariri N, Thibault L. High-fat diet-induced obesity in animal models. *Nutr Res Rev.* (2010) 23:270–99. doi: 10.1017/S0954422410000168

frontiers | Frontiers in Nutrition

TYPE Original Research
PUBLISHED 28 September 2022
DOI 10.3389/fnut.2022.925390

OPEN ACCESS

EDITED BY
Gratiela Gradisteanu Pircalabioru,
University of Bucharest, Romania

REVIEWED BY
Yatian Yang,
University of California, Davis,
United States
Chen Chen,
The University of Queensland, Australia

*CORRESPONDENCE
Xinhua Xiao
xiaoxh2014@vip.163.com

SPECIALTY SECTION
This article was submitted to Nutrition and Metabolism, a section of the journal Frontiers in Nutrition

RECEIVED 21 April 2022
ACCEPTED 24 August 2022
PUBLISHED 28 September 2022

CITATION
Ding L, Liu J, Zhou L, Jia X, Li S, Zhang Q, Yu M and Xiao X (2022) A high-fat diet disrupts the hepatic and adipose circadian rhythms and modulates the diurnal rhythm of gut microbiota-derived short-chain fatty acids in gestational mice. *Front. Nutr.* 9:925390. doi: 10.3389/fnut.2022.925390

A high-fat diet disrupts the hepatic and adipose circadian rhythms and modulates the diurnal rhythm of gut microbiota-derived short-chain fatty acids in gestational mice

Lu Ding[1], Jieying Liu[1,2], Liyuan Zhou[1], Xinmiao Jia[2], Shunhua Li[1], Qian Zhang[1], Miao Yu[1] and Xinhua Xiao[1]*

[1]Department of Endocrinology, Key Laboratory of Endocrinology, Ministry of Health, Peking Union Medical College Hospital, Chinese Academy of Medical Sciences and Peking Union Medical College, Beijing, China, [2]Department of Medical Research Center, Peking Union Medical College Hospital, Chinese Academy of Medical Sciences and Peking Union Medical College, Beijing, China

The prevalence of gestational obesity has reached epidemic proportions. Evidence supported that the interactions between the gut microbiota and circadian clocks far reached, affecting host metabolism. Our study aimed to investigate the effect of a high-fat diet (HF) on the hepatic and adipose circadian rhythms in gestational mice and to explore the role of gut microbiota-derived short-chain fatty acids (SCFAs) in mediating the effects. C57BL/6 female mice were randomly fed a standard chow diet (Ctr) or HF prior to and during pregnancy. Samples were collected every 4 h over 24 h (six time points), and 16S rRNA and metabonomics were carried out. Rhythmic patterns were identified and compared using CircaCompare. The results showed that the HF before and during pregnancy significantly induced obesity and worsen glucose tolerance, insulin sensitivity, and lipid metabolism in the gestational mice. Furthermore, the HF significantly disrupted the rhythmic pattern of hepatic and adipose circadian clock genes and downstream metabolic genes. Importantly, our results revealed that the HF altered the diurnal rhythm of the gut microbiota in a diverse manner, which was assessed across three categories: phase shift, loss rhythmicity, and gained rhythmicity. We report here, for the first time, a parallel alteration of the rhythmic phase of butyric acid and butyrate-producing *Clostridiaceae_1*, which was confirmed by a positive correlation between them. Overall, our research emphasized the importance of the rhythmicity of gut microbiota-derived SCFAs in mediating circadian disruption in response to the HF in gestational mice, which may provide novel insights into the prevention and treatment of gestational obesity.

KEYWORDS

gut microbiota, circadian rhythm, SCFAs, high-fat diet, glucose and lipid metabolism, gestational obesity

Introduction

The prevalence of gestational obesity has reached epidemic proportions (1). Epidemiologic and animal studies have demonstrated that gestational obesity increased not only the risk of developing gestational diabetes mellitus (2), lipid disorders (3), congenital heart disease (4), and preterm delivery (5, 6) but also the risk of progressing chronic metabolic diseases in the later life of offspring (7–9). With its increasing prevalence and subsequent health outcomes, it is of great importance to uncover the critical mechanisms of gestational obesity.

In mammals, the circadian clock system synchronizes daily rhythms of homeostasis, enabling organisms to temporally coordinate physiology and to align it with geophysical time (10, 11). The ubiquitous rhythmic transcriptional program is controlled by a network of core clock transcription factors, including *circadian locomotor output cycles kaput* (*CLOCK*), *brain and muscle Arnt-like protein* (*Bmal1*), *period* (*Per*), and *cryptochrome* (*Cry*), with *nuclear receptor subfamily 1*, *group D*, and *member 1* (*Rev-erbα*) family stabilizing the core oscillator (12). While the hypothalamic central clock is controlled by light, food consumption is widely considered a major stimulus for peripheral clocks in different organs (13). A high-fat diet (HF) was found to reprogram hepatic circadian clocks *via* the rewiring of specific transcriptional pathways (14). Moreover, an HF induced obesity and inhibited the expression of clock genes in adipose tissues (14). However, tissue responses to an HF are still controversial due to different nutritional compositions, intervention times, and animal models (15–18). Intriguingly, a recent study reported a poor association between the response of local clocks and the tissue rhythmic transcriptome (19). Consequently, the specific underlying mechanism responsible for the disruption of peripheral circadian rhythm remains unclear.

As a non-canonical oscillator, the gut microbiota mainly entrains dietary cues to regulate host metabolism (20). Frazier et al. newly reported that the host C-type lectin antimicrobial peptide *Reg3g* worked with key ileal microbes to induce metabolic disruption in the HF-treated mice model (21). Moreover, accumulating evidence supported that the interactions between the gut microbiota and peripheral circadian rhythm far reached, affecting host metabolism (18, 22). A recent study showed that the diurnal alteration of the gut microbiota in response to an HF reprogrammed hepatic circadian clocks and contributed to obesity in mice compared with mice fed a normal chow diet or a low-fat diet (17). Although some of the hepatic core clock genes (*Bmal1* and *Per2*) remained comparable between groups, the rhythmic transcription of PPAR signaling was altered in the HF-fed mice (17). Importantly, these effects were replicated in germ-free mice that received fecal transplantation of the gut microbiota derived from HF-fed mice, which further confirmed that the gut microbiota modulated hepatic lipid metabolism in response to the HF mainly by activating the host's circadian rhythmicity of PPAR signaling (14). Research on how the gut microbiota modulates host metabolism by interacting with host circadian clocks has focused on microbially produced metabolites, particularly including short-chain fatty acids (SCFAs). Studies have continued to show that the circadian rhythm of gut microbiota-derived SCFAs has vital effects on the host's circadian control of metabolism (14, 23). However, research on the mechanism underlying the interaction of gut microbiota and peripheral clocks and how they affect the glucose and lipid metabolism in gestational mice is limited. A clear understanding of the mechanistic changes underlying these processes could have a profoundly beneficial impact on the prevention and treatment of gestational obesity.

Therefore, in the current study, we established a gestational obesity model by feeding mice an HF prior to and during pregnancy. We aimed to investigate the effects of the HF on hepatic and adipose circadian rhythms, emphasizing alterations of the rhythmic pattern of metabolic parameters. In addition, we explored the role of gut microbiota-derived SCFAs in mediating circadian disruption in response to HF in gestational mice.

Materials and methods

Animals and experimental scheme

A total of 80 4-week-old C57BL/6 female mice were purchased from Beijing Huafukang Biotechnology Co., Ltd., (Beijing, China, SYXC-2014-0029). The mice were maintained in a specific pathogen-free (SPF) environment at a controlled temperature of 22 ± 2°C and subjected to a 12:12 light/dark cycle (lights on at 06:00 am, ZT0 = 06:00). After acclimation for 1 week, 5-week-old mice with similar body weights were randomly assigned to one of two groups: a control group (Ctr, $n = 40$), which was fed a standard chow diet (AIN-93G) (15.8% of the calories as fat), and a high-fat diet group (HF, $n = 40$), which was fed a high-fat diet (D12492) (60% of the calories as fat). After 5 weeks of intervention, the C57BL/6 female mice were mated with normal 9-week-old C57BL/6 male control mice. Pregnancy was timed based on vaginal plug formation. The morning of vaginal plug was considered E0.5. Weekly body weight and food consumption were recorded. The pregnant mice continued on their respective diets throughout the pregnancy and were killed every 4 h over 24 h at six different time points of 07:00 (ZT1), 11:00 (ZT5), 15:00 (ZT9), 19:00 (ZT13), 23:00 (ZT17), or 03:00 (ZT21) on E18.5 (**Figure 1A**). All procedures were performed in accordance with the protocol approved by the Animal Care and Ethics Committee at Peking Union Medical College Hospital (Beijing, China, XHDW-2019-012). All animal operations were conducted in compliance with the National Institutes of Health Guide for the Care and Use of Laboratory Animals.

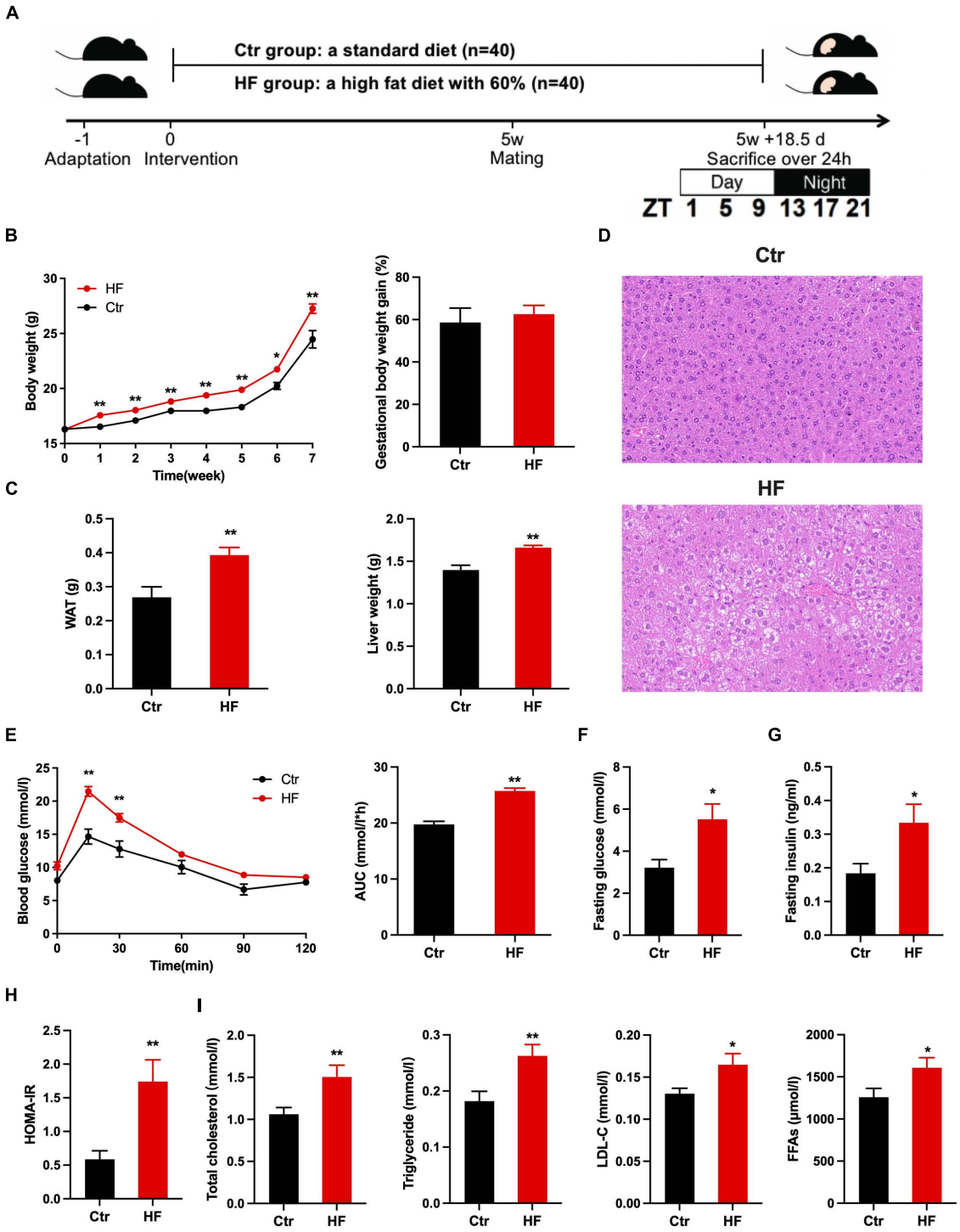

FIGURE 1
High fat diet induced obesity and metabolic disorders in gestational mice. Mice were fed with a standard chow diet, or a high-fat diet prior to and throughout pregnancy. The morning of vaginal plug confirmed the pregnancy and was considered E0.5. The pregnant mice continued to feed on their respective diets until E18.5. **(A)** Experimental design; **(B)** body weight alteration during the high-fat diet treatment (left) and gestational weight gain (right); **(C)** weight of the WAT (left) and liver (right); **(D)** histological examination of liver tissues; **(E)** oral glucose tolerance test after fasting for 6 h (left) and the area under the curve (right); **(F)** fasting glucose level; **(G)** fasting insulin level; **(H)** HOMA-IR; **(I)** level of TC, TG, LDL-C, and FFAs. Ctr, standard chow diet-fed pregnant mice; HF, high-fat diet-fed pregnant mice; HOMA-IR, homeostasis model assessment of insulin resistance; TC, total cholesterol; TG, triglyceride; LDL-C, low-density lipoprotein cholesterol; FFAs, free fatty acids. Data are expressed as means ± S.E.M. (n = 8–12/group). Student's t-test and two-way ANOVA; *$p < 0.05$ and **$p < 0.01$.

Hematoxylin and eosin staining

In brief, liver tissues were fixed in 4% PFA and embedded in paraffin. Then, 4-μm-thick sections of the tissues were prepared and stained with hematoxylin and eosin (HE) for morphological analysis.

Glucose tolerance tests

For the glucose tolerance test (GTT), the mice fasted for 6 h were orally administered a glucose load (2 g/kg of body weight). Blood glucose levels were monitored by the tail bleeding time before intervention (0 min) and 15, 30, 60, 90, and 120 min after intervention using a glucometer (Bayer, Leverkusen, Germany). The area under the curve (AUC) was calculated, as previously described (24).

Serum biochemical analyses

For serum isolation, blood samples were collected from the infraorbital retrobulbar plexus of the mice, separated by centrifugation at 3,000 × *g* for 10 min at 4°C, and then stored at −80°C. Total triglyceride (TG), total cholesterol (TC), low-density lipoprotein cholesterol (LDL-C), and free fatty acids (FFAs) were measured, as previously described (25).

Enzyme-linked immunosorbent assay

Serum insulin was measured using an enzyme-linked immunosorbent assay (ELISA) kit (80-INSMSU-E01, Salem, NH, United States) following the manufacturer's protocol. The homeostasis model assessment–insulin resistance (HOMA-IR) index was calculated according to the following formula: [fasting insulin concentration (mU/L) × fasting glucose concentration (mg/dL)]/22.5.

Reverse transcription quantitative PCR (RT-qPCR) experiment

An E.Z.N.A. Total RNA Kit (Life Technologies In., Carlsbad, CA, United States) was used to extract total RNA from liver tissues. cDNA synthesis was performed with 1 μg total RNA using the PrimeScriptTM RT Reagent Kit with gDNA Eraser (RR047A, TaKaRa Bio Inc., Otsu, Shiga, Japan). RT-qPCR was performed using SYBR® Green Master Mix (RR820A, Takara Bio Inc., Otsu, Shiga, Japan) in an ABI PRISM® 7500 Sequence Detection System (Applied Biosystems Inc.). The relative expression levels of mRNAs were calculated using the $2^{-\Delta\Delta Ct}$ method. The first normalization was to the geometrical mean of reference genes. The second normalization was to the mean expression of each condition. Log2 transformation was applied to the mRNA expression for presentation purposes (19). The primer sequences used for RT-qPCR are detailed in **Supplementary Table 1**.

Fecal microbiota analysis

Microbial DNA was extracted from the cecal content using a cecal DNA isolation kit (MN NucleoSpin 96 Soi, Germany) following the manufacturer's protocol. The V3-V4 regions of bacterial 16S rRNA genes were amplified using the primers 338F, 5′-ACTCCTACGGGAGGCAGCA-3′ and 806R, 5′-GGACTACVVGGGTATCTAATC-3′ with the barcode. PCR products were purified using the Qiagen Gel Extraction Kit (Qiagen, Germany) and quantified using a Qubit@ 2.0 Fluorometer (Thermo Scientific, United States). Tags were sequenced on the Illumina NovaSeq platform. Raw tags were quality-filtered under specific filtering conditions to obtain high-quality clean tags (26) according to the QIIME (version 1.9.1[1]) quality control process (27). Operational taxonomic units (OTUs) were clustered with a 97% similarity cutoff using UPARSE (version 7.0.1001[2]) (28). The Silva Database[3] was used to annotate representative sequences based on the Mothur algorithm (29).

Short-chain fatty acid measurement

Liver tissues were immediately collected and frozen in liquid nitrogen before GC–MS analysis. The concentration of SCFA metabolites was measured at Shanghai Biotree Biotech Co., Ltd., (Shanghai, China), as described in previous studies (30, 31). In brief, SCFAs, including acetic acid, propionic acid, butyric acid, valerate acid, isobutyric acid, isovaleric acid, and hexanoic acid, were extracted from liver tissues using solvent mixtures containing methyl tert-butyl ether and 2-methylvaleric acid. The aliquot (1 μL) was analyzed by an HP-FFAP capillary column (Agilent, Folsom, CA, United States). With helium as the carrier gas, the initial temperature was set to 80°C for 1 min, subsequently increased to 200°C for 5 min, and then maintained at 240°C for 1 min. The injection, transfer line, quad, and ion source temperatures were 240°C, 240°C, 150°C, and 200°C, respectively, and the electron impact energy was −70 eV. Mass spectrometry data were acquired in the Scan/SIM mode, with an m/z range of 33–150 after a solvent delay of 3.5 min.

1 http://qiime.org/scripts/split_libraries_fastq.html
2 http://drive5.com/uparse/
3 http://www.arb-silva.de/

Statistical analyses

Statistics were analyzed by Student's *t*-test or two-way ANOVA with Tukey's *post hoc* analyses. A *P*-value < 0.05 was considered statistically significant. Rhythmic features were defined as any feature with periods of 24 h by a *P*-value < 0.05. Specifically, loss in rhythmicity indicated a parameter which was significantly oscillated in the Ctr group, but not significantly oscillated in the HF group (Ctr $p < 0.05$, HF $p > 0.05$). Contrarily, gain rhythmicity indicated a parameter which was not significantly oscillated in the Ctr group but significantly oscillated in the HF group (Ctr $p > 0.05$, HF $p < 0.05$) (32). Phase, MESOR, and amplitude were monitored and compared using the non-linear cosinor regression tool CircaCompare when the parameters significantly oscillated in the two groups (33). Correlation analyses were performed by Spearman and Pearson correlation coefficient tests. All statistical analyses and data visualization were performed with either R v.4.1.1 or GraphPad Prism version 8.0 (GraphPad Software Inc., San Diego, CA, United States). In all bar and line plots, data were presented as the mean ± standard error of mean (S.E.M.).

Results

High-fat diet induced obesity in gestational mice

The experimental design of the study is illustrated in **Figure 1A**. To determine the effects of the HF on gestational mice, female mice were fed with an HF prior to pregnancy for 5 weeks and throughout pregnancy. The results showed that the HF significantly induced body weight gain prior to and throughout pregnancy ($P < 0.05$), although gestational body weight gain was not obviously different between the two groups (**Figure 1B**). The subcutaneous white adipose tissue (WAT) was significantly increased in the HF group compared with the Ctr group ($P < 0.01$, **Figure 1C**). Simultaneously, the liver weight was dramatically increased in the gestational mice of the HF group compared with that of the Ctr group ($P < 0.01$, **Figure 1C**), which was consistent with the increase in hepatocyte size (**Figure 1D**). These results revealed that the HF increased body weight gain, liver weight, and subcutaneous WAT weight, leading to obesity in the gestational mice.

The effects of high-fat diet on glucose and lipid metabolism in gestational mice

Since the HF significantly programmed the body weight and body composition in the gestational mice, we further detected the effects of the HF on glucose and lipid metabolism in the gestational obese mice. In mice on the HF, the oral GTT significantly elevated blood glucose at 15 min and 30 min after the administration of glucose ($P < 0.01$), and the calculated AUC of the OGTT result was also dramatically elevated in the HF group compared with the Ctr group ($P < 0.01$, **Figure 1E**). In addition, the HF led to significantly increased fasting glucose and insulin levels in the gestational mice ($P < 0.05$, **Figures 1F,G**), which resulted in a remarkable elevation in the HOMA-IR index ($P < 0.01$, **Figure 1H**). Concomitantly, TC, TG, LDL-C, and FFA levels were significantly elevated in the HF group ($P < 0.05$, **Figure 1I**). These results demonstrated that the HF markedly impaired glucose and lipid homeostasis and insulin sensitivity in the gestational obese mice.

High-fat diet disrupted the hepatic and adipose circadian rhythms in gestational mice

To address the role of the circadian rhythm in response to the HF, we first characterized the oscillation of the circadian clock genes of metabolic peripheral tissues liver and WAT and compared their rhythmic pattern in the gestational mice. The expression of *Clock*, *Bmal1*, *Per2*, *Cry2*, and *Rev-ervα* exhibited periodic oscillations after both feeding intervention in the liver and WAT (all $P < 0.05$, **Figure 2**). As shown in **Figure 2A**, the rhythmic pattern of hepatic *Cry2* and *Rev-erbα* was significantly phase-advanced in the HF group compared with the Ctr group (both $P < 0.05$). Consistently, the *Clock*, *Bmal1*, *Cry2*, and *Rev-erbα* phases were significantly advanced in the WAT (all $P < 0.05$, **Figure 2B**). However, the rhythmic pattern of clock genes also displayed tissue specificity: the MESOR of hepatic *Rev-erbα* revealed significant elevation after HF treatment compared with the Ctr group ($P < 0.05$, **Figure 2A**), while the amplitude of *Cry2* was strikingly higher in the HF group than in the Ctr group in the WAT ($P < 0.05$, **Figure 2B**). There was no dramatic difference between the feeding protocols for either phase, MESOR or amplitude for the rhythmic pattern of hepatic *Clock*, *Bmal1*, and *Per2* and adipose *Per2*.

We next determined the expression of selected genes involved in glucose and lipid metabolic physiology in the liver and WAT. The results showed that the rhythmic patterns vary among different metabolic genes in different tissues. In the liver (**Figure 3A**), the expression of *PPARα* and *SREBP1* exhibited rhythmic patterns in both feeding protocols, and both were significantly phase-advanced in the HF group compared with the Ctr group (all $P < 0.05$). By contrast, the expression of *FASN*, *Glut2*, and *G6P* lost diurnal rhythmicity after HF treatment, while the expression of *PGC-1α* merely oscillated in the HF group. In the WAT (**Figure 3B**), the expression

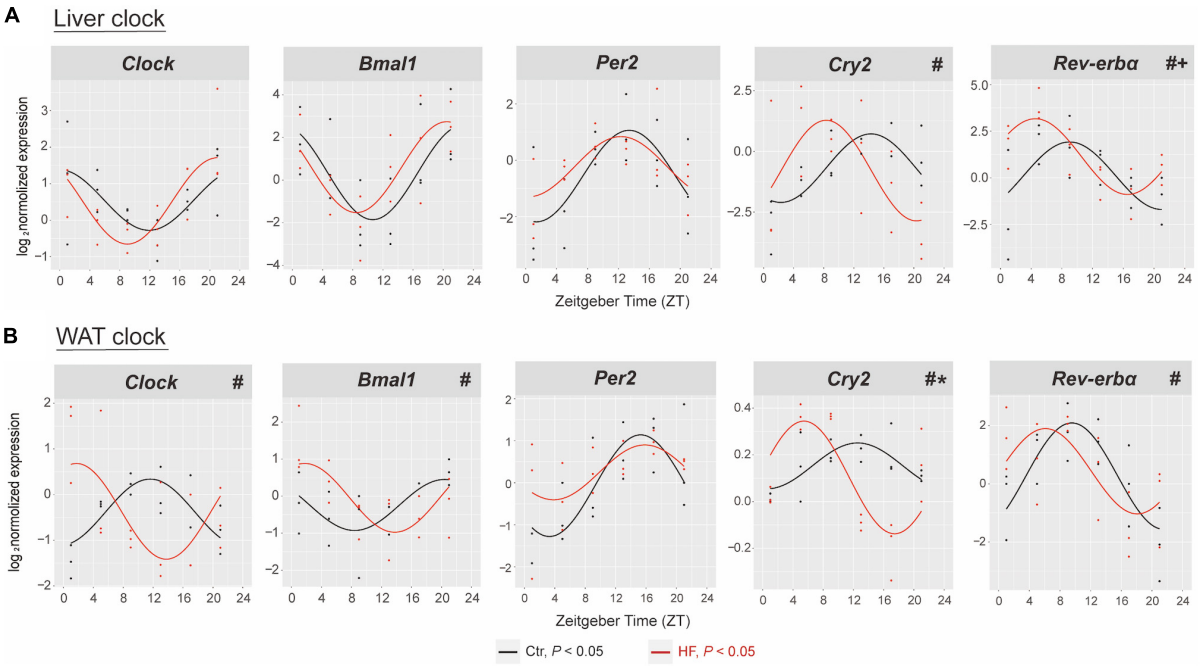

FIGURE 2
High-fat diet disrupted the hepatic and adipose circadian rhythm in gestational mice. Mice were fed with a standard chow diet or a high-fat diet prior to pregnancy for 5 weeks, and throughout pregnancy. The morning of vaginal plug confirmed the pregnancy and was considered E0.5. On E18.5, the mice were killed at 4-h intervals over 24 h. Rhythmic pattern of circadian clock genes in the **(A)** liver and **(B)** WAT. The dots mark individual measurements in each zeitgeber time (ZT), and line represents cosinor regression fit. Rhythmic pattern of genes with significant differences in phase (#), amplitude (*), or MESOR (+) derived from CircaCompare ($n = 2–3$/time point). Ctr, standard chow diet-fed pregnant mice; HF, high-fat diet-fed pregnant mice; WAT, white adipose tissue.

of *SREBP1* and *FASN* merely oscillated in the HF group, and the expression of *PPARγ*, *ACC*, *HSL*, and *ATGL* did not exhibit statistical diurnal rhythmicity on either feeding intervention. These observations suggested that disruption of the peripheral circadian rhythm had a significant impact on metabolic physiology.

The diurnal rhythm of gut microbiota was altered in a diverse manner in high-fat-treated gestational mice

The gut microbiota has been identified as a crucial participant involved in host circadian rhythms in response to dietary cues and itself also undergoes diurnal oscillation (20). We next performed 16S rRNA gene sequencing to examine whether the gut microbiota plays a role in regulating the peripheral circadian rhythm in the gestational mice. PCoA showed that the HF markedly altered the microbial community composition across different time points compared with the Ctr group (**Figure 4A**). The rhythmic patterns of the relative abundance varied among the different microbial families, although there was no significant difference in family-level relative abundance between the two groups (**Figure 4B**). One of the families, *Clostridiaceae_1*, exhibited a diurnal rhythm on both feeding protocols, and its rhythmic pattern was dramatically phase-delayed in the HF group compared with that in the Ctr group ($P < 0.05$, **Figure 4C**). Simultaneously, *Veillonellaceae* and *Prevotellaceae* lost rhythmicity in the HF treatment group (**Figure 4D**), while *Erysipelotrichaceae* and *Ruminococcaceae* gained rhythmicity in the HF group (**Figure 4E**). Collectively, these data revealed that the HF altered the diurnal rhythm of gut microbiota in a complex and diverse manner in the gestational mice.

High-fat diet modulated the diurnal rhythm of gut microbiota-derived short-chain fatty acids

Microbiota-derived SCFAs are regulatory controllers of host metabolism, and they are transported by the portal vein (34). Since SCFAs are mainly absorbed by the liver, we monitored the hepatic SCFA concentration by GC-MS. As indicated in **Figure 5A**, PCoA demonstrated that the HF altered the concentration of SCFAs across different time points compared with that of the Ctr group (**Figure 5A**). The hepatic concentration of propionic acid, valeric acid, and

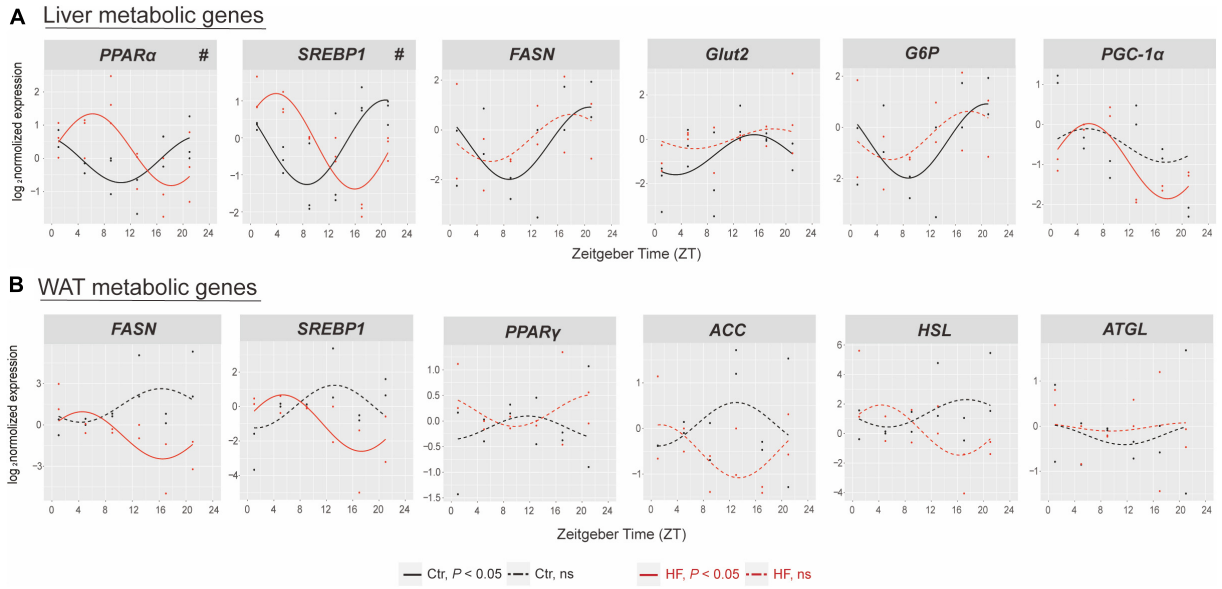

FIGURE 3
The effects of high-fat diet on metabolic genes of liver and white adipose tissue in gestational mice. Mice were fed with a standard chow diet or a high-fat diet prior to pregnancy for 5 weeks, and throughout pregnancy. The morning of vaginal plug confirmed the pregnancy and was considered E0.5. On E18.5, the mice were killed at 4-h intervals over 24 h. Rhythmic pattern of metabolic genes in the **(A)** liver and **(B)** WAT. Significant rhythms ($P < 0.05$) are denoted by the continuous line, and non-significant rhythms are denoted by the dotted line. The dots mark individual measurements in each zeitgeber time (ZT), and line represents cosinor regression fit. Rhythmic pattern of genes with significant differences in phase (#) derived from CircaCompare ($n = 2–3$/time point). Ctr, standard chow diet-fed pregnant mice; HF, high-fat diet-fed pregnant mice; WAT, white adipose tissue.

hexanoic acid was significantly increased in the HF group compared with the Ctr group (all $P < 0.05$), while acetic acid, isobutyric acid, butyric acid, and isovaleric acid showed no difference between the groups (**Figure 5B**). Among all the SCFAs (**Figure 5C**), butyric acid exhibited a diurnal rhythm in both feeding protocols and was significantly phase-delayed in the HF group compared with the Ctr group ($P < 0.05$). In addition, isovaleric acid increased rhythmically after HF treatment. Other SCFAs did not exhibit a statistically significant diurnal rhythm in either feeding intervention. The association between SCFAs and the gut microbiota was confirmed by correlation analysis (**Figures 5D,E**). The results showed that butyric acid and isovaleric acid were significantly positively correlated with *Clostridiaceae_1*.

Discussion

An adverse gestational metabolic status exposes the fetus to a suboptimal intrauterine environment, which can disrupt fetal development and influence long-term impacts on health and disease in offspring (35, 36). Such a causal relationship is encompassed in the concept of the Developmental Origins of Health and Disease (DOHaD) (37). Our previous studies suggested that a maternal HF before and during pregnancy and lactation contributed to glucose and lipid metabolic disorders in dams and offspring (24, 38). Here, we further confirmed that the HF before and during pregnancy significantly induced obesity and dramatically worsen glucose tolerance, insulin sensitivity, and lipid metabolism in the gestational mice.

The liver and adipose tissues are core sites for the central control of glucose and lipid metabolism (13). Studies have suggested that among different peripheral tissues, daytime feeding strongly inverted the local clocks in the liver and WAT compared with freely fed animals (19), indicating that the circadian clock in the liver and adipose tissue are most susceptible to different nutritional regimes. To date, the effects of an HF on the circadian clock in the liver and WAT are still controversial due to complexity imposed by different nutritional compositions, intervention times, and animal models (15–18). In this study, we fed the C57BL/6 female mice a 60% (kcal) fat diet prior to and during pregnancy. Our results showed that the HF significantly advanced the rhythmic phase of hepatic *Cry2* and *Rev-erbα* and adipose *Clock*, *Bmal1*, *Cry2*, and *Rev-erbα* in the gestational mice. As one of the core clock machineries, *Cry* regulated hepatic gluconeogenesis through activating the G protein-coupled receptor, which blocked the glucose-mediated increases in the intracellular adenosine 3′,5′-cyclic monophosphate (cAMP) concentrations and in the PKA-mediated phosphorylation of Creb (39). The nuclear receptor *Rev-erbα* has been shown to unite with core circadian

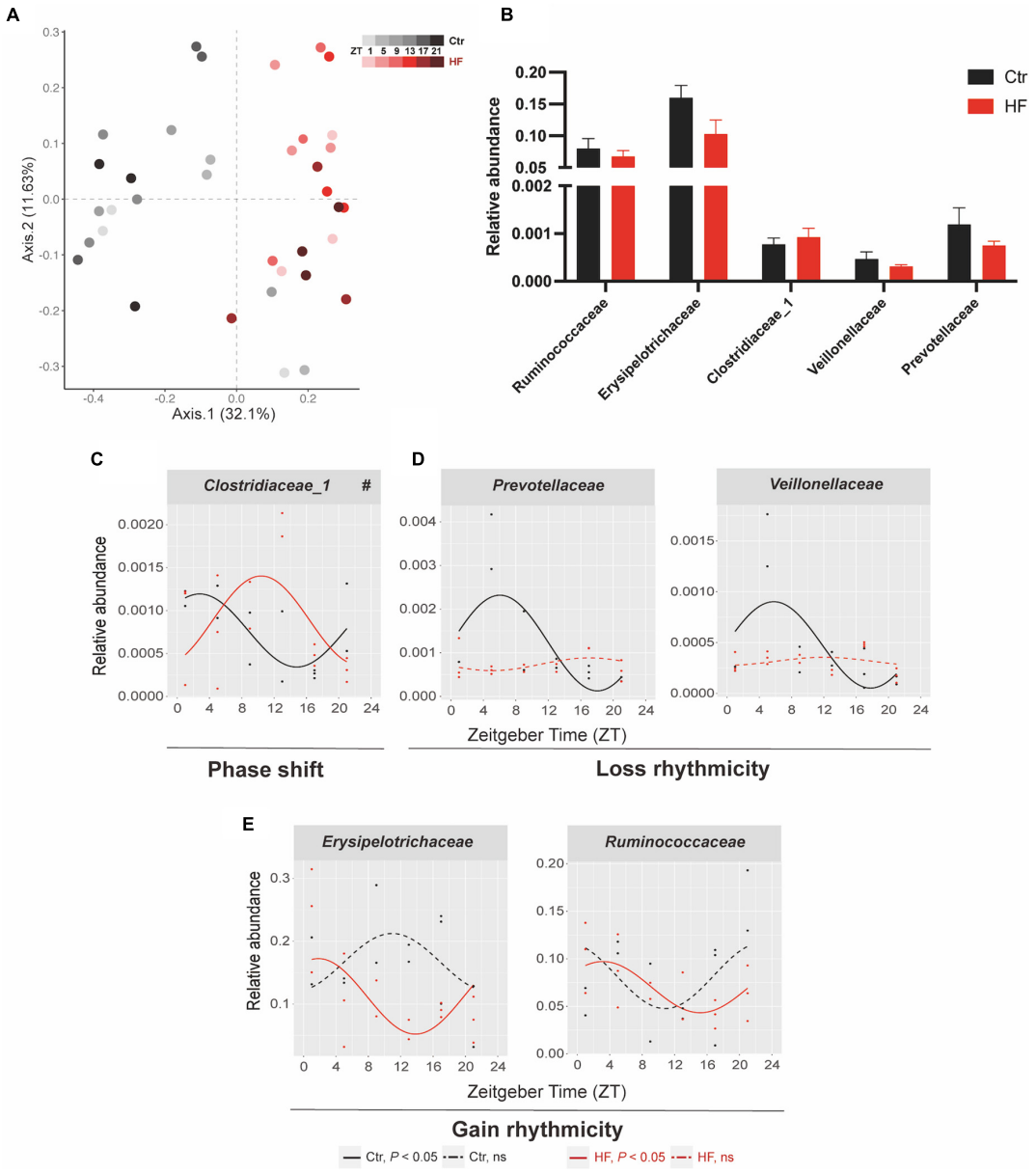

FIGURE 4
Diurnal rhythm of gut microbiota was altered in a diverse manner in HF-treated gestational mice. Mice were fed with a standard chow diet, or a high-fat diet prior to pregnancy for 5 weeks, and throughout pregnancy. The morning of vaginal plug confirmed the pregnancy and was considered E0.5. On E18.5, the pregnant mice were killed at 4-h intervals over 24 h. **(A)** Bray–Curtis PCoA. Shading represents different time points as indicated. **(B)** The relative abundance and **(C–E)** the diurnal patterns of microbiota. Significant rhythms ($P < 0.05$) are denoted by the continuous line, and non-significant rhythms are denoted by the dotted line. The dots mark individual measurements in each zeitgeber time (ZT), and line represents cosinor regression fit. Rhythmic pattern of genes with significant differences in phase (#) derived from CircaCompare ($n = 2–3$/time point). Data of bar chart are expressed as means ± S.E.M. ($n = 12$/group) using Student's *t*-test. Ctr, standard chow diet-fed pregnant mice; HF, high-fat diet-fed pregnant mice.

clock genes and other components of the principal feedback loop, contributing to the clock function in driving rhythmic expression patterns (40). Cistromic analysis has shown that dual depletion of *Rev-erbα/β* in mice profoundly disrupts lipid metabolic gene networks, emphasizing its vital role in maintaining lipid homeostasis (12). Moreover, diverse nutrients may activate different metabolic and physiological signals, all of which are potential zeitgebers (41, 42). The responses and interactions between different signals can vary for different organs. Therefore, this partly explains the varied extent of the phase shift of the circadian clock in the liver and WAT. To the best of our knowledge, this is the first study to report a phase

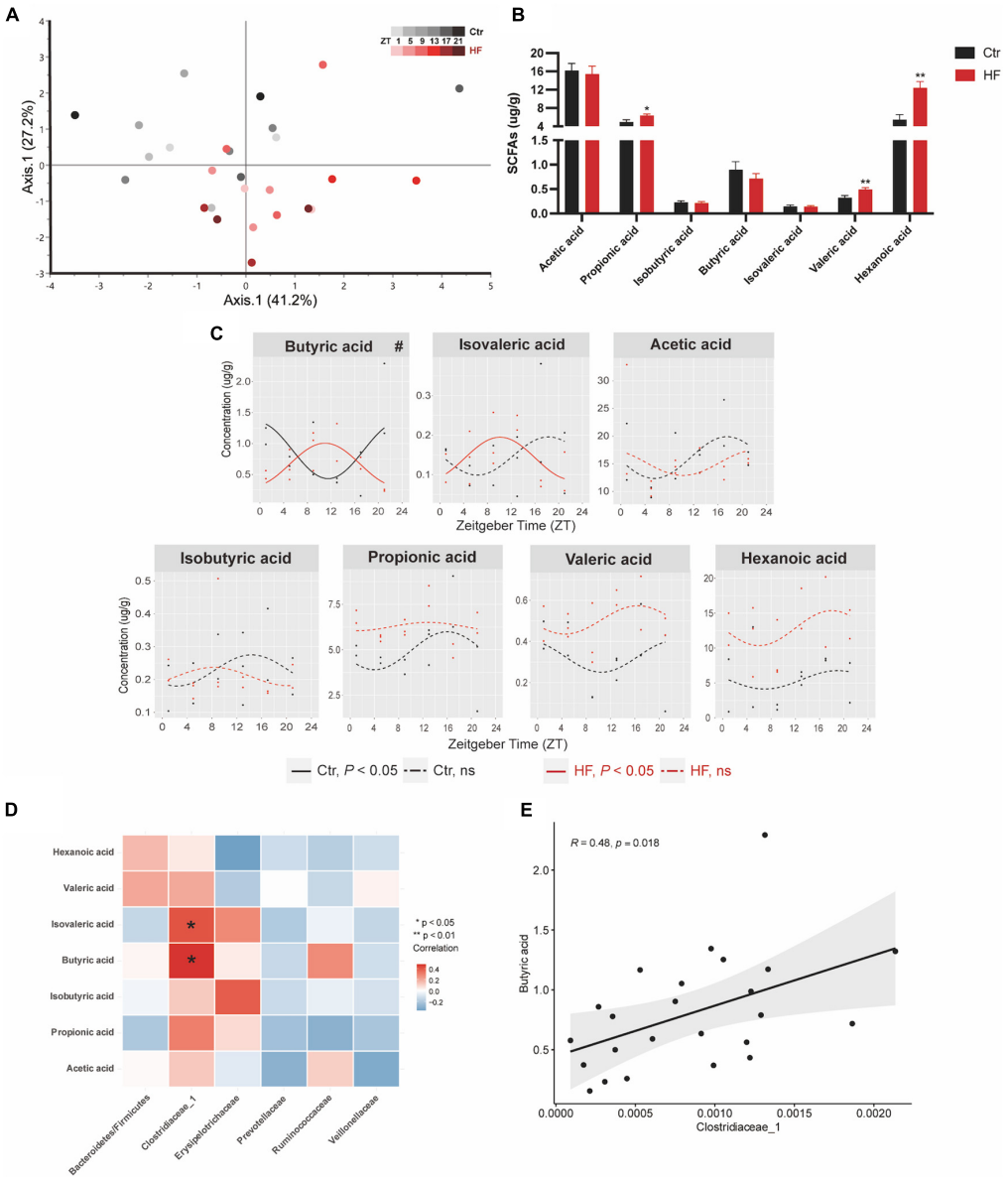

FIGURE 5
High-fat diet modulated the diurnal rhythm of gut microbiota-derived short-chain fatty acids. Mice were fed with a standard chow diet, or a high-fat diet prior to pregnancy for 5 weeks, and throughout pregnancy. The morning of vaginal plug confirmed the pregnancy and was considered E0.5. On E18.5, pregnant mice were killed at 4-h intervals over 24 h. **(A)** Euclidean distance PCoA. Shading represents different time points as indicated. **(B)** Relative abundance and **(C)** diurnal patterns of SCFAs. **(D)** Heatmap of correlation analysis between SCFAs and the altered family. **(E)** Correlation analysis between butyric acid and *Clostridiaceae_1*. Significant rhythms ($P < 0.05$) are denoted by the continuous line, and non-significant rhythms are denoted by the dotted line. The dots mark individual measurements in each zeitgeber time (ZT), and line represents cosinor regression fit. Rhythmic pattern of genes with significant differences in phase (#) derived from CircaCompare ($n = 2–3$/time point). Data of bar chart are expressed as means ± S.E.M. ($n = 12$/group) using Student's *t*-test; $^*p < 0.05$ and $^{**}p < 0.01$. Ctr, standard chow diet-fed pregnant mice; HF, high-fat diet-fed pregnant mice; SCFAs, short-chain fatty acids.

shift in the hepatic and adipose circadian clock in HF-treated gestational mice. These outcomes may extend the understanding of how peripheral circadian clocks respond to the HF in the gestational mice.

Oscillations of the core circadian clock must be transmitted *via* transcriptional signals among multiple clock-controlled genes to drive downstream rhythmic outputs (11). However, a recent study reported a poor association between the response of the clock and the tissue rhythmic transcriptome (19). Consistent with this study, our findings revealed that the alteration of metabolic genes did not perfectly match the change in the tissue clock on the HF. In the liver, the

nuclear receptor *PPARα*, a crucial factor in regulating dynamic lipid metabolism (43), and the lipogenesis gene *SREBP1* were phase-advanced in the HF group. Furthermore, the fatty acid synthase *FASN*, glucose transporter *Glut2*, and the glycolysis key enzyme *G6P* lost rhythmicity statistically, while the gluconeogenesis gene *PGC-1α* gained rhythmicity in the liver of the HF group compared with that of the Ctr group. In the WAT, *FASN* and *SREBP1* gained rhythmicity in the HF group compared with the Ctr group. Neither the master regulator of adipogenesis, *PPARγ*, nor the lipogenesis gene *ACC*, and the lipidolysis genes *HSL* and *ATGL* exhibited rhythmicity statistically in both groups. Taken together, we found that the HF resulted in a significant phase shift in hepatic and adipose circadian clock genes and downstream metabolic genes, which is different from the non-pregnant HF-fed mice (44, 45). Studies have confirmed that progesterone and estrogen exhibited rhythmicity (46, 47). Simultaneously, evidence has showed that progesterone altered genes along circadian rhythm signaling and hypothalamic–pituitary–gonadal axes (48). Since the gestational mice experience dramatic change in the level of sex hormone, these may partially explain the difference between the circadian manner in the pregnant mice and non-pregnant mice, although the circadian rhythm of the sex hormone need to be further determined.

The gut microbiota is confirmed to exhibit diurnal rhythmicity in relative abundance and functional level, which has a major influence on the circadian clock network and host metabolism (17, 49). Unlike other peripheral organs, microbial oscillators neither entrain on photic cues nor follow the control of the core clock machinery. Dietary cues are the primary driver in modulating the rhythmic pattern of the gut microbiota (20). Since the rhythmic patterns of metabolic genes were not entirely regulated by their core clock, we hypothesized that the gut microbiota played a role in modulating the host peripheral circadian clock and downstream genes. Intriguingly, we found that the HF altered the diurnal rhythm of gut microbiota in a diverse manner, which we classified into three categories: (1) phase shift: contrary to the phase-advanced circadian clock in the liver and WAT, the relative abundance of butyric acid-producing family *Clostridiaceae_1* was significantly phase-delayed in the HF group compared with the Ctr group (50); (2) loss rhythmicity: *Veillonellaceae* and *Prevotellaceae* have been confirmed to be responsible for producing SCFAs (51, 52), and both lost rhythmicity in the HF group; (3) gain rhythmicity: the families *Erysipelotrichaceae* and *Ruminococcaceae* both gained rhythmicity in the HF group compared with the Ctr group. The study has revealed that *Erysipelotrichaceae* accelerated cholesterol accumulation by producing trimethylamine *N*-oxide, indicating its role in modulating lipid metabolism (53). Furthermore, many genera from the *Ruminococcaceae* family are SCFA producers that alter SCFA production and thereby influence systemic circulation (54). Studies have the alteration of the gut microbiota in the HF in the gestational mice (44, 45). To date, several studies have explored the diurnal rhythm of the gut microbiota in response to the HF (17, 18, 23). However, data identifying the classical markers in the circadian rhythm in the HF directly in the pregnant mice are lacking. Hence, for the first time, our study revealed that the HF distinctively altered the rhythmic pattern of the gut microbiota. Given that all of the altered families belong to the SCFA-producing bacteria, we were triggered to detect the concentration and rhythmic pattern of SCFAs.

SCFAs, produced by intestinal microbial fermentation of dietary fibers and complex carbohydrates, consist primarily of acetic acid, propionic acid, and butyric acid (55). SCFAs can be transported by the portal vein to peripheral tissues, serving as mediators of the cross talk between the gut microbiome and other organs (56). Since SCFAs are mainly absorbed by the liver (17, 34), we monitored the hepatic SCFA content. Among all the SCFAs, butyric acid exhibited a diurnal rhythm in both feeding protocols, and its rhythmic phase was significantly delayed in the HF group compared with the Ctr group. As a kind of energy source, butyric acid is considered an important regulator of gene expression and appears to play essential roles in gut health and host metabolism (57). In human and mouse B cells, butyric acid inhibited the expression of genes *Aicda* and *Prdm1* by acting as histone deacetylation inhibitor (58). Leone et al. reported that butyric acid caused alteration of the diurnal pattern of the hepatic circadian clock, mainly by impacting the expression of *Per2* and *Bmal1* in mouse hepatic organoids (17). A recent study revealed that increased butyric acid dramatically expanded the phase and amplitude of hepatic *Per2* expression, thus enhancing the expression of the downstream phospholipid metabolic genes, enabling the host to maximize caloric uptake (59). Interestingly, for the first time, our study found that the phase alteration of butyric acid was consistent with that of the butyrate-producing family *Clostridiaceae_1* in the gestational mice. The correlation analysis further confirmed the association between them by showing that butyric acid was significantly positively correlated with *Clostridiaceae_1*. These data may provide support for the hypothesis that the HF modulates the peripheral circadian rhythm by modulating gut microbiota-derived SCFAs, although assertion of a cause and effect relationship will require further investigation.

Overall, this study showed that the HF before and during pregnancy significantly induced obesity and worsen glucose tolerance, insulin sensitivity, and lipid metabolism in the gestational mice. Furthermore, we first established a gestational mice model in a circadian manner, and we found the HF resulted in a significant phase shift in hepatic and adipose circadian clock genes and downstream metabolic genes. Moreover, we performed the analysis of rhythmicity using the latest and highly sensitive tool CircaCompare. Compared with the traditional tools for rhythmicity detection, such as JTK_Cycle, Bio_Cycle, and RAIN, CircaCompare provides a means to quantify and

statistically support differences between rhythms, specific to the characteristic desired (MESOR, amplitude, and phase) with high sensitivity (33). To the best of our knowledge, it is the latest tool for comparison between rhythms directly (60, 61). We took advantage of this tool to explore the circadian characteristics in the gestational mice. Importantly, our results revealed that the HF altered the diurnal rhythm of gut microbiota in a diverse manner in the gestational mice, which we classified into three categories: phase shift, loss rhythmicity, and gain rhythmicity. More fundamentally, this study reported a parallel alteration of the rhythmic phase of butyric acid- and butyrate-producing *Clostridiaceae_1*, which was further confirmed by a significant positive correlation between them. Since chronotherapeutics holds great promise for improving efficacies, these data provided support for the consideration of applying the timed treatments for managed health during gestation.

Consequently, our research emphasized the importance of the rhythmicity of gut microbiota-derived SCFAs in mediating circadian disruption in response to an HF in gestational mice, which may provide novel insights into the prevention and treatment of gestational obesity.

Data availability statement

The data presented in this study are deposited in the NCBI repository https://www.ncbi.nlm.nih.gov/, accession number: PRJNA846143.

Ethics statement

The animal study was reviewed and approved by the Animal Care and Ethics Committee at Peking Union Medical College Hospital (Beijing, China, XHDW-2019-012).

Author contributions

LD was responsible for the animal experiments, data analysis, making figures, drafting, and revising the manuscript. JL helped with the study design and reviewed the manuscript. XJ helped with the data analysis. LZ, SL, QZ, and MY helped with the animal experiments. XX contributed to the whole study design, data interpretation, and reviewed the manuscript. All authors have read and approved the final version of the manuscript.

Funding

This work was supported by the grants from National Natural Science Foundation of China (Nos. 81870579, 81900723, 82170854, and 81870545), Beijing Natural Science Foundation (7202163), Beijing Municipal Science and Technology Commission (Z201100005520011), National Key Research and Development Program of China (2018YFC2001100), CAMS Innovation Fund for Medical Sciences (CIFMS2021-1-I2M-002 and CIFMS2017-I2M-1-008).

Conflict of interest

The authors declare that the research was conducted in the absence of any commercial or financial relationships that could be construed as a potential conflict of interest.

Publisher's note

All claims expressed in this article are solely those of the authors and do not necessarily represent those of their affiliated organizations, or those of the publisher, the editors and the reviewers. Any product that may be evaluated in this article, or claim that may be made by its manufacturer, is not guaranteed or endorsed by the publisher.

Supplementary material

The Supplementary Material for this article can be found online at: https://www.frontiersin.org/articles/10.3389/fnut.2022.925390/full#supplementary-material

References

1. World Health Organization. *Obesity and Overweight (World Health Organization)*. Geneva: WHO (2021).

2. Sweeting A, Wong J, Murphy HR, Ross GP. A clinical update on gestational diabetes mellitus. *Endocr Rev*. (2022) bnac003. doi: 10.1210/endrev/bnac003

3. Bidne KL, Rister AL, McCain AR, Hitt BD, Dodds ED, Wood JR. Maternal obesity alters placental lysophosphatidylcholines, lipid storage, and the expression of genes associated with lipid metabolism‡. *Biol Reprod*. (2021) 104:197–210. doi: 10.1093/biolre/ioaa191

4. Helle E, Priest JR. Maternal obesity and diabetes mellitus as risk factors for congenital heart disease in the offspring. *J Am Heart Assoc*. (2020) 9:e011541. doi: 10.1161/JAHA.119.011541

5. Bellamy L, Casas JP, Hingorani AD, Williams D. Type 2 diabetes mellitus after gestational diabetes: a systematic review and meta-analysis. *Lancet*. (2009) 373:1773–9. doi: 10.1016/S0140-6736(09)60731-5

6. Buchanan TA, Xiang AH, Page KA. Gestational diabetes mellitus: risks and management during and after pregnancy. *Nat Rev Endocrinol*. (2012) 8:639–49. doi: 10.1038/nrendo.2012.96

7. Johns EC, Denison FC, Norman JE, Reynolds RM. Gestational diabetes mellitus: mechanisms, treatment, and complications. *Trends Endocrinol Metab.* (2018) 29:743–54.

8. Jaskolka D, Retnakaran R, Zinman B, Kramer CK. Sex of the baby and risk of gestational diabetes mellitus in the mother: a systematic review and meta-analysis. *Diabetologia.* (2015) 58:2469–75. doi: 10.1007/s00125-015-3726-1

9. Damm P, Houshmand-Oeregaard A, Kelstrup L, Lauenborg J, Mathiesen ER, Clausen TD. Gestational diabetes mellitus and long-term consequences for mother and offspring: a view from Denmark. *Diabetologia.* (2016) 59:1396–9. doi: 10.1007/s00125-016-3985-5

10. Bass J, Lazar MA. Circadian time signatures of fitness and disease. *Science.* (2016) 354:994–9. doi: 10.1126/science.aah4965

11. Panda S, Antoch MP, Miller BH, Su AI, Schook AB, Straume M, et al. Coordinated transcription of key pathways in the mouse by the circadian clock. *Cell.* (2002) 109:307–20.

12. Cho H, Zhao X, Hatori M, Yu RT, Barish GD, Lam MT, et al. Regulation of circadian behaviour and metabolism by REV-ERB-α and REV-ERB-β. *Nature.* (2012) 485:123–7. doi: 10.1038/nature11048

13. Reinke H, Asher G. Crosstalk between metabolism and circadian clocks. *Nat Rev Mol Cell Biol.* (2019) 20:227–41. doi: 10.1038/s41580-018-0096-9

14. Murakami M, Tognini P, Liu Y, Eckel-Mahan KL, Baldi P, Sassone-Corsi P. Gut microbiota directs PPARγ-driven reprogramming of the liver circadian clock by nutritional challenge. *EMBO Rep.* (2016) 17:1292–303. doi: 10.15252/embr.201642463

15. Yanagihara H, Ando H, Hayashi Y, Obi Y, Fujimura A. High-fat feeding exerts minimal effects on rhythmic mRNA expression of clock genes in mouse peripheral tissues. *Chronobiol Int.* (2006) 23:905–14. doi: 10.1080/07420520600827103

16. Paschos GK, Ibrahim S, Song WL, Kunieda T, Grant G, Reyes TM, et al. Obesity in mice with adipocyte-specific deletion of clock component Arntl. *Nat Med.* (2012) 18:1768–77. doi: 10.1038/nm.2979

17. Leone V, Gibbons SM, Martinez K, Hutchison AL, Huang EY, Cham CM, et al. Effects of diurnal variation of gut microbes and high-fat feeding on host circadian clock function and metabolism. *Cell Host Microbe.* (2015) 17:681–9. doi: 10.1016/j.chom.2015.03.006

18. Kohsaka A, Laposky AD, Ramsey KM, Estrada C, Joshu C, Kobayashi Y, et al. High-fat diet disrupts behavioral and molecular circadian rhythms in mice. *Cell Metab.* (2007) 6:414–21. doi: 10.1016/j.cmet.2007.09.006

19. Manella G, Sabath E, Aviram R, Dandavate V, Ezagouri S, Golik M, et al. The liver-clock coordinates rhythmicity of peripheral tissues in response to feeding. *Nat Metab.* (2021) 3:829–42. doi: 10.1038/s42255-021-00395-7

20. Choi H, Rao MC, Chang EB. Gut microbiota as a transducer of dietary cues to regulate host circadian rhythms and metabolism. *Nat Rev Gastroenterol Hepatol.* (2021) 18:679–89. doi: 10.1038/s41575-021-00452-2

21. Frazier K, Kambal A, Zale EA, Pierre JF, Hubert N, Miyoshi S, et al. High-fat diet disrupts REG3g and gut microbial rhythms promoting metabolic dysfunction. *Cell Host Microbe.* (2022) 30:809–23. doi: 10.1016/j.chom.2022.03.030

22. Chaix A, Lin T, Le HD, Chang MW, Panda S. Time-restricted feeding prevents obesity and metabolic syndrome in mice lacking a circadian clock. *Cell Metab.* (2019) 29:303–19.e4. doi: 10.1016/j.cmet.2018.08.004

23. Han S, Gao H, Song R, Zhang W, Li Y, Zhang J. Oat fiber modulates hepatic circadian clock via promoting gut microbiota-derived short chain fatty acids. *J Agric Food Chem.* (2021) 69:15624–35. doi: 10.1021/acs.jafc.1c06130

24. Zheng J, Xiao X, Zhang Q, Yu M, Xu J, Wang Z. Maternal high-fat diet modulates hepatic glucose, lipid homeostasis and gene expression in the PPAR pathway in the early life of offspring. *Int J Mol Sci.* (2014) 15:14967–83. doi: 10.3390/ijms150914967

25. Zhou LY, Xiao XH, Zhang Q, Zheng J, Li M, Deng MQ. A Possible mechanism: genistein improves metabolism and induces white fat browning through modulating hypothalamic expression of Ucn3, Depp, and Stc1. *Front Endocrinol.* (2019) 10:478. doi: 10.3389/fendo.2019.00478

26. Bokulich NA, Subramanian S, Faith JJ, Gevers D, Gordon JI, Knight R, et al. Quality-filtering vastly improves diversity estimates from Illumina amplicon sequencing. *Nat Methods.* (2013) 10:57–9. doi: 10.1038/nmeth.2276

27. Caporaso JG, Kuczynski J, Stombaugh J, Bittinger K, Bushman FD, Costello EK, et al. QIIME allows analysis of high-throughput community sequencing data. *Nat Methods.* (2010) 7:335–6.

28. Edgar RC. UPARSE: highly accurate OTU sequences from microbial amplicon reads. *Nat Methods.* (2013) 10:996–8. doi: 10.1038/nmeth.2604

29. Quast C, Pruesse E, Yilmaz P, Gerken J, Schweer T, Yarza P, et al. The SILVA ribosomal RNA gene database project: improved data processing and web-based tools. *Nucleic Acids Res.* (2013) 41:D590–6. doi: 10.1093/nar/gks1219

30. Wei Z, Zhou N, Zou L, Shi Z, Dun B, Ren G, et al. Soy protein alleviates malnutrition in weaning rats by regulating gut microbiota composition and serum metabolites. *Front Nutr.* (2021) 8:774203. doi: 10.3389/fnut.2021.774203

31. Shi Z, Zhu Y, Teng C, Yao Y, Ren G, Richel A. Anti-obesity effects of α-amylase inhibitor enriched-extract from white common beans (*Phaseolus vulgaris* L.) associated with the modulation of gut microbiota composition in high-fat diet-induced obese rats. *Food Funct.* (2020) 11:1624–34. doi: 10.1039/c9fo01813a

32. Gutierrez Lopez DE, Lashinger LM, Weinstock GM, Bray MS. Circadian rhythms and the gut microbiome synchronize the host's metabolic response to diet. *Cell Metab.* (2021) 33:873–87. doi: 10.1016/j.cmet.2021.03.015

33. Parsons R, Parsons R, Garner N, Oster H, Rawashdeh O. CircaCompare: a method to estimate and statistically support differences in mesor, amplitude and phase, between circadian rhythms. *Bioinformatics.* (2020) 36:1208–12. doi: 10.1093/bioinformatics/btz730

34. Cummings JH, Pomare EW, Branch WJ, Naylor CP, Macfarlane GT. Short chain fatty acids in human large intestine, portal, hepatic and venous blood. *Gut.* (1987) 28:1221–7. doi: 10.1136/gut.28.10.1221

35. Campodonico-Burnett W, Hetrick B, Wesolowski SR, Schenk S, Takahashi DL, Dean TA, et al. Maternal obesity and western-style diet impair fetal and juvenile offspring skeletal muscle insulin-stimulated glucose transport in nonhuman primates. *Diabetes.* (2020) 69:1389–400. doi: 10.2337/db19-1218

36. Sun Y, Wang Q, Zhang Y, Geng M, Wei Y, Liu Y, et al. Multigenerational maternal obesity increases the incidence of HCC in offspring via miR-27a-3p. *J Hepatol.* (2020) 73:603–15. doi: 10.1016/j.jhep.2020.03.050

37. Barker DJ. The origins of the developmental origins theory. *J Intern Med.* (2007) 261:412–7. doi: 10.1111/j.1365-2796.2007.01809.x

38. Zhou LY, Xiao XH, Zhang Q, Zheng J, Li M, Wang XJ, et al. Gut microbiota might be a crucial factor in deciphering the metabolic benefits of perinatal genistein consumption in dams and adult female offspring. *Food Funct.* (2019) 10:4505–21. doi: 10.1039/c9fo01046g

39. Zhang EE, Liu Y, Dentin R, Pongsawakul PY, Liu AC, Hirota T, et al. Cryptochrome mediates circadian regulation of cAMP signaling and hepatic gluconeogenesis. *Nat Med.* (2010) 16:1152–6. doi: 10.1038/nm.2214

40. Solt LA, Wang Y, Banerjee S, Hughes T, Kojetin DJ, Lundasen T, et al. Regulation of circadian behaviour and metabolism by synthetic REV-ERB agonists. *Nature.* (2012) 485:62–8.

41. Pezük P, Mohawk JA, Wang LA, Menaker M. Glucocorticoids as entraining signals for peripheral circadian oscillators. *Endocrinology.* (2012) 153:4775–83. doi: 10.1210/en.2012-1486

42. Crosby P, Hamnett R, Putker M, Hoyle NP, Reed M, Karam CJ, et al. Insulin/IGF-1 drives PERIOD synthesis to entrain circadian rhythms with feeding time. *Cell.* (2019) 177:896–909.e20. doi: 10.1016/j.cell.2019.02.017

43. Oishi K, Shirai H, Ishida N. CLOCK is involved in the circadian transactivation of peroxisome-proliferator-activated receptor alpha (PPARalpha) in mice. *Biochem J.* (2005) 386(Pt 3):575–81.

44. Miao M, Wang Q, Wang X, Fan C, Luan T, Yan L, et al. The protective effects of inulin-type fructans against high-fat/sucrose diet-induced gestational diabetes mice in association with gut microbiota regulation. *Front Microbiol.* (2022) 13:832151. doi: 10.3389/fmicb.2022.832151

45. Chung E, Grue KA, Kaur G, Mallory B, Serrano CR, Ullevig SL, et al. Maternal exercise before and during pregnancy alleviates metabolic dysfunction associated with high-fat diet in pregnant mice, without significant changes in gut microbiota. *Nutr Res.* (2019) 69:42–57. doi: 10.1016/j.nutres.2019.08.002

46. Anderson ST, FitzGerald GA. Sexual dimorphism in body clocks. *Science.* (2020) 369:1164–5.

47. Junkermann H, Mangold H, Vecsei P, Runnebaum B. Circadian rhythm of serum progesterone levels in human pregnancy and its relation to the rhythm of cortisol. *Acta Endocrinol.* (1982) 101:98–104. doi: 10.1530/acta.0.1010098

48. Xia X, Wang P, Wan R, Chang Z, Du Q. Progesterone affects sex differentiation and alters transcriptional of genes along circadian rhythm signaling and hypothalamic-pituitary-gonadal axes in juvenile Yellow River Carp (*Cyprinus carpio* var.). *Environ Toxicol.* (2019) 34:1255–62. doi: 10.1002/tox.22826

49. Bishehsari F, Voigt RM, Keshavarzian A. Circadian rhythms and the gut microbiota: from the metabolic syndrome to cancer. *Nat Rev Endocrinol.* (2020) 16:731–9. doi: 10.1038/s41574-020-00427-4

50. Fu X, Liu Z, Zhu C, Mou H, Kong Q. Nondigestible carbohydrates, butyrate, and butyrate-producing bacteria. *Crit Rev Food Sci Nutr.* (2019) 59(Suppl. 1): S130–52.

51. Louis P, Flint HJ. Formation of propionate and butyrate by the human colonic microbiota. *Environ Microbiol.* (2017) 19:29–41. doi: 10.1111/1462-2920.13589

52. Gierse LC, Meene A, Schultz D, Schwaiger T, Schröder C, Mücke P, et al. Influenza A H1N1 induced disturbance of the respiratory and fecal microbiome of german landrace pigs – A multi-omics characterization. *Microbiol Spect.* (2021) 9:e0018221. doi: 10.1128/Spectrum.00182-21

53. Zhang X, Wu Q, Zhao Y, Yang X. *Decaisnea insignis* seed oil inhibits trimethylamine-N-oxide formation and remodels intestinal microbiota to alleviate liver dysfunction in L-carnitine feeding mice. *J Agric Food Chem.* (2019) 67:13082–92. doi: 10.1021/acs.jafc.9b05383

54. Tang W, Yao X, Xia F, Yang M, Chen Z, Zhou B, et al. Modulation of the Gut microbiota in rats by Hugan Qingzhi tablets during the treatment of high-fat-diet-induced nonalcoholic fatty liver disease. *Oxid Med Cell Longev.* (2018) 2018:7261619. doi: 10.1155/2018/7261619

55. Zhou L, Xiao X, Li M, Zhang Q, Yu M, Zheng J, et al. Maternal exercise improves high-fat diet-induced metabolic abnormalities and gut microbiota profiles in mouse dams and offspring. *Front Cell Infect Microbiol.* (2020) 10:292. doi: 10.3389/fcimb.2020.00292

56. den Besten G, van Eunen K, Groen AK, Venema K, Reijngoud DJ, Bakker BM. The role of short-chain fatty acids in the interplay between diet, gut microbiota, and host energy metabolism. *J Lipid Res.* (2013) 54: 2325–40.

57. Louis P, Flint HJ. Diversity, metabolism and microbial ecology of butyrate-producing bacteria from the human large intestine. *FEMS Microbiol Lett.* (2009) 294:1–8. doi: 10.1111/j.1574-6968.2009.01514.x

58. Sanchez HN, Moroney JB, Gan H, Shen T, Im JL, Li T, et al. B cell-intrinsic epigenetic modulation of antibody responses by dietary fiber-derived short-chain fatty acids. *Nat Commun.* (2020) 11:60. doi: 10.1038/s41467-019-13603-6

59. Huang G, Wang L, Li J, Hou R, Wang M, Wang Z, et al. Seasonal shift of the gut microbiome synchronizes host peripheral circadian rhythm for physiological adaptation to a low-fat diet in the giant panda. *Cell Rep.* (2022) 38:110203. doi: 10.1016/j.celrep.2021.110203

60. Ellison AR, Wilcockson D, Cable J. Circadian dynamics of the teleost skin immune-microbiome interface. *Microbiome.* (2021) 9:222. doi: 10.1186/s40168-021-01160-4

61. Lundell LS, Parr EB, Devlin BL, Ingerslev LR, Altıntaş A, Sato S, et al. Time-restricted feeding alters lipid and amino acid metabolite rhythmicity without perturbing clock gene expression. *Nat Commun.* (2020) 11:4643. doi: 10.1038/s41467-020-18412-w

Frontiers in Nutrition

Explores what and how we eat in the context of health, sustainability and 21st century food science

A multidisciplinary journal that integrates research on dietary behavior, agronomy and 21st century food science with a focus on human health.

Discover the latest Research Topics

See more →

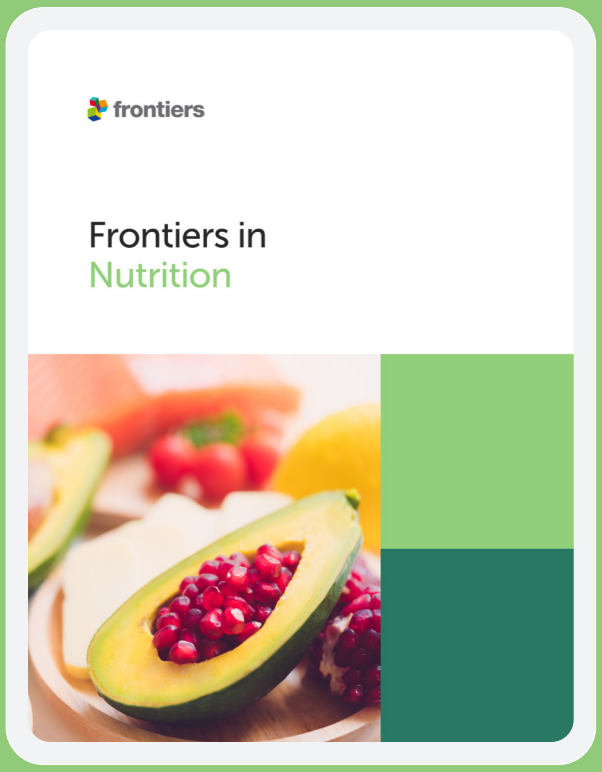

Frontiers

Avenue du Tribunal-Fédéral 34
1005 Lausanne, Switzerland
frontiersin.org

Contact us

+41 (0)21 510 17 00
frontiersin.org/about/contact